VOLUME 5 MARCH 1961 No. 1

COMBUSTION

AND

FLAME

QUARTERLY JOURNAL OF THE COMBUSTION INSTITUTE

Editors

F. H. GARNER BERNARD LEWIS (U.S.A.)

Editorial Board

L. Deffet (BELGIUM)
W. Jost (GERMANY)
P. Laffitte (FRANCE)
J. W. Linnett (U.K.)
P. Lloyd (U.K.)
J. P. Longwell (U.S.A.)
F. E. Marble (U.S.A.)
W. T. Olson (U.S.A.)
D. T. A. Townend (U.K.)
S. Yagi (JAPAN)
E. F. M. van der Held (NETHERLANDS)

LONDON
BUTTERWORTHS
1961

COMBUSTION

AND

FLAME

QUARTERLY JOURNAL OF THE COMBUSTION INSTITUTE

VOLUME V

Editors

F. H. GARNER BERNARD LEWIS (U.S.A.)

Editorial Board

L. Deffet (BELGIUM)
W. Jost (GERMANY)
P. Laffitte (FRANCE)
J. W. Linnett (U.K.)
P. Lloyd (U.K.)
J. P. Longwell (U.S.A.)
F. E. Marble (U.S.A.)
W. T. Olson (U.S.A.)
D. T. A. Townend (U.K.)
S. Yagi (JAPAN)
E. F. M. van der Held (NETHERLANDS)

LONDON
BUTTERWORTHS
1961

BUTTERWORTHS AND CO. (PUBLISHERS) LTD
88 Kingsway, London, W.C.2

U.S.A. Distributors:
BUTTERWORTHS INC., 7235 WISCONSIN AVENUE, WASHINGTON 14, D.C.

Commonwealth Offices:

AUCKLAND:	35 High Street
BRISBANE:	240 Queen Street
DURBAN:	33/35 Beach Grove
MELBOURNE:	430 Bourke Street
SYDNEY:	8 O'Connell Street
TORONTO:	1367 Danforth Avenue
WELLINGTON:	49/51 Ballance Street

PRINTED IN GREAT BRITAIN BY THE LEWES PRESS, WIGHTMAN & CO. LTD., LEWES, SUSSEX.

Thermal Radiation from Fluorine–Ammonia Flames

R. EULNER, J. MERTENS and R. L. POTTER*

Bell Aircraft Corporation, Post Office Box One, Buffalo 5, New York

(*Received June 1959*)

The radiation from stoichiometric fluorine–ammonia flames has been measured at atmospheric pressure and at two optical densities. From these measurements an engineering emissivity has been calculated and the effective charge of HF *has been deduced.*

Introduction

RADIATION by high temperature combustion gases may contribute a substantial portion of the total heat transferred to the walls of a combustion chamber. This is especially true if the major products of combustion radiate in the infra-red, such as HF. An approximate theoretical method for estimating engineering emissivities of hot gases has been developed by S. S. PENNER[1] for high pressures where rotational overlapping is complete and by S. S. PENNER, M. H. OSTRANDER and H. S. TSIEN[2] at low pressures where non-overlapping of rotational lines occurs. The simple method developed for high pressures although giving high results, appears to be very good even at low pressures, while the method for low pressures appears to be very sensitive to assumed line widths and line shapes. In view of the importance of HF as a combustion product in high temperature flames, measurements of the thermal radiation from stoichiometric fluorine–ammonia flames have been made at two optical densities at atmospheric pressure. Fluorine–ammonia flames were used because of the relative simplicity in handling the fuel.

Experimental

The method of measuring the thermal radiation from the fluorine–ammonia flames was similar to that used by H. C. HOTTEL and V. C. SMITH[3]. If the radiation from a flame, arising from a surface dS_2 at an angle θ_2 from the normal to the surface, passing a distance R into a detector of receiving area dS_1, at an angle θ_1 to the normal to the surface of the detector gives the same response to the detector as a black body at some temperature T_{BB} at the same distance R, then

$$\int_{S_1}\int_{S_2}\int_{0}^{\infty} i_F(\lambda, T_F)\cos\theta_1\cos\theta_2\frac{dS_1\,dS_2}{R^2}\,d\lambda$$

$$=\int_{S_1}\int_{S_2}\int_{0}^{\infty} i_{BB}(\lambda, T_{BB})\cos\theta_1\cos\theta_2\frac{dS_1\,dS_2}{R^2}\,d\lambda$$

where $i(\lambda)$ is the monochromatic intensity of radiation, and λ is the wavelength. Since the detector fixes θ_1, θ_2 and dS_1, dS_2, then

$$I_{BB}(\lambda, T_{BB})=2\pi hc^2/\lambda^5\,[\exp(hc/\lambda kT)-1]$$

where the following relation holds

$$\int_0^\infty I_F(\lambda, T_F)\,d\lambda=\int_0^\infty I_{BB}(\lambda, T_{BB})\,d\lambda=\sigma T_{BB}^4$$

where σ is the Stefan–Boltzmann constant. Finally in terms of the emissivity of the flame, there is obtained

$$\varepsilon T_F^4=T_{BB}^4$$

Hence an engineering emissivity ε of the flame can be found by obtaining the temperature of a black body that gives the same radiation as the flame at temperature T_F.

The preceding analysis presupposes that no absorbing medium is interposed between the source of radiation and the detector. However, detectors of the thermopile type used in the present investigations are enclosed and evacuated to ensure proper functioning of the receiving element independently of the

*Present address: American Cyanamid Company, Stamford, Connecticut.

surrounding atmosphere. Hence the preceding discussion must be amended to allow for the window in the detector. If the transmittance of the window material is $\tau(\lambda)$, then when the energy received by the detector is the same for both flame and black body,

$$\int_0^\infty \tau(\lambda) I_F(\lambda, T_F)\, d\lambda = \int_0^\infty \tau(\lambda) I_{BB}(\lambda, T_{BB})\, d\lambda$$

The detector used in this investigation was a specially built Leeds and Northrup double mirror evacuated Rayotube, Type 8890–U having a calcium fluoride window 1·5 mm thick with a rectangular aperture. The transmittance of the window used in the Rayotube was measured with a Beckman Model IR2 infra-red spectrophotometer as a function of wavelength,

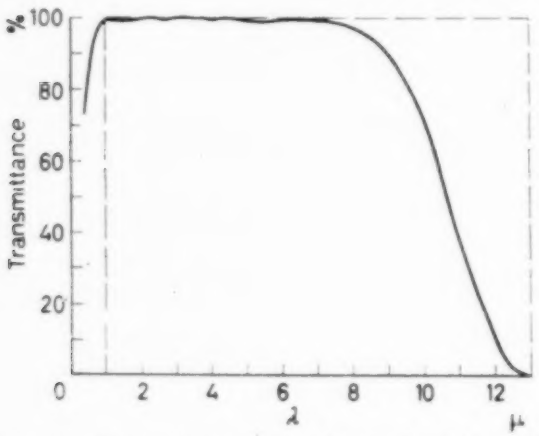

Figure 1. Transmittance of calcium fluoride window

and is shown in *Figure 1*. In the region of the fundamental and first overtone of HF[1], the transmittance is 99·5 per cent, while above 13 microns the transmittance is essentially zero. Hence

$$0{\cdot}995\, \varepsilon T_i^4 = \frac{1}{\sigma} \int_0^\infty \tau(\lambda) I_{BB}(\lambda, T_{BB})\, d\lambda$$

was used to obtain ε from the measurements. The integral was obtained by graphical integration.

The Rayotube was calibrated by sighting on an approximate black body, namely a hole in a plug inserted in a silicon carbide target tube supplied by Leeds and Northrup. The effective emissivity of the hole in the ceramic plug was estimated according to

$$\varepsilon' = \varepsilon / [\varepsilon + f(1 - \varepsilon)]$$

where ε is the emissivity of the wall material, and f is the fraction of the inner surface of the black body enclosure that is cut away by the opening. From the geometry of the plug and tube ε' was estimated to be 0·993 which was assumed to be effectively unity. The details of the black body device and the Rayotube in operating position are shown in *Figure 2*. The temperature of the black body was measured by thermocouple and optical pyrometry, and the results agreed within a few degrees centigrade of each other. A calibration curve of Rayotube e.m.f. versus black body temperature was obtained in this manner. The e.m.f. generated by the radiation falling upon the thermopile in the Rayotube was measured on a Leeds and Northrup K–2 Potentiometer.

The fluorine was purchased in cylinders from the General Chemical Co., while the ammonia came from the Henry Bower Chemical Mfg Co. The ammonia was better than 99·15 per cent ammonia, the balance being water. The fluorine was 98·8 per cent fluorine, the balance being 0·4 per cent HF, CO_2 and 0·8 per cent O_2, N_2 and other non-condensables. Both ammonia and fluorine were used without purification.

In order to provide a suitable flame, a rectangular diffusion burner was constructed with fluorine tubes alternating with ammonia tubes. By making the distance between tubes as small as possible, a premixed flame was approached. It was necessary to cool the face of the burner, and a special jacket was provided so that water could be circulated below the face of the burner. The flame was surrounded by nitrogen to exclude atmospheric oxygen. Special nitrogen jets were provided at each end of the burner to control the path length. The path length was estimated by means of a schlieren system set at right angles to the optical path of the Rayotube. Fisher–Porter flowmeters were used to monitor the fluorine and ammonia flows. The burner could be raised or lowered and, by changing the vertical position of the burner, the region of maximum emission could be determined.

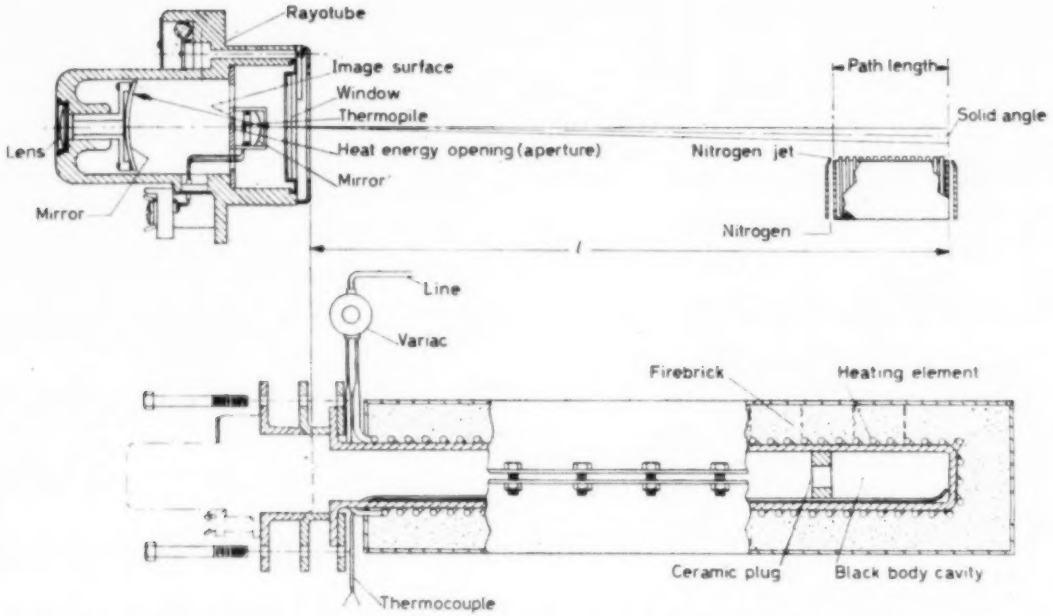

Figure 2. Arrangement of block body device with Rayotube in operating position

The general experimental layout is shown in *Figure 3.*

Measurements were made of stoichiometric fluorine–ammonia flames of 3·2 and 4·75 cm path length. With no nitrogen flowing from the jets at either end of the burner, the burnt gases expanded, and the cold outer layers absorbed some of the radiation. By adjusting the nitrogen flow at each end of the burner, it was possible to confine the flame between sharp, vertical boundaries, as indicated by the schlieren image. This procedure reduced the layer in which self-absorption occurred to a minimum and at the same time provided a simple means of obtaining

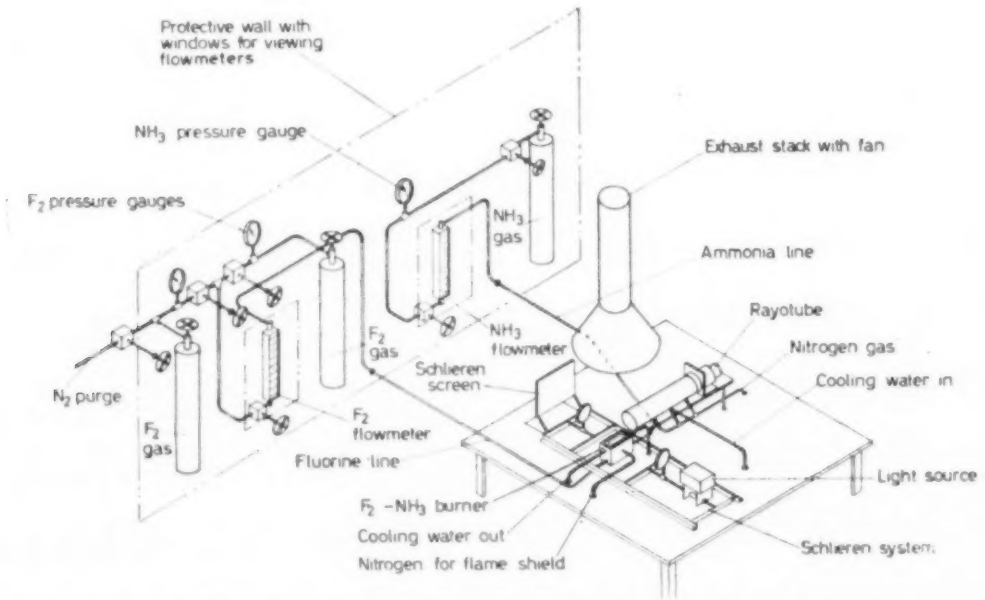

Figure 3. Schematic of fluorine–ammonia burner system for radiant heat transfer studies

an accurate estimate of the path length. As the HF fundamental occurs in, and is nearly obscured by, the 2·7 micron atmospheric water vapour band, a tube suitably blackened was placed between the flame and the Rayotube. Dry nitrogen was continuously flushed through the tube to eliminate water vapour.

Results

The emissivities for stoichiometric fluorine–ammonia flames at atmospheric pressure are given in *Table 1*. The reproducibility of the measurements may be seen by inspection of the emissivities. The random errors in the experiments account for the variations in the tabulated emissivities. The systematic errors are not believed to be serious. Thus, the flame temperature was calculated on an IBM 704 digital computer, and since the thermodynamic data are good, the flame temperature should also be good because the only piece of information in doubt is the dissociation energy of F_2. This was taken to be 36·7 kcal/mole, following W. H. Evans, T. R. Munson and D. D. Wagman[3]. However, in the combustion products of a stoichiometric mixture of fluorine and ammonia there is very little F_2 present, although there is a considerable amount of F (about 0·149 mole fraction) which has come from dissociation of HF. Another systematic error may be the temperature assigned to the black body, which may not be the true thermodynamic temperature. However, because of the close agreement between temperatures obtained by thermocouple and optical pyrometer, with independent calibrations, it is believed that the temperatures are correct to ±10° at 1 000°K. The burners were wide enough so that the gases should not depart appreciably from equilibrium by radiation at right angles to the path cut out by the Rayotube[6]. It was assumed that no absorption of radiation occurred between the flame and the detector, except for the calcium fluoride window, and that the radiation reflected from the detector itself was negligible. The random errors are in the path length determinations, mixture strength of the combustible gases, and difficulties encountered due to deposition of ammonium fluoride salts on the burner tips. Estimation of all these effects together indicates that the emissivities are reliable to about ±10 per cent.

Table 1. Emissivities of stoichiometric fluorine-ammonia flames at atmospheric pressure

l *cm*	T_{BB} °K	T_F °K	X *cm.atm*	ϵ	k_p *(calc.)* $(cm.atm)^{-1}$
3·2	783	3835	1·885	0·00156	0·00802
3·2	783	3835	1·885	0·00156	0·00802
3·2	783	3835	1·885	0·00156	0·00802
3·2	782	3835	1·885	0·00155	0·00800
3·2	783	3835	1·885	0·00156	0·00802
4·75	878	3835	2·798	0·00251	0·00865
4·75	875	3835	2·798	0·00248	0·00855
4·75	867	3835	2·798	0·00238	0·00820
4·75	871	3835	2·798	0·00243	0·00838
4·75	867	3835	2·798	0·00238	0·00820
4·75	862	3835	2·798	0·00232	0·00800
4·75	856	3835	2·798	0·00226	0·00780
4·75	868	3835	2·798	0·00238	0·00821
4·75	868	3835	2·798	0·00238	0·00821
					Average k_p=0·00816

Discussion

S. S. Penner *et al.*[1,2] have made theoretical calculations of emissivities of radiating gases under several assumptions. First, they took up the simple case where the rotational lines completely overlap. Later the case of non-overlapping rotational lines was examined. According to the curves exhibited by S. S. Penner[7], the limiting emissivities based on the first assumption where complete rotational overlapping occurs, give an excellent repre-

sentation of the emissivity based on non-overlapping lines at higher temperatures even at rather low values of the optical density, $X = pl$, where p is in atmospheres and l is in centimetres. Hence, even though X in the present experiments was not larger than 2·85 cm atm, it appears best to compare the measured emissivities with the emissivities estimated on the basis of complete overlapping of rotational lines because the temperatures in the stoichiometric fluorine–ammonia flame are very high, about 3 835° K. In so doing, it is assumed that the other gases present in the flame do not change the transition probabilities of HF and that the effective band widths for HF as given by Penner *et al.*[1] can be applied at atmospheric pressure.

If the emissivity is calculated according to this method, one finds that the contribution of the first overtone amounts to less than five per cent of the total emissivity for the conditions under which the experiments were carried out. If one uses the relation suggested by J. E. ROSENTHAL[8] for k_v in terms of k_F, where k_F and k_v are the average absorption coefficients of the fundamental and first overtone respectively, there can be derived the approximate relation for small values of pl, since k_F is also small

$$\varepsilon \simeq [k_F pl \cdot \varepsilon'_F + k_O pl \cdot \varepsilon'_O] - \tfrac{1}{2}[(k_F pl)^2 \cdot \varepsilon'_F + (k_O pl)^2 \cdot \varepsilon'_O] + \ldots$$

where ε'_F and ε'_O are the limiting emissivities of the fundamental and first overtone respectively. Then $k_O = 2{\cdot}18 \times 10^{-2} k_F$, hence

$$\varepsilon \simeq k_F pl\,[0{\cdot}0994 - k_F pl\,0{\cdot}049 + \ldots]$$

If the values of ε obtained experimentally are assumed correct, then it is possible to obtain a new value of k_F. These are tabulated in *Table 1*.

Accepting as correct the experimentally derived value of k_F, it is possible to arrive at a new value for the effective charge of HF from the relation

$$k_F = \frac{N_I \pi e_F^2}{3\mu c^2} \times \frac{1}{\Delta\nu_{n \to n+1}}$$

where N_I is the number of molecules per cubic centimetre, μ the reduced mass, c the velocity of light, $\Delta\nu_{n \to n+1}$ is the effective band width of the fundamental of HF in wave numbers and e_F is the effective charge. The effective charge calculated in this manner is 0·244 e as compared with 0·262 e given by Penner *et al.*[1] where e is the charge on the electron. The standard deviation in the calculated values of k_F is about nine per cent which is of the order estimated for the random error in the experiments. The reduction of the effective charge by approximately eight per cent is not surprising since the value adopted by Penner *et al.*[1] was obtained as the result of extrapolation plus another correction. For high temperature emissivity estimates of combustion gases containing HF, it is recommended that Penner *et al.*'s[1] simple method of obtaining limiting emissivities be used with the effective charge of HF taken as 0·244 e.

References

1 PENNER, S. S. *J. appl. Phys.* 1950, **21**, 685
2 PENNER, S. S., OSTRANDER, M. H. and TSIEN, H. S. *J. appl. Phys.* 1952, **23**, 256
3 HOTTEL, H. C. and SMITH, V. C. *Trans. Amer. Soc. mech. Engrs*, 1935, **57**, 463
4 TALLEY, R. M., KAYLOR, H. M. and NIELSEN, A. H. *Phys. Rev.* 1950, **77**, 529
5 EVANS, W. H., MUNSON, T. R. and WAGMAN, D. D. *J. Res. Nat. Bur. Stand.* 1955, **55**, 147
6 GAYDON, A. G. and WOLFHARD, H. G. *Flames*. Chapman and Hall: London, 1953
7 PENNER, S. S. *J. appl. Phys.* 1952, **23**, 825
8 ROSENTHAL, J. E. *Proc. Nat. Acad. Sci., Wash.* 1935, **21**, 281

an accurate estimate of the path length. As the HF fundamental occurs in, and is nearly obscured by, the 2·7 micron atmospheric water vapour band, a tube suitably blackened was placed between the flame and the Rayotube. Dry nitrogen was continuously flushed through the tube to eliminate water vapour.

Results

The emissivities for stoichiometric fluorine–ammonia flames at atmospheric pressure are given in *Table 1*. The reproducibility of the measurements may be seen by inspection of the emissivities. The random errors in the experiments account for the variations in the tabulated emissivities. The systematic errors are not believed to be serious. Thus, the flame temperature was calculated on an IBM 704 digital computer, and since the thermodynamic data are good, the flame temperature should also be good because the only piece of information in doubt is the dissociation energy of F_2. This was taken to be 36·7 kcal/mole, following W. H. Evans, T. R. Munson and D. D. Wagman[5]. However, in the combustion products of a stoichiometric mixture of fluorine and ammonia there is very little F_2 present, although there is a considerable amount of F (about 0·149 mole fraction) which has come from dissociation of HF. Another systematic error may be the temperature assigned to the black body, which may not be the true thermodynamic temperature. However, because of the close agreement between temperatures obtained by thermocouple and optical pyrometer, with independent calibrations, it is believed that the temperatures are correct to ±10° at 1 000°K. The burners were wide enough so that the gases should not depart appreciably from equilibrium by radiation at right angles to the path cut out by the Rayotube[6]. It was assumed that no absorption of radiation occurred between the flame and the detector, except for the calcium fluoride window, and that the radiation reflected from the detector itself was negligible. The random errors are in the path length determinations, mixture strength of the combustible gases, and difficulties encountered due to deposition of ammonium fluoride salts on the burner tips. Estimation of all these effects together indicates that the emissivities are reliable to about ±10 per cent.

Table 1. Emissivities of stoichiometric fluorine-ammonia flames at atmospheric pressure

l *cm*	T_{BB} °*K*	T_F °*K*	X *cm.atm*	ϵ	k_F *(calc.)* $(cm.atm)^{-1}$
3·2	783	3835	1·885	0·00156	0·00802
3·2	783	3835	1·885	0·00156	0·00802
3·2	783	3835	1·885	0·00156	0·00802
3·2	782	3835	1·885	0·00155	0·00800
3·2	783	3835	1·885	0·00156	0·00802
4·75	878	3835	2·798	0·00251	0·00865
4·75	875	3835	2·798	0·00248	0·00855
4·75	867	3835	2·798	0·00238	0·00820
4·75	871	3835	2·798	0·00243	0·00838
4·75	867	3835	2·798	0·00238	0·00820
4·75	862	3835	2·798	0·00232	0·00800
4·75	856	3835	2·798	0·00226	0·00780
4·75	868	3835	2·798	0·00238	0·00821
4·75	868	3835	2·798	0·00238	0·00821
				Average k_F =	0·00816

Discussion

S. S. Penner *et al.*[1,2] have made theoretical calculations of emissivities of radiating gases under several assumptions. First, they took up the simple case where the rotational lines completely overlap. Later the case of non-overlapping rotational lines was examined. According to the curves exhibited by S. S. Penner[7], the limiting emissivities based on the first assumption where complete rotational overlapping occurs, give an excellent repre-

sentation of the emissivity based on non-overlapping lines at higher temperatures even at rather low values of the optical density, $X = pl$, where p is in atmospheres and l is in centimetres. Hence, even though X in the present experiments was not larger than 2·85 cm atm, it appears best to compare the measured emissivities with the emissivities estimated on the basis of complete overlapping of rotational lines because the temperatures in the stoichiometric fluorine–ammonia flame are very high, about 3 835°K. In so doing, it is assumed that the other gases present in the flame do not change the transition probabilities of HF and that the effective band widths for HF as given by Penner *et al.*[1] can be applied at atmospheric pressure.

If the emissivity is calculated according to this method, one finds that the contribution of the first overtone amounts to less than five per cent of the total emissivity for the conditions under which the experiments were carried out. If one uses the relation suggested by J. E. Rosenthal[8] for k_o in terms of k_F, where k_F and k_o are the average absorption coefficients of the fundamental and first overtone respectively, there can be derived the approximate relation for small values of pl, since k_F is also small

$$\varepsilon \simeq [k_F pl \cdot \varepsilon'_F + k_O pl \cdot \varepsilon'_O] - \tfrac{1}{2}[(k_F pl)^2 \cdot \varepsilon'_F + (k_O pl)^2 \cdot \varepsilon'_O] + \ldots$$

where ε'_F and ε'_O are the limiting emissivities of the fundamental and first overtone respectively. Then $k_o = 2{\cdot}18 \times 10^{-2} k_F$, hence

$$\varepsilon \simeq k_F pl\,[0{\cdot}0994 - k_F pl\, 0{\cdot}049 + \ldots]$$

If the values of ε obtained experimentally are assumed correct, then it is possible to obtain a new value of k_F. These are tabulated in *Table 1*. Accepting as correct the experimentally derived value of k_F, it is possible to arrive at a new value for the effective charge of HF from the relation

$$k_F = \frac{N_I \pi e_F^2}{3\mu c^2} \times \frac{1}{\Delta\nu_{n\to n+1}}$$

where N_I is the number of molecules per cubic centimetre, μ the reduced mass, c the velocity of light, $\Delta\nu_{n\to n+1}$ is the effective band width of the fundamental of HF in wave numbers and e_F is the effective charge. The effective charge calculated in this manner is 0·244 e as compared with 0·262 e given by Penner *et al.*[1] where e is the charge on the electron. The standard deviation in the calculated values of k_F is about nine per cent which is of the order estimated for the random error in the experiments. The reduction of the effective charge by approximately eight per cent is not surprising since the value adopted by Penner *et al.*[1] was obtained as the result of extrapolation plus another correction. For high temperature emissivity estimates of combustion gases containing HF, it is recommended that Penner *et al.*'s[1] simple method of obtaining limiting emissivities be used with the effective charge of HF taken as 0·244 e.

References

1 Penner, S. S. *J. appl. Phys.* 1950, **21**, 685
2 Penner, S. S., Ostrander, M. H. and Tsien, H. S. *J. appl. Phys.* 1952, **23**, 256
3 Hottel, H. C. and Smith, V. C. *Trans. Amer. Soc. mech. Engrs.* 1935, **57**, 463
4 Talley, R. M., Kaylor, H. M. and Nielsen, A. H. *Phys. Rev.* 1950, **77**, 529
5 Evans, W. H., Munson, T. R. and Wagman, D. D. *J. Res. Nat. Bur. Stand.* 1955, **55**, 147
6 Gaydon, A. G. and Wolfhard, H. G. *Flames.* Chapman and Hall: London, 1953
7 Penner, S. S. *J. appl. Phys.* 1952, **23**, 825
8 Rosenthal, J. E. *Proc. Nat. Acad. Sci., Wash.* 1935, **21**, 281

Burning Velocities of Hydrogen–Air and Hydrogen–Oxygen Mixtures

Determination by Burner Method with Schlieren Photography

D. A. SENIOR*

Department of Chemical Engineering, Imperial College of Science and Technology, London, S.W. 7

(*Received July 1959*)

A schlieren system for photographing the inner cone in bunsen flames used in burning velocity measurements is described. A useful magnification factor of 20 to 25 times measured from the burning cone to its photograph is obtainable; so the system can be used with the small burners needed for such fast burning flames as those of hydrogen–oxygen mixtures. Some results for hydrogen–oxygen and hydrogen–air flames are given which accord with Jahn's values at the lean end, though the results for the richer hydrogen–oxygen mixtures agree with the higher values determined by Bartholomé.

A SEARCH through the literature for burning velocity measurements of hydrogen, carbon monoxide, methane, ethylene and propane mixed with air or oxygen gave 67 separate determinations (see ref. 1). Of these only 14 related to mixtures containing oxygen and only 8 related to mixtures containing hydrogen. The reason for the scarcity of measurements on mixtures containing oxygen or hydrogen derives in part from their high burning velocity which leads to experimental difficulty whatever method of measurement is used.

In measurements based on the inner cones in bunsen flames, for example, the difficulty lies in the need to use burning tubes of a very small diameter in order to preserve laminar flow at the high flow rates required to prevent flash-back. Thus, for hydrogen–oxygen mixtures around stoichiometric, the tube diameter cannot exceed 1 mm, though E. BARTHOLOMÉ[2] has succeeded in increasing this somewhat by means of a specially shaped nozzle. With such small burners, accurate measurement of the burning cone is impossible unless very good optical arrangements are employed.

The need was clear, however, for further data on hydrogen–air and particularly on hydrogen–oxygen flames and attention was therefore given to producing an optical system which would give useful enlargements at 20 to 25 times linear magnification. At the same time it was decided to employ a schlieren system, since an examination of the structure of the bunsen inner cone by both H. R. CONAN and J. W. LINNETT[3] and by F. J. WEINBERG[4,5] demonstrated that the schlieren cone was the most satisfactory surface on which to base the measurement.

This paper is concerned with the optical system and with some burning velocities for hydrogen–oxygen and hydrogen–air mixtures which have been determined by means of it.

The Optical System

This is shown diagrammatically in *Figure 1*. The light source is a 150 CP Ediswan Pointolite Lamp P and an image is focused by means of a Dallmeyer type B condenser lens L_1 of focal length 3 in. and diameter 2·75 in. on to a horizontal slit S 2 mm in width. Parallel light is provided at the location of the flame by means of an achromatic telescope objective L_2, of 27 in. focal length and 4 in. diameter. An identical lens L_3 brings the light to a focus at a horizontal knife edge K. A 21 in. focal length, 1·5 in. diameter, achromatic lens L_4 which could be smaller produces an aerial image I of the burner and burning cone at a point where it is conveniently magnified on to the photographic plate Ph by means of the Schneider–Kreuznach Xenon F 1·5 in. diameter lens, L_5, of 5·5 cm

*Formerly of Admiralty Research Laboratory, Teddington, Middlesex. Now Scientific Attaché to British Embassy, Moscow.

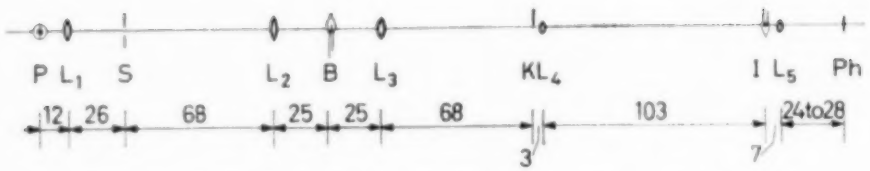

Figure 1. Optical layout. Dimensions given to nearest centimetre

focal length arranged with the rear component of the lens facing the aerial image. The photographic plate is held in a press camera with lens and lens plate removed, and exposures are made by means of the roller blind shutter in the camera. The resulting image on the plate has five to six times the dimensions of the object. A further enlargement of four times on to a dimensionally stable* printing paper is employed and measurements are made on the photographic print.

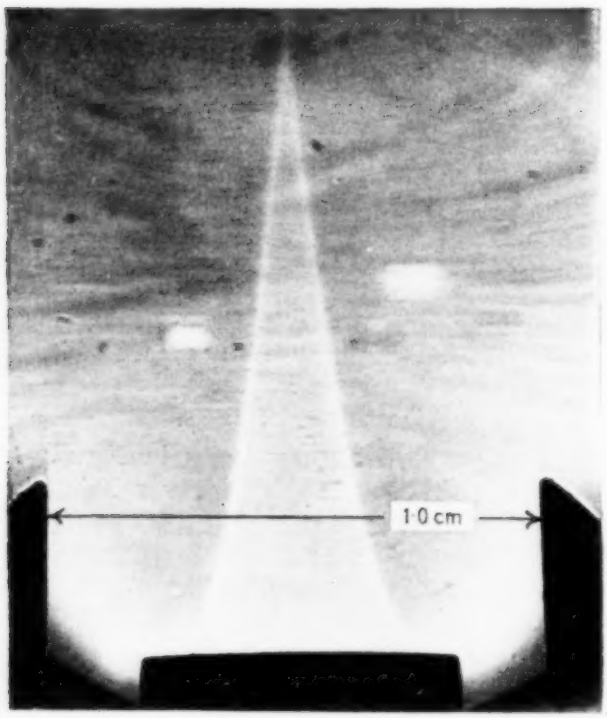

Figure 2. Enlargement of burning cone picture. Tube i.d. 0·482 cm. Gas mixture 24·9 per cent hydrogen, 75·1 per cent air

A picture of a burning cone is shown in *Figure 2*. Two vertical knife edges spaced 1 cm apart were attached to the burner as shown in order to facilitate calculation of scale.

*Kodak Bromide Foil Card.

Some optical distortion is unavoidable. This is seen in the picture of a graticule inserted at the location of the burner (*Figure 3*). Over

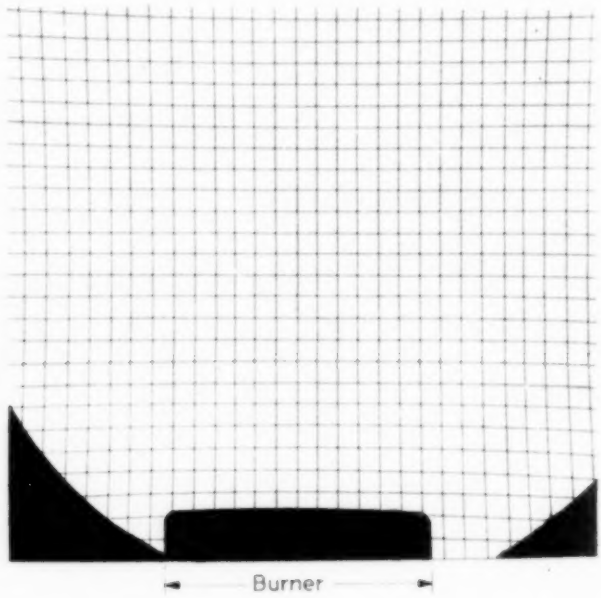

Figure 3. Some barrel distortion occurs

the region occupied by the burning cone, the distortion amounts to a few per cent and allowance is readily made for its effect.

Experimental Arrangements for Burner and Gas Supply

Tubes of internal diameter 0·099, 0·166, 0·333 and 0·482 cm were used, the smallest two being found convenient for hydrogen–oxygen mixtures and the largest three for hydrogen–air mixtures.

Hydrogen and air or oxygen were taken from cylinders through rotameters and rubber tubing to a T-junction and thence to the burner tube which was made long enough to ensure laminar flow at exit†. A water manometer was arranged

†Reynolds numbers did not exceed 1500, except for the richest two hydrogen–oxygen mixtures where the values were 1700 and 2100.

to measure excess gas pressure at exit from the rotameters.

The rotameters were calibrated and the effect of the excess gas pressure on the calibration curves was determined from measurements using a bubble meter. No allowance was made for water vapour pressure in the bubble meter and the gases were not dried during calibration or burning velocity measurements as errors from these causes were likely to be considerably less than those in the measurement of the burning cones.

The burner tube was not cooled. Measurements showed that the height of the cone in the worst case (smallest tube diameter and slowest burning mixture) was unaffected when water was poured into a small can arranged to be concentric with the tube. The complications of a cooling jacket and continuous flow of cooling water were therefore avoided.

Gas flow conditions were varied as widely as possible for each tube. With too lean a mixture at a given flow rate the cone became too long for accurate measurement. When the mixture was too rich the flame became fluted prior to lighting back. A useful range of mixtures could generally be found between the limits set by these two effects.

Measurement of Burning Cone Pictures

The scale of the picture at the base of the cone was determined from the distance between the images of the knife edges. The dimensions of the cone were then determined as though the scale were constant over the whole picture. The total cone area was derived by graphical integration and a correction factor was applied depending simply on the height of the cone. The correction factor was previously determined (from the graticule picture) for the errors due to optical distortion for right cones of various heights. This procedure was accurate enough as the correction amounted to only a few per cent.

A simple form of graphical integration was employed. The centre line of the cone and the outer edge of one side of the cone were drawn in on the photographic print. Then, with a suitable interval, marks were made by means of dividers along the outer edge of the cone.

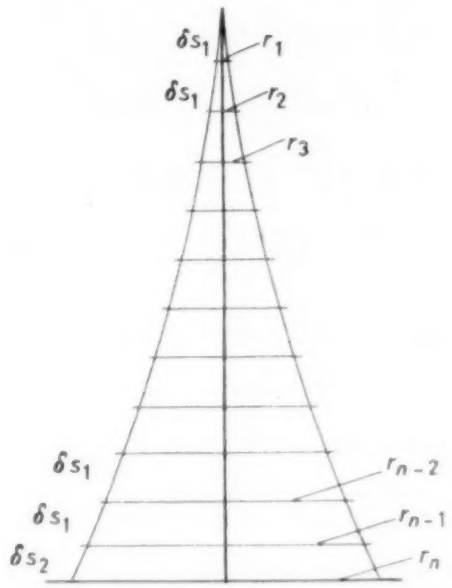

Figure 4. Method of integration of area of cone

Lines were then drawn at right angles to the centre line through these marks as shown in *Figure 4*. The area of the cone was assumed to be equal to the sum of the conical frusta determined by these lines and marks. The total surface area, A, was then given by the expression

$$A = 2\pi\delta s_1 \{r_1 + r_2 + \ldots + r_{n-2} + \tfrac{1}{2}r_{n-1}\} + \pi\delta s_2 \{r_{n-1} + r_n\}$$

The errors involved in this procedure with a reasonable number of intercepts (15 to 20) seemed unlikely to be any greater than those involved in the more usual 'corrected cone' and planimeter method[4] which involves the difficult measurement of the gradient at various points of the cone.

Calculation of Burning Velocity

The gas flow rate determined by the corrected rotameter readings divided by the area A was taken as the burning velocity. Alternative methods[6] such as those of Dery and those employing the cone apex angle, the cone gradient at various points (Smith and Pickering) and cone gradients deduced from a mathematical approximation to the shape of the curve were applied in a few cases. These, however, seemed to show no improvement on the total area

method. Thus Dery's method gave differing answers when applied to a larger or smaller section of the burning cone; the cone apex angle could not be determined accurately enough; the gradient method of Smith and Pickering gave increasing values of the burning velocity as the point at which the gradient was measured moved from the tip to the base of the cone (contrary to expectations); and the gradient method based on the mathematical approximation to the curve gave the same result though the actual values differed from those based on graphical measurements of the gradient by ±5 per cent. The total area method and the method of deducing the area seemed adequate therefore within the accuracy of the experiment.

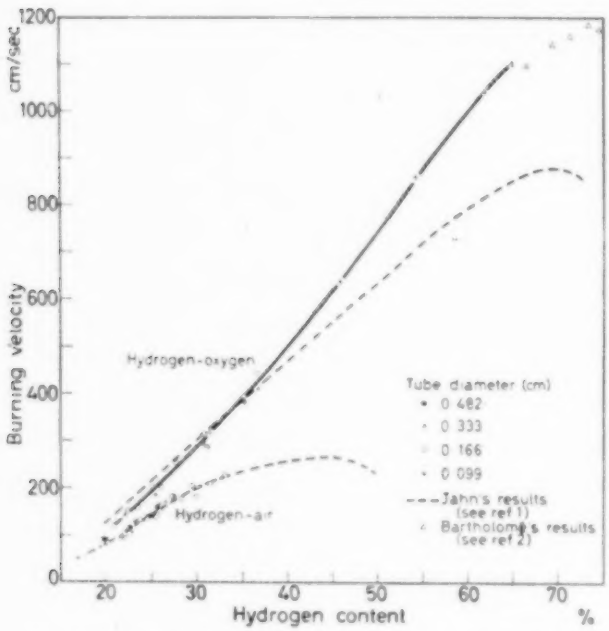

Figure 5. Burning velocities by total area method

Results

Results are shown graphically in *Figure 5*. It is seen that the values of burning velocities do not depend significantly on tube diameter and the scatter is reasonably small. Surprisingly, the values are not far removed from those of Jahn for lean mixtures although the higher value obtained by Bartholomé for the maximum burning velocity with hydrogen–oxygen mixtures is supported by the present results.

The author wishes to thank Dr F. J. Weinberg of the Imperial College who suggested the possibility of enlarging the schlieren image and Dr J. H. Burgoyne also of the Imperial College under whose supervision the work was carried out in the Department of Chemical Engineering.

References

[1] LEWIS, B. and VON ELBE, G. *Combustion, Flames and Explosions of Gases*. McGraw-Hill: New York, 1951

[2] BARTHOLOMÉ, E. 'Zur Methodik der Messung von Flammengeschwindigkeiten'. *Z. Elektrochem.* 1949, **53**, 191

[3] CONAN, H. R. and LINNETT, J. W. 'Burning velocity determinations, Part V—The use of schlieren photography in determining burning velocities by the burner method'. *Trans. Faraday Soc.* 1951, **47**, 981

[4] WEINBERG, F. J. 'Location of the schlieren image in a flame'. *Fuel, Lond.* 1955, **34**, 584

[5] WEINBERG, F. J. 'Location of the schlieren image in a flame'. *Fuel, Lond.* 1956, **35**, 161

[6] GAYDON, A. G. and WOLFHARD, H. G. *Flames, their Structure and Radiation*. Chapman and Hall: London, 1953

The Theory of Steady Laminar Spherical Flame Propagation: Analytical Solutions

D. B. SPALDING and V. K. JAIN

Mechanical Engineering Department, Imperial College of Science and Technology, London, S.W.7

(*Received August 1959*)

Spherical steady laminar flame propagation is considered. Analytical solutions have been obtained for the cases of (a) *Step-function reaction-rate curves, and* (b) *Adams-type reaction-rate curves. It is shown that the effective radius of a spherical flame is under-estimated if one uses the thin-flame approximation. The error decreases as the rate of injection and the laminar flame speed of the mixture increase. Graphical comparison has been made with numerical and analogue solutions. Curves are presented which can be used with fair accuracy with any realistic reaction-rate function.*

Introduction

Purpose of the paper

THE theory of one-dimensional laminar steady flame propagation has been rather extensively studied and is well understood. The phenomenon of spherical steady laminar flame propagation has been investigated by numerical means[2]. In the spherical flame problem, we assume that combustible gas flows uniformly and steadily from a point source into an atmosphere which comprises the products of combustion. Ref. 2 gives a description of the spherical flame, a formulation of the theoretical problem, and particular numerical solutions. This problem has also been solved by the resistance network analogue computer[3]. The purpose of the present paper is to present analytical solutions to the problem for artificial reaction-rate functions and to compare the results with those obtained by the resistance network analogue computer and by numerical means.

Notation

The following symbols are used:

- c Specific heat of gases at constant pressure, assumed constant (cal/g.°C)
- k Thermal conductivity of gases, assumed constant (cal/cm.s.°C)
- $\dot{m}$ Strength of point source (mass injection rate) (g/s)
- $\dot{m}''_f$ Mass burning rate per unit area in a plane laminar flame propagating through the injected mass (g/cm².s)
- r Radius from point of injection (cm)
- r_f Radius of flame calculated from the thin-flame approximation, equation 45 (cm)
- r^* Radius of effective thin flame (cm)
- $\dot{q}'''$ Volumetric reaction rate in flame, dependent on T alone (cal/cm³.s)

$$\overline{\dot{q}'''} = \int_{T_u}^{T_b} \dot{q}''' \mathrm{d}T / (T_b - T_u) \quad (\mathrm{cal/cm^3.s})$$

- T Gas temperature (°C)
- T_u Temperature of unburnt combustible (°C)
- T_b Temperature of adiabatic combustion products (°C)

$$\delta = \frac{k 4\pi r^{*2}}{c\dot{m}} \text{ thickness of flame (cm)}$$

$$\lambda = \overline{\dot{q}'''} k\,(4\pi r^{*2})^2 / \dot{m}^2 c^2\,(T_b - T_u)$$

$$\mu = \dot{q}''' \dot{m}^2 c^2 / k\,(T_b - T_u)\,(4\pi k)^2$$

$$\eta = \frac{4\pi k r}{\dot{m}c}, \text{ dimensionless radius}$$

$$\eta^* = \frac{4\pi k r^*}{\dot{m}c}, \text{ dimensionless effective radius}$$

$$y = -\frac{\dot{m}c}{4\pi k r}$$

$$y^* = -\frac{\dot{m}c}{4\pi k r^*}$$

$$\xi = \exp(-\dot{m}c / 4\pi k r)$$

$$\xi^* = \exp(-\dot{m}c / 4\pi k r^*)$$

$$\tau = (T - T_u) / (T_b - T_u)$$

$$\phi(\tau) = \dot{q}''' / \overline{\dot{q}'''}$$

Equation and boundary conditions

It is shown in ref. 2 that the problem is defined by the following differential equation

$$\frac{1}{r^2}\frac{\mathrm{d}}{\mathrm{d}r}\left(kr^2\frac{\mathrm{d}T}{\mathrm{d}r}\right)-\frac{\dot{m}c}{4\pi r^2}\frac{\mathrm{d}T}{\mathrm{d}r}+\dot{q}'''=0 \quad \ldots [1]$$

Boundary conditions

$$r=0: T=T_u \quad \ldots . [2]$$

$$r=\infty: T=T_b \quad \ldots . [3]$$

Reaction-rate functions

To solve the differential equation 1 under the boundary conditions 2 and 3 analytically, we have to assume artificial reaction-rate functions, i.e. $\dot{q}'''(T)$. Two families of such reaction-rate functions have been studied and are represented graphically in *Figures 1* and *2*.

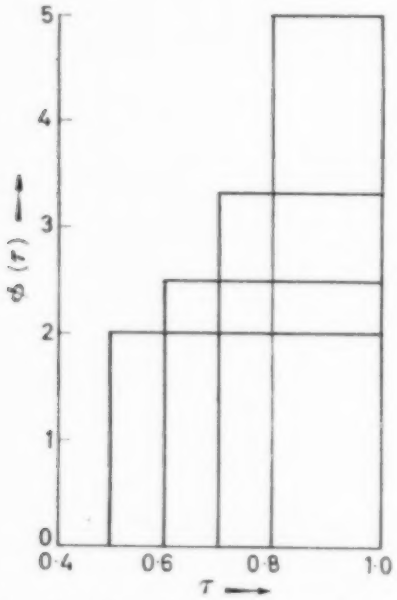

Figure 1. Step-function reaction-rate curves for $\tau_f=0{\cdot}5$, 0·6, 0·7 and 0·8

Summary of main results of analysis

We have discussed the results in terms of an 'effective thin-flame radius' r^* which is the radius obtained by extrapolating, through the region where reaction is taking place, the temperature curve valid for the region upstream of the reaction zone; r^* is the radius at which this curve intersects the temperature of combustion products. We define r_f as the radius which the flame would have for the given $\dot{m}$, if the flame were very thin and so had the same mass burning rate per unit area as a plane flame; this is called the 'thin-flame approximation'. The

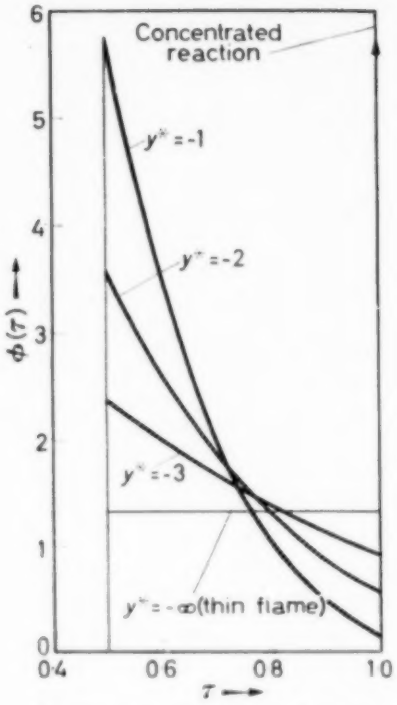

Figure 2. Adams-type reaction-rate curve for $\tau_f=0{\cdot}5$

analysis below shows that, for thick flames, the ratio r^*/r_f is a function of the dimensionless parameter $\dot{m}\dot{m}_f''c^2/4\pi k^2$, where $\dot{m}_f''$ is the mass burning rate per unit area of the combustible gas in question in a plane flame. *Figures 5* and *6* show how r^*/r_f rises above unity as $\dot{m}\dot{m}_f''c^2/4\pi k^2$ tends to zero. Hence the thin-flame approximation is asymptotically correct for high injection rates and highly reactive gases, otherwise the effective flame radius is always under-estimated.

Method of Solution

Dimensionless form

For simplicity, we suppose that the conductivity k is constant. We then render equation 1 dimensionless by the following transformations:

$$\tau \equiv (T-T_u)/(T_b-T_u) \quad \ldots . [4]$$

$$\eta \equiv 4\pi kr/\dot{m}c \quad \ldots . [5]$$

$$\phi(\tau) \equiv \dot{q}'''/\overline{\dot{q}'''} \quad \ldots . [6]$$

$$\mu \equiv \overline{\dot{q}'''}\dot{m}^2c^2/k\,(T_b-T_u)\,(4\pi k)^2 \quad \ldots . [7]$$

$$\overline{\dot{q}'''} \equiv \int_{T_u}^{T_b} \dot{q}'''\mathrm{d}T/(T_b-T_u) \quad \ldots . [8]$$

There results the following differential equation

$$\frac{1}{\eta^2}\frac{\mathrm{d}}{\mathrm{d}\eta}\left(\eta^2\frac{\mathrm{d}\tau}{\mathrm{d}\eta}\right)-\frac{1}{\eta^2}\frac{\mathrm{d}\tau}{\mathrm{d}\eta}+\mu\phi(\tau)=0 \quad \ldots [9]$$

The boundary conditions are:

$$\eta=0:\tau=0 \quad \ldots [10]$$

$$\eta=\infty:\tau=1 \quad \ldots [11]$$

Solution for μ

Step-function reaction-rate curve—We consider a reaction-rate curve defined by:

$$0\leqslant\tau\leqslant\tau_i:\phi(\tau)=0 \quad \ldots [12]$$

$$\tau_i<\tau\leqslant 1:\phi(\tau)=\frac{1}{1-\tau_i} \quad \ldots [13]$$

For such a system it is necessary to consider the solution of equation 9 in two regions, i.e. the region of no reaction and the region of finite reaction, and to join the solutions at τ_i. τ_i might be called the ignition temperature.

(*i*) In the region $0\leqslant\tau\leqslant\tau_i$, we can easily show that

$$\frac{\mathrm{d}\tau}{\mathrm{d}\eta}=\frac{\tau}{\eta^2} \quad \ldots [14]$$

which yields

$$\tau=\tau_i\exp\left\{\frac{1}{\eta_i}-\frac{1}{\eta}\right\} \quad \ldots [15]$$

where η_i is the value of η at $\tau=\tau_i$.

We note that, following the definition of r^* (see above), η^* is the value of the variable η which gives $\tau=1$ and satisfies the equation 15.

$$\therefore\frac{1}{\eta^*}-\frac{1}{\eta_i}=\ln\tau_i \quad \ldots [16]$$

(*ii*) In the region where reaction rate is finite, we have

$$\frac{\mathrm{d}}{\mathrm{d}\eta}\left(\eta^2\frac{\mathrm{d}\tau}{\mathrm{d}\eta}\right)-\frac{\mathrm{d}\tau}{\mathrm{d}\eta}+\frac{\mu\eta^2}{1-\tau_i}=0 \quad \ldots [17]$$

Integrating the above differential equation and applying the condition that the slope at $\tau=\tau_i$ is continuous, we obtain

$$\frac{\mathrm{d}\tau}{\mathrm{d}\eta}-\frac{\tau}{\eta^2}+\frac{\mu}{3(1-\tau_i)}\cdot\eta=\frac{\mu}{3(1-\tau_i)}\frac{\eta_i^3}{\eta^2} \quad \ldots [18]$$

Integrating equation 18, we obtain

$$\tau\mathrm{e}^{1/\eta}-\tau_i\mathrm{e}^{1/\eta_i}=-\frac{\mu}{3(1-\tau_i)}\eta_i^3\mathrm{e}^{1/\eta}+\frac{\mu}{3(1-\tau_i)}\eta_i^3\mathrm{e}^{1/\eta_i}-\frac{\mu}{6(1-\tau_i)}\left[\eta^2\mathrm{e}^{1/\eta}+\eta\mathrm{e}^{1/\eta}-\int\frac{\mathrm{e}^{1/\eta}}{1/\eta}\mathrm{d}(1/\eta)\right]_{\eta_i}^{\eta} \quad \ldots [19]$$

Applying the condition that the slope at $\tau=1$ is zero in equation 18, we obtain

$$\eta_1=\left[\frac{3(1-\tau_i)}{\mu}+\eta_i^3\right]^{1/3} \quad \ldots [20]$$

where η_1 is the value of η where τ reaches unity.

Also applying the condition that $\tau=1$, $\eta=\eta_1$, we obtain as our final result

$$\frac{\mu}{6(1-\tau_i)}\int_{1/\eta_1}^{1/\eta_i}\frac{\mathrm{e}^{1/\eta}}{1/\eta}\mathrm{d}(1/\eta)=\tau_i\mathrm{e}^{1/\eta_i}+\frac{\mu\mathrm{e}^{1/\eta_i}}{3(1-\tau_i)}\left[\eta_i^3+\eta_i^2/2+\eta_i/2\right]-\frac{\mu\mathrm{e}^{1/\eta_1}}{3(1-\tau_i)}\left[\eta_1^3+\eta_1^2/2+\eta_1/2\right] \quad \ldots [21]$$

The task of calculating μ with τ_i as a parameter for various values of η^* can be accomplished with the help of equations 16, 20 and 21. The results will be discussed below.

Adams-type reaction-rate function—In an early analysis of the present problem, G. K. ADAMS[1] used the assumption of a constant temperature gradient in the reaction zone while solving the problem of monopropellant droplet combustion. He used a space variable which was inversely proportional to the radial distance. We, therefore, have made the same assumption and have worked backwards to find out the reaction-rate function. It will appear that this reaction-rate function, represented in *Figure 2*, depends on the dimensionless effective flame radius, η^*.

We re-write equation 9 by using the transformation, $y=-1/\eta$, which gives

$$\frac{\mathrm{d}^2\tau}{\mathrm{d}y^2}-\frac{\mathrm{d}\tau}{\mathrm{d}y}=-\lambda\frac{y^{*4}}{y^4}\phi(\tau) \quad \ldots [22]$$

where

$$\lambda\equiv\frac{\mu}{y^{*4}}\equiv\frac{\dot{q}'''k(4\pi r^{*2})^2}{\dot{m}^2c^2(T_b-T_u)} \quad \ldots [23]$$

and y^* has been defined in the same way as η^* (see previous section). λ is identical in definition to the eigenvalue of the plane flame problem used in ref. 5.

In this case, following Adams, we assume that the reaction starts at a temperature τ_i and that, in the reaction zone, the temperature gradient $d\tau/dy$ is constant, having its value equal to that at the temperature τ_i.

When $\phi(\tau)=0$, the treatment is similar to that of the previous section and we obtain

$$d\tau/dy=\tau \quad \ldots . [24]$$

which gives

$$\tau=\tau_i e^{y-y_i} \quad \ldots . [25]$$

$$\therefore y_i-y^*=\ln \tau_i \quad \ldots . [26]$$

When the reaction rate is finite we have

$$\frac{d^2\tau}{dy^2}-\frac{d\tau}{dy}=-\lambda\frac{y^{*4}}{y^4}\cdot\phi(\tau) \quad \ldots . [22]$$

The boundary conditions are:

$$y=y_i:\tau=\tau_i;\ d\tau/dy=\tau_i \quad \ldots . [27]$$

$$y=y_1:\tau=1;\ d\tau/dy=0 \quad \ldots . [28]$$

Integrating equation 22 under the above boundary conditions, and using Adams's assumption of constant $d\tau/dy$ in the reaction zone, we have

$$\lambda=\frac{\tau_i^2 y_1^4}{2y^{*4}}+\frac{\tau_i^2}{5y^{*4}}(y_1^5-y_i^5) \quad \ldots [29]$$

where, by definition of ϕ,

$$\int_0^1 \phi(\tau)\,d\tau=1 \quad \ldots . [30]$$

We also have, using the basic assumption of Adams, $d\tau/dy=\tau_i$ in the reaction zone. This yields

$$\tau=\tau_i(y-y_1)+1 \quad \ldots . [31]$$

Since $y=y_i$ for $\tau=\tau_i$, we have

$$\tau_i=\tau_i(y_i-y_1)+1 \quad \ldots . [32]$$

With the help of equations 26, 29 and 32, we can obtain a series of values of λ versus y^* with τ_i as a parameter.

The reaction-rate curve can finally be deduced as:

$$0\leqslant\tau\leqslant\tau_i:\phi(\tau)=0 \quad \ldots . [33a]$$

$$\tau_i<\tau\leqslant 1:\phi(\tau)=\frac{y^4}{\frac{\tau_i y_1^4}{2}+\frac{\tau_i}{5}(y_1^5-y_i^5)}+\frac{\tau_i y_1^4 f(\tau-1)}{\frac{\tau_i y_1^4}{2}+\frac{\tau_i}{5}(y_1^5-y_i^5)} \quad \ldots . [33b]$$

where $f(\tau-1)$ is a 'delta function', i.e. the function is such that it is zero everywhere except at $\tau=1$ where its value is infinite, and

$$\int_0^x f(\tau-1)\,d\tau=1,\ (x>1) \quad \ldots . [34]$$

The reaction-rate curves of the above type are represented graphically in *Figure 2*.

The centroid of the reaction-rate function, τ_c, is given by:

$$\tau_c=\int_0^1 \tau\phi(\tau)\,d\tau=\frac{\frac{\tau_i}{6}(y_1^6-y_i^6)-\frac{\tau_i y_1}{5}(y_1^5-y_i^5)+\frac{y_1^5-y_i^5}{5}+\frac{y_1^4}{2}}{\frac{y_1^4}{2}+\frac{y_1^5-y_i^5}{5}} \quad \ldots . [35]$$

The results will be discussed below.

Degeneration of a spherical flame into a plane flame

Step-function reaction rate—Let us first define the flame thickness δ by

$$\delta\equiv(k/c\dot{m})\,4\pi r^{*2} \quad \ldots . [36]$$

The physical significance of this is as follows: δ is the thickness of gas through which just sufficient heat could pass by conduction to raise the gas flow through the prevailing temperature difference; it is a measure of the thickness of the 'pre-heat zone' of a flame.

Then

$$\frac{r^*}{\delta}=\frac{\dot{m}c}{4\pi k r^*}=\frac{1}{\eta^*} \quad \ldots . [37]$$

The spherical flame must degenerate into a plane flame when the flame thickness is very small compared with the flame radius, i.e. when r^*/δ or $1/\eta^*$ tends to infinity. It is to be noted that both $1/\eta_1$ and $1/\eta_i$ tend to infinity as $1/\eta^*\longrightarrow\infty$.

Equation 21 can be written as

$$\frac{\mu}{6(1-\tau_i)}\left[e^{1/\eta}\{\eta+\eta^2+2!\eta^3+3!\eta^4+4!\eta^5+\ldots.\}\right]_{\eta_1}^{\eta_i}$$

$$=\tau_i e^{1/\eta_i}+\frac{\mu}{3(1-\tau_i)}e^{1/\eta_i}\left[\eta_i^3+\frac{\eta_i^2}{2}+\frac{\eta_i}{2}\right]-\frac{\mu e^{1/\eta_1}}{3(1-\tau_i)}\left[\eta_1^3+\frac{\eta_1^2}{2}+\frac{\eta_1}{2}\right] \quad \ldots [21a]$$

It is a well known property[4] of asymptotic expansions such as that which forms the LHS of equation 21a that the difference between the true value of the function and the sum of a finite number of terms is of the order of magnitude of the last term retained.

Hence for η^*, η_1 and η_i all tending to zero, we neglect terms which are of order higher than η^4 and we obtain

$$\frac{\lambda_0}{1-\tau_i}(e^{1/\eta_i}-e^{1/\eta_1})=\tau_i e^{1/\eta_i} \quad \ldots [38]$$

where λ_0 is the value of λ for a plane flame. It is easy to see from equation 20 that in the limit

$$\frac{1}{\eta_i}-\frac{1}{\eta_1}=\frac{1-\tau_i}{\lambda_0} \quad \ldots [39]$$

Equations 38 and 39 combine to give

$$\frac{\lambda_0}{1-\tau_i}=1/\ln\left\{\frac{\lambda_0}{\lambda_0-\tau_i+\tau_i^2}\right\} \quad \ldots [40]$$

This equation is identical with Spalding's result[3] for a plane flame for a step-function reaction rate, as it should be.

Adams-type reaction-rate function—In this case, inspection of equations 29, 33a, 33b and 35 shows that for a plane flame, for which $y^* \to -\infty$, we have:

$$\lambda_0=\tau_i(1-\tau_i/2) \quad \ldots [41]$$

$$0\leqslant\tau\leqslant\tau_i:\phi(\tau)=0 \quad \ldots [42a]$$

$$\tau_i\leqslant\tau\leqslant 1:\phi(\tau)=\frac{1}{1-\tau_i/2}+\frac{\tau_i f(\tau-1)}{1-\tau_i/2} \quad \ldots [42b]$$

$$\tau_c=\frac{1+\tau_i-\tau_i^2}{2(1-\tau_i/2)} \quad \ldots [43]$$

It is worthwhile to point out that the Adams type of reaction-rate function seems to be a combination of step-function and concentrated[5] reaction-rate function.

Results

Table 1 gives the values of λ versus $1/\eta^*$ for various values of τ_i for the step-function reaction rate. The table has been evaluated with the help of equations 16, 20 and 21 and noting that $\lambda=\mu\eta^{*4}$.

Table 1. Values of λ versus $1/\eta^*$ for various values of τ_i for the step-function reaction rate

$\frac{1}{\eta^*}$	$\tau_i=0.5$	$\tau_i=0.6$	$\tau_i=0.7$	$\tau_i=0.8$
	λ	λ	λ	λ
∞	0·3138	0·3552	0·3942	0·4309
5·2980	0·3717	0·4024	0·4302	0·4553
4·0000	0·3906	0·4180	0·4414	0·4609
3·0000	0·4198	0·4395	0·4593	0·4741
2·0000	0·4719	0·4838	0·4875	0·4969
1·5000	0·5286	0·5274	0·5262	0·5175
1·2500	0·5747	0·5653	0·5550	0·5345
1·0000	0·6450	0·6190	0·5940	0·5628
0·7994	0·7346	0·6918	0·6465	0·5987
0·6250	0·8631	0·7938	0·7229	0·6477

Table 2 gives the values of λ versus y^* for various values of τ_i for the Adams-type reaction-rate function. The table has been evaluated with the help of equations 26, 29 and 32.

Table 2. Values of λ versus y^* for various values of τ_i for Adams-type reaction-rate curves

y^*	$\tau_i=0.5$	$\tau_i=0.6$	$\tau_i=0.7$	$\tau_i=0.8$
	λ	λ	λ	λ
$-\infty$	0·3750	0·4200	0·4550	0·4800
−4·0000	0·4013	0·4427	0·4707	0·4881
−3·0000	0·4178	0·4514	0·4774	0·4905
−2·0000	0·4635	0·4832	0·4937	0·4983
−1·5000	0·5273	0·5212	0·5134	0·5064
−1·2500	0·5926	0·5586	0·5320	0·5136
−1·0000	0·7165	0·6273	0·5647	0·5257
−0·7994	0·9214	0·7369	0·6147	0·5433
−0·6250	1·3113	0·9384	0·7026	0·5724

The results of refs. 2 and 3 are expressed as plots of λ versus ξ^*, the latter quantity being related to the present space variables by:

$$\xi^*=e^{-1/\eta^*}=e^{y^*} \quad \ldots [44]$$

Figures 3 and *4* show the plots of λ versus ξ^*

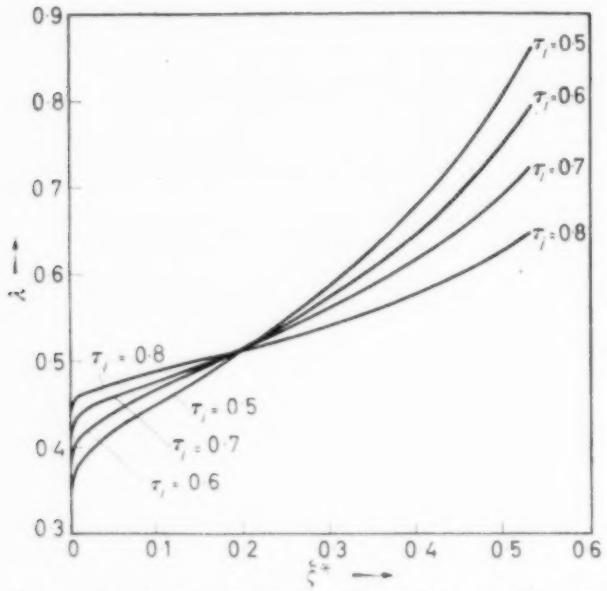

Figure 3. Variation of λ with ξ for step-function reaction-rate curves*

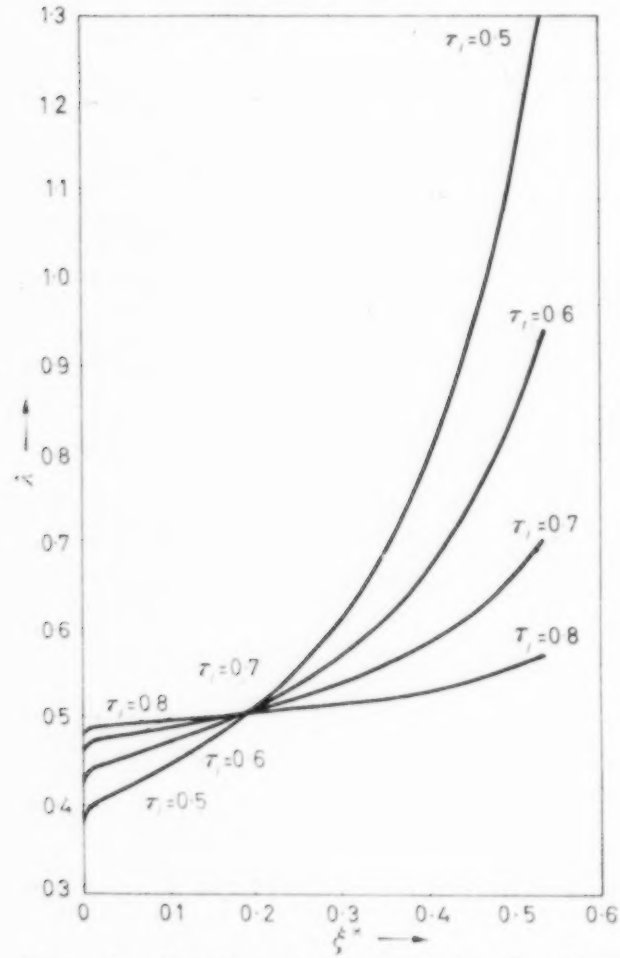

Figure 4. Variation of λ with ξ for the Adams reaction-rate function*

with τ_i as a parameter for the step-function reaction-rate and the Adams-type reaction-rate functions respectively.

From the thin-flame approximation, given above, we have

$$\dot{m} = \dot{m}_f'' 4\pi r^2 \qquad \ldots [45]$$

It can be easily seen that

$$\frac{r^*}{r_f} = \left(\frac{\lambda}{\lambda_0}\right)^{\frac{1}{4}} \qquad \ldots [46]$$

We can also easily show that

$$\dot{m}\dot{m}_f'' c^2 / 4\pi k^2 = \left(\frac{\lambda}{\lambda_0}\right)^{1/2} \left(\ln \frac{1}{\xi^*}\right)^2 \quad \ldots [47]$$

where $\dot{m}\dot{m}_f'' c^2 / 4\pi k^2$ is the square of the ratios of flame radius and flame thickness in a thin flame.

Figures 5 and 6 show the plot of r^*/r_f versus

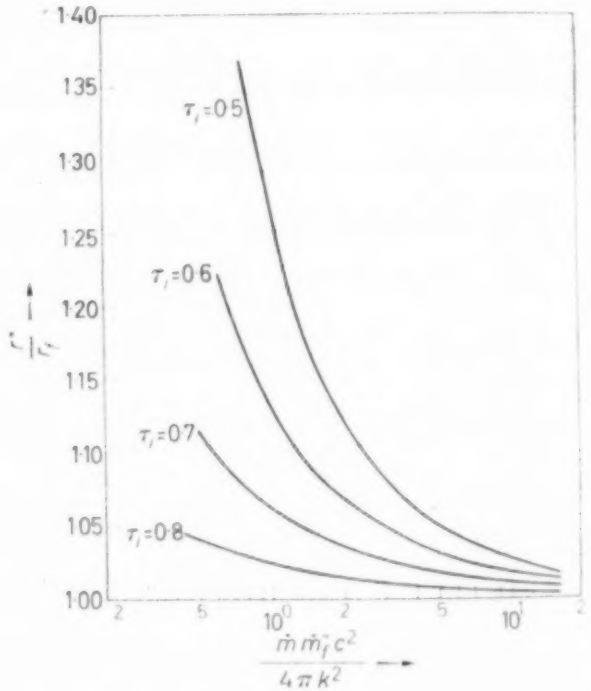

Figure 5. Variation of r^*/r_f with $\dot{m}\dot{m}_f'' c^2/4\pi k^2$ for step-function reaction-rate curves

$\dot{m}\dot{m}_f'' c^2 / 4\pi k^2$ with τ_i as a parameter, for the step-function and the Adams reaction-rate function respectively.

Discussion

Comparison with numerical (ref. 2) and analogue (ref. 3) results

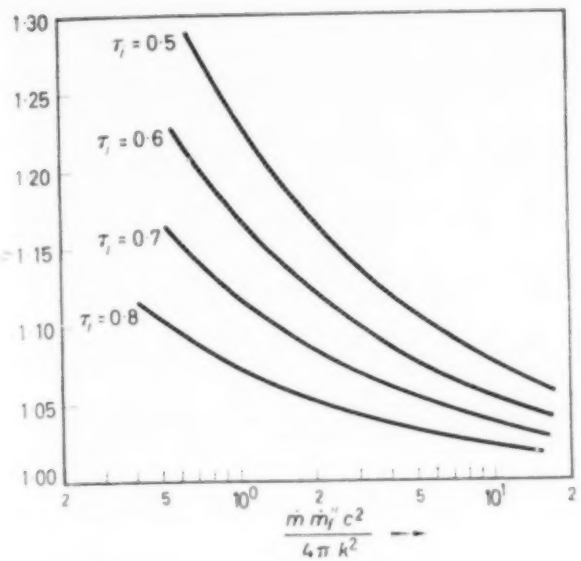

Figure 6. Variation of r^*/r_f with $\dot{m}\dot{m}_f''c^2/4\pi k^2$ for Adams-type reaction-rate function

The problem of the spherical flame has been solved by numerical means in ref. 2 for the following reaction-rate function

$$\phi(\tau) = 30(1-\tau)\tau^4 \quad \ldots\ldots [48]$$

The problem has also been solved by the resistance network analogue computer in ref. 3 for the following family of reaction-rate functions:

$$\phi(\tau) = (n+1)(n+2)(1-\tau)\tau^n \quad \ldots [49]$$

with $n = 2$, 4, 6 and 8. The case of $n = 4$ is, of course, that of ref. 2.

For the comparison of the analytical solutions with the numerical (ref. 2) and analogue (ref. 3) solutions, we plot r^*/r_f versus τ_c with $\dot{m}\dot{m}_f''c^2/4\pi k^2$ as a parameter, using equations 45, 46 and 47. τ_c is the centroid of the reaction-rate function.

Figure 7 shows the plot of r^*/r_f versus τ_c with $\dot{m}\dot{m}_f''c^2/4\pi k^2$ as a parameter. This figure contains the analytical solutions corresponding to the step-function reaction-rate curves, the analogue solutions (ref. 3) and the numerical solutions (ref. 2). The disagreement between the corresponding results of numerical solutions and analogue solutions is due to slight inaccuracies in the latter apparatus. The difference between the analytical results for the step-function reaction-rate and the reaction-rate

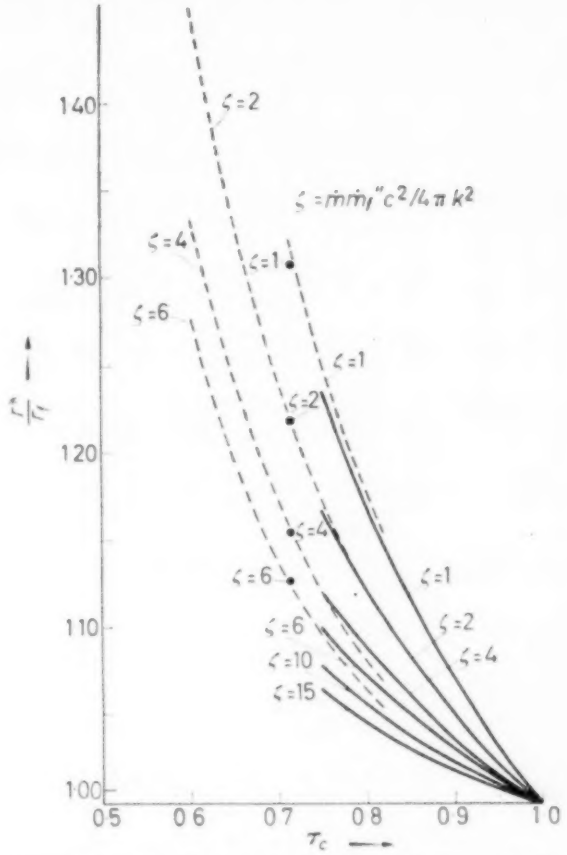

Figure 7. Variation of r^*/r_f with τ_c. Full lines indicate analytical solutions for step-function reaction-rate curves. Broken lines indicate solutions obtained by analogue for family of reaction-rate curves given by $\phi = (n+1)(n+2)\tau^n(1-\tau)$

• indicate solutions obtained by numerical means for reaction-rate curve given by $\phi = 5 \times 6\tau^4(1-\tau)$

family given by equation 49 is small, of the order of two per cent.

Figure 8 shows the plot of r^*/r_f versus τ_c with $\dot{m}\dot{m}_f''c^2/4\pi k^2$ as a parameter for the Adams-type reaction-rate function. The latter gives results which agree less well with the step-function reaction-rate results.

Real combustible gases do not have reaction-rate curves possessing the spikes of the Adams curves, but have the same general shape as the equation 49 family. The step-function is unrealistic in shape but less so than the Adams reaction-rate function. The step-function reaction-rate results, when expressed in terms of the centroid position τ_c, do not differ appreciably from those of the realistic reaction-rate family given by equation 49. Hence we may

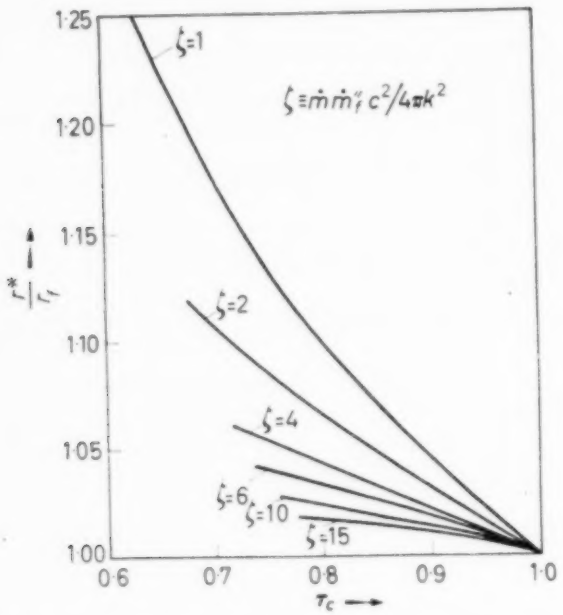

Figure 8. Variation of r^*/r_f with τ_c for Adams-type reaction-rate function

conclude that the dependence of r^*/r_f on $\dot{m}\dot{m}''_f c^2/4\pi k^2$ is not greatly dependent on the detailed shape of the reaction-rate curve; the main influence is the centroid of this curve, τ_c.

Figure 9 shows r^*/r_f versus $\dot{m}\dot{m}''_f c^2/4\pi k^2$ for various τ_c based on the analogue results. The curves in *Figure 9* can, probably, be taken as valid with two per cent accuracy for real combustible gases.

Conclusions

(*a*) The effective radius of a spherical flame r^* is always greater than r_f, defined by equation 45. However, for typical reaction-rate functions, r^*/r_f does not exceed unity by more than 25 per cent if the parameter $\dot{m}\dot{m}''_f c^2/4\pi k^2$ exceeds about 10. This parameter has the physical significance of [flame radius/flame thickness]^2.

(*b*) The dependence of r^*/r_f on $\dot{m}\dot{m}''_f c^2/4\pi k^2$ is not greatly dependent on the detailed shape of the reaction-rate curve; the main influence is the position of the centroid of this curve.

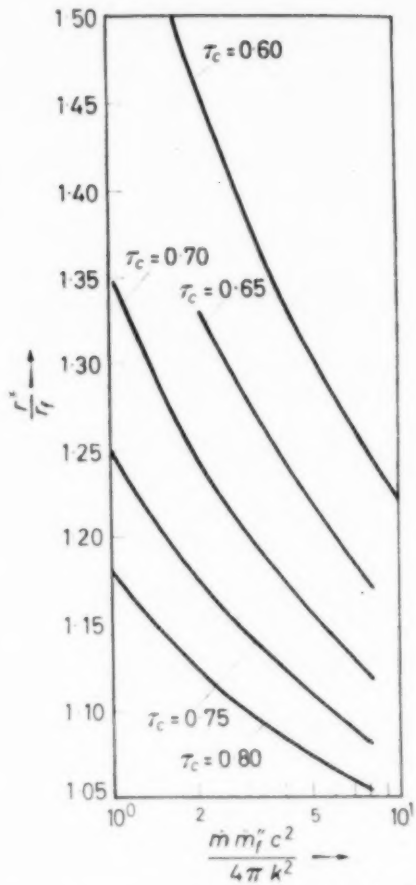

Figure 9. Variation of r^*/r_f with $\dot{m}\dot{m}''_f c^2/4\pi k^2$: curves recommended for general use

(*c*) The curves for this dependence shown in *Figure 9* can probably be used with two per cent accuracy for any realistic reaction-rate function.

References

[1] Adams, G. K. Private communication

[2] Spalding, D. B. *Combustion & Flame*, 1960, **4**, 51

[3] Spalding, D. B., Jain, V. K. and Samain, M. D. 'The theory of steady laminar spherical flame propagation: analogue solutions'. *Combustion & Flame*, 1961, **5**, 19

[4] Federal Works Agency. *Tables of Sine, Cosine and Exponential Integrals*, Vol. II, page xiii, 1940

[5] Spalding, D. B. *Combustion & Flame*, 1957, **1**, 296

The Theory of Steady Laminar Spherical Flame Propagation: Analogue Solutions

D. B. SPALDING, V. K. JAIN and M. D. SAMAIN

Mechanical Engineering Department, Imperial College of Science and Technology, London, S.W.7

(*Received August 1959*)

Steady spherical laminar flame propagation is considered in gases with temperature-explicit reaction-rate curves. The temperature distribution has been calculated by means of a resistance network analogue computer. It is shown that the effective radius of a spherical flame is under-estimated by the thin-flame approximation. The error decreases as the rate of injection and the laminar flame speed of the mixture increase. Comparison has been made with the results obtained by numerical means.

Introduction

Purpose of the paper

THE phenomenon of steady spherical laminar flame propagation has been studied by numerical means in ref. 1 which gives a description of the flame, a formulation of the theoretical problem, and particular solutions. Analytical solutions to this problem for artificial reaction-rate curves have also been presented in ref. 2. The purpose of this paper is to present solutions to the spherical flame problem obtained by means of a resistance network analogue computer and to compare the results with those obtained by numerical means[1]. In this problem, we assume that combustible gas flows uniformly and steadily from a point source into an atmosphere which comprises the products of combustion.

Notation

The following symbols are used:

(a) *Flame notation—*

- c Specific heat of gases at constant pressure, assumed constant (cal/g.°C)
- k Thermal conductivity of gases, assumed constant (cal/cm.s.°C)
- $\dot{m}$ Strength (mass injection rate) of point source of combustible gas (g/s)
- $\dot{m}_f''$ Mass burning rate per unit area in a plane laminar flame propagating through the injected mass (g/cm².s)
- r Radius from point of injection (cm)
- r_f Radius of flame calculated from the thin-flame approximation, i.e. equation 25 (cm)
- r^* Radius of effective thin flame (cm)
- $\dot{q}'''$ Volumetric reaction rate in flame (cal/cm³.s)
- $\overline{\dot{q}'''} = \int_{T_u}^{T_b} \dot{q}''' \mathrm{d}T / (T_b - T_u)$ (cal/cm³.s)
- T Gas temperature (°C)
- T_u Temperature of unburnt combustible (°C)
- T_b Temperature of adiabatic combustion products (°C)
- $\delta = k / c\dot{m}_f''$, thickness of plane flame (cm)
- $\lambda = \overline{\dot{q}'''} k (4\pi r^{*2})^2 / \dot{m}^2 c^2 (T_b - T_u)$
- $\xi = \exp(-\dot{m}c / 4\pi k r)$
- $\xi^* = \exp(-\dot{m}c / 4\pi k r^*)$
- $\tau = (T - T_u) / (T_b - T_u)$
- $\varphi(\tau) = \dot{q}''' / \overline{\dot{q}'''}$

(b) *Electrical notation—*

- E_j Voltage across the branch resistance corresponding to node j (V)
- $\bar{E}_j$ Mean height of the diagram of E_j versus V_j (V)
- R_0 Constant series resistances (ohms)
- V_j Voltage at node j (V)
- V_0 Maximum node voltage (V)
- $p+1$ Number of nodes on network
- σ_j Branch resistance corresponding to node j (ohms)
- σ_0 Scaling factor in the case of branch resistances (ohms)

Equation and boundary conditions

It is shown in ref. 1 that the problem is defined by the following differential equation

$$\frac{1}{r^2}\frac{\mathrm{d}}{\mathrm{d}r}\left(kr^2\frac{\mathrm{d}T}{\mathrm{d}r}\right)-\frac{\dot{m}c}{4\pi r^2}\frac{\mathrm{d}T}{\mathrm{d}r}+\dot{q}'''(T)=0 \quad \ldots [1]$$

The boundary conditions are:

$$r=0 \;:T=T_u \qquad \ldots . [2]$$

$$r=\infty : T=T_b \qquad \ldots . [3]$$

Reaction-rate function

Below we study the spherical flame problem for a family of temperature-explicit reaction-rate curves, given by the following equation:

$$\phi(\tau)=(n+1)(n+2)(1-\tau)\tau^n \qquad \ldots . [4]$$

where τ is given by

$$\tau \equiv (T-T_u)/(T_b-T_u) \qquad \ldots . [5]$$

The cases of $n=2$, 4, 6 and 8 are considered.

Main results

It is convenient to discuss the results in terms of an effective 'thin-flame radius' r^* which is the radius obtained by extrapolating, through the region where reaction is taking place, the temperature curve valid for the region upstream of the reaction zone; r^* is the radius at the point on this curve having the temperature of the combustion products. We define r_f as the radius which the flame would have for the given $\dot{m}$, if the flame were very thin and had the same mass burning rate per unit area as a plane flame with the same combustible material. The assumption that r^* equals r_f is called the 'thin-flame approximation'. The analysis below shows that, for thick flames, r^*/r_f is a function of the dimensionless parameter $\dot{m}\dot{m}_f''c^2/4\pi k^2$. *Figure 5* shows how r^*/r_f rises above unity as $\dot{m}\dot{m}_f''c^2/4\pi k^2$ tends to zero. Hence the thin-flame approximation is asymptotically correct for high injection rates and highly reactive gases; otherwise the effective flame radius is always under-estimated.

Method of Solution

Dimensionless form

For simplicity, we suppose that the gas conductivity k is a constant. We then render equation 1 dimensionless by equation 5 and the following transformations:

$$\xi \equiv \exp(-\dot{m}c/4\pi k r) \qquad \ldots . [6]$$

$$\phi(\tau)\equiv \dot{q}'''/\overline{\dot{q}'''} \qquad \ldots . [7]$$

$$\overline{\dot{q}'''}\equiv \int_{T_u}^{T_b}\dot{q}'''\,\mathrm{d}T/(T_b-T_u) \qquad \ldots . [8]$$

$$\lambda \equiv \overline{\dot{q}'''}k(4\pi r^{*2})^2/\dot{m}^2c^2(T_b-T_u) \quad \ldots [9]$$

There results the following differential equation

$$\frac{\mathrm{d}^2\tau}{\mathrm{d}\xi^2}=-\lambda\left(\frac{\ln\xi^*}{\ln\xi}\right)^4\frac{1}{\xi^2}\phi(\tau) \qquad \ldots . [10]$$

The boundary conditions are:

$$\xi=0:\tau=0 \qquad \ldots . [11]$$

$$\xi=1:\tau=1 \qquad \ldots . [12]$$

ξ^* is the dimensionless effective flame radius defined in the same way as r^* (previous section). ξ^* is, therefore, mathematically defined as

$$\xi^*=1/(\mathrm{d}\tau/\mathrm{d}\xi)_{\xi=0} \qquad \ldots . [13]$$

Finite difference form of differential equation and boundary conditions

The finite difference form of differential equation 10, taking equal intervals $\Delta\xi$, is

$$\frac{\tau_{j+1}+\tau_{j-1}-2\tau_j}{\Delta\xi^2}=-\frac{\lambda}{\xi_j^2}\left(\frac{\ln\xi^*}{\ln\xi_j}\right)^4\phi(\tau_j) \quad . . [14]$$

The boundary conditions are:

$$\xi_j=0:\tau_j=0 \qquad \ldots . [15]$$

$$\xi_j=1:\tau_j=1 \qquad \ldots . [16]$$

Analogue network

To solve the finite difference equation 14 under the boundary conditions 15 and 16, we set up the electrical resistance network illustrated in *Figure 1*. Let V_j denote the voltage at node j of the series line of resistances, while E_j denotes

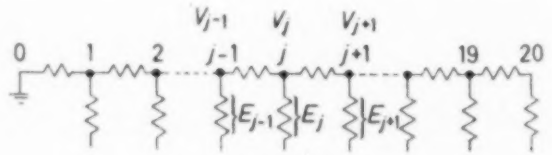

Figure 1

the voltage across the corresponding branch resistance.

Kirchhoff's law applied to the node j yields

$$\frac{(V_{j+1}-V_j)}{R_{j+1}} - \frac{(V_j-V_{j-1})}{R_{j-1}} = -\frac{E_j}{\sigma_j} \quad \ldots.[17]$$

where Rs and σs are the series and branch resistances respectively.

Putting:

$$R_{j+1} = R_{j-1}R_0 \text{ (constant)} \quad \ldots.[18]$$

$$\sigma_j = \sigma_0 \xi_j^2 (\ln \xi_j)^4 \quad \ldots.[19]$$

where σ_0 is a constant, we have

$$\frac{V_{j+1}+V_{j-1}-2V_j}{R_0} = -\frac{E_j}{\sigma_0 \xi_j^2 (\ln \xi_j)^4} \quad \ldots.[20]$$

Equations 14 and 20 become identical if the following relations are satisfied between the thermal and electrical quantities.

$$\tau_j = V_j / V_0 \quad \ldots.[21]$$

$$\phi(\tau) = E_j / \bar{E}_j \quad \ldots.[22]$$

$$\lambda = (\bar{E}_j p^2 R_0) / \sigma_0 V_0 (\ln \xi^*)^4 \quad \ldots.[23]$$

$$p = 1/\Delta\xi \quad \ldots.[24]$$

where V_0 is the maximum to which V_j goes. Note that there are $(p+1)$ nodes in the network.

Outline description

The practical arrangement is shown in the block diagram [*Figure 2*(a)]. The voltage V_j on node j

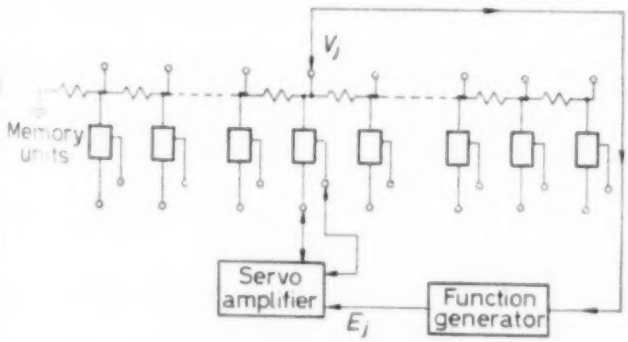

Figure 2(a)

of the electrical network is fed to a function generator which has an input/output curve of the same shape as the reaction-rate curve. The function-generator output voltage E_j is

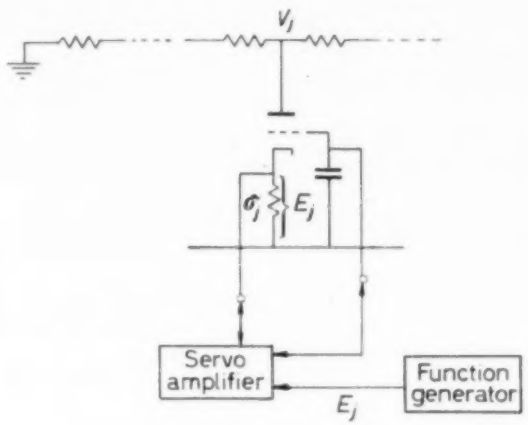

Figure 2(b)

connected to a memory unit containing the resistance σ_j. The function generator is connected to each point in turn by a rotary switch and the memory units, one to each node, maintain the voltages previously set by the function-generator. After a few cycles of operation Kirchhoff's equation for the points of the network becomes equivalent to the finite difference equation 14 which the flame must satisfy.

Brief Description of the Apparatus

Resistance network

The apparatus has been described in an earlier paper by D. B. SPALDING and M. D. SAMAIN[3]. The network resistances have not been built into the analogue computer but assembled on detachable tagboards. They are selected from stabilized carbon resistances and, in the case of the branch resistances, are usually made up of two or more in series.

To cover the required range of λ, two sets of branch resistances were made. The first set was calculated for a 21-point network from equations 18 and 19. This gives the solution for larger values of λ. It is not possible to get sufficient current into the network to give results when the reaction is near the inner limit. The second set was made with different scaling factors σ_0 and R_0 to give the solutions for smaller values of λ; since the reaction would be concentrated near the left (inner limit; low values of ξ^*) and current would only be flowing into the first few points, it was designed on a

basis of 41 points but only the first 21 were set up.

The usable range of resistances is large and difficulties may arise if the branch resistances fall below a few hundred ohms or exceed a few megohms. This difficulty has been avoided by a suitable choice of scale. *Table 1* gives the numerical values of the branch resistances for the 21-point network.

Table 1. Branch resistance values from $\sigma=\sigma_0\xi^2(\ln\xi)^4$ *and* $\Delta\xi=0{\cdot}05$ *for 21-point network, where* σ_0 *is* 1×10^6 *ohms*

Network junction	ξ	*Resistance* σ *(ohms)*
0	0·0	0·0
1	0·05	201 000
2	0·10	281 000
3	0·15	291 000
4	0·20	268 000
5	0·25	231 000
6	0·30	190 000
7	0·35	149 000
8	0·40	113 000
9	0·45	82 300
10	0·50	57 700
11	0·55	38 700
12	0·60	24 500
13	0·65	14 500
14	0·70	7 920
15	0·75	3 840
16	0·80	1 580
17	0·85	503
18	0·90	99
19	0·95	8·9
20	1·00	0·0

Function generator

The function generator is of the cathode ray tube type. The reaction-rate curve is cut out from cardboard and placed over the face of the tube. A photocell and amplifier move the spot vertically so that it is always on the edge of the cardboard mask. The input voltage deflects the spot horizontally.

The mask has to be positioned carefully both by rotating and moving vertically until the output is zero at $\tau=0$ and $\tau=1$; after adjustment the correctness of the position is checked by plotting the output/input curve of the function generator.

Memory units

Each network point is fed from a simple memory unit containing the branch resistances. The memory unit consists of a condenser and a cathode follower as shown in *Figure 2*(b). The function generator sets the voltage on the condenser which has a very high leakage resistance. This voltage remains until the function generator is connected again.

Servo-amplifier

The servo-amplifier is a high-gain d.c. amplifier which compares the voltage on the cathode of each memory valve with the function generator voltage and feeds an error signal to the grid to make these two voltages equal. By having high gain ($>1\,000$) the effects of differences between valve characteristics are minimized.

Operation and measurement

When the function generator has been set up, the rotary switch, a uniselector, is started. The uniselector is driven by a valve circuit and can be set to run at any convenient speed, usually $12\frac{1}{2}$ steps/second.

The network voltages are displayed on a long-persistence cathode ray tube. This shows whether stability has been reached or not. About five to ten uniselector rotations are required for stability. A fault, such as a dirty switch contact or a valve failure, gives a characteristic indication on the cathode ray tube.

The amplitude of the function generator output, i.e. the height of the reaction-rate curve, can be changed and after each change the analogue takes a few seconds to settle down; measurements are then made. To avoid 'loading' a null method is used.

Voltages on the network are read to an accuracy of one per cent by means of a moving coil meter used in a null circuit.

The variation of the amplitude of the function generator output, i.e. the height of the reaction-rate curve, corresponds to varying the quantity $E_1p^2R_0/\sigma_0V_0$. For a given height of the reaction-rate curve, we can find ξ^* by reading the voltage at node No. 1 (see *Figure 1*) and using equations 13 and 21. λ can now be evaluated with the help of equation 23.

Results

The results have been presented in *Figure 3* as plots of λ versus ξ^*. *Figure 4* shows some typical curves of τ versus ξ.

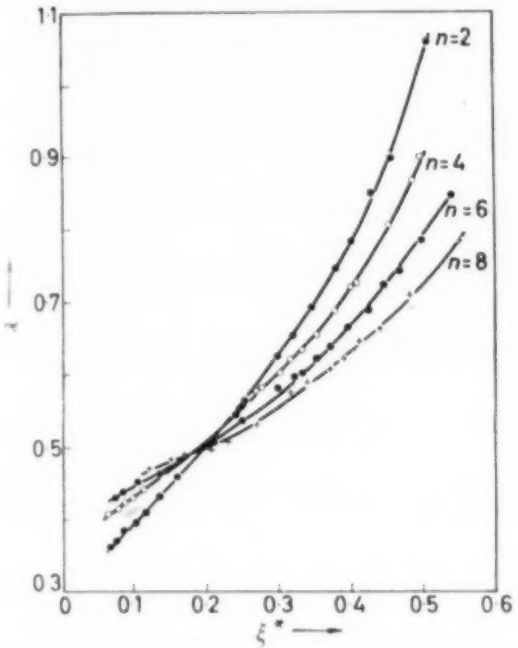

Figure 3. Variation of λ with ξ^*, with n as a parameter

Following the definitions of r_f, given above, we have

$$\dot{m} = 4\pi r_f^2 \dot{m}_f'' \qquad \ldots . [25]$$

It can easily be seen from equations 6, 9 and 25 that

$$\frac{r^*}{r_f} = \left(\frac{\lambda}{\lambda_0}\right)^{1/4} \qquad \ldots . [26]$$

and

$$\frac{\dot{m}\dot{m}_f'' c^2}{4\pi k^2} = \left(\frac{\lambda}{\lambda_0}\right)^{1/2} \left(\ln \frac{1}{\xi^*}\right)^2 \qquad \ldots . [27]$$

where λ_0 is the value of λ at which $\xi^* = 0$.

Figure 5 shows the plots of r^*/r_f versus $\dot{m}\dot{m}_f'' c^2/4\pi k^2$ with n, the exponent in the reaction-rate function, as a parameter.

The quantity $\dot{m}\dot{m}_f'' c^2/4\pi k^2$ can be interpreted physically. If we define a 'flame thickness' δ by

$$\delta \equiv k/c\dot{m}_f'' \qquad \ldots . [28]$$

it is easy to show that

$$\dot{m}\dot{m}_f'' c^2/4\pi k^2 = r_f^2/\delta^2 \qquad \ldots . [29]$$

Discussion

Comparison with numerical solution

The problem of spherical flame propagation has also been solved by numerical means in ref. 1 for the following reaction-rate curve

$$\phi = 30\,(1-\tau)\,\tau^4 \qquad \ldots . [30]$$

Equation 30 is, of course, the case of $n = 4$ of the equation 4 reaction-rate family studied in the present paper.

For the comparison of the results obtained (*1*) by the analogue method, (*2*) by numerical means, we plot r^*/r_f versus $\dot{m}\dot{m}_f'' c^2/4\pi k^2$ for $n = 4$ in both cases. The plot has been shown

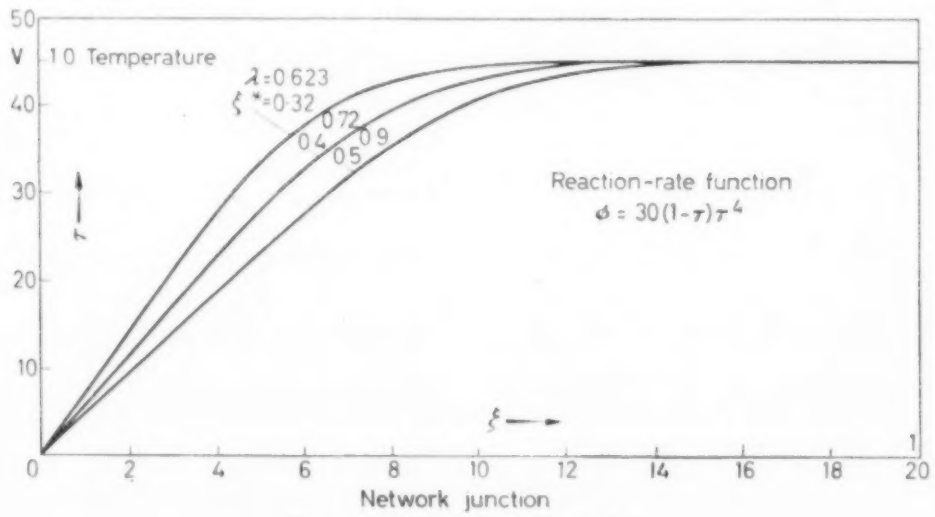

Figure 4. Variation of τ with ξ

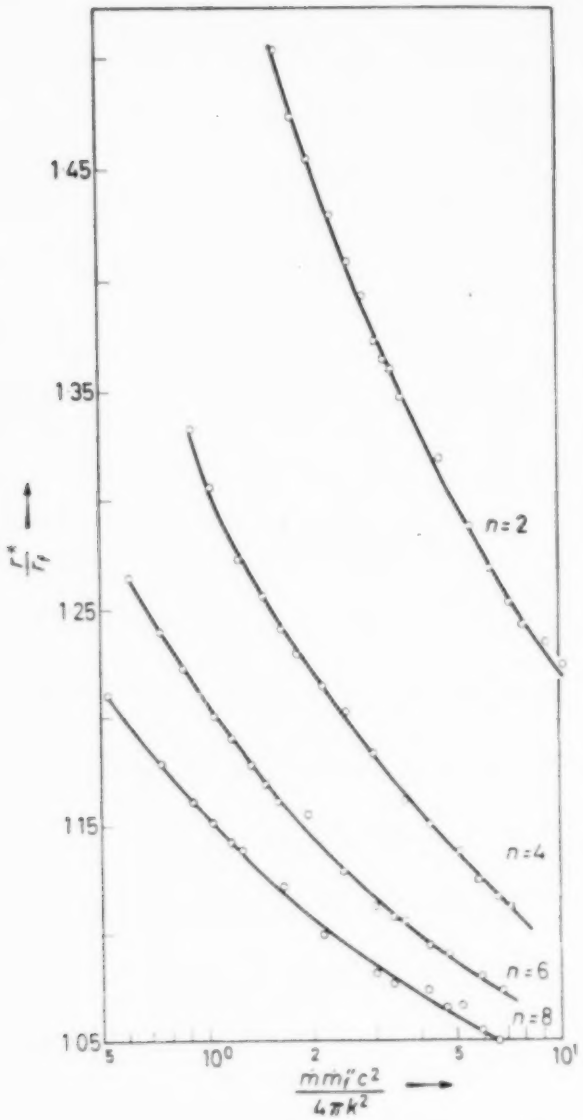

Figure 5. Variation of r^*/r_f with $\dot{m}\dot{m}''_f c^2/4\pi k^2$, with n as a parameter

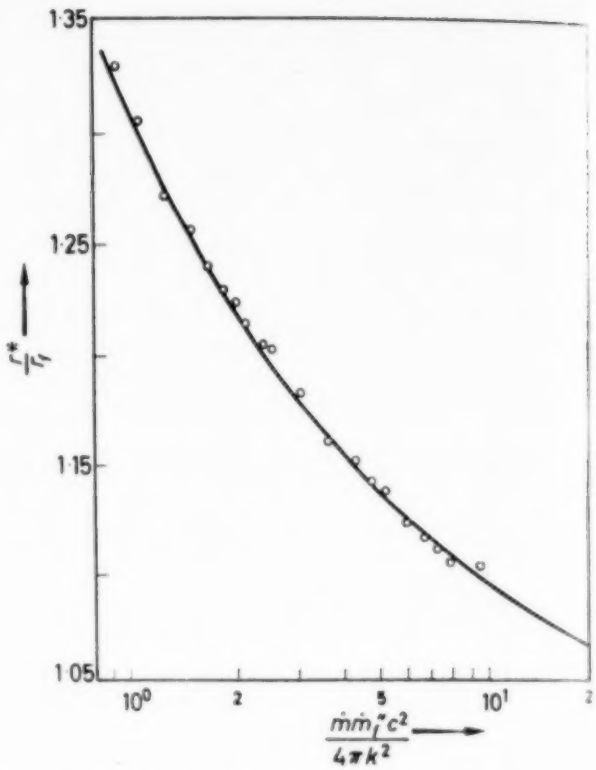

Figure 6. Variation of r^*/r_f with $\dot{m}\dot{m}''_f c^2/4\pi k^2$. The marked points indicate the solutions obtained by analogue for the reaction-rate curve given by $\phi = 30\,(1-\tau)\tau^4$. The full line indicates the solutions obtained by numerical means for the same reaction-rate curve[1]

in *Figure 6*. The disagreement between the two results is due to slight inaccuracies in the analogue apparatus. However, the disagreement is small, of the order of two per cent.

Since the disagreement between the analogue and numerical results for the case of $n=4$ of the equation 4 reaction-rate family is small, we conclude, therefore, that *Figure 5* could probably be used with 2 per cent accuracy for the reaction-rate family given by equation 4.

Influence of n

Figure 5 shows that as n increases r^*/r_f comes closer to unity. n is related to the centroid, τ_c, of a member of the reaction-rate family of equation 4 as follows:

$$\tau_c = \int_0^1 \tau\phi\,(\tau)\,\mathrm{d}\tau \qquad \ldots.[31]$$

i.e.

$$\tau_c = (n+1)/(n+3) \qquad \ldots.[32]$$

As n tends to infinity τ_c tends to unity; hence, as is to be expected, the thin-flame approximation is asymptotically correct for gases with a steep dependence of reaction rate on temperature.

Conclusions

(*a*) The effective radius of a spherical flame r^* is always greater than r_f, defined by equation 25. However, r^*/r_f does not exceed unity by more than 10 per cent if the parameter $\dot{m}\dot{m}''_f c^2/4\pi k^2$ exceeds about 10 and if the centroid of the reaction-rate curve, τ_c, exceeds

0·70. The above parameter has the physical significance of (flame radius/flame thickness)^2.

(*b*) The analogue can be used to solve the spherical flame problem for any temperature-explicit reaction-rate curve with a fair degree of accuracy.

The authors' thanks are due to Mr P. Dale who made most of the apparatus and did some of the measurements, and to the Department of Scientific and Industrial Research for providing financial support.

References

[1] SPALDING, D. B. 'The theory of steady laminar spherical flame propagation: equations and numerical solutions'. *Combustion & Flame*, 1960, **4**, 51

[2] SPALDING, D. B. and JAIN, V. K. 'The theory of steady laminar spherical flame propagation: analytical solutions'. *Combustion & Flame*, 1961, **5**, 11

[3] SPALDING, D. B. and SAMAIN, M. D. 'The analogue solution of temperature distribution and extinction in an idealized cylindrical flame'. *Rep. No. AFOSR TN–58–216*, Contract AF 61(514)–1014, January 1958

Shock Waves from Preflame Reactions in a Motored Engine

J. C. FIREY and R. R. LAVI

Department of Mechanical Engineering, University of Washington, Seattle 5, Washington

(Received August 1959)

Engine experiments with an impact pressure detector and a rate of change of pressure indicator demonstrate that preflame reactions are capable of generating impact pressures. Two-stage preflame reactions of normal heptane were observed with both stages developing impact pressures. It is proposed that these impact pressures are due to a shock wave formed by the preflame reaction and that this shock wave may lead to a detonation wave which is the compression ignition process.

THE compression ignition process, occurring in the normal running of a diesel engine or the knocking of a gasoline engine, is incompletely understood today. Several theories have been proposed to explain the process, notably the autoignition theory and the detonation wave theory[1]. In a previous article[2], it was shown that the compression ignition process exhibited strong and directional impact pressures in conformity with the detonation wave theory, and that the detonation wave theory can be harmonized with the available data on compression ignition by assuming that the shock wave needed to initiate the detonation wave is created by preflame reactions (e.g. cool flame reactions) occurring in the compressed mixture of air and fuel. In this paper further evidence is presented that preflame reactions are capable of generating shock waves in a motored engine.

Engine experiments were run, first, to ascertain whether the occurrence of a preflame reaction creates impact pressure waves and, secondly, to estimate the Mach number of these pressure waves from gas vibration frequency measurements. If the preflame reaction generates a shock wave then impact pressures should be present, as they were found to be, and the Mach number of the wave should be greater than one, as it was found to be.

The Impact Pressure Detector

The impact pressure detector consisted of a small steel cantilever beam suspended in the engine combustion chamber in such a manner that, when the beam was deflected by an impact pressure, an electric circuit was completed. The resulting electric signal was then displayed on a cathode ray oscilloscope. In this manner the occurrence and timing of the impact pressure pulse could be measured.

The beam and holder are sketched in *Figure 1* together with the simple electric circuit. A

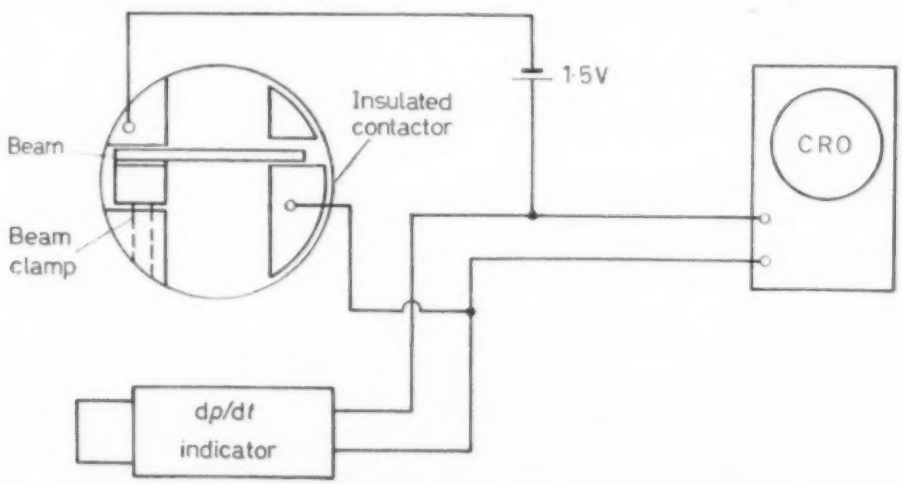

Figure 1. Sketch of beam and holder and circuit for impact pressure detector

deflection of the cantilever beam can only be caused by impact pressure since static pressure acts equally on both faces of the beam. When the beam is deflected by an amount equal to the preset clearance the electric circuit is completed and the oscilloscope trace is deflected vertically by 1·5 V. The beam holder was so constructed that beams of various thicknesses could be used, the preset clearance could be varied and, when inserted into the engine, the beam faced directly across a cylinder diameter, being about 0·75 in. in from the cylinder wall. Steel beams were used of 0·125 in. width, 0·500 in. free length and of thickness varying from 0·0015 in. to 0·020 in.

If we accept for the moment the detonation wave theory of compression ignition, then we expect the generation of a shock wave by the preflame reaction to be followed by the detonation wave of compression ignition. The detector is thus required to be sufficiently sensitive to respond to the presumably weak impact pressure of the shock wave while being strong enough to withstand the very strong impact pressure of the subsequent detonation wave. It is further necessary to determine the time of occurrence of the impact pressure since shock wave formation by the preflame reaction will only be indicated by impact pressure occurring after the start of the preflame reaction but prior to the onset of the detonation wave. These two requirements were met in the following manner. The beam holder was constructed so that after deflecting a certain amount the beam came to rest against two stops and was thus prevented from undergoing damaging deformations. The electric signal from the impact pressure detector was superimposed upon the signal of a Phillips magnetostrictive rate-of-change-of-pressure (dp/dt) indicator so that the time of occurrence of the impact pressure could be determined relative to the preflame reaction and the detonation wave.

Calibration of the Impact Pressure Detector

The response of the impact pressure detector to shock waves of known strength was measured in the shock tube sketched schematically in *Figure 2*. In this device the driver volume is isolated from the test section of the tube by a plastic diaphragm. Regulated pressure is applied from a nitrogen cylinder to the driver volume until the plastic diaphragm bursts. The resulting shock wave travels down the test section and acts in turn upon the impact pressure detector and the two quartz piezoelectric

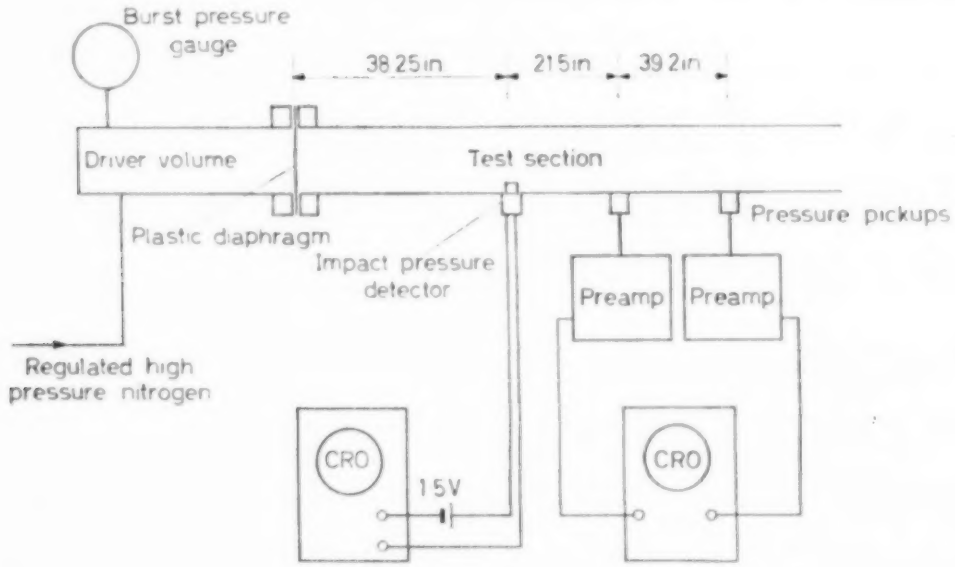

Figure 2. Schematic diagram of shock tube for calibration of the impact pressure detector

pressure detectors. The time required by the shock wave to travel the known distance between the quartz pressure detectors is measured with the calibrated sweep of a cathode ray oscilloscope in order to determine the wave velocity. The wave velocity was also calculated from the measured pressure in the driver volume at the moment of bursting. The calculated and measured values of wave velocity agreed within five per cent. Plastic diaphragms of various materials and thicknesses were used to vary the shock wave velocity. Nevertheless only certain values of shock wave velocity could be obtained. The end of the test section was open so that for each run the test section was initially filled with air at one atmosphere pressure and room temperature of 70°F ±3°F.

In *Table 1* below are listed the minimum shock wave Mach number to which the impact pressure detector responded and the next lower value of available Mach number to which the impact pressure detector did not respond for several values of beam thickness and preset clearance.

Table 1. Results of shock tube calibration of impact pressure detector

Impact pressure detector		*Shock wave Mach number to which:*	
Beam thickness in.	*Preset clearance in.*	*The detector did not respond*	*The detector did respond*
0·003	0·008	1·08	1·12
0·005	0·005	1·08	1·12
0·008	0·008	1·28	1·42
0·012	0·009	1·28	1·42

These results demonstrate that the impact pressure detector is capable of responding to shock waves.

Since the beam in the impact pressure detector is statically balanced it is the impact pressure of the shock wave which causes the beam to move and the detector to respond. This impact pressure is created by the forward velocity of the gas immediately behind the front of the shock wave.

To respond, the beam in the impact pressure detector must be deflected through the preset clearance. This requires the impact pressure not only to be sufficient to cause this deflection when acting steadily but also to act for a sufficient length of time that the total work done on the beam by the impact pressure equals the elastic strain energy of the beam in the deflected position for response. Hence the response of the impact pressure detector may vary not only with the magnitude but also with the duration of the impact pressure pulse of the shock wave.

The Test Engine

All of the experiments described herein were carried out in a Waukesha CFR engine equipped with a four hole cylinder. The engine was motored without spark ignition at the following conditions:

975 rev/min

170°F jacket temperature

170°F intake air temperature

Various compression ratios and fuel/air ratios were used.

The impact pressure detector was inserted in the top hole of the cylinder and the dp/dt indicator was inserted in a side hole so as to face directly across a cylinder diameter. The positions of the indicators within the engine cylinder are shown diagrammatically in *Figure 3*.

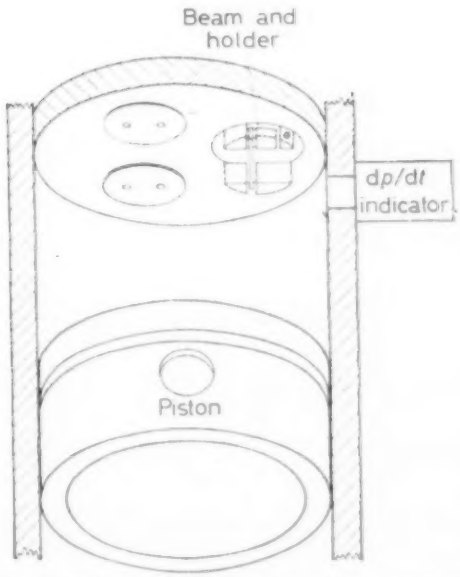

Figure 3. Location of indicators within the engine cylinder

Normal heptane fuel was used for all of the experiments except where otherwise stated.

Impact Pressure from Preflame Reaction

An impact pressure signal was frequently, though not always, observed when only a single preflame reaction was occurring in the engine cylinder. A typical oscilloscope diagram of such an event is shown in *Figure 4*. The

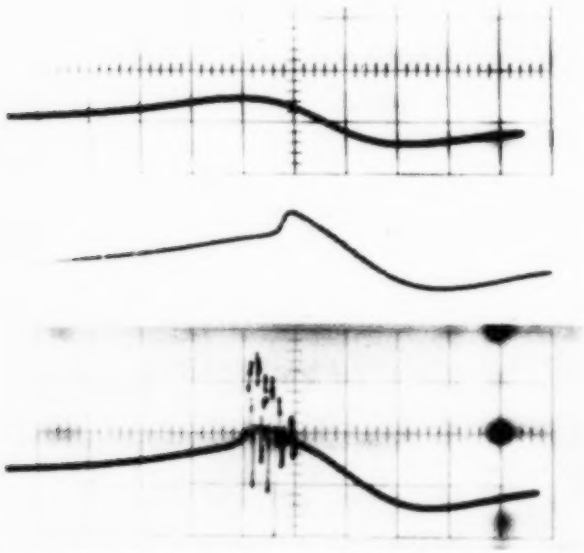

Figure 4. Rate of change of pressure diagrams from preflame reaction, upper, compression of air only; centre, preflame reaction; lower, preflame reaction with impact pressure signal; time scale 0·002 sec per interval; compression ratio 9·9/1; fuel/air ratio 0·04

impact pressure signal occurs within less than 0·0004 sec after the start of the preflame reaction. Also shown in *Figure 4*, for purposes of comparison, are oscilloscope diagrams for compression of air only and for preflame reaction without an impact pressure signal. The latter diagram shows preflame reaction occurring about 15° to 20° before top dead centre.

When compression ignition took place an impact pressure signal was very frequently, though not invariably, obtained from the first preflame reaction. An impact pressure signal occurred shortly after the preflame reaction and well before compression ignition. The compression ignition process also produces an impact pressure signal.

Despite the stops the test beams were often damaged when compression ignition occurred. Beams of 0·010 in. or greater thickness did not appear to be damaged. The thinner beams (0·003 in. and 0·005 in.) which responded well to the impact pressure of the preflame reaction were damaged so quickly that a photograph of the above sequence was not obtainable.

Impact pressures as described above were observed from preflame reactions over a wide range of fuel/air ratios (0·06 to 0·02 by weight) and engine compression ratios (7/1 to 10/1 by volume) on both clear normal heptane fuel and normal heptane plus 6 ml/gallon of tetraethyllead. Lean fuel/air ratios were used as it was found that under these conditions steady preflame reactions could be obtained with a long time interval before compression ignition. At richer fuel/air ratios preflame reaction occurs but tends to be erratic and precedes compression ignition by only a short time rendering difficult a study of the properties of the preflame reaction.

Impact pressure signals from the first preflame reaction were only obtained from beams of 0·005 in. thickness or less with preset clearance of 0·005 in. or less. Thinner beams responded at greater preset clearances, the 0·003 in. beam responding up to a preset clearance of 0·010 in.

The foregoing experiments show that the first preflame reaction generates impact pressures in a motored engine.

Impact Pressure from Compression Ignition

An impact pressure signal was invariably obtained when compression ignition occurred, provided the beam was of 0·015 in. thickness or less with a preset clearance of 0·008 in. or less. This experiment confirms the previous observation[2] that compression ignition creates an impact pressure. We also see, as expected, that the impact pressure of compression ignition is stronger than the impact pressure of the preflame reaction.

The Two-stage Preflame Reaction

One of the more interesting observations made during the course of these experiments was that a two-stage preflame reaction can readily

obtained and that it is the second stage preflame reaction which causes compression ignition of normal heptane in these experiments.

To observe this two-stage process it was found necessary to operate the engine at lean mixtures (0·04 fuel/air ratio by weight) and high compression ratio (9·9/1 by volume). At these conditions a dp/dt indicator diagram as shown in *Figure 5* is obtained. Also shown in *Figure 5*, for purposes of comparison, are dp/dt indicator diagrams for compression of air only and for a single stage preflame reaction. Following the first preflame reaction a second preflame reaction is seen to occur some 0·004 to 0·005 sec later.

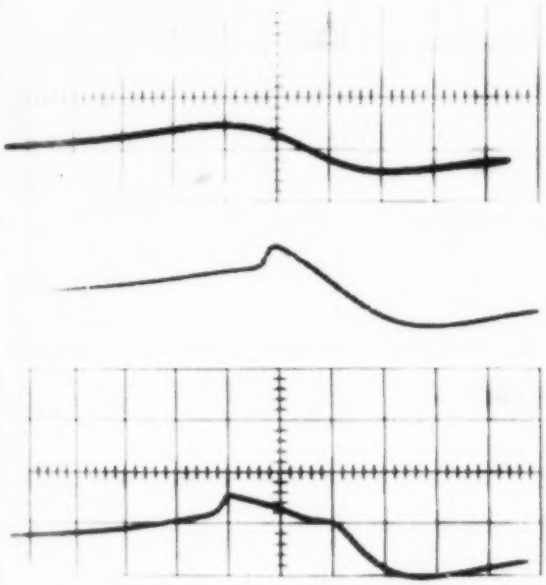

Figure 5. Rate of change of pressure diagram from two-stage preflame reaction; upper, compression of air only; centre, single-stage preflame reaction; lower, two-stage preflame reaction; time scale 0·002 sec per interval; compression ratio 9·9/1; fuel/air ratio 0·04

The intensity of the second stage preflame reaction varied greatly from cycle to cycle in contrast to the first stage preflame reaction which was relatively steady. In *Figure 6* are shown several dp/dt indicator diagrams obtained in sequence at apparently identical engine operating conditions. The height of the dp/dt trace and hence the energy release rate created by the second stage preflame reaction is seen to vary from almost none at all to complete compression ignition.

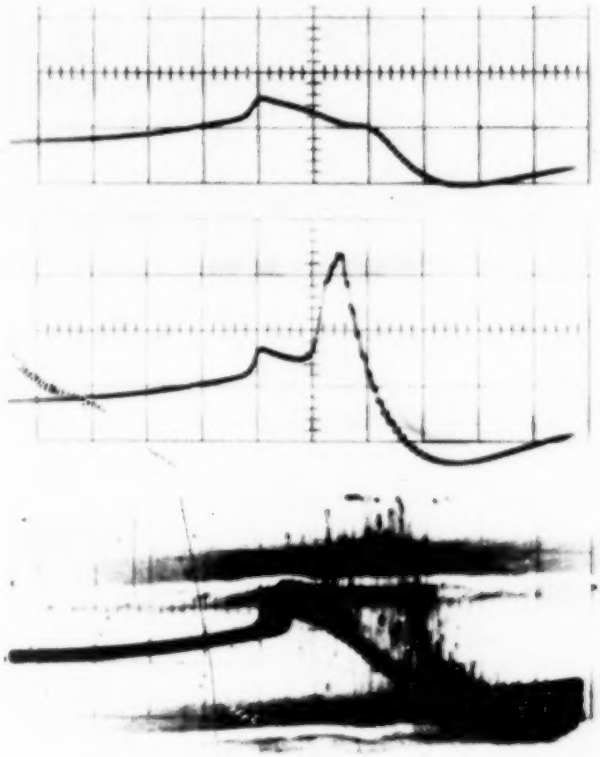

Figure 6. Rate of change of pressure diagrams from two-stage preflame reaction; upper, weak second-stage reaction; centre, moderate second-stage reaction; lower, compression ignition; time scale 0·002 sec per interval; compression ratio 9·9/1; fuel/air ratio 0·04

Whatever the cause of these cycle to cycle variations, the resulting sequence of indicator diagrams provides a clear picture of the transformation from slow preflame reaction to rapid compression ignition. Compression ignition is seen to be caused by the second stage preflame reaction and to occur very nearly concurrently with it.

The second stage preflame reaction is also capable of generating impact pressure as is shown in *Figure 7* which is another sequence of dp/dt indicator diagrams obtained at apparently identical engine operating conditions with the impact pressure detector connected. In upper *Figure 7* the second stage preflame reaction is insufficiently rapid to create an impact pressure, even though the first stage preflame reaction did cause an impact pressure signal. In lower *Figure 7* the second stage preflame reaction was rapid enough to create an impact pressure.

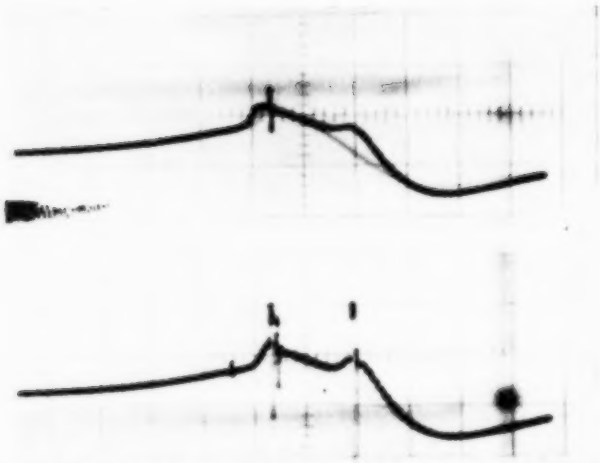

Figure 7. Rate of change of pressure and impact pressure diagrams from two-stage preflame reaction; upper, weak second-stage reaction; lower, strong second-stage reaction; time scale 0·002 sec per interval; compression ratio 9·9/1; fuel/air ratio 0·04

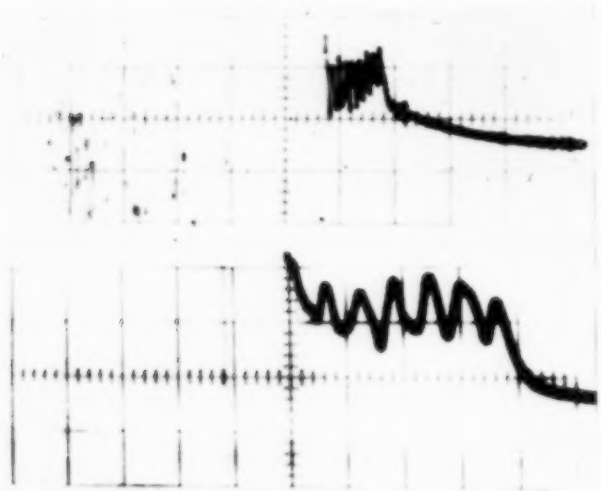

Figure 8. Rate of change of pressure diagrams showing pressure waves from preflame reaction; lower, expanded scale 0·0004 sec per interval, 0·1 V per interval; upper, normal scale 0·002 sec per interval, 0·5 V per interval; compression ratio 9·9/1; fuel/air ratio 0·04. Time scale from right to left

These results indicate that a two-stage preflame reaction can occur in a motored engine, that both stages of the preflame reaction generate impact pressures and that compression ignition of normal heptane is caused by the second stage reaction in these experiments.

Analysis of Impact Pressure Results

A quantitative measure of the strength of the impact pressure cannot readily be obtained from the impact pressure gauge results since the natural beam periods are longer than the time between successive reflections of the pressure wave. In *Table 2* below are listed the calculated natural frequencies and half periods for several of the beams used in the gauge.

Table 2. Natural frequencies of gauge beams

Beam thickness in.	*Natural frequency c/s*	*Beam half period sec*
0·003	391	0·00128
0·005	653	0·00077
0·008	1050	0·00043
0·012	1560	0·00032

The beam half period is of interest here as the time required by the beam to move from the rest position to make contact when the applied impact pressure is just barely able to cause gauge response. Any higher impact pressure causes response and hence cannot be measured. The minimum responding impact pressure could perhaps be estimated from the beam mechanical properties were the beam half period shorter than the time between successive applications of the pressure wave upon the beam. As discussed in the next section the time between successive wave reflections is a maximum of 0·00025 sec which is less than the half periods of the beams. Under these conditions an impact pressure greater than the minimum must be applied to bring about gauge response.

The response of the impact pressure gauge was also evaluated in the test engine when run with normal, spark ignited combustion without knock. *iso*Octane fuel was used at a compression ratio of 7/1 and a spark timing of 10° before top dead centre. No response of the impact pressure gauge was obtained under these conditions. These results demonstrate that the gauge does not respond to such impact pressures as are generated by normal combustion and that the gauge is not functioning as an ionization gap.

Pressure Waves from Preflame Reactions

Marked pressure waves have been observed to follow the first preflame reaction when an impact

pressure signal was obtained. These are perhaps a reverberation of the shock wave within the engine combustion chamber. A typical dp/dt indicator trace of such a reverberation is shown in lower *Figure 8* wherein a high horizontal and vertical oscilloscope gain has been used to show the pressure waves more clearly. The relative magnitude of these pressure waves is more readily seen in upper *Figure 8* wherein the same oscilloscope gain has been used as for the previous diagrams of preflame reaction. The pressure wave magnitude varied greatly from cycle to cycle.

If these pressure waves are shock waves their velocity must exceed acoustic velocity in the cylinder gases (i.e. the wave Mach number must exceed unity). For this comparison both the acoustic velocity and the pressure wave velocity must be determined.

The acoustic velocity was estimated by two different methods. In the first method the temperature, pressure and composition of the gas within the engine cylinder at maximum compression were calculated from the known values of intake air temperature, fuel/air ratio, compression ratio and engine speed. These calculated values were then corrected for speed and preflame reaction effects as observed experimentally by J. C. LIVENGOOD, C. F. TAYLOR and P. C. WU[3]. These calculations gave an acoustic velocity of 1 885 ft/sec. In the second method the slowest observed pressure wave velocity was assumed to be the acoustic velocity. This assumption gave an acoustic velocity of 1 909 ft/sec which agrees within 1 per cent with the calculated value.

The pressure wave velocity was calculated from the measured wave frequency and the known combustion chamber dimensions. The measured frequency of the gas vibration caused by the first preflame reaction varied from 4 150 to 5 000 c/s with an average value of 4 425 c/s. The frequency varied not only from one engine cycle to the next but also during the course of any one engine cycle.

If we assume the slowest pressure wave to be a sound wave then the observed pressure waves have the following Mach numbers:

Observed frequency, c/s	Mach No.
4 150	1·00
4 425	1·07
5 000	1·21

Alternatively we can assume the calculated acoustic velocity of 1 885 ft/sec to be correct and that the shock waves travel a full cylinder diameter between reflections. For this assumption the pressure waves have the following Mach numbers:

Observed frequency, c/s	Mach No.
4 150	1·21
4 425	1·29
5 000	1·45

The authors were unable to find in the literature a detailed analysis of the reverberation modes of shock waves in a cylindrical chamber. Hence no decision was made as to which of the above sets of Mach numbers is correct. In any event all values of the Mach numbers are in excess of unity indicating that the pressure waves created by the preflame reaction are shock waves.

The second stage preflame reaction also generates marked pressure waves of a distinctly higher frequency than those generated by the first preflame reaction (*ca.* 5 500 c/s as compared with 4 400 c/s). The Mach number of these second stage pressure waves was not estimated, however, since the gas temperature and composition following the second stage reaction are unknown.

Discussion

The foregoing experimental observations can be interpreted in terms of the detonation wave theory of compression ignition in the following manner. As discussed in ref. 2, to initiate a detonation wave in the engine a prior shock wave is needed and the preflame reaction is a likely source of this shock wave. The preflame reaction is seen to generate pressure waves whose Mach numbers are greater than unity and which possess an impact pressure. It appears reasonable therefore to presume that these pressure waves are shock waves created by the

preflame reaction. If sufficiently strong these shock waves may cause the detonation wave which is compression ignition.

Presumably either the first or second preflame reaction is capable of initiating compression ignition provided a sufficiently strong shock wave is generated. The sequence of *Figures 6* and *7* can be interpreted in the following manner. A weak second stage preflame reaction possesses an insufficient energy release rate to create a shock wave and an impact pressure signal is not obtained. A moderate second stage preflame reaction can create a shock wave and impact pressure but the shock is not strong enough to initiate detonation. A strong second stage preflame reaction creates a strong shock wave which causes the detonation wave. The time interval between creation of a strong shock wave and occurrence of the consequent detonation wave must be very short and we cannot expect to see these processes separately on a single indicator diagram. Hence, compression ignition appears to take place concurrently with the second stage preflame reaction. Under some engine operating conditions normal heptane undergoes compression ignition without evidence of a prior preflame reaction. Perhaps in this latter case the first preflame reaction generated a shock wave adequate to detonate the mixture. Further studies of these possibilities are planned.

Gasoline engine knock, such as may occur with normal, spark ignited combustion, is generally considered to be compression ignition of the compressed but unburnt end gas ahead of the flame front. D. L. PASTELL[4] has shown that knock in a spark ignited engine and compression ignition in a motored engine are remarkably similar. Thus if compression ignition in a motored engine is a detonation wave process it is likely that knock in a spark ignited engine is also a detonation wave process.

We wish to thank the Engineering Experiment Station and the Department of Mechanical Engineering at the University of Washington for the generous financial assistance which made this research possible. We wish also to express our appreciation of the generosity of the California Research Corporation in making available the CFR engine with which these experiments were performed.

References

[1] SOKOLIK, A. and VOINOV, C. *Bull. Acad. Sci. Russ.* **1927,** 123

[2] FIREY, J. C. *Sixth Symposium (International) on Combustion,* p 878–886. Reinhold: New York, 1957

[3] LIVENGOOD, J. C., TAYLOR, C. F. and WU, P. C. 'Measurement of gas temperature in an engine by the velocity of sound method', presented at the S.A.E. Annual Meeting, 13–17 January 1958, Detroit, Michigan

[4] PASTELL, D. L. 'Precombustion reactions in a motored engine', *S.A.E. quart. Trans.* 1950, **4,** 571

Scale Effect in a Gas Turbine Combustion Chamber fitted with a Swirl Atomizer—Part II

M. V. HERBERT and J. A. BAMFORD

National Gas Turbine Establishment, Pyestock, Hampshire

(*Received October 1959*)

Primary zone wall temperatures have been measured on two aircraft-pattern combustion chambers with a scale ratio of two. Analysis of the heat transfer processes with respect to linear scale and pressure enables trends to be established over a wide range of conditions. It is demonstrated that the established scaling technique—in which pressure is varied inversely as linear scale, and gas temperatures and velocities kept constant—does not give exact similarity in wall temperatures. However, the discrepancy is not very great, and much less than would result from holding pressure constant with varying scale.

Introduction

IT HAS been accepted in principle for some time that the most satisfactory technique for scaling gas turbine combustion systems is to maintain constant the following terms:

(*i*) pressure × linear scale
(*ii*) velocities throughout
(*iii*) temperatures throughout.

This was proposed from theoretical considerations by D. G. STEWART[1], who analysed a large number of relevant chemical and physical processes. These were not all compatible, and a compromise between conflicting factors was found to be necessary. Constant Reynolds number is implicit in the above rules, while an extensive survey of stability data on simple premixed combustion systems[2] has shown that in practice combustion loading will also be preserved. Thus the basic similarity requirements for aerodynamic and combustion performance are satisfied, but not those of all the contributory processes such as heat transfer and fuel atomization.

Some additional criteria relating to the scaling of atomizers were derived in ref. 3, supported by test results under conditions where performance is highly sensitive to quality of atomization. However, this still leaves the presumption that metal surfaces are, like the contained gases, at the same temperatures in different scales of chamber; and this, in the light of elementary heat transfer considerations, would not appear to be justified. The success demonstrated[3] in the matching of chambers having a scale ratio of two suggests that no very serious discrepancy in metal temperatures can exist at least under low pressure conditions; but some more specific investigation of this point is required for the general case.

Test Apparatus

The same two scales of tubular aircraft-pattern combustion chamber were used as in the earlier tests[3], but with different atomizers to suit the new range of higher flows required. All the present tests were carried out at pressures above 1 atm and with high fuel/air ratios, as it was felt that a high level of wall temperature would offer the most satisfactory comparison. At these conditions combustion efficiency is always close to 100 per cent.

In the full-size chamber a standard twin-orifice Duple atomizer was used, with fuel always passing through both orifices. For the half-size version a single orifice atomizer of similar internal arrangement was constructed, as it was not mechanically feasible to make a half-size Duple. The spray cone angle of this half-size atomizer corresponded well with the overall cone angle of the full-size Duple. Fuel used throughout was kerosine RDE/F/KER. SR.312.

The pilot and main orifices of the full-size Duple atomizer had 'flow numbers' of 0·47 and

3·6 respectively. No 'pressurizing valve', such as is used on the engine to regulate the distribution of flow between the two orifices, was used on the rig. The supply pressures to each were still generally different, the pilot being held at a pressure drop of about 300 lb/in², and the required fuel flow obtained by manual regulation of the main supply. This implied that strict matching of spray qualities would call for a range of half-size atomizers of varying flow number, each suited to a narrow band of fuel flows only. However, since operation near either extinction limit of fuel/air ratio was not contemplated, and combustion performance in the region of high efficiency is generally rather insensitive to atomization, it was felt that some relaxation of this requirement could be accepted. The precise scale matching of fuel droplet size and penetration sought in previous work[3] becomes less essential. For this reason, a single half-size atomizer of flow number = 0·83 was chosen as a fair compromise.

The test rig is shown diagrammatically in *Figure 1*. A 'hack' combustion chamber was used to preheat the air supply for all tests. Both scales of chamber were fitted with upstream adaptors each shaped in the segment of an annulus, carrying a row of straight vanes to simulate compressor outlet conditions on the engine. Further adaptors fitted downstream of the chambers enabled outlet temperature to be measured by sonic pyrometers traversing annular segments. A description of the scale matching of air distribution within the chambers and their inlet velocity and outlet temperature profiles was given in ref. 3.

Thermocouple attachment

A total of nine thermocouples was fitted to the flame-tube of each chamber, distributed around the primary zone. Three circumferential stations 120° apart each comprised three couples at equal axial spacing: at each station, the first and second couples were respectively level with the first and second rows of radial air injection holes, and the third couple was between the second row of holes and the cooling louvres. These positions are illustrated in *Figures 2* and *3*.

On both chambers the thermocouples were formed from Pyrotenax cable of 0·0625 in. outside diameter carrying twin chromel–alumel wires of 0·013 in. diameter. The metal sheath was cut back for a length of about 0·1 in, and the two wires welded together to form a bead. This bead was then inserted in a hole in the flame-tube wall and attached by high-temperature brazing, the braze being dressed off flush on the inside. The end of the cable adjacent to the thermocouple junction was held down flat against the outside of the flame-tube wall by means of a small strap of Nimonic wire welded in place. The three cables in each group were then strapped together and passed down the secondary air annulus and through a stub-pipe fixed to the downstream end of the

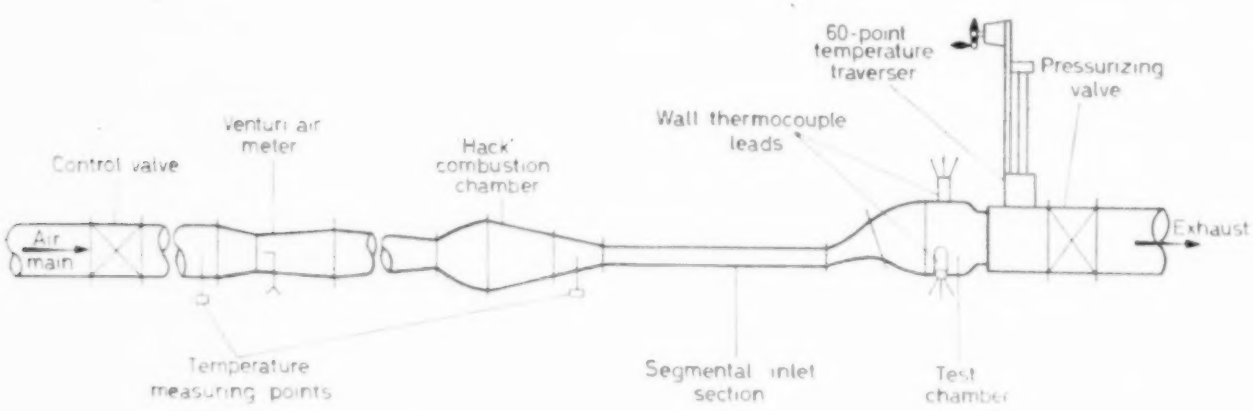

Figure 1. Layout of test rig (not to scale)

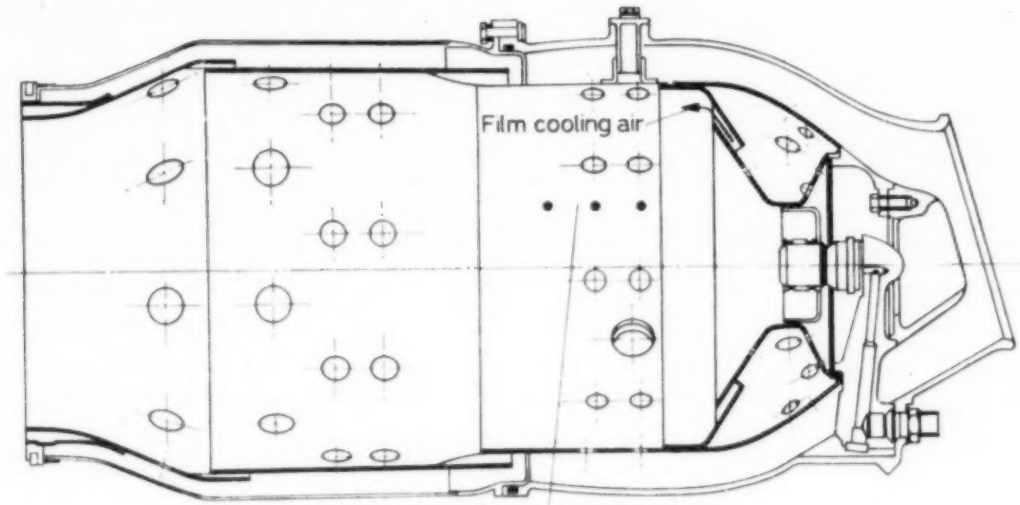

Figure 2. Thermocouple positions

air casing. This was made pressure-tight by a Sindanyo gland into which the cables were cemented.

As the half-size flame-tube wall was only 0·028 in. thick, this form of attachment required considerable finesse, and the resulting assembly was not as robust as could be desired. Failure of thermocouples in service was in fact a fairly frequent occurrence. A further problem was to make sure that none of the thermocouple beads projected into the airstream in the secondary annulus: although every possible care was taken in assembly, the scale of the apparatus was such that the precise location of the effective couple junction could not be determined with certainty. In order to allow a better result to be achieved by statistical averaging, more numerous couples would have been very desirable. It was feared, however, that excessive blockage of the annulus by a large mass of cables would interfere with the secondary airflow, and affect the temperature of the flame-tube locally. In addition, the chamber had to be capable of being dismantled fairly readily, so that too much complication could not be entertained.

It should be emphasized that in view of these factors—i.e. scarcity of couples, difficulties of installation, and uncertainty of behaviour—it is not possible to claim any high accuracy of measurement.

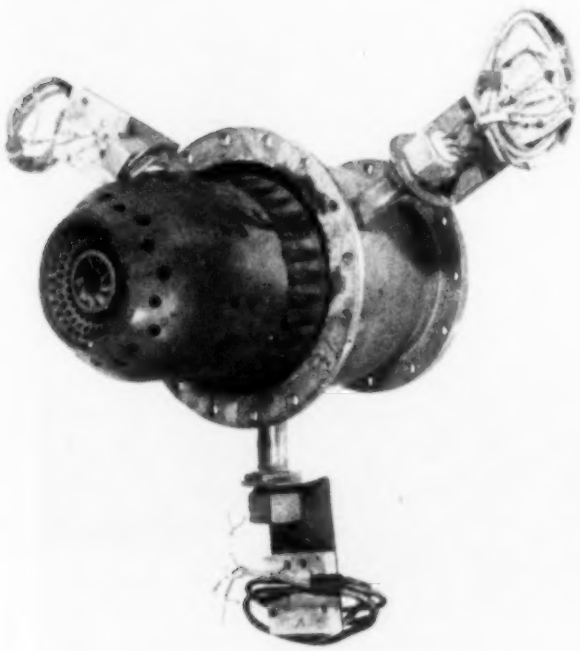

Figure 3. Half-size test chamber, showing location of thermocouples

Test conditions

In all tests the inlet air was raised from about 25 °C to 250 °C in the 'hack' chamber, and an 'air'/fuel ratio of 60 (within ±2 per cent) was

used in the test chamber. This corresponds very closely to stoichiometric conditions in the primary zone. The following relations between mass flow and pressure were maintained within ± 1·5 per cent:

$$\text{Full-size:} \quad Q = 2{\cdot}35\,P$$
$$\text{Half-size:} \quad Q = 0{\cdot}588\,P$$

This led to plant capacity setting a limit at 3·8 atm on the pressure attainable in the full-size chamber. In the half-size, which had originally been built for sub-atmospheric tests only[3], the upstream end of the air casing was formed of a bronze casting (correctly scaled on the inside only), and it was deemed unsafe to operate at pressures above 4·4 atm.

In each test wall temperatures were recorded at the beginning and end of a period of some 15 minutes during which steady running conditions were maintained. The value presented is the average of these two readings, but very little tendency to wander was exhibited.

Test Results

The test data are given in *Table 1*. In the later tests on the half-size chamber, all the thermocouples in the row farthest upstream had failed, but limited interest in temperatures at this station did not warrant further replacement.

It is immediately clear from *Table 1* that, even preserving the scaling technique given by PD = constant, the full-size chamber wall temperatures are somewhat higher than those on the half-size. The exact level of difference is difficult to estimate from the table, as a certain amount of random scatter exists in the results, both on individual scales and in comparison between them. This could arise from a number of causes. On each scale the patterns of airflow and fuel distribution may change to a small extent with pressure, leading to some variation in local conditions at each thermocouple position. Then the matching of air and fuel flows between scales—although evidently good in a general way—may not be perfect in detail, nor the thermocouples attached in exactly identical relative positions. Other work using thermal-sensitive paint has given evidence of very uneven wall temperature distribution

Table 1. Test results

Test No.	Chamber	Inlet pressure (atm)	Air flow (lb/sec)	Air/fuel ratio	Combustion efficiency (%)	Exhaust temp. (°C)	Wall temperatures (°C)										
							1	2	3	4	5	6	7	8	9	Average of first row (1, 4, 7)	Average of second row (2, 5, 8)	Average of third row (3, 6, 9)
I	Half size	1·1	0·642	59·3	93·7	830	282	278	340	193	336	400	226	308	384	234	307	375
II		2·2	1·310	60·5	100	868	228	294	359	206	319	403	287	359	430	240	324	397
III		3·3	1·915	58·9	100	885	—	331	403	—	359	417	—	303	382	—	331	401
IV		4·4	2·59	59·8	98·9	860	—	336	392	—	386	422	—	325	428	—	349	414
V	Full-size	1·1	2·59	60·0	100	873	311	370	442	288	326	413	288	337	378	296	344	411
VI		1·65	3·88	60·0	97·0	847	305	379	469	282	332	433	305	362	402	297	358	435
VII		2·2	5·17	60·0	96·8	847	311	378	493	292	340	458	297	356	390	300	358	447
VIII		2·7	6·32	59·7	100	869	316	419	503	292	344	449	345	429	463	318	397	471
IX		3·3	7·76	60·0	98·8	859	338	446	546	300	350	465	339	422	451	326	406	487
X		3·8	8·90	60·0	100	867	350	490	514	296	343	467	371	468	483	339	434	488

around a flame-tube. It is doubtful if this pattern on one scale of chamber can be exactly matched on another, however carefully the atomizers may be chosen: the spray parameters can be matched as to overall values, but scarcely the distribution pattern individual to any one atomizer. This can be seen on an annular chamber with several nominally identical atomizers, but without necessarily having precise circumferential symmetry. A piece of apparatus as complex as a gas turbine combustion chamber is far from the ideal vehicle for conducting a heat transfer investigation.

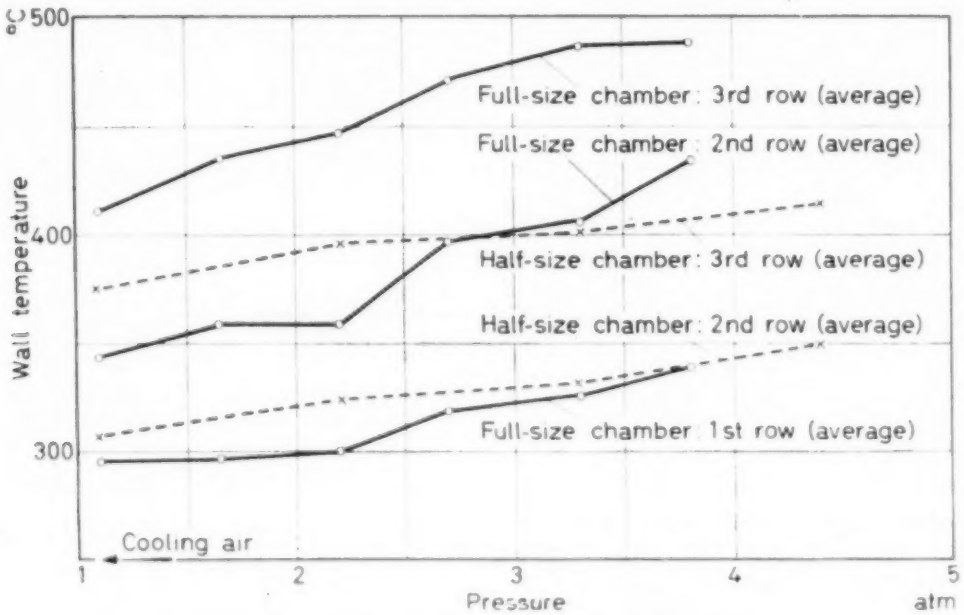

Figure 4(a). *Some experimental results*

However, the results of averaging each row of thermocouple temperatures, given on the right of *Table 1* and plotted in *Figure 4*(a), show an encouraging consistency in trend with both pressure and downstream movement on each scale, and these average values will be used for the purpose of the comparison. Their ultimate utility depends very largely on finding some correspondence with a reasonable analytical picture, and to that we must now turn.

Heat Transfer Analysis

In ref. 4 a method of assessment of the various heat transfer quantities was derived, based on tests using an aircraft combustion chamber identical with the full-size one in this work, except for a modification to the cooling arrangements. This difference unfortunately prevents direct application of the method to this case. In the chamber used in ref. 4, no internal 'blanket' or 'film' of inlet air was injected upstream of the primary zone for cooling purposes, so that the convective heat transfer from the gases to the flame-tube wall depended on a local gas temperature which could be established within fairly close limits. The scaled chambers used in these tests, however, incorporated the standard method of 'film cooling' by means of air injected around the conical 'flare' surrounding the atomizer assembly (see *Figure 2*). The presence of this air renders quite uncertain the local gas temperature upon which convection to the wall depends, but it is natural to expect that a lower level of wall temperature will be obtained with this arrangement.

This is confirmed by comparison with calculation following the method of ref. 4. Corresponding to a primary zone combustion efficiency of 80 per cent, the bulk gas temperature varies with pressure due to dissociation as follows:

Table 2

Pressure P *atm*	*Gas temp.* T_f °K
$\frac{1}{4}$	1925
$\frac{1}{2}$	1940
1	1955
2	1970
4	1985

Ref. 4 gives the following expression for flame emissivity:

$$e_f = 1 - \exp\{-1{\cdot}6 \times 10^{1} P (rl)^{0{\cdot}5} T_f^{-1{\cdot}5}\}$$

In the range of low emissivities in question it is possible to write

$$e_f \simeq 1 - \exp(-e_f)$$

whence

$$e_f \simeq 1{\cdot}6 \times 10^{1} P (rl)^{0{\cdot}5} T_f^{-1{\cdot}5}$$

In our case

$$e_f \simeq 0{\cdot}05 P D^{0{\cdot}5}$$

where D is the linear scale factor, which is unity on the full-size chamber (for notation, see Appendix). Thus, following the argument developed in ref. 4 for internal radiation:

$$\begin{aligned} R_1 &= S.\tfrac{1}{2}(1+e_s)(e_f T_f^4 - a_f T_w^4) \\ &\simeq S.\tfrac{1}{2}(1+e_s)\, e_f T_f^{1{\cdot}5}(T_f^{2{\cdot}5} - T_w^{2{\cdot}5}) \\ &= 1{\cdot}19 \times 10^{-13} P D^{0{\cdot}5} T_f^{1{\cdot}5}(T_f^{2{\cdot}5} - T_w^{2{\cdot}5}) \\ &\qquad \text{C.h.u./sec ft}^2 \end{aligned}$$

Also, for external radiation:

$$\begin{aligned} R_2 &= S\left\{\frac{e_w e_c}{e_c + e_w(1-e_c)(d_w/d_c)}\right\}(T_w^4 - T_i^4) \\ &\simeq 0{\cdot}4 S (T_w^4 - T_i^4) \\ &= 1{\cdot}12 \times 10^{-12}(T_w^4 - 523^4)\ \text{C.h.u./sec ft}^2 \end{aligned}$$

Next take the convection components. Ref. 4 shows that the following general expressions are applicable:

$$\begin{cases} C_1 = 0{\cdot}017\left(\dfrac{\lambda}{\mu^{0{\cdot}8}}\right)\left(\dfrac{Q_f^{0{\cdot}8}}{A_p^{0{\cdot}8} d_p^{*0{\cdot}2}}\right)(T_f - T_w) \\ C_2 = 0{\cdot}02\left(\dfrac{\lambda}{\mu^{0{\cdot}8}}\right)\left(\dfrac{Q_a^{0{\cdot}8}}{A_a^{0{\cdot}8} d_a^{*0{\cdot}2}}\right)(T_w - T_i) \end{cases}$$

Introducing the chamber geometry and aerodynamic arrangements, this led to:

$$\begin{cases} C_1 = 0{\cdot}0119\left(\dfrac{\lambda}{\mu^{0{\cdot}8}}\right) Q^{0{\cdot}8}(T_f - T_w) \\ C_2 = 0{\cdot}106\left(\dfrac{\lambda}{\mu^{0{\cdot}8}}\right) Q^{0{\cdot}8}(T_w - T_i) \end{cases}$$

The mass flow relations given under 'test conditions' above can now be used to give finally:

$$\begin{cases} C_1 = 1{\cdot}32 \times 10^{-3} P^{0{\cdot}8} D^{-0{\cdot}2}(T_f - T_w) \\ \qquad\qquad \text{C.h.u./sec ft}^2 \\ C_2 = 8{\cdot}27 \times 10^{-3} P^{0{\cdot}8} D^{-0{\cdot}2}(T_w - 523) \\ \qquad\qquad \text{C.h.u./sec ft}^2 \end{cases}$$

For equilibrium, one then equates

$$R_1 + C_1 = R_2 + C_2$$

where all four quantities are expressed in terms of P, D, T_f and T_w. Substituting for T_f from *Table 2* above, a value of T_w can be found for any combination of P and D. At the datum of $P=1$, $D=1$, we get $T_w = 830$°K, compared with a maximum measurement of about 710°K, or an average of the third row couples of about 680°K. In taking account of this discrepancy it is only reasonable to assume that the internal radiation is unaffected by the presence of film cooling air. It is clear from *Figure 4*(a) that the temperature of this film increases as it passes downstream, but as it evidently continues to limit the convective heat flow to the wall, it apparently never reaches the level of the gas temperature.

The most obvious starting point, then, is to find the level of wall temperature corresponding to zero internal convection, and check where this lies in relation to the average measured wall temperature at each row of thermocouples. Taking the same datum conditions as before, the assumption that $R_1 = R_2 + C_2$ gives $T_w = 695$°K, which in fact agrees quite well with the average of the third row. Results over the full range of conditions tested are shown in *Figure 4*(b), which demonstrates substantial agreement throughout the range. This early success is both fortuitous and fortunate, offering immediately a simple method of general procedure.

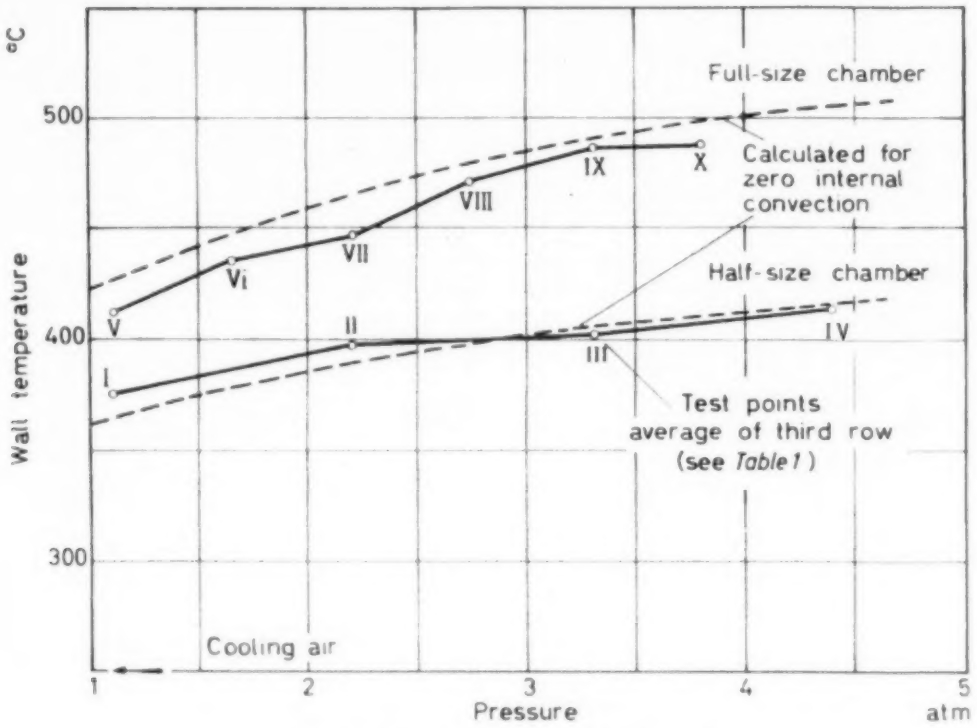

Figure 4(b). *Some experimental results*

Thus we observe that the temperature of the internal cooling film is below that of the adjacent wall at the first and second row positions, and reaches a value equal to the wall temperature level with the third row. From the results of the first and second rows of couples—which show substantial similarity in pattern to the third row [*Figure 4*(a)]—a measure of the change in negative internal convection (i.e. heat transfer from wall to cooling air film) with downstream movement can be obtained.

General scale results

Applying the condition of zero internal convection to a wider range of P and D, for the same conditions of inlet temperature and fuel/air ratio, we get maximum primary zone wall temperatures as in *Figure 5*, and corresponding heat transfer rates as in *Figure 6*. It is not in fact possible to justify the continued assumption of a primary zone combustion efficiency of 80 per cent at conditions which combine low values of both P and D, since this efficiency depends on the product $P \times D$ and below a critical value starts to fall with it (see Figure 2 of ref. 4). Along the line marked 'PD = constant' in *Figures 5* and *6*, corresponding to the normal scaling method, the efficiency is of course constant.

Examination of *Figure 5* shows the extent to which the scaling rule of PD = constant fails to preserve similarity of wall temperatures. While it is clearly much closer than changing scale at constant pressure (PD^0 = constant), a nearer match (of wall temperature only) would in this case be obtained with PD^2 = constant. Other calculations for the case of zero internal cooling air produce a picture broadly similar to *Figure 5*, so that we may conclude the above results to be of a fairly general nature.

Conclusion

The experiment indicates that, in the combustion chambers tested, the internal cooling air film reaches the flame-tube wall temperature near the downstream end of the primary zone. At this station, internal convection is then zero. Using this picture, a general analysis shows that scaling according to the rule 'pressure × linear

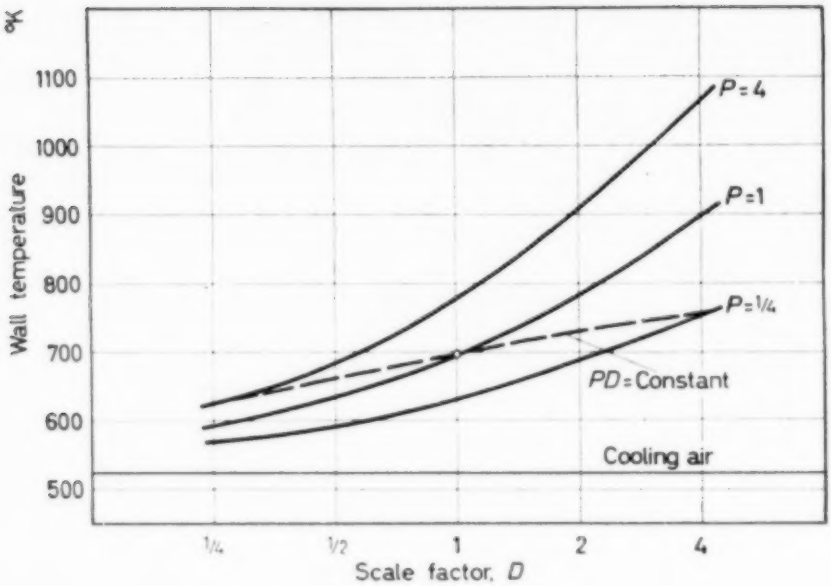

Figure 5. Calculated wall temperatures

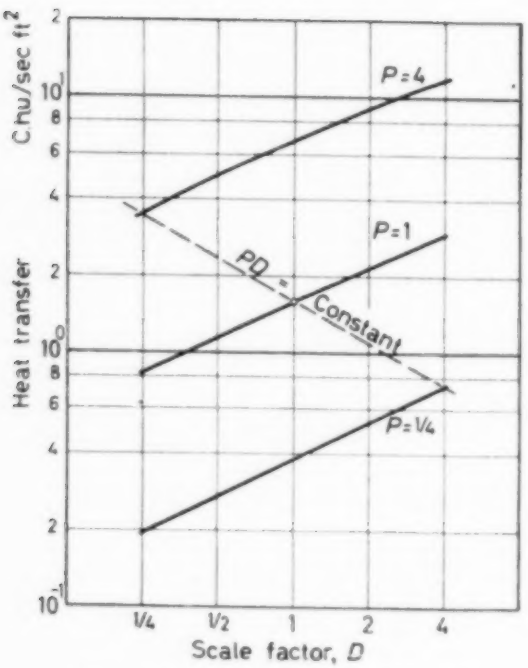

Figure 6. Calculated heat transfer

scale = constant' gives maximum wall temperatures which increase somewhat with scale factor. Very much larger discrepancies would exist, however, if pressure was not varied with scale.

Crown Copyright reserved. Reproduced by permission of the Controller, H.M. Stationery Office.

Appendix: Notation

a	absorptivity
A	cross sectional area, ft²
C	convection heat transfer coefficient, C.h.u./sec ft²
d	diameter, ft
d^*	hydraulic mean diameter, ft
D	scale factor (= unity on full-size chamber used in tests)
e	emissivity
l	radiation beam length, ft
P	pressure, atm
Q	mass flow (used without suffix for total flow), lb/sec
r	fuel/air ratio by weight
R	radiation heat transfer coefficient C.h.u./sec ft²
S	Stefan–Boltzmann constant, C.h.u./sec ft² (°K)⁴
T	temperature, °K
λ	gas conductivity, C.h.u./sec ft °K
μ	gas viscosity, lb/sec ft

Suffixes

$_1$	internal
$_2$	external
$_a$	cooling air annulus
$_c$	air casing wall
$_f$	flame
$_i$	air entry condition
$_p$	primary zone
$_w$	flame-tube wall

References

[1] STEWART, D. G. 'Scaling of gas turbine combustion systems'. *Selected Combustion Problems*, Vol. II. (G.A.R.D.; Butterworths: London, 1956

[2] HERBERT, M. V. 'Aerodynamic influences on flame stability'. *Progress in Combustion Science and Technology*. Pergamon: London, 1960

[3] HERBERT, M. V. and BAMFORD, J. A. 'Scale effect in a gas turbine combustion chamber fitted with a swirl atomizer, Part I'. *Combustion & Flame*, 1957, **1**, 360

[4] LEFEBVRE, A. H. and HERBERT, M. V. 'Heat transfer processes in gas turbine combustion chambers'. Institution of Mechanical Engineers: London, 1960

Perturbation Studies of Flames by Changes in Composition

ROSE L. SCHALLA

Lewis Research Center, National Aeronautics and Space Administration, Cleveland, Ohio

(*Received September 1959*)

The nature of perturbations created by abrupt changes in composition and their effects on flame propagation have been investigated for ethylene–air mixtures in a 1 in. square flame tube. The time required for the flame to establish a new linear velocity in a mixture of given composition and flame speed, after propagating through a preceding mixture of either higher or lower flame speed, was determined. When propagation was from a slow to a fast flame-speed mixture, oscillations in flame structure and velocity along with accompanying pressure disturbances were observed across the transition region. A small pressure decrease but no oscillatory behaviour was observed for propagation from a fast to a slow flame-speed mixture.

Introduction

HOMOGENEOUS fuel–oxidant mixtures are seldom obtained throughout a combustion chamber; in fact, in many combustors compositions may vary from almost pure fuel to pure oxidant. The variation of flame speed and other combustion properties with composition has been extensively investigated. However, a flame propagating from one composition into another will be affected by sudden changes in such variables as flame temperature, density and heat-release rate. The extent of the influence of these and other factors on the flame properties is not well understood. For example, a flame propagating from one mixture to another must undergo a change of burning velocity in going from one steady state to another. It is not known how long this transition will take or what happens to the flame during the transition period. Theoretical studies by BOA-TEH CHU[1, 2] have indicated that a discontinuity in composition would create a compression or expansion wave. As described in refs. 2 and 3, any pressure waves formed would be reflected from the ends of the tube and thereby could result in oscillating flow.

To gain more insight into these phenomena, an experimental study was undertaken to examine the nature of the perturbations created by an abrupt change in composition. The work was carried out in horizontal 1 in. square flame tubes with ethylene–air mixtures. A sliding metal diaphragm divided the tube into two equal lengths and separated the different compositions prior to ignition. Shadowgraph and schlieren photographs with high-speed cameras were taken to observe the changes in flame structure across the transition region. The amplitude and frequency of the pressure disturbances were also measured. Streak-film motion pictures were taken to follow the spatial velocities of the flame throughout the tube, and from these photographs times for establishing a uniform flame speed in the second composition were obtained. Hereinafter, this time will be referred to as the response time.

The existing theories and their relation to the results obtained are briefly examined.

Experimental

A conventional vacuum line was used for preparing the different ethylene–air mixtures and for evacuating and filling the flame tube. A 4 ft long Lucite tube of 1 in. square cross sectional area, mounted horizontally, was used as the flame tube [see *Figure 1*(a)]. A few experiments were conducted with tubes 3 ft and $1\frac{1}{2}$ ft long. The standard 4 ft tube was separated

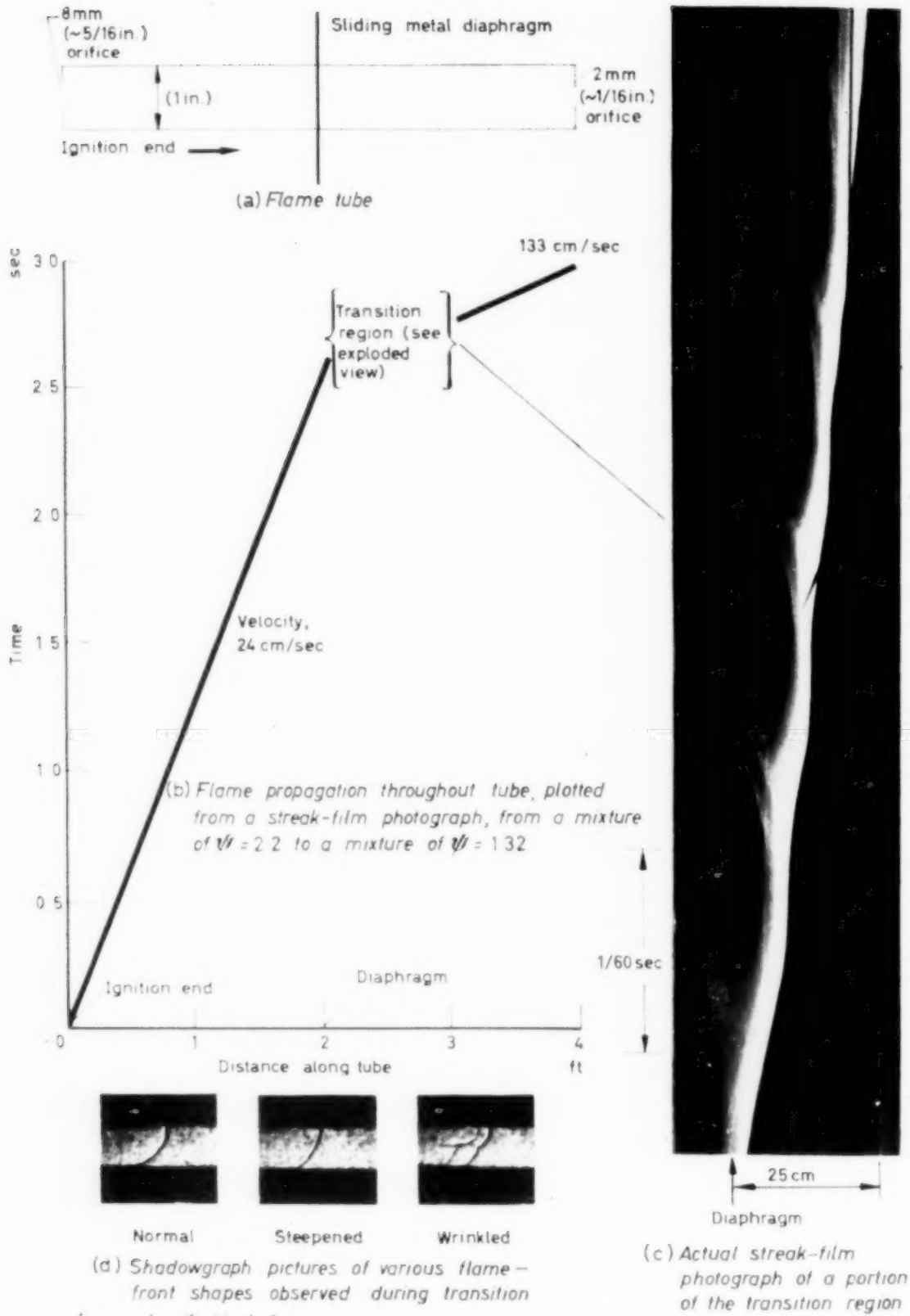

Figure 1. Typical flame travel and transition phenomena for propagation from a slow to a fast flame-speed mixture in a 1 in. flame tube

into two equal lengths by a manually operated sliding metal diaphragm, which was removed just prior to ignition. To obtain unequal lengths of gas column, another 4 ft tube was divided into a 3 ft and a 1 ft section. Orifices at the ends of the tubes were always 8 mm (~5/16 in.) and 2 mm (~1/16 in.) in diameter, with ignition at the larger orifice. As described in ref. 4, the use of orifices tends to produce uniform flame travel. Ignition was achieved by either an alcohol lamp or a bunsen burner, with no apparent variation among identical runs between these two igniters.

Mixtures of ethylene and filtered air were used throughout the investigation. Ethylene was selected because its flame speed in air over a wide composition range had already been reported for a tube of similar size in ref. 5. The high spatial flame speeds and wide flammability range of ethylene permit greater differences in flame speeds and temperatures to be obtained with various compositions than would be possible with aliphatic hydrocarbons. The general method of study was to select a given ethylene–air composition to be used as a reference mixture in the second half of the tube and to vary the composition of the mixture in the first half over the ignitable range. A new reference mixture was then chosen, and the procedure was repeated.

To follow the flame travel throughout the tube, a DuMont 35 mm streak-film oscilloscope camera was adapted to cover the 4 ft tube length. Camera speed was 30 in./sec. By using very fast film, the visible light of the flame was detectable at this speed. Streak-film traces facilitate detection of changes from uniform to non-uniform flame velocity and also furnish fairly accurate spatial flame velocities.

A high-sensitivity SLM quartz-crystal pressure pickup with a natural frequency of 7 kc/s was used for detecting pressure disturbances. For most of the runs the pickup was located about 2·5 in. from the exit end of the tube; some studies were made varying the location to 9 in. before and after the diaphragm and 2·5 in. from the ignition end. The electrical output from the pickup was displayed on a dual-beam cathode ray oscilloscope and was photographed; a wave of known frequency on the second channel served as a time base. A photomultiplier tube ahead of the diaphragm was used to trigger the oscilloscope.

A shadowgraph system with a high-speed camera was used to observe changes in flame structure across the interface. A two-lens camera was also used to photograph simultaneously the flame and the pressure displacement displayed on the oscilloscope screen. Thus, a direct comparison between flame structure and the pressure oscillations was obtained.

Results and Discussion

Determination of spatial flame speeds

In *Figure 2* the spatial flame velocities of ethylene–air mixtures determined in this investigation are plotted against fuel concentration expressed as fraction of stoichiometric, denoted

$$\left(\psi = \frac{f/f+a}{(f/f+a)_{\text{stoich}}}\right)$$

Calculated equilibrium flame temperatures from ref. 5 are plotted against composition in *Figure 3*. The spatial velocities were usually obtained by using a single composition through the 4 ft tube; no attempt was made to convert spatial velocities to fundamental flame speeds.

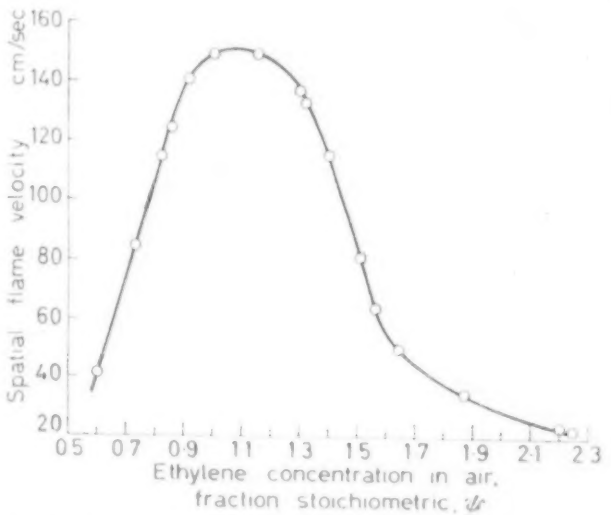

Figure 2. Variation of spatial flame velocities of ethylene–air mixtures over a wide range of compositions

The flame velocity was uniform over the 4 ft tube length except for mixtures between $\psi = 0{\cdot}8$

and $\psi = 1{\cdot}5$, in which the flame propagation displayed oscillatory motion in the initial portion of the tube. Only flames of spatial velocities very near the maximum continued to oscillate past the first quarter of the tube. This initial non-uniform behaviour can probably be explained on the basis that ignition was achieved by a flame of lower flame temperature, namely the outer edge of an alcohol lamp or bunsen burner. As will be shown later, a flame

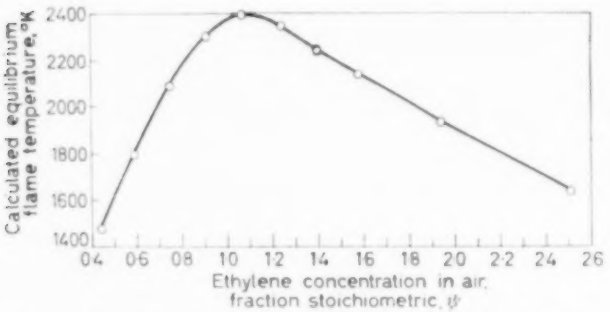

Figure 3. Variation of calculated equilibrium flame temperatures of ethylene–air mixtures over a wide range of compositions (ref. 5)

of low burning velocity and temperature sets up oscillations when it propagates into (i.e. ignites) a mixture of higher flame speed and temperature. Other factors, however, may be involved. Since a uniform velocity was established before the flame reached the second half of the tube, these initial disturbances did not interfere with the experiment proper. Several investigators[6–8] have reported the occurrence of self-induced oscillations in the centre section of tubes. In this study, uniform travel was obtained in that area because orifices instead of the customary open- to closed-end tube were used.

It is also interesting to note that premixed-rocket studies by J. R. Osborn and R. M. Schiewe[9] show smooth burning for very lean or rich ethylene–air mixtures and increasing instability for mixtures approaching stoichiometric ratios. The same mixtures that burned without oscillations in the rocket tests were those that did not start out oscillating in the present tube study.

General transition behaviour

Initial studies with a change in composition were undertaken with propagation from a low-flame-speed mixture ($\psi = 2{\cdot}2$) to a faster mixture ($\psi = 1{\cdot}32$), with spatial velocities of 24 and 133 cm/sec, respectively. The streak-film traces showed uniform flame travel of this first mixture to, or slightly past, the centre of the tube [see *Figure 1*(b)]. How far the flame velocity of the first mixture will extend past the centre probably depends on the gas velocity, U_g, ahead of the flame. A determination of U_g in ref. 4 has shown that, in a 1 in. diameter tube, U_g is very small for spatial velocities lower than 70 cm/sec and increases to about 25 cm/sec at the maximum spatial velocity of 150 cm/sec. After the interface between the two mixtures was crossed, the streak-film trace indicated that the flame velocity went through a series of oscillations for about 160 msec over a distance of about 1 ft. The uniform velocity of the second mixture was then established for the remainder of the tube. An exploded view of a portion of the actual film trace showing the oscillatory movement can be seen in *Figure 1*(c). Shadowgraph pictures [*Figure 1*(d)] show the changes in the flame front that occurred throughout this transition region. The typical flame-front structures observed were the normal flame structure, a more steepened shape, and a wrinkled surface.

The frequency of the oscillations was about 56 c/s. The natural frequency of the tube with air at room temperature was determined to be 71 c/s. The frequency under test conditions cannot be determined unambiguously, because the temperature of the hot gas in the first half is not accurately known. An estimate of the frequency assuming the gas in the first half is near flame temperature and that the tube is closed at one end would be about 170 c/s.

When the flame travel was from the faster flame-speed mixture into the slower, neither the shadowgraph nor the streak-film photographs indicated the presence of any oscillations for the two mixtures involved. Across the interface the flame speed decreased smoothly from 133 to 24 cm/sec in about 50 msec.

Effect of tube length and position of diaphragm

Using the same two mixtures as before, propagation from the slow to the fast flame-speed mix-

ture was repeated in a 3 ft and a 1½ ft tube. Similar oscillatory behaviour was observed, and there was a slight increase in the frequency of the oscillations as tube length was varied from 4 ft to 1½ ft. The duration of the oscillations decreased with decreasing tube length as shown in *Figure 4*. No oscillations were observed for propagation from the fast to the slow flame-speed mixtures with a shorter tube, and corresponding response times are shown in *Figure 4*.

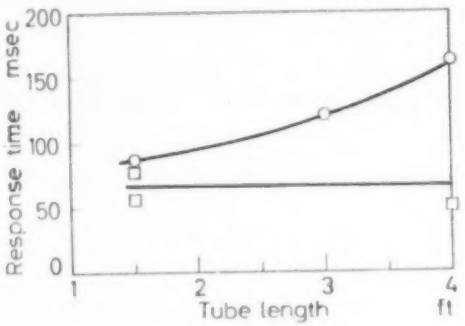

Figure 4. Effect of variation in tube length on the response time. ○ Propagation from a mixture of $\psi=2{\cdot}2$ (24 cm/sec) to a mixture of $\psi=1{\cdot}32$ (133 cm/sec). □ Propagation from a mixture of $\psi=1{\cdot}32$ (133 cm/sec) to a mixture of $\psi=2{\cdot}2$ (24 cm/sec)

To make certain that the position of the diaphragm was not significant to the results being obtained, studies were made with the first section 1 ft long and the second 3 ft, and vice versa. Essentially the same results were obtained as with the diaphragm at the centre. Subsequent experiments were all conducted in a 4 ft tube divided into two equal lengths.

Duration of oscillation and maximum pressure rise with three reference mixtures

A more extensive study of the duration of the oscillatory motion and accompanying pressure changes was conducted by selecting three different reference compositions to be used in the second half of the tube and varying the composition of the mixtures in the first half over the ignitable fuel–air range. In *Figure 5*, three schematic sketches show the typical situations of composition and flame speeds being considered. The three reference compositions were $\psi=0{\cdot}73$, 1·09 and 1·8, with spatial velocities of 85, 150 and 40 cm/sec, respectively. The maximum velocity mixture of 150 cm/sec was studied first [see *Figure 5*(a)]. Propagation from any mixture such as B or C into the reference mixture A resulted in oscillations across the transition region. Of necessity all mixtures used in the first half of the tube were of lower flame speed. The streak-film trace in *Figure 1* was typical of the results obtained. From the streak-film photographs, the duration

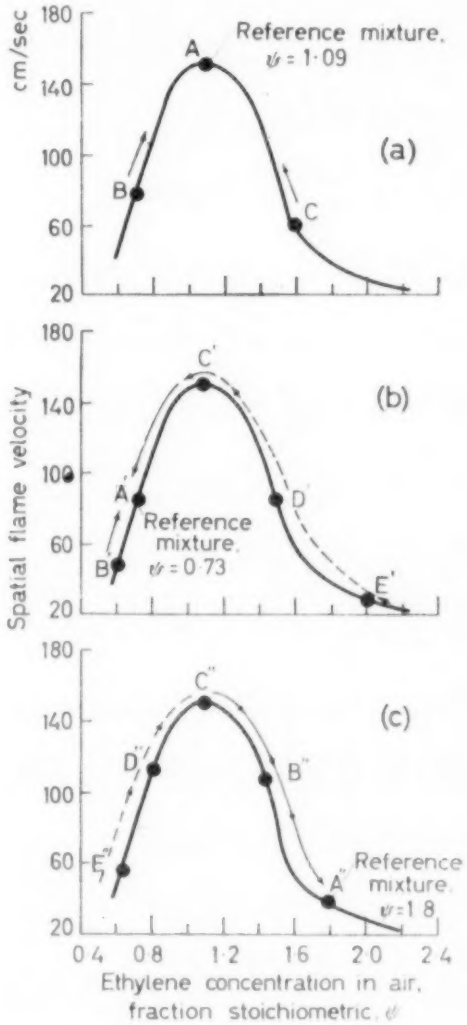

Figure 5. Schematic sketches showing the typical situation of composition and flame speed for three different reference mixtures

of the oscillations created by each composition used in the first half of the tube was obtained, and the results are shown in *Figure 6*(a). Pressure disturbances were also measured; the maximum pressure rises obtained are shown in

Figure 7(a). The square symbols in *Figure 6*(a) represent the oscillation times obtained from the pressure traces. The response times from the film traces and the pressure curves are in good agreement. As shown in *Figures 6*(a) and *7*(a), the duration of the oscillations and the pressure decreased as the flame speed of the first mixture was increased, or, in other words, as the diffe

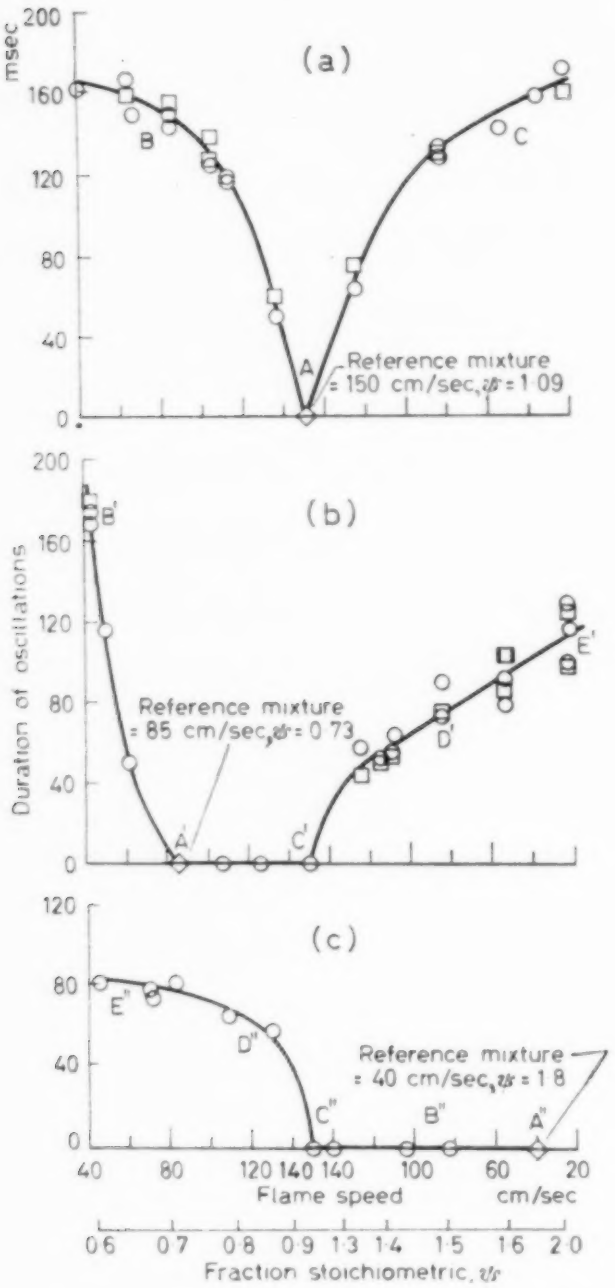

Figure 6. Duration of oscillations created by propagation from various flame-speed mixtures into three constant reference mixtures of (a) $\psi=1{\cdot}09$ *(150 cm/sec),* (b) $\psi=0{\cdot}73$ *(85 cm/sec), and* (c) $\psi=1{\cdot}8$ *(40 cm/sec).* ○ *Oscillation times from streak-film photographs.* □ *Oscillation times from pressure traces*

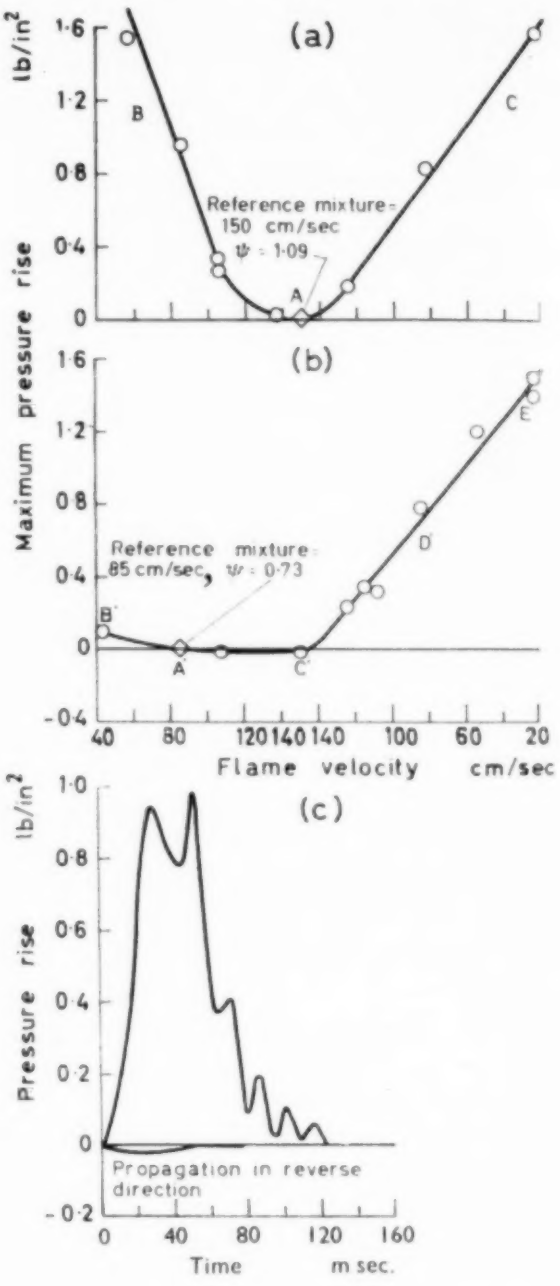

Figure 7. Maximum pressure rises resulting from propagation through various flame-speed mixtures into two constant reference mixtures of (a) $\psi=1{\cdot}0$ *(150 cm/sec), and* (b) $\psi=0{\cdot}73$ *(85 cm/sec); and* (c) *the pressure rise against time during the transition from a flame speed of 85 cm/sec* ($\psi=0{\cdot}73$) *to the maximum velocity of 150 cm/sec*

ence in flame speeds between the two compositions decreased. With the maximum difference in flame speed obtainable, the oscillations lasted about 170 msec, and the maximum pressure rise was about 1·6 lb/in². The oscillatory motion in this case covered about 16 in. of the tube.

A lean mixture of $\psi = 0{\cdot}73$ (85 cm/sec) was selected as the second reference mixture. The typical composition variations that can be achieved are shown schematically in *Figure* 5(b). Propagation from a lower flame speed, lean mixture, B′, into the reference mixture, A′, produced very low-amplitude oscillations and a small pressure rise. The duration of oscillations and maximum pressure rises are shown in *Figures* 6(b) and 7(b), respectively. With any composition between A′ and C′ in the first half of the tube, no oscillations were observed. These results are in agreement with the case considered previously for propagation from a high flame-speed ($\psi = 1{\cdot}32$) to a lower flame-speed mixture ($\psi = 2{\cdot}2$). Since only the duration of the oscillations was being measured, any time involved for this transition was neglected; and thus these data are reported as zero oscillation time. As shown in *Figure* 7(b), a very small pressure decrease was obtained with these mixtures between A′ and C′.

When any mixture on the rich side of stoichiometric (i.e. D′ or E′) was used in the first half of the tube, the typical oscillatory flame travel shown in *Figure 1* was again observed. The duration of oscillations is less than for the maximum-velocity reference mixture; however, the maximum pressure rises obtained are very similar. Compositions between D′ and C′ have flame speeds higher than the reference mixture and yet gave rise to oscillations unlike the cases considered earlier, namely, the compositions between A′ and C′ and propagation from a mixture of $\psi = 1{\cdot}32$ to $\psi = 2{\cdot}2$. There appears to be a contradiction therefore in a statement that propagation from a fast to a slow flame-speed mixture is free of oscillations. However, this anomaly can be resolved if it is realized that in travelling from these rich mixtures into the lean reference composition, the flame must momentarily encounter all compositions and flame speeds in between the two, including the maximum-velocity composition. In crossing from the rich to the lean side, the flame velocity is really being increased to the maximum velocity (i.e. from a slower to a higher flame speed) before reaching the reference-velocity mixture, and consequently oscillations should be observed. If it were possible to avoid this initial acceleration to the maximum velocity (as is the case with mixtures between C′ and A′) before entering the leaner reference flame speed mixture, it is believed that no oscillations would result. When mixtures between D′ and E′ are used in the first half of the tube, oscillations are observed because of this transition across the maximum-velocity mixture; however, oscillations would be expected in this case even if it were possible to avoid obtaining the maximum velocity because they are of lower flame speed. The preceding explanation would also account for the fact that the maximum pressure rise is the same on the rich side in *Figures* 7(a) and (b).

A very rich, low flame-speed mixture ($\psi = 1{\cdot}8$, 40 cm/sec) was selected as a third reference composition. The combinations of compositions that can be obtained are shown in *Figure* 5(c). Propagation from any mixture of higher flame speed on the rich side (i.e. between A″ and C″) did not create oscillations during the transition. When lean mixtures (i.e. D″ and E″) were present in the first half of the tube, the typical oscillatory transition was observed. The duration of these oscillations is shown in *Figure* 6(c). The results are in agreement with those obtained for the second reference mixture; namely, that no oscillations were obtained with mixtures of higher flame speed on the same side of stoichiometric, but propagation from any mixture on the opposite side of stoichiometric resulted in oscillations. The latter situation is again attributed to the fact that the flame speed first increased to the maximum velocity before encountering the reference-velocity mixture.

The two factors that seem to determine the duration of the oscillations are: (*1*) the initial difference in flame speed between the two mixtures, as illustrated by the data in *Figure* 6(a), and (*2*) the magnitude of the flame speed

of the second mixture as shown in *Figures* 6(b) and (c). Once started, the oscillations can be maintained longer in a high-flame speed, near-stoichiometric mixture. For example, when rich mixtures were used in the first half of the tube, the oscillations were about 30 per cent shorter with the lean reference mixture of 85 cm/sec than with maximum velocity mixture. With lean mixtures that produced oscillations, the times ranged from 75 per cent less at $\psi = 0{\cdot}67$ (64 cm/sec) to approximately the same value at $\psi = 0{\cdot}6$ (42 cm/sec). In the rich reference mixture (40 cm/sec), the duration of oscillations was about 50 per cent less than with the maximum-velocity reference mixture. These findings may also explain why, of the various mixtures that started out oscillating in the tube when ignited by the alcohol lamp, those with the highest flame speeds oscillated the longest.

The maximum rise in pressure does not appear to be related to the magnitude of the flame velocity, but to the initial difference in flame speed encountered between the two mixtures. The absolute value of the pressure rise is influenced by the size of the orifices.

Description of pressure traces and relation with changes in flame structure

To study the pressure disturbances in greater detail, the curve of pressure rise against time is shown in *Figure* 7(c) for a mixture of $\psi = 0{\cdot}73$ (85 cm/sec) in the first half of the tube and the maximum-velocity mixture (150 cm/sec) in the second. The pressure curve for propagation in the opposite direction is also shown. These plots were obtained from still-camera photographs of oscilloscope traces, and these small photographs greatly limit the degree of accuracy in plotting. There was no detectable detail in the pressure traces obtained for propagation from the fast to the slow flame-speed mixtures. For propagation in the slow to the fast direction, the frequency of the pressure oscillations is about 60 c/s, or about the same as the frequency of flame oscillations discussed previously. The pressure rises therefore coincide with the gross oscillations in flame structure. This was also established experimentally by photographing the pressure change and flame simultaneously with a high-speed two-lens camera. It was observed that the pressure increased as the flame wrinkled and decreased as it resumed its normal to steepened shape. The camera speed was too slow to detect formation and interaction of any wave phenomena that might be associated with these reactions.

To determine whether there was much variation in the amplitude and frequency of the pressure curves at different positions along the tube, pressure traces were also obtained with the pickup located $2\frac{1}{2}$ in. from the ignition end and 6 in. after and before the diaphragm. While some slight variations among the curves were noted, the maximum pressure and frequency were substantially the same at all four stations.

General discussion

The obviously complex nature of the action and interaction of chemical, aerodynamic and other factors that occur at the transition region makes any analysis of the experimental findings highly speculative. Theoretical studies by Chu[1,2] have indicated that propagation across a composition gradient that involves an increase in velocity will generate a compression wave, while a decrease in velocity will produce an expansion wave. These compression or expansion waves are postulated to occur as a result of the differences in heat-release rates between the two compositions, and to be of the same magnitude if the difference in flame speeds between the mixtures is held constant. As discussed in refs. 2 and 3, any acoustic waves formed would reflect from the ends of the tube and cause additional interaction with the flame.

For propagation from the fast to the slow flame-speed mixtures, the slight pressure decreases observed experimentally may be accounted for by assuming the formation of an expansion wave as predicted by Chu's theory. The use of orifices and finite tube length prevents a quantitative comparison of this pressure decrease with that predicted by theory. The absence of any detail in the pressure traces or streak-film pictures prevents any frequency measurements and restricts further analysis in this case.

For propagation from the slow to the fast flame-speed mixtures, a compression wave is probably formed at the interface and is responsible for the flame becoming wrinkled. Since a rise in pressure is observed when the flame wrinkles, it is assumed that the increased surface area created by this wrinkled condition increases the burning rate and consequently leads to the observed pressure disturbances. Motion pictures show that the flame does not remain in its wrinkled or ruffled form indefinitely, but goes through several cycles of wrinkled surface, normal flame structure, and then a steepened shape. These cycles are also indicated by the velocity changes shown in the streak-film trace [*Figure 1*(c)]. The nearly vertical portions of the trace indicate that at times the velocity is reduced to much less than the normal velocity of the reference mixture.

These periodic reductions of apparent flame velocity may be due to the motion of the gas opposite to the direction of the flame travel. *Figure 1*(c) shows numerous breakups in the flame indicated by the 'tail' moving backward into the burnt gas. This is quite typical for interaction of a flame with a pressure wave coming from the unburnt side. Hydrodynamic effects may also be important. The cycle is continued because the flame must again accelerate to the higher flame velocity of the reference mixture, and consequently another wrinkled surface and rise in pressure are generated. The pressure and film traces show that the frequency of the oscillations was similar throughout the vibratory region but the amplitude decreased. Shadowgraph pictures showed that the flame surface wrinkled less during each succeeding oscillation, and consequently the ensuing pressure rises were never as great. Apparently, when the decelerating effects no longer reduce the flame speed below the reference mixture velocity, the flame propagates at the reference mixture velocity for the remainder of the tube.

The findings of this experimental study therefore suggest that propagation across a composition gradient that involves an increase in flame speed is a source of pressure oscillations. The flame supplies the energy for these oscillations as a result of the formation of a wrinkled shape and therefore an increased surface area. Under the experimental conditions employed, the oscillations cease after a definite time interval. The length of this time interval seems to be a function of the magnitude of the flame velocity of the second mixture and the initial difference in velocity between the two compositions.

References

[1] Chu, Boa-Teh. *Fourth Symposium (International) on Combustion*, p 603. Williams and Wilkins: Baltimore, 1953

[2] Chu, Boa-Teh. *Tech. Note Nat. Adv. Comm. Aero., Wash., No. 3683*, 1956

[3] Rudinger, G. *Third AGARD Combustion and Propulsion Colloquium* (Palermo, Sicily, 17–21 March 1958)

[4] Gerstein, M., Levine, O. and Wong, E. L. *J. Amer. chem. Soc.* 1951, **73**, 418

[5] Simon, D. M. and Wong, E. L. *Rep. Nat. Adv Comm. Aero., Wash., No. RM E51H09*, 1951

[6] Markstein, G. H. *Fourth Symposium (International) on Combustion*, p 527. Williams and Wilkins: Baltimore, 1953

[7] Behrens, H. *Fourth Symposium (International) on Combustion*, p 538. Williams and Wilkins: Baltimore, 1953

[8] Guenoche, H. and Jouy, M. *Fourth Symposium (International) on Combustion*, p 403. Williams and Wilkins: Baltimore, 1953

[9] Osborn, J. R. and Schiewe, R. M. *Report No. 1–58–1*: Purdue University, 1958

The High Temperature Pyrolysis of Acetylene 1 400° to 2 500°K

C. F. ATEN and E. F. GREENE

Metcalf Chemical Laboratories, Brown University, Providence 12, R. I.

(*Received October 1959*)

The pyrolysis of acetylene–argon mixtures has been investigated in the temperature range 1400° to 2500° K using shock wave heating. Time resolved emission and absorption spectra, measurements of reflected shock velocities, and analysis of the products of the reaction have been used to follow the rate of loss of acetylene. The average activation energy over the temperature range from 600° to 2500° K is approximately 39 kcal/mole and there is evidence that the same mechanism is dominant over the whole range.

Introduction

IN THE study of the pyrolysis of hydrocarbons the investigation of the reaction of acetylene with itself has had a particular importance. This has been so because acetylene is often found as an intermediate in the pyrolysis reactions of other hydrocarbons and because K. KNOX, R. G. W. NORRISH and G. PORTER[1] have found evidence that some hydrocarbons originally react to form acetylene and that it is through this compound that the final products, hydrogen and solid carbon, are formed. Thus studies of the reaction of acetylene with itself may be useful in shedding light on steps which occur in a number of hydrocarbon pyrolyses.

Much of the previous work on acetylene pyrolysis has been summarized by E. W. R. STEACIE[2], but there are some more recent careful studies which have added new information. In the temperature range 625° to 745°K C. G. SILCOCKS[3] has done experiments in which he followed the pressure change with time and analysed the products of the reaction. G. J. MINKOFF, D. M. NEWITT and P. RUTLEDGE[4] also measured the pressure as a function of time in a static system in the range 698° to 798°K. They found no evidence for benzene in the ultra-violet spectrum of the products. They reported an activation energy of 47 kcal/mole for the second order reaction. Silcocks's value was 50 kcal/mole for the homogeneous reaction and both groups noticed a strong inhibition by small concentrations of nitric oxide.

At higher temperatures the reaction is too rapid for study in conventional flow systems, but three papers have reported studies of acetylene reactions carried out in shock tubes.

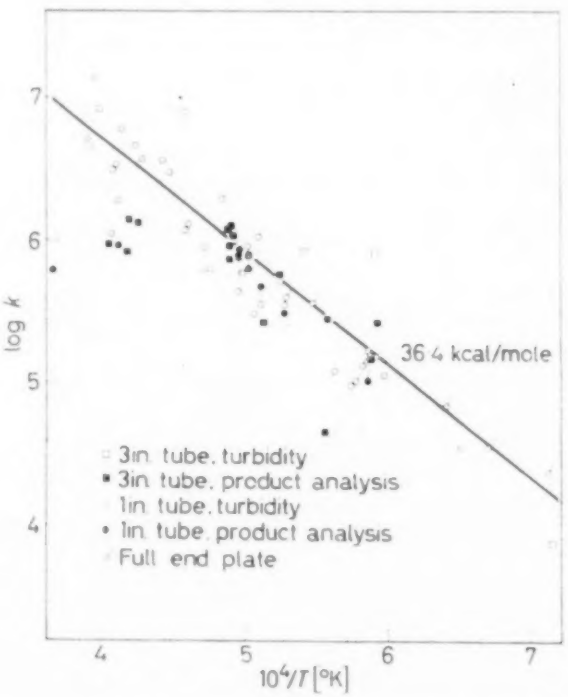

Figure 1. log *k* [*l. mole*$^{-1}$ *. sec*$^{-1}$] *versus* $1/T$ [$^{\circ}K^{-1}$] *for shocks in acetylene–argon mixtures* (*see* Table 1)

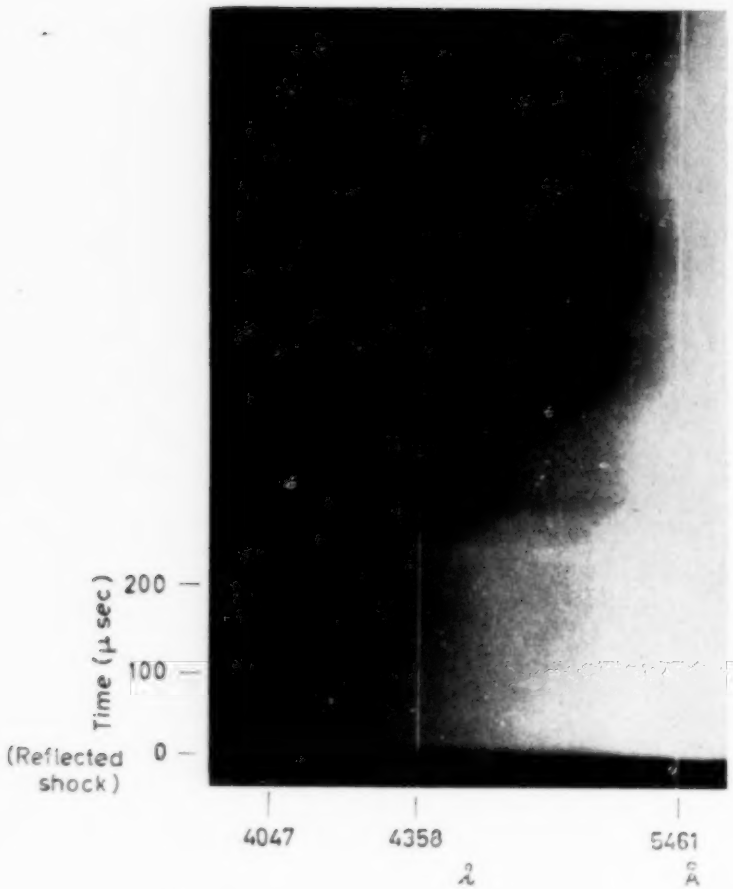

Figure 2. Time resolved emission spectrum.
20% C_2H_2, 80% A
$P_1 = 20mm$ Hg
$T_5 \sim 3100°K$
$N_0 \sim 0{\cdot}08$ mole/l.

W. J. HOOKER[5] found the order of the reaction to be roughly first or second with an activation energy of 39 kcal/mole for the second order reaction. (He quotes 33 kcal/mole based on a rate constant defined in terms of pressure instead of concentrations.) He did not measure the absolute rate. Other workers have given some evidence for a second order reaction with an activation energy of about 30 kcal/mole[6,7]. The present work represents an effort to get more precise results in the temperature range 1 400° to 2 500°K and to examine the reacting system with several different measuring techniques.

Experimental

The shock tubes used, only slightly modified from those of previous studies[6,7], had Pyrex test sections of dimensions 3 in. i.d. × 84 in. and 1 in. i.d. × 60 in. The incident shock velocities were measured by timing the signals from three schlieren stations at 8 in. intervals near the end of the tube. These signals were easily usable (about ten times the noise background) down to initial pressures of acetylene of 1 cm and $\rho_2/\rho_1 = 5$ in the 1 in. tube. For this tube the shock velocities were extrapolated to the end plate using the measured 8 per cent average attenuation per metre. In the 3 in. tube the average shock accelerated 4 per cent per metre and the average of the velocities in the two intervals was used. The initial temperature was 300 ± 2°K.

The acetylene, Matheson, 99·5 per cent, was bubbled through a 16 in. column of concentrated sulphuric acid to remove solvent acetone. A gas chromatogram showed that there was less than 0·05 per cent acetone in the effluent and this was used in the experiments. The remaining gases were used as supplied: argon, Air Reduction, 99·9 per cent; oxygen, Air Reduction, 99·7 per cent; and nitric oxide, Matheson, 99·0 per cent. Hydrogen was the driver gas for all the shocks but one in which helium was used. The gases were assumed to

Table 1. Properties of reflected shocks in acetylene–argon mixtures—Turbidity measurements

Mole % C_2H_2 in A	Shock tube i.d. minus end plate dia. mm	u_1† mm/μsec ±1%	P_1 mm Hg	N_0 mole/l. $\times 10^2$	T_5 °K	t_ϵ μsec $\epsilon=0{\cdot}139$	$\epsilon=1{\cdot}77$	$\epsilon=17{\cdot}7$
20	1·6	1·36	28·5	0·48	2576	—	4	9·5
100	3*	2·44	1·9	0·88	2570	—	2·5	>3
20	1·6	1·31	8·0	0·13	2540	—	5	15
100	3*	2·40	0·98	0·44	2520	—	2·1	8
37	1·6	1·50	41·4	2·02	2470	—	3·1	15
20	1·6	1·28	20·0	0·33	2462	—	7	32
20	1·6	1·28	20·2	0·33	2449	—	9	22
20‡	1·6	1·28	45·5	0·73	2436	3	9	14
20	1·6	1·27	9·9	0·16	2420	—	11	22
20	1·6	1·26	17·8	0·28	2374	—	7	18
20	1·6	1·25	11·6	0·23	2345	—	10	32
20	1·6	(1·23)	31·4	0·49	2270	—	5	15
20	1·6	1·22	17·5	0·27	2247	—	10	32
100	3*	2·19	2·9	0·46	2200	—	2·7	—
20	1·6	1·20	56·5	0·74	2187	—	12	27
20	1·6	1·19	38·8	0·59	2185	—	12	33
20	1·6	(1·18)	30·2	0·45	2128	—	25	58
20	1·6	1·17	32·7	0·49	2108	—	35	70
20	0	1·16	15·2	0·22	2075	—	18	70
20	1·6	1·14	57·9	0·83	2026	—	29	60
20	1·6	1·14	28·7	0·42	2023	—	44	85
20§	1·6	1·13	51·1	0·72	1998	—	16	34
20	1·6	1·13	94·8	1·42	1978	—	25	49
100	0	2·01	3·7	1·37	1968	—	6·5	16
20‖	1·6	1·12	49·9	0·71	1967	—	41	85
20	1·6	1·10	48·3	0·68	1912	—	32	60
20	1·6	(1·10)	18·4	0·76	1902	—	41	80
20	0	1·10	38·8	0·54	1897	—	49	100
100	3*	1·95	3·7	0·54	1850	—	21	55
100	0	1·92	4·2	1·45	1835	—	17·5	45
20	1·6	1·05	97·7	1·31	1782	—	65	135
20	1·6	1·07	176·5	2·33	1746	—	42	105
20	0	(1·06)	83·2	1·08	1736	—	88	—
20	0	1·03	85·1	1·10	1720	—	66	170
37	1·6	1·18	24·2	0·93	1713	—	70	140
100	3*	1·84	6·6	0·59	1700	—	22	48
100	0	1·81	9·1	2·90	1693	7	21	—
20	1·6	1·02	60·9	0·78	1679	31	115	—
100	0	1·71	13·8	4·06	1567	11	33	—
20	1·6	0·99	174·5	2·10	1536	41	120	—
100	0	(1·67)	9·3	2·61	1495	32	—	—
100	0	1·58	12·5	3·25	1406	38	—	—
100	3*	1·58	15·0	3·87	1400	100	—	—

*Tube diameter 3 in. Others all 1 in.
†Velocities in parentheses interpolated on plot of u_1 versus bursting pressure ratio.
‡0·4 per cent nitric oxide added. §0·9 per cent oxygen added. ‖0·2 per cent oxygen added added.

be ideal and mixtures were stirred for 30 min. before they were used.

The end plates used in the tubes varied. Some left as much as 1 mm clearance between themselves and the tube wall for pumping, while others completely blocked the tube which was pumped from a port near the diaphragm. The full end plate seems to have led to a little more reaction but the increase was small compared to the scatter of the results (see *Figure 1* and *Table 1*).

The products of reaction which remained after the gases cooled to room temperature were quantitatively trapped at *ca.* 78°K[8]. The

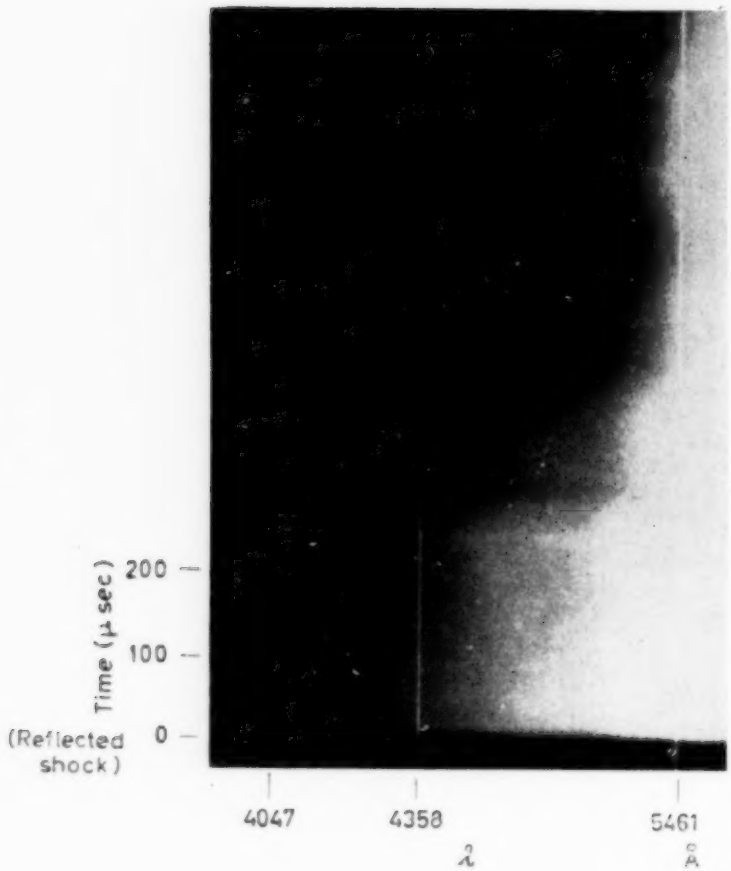

Figure 2. Time resolved emission spectrum.
20% C_2H_2, 80% A
$P_1 = 20mm$ Hg
$T_5 \sim 3100°K$
$N_0 \sim 0{\cdot}08$ mole/l.

W. J. HOOKER[5] found the order of the reaction to be roughly first or second with an activation energy of 39 kcal/mole for the second order reaction. (He quotes 33 kcal/mole based on a rate constant defined in terms of pressure instead of concentrations.) He did not measure the absolute rate. Other workers have given some evidence for a second order reaction with an activation energy of about 30 kcal/mole[6,7]. The present work represents an effort to get more precise results in the temperature range 1 400° to 2 500°K and to examine the reacting system with several different measuring techniques.

Experimental

The shock tubes used, only slightly modified from those of previous studies[6,7], had Pyrex test sections of dimensions 3 in. i.d. × 84 in. and 1 in. i.d. × 60 in. The incident shock velocities were measured by timing the signals from three schlieren stations at 8 in. intervals near the end of the tube. These signals were easily usable (about ten times the noise background) down to initial pressures of acetylene of 1 cm and $\rho_2/\rho_1 = 5$ in the 1 in. tube. For this tube the shock velocities were extrapolated to the end plate using the measured 8 per cent average attenuation per metre. In the 3 in. tube the average shock accelerated 4 per cent per metre and the average of the velocities in the two intervals was used. The initial temperature was 300 ± 2°K.

The acetylene, Matheson, 99·5 per cent, was bubbled through a 16 in. column of concentrated sulphuric acid to remove solvent acetone. A gas chromatogram showed that there was less than 0·05 per cent acetone in the effluent and this was used in the experiments. The remaining gases were used as supplied: argon, Air Reduction, 99·9 per cent; oxygen, Air Reduction, 99·7 per cent; and nitric oxide, Matheson, 99·0 per cent. Hydrogen was the driver gas for all the shocks but one in which helium was used. The gases were assumed to

Table 1. Properties of reflected shocks in acetylene–argon mixtures—Turbidity measurements

Mole % C_2H_2 in A	Shock tube i.d. minus end plate dia. mm	u_1† mm/μsec ±1%	P_1 mm Hg	N_0 mole/l. ×10²	T_5 °K	t_ϵ μsec		
						$\epsilon=0.139$	$\epsilon=1.77$	$\epsilon=17.7$
20	1·6	1·36	28·5	0·48	2576	—	4	9·5
100	3*	2·44	1·9	0·88	2570	—	2·5	>3
20	1·6	1·31	8·0	0·13	2540	—	5	15
100	3*	2·40	0·98	0·44	2520	—	2·1	8
37	1·6	1·50	41·4	2·02	2470	—	3·1	15
20	1·6	1·28	20·0	0·33	2462	—	7	32
20	1·6	1·28	20·2	0·33	2449	—	9	22
20‡	1·6	1·28	45·5	0·73	2436	3	9	14
20	1·6	1·27	9·9	0·16	2420	—	11	22
20	1·6	1·26	17·8	0·28	2374	—	7	18
20	1·6	1·25	11·6	0·23	2345	—	10	32
20	1·6	(1·23)	31·4	0·49	2270	—	5	15
20	1·6	1·22	17·5	0·27	2247	—	10	32
100	3*	2·19	2·9	0·46	2200	—	2·7	—
20	1·6	1·20	56·5	0·74	2187	—	12	27
20	1·6	1·19	38·8	0·59	2185	—	12	33
20	1·6	(1·18)	30·2	0·45	2128	—	25	58
20	1·6	1·17	32·7	0·49	2108	—	35	70
20	0	1·16	15·2	0·22	2075	—	18	70
20	1·6	1·14	57·9	0·83	2026	—	29	60
20	1·6	1·14	28·7	0·42	2023	—	44	85
20§	1·6	1·13	51·1	0·72	1998	—	16	34
20	1·6	1·13	94·8	1·42	1978	—	25	49
100	0	2·01	3·7	1·37	1968	—	6·5	16
20‖	1·6	1·12	49·9	0·71	1967	—	41	85
20	1·6	1·10	48·3	0·68	1912	—	32	60
20	1·6	(1·10)	18·4	0·76	1902	—	41	80
20	0	1·10	38·8	0·54	1897	—	49	100
100	3*	1·95	3·7	0·54	1850	—	21	55
100	0	1·92	4·2	1·45	1835	—	17·5	45
20	1·6	1·05	97·7	1·31	1782	—	65	135
20	1·6	1·07	176·5	2·33	1746	—	42	105
20	0	(1·06)	83·2	1·08	1736	—	88	—
20	0	1·03	85·1	1·10	1720	—	66	170
37	1·6	1·18	24·2	0·93	1713	—	70	140
100	3*	1·84	6·6	0·59	1700	—	22	48
100	0	1·81	9·1	2·90	1693	7	21	—
20	1·6	1·02	60·9	0·78	1679	31	115	—
100	0	1·71	13·8	4·06	1567	11	33	—
20	1·6	0·99	174·5	2·10	1536	41	120	—
100	0	(1·67)	9·3	2·61	1495	32	—	—
100	0	1·58	12·5	3·25	1406	38	—	—
100	3*	1·58	15·0	3·87	1400	100	—	—

*Tube diameter 3 in. Others all 1 in.
†Velocities in parentheses interpolated on plot of u_1 versus bursting pressure ratio.
‡0·4 per cent nitric oxide added. §0·9 per cent oxygen added. ‖0·2 per cent oxygen added added.

be ideal and mixtures were stirred for 30 min. before they were used.

The end plates used in the tubes varied. Some left as much as 1 mm clearance between themselves and the tube wall for pumping, while others completely blocked the tube which was pumped from a port near the diaphragm. The full end plate seems to have led to a little more reaction but the increase was small compared to the scatter of the results (see *Figure 1* and *Table 1*).

The products of reaction which remained after the gases cooled to room temperature were quantitatively trapped at *ca.* 78°K[8]. The

recovered products were analysed with a gas chromatograph for C_2–C_4 compounds. The products found were acetylene, diacetylene and vinyl acetylene (identified by infra-red spectra) although unstable, higher boiling materials were also present (visible in the cold traps).

Because the drum spectra appeared to be continuous, the loss in spectral resolution was considered to be unimportant. The intensity of the tungsten source was determined before each run by using a mechanical chopper to interrupt the light beam. The transit time

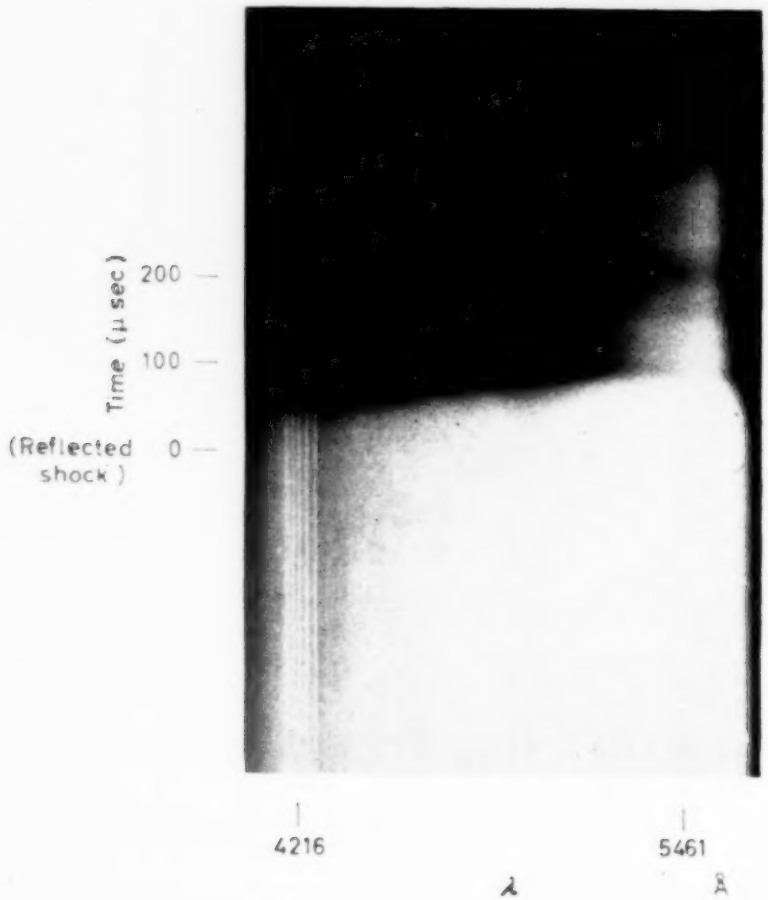

Figure 3. Time resolved absorption spectrum. CN bands of the source appear at the left before the shock. The light visible after the shock is probably emitted by the reaction.
100% C_2H_2
$T_5 \sim 1600°K$
$P_1 = 9mm$ Hg
$N_0 = 0{\cdot}028$ mole/l.

The whole procedure required that the products be at room temperature for about one hour.

Time resolved emission and absorption spectra were taken of the hot acetylene (see *Figures 2* and *3*). The resolving time was about 10 μsec, the ultra-violet is at the left, and time increases upwards. The spectrograph was Hilger E612, $f/1{\cdot}5$ camera, with Tri-X film mounted on a rotating drum with film velocity of 0·03 mm/μsec. More precise measurements of emission and absorption were made with phototube–filter combinations and a tungsten source. These consisted of 931 A tubes and filters with a 150 Å half-width peaked at 3 900 Å.

the shock through the 0·3 mm light beam was the limiting factor in giving a response time of 1 μsec or less. *Figure 4* shows simultaneous traces on a double beam oscilloscope of (above) emission and (below) absorption versus time.

The final measurement was a general view of the reacting gas obtained as a drum camera or smear photograph in which a slit on the shock tube wall and parallel to its axis was imaged on a moving film. Schlieren, shadow and simple emission records were obtained. Here the time resolution was again about 10 μsec. Variations in the reflected shock velocity could give rough information about the heat release

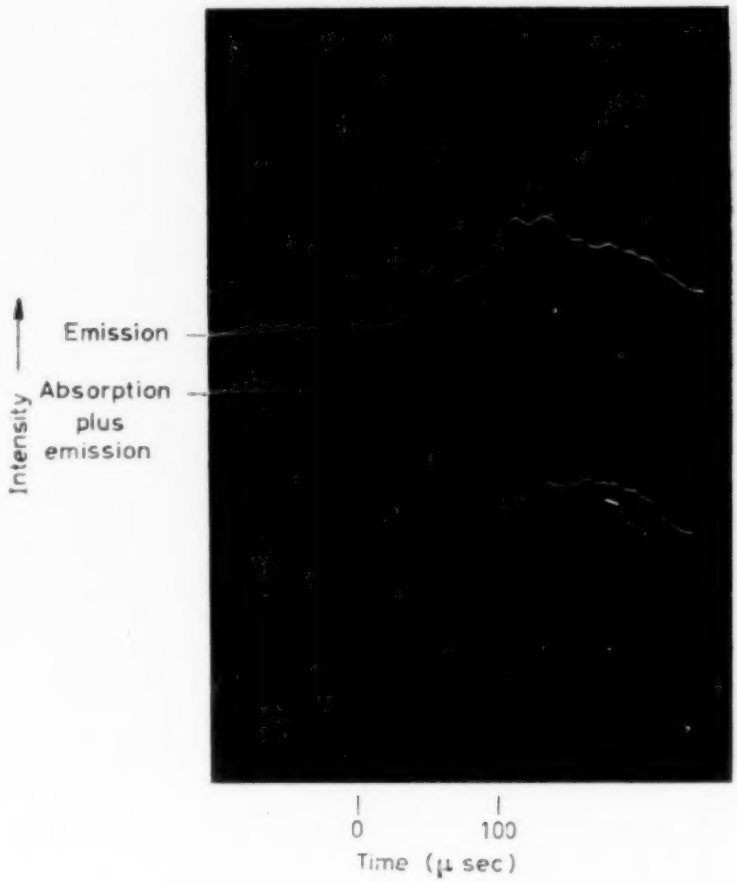

Figure 4. Emission (above) *and absorption plus emission* (below) *at 3900Å recorded with phototube and light filter. There is a small kick in absorption when the reflected shock arrives. At maximum absorption* $I/I_0 = 0.3$.
20% C_2H_2, 0·9% O_2, 79% A
$P_1 = 58$ *mm* Hg
$T_5 = 2026°K$
$N_0 = 0.008$ *mole/l.*
$t_m = 255$ *μsec*

in any reaction which was occurring. *Figure 5* shows a shock in pure acetylene in which a luminous reaction started about 10 μsec after the shock reflected from the end plate but in which the reflected shock velocity (0·36 mm/μsec) is only 0·02 mm/μsec faster than that calculated for no reaction.

Results

List of symbols

- d tube diameter
- E_a activation energy
- I light intensity
- k second order reaction rate constant
- N concentration of acetylene in state 5 (see subscripts)
- P pressure
- T temperature
- t_r time for ε of reacting acetylene to reach a given value
- t_m calculated time for reflected shock to meet contact surface, a minimum time for reaction

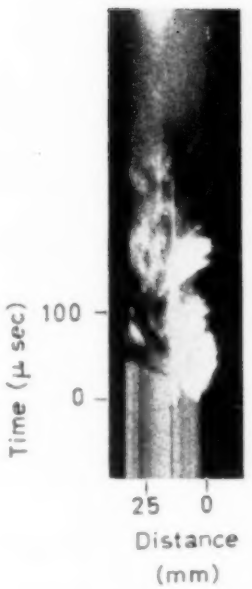

100% C_2H_2
$P_1 = 6$ *mm* Hg
$T_5 \sim 2500°K$
$N_0 = 0.010$ *mole/l.*
$t_m = 76$ *μsec*

Figure 5. Schlieren picture of incident shock (dark line) and reflected shock (emission edge). The end plate is at the right (0mm).

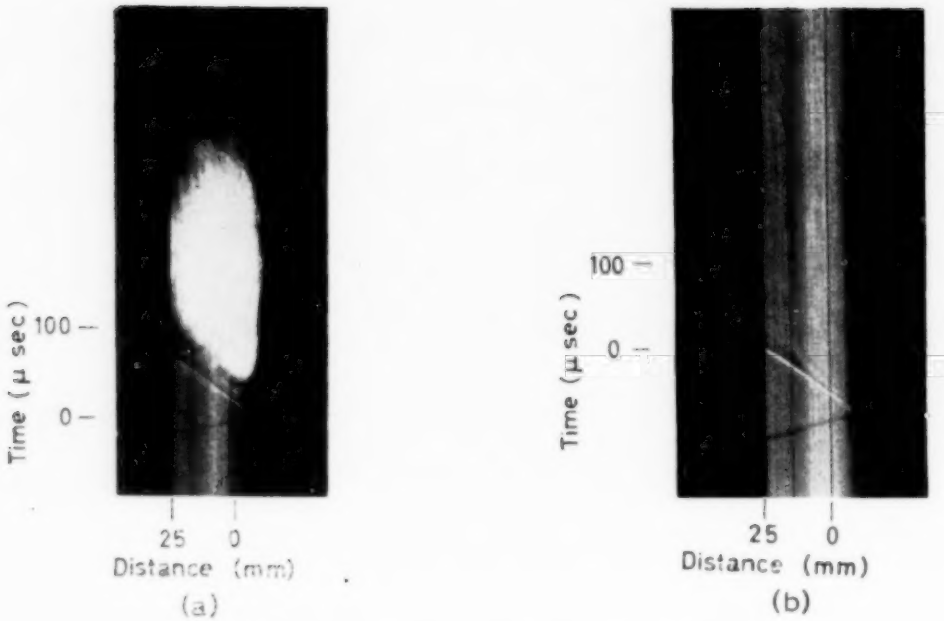

Figure 6. Reflected shocks in 1 in. diameter inner tube.
(a) *35% C_2H_2, 65% A* (b) *26% C_2H_2, 74% A*
$P_1 = 35mm$ Hg *$P_1 = 81mm$ Hg*
$T_5 = 2500°K$ *$T_5 = 1660°K$*
$N_0 = 0{\cdot}015$ mole/l. *$N_0 = 0{\cdot}013$ mole/l.*
$t_{1/2} = 22$ μsec

u velocity relative to shock front
z fractional extent of reaction
ΔH enthalpy increment
ε extinction coefficient
ρ density

Subscripts—

0 an initial value before reaction (acetylene concentration and light intensity)
1 refers to gas ahead of incident shock
2 refers to gas behind incident shock
5 refers to gas behind reflected shock (gas ahead of reflected shock is in state 2)

Description

The measurements were made on the reacting gas behind the reflected shock. The temperature and density of this gas were estimated with one-dimensional calculations assuming ideal gases, vibrational equilibrium and no chemical reaction. The latter assumption is good for the cooler shocks and is reasonable for the hotter ones since always more than 50 per cent of the acetylene could be recovered. Furthermore, the drum camera pictures indicated little change in reflected shock velocity during the time the turbidity measurements were made. Vibrational relaxation has been reported to be complete well before absorption of visible light occurs[6]. The argon–acetylene mixtures gave clean reflected shocks [see *Figures 6*(a) and 6(b)] in both the 1 in. and 3 in. tubes. Deviations from ideal flow are considered to be negligible among the other experimental errors such as interpreting the turbidity results and correlating them with the product analyses. The shocks in *Figure 6* were run in the 3 in. tube but were reflected within a concentric, 1 in. i.d. Lucite tube (3 in. long) mounted on a 1 in. diameter end plate. When the reflected shock emerged from the inner tube a strong rarefaction cooled the reacting mixture much more than in the normal runs (as in *Figure 5*).

Earlier work[8] suggested that high temperature acetylene pyrolysis is a second order reaction and that polyacetylenes may be intermediates in the formation of solid carbon. Therefore it is interesting to look at the results of the present work in this light.

Unfortunately, there is relatively little known about the spectra of the higher polyacetylenes because these compounds are so unstable. Nevertheless, the evidence available[9] indicates that with our low resolution the absorption of polymerizing polyacetylenes would appear as a continuum first in the ultra-violet and then in the visible. This is just what was found (see *Figure 3*). The light after the main absorption is probably not transmitted but emitted as essentially black body radiation from regions of higher temperature and more advanced polymerization. In wavelength distribution it is quite similar to the emission spectrum shown in *Figure 2*. However, because other conjugated systems may well be present in the hot gas and because in general the spectrum to be expected would be very much the same, the actual observations cannot give detailed information about the intermediates in the reaction.

The main problem is to relate the turbidity measurements, listed in *Table 1*, to the extent of reaction. One simple approach is to assume that the polymerization reaction follows the same mechanism throughout the temperature range of these experiments (1400° to 2500°K) and that the extent of the reaction at any temperature may be uniquely characterized by specifying an extinction coefficient for the reacting mixture. The species absorbing at 3900 Å are presumed to be either polyacetylenes or related substances. The procedure used was as follows. For each turbidity run the transmitted light was corrected for the measured emission to give I^0/I versus time after the passage of the reflected shock for the particular temperature and concentration of acetylene (N_0) of that run. T and N_0 were calculated on the basis of no reaction from the initial pressure and composition and the measured shock velocity. Then with Beer's law

$$\log I^0/I = \varepsilon N_0 d$$

ε was obtained as a function of time. Three suitable values of $\varepsilon = 0{\cdot}139$, $1{\cdot}77$, and $17{\cdot}7$ l. mole^{-1} cm^{-1} were chosen and the times t_ε required to reach these εs were listed for each run as far as possible. For a bimolecular reaction the rate constant is proportional to $1/N_0 t_\varepsilon$ so that activation energies could be obtained by plotting $\log(1/N_0 t_\varepsilon)$ versus $1/T$ for each ε. The activation energy was also found for the product analysis results (see *Table 2*). These were treated as described earlier[8]. That is, the reaction was assumed to be stopped completely by the first cooling of the rarefaction wave. This rarefaction was generated at the contact surface when the reflected shock moved from the denser acetylene–argon mixture into the less dense driver gas (hydrogen). The time estimated in this way is generally consistent within a factor of two with the duration of the emission from the hot gases (see *Figures 4* and *5*). The earlier product analysis results[8] in the 3 in. tube were also included to provide more points, but no runs at temperatures over 2200°K were used because the approximations made in the interpretation are less satisfactory

Table 2. Properties of reflected shocks in acetylene–argon mixtures—Product analysis (2·5 cm diameter tube, end plate diameter 1·6 mm less than tube)

Mole % C_2H_2 in A	u_1 mm/μsec ±1%	P_1 mm Hg	N_0 (moles/l.) ×10²	T_5 °K	Mole fraction of original C_2H_2 recovered as			* t_m μsec	log k l. mole^{-1} sec^{-1}
					C_2H_2	C_4H_2	C_4H_4		
37	1·60	16·9	0·89	2750	0·75	0·080	0·012	131	5·79
20+0·4% NO	1·28	45·5	0·73	2436	0·62	0·069	0·009	214	5·96
20+0·4% NO	1·14	57·9	0·83	2026	0·56	0·050	0·007	255	5·96
20+0·9% O_2	1·13	51·1	0·72	1998	0·66	0·059	0·019	259	5·80
20+0·4% O_2	1·12	49·9	0·71	1967	0·71	0·033	0·010	262	5·69
20	(1·10)	18·4	0·76	1902	0·83	0·046	0·009	188	5·50
37	1·18	24·2	0·93	1713	0·92	0·022	0·011	212	5·01

*t_m time calculated on basis of no reaction for reflected shock to reach contact surface.

at higher temperatures and also because the calculated rate constants begin to fall off markedly compared to the values expected from the lower temperature runs. Least square fits to the four sets of results are given in *Table 3*.

The product analysis results were used to calibrate the turbidity measurements by shifting the vertical scale of the latter lines so that they all matched at 1667°K for the average of the five runs for which both turbidity and product analysis measurements were made. The open points plotted in *Figure 1* are turbidity runs (the values for different εs are averaged) after the vertical displacement. The solid points indicate the product analysis runs and the five runs used for the calibration are shown with the two points joined by a vertical line. After the vertical displacement required, the product analysis results provide a value of k and then for each of the three εs one can derive an estimate of the extent of reaction, z. For a second order reaction

$$z = \frac{N_0 - N}{N_0} = \frac{ktN_0}{1 + ktN_0}$$

For $N_0 = 0{\cdot}010$ moles/l. and $T = 1910$°K, an intermediate value, the rate constant is $k = 5{\cdot}26 \times 10^5$ l. mole^{-1} sec^{-1} and this gives $z = 0{\cdot}030$, $0{\cdot}067$ and $0{\cdot}201$ for $\varepsilon = 0{\cdot}139$, $1{\cdot}77$ and $17{\cdot}7$ l. mole^{-1} cm^{-1}. The Arrhenius frequency factor and activation energy for all the runs together are $7{\cdot}8 \times 10^9$ l. mole^{-1} sec^{-1} and $36{\cdot}4 \pm 3$ kcal/mole. The frequency factor is about $0{\cdot}05$ of the collision frequency.

In three runs indicated in *Tables 1* and *2* small amounts of nitric oxide and oxygen were added to the acetylene. There was no noticeable change in either the product analysis or turbidity results.

To check the assumption of a second order reaction, we corrected all the rate constants to 2000°K by using the definition

$$k_{2000} = k_f \exp\left(\frac{36\,400}{1{\cdot}99}\left[\frac{1}{T} - \frac{1}{2000}\right]\right)$$

and then plotted $\log k_{2000}$ versus $\log N_0$, the concentration of the hot acetylene. The slope should be zero for a second order reaction or $n-2$ for an nth order reaction. The actual slope is $-0{\cdot}28 \pm 0{\cdot}10$ (by least squares) and so the original assumption of a second order rate law seems plausible until more precise results are available.

One can obtain a rough estimate of the heat liberated in the reaction by measuring the acceleration of the reflected shock. If the

Table 3. Activation energies obtained from extinction coefficients and product analysis

ε l. mole^{-1} cm^{-1}	No. of runs	E_a kcal/mole
0·139	7	37·6 ± 7
1·77	40	36·8 ± 3
17·7	33	32·8 ± 4
Product analysis	18	40·0 ± 10

Table 4. Observed reflected shock velocities and estimated heats of reaction

P_1 mm Hg	u_1 mm/μsec	$u_{2,\text{calc.}}$ mm/μsec	$u_{2,\text{meas.}}$ end plate mm/μsec	ΔH reaction kcal/mole	T_2°K	N_0 mole/l. ×10^2
5·8	2·4 ±0·2	0·34	0·36	0·3	2500	2·5
6·1	2·2 ±0·1	0·32	0·37	0·4	2200	2·5
10·2	2·1 ±0·1	0·32	0·36	0·5	2100	4·0
20·6	2·1 ±0·1	0·32	0·43	1·3	2100	8·1
14·8	2·0 ±0·1	0·31	0·36	0·5	1960	5·5
24·8†	1·78 ±0·06	0·30	0·34	0·4	1620	7·6
20·4*†	1·41 ±0·03	0·39	0·41	0·6	2500	2·5
16·6*†	1·02 ±0·01	0·39	0·42	0·8	1660	1·1

*Partial pressure of acetylene in argon–acetylene mixture 35% C_2H_2, 26% C_2H_2 respectively for last two runs.
†Using inner tube.

velocity of the shock leaving the end plate is constant then the enthalpy change through the reflected shock is given by

$$\Delta H = \tfrac{1}{2}\left[(u_1 - u_2 + u_5)^2 - u_5^2\right] \quad \ldots . [1]$$

where u stands for velocity with respect to the shock front and the subscripts 1, 2 and 5 indicate the regions before and behind the incident shock, and behind the reflected shock, respectively. Then the estimated heat of reaction is just $\Delta H - \Delta H_{\text{calc. for no reaction}}$ which becomes $\Delta H_{\text{reaction}} = (u_1 - u_2)\,(u_{5,\text{obs.}} - u_{5,\text{calc.}})$. In a typical drum camera picture the original reflected shock had an approximately constant velocity leaving the end plate and then speeded up to a higher value when the shock reached the hydrogen behind the contact surface. *Table 4* lists the measured incident and reflected velocities and the heats of reaction derived from them using equation 1. *Table 4* shows that only about 0·5 kcal appears per mole of original acetylene before the reflected shock reaches the contact surface.

Although there is little definitely known about the course of the reaction, one can make some guesses about the heat given off at various stages. The heat of formation of acetylene from hydrogen and graphite is 54·2 kcal/mole at 25°C so that about one per cent of the total heat available appears at the beginning. Another interesting quantity is the heat of reaction of acetylene to form diacetylene. This has not as yet been measured directly but T. Flitcroft, H. A. Skinner and M. C. Whiting[9] have measured the heats of hydrogenation of conjugated triply bonded hydrocarbons. After a correction for hyperconjugation their result leads to a resonance energy of about 7 kcal/mole for diacetylene. This should be close to the heat of reaction

$$2C_2H_2 \longrightarrow C_4H_2 + H_2$$

A simple particle-in-a-box calculation indicates that energy of formation of conjugated triple bond systems from acetylene increases from its value of −5 kcal per C_2 unit to about 18 cal/(mole acetylene) for H_2C_{20}. The observed enthalpies and the amount of acetylene converted therefore would be consistent with about a tenth of the original acetylene forming polyacetylenes.

Discussion

The results of the present work are compared with earlier work[3,4] in *Figure 7*. Each shock wave point is the average of five runs.

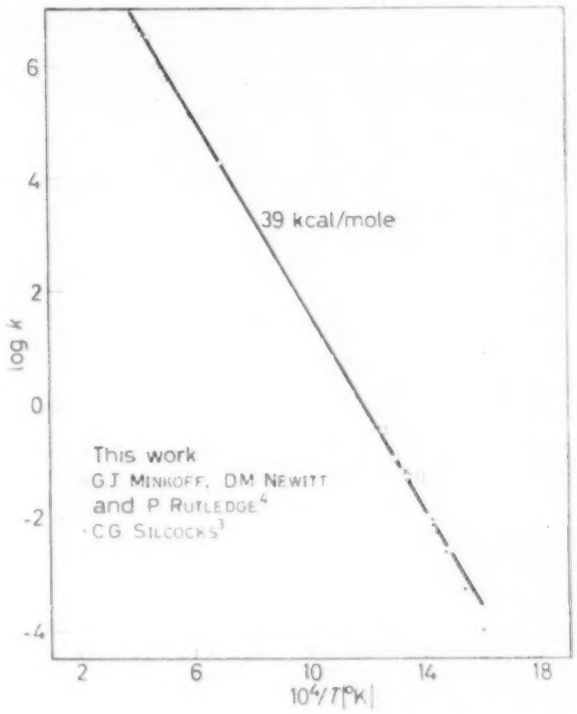

Figure 7. log k [$l.\ mole^{-1}\ .\ sec^{-1}$] *versus* $1/T$ [$°K^{-1}$] *on a condensed scale*

Although the reaction time can be determined only approximately in the present work the method used[8] should yield a rough lower limit or correspondingly an upper limit for the rate constant. Slower cooling or self-heating during the reaction would lead to larger extents of reaction. Presumably back reaction to regenerate acetylene is unlikely under these conditions. However, one exception to this argument arises in the case of product analyses at low initial pressures and high shock strengths where the yield actually does drop. This is probably because these are the conditions in which a significant fraction of the acetylene is in the cooler boundary layer or mixed with the driver gas and therefore is not available for reaction. To the extent that the rate constants given are

upper limits the results are evidence for either a change of mechanism at higher temperatures or else a decrease of activation energy with temperature. However, the reaction is probably second order throughout the range and the absolute concentrations used in the high and low temperature work are almost identical which suggests that the mechanism up to the rate-determining step may be the same in both temperature ranges. This is so because if two competing reactions occur simultaneously the one with the higher, not the lower, activation energy should tend to become dominant at high temperatures.

The inhibition of the acetylene pyrolysis by nitric oxide at lower temperatures, e.g. see refs. 4 and 5, has led to the introduction of a free radical mechanism, either through the formation of HC_2 or the acetylene diradical, even though these steps require approximately 121 and 42 to 67 kcal/mole[10]. As Minkoff points out the first is probably much too high to be important in a reaction with a measured activation energy of about 40 kcal/mole. The observed lack of effect on the rate by nitric oxide and oxygen in our experiments may be merely an indication that near 2000°K the radical trapping reactions are less effective than those at lower temperatures.

The observation of significant quantities of diacetylene and an enthalpy release consistent with its formation suggest that diacetylene may be a primary intermediate in the reaction. The reason that relatively little of it is recovered from reactions at temperatures below about 1000°K may be merely that it subsequently reacts with hydrogen to form any of the thermodynamically favoured substances among which are ethylene, benzene, methane and ethane. This would also provide an interpretation of the pressure drop in the low temperature reaction which is often used as a measure of the loss of acetylene.

It would be interesting to study the pyrolysis of diacetylene with some of the methods which have been used for acetylene.

This research was supported in part by the United States Air Force through the Air Force Office of Scientific Research of the Air Research and Development Command, under contract No. 49(638)–167. Reproduction in whole or in part is permitted for any purpose of the United States Government.

It is a pleasure to thank Texaco Inc. for the award of a fellowship to C.F.A.

References

[1] Knox, K., Norrish, R. G. W. and Porter, G. *J. chem. Soc.* **1952,** 1477
[2] Steacie, E. W. R. *Atomic and Free Radical Reactions,* Vol. I, 2nd ed. Reinhold: New York, 1954
[3] Silcocks, C. G. *Proc. Roy. Soc. A,* 1957, **242,** 411
[4] Minkoff, G. J., Newitt, D. M. and Rutledge, P. *J. appl. Chem.* 1957, **7,** 406
[5] Hooker, W. J. *Seventh Symposium (International) on Combustion,* p 949. Butterworths: London, 1959
[6] Aten, C. F. and Greene, E. F. *Disc. Faraday Soc.* 1956, **22,** 162
[7] Greene, E. F., Taylor, R. L. and Patterson, W. L., Jr. *J. phys. Chem.* 1958, **62,** 238
[8] Armitage, J. B., Cook, C. L., Entwhistle, N., Jones, E. R. H. and Whiting, M. C. *J. chem. Soc.* **1952,** 1998, 2010, 2014 and 2883
[9] Flitcroft, T., Skinner, H. A. and Whiting, M. C. *Trans. Faraday Soc.* 1957, **53,** 784
[10] Minkoff, G. J. *Canad. J. Chem.* 1958, **36,** 131 and Laidler, K. J. *Chemical Kinetics of Excited States,* p 93. Oxford University Press: London, 1955 but using *ca.* 44 instead of 85 kcal/mole as the difference in heats of formation of C_2H_4 and C_2H_2 at 1500°K

Evidence for Carbon Suboxide, C_3O_2, as an Intermediate Product in the Cool Flame Oxidation Products of Diethyl Ether

L. H. S. ROBLEE, Jr, J. T. AGNEW and K. WARK, Jr

Purdue University, W. Lafayette, Ind.

(*Received December 1959*)

Emission spectra of two-stage cool flames of a mixture of diethyl ether and air with an equivalence ratio of four have been obtained in the spectral region 3·5 to 18·5 microns. Four emission bands corresponding to known vibrational frequencies for carbon suboxide have been obtained in these spectra. Two additional experiments confirming the presence of carbon suboxide in the products are described, and a reaction mechanism is outlined for the formation of carbon suboxide.

Introduction

THE importance of low temperature reactions in the oxidation of hydrocarbons has been well established. These reactions and the intermediate species which result from them play a fundamental role in determining the course of the combustion process. Our knowledge of the intermediates produced in these reactions is far from complete. The work described here is concerned with identification of intermediates produced in these combustion reactions which are, in some cases, termed cool flame reactions.

The terminology in the literature concerning these cool flames has been somewhat confusing during the past ten years. The pioneer work was done by H. J. EMELEUS[1], A. R. UBBELOHDE[2], and by V. A. KONDRATIEV[3], in which the faint blue emission from the cool flame was confirmed as being due to the existence of excited formaldehyde molecules. Since then, subsequent investigations have led to the use of the term 'two-stage' cool flames. This terminology was used to describe the existence of two pale blue flames which can be observed in the steady flow combustion of certain hydrocarbon fuels. W. G. AGNEW, J. T. AGNEW and K. WARK, Jr[4], using diethyl ether as the fuel, have shown that the emission spectrum of the first-stage flame is truly that of excited formaldehyde, whereas that of the second-stage flame may be due to either the excited formaldehyde or the formyl radical, HCO, depending primarily on the initial mixture ratio.

Since the characteristic vibrational frequencies of most molecular species lie in the infra-red (i.r.) region of the electromagnetic spectrum, spectroscopic studies of the emission characteristics of two-stage flames in the i.r. region should provide useful information as to the identity of molecular species present in these reactions. Several investigations of this type have been carried out[4–7] with the result that in addition to formaldehyde, further species identified have been methane, ethylene and methyl alcohol.

The work reported here was undertaken to extend the work reported by K. WARK, Jr, *et al.*[7], thereby providing better and more extensive emission spectra for the identification of transient molecular species produced in low-temperature oxidation processes.

Equipment and Procedure

The equipment used to obtain the i.r. emission spectra was essentially the same as used by Agnew, Agnew and Wark[4], with a few major improvements. The reader is referred to that paper for a general description of the experimental technique.

For spectroscopic studies it is desirable to obtain a large depth of radiating gases in order

to have sufficient emission intensity. There is, however, a practical restriction on this depth since it is mandatory that all of the gases 'seen' by the spectrometer be in essentially the same state of reaction. For this purpose, a new flat flame burner of rectangular cross section was built so that the above conditions could be optimized when the burner was used in conjunction with the Perkin–Elmer Model 99 spectrometer. A further optical improvement was the use of an external off-axis paraboloidal mirror to focus the radiation from the flame zone on the entrance slit of the spectrometer. The use of this external paraboloidal focusing mirror had the added advantage that the two mirrors used to rotate the image of the flame zone from a horizontal plane to a vertical plane were of much smaller dimensions and could be mounted as a single unit directly in front of the entrance slit of the spectrometer.

An improvement was also made on the method of supplying and controlling the fuel–air mixture supplied to the burner. Compressed air was passed through a pressure regulator and a rotameter. The desired fuel–air ratio was obtained by mixing this air with diethyl ether vapour produced in a fuel reservoir suspended in a constant temperature water bath. The air flow rotameter was calibrated with a wet test meter and the ether flow rotameter was calibrated by measuring the amount of condensed ether vapour collected in a given time interval.

The results shown in this paper are for several different positions in the flame zone. All of the spectra are for rich mixtures of diethyl ether and air with an equivalence ratio of four. Position 1 is in the cool flame; position 2, between the cool flame and the second-stage flame; position 3, in the second-stage flame; and position 4 above the second-stage flame. It is in this region (position 4) that a yellow column forms as the fuel–air ratio is leaned. In addition to two-stage flames with rich mixtures, several other flame structures can be observed depending mainly on the fuel–air ratio. A comprehensive review of these structures is given by W. G. Agnew and J. T. Agnew[3].

Emission spectra were taken with both sodium chloride and KRS–5 prisms, the use of the latter prism being new in this work.

Results and Discussion

For the sake of brevity, the reader is referred to the original work by L. H. S. Roblee[9] for a complete presentation of the many emission spectra recorded with the improved equipment described above. None of the spectra obtained with the sodium chloride prism will be shown in this paper. These spectra were essentially a confirmation of the work done by Wark[7] except that the bands were more distinct and wavelength assignments were more readily made. Specifically, long wavelength bands were observed at 11·00, 11·56, 11·63, 11·74, 12·09, 12·26, 12·43, 12·77, 13·04, 13·29, 13·47, 13·63, 13·70, 13·85, 14·17, 14·41 and 14·84 microns. The band at 13·70 microns is believed to be due to acetylene. This was partially confirmed by the observation that the 13·70 band was enhanced when traces of acetylene were added to the air stream. A search of the literature revealed that the wavelengths 11·00 and 12·77 microns corresponded to two of the vibrational frequencies of the species C_3O_2, carbon suboxide, a linear molecule of di-ketene nature, with the structure O=C=C=C=O. In addition to the bands at 11·00 and 12·77 microns, carbon suboxide has several other strong bands at 4·15, 4·36, 4·57, 6·37, 15·70, 17·95 and 18·39 microns. Of these bands, only the last three lie in a spectral region relatively free of water and carbon dioxide emission. Since these long wavelengths are beyond the useful range of sodium chloride optics, a KRS–5 prism was used to obtain emission spectra in the long wavelength region.

Figure 1 shows the emission spectra of a two-stage flame of a diethyl ether–air mixture with an equivalence ratio of four. The slit width used in the various spectral regions is indicated in the figure.

Since bands in the 3·5 to 13·0 μ region are not highly resolved, an indication of the relative strength of large group frequencies can be obtained. The first region centred at 3·5 μ is one of the strongest for the fuel spectrum but

is also characteristic of C—H group stretching frequencies. Thus, this band is due to fuel residual and/or new molecules containing the basic C—H structure. This band intensity increases through the stages.

The next prominent band centred at about 4·68 μ and due primarily to carbon dioxide completely masks the carbon monoxide band in this same region which was observed with sodium chloride optics. Fairly strong atmospheric carbon dioxide absorption is observed on the short wavelength side of this band. Corresponding with completeness of combustion, the carbon dioxide band increases through the stages.

The next intense band is the C=O group frequency at 5·65 μ. This band is of special interest: its intensity increases from position 1 to position 2 then decreases from position 2 to position 4. In contrast to this trend, the band at 7·94 μ, characteristic of the aldehyde structure, progressively increases through the stages. Thus, it is evident that species containing a C=O structure, *other* than formaldehyde, must be formed in the cool flame region which undergo further reaction in the second-stage flame.

Similar to the 5·65 μ band, the band at 9·40 μ shows the same intensity variations through the stages. This region is associated with alcohols and open chain anhydrides and is characteristic of the C—O group frequency. The production of ethylene, as evidenced by the 10·41 μ band, steadily increases through the stages.

Bands at 13·52 and 15·00 μ are believed to be due principally to carbon dioxide. Since these bands are not well resolved by the KRS–5 prism, the less intense acetylene band at 13·72 μ is masked. The intensity of these bands like the carbon dioxide band at 4·7 μ increases through the stages. Also, the unidentified band at 16·69 μ exhibits the same behaviour.

As mentioned earlier, the spectrum for wavelengths greater than 15 μ was recorded to determine if longer wavelength bands of carbon suboxide would be present. The fact that bands at 15·70 and 17·95 μ show up clearly, provides strong evidence for the presence of this emitter. There is no evidence of carbon suboxide emission at 18·39 μ.

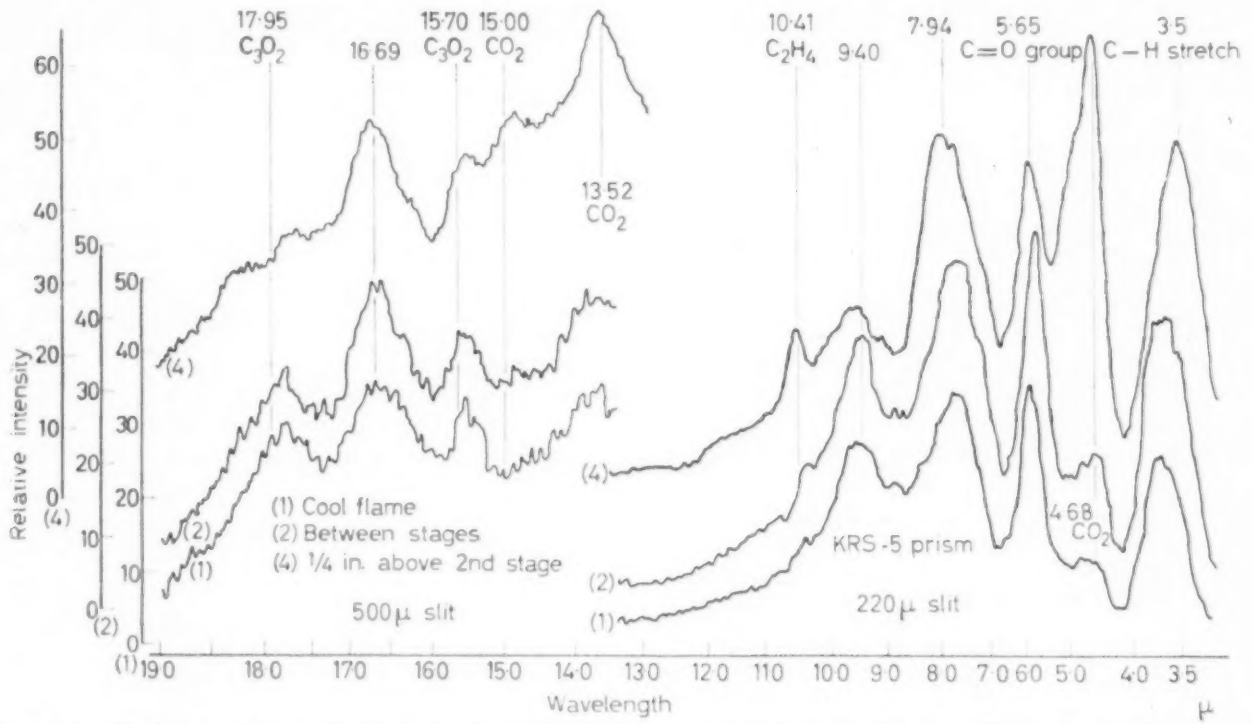

Figure 1. Emission spectra of diethyl ether–air mixture as a function of flame position: 3·5 to 19 microns

It is possible that the combination of low emission intensity from this band and decreased prism transmission at this wavelength make the band at 18·39 microns undetectable.

Further Tests to Support the Identification of Carbon Suboxide

Two additional experimental procedures were used to support the assignment of carbon suboxide as the emitter responsible for the emission bands at 11·00, 12·85, 15·70 and 17·95 μ. One technique involved introducing pure carbon suboxide into a two-stage flame and observing changes in spectral activity. In the second technique, exhaust gases from a two-stage flame were analysed spectroscopically.

Pure carbon suboxide for addition to an established two-stage flame was prepared after the method described by C. D. HURD and F. D. PILGRIM[9]. Carbon suboxide has a boiling point of 6·3°C and, therefore, was easily vaporized into the fuel stream when removed from storage in a dry ice bath. *Figure 2* shows the spectra in the range 15·0 to 18·5 μ taken between stages in a two-stage flame both with and without the addition of a small quantity of carbon suboxide.

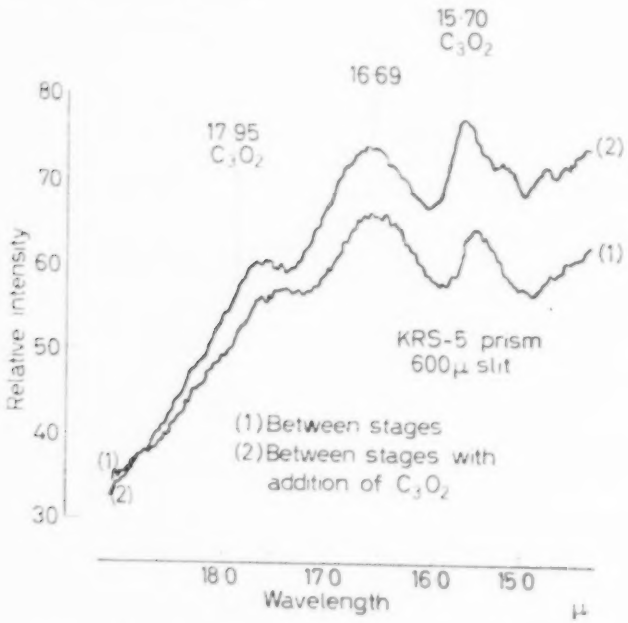

Figure 2. Emission spectrum of diethyl ether–air mixture between stages with and without addition of carbon suboxide; 15·0 to 18·5 microns

It is obvious that the addition of small quantities of carbon suboxide to the fuel stream has resulted in enhancement of the radiation and the 15·70 μ wavelength. In the upper spectrum the intensity of the 15·70 micron band exceeds that of the 16·69 μ band, while in the lower spectrum, with no carbon suboxide addition, the reverse is true. The fact that the 17·95 μ band, also characteristic of the carbon suboxide molecule, does not exhibit this tendency as strongly as does the 15·70 μ band was rather disconcerting, and it was felt that further experimental evidence for the existence of the carbon suboxide was required. Accordingly, the absorption spectrum of the exhaust gases from the two-stage flame was recorded and analysed for carbon suboxide.

Since carbon suboxide reacts with water to form malonic acid, the exhaust gases collected were first passed over calcium chloride and phosphorus pentoxide to remove water before being passed through dry ice and liquid nitrogen baths. Vapours from the collected gases were allowed to expand into an evacuated absorption cell of 1 m path length, and the absorption spectrum recorded with a lithium fluoride prism as the dispersing medium. *Figure 3* shows a

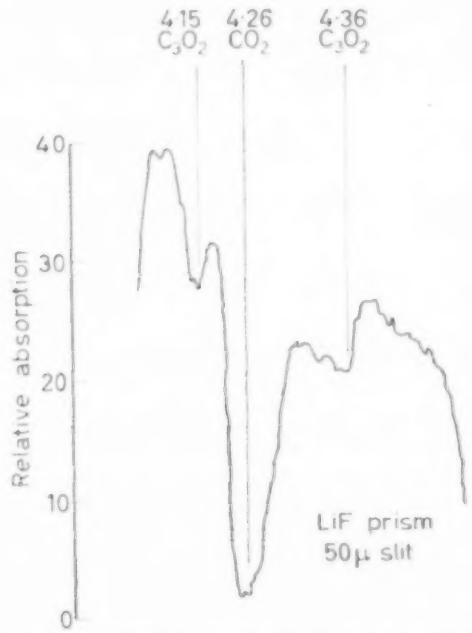

Figure 3. Absorption spectrum of condensed exhaust gases; 4 to 4·4 microns

part of the absorption spectrum for the exhaust products collected in the dry ice trap. The bands appearing at 4·15 and 4·36 μ on either side of the strong 4·26 μ carbon dioxide absorption band provide further confirmation of the existence of carbon suboxide in the products of the two-stage diethyl ether–air flame. As a further check, an absorption spectrum of pure carbon dioxide in the 1 m absorption cell was obtained, with the carbon dioxide at a concentration such that the absorption at 4·26 microns was the same as in *Figure 3*.

A final and admittedly rather tenuous indication of the existence of carbon suboxide in the products of the low temperature oxidation of diethyl ether with air is a physical phenomenon which can be appreciated only by personal experience. The exhaust products of the low temperature oxidation, particularly those of the first-stage flame, have a very offensive odour and a strong lachrymal effect. It was observed that carbon suboxide itself has this very same effect when present in small quantities in the atmosphere.

Reaction Mechanism

The spectroscopic evidence presented strongly indicates that carbon suboxide is generated in two-stage flames of diethyl ether–air mixtures. A possible reaction mechanism to account for the production of carbon suboxide is presented below. Based on the peroxidation theory of combustion, the formation of acetone is postulated from which ketene and, subsequently, carbon suboxide is formed.

$$(C_2H_5)_2O + {}^{\circ}OH \longrightarrow CH_3\dot{C}HOCH_2CH_3 + H_2O \quad \ldots . [1]$$

$$CH_3\dot{C}HOCH_2CH_3 + O_2 \longrightarrow CH_3C(OO_{\circ})HOCH_2CH_3 \quad \ldots . [2]$$

$$CH_3C(OO^{\circ})HOCH_2CH_3 + RH \longrightarrow CH_3C(OOH)HOCH_2CH_3 + R^{\circ} \quad \ldots . [3]$$

$$CH_3C(OOH)HOCH_2CH_3 \longrightarrow CH_3C(O^{\circ})HOCH_2CH_3 + {}^{\circ}OH \quad \ldots . [4]$$

The alkyl peroxy radical formed in steps 1 and 2 is generally accepted as an initial step of the hydrocarbon oxidation chain reaction. The formation of the butoxy radical through an alkyl hydroperoxide in steps 3 and 4 is probable in oxidation reactions according to J. T. Neu[10]. On the basis of products which have been found in low temperature reactions, the radical formed in equation 4 may decompose to acetaldehyde and a primary ethoxy radical as follows

$$CH_3C(O^{\circ})HOCH_2CH_3 \longrightarrow CH_3CHO + {}^{\circ}OC_2H_5 \quad \ldots . [5]$$

Aldehydes, in general, oxidize faster than hydrocarbons and would further react, as follows

$$CH_3CHO + R^{\circ} \longrightarrow CH_3CO^{\circ} + RH \quad \ldots . [6]$$

In equation 6 the R° group is any hydrogen acceptor. The reaction of the acetyl radical with a methyl radical is postulated for the formation of acetone

$$CH_3CO^{\circ} + CH_3^{\circ} \longrightarrow CH_3COCH_3 \quad \ldots . [7]$$

This reaction occurs only when the oxygen supply is low since methyl radicals preferentially react with oxygen. By pyrolysis of acetone, ketene is produced

$$CH_3COCH_3 \xrightarrow{\Delta} H_2C{=}C{=}O + CH_4 \quad \ldots . [8]$$

The highly reactive ketene undergoes the well-known dimerization reaction[11] and subsequently adds water[12] to give acetoacetic acid

$$2(H_2C{=}C{=}O) \longrightarrow CH_2{=}C(-O-)-CH_2-C(=O)- \xrightarrow{+H_2O} CH_3C(=O)-CH_2CO_2H \quad \ldots . [9]$$

It is then assumed that the acetoacetic acid formed in step 9 undergoes intramolecular dehydration and the loss of a methane molecule to form carbon suboxide, as follows

$$CH_3COCH_2CO_2H \longrightarrow C_3O_2 + CH_4 + H_2O \quad \ldots . [10]$$

One of the authors (L.H.S.R.) would like to express his appreciation to the Standard Oil Company of Indiana for assistance while carrying out this work.

References

1 Emeleus, H. J. *J. chem. Soc.* 1926, **128,** 2498; 1929, **131,** 1733

2 Ubbelohde, A. R. *Proc. Roy. Soc. A,* 1935, **152,** 354

3 Kondratiev, V. A. *Acta phys.-chim. U.R.S.S.* 1936, **4,** 556

4 Agnew, W. G., Agnew, J. T. and Wark, K., Jr. *Fifth Symposium (International) on Combustion,* p 766. Reinhold: New York, 1955

5 Agnew, W. G. and Agnew, J. T. *Industr. Engng Chem. (Industr.),* 1956, **48,** 2224

6 Donovan, R. E. and Agnew, W. G. *J. chem. Phys.* 1955, **23,** 1952

7 Wark, K., Jr, Agnew, J. T. and Agnew, W. G. *Chem. Engng Data, Ser. 3,* (October 1958) 313

8 Roblee, L. H. S. 'Infra-red spectroscopic studies of cool flames in a flat flame burner'. *Ph.D. Thesis* Purdue University: Lafayette, Indiana, 1958

9 Hurd, C. D. and Pilgrim, F. D. *J. Amer. chem. Soc.* 1933, **55,** 757

10 Neu, J. T. *General Papers,* Division of Petroleum Chemistry of the American Chemical Society, 1953, **33,** 233

11 Whiffen, D. H. *et al. J. chem. Soc.* **1946,** 1005

12 Boese, A. B., Jr. *Industr. Engng Chem. (Industr.)* 1940, **32,** 16

Inhibition of Combustion Reactions by Inorganic Lead Compounds

J. BARDWELL

Department of Chemistry, University of Saskatchewan, Saskatoon, Canada

(*Received January 1960*)

The effects of lead oxide and other inorganic lead compounds on combustion processes have been investigated by the use of coated vessels. With n*-butane, lead oxide acts as a powerful inhibitor ; it suppresses cool flames and low-temperature ignitions over a wide range of experimental conditions. The pervasive nature of the inhibition supports the proposal, made previously by Walsh and others, that lead oxide plays a central role in the anti-knock action of lead tetraethyl.*

Introduction

ALTHOUGH lead tetraethyl is well known as an effective anti-knock agent in engine combustion, there has been much disagreement about the mechanism of its action. Among the questions on which differences of opinion have occurred are:

(*1*) Whether lead tetraethyl is basically a positive catalyst or an inhibitor[1,2].

(*2*) Whether the metallic or organic part of the molecule is responsible[3,4].

(*3*) Whether the processes are homogeneous or heterogeneous[5,6].

Such lack of agreement is understandable when one considers the seeming contradictions in experimental results with this additive. Although it is an extremely effective anti-knock agent with some hydrocarbon fuels, e.g. *n*-paraffins, lead tetraethyl is actually a pro-knock agent with others[7,8]. Even with *n*-paraffins, the anti-knock action is not associated with pervasive inhibition of the combustion process; the early stages of the reaction are apparently little affected[7,9], and under some experimental conditions the net effect is acceleration rather than inhibition[2,4].

A possible clue to the mode of action of lead tetraethyl and other metallic anti-knocks is to be found in the observation that their effects on combustion rate tend to persist even after their use has been discontinued; when experiments are resumed with untreated fuel, reaction rates do not return to their normal values[2,4,10,11]. These effects have been ascribed to contamination of surfaces by deposits of metals or metal oxides and it has been suggested that when lead tetraethyl is used, the deposit is lead oxide (PbO)[2,11]. Tests of this hypothesis by deliberate treatment of vessel surfaces with lead oxide have yielded contradictory results. Static experiments with methane[5], ethers[11], and hydrogen[12] have shown lead oxide to have an inhibiting effect, but flow experiments with *n*-heptane have suggested a catalytic effect[13].

Recent work in this laboratory has yielded information on the influence of various surfaces on the rate of hydrocarbon combustion. This paper describes observations made when a silica surface was treated with three inorganic lead compounds, lead oxide (PbO), lead tetroxide (Pb_3O_4) and lead chloride ($PbCl_2$). The relevance of these observations to the problem of anti-knock action is discussed.

Experimental

A silica reaction vessel, cylindrical in shape, 6 cm in diameter and 9 cm long, was supported vertically in a furnace and connected to a manometer, a pumping system and storage vessels. The reactant gases, *n*-butane and oxygen, were admitted in succession to the vessel and the progress of reaction was followed by pressure measurements and by observation through a window.

After some experimentation it was found that the following procedure for treating the inner

surface of the vessel gave deposits of satisfactory uniformity and tenacity. The solids (lead oxide, lead tetroxide and lead chloride) were screened and the portion that passed a 200-mesh screen was then suspended in a small volume of water and transferred to the clean vessel. The vessel was heated to 80°C by immersion in a water-bath, then connected to an aspirator, and continuously rotated in such a way as to bring the suspension in contact with all parts of the inner surface. As the water evaporated a dry deposit was left clinging to the surface. Deposits amounting to 0·9 mg/cm² were used in most experiments; observations with other amounts are described below.

Results

Effect of deposits on reaction in the cool flame region

The oxidation of *n*-butane in a clean silica vessel gives rise to cool flames and two-stage ignition over a considerable temperature range starting at about 275°C[14,15]. The occurrence of these phenomena was greatly affected by the presence of the surface deposits; the general effects may be judged by the following observations. (All pressures given refer to the total initial pressure of equimolar mixtures of *n*-butane and oxygen.)

(*a*) 300°C, 100 mm: with the clean silica vessel two cool flames occurred, the first after an induction period of 65 sec and the second after a further interval of 25 sec. The rate of pressure change immediately before the passing of each flame was about 30 mm/min. With all three coatings (lead oxide, lead tetroxide and lead chloride) the reaction was completely inhibited, the maximum rate of pressure change being less than 0·01 mm/min.

(*b*) 300°C, 300 mm: with the clean silica vessel, a two-stage ignition occurred; after an induction period of 12 sec there was a cool flame, followed after 1 sec by ignition. With the coated vessels reaction was quite slow, the maximum rate being 1 mm/min with lead tetroxide and lead chloride and only 0·4 mm/min with lead oxide.

(*c*) 350°C, 200 mm: under these conditions of temperature and pressure the same general type of reaction was found with all four surfaces, namely a pressure increase interrupted by a single, weak, pressure pulse. Large differences did, however, occur in the induction period preceding the pressure pulse. With the clean silica vessel it was 1 sec, with the vessel coated with lead tetroxide or lead chloride it was 3 sec, and with the lead oxide-coated vessel it was 130 sec.

Effect of deposits on cool flame limits

The pressure/temperature limits for the occurrence of cool flames with the various surfaces are shown in *Figure 1*. The curves there give

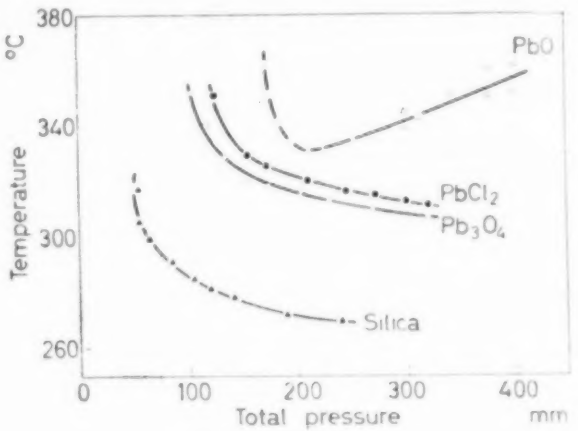

Figure 1. Cool flame limits for equimolar mixtures of n-butane and oxygen with a silica vessel, uncoated and with coatings of lead tetroxide, lead chloride and lead oxide

the lower boundary of the cool flame region; slow reaction is found at temperatures below those plotted. The large shifts in these limits provide further evidence for the marked retardation induced by these coatings. It was also noted that when cool flames did occur with the coated vessels, the associated pressure surge was usually much weaker than with the clean vessel.

Figure 1 shows that the lead oxide coating was especially effective in shifting the cool flame limit to higher temperatures. Some experiments were done with different amounts of lead oxide; the results showed that even small amounts were quite effective. For example, at 300 mm pressure, the cool flame limit without any lead oxide was 268°C, but with 0·1 mg/cm² of

lead oxide it was 321°C. The corresponding limit with 0·9 mg/cm² was 344°C and this value remained unchanged when the amount of lead oxide was increased to 2·2 mg/cm².

Effect of deposits on ignition limits

Ignition limits were also shifted by the presence of the deposits. *Figure 2* shows the minimum

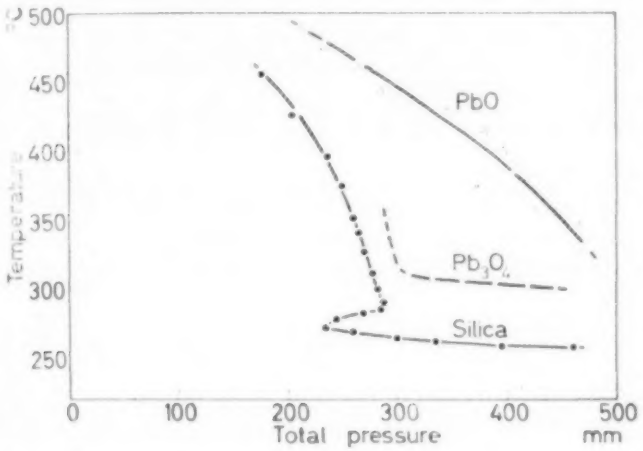

Figure 2. Ignition limits for equimolar mixtures of n-butane and oxygen with a silica vessel, uncoated and with coatings of lead tetroxide and lead oxide

pressures and temperatures for ignition with the clean vessel and the vessel coated with lead tetroxide and with lead oxide. The results with lead chloride were practically identical with those shown for lead tetroxide and the experimental points have been omitted from *Figure 2*. It is noteworthy that the ignition peninsula at about 275°C, which is a prominent feature of the ignition diagram with many fuels oxidized in clean vessels[7], was not detectable with the coated vessels. The results with lead oxide again illustrate this compound's potent inhibiting effect; its presence on the walls raises ignition pressure by about 70 per cent.

Discussion

Although all three lead compounds tested have a considerable inhibiting effect on the oxidation of *n*-butane, it is clear that lead oxide is the most effective. The results with lead tetroxide and lead chloride are, in fact, comparable with those obtained[16] with many other inorganic compounds including nickelous oxide, ferric oxide, manganous chloride and potassium iodide. The exceptionally potent inhibition found with lead oxide is of particular interest because of its relevance to the mechanism of the anti-knock action of lead tetraethyl. Before this aspect is considered, however, it is worth while to compare the effect of lead oxide on butane oxidation with its effect on other gas phase oxidations. D. R. WARREN[12] has found that a lead oxide surface inhibits the oxidation of hydrogen at about 500°C much more effectively than does a silica surface, and A. D. WALSH and co-workers[5,17] have reached a similar conclusion with methane. With *n*-heptane, however, the opposite conclusion was reached by E. C. HUGHES and co-workers[13] who studied the reaction in the temperature range 371° to 427°C with a flow system. Interesting results with ethers were obtained by G. H. N. CHAMBERLAIN and A. D. WALSH[11] who employed a static system and observed oxidation phenomena with diethyl ether and di*iso*propyl ether at various temperatures between 210°C and 500°C. Their results are summarized in *Table 1* and are compared with those obtained with *n*-butane in the present investigation.

Table 1. Effect of a surface-coating of lead oxide on combustion behaviour of ethers and of n*-butane*

Characteristic	*With ethers (ref. 11)*	*With* n*-butane (this work)*
Rate of slow combustion	*Reduced*	*Reduced*
Cool flame pressure kicks	*Reduced*	*Reduced*
Ignition pressures	*Raised by 10 to 15%*	*Raised by 65 to 75%*
Pressure limit for a cool flame	*Little effect*	*Large effect*
Induction period to cool flame	*Unaffected*	*Increased about 100-fold*

It appears from *Table 1* that lead oxide brings about a more pervasive inhibition of the oxidation of *n*-butane than that of ethers. The differences in response to lead oxide are particularly noticeable in the low temperature reaction leading to cool flames; with *n*-butane lead oxide suppresses cool flames over a wide range of experimental conditions (see *Figure 1*) but with ethers there is little effect[11]. A possible explanation of this difference is that the free radical chains are of much greater

length in butane oxidation than in ether oxidation. In any event, the conclusion of Chamberlain and Walsh[11] that lead oxide has little effect on the chains leading to cool flames appears to be inapplicable to butane oxidation.

The inhibition by lead oxide of the oxidation of methane[17] and ethers[11] led Walsh and co-workers to propose a detailed mechanism for the anti-knock action of lead tetraethyl[1,11]. According to this theory the anti-knock action is a consequence of the destruction of free radicals, such as HO_2, at the surface of lead oxide smoke particles, formed from lead tetraethyl in the cylinder. Although this theory has been vigorously defended by Walsh and co-workers[1-5], it does not appear to have won universal acceptance[6,18,19]. The results with *n*-butane inasmuch as they show that lead oxide exerts a profound effect on the combustion of a typical hydrocarbon, lend support to the view that lead oxide is the active anti-knock species when lead tetraethyl is used. It is interesting to compare the results given above with those of D. T. A. Townend and M. R. Mandlekar[15,20] who measured ignition pressures for *n*-butane (and *n*-pentane) with and without lead tetraethyl. They found that 0·1 per cent of this additive (a concentration similar to that used for effective anti-knock action) raised minimum ignition pressures by about 5 per cent. This is much less than the increase of about 70 per cent found with a surface deposit of lead oxide (0·9 mg/cm^2). If solid lead oxide in the form of a smoke is in fact present in an engine cylinder as suggested by Walsh and co-workers[1,11], it would seem that very little would be needed for marked anti-knock action.

In one respect the effect of lead oxide on the combustion of paraffins appears to differ from the effect of lead tetraethyl: with *n*-butane lead oxide greatly lengthens the induction period preceding a cool flame; lead tetraethyl, however, has little effect, at least with *n*-heptane[7,9]. This difference is readily explained if, as supposed, the true inhibitor is lead oxide, and if there is an appreciable delay in its formation from lead tetraethyl.

The possibility that lead oxide vaporizes appreciably and that the observed inhibition is due to lead oxide molecules in the vapour stat must be considered[6]. This possibility was di cussed by Chamberlain and Walsh[11] w rejected it because of their observation that, ether oxidation with a lead oxide-coated vess inert gas additions accelerate the reaction. similar result has been obtained in buta oxidation[16]. Reliable vapour pressure valu for lead oxide in the temperature range o interest do not appear to be obtainable, bu available data[21] suggest that the vapour pressur is very low. Furthermore, if vapour molecule were largely responsible for the observed inhibition its magnitude would be expected to increase sharply with increasing temperature and this does not appear to be so (see *Figure 2*). The role of lead oxide vapour in the range of temperature considered here seems likely to be a very minor one.

The author is indebted to the National Research Council of Canada for a grant in aid of this research, and to M. Cherneskey for assistance with the experimental work.

References

1 Chamberlain, G. H. N., Hoare, D. E. and Walsh, A. D. *Disc. Faraday Soc.* 1953, **14**, 89

2 King, R. O. *Canad. J. Res. F*, 1948, **26**, 125, 226

3 Badin, E. J. *Third Symposium on Combustion, Flame and Explosion Phenomena*, p 386. Williams and Wilkins: Baltimore, 1949

4 Pidgeon, L. M. and Egerton, A. C. *J. chem. Soc.* **1932**, 676

5 Cheaney, D. E., Davies, D. A., Davis, A., Hoare, D. E., Protheroe, J. and Walsh, A. D. *Seventh Symposium (International) on Combustion*, p 183. Butterworths: London, 1959

6 Norrish, R. G. W. *Seventh Symposium (International) on Combustion*, p. 203. Butterworths: London, 1959

7 Lewis, B. and von Elbe, G. *Combustion, Flames and Explosions of Gases*, pp 126–199. Academic Press: New York, 1951

8 Zang, W. I. and Lovell, W. G. *Industr. Engng Chem. (Industr.)*, 1951, **43**, 2826

9 Pahnke, A. J., Cohen, P. M. and Sturgis, B. *Industr. Engng Chem. (Industr.)*, 1954, **46**, 10

10 Barusch, M. R. and Payne, J. Q. *Industr. Engng Chem. (Industr.)*, 1951, **43**, 2329

11 Chamberlain, G. H. N. and Walsh, A. D. *Proc. Roy. Soc. A*, 1952, **215**, 175

12 Warren, D. R. *Proc. Roy. Soc. A*, 1952, **211**,

13 Hughes, E. C., Darling, S. M., Bartleson, J. D. and Klingel, A. R. *Industr. Engng Chem. (Industr.)*, 1951, **43**, 2841

[4] BARDWELL, *J. Fifth Symposium (International) on Combustion*, p 529. Reinhold: New York, 1955
[5] TOWNEND, D. T. A. and MANDLEKAR, M. R. *Proc. Roy. Soc. A*, 1933, **141**, 484
[6] CHERNESKEY, M. and BARDWELL, J. *Canad. J. Chem.* In press
[7] HOARE, D. E. and WALSH, A. D. *Fifth Symposium (International) on Combustion*, p 467. Reinhold: New York, 1955
[18] PAHNKE, A. J. *Advances in Chemistry Series, No. 20*, p 202. American Chemical Society: Washington 6, D.C., 1958
[19] ROSS, A. and RIFKIN, E. B. *Industr. Engng. Chem. (Industr.)* 1956, **48**, 1528
[20] TOWNEND, D. T. A. and MANDLEKAR, M. R. *Proc. Roy. Soc. A*, 1934, **143**, 168
[21] MELLOR, J. W. *A Comprehensive Treatise on Inorganic and Theoretical Chemistry*, Vol. VII, p 647, Longmans, Green: London, 1930

The Relationship between Burning Velocity and Space Velocity of a Spherical Combustion Wave in a Closed Spherical Chamber

S. D. RAEZER

Applied Physics Laboratory, The Johns Hopkins University, Silver Spring, Maryland

(*Received February 1960*)

A relationship between burning velocity and space velocity of a centrally ignited spherical combustion wave with reaction zone of zero thickness is derived for expansion in a closed spherical chamber, on the assumption that the velocity of the gas is sufficiently small compared to that of sound that the pressure remains uniform throughout the chamber, and that temperature equilibrium exists in the cold gas and hot gas regions. It is shown that if, in addition, the specific heats and average gramme molecular weight are constant, the ratio v_s/v_f may be expressed as a function of the flame radius.

List of Symbols

THE following symbols are used:

- C_v Specific heat at constant volume (cal g^{-1} °C^{-1})
- M Gramme molecular weight (g mole^{-1})
- m Mass (g)
- m_0 Total mass
- n Mass fraction of gas consumed
- P Pressure (dyne cm^{-2})
- R Chamber radius (cm)
- r Flame radius (cm)
- S Ratio of burning velocity to space velocity
- t Time (sec)
- V Volume (cm^3)
- V_0 Bomb volume
- v_f Burning velocity (cm sec^{-1})
- v_s Space (or flame front) velocity (cm sec^{-1})
- γ Ratio of specific heats of unburnt gas
- ρ Density (g cm^{-3})
- θ Temperature (°C)
- θ_e Final temperature for combustion at constant volume
- θ_0 Initial temperature in bomb before ignition
- θ_f Flame temperature

Unless otherwise assigned, subscript $_0$ denotes the initial, $_e$ the final, state; $_1$ and $_2$ refer to the cold and hot gas regions, respectively.

Introduction

A method of measuring burning velocity developed by E. F. FIOCK *et al.*[1] depends upon both a measurement of the velocity with which a spherical flame, ignited at the centre of a spherical chamber, moves toward the wall and upon a measurement of the resulting pressure rise in the chamber. On the basis of conditions in the unburnt gas region ahead of the flame front they derived, with the assumption that the law of adiabatic compression of an ideal gas applied in this region, the following relationship

$$v_f = v_s\left[1 - \frac{R^3 - r^3}{3\gamma P r^2}\frac{\mathrm{d}P}{\mathrm{d}r}\right] \qquad \ldots . [1]$$

where the symbols have the meanings listed above.

Employing the same physical considerations, B. LEWIS and G. VON ELBE[2] have derived the equivalent relationship

$$v_f = \tfrac{1}{3}\frac{\mathrm{d}n}{\mathrm{d}t}\frac{R^3}{r^2}\left(\frac{P_0}{P}\right)^{1/\gamma} \qquad \ldots . [2]$$

where

$$r = [1 - (1 - n)\,(P_0/P)^{1/\gamma}]^{1/3} \qquad \ldots . [3]$$

By including the approximate expression

$$n = (P - P_0)/(P_e - P_0) \qquad \ldots . [4]$$

they eliminated all but one variable, the pressure. Equation 4, derived from energy considerations and conditions in the burnt gas region, is valid only in the early stages of burning where the pressure rise is small. P_e refers to the final pressure in the bomb computed thermo-

dynamically for combustion at constant volume using average specific heats and dissociation equilibria.

From equations 2, 3 and 4 the expression (attributed[3] to R. J. Dery)

$$v_f = \frac{v_s}{1+(1/\gamma)(P_e/P-1)} \quad \ldots\ldots [5]$$

may be derived.

Using the same physical assumptions but following a different mathematical approach, a more complete solution will be obtained from which equation 5 follows as a limiting case. In addition, an approximate formula will be derived which expresses the ratio v_f/v_s in terms of the flame radius.

Derivation of the Ratio v_f/v_s

The physical characteristics of the real case and justification for the assumptions used by the author have been adequately presented in the references cited, so that the following will be confined mainly to the analysis. Since the ratio v_f/v_s appears in a natural manner throughout the derivation and is a quantity which is independent of flame kinetics, the derivation will be carried out in terms of this ratio, designated for convenience as S.

The case considered is that of a spherical flame front of zero thickness, originating at the centre of a closed spherical chamber and burning toward the wall. Actually, the analysis is general and applies to any thin flame subject to one-dimensional analysis where the gas velocity goes to zero at fixed boundaries ahead of and behind the flame.

The chamber will be divided into two regions, the unburnt region between the flame front and wall (1), and the burnt gas region where combustion is complete (2). It will be assumed that the pressure is uniform throughout the chamber and varies only with the time; that the temperatures in regions (1) and (2) vary only with the time, a discontinuous change occurring at the reaction zone separating the two regions; that the gas is ideal; and that the specific heat within each region may be adequately approximated by some average value over the course of the reaction.

If in region (1) no heat is lost to the wall or gained from region (2), it follows from this and preceding assumptions that

$$dP_1/P_1 = \gamma d\rho_1/\rho_1 \quad \ldots\ldots [7]$$

Since

$$\frac{d\rho_1}{\rho_1} = \frac{1}{V_1}\left(\frac{dm_1}{\rho_1} - dV_1\right) \quad \ldots\ldots [7]$$

where $dV_1 = -dV_2$, and by definition of the flame speed $dm_1 = \rho_1 S\, dV_2$, it follows that

$$\frac{d\rho_1}{\rho_1} = (1-S)\frac{dV_2}{V_0 - V_2} \quad \ldots\ldots [8]$$

and

$$\frac{dP_1}{P_1} = \gamma_1 (1-S)\frac{dV_2}{V_0 - V_2} \quad [9]$$

Equation 9 is identical with equation 1.

In region (2), again making use of equation 7

$$\frac{d\rho_2}{\rho_2} = \frac{1}{V_2}\left(\frac{dm_2}{\rho_2} - dV_2\right)$$

where $dm_2 = \rho_1 S\, dV_2$, we obtain

$$\frac{d\rho_2}{\rho_2} = \left(\frac{\rho_1}{\rho_2}S - 1\right)\frac{dV_2}{V_2} \quad \ldots\ldots [10]$$

Since from the ideal gas law

$$\frac{dP_2}{P_2} = \frac{d\theta_2}{\theta_2} + \frac{d\rho_2}{\rho_2}$$

then

$$\frac{dP_2}{P_2} = \left(\frac{\rho_1}{\rho_2}S - 1\right)\frac{dV_2}{V_2} + \frac{d\theta_2}{\theta_2} \quad \ldots\ldots [11]$$

Because the pressure remains uniform, $dP_1/P_1 = dP_2/P_2$, giving from equations 9 and 11

$$\gamma(1-S)\frac{V_2}{V_0 - V_2} = \frac{\rho_1}{\rho_2}S - 1 + \frac{V_2}{\theta_2}\frac{d\theta_2}{dV_2} \quad \ldots\ldots [12]$$

Considering a small element of reacting mass dm passing through the flame front, if no heat of reaction is lost by transfer, the chemical energy released raises the internal energy of the element, expanding its volume and doing work of compression on the gas in regions (1) and (2). If the gas were completely reacted adiabatically at constant volume, the energy of reaction per mass of gas mixture would be given

$C_{vf}(\theta_e-\theta_0)$, C_{vf} being the average specific heat over the temperature range $(\theta_e-\theta_0)$. Except for the case where predissociation in the cold gas occurs, the same reaction energy should be obtained and the same specific heat approximately apply for the reaction of the mass element dm, so that

$$C_{vf}(\theta_e-\theta_0)\,dm_2=C_{vf}(\theta_f-\theta_1)\,dm_2 + m_1C_{v1}d\theta_1+m_2C_{v2}d\theta_2 \quad \ldots.[13]$$

where θ_f is the maximum temperature reached in the reaction zone. In general, the flame temperature θ_f will be lower than the mean temperature of the burnt gas θ_2 since the gas in region (2) is receiving energy of compression. The elevation of the initial temperature of the reacting gas resulting from compression of the gas in region (1) tends to offset this effect by raising θ_f in an approximately additive fashion. Initially, for small flame radii compression is slight and θ_2 is very close to θ_f. As the flame radius increases, θ_f increases in step with but is lower than θ_2. For purposes of obtaining a closed solution the approximation $\theta_f=\theta_2$ will be made and justified later. With this approximation, using equation 13 the last term in equation 12 is given by

$$\frac{V_2}{\theta_2}\frac{d\theta_2}{dV_2}=\frac{C_{vf}}{C_{v2}}\left[(\theta_e-\theta_0)-(\theta_2-\theta_1)\right]\frac{V_2}{m_2\theta_2}\frac{dm_2}{dV_2}-\frac{C_{v1}}{C_{v2}}\frac{m_1V_2}{m_2\theta_2}\frac{d\theta_1}{dV_2} \quad \ldots.[14]$$

Since

$dm_2/dV_2=\rho_1S$ and $(V_1/\rho_1)(d\rho_1/dV_2)=(1-S)$,

using ideal gas relationships, it may be shown that

$$\frac{V_2}{\theta_2}\frac{d\theta_2}{dV_2}=\frac{C_{vf}}{C_{v2}}\frac{M_1}{M_2}S\left[\left(\frac{\theta_e}{\theta_0}-1\right)\left(\frac{\rho_0}{\rho_1}\right)^{\gamma-1}-\left(\frac{\theta_2}{\theta_1}-1\right)\right]-\frac{C_{v1}}{C_{v2}}\frac{M_1}{M_2}(\gamma-1)(1-S) \quad \ldots.[15]$$

Combining equations 15 and 12 and solving for S gives

$$S=\left\{1-\left(\frac{V_2}{V_0-V_2}\right)+\frac{C_{v1}}{C_{v2}}\frac{M_1}{M_2}(\gamma-1)\right\}\Big/\left\{\gamma\left(\frac{V_2}{V_0-V_2}\right)+\frac{\rho_1}{\rho_2}\left(1-\frac{C_{vf}}{C_{v2}}\right)+\frac{C_{vf}}{C_{v2}}\frac{M_1}{M_2}\left[1+\left(\frac{\theta_e}{\theta_0}-1\right)\left(\frac{\rho_0}{\rho_1}\right)^{\gamma-1}\right]+\frac{C_{v1}}{C_{v2}}\frac{M_1}{M_2}(\gamma-1)\right\} \quad \ldots.[16]$$

Using equation 8

$$d\rho_1/\rho_1=(1-S)\,dV_2/(V_0-V_2)$$

and conservation of mass in the form

$$\rho_2=(\rho_0V_0-\rho_1V_1)/V_2$$

S and the thermodynamic variables may be easily obtained for stepwise increments of V_2 over the entire range of V_2.

If the average molecular weight does not change during reaction and the specific heat at constant volume remains constant, equation 16 can be reduced to

$$S=\frac{1}{1+\frac{1}{\gamma}\left(\frac{P_e-P_0}{P}\right)\left(1-\frac{m_2}{m_0}\right)} \quad \ldots.[17]$$

Using the approximation

$$m_2/m_0=(P-P_0)/(P_e-P_0) \quad \text{(equation 4)}$$

or the equivalent approximation, $m_2/m_0\ll 1$ and $(P-P_0)\ll P_0$, equation 17 can be reduced to equation 5

$$S=1/\{1+(1/\gamma)(P_e/P-1)\}$$

Equations 17 and 8 may be combined to yield a relationship between S and V_2.

Re-writing equation 17 in its equivalent form

$$S=\frac{1}{1+\frac{1}{\gamma}\left(\frac{\theta_e}{\theta_0}-1\right)\left(1-\frac{V_2}{V_0}\right)\left(\frac{\rho_0}{\rho_1}\right)^{\gamma-1}} \quad \ldots.[18]$$

combining with equation 8, and re-arranging, one obtains

$$\frac{\rho_1^{\gamma-2}}{\rho_0^{\gamma-1}}d\rho_1=\frac{S}{\gamma}\left(\frac{\theta_e}{\theta_0}-1\right)\frac{dV_2}{V_0} \quad \ldots.[19]$$

which upon integration yields

$$\left(\frac{\rho_1}{\rho_0}\right)^{\gamma-1}=\frac{\gamma-1}{\gamma V_0}\left(\frac{\theta_e}{\theta_0}-1\right)\int S\,dV_2 \quad \ldots.[20]$$

Inserting this expression in equation 18 there results

$$S^{-1}-1=(\gamma-1)(V_0-V_2)/\int S\,dV_2 \quad \ldots.[21]$$

which upon differentiating gives

$$S=(1-\gamma)\left[\frac{1}{S^{-1}-1}+\frac{V_0-V_2}{(S^{-1}-1)^2}\frac{\mathrm{d}(S^{-1})}{\mathrm{d}V_2}\right]\ldots.[22]$$

Equation 22 can be arranged into the integrable form

$$-\frac{\mathrm{d}V_2}{V_0-V_2}=\frac{(\gamma-1)S^{-1}\,\mathrm{d}(S^{-1})}{(\gamma S^{-1}-1)(S^{-1}-1)}\quad\ldots.[23]$$

which upon integration yields

$$V_0-V_2=C\left[(1-S^{-1})/(1-\gamma S^{-1})^{1/\gamma}\right]\ldots[24]$$

In the ideal case of a reaction zone of zero thickness starting fully developed at the origin, one may impose the boundary condition that as $V_2\longrightarrow 0$, $S^{-1}=v_s/v_f\longrightarrow\theta_f/\theta_0$ where θ_f is the normal flame temperature.

Evaluating C and substituting its value in equation 24 gives

$$\frac{V_2}{V_0}=1-\left(\frac{v_s/v_f-1}{\theta_f/\theta_0-1}\right)\left(\frac{\gamma(\theta_f/\theta_0)-1}{\gamma(v_s/v_f)-1}\right)^{1/\gamma}\quad\ldots.[25]$$

Discussion

Since the value of the spherical bomb method lies chiefly in the fact that by this method the burning velocity can be obtained over a wide range of variation in temperature and pressure in a single experiment, an accurate experimental determination of these variables is necessary. For this reason, their elimination from the formula for burning velocity may be of limited practical value.

How large an error is introduced by the approximation $\theta_f=\theta_2$ could be best determined by comparison of particular results obtained by the method of Fiock with those calculated from equation 16. Equation 25, which applies where the ratio of molecular weights and specific heats of unburnt to burnt gas are both close to unity, could be employed as a convenient cross-check with other methods. In any case, the author feels that the calculations may be of some interest and that the approach, being general and straightforward, may serve to clarify the basic thermodynamics of the problem.

References

[1] Fiock, E. F., Marvin, C. F., Caldwell, F. R. and Roeder, C. H. *Nat. Adv. Comm. Aero. Wash., Rep. No. 682* (1940)

[2] Lewis, B. and von Elbe, G. *Combustion, Flames and Explosions of Gases*, pp 453–457. Academic Press: New York, 1951

[3] Manton, J., von Elbe, G. and Lewis, B. *Fourth Symposium (International) on Combustion*, p 358. Williams and Wilkins: Baltimore, 1953

The Quenching Diameter of Ozone Flames*

A. G. STRENG and A. V. GROSSE

Research Institute of Temple University, Philadelphia 44, Pa

(*Received February 1960*)

The quenching diameters of various ozone–oxygen and pure ozone flames have been determined experimentally, as a function of composition, temperature and pressure. The quenching diameter, d_c, for pure ozone equals 90μ at 298°K and 1·0 atm ; it is the smallest of all known flames.

THE knowledge of the quenching diameter of ozone flames is of great practical importance for the safe and successful handling of concentrated and pure ozone. In addition, it has a large theoretical interest. It lends itself to theoretical treatment more easily than any other flame. Thus the theoretical relationship between the kinetics of ozone decomposition and the burning velocity has been fully developed in recent years[1–3].

The combustion wave theory as developed by B. LEWIS and G. VON ELBE[4] gives, among others, the relationship between the minimum ignition energy, the quenching diameter and the burning velocity of a flame. The quenching diameter of the 25 mole per cent ozone flame has also been calculated directly from theory[5].

In view of these relationships, an experimental determination of the quenching diameter, coupled with the knowledge of the burning velocity, makes it possible to calculate readily the minimum ignition energy and also the boundary velocity gradient for flashback. All of these parameters are of importance for the practical handling of pure or concentrated ozone gas.

The quenching diameter of various ozone–oxygen flames in the range of 10 to 100 volume per cent ozone was determined by using the accumulated experience of the Institute in handling concentrated and pure ozone. It was anticipated that the quenching diameter for pure ozone would be *smaller* than that of any other previously measured quenching diameter of a combustible mixture. This proved to be so. The quenching diameter for pure ozone was found to equal 90 microns at 298° K (25° C) and 1·0 atm.

Experimental Method

The method used by us for the determination of the quenching diameter is simple and well established. It is based on the determination of the minimum tube diameter which prevents the propagation of a flame front, i.e. quenches the flame. The apparatus is illustrated in *Figure 1*; the details are apparent. Ozone–oxygen mixtures of the desired composition were prepared. The apparatus was evacuated and filled with the mixture to slightly above atmospheric pressure. The flame was initiated by inserting a hot platinum wire into the open part of the tube. The ozone flame was propagated to the capillary and *either* was quenched, if its diameter was *below* the quenching diameter, *or* exploded the ozone mixture in the sealed part of the tube if its diameter was *greater* than the quenching diameter. In the case of successful quenching the sealed part of the tube could be cut off at the capillary, attached to a measuring system and the survival or non-combustion of ozone demonstrated by condensing it in a bath of liquid oxygen; the amount of ozone could be determined either by volumetric or titration analysis.

In the above experiments the quenching diameter for cylinders, d_c, was determined. The quenching distance between two parallel plane surfaces, $d_{||}$, and the quenching diameter

*Presented at the Seventeenth International Congress of Pure and Applied Chemistry, Munich, Germany, September 1959

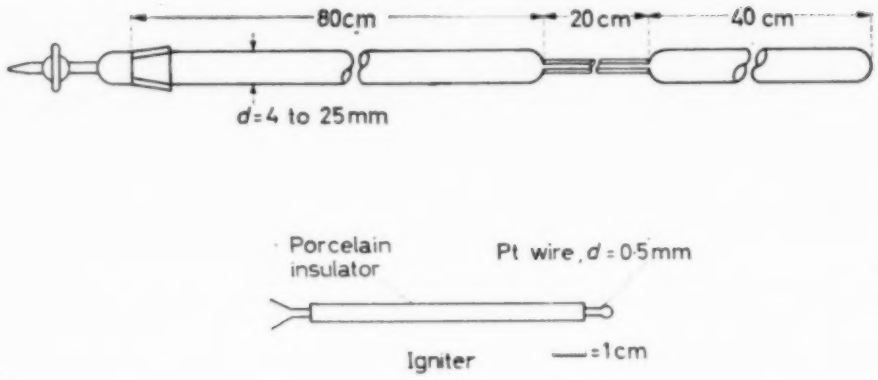

Figure 1. Apparatus for the determination of the quenching diameter of flames

of hollow spheres or bubbles, d_s, bear a simple relationship to d_c. Thus:

$$d_c = 1{\cdot}639\, d_{||}$$

$$d_s = 2{\cdot}24\ \ d_{||}$$

and

$$d_s = 1{\cdot}37\ \ d_c$$

Purity of Ozone

The purity of ozone is an important factor in obtaining reproducible results. Our pure ozone was prepared by the method described previously[6-8] based on the Clark Thorp patent (*U.S. Patent No. 2700648*), which leaves less than 5 p.p.m. by weight of organic impurities, expressed as carbon dioxide, in the oxygen used. The presence of organic impurities sensitizes the ozone. The high heat release occurring during the combustion of these impurities may cause the flame to propagate through capillaries below the quenching diameter for pure ozone.

The ozone–oxygen mixtures were prepared by measuring both the ozone and oxygen volumes. The accuracy of the mixture composition was carried to $\pm 0{\cdot}2$ mole per cent.

Experimental Results

Effect of ozone concentration, temperature and pressure on quenching diameter

The results of the quenching experiments at 298°K and at 1 atm pressure are shown graphically in *Figure 2* which delineates the region of flame propagation from the region where the flame is quenched in the capillary. The boundary line is a straight line function of $\log d_c$ versus ozone concentration.

The equation is

$$\log d_c = 6{\cdot}189 - 2{\cdot}118 \log x \qquad \ldots . [1]$$

where d_c is in microns, and x denotes mole per cent ozone. Cook's data, based on his minimum energy determinations for 9·5, 11·1 and 15·5

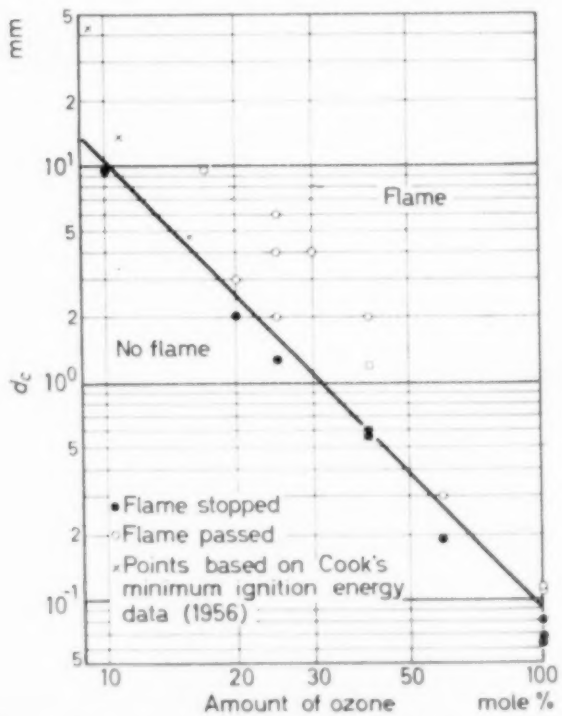

Figure 2. Quenching diameter, d_c, versus ozone concentration for ozone—oxygen mixtures at 298°K and 1 atm

mole per cent ozone[9], are in reasonable agreement with our data, particularly if it is remembered that they are obtained by a different method.

Similar experiments were carried out in tubes surrounded along their entire length by dry ice, i.e. at a temperature of 195°K and 1 atm pressure. The equation for d_c (same units as in equation 1) at 195°K is

$$\log d_c = 6{\cdot}403 - 2{\cdot}113 \log x \quad \ldots . [2]$$

The effect of temperature for the quenching diameter of *pure 100 per cent ozone* can be expressed as

$$d_c = 347{\cdot}5 - 0{\cdot}864\,T \quad \ldots . [3]$$

where T is the absolute temperature and d_c again is in microns.

In order to investigate the effect of pressure on the quenching of ozone flames it was found preferable to use hollow spheres of catalytically inert material instead of tubes. The study was made at 195°K in the pressure range from 1 atm to about 6 atm; the latter corresponds to the saturation pressure of pure ozone at 195°K. The results are plotted in *Figure 3*. As in *Figure 2*, the black dots indicate that the flame was quenched while the open circles show that the flame propagated. The quenching diameter, d_x, at 195°K is shown as a solid line. Based on our other data, the pressure relationship can be extrapolated to *room* temperature and the extrapolated line for 298°K is shown as a broken line in *Figure 3*. The relationship between the quenching diameter of pure ozone versus pressure converted to d_c values at 298°K is given by the expression

$$\log d_c = 1{\cdot}953 - 1{\cdot}111 \log P \quad \ldots . [4]$$

where P is in atmospheres and d_c again in microns.

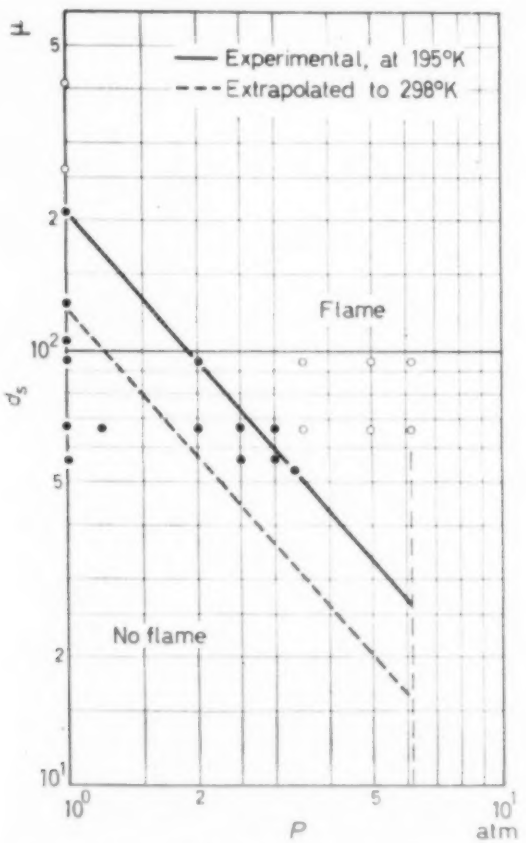

Figure 3. Quenching diameter, d_x, versus pressure for 100 per cent ozone

Comparison of Quenching Distance of Ozone versus Other Explosive Mixtures

It is of interest to compare ozone with a number of other well known combustion mixtures. Pertinent data are given in *Table 1*. The ethane–oxygen mixture has the smallest quenching distance in Lewis and von Elbe's compilation (*loc. cit.* ref. 4, pp 408–412). It can be readily seen that ozone has an even smaller quenching distance. Such an explosive mixture as hydrogen and oxygen (70:30 per cent) has a quenching distance roughly four times larger.

Flame Velocity Measurements at Low Ozone Concentrations

Our earlier measurements[7] on the burning velocity of ozone–oxygen mixtures may have been carried out in tubes narrower than the quenching diameter, since the latter was not known at that time.

We thus repeated our burning velocity measurements in wider tubes, up to 34 mm i.d. However, in such a wide tube we *failed* to ignite a 9·0 mole per cent ozone–oxygen mixture at 1·00 atm and 298°K ($d_{c\,(calc.)} = 14$ mm), by using a glowing platinum wire.

Minimum Ignition Energy and Quenching Diameter

Lewis and von Elbe (*loc. cit.* ref. 4, p 413) have developed the relationship between the minimum ignition energy, $E_{min.}$ (i.e. the minimum energy necessary to initiate a flame front), the burning velocity, temperature and quenching diameter of the flame. The relationship is

$$E_{min.} = \pi d^2 (\mu / S_u) (T_b - T_u) \quad \ldots . [5]$$

where $E_{min.}$ denotes energy in calories, d is the quenching distance between parallel walls in centimetres ($d = 0{\cdot}61\, d_c$), μ is the thermal conductivity, cal/cm. sec. °K, S_u is the burning velocity, cm/sec, T_b is the flame temperature, °K, and T_u is the initial gas temperature, °K.

Table 1. Quenching distances of various gas mixtures

Gas	Quenching distance $d_{\parallel}$ microns
100% *Ozone*	55
17% *Ethane+oxygen*	200
70% *Hydrogen*+30% *oxygen*	380
90% *Hydrogen*+10% *oxygen*	2030
12% *Methane+air*	8890

Since we have determined S_u for the whole range of ozone concentrations[6–8] and μ and T_b can be readily calculated, we now have a simple way of obtaining $E_{min.}$ from d_c and vice versa. The flame temperatures were given in our earlier publication[7], and μ was calculated following Lewis and von Elbe (*loc. cit.* ref. 4, p 415).

The calculated minimum ignition energies, both in calories and millijoules, for various mole percentages of ozone, are given in *Table 2*.

$E_{min.}$ versus d_c on a log versus log plot is a straight line and the relationship can be expressed simply in the form of the equation

$$\log E_{min.} = 2{\cdot}574 \log d_c - 1{\cdot}463 \quad \ldots . [\,]$$

where $E_{min.}$ is in mJ, and d_c in mm.

The above relationship permitted us to use Cook's data on the minimum ignition energies and to compare them with our quenching diameters. Cook and his co-workers performed spark explosion tests in a 9·9 cm i.d. glass bulb. They found that at room temperatures and 1 atm pressure an electric spark of 0·004 J ignites a 15·5 mole per cent ozone–oxygen mixture but does not ignite a 15·0 mole per cent mixture. A spark of 0·05 J initiated the combustion of a mixture containing 11·1 mole per cent ozone, but failed with 10·4 mole per cent. In a third experiment a 0·47 J spark initiated a 9·5 mole per cent ozone but did not initiate a 9·1 mole per cent ozone mixture. Using the Lewis and von Elbe equation, it follows that the quenching diameter for the 9·5 mole per cent ozone mixture is 41 mm, for the 11·1 per cent 14 mm and for the 15 per cent 5 mm. These results are in reasonable agreement with our own quenching diameter determinations as can be seen from *Figure 2*, where Cook's data are plotted along with ours.

Relation of Boundary Velocity Gradient for Flashback to Burning Velocity and Quenching Diameter

Recently, A. L. Berlad and A. E. Potter[10] established a general relationship between the boundary velocity gradient for flashback, i.e. g_f, the burning velocity, S_u, and the quenching

Table 2. Minimum ignition energies for ozone and ozone–oxygen mixtures at 1 atm and 298°K initial gas temperature

Mole % O_3	Quenching diameter mm d_c	Heat conductivity cal/cm. sec. °C	Burning velocity cm/sec S_u	Flame temperature, °K T_b	Minimum ignition energy cal	mJ
100·0	0·090	$3{\cdot}3 \times 10^{-5}$	472	2677	16×10^{-9}	$0{\cdot}7 \times 10^{-4}$
75·0	0·165	$3{\cdot}9 \times 10^{-5}$	334	2425	$7{\cdot}8 \times 10^{-8}$	$3{\cdot}3 \times 10^{-4}$
50·0	0·390	$4{\cdot}55 \times 10^{-5}$	193	1950	$0{\cdot}7 \times 10^{-6}$	$2{\cdot}9 \times 10^{-3}$
25·0	1·65	$5{\cdot}2 \times 10^{-5}$	52	1250	$0{\cdot}3 \times 10^{-4}$	$1{\cdot}25 \times 10^{-1}$

diameter, d_c. This relationship is

$$g_f = 1{\cdot}4125\,(S_u/d_c)^{1{\cdot}168} \quad \ldots . [7]$$

Assuming that this relationship applies also to ozone flames, at least in first approximation, we can calculate the velocity gradients for flashback for various ozone flames. The calcu-

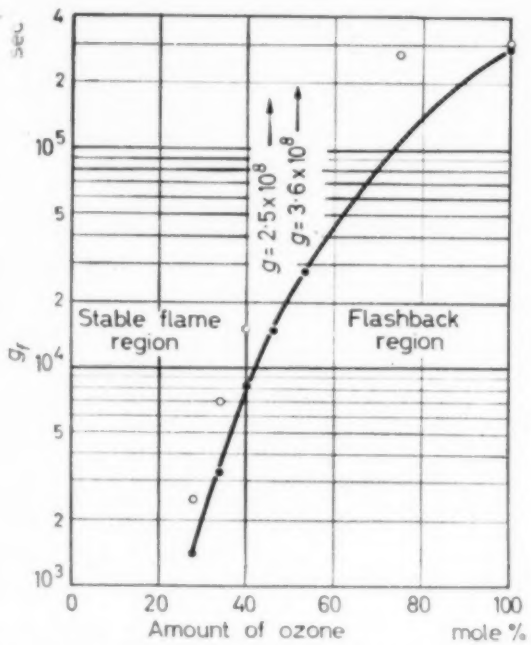

Figure 4. Critical boundary velocity gradient for flashback, g_f, versus ozone concentration in ozone–oxygen mixtures at 298°K and 1 atm

lated g_f values are the black dots plotted in *Figure 4* and are also given in *Table 3*. The calculated velocity gradients of our experimental ozone flames are designated by open circles in *Figure 4*. It can be seen that the calculated flashback gradients, g_f, are in agreement, at least in first approximation, with the experimental velocity gradients.

Using the flashback gradient values calculated from the Berlad and Potter relationship, we are now in a position to calculate the minimum volumetric flow or 'flashback flow' for various ozone–oxygen mixtures and cylindrical tubes of a given *inside diameter*.

Generally, the boundary velocity gradient, g,

$$g = 4V/R^3, \text{ sec}^{-1} \quad \ldots . [8]$$

if V is the volumetric flow in cm³/sec, and R denotes radius of tube in cm.

These calculated values are of great practical importance to anyone experimenting with ozone or ozone mixtures, and are presented in *Table 3*, for ready reference.

References

[1] VON KÁRMÁN, T. and PENNER, S. S. *Selected Combustion Problems*, pp 5–41. AGARD; Butterworths: London, 1954
VON KÁRMÁN, T. *Sixth Symposium (International) on Combustion*, pp 1–11. Reinhold: New York, 1957

[2] HIRSCHFELDER, J. O., CURTISS, C. F. and CAMPBELL, D. E. *J. phys. Chem.* 1953, **57**, 403
HIRSCHFELDER, J. O., CURTISS, C. F. and BIRD, R. B. *Molecular Theory of Gases and Liquids*, pp 756–783. Wiley: New York, 1954

[3] SANDRI, R. *Canad. J. Chem.* 1956, **34**, 313 and 324; 1957, **35**, 474

[4] LEWIS, B. and VON ELBE, G. *Combustion, Flames and Explosions of Gases*, Chapter 7. Academic Press: New York, 1951; see also *Z. Elektrochem.* 1957, **61**, 574–78; *Advances in Chemistry Series No. 20*, pp 15–21. American Chemical Society, Washington 6, D.C., 1958; *Seventh Symposium (International) on Combustion, London–Oxford, 1958*. Butterworths: London, 1959

[5] GERSTEIN, M. and POTTER, A. E. 'Considerations related to the quenching of flames with simple

Table 3. Minimum gas flow or 'flashback' flow for ozone and ozone–oxygen mixtures

Burner tube, i.d. cm	*Minimum gas flow, cm³/sec at 1·0 atm and 298°K*				
	25 *mole %* O_3	40 *mole %* O_3	50 *mole %* O_3	75 *mole %* O_3	100% O_3
0·065	—	—	—	3	7
0·1	—	—	2	11	29
0·2	—	7	17	88	232
0·3	—	21	53	275	725
0·6	17	174	441	2310	6090
0·8	40	415	1050	5500	14500
1·0	80	830	2100	11000	29000
2·0	640	6640	16800	88000	232000
g_f, sec^{-1}	$8{\cdot}0 \times 10^2$	$8{\cdot}3 \times 10^3$	$2{\cdot}1 \times 10^4$	$1{\cdot}1 \times 10^5$	$2{\cdot}9 \times 10^5$

kinetics'. *Heat Transfer and Fluid Mechanics Institute Symposium*, 19–21 June 1958, pp 69–79. University of California: Berkeley, Calif.

[6] GROSSE, A. V. and STRENG, A. G. 'Pure ozone flames, alone and with various fuel gases'. *Technical Note No. 4, Contract* AF 18(600)–1475, The Research Institute of Temple University, 1 August 1957, Philadelphia; PB131732, U.S. Department of Technical Services, Washington, D.C.

[7] STRENG, A. G. and GROSSE, A. V. *Sixth Symposium (International) on Combustion*, pp 268–73. Reinhold: New York, 1957; see also *J. Amer. chem. Soc.* 1957, **79**, 1517

[8] STRENG, A. G. and GROSSE, A. V. 'The pure ozone flame and the combustion of various fuel gases in pure ozone'. *Advances in Chemistry Series No. 21*, pp 38–43. American Chemical Society, Washington 6, D.C. 1959. (Paper presented at the International Ozone Conference, Chicago, Ill., 28 November 1956.)

[9] COOK, G. A., SPANDINGER, E., KIFFER, A. S. and CLUMPP, C. V. *Industr. Engng Chem. (Industr.)*, 1956, **48**, 736

[10] BERLAD, A. L. and POTTER, A. E. *Combustion and Flame*, 1957, **1**, 127

Knock Resistance and Anti-knock with Hydrocarbon Fuels

J. CARTLIDGE and C. F. H. TIPPER

Department of Inorganic and Physical Chemistry, University of Liverpool

(Received June 1960)

On the basis of the results of studies by the authors of the peroxidic products of the gas-phase oxidation of a number of hydrocarbons it is suggested that an increasing tendency to knock is related to an increased tendency for the fuel to form hydroperoxides and in particular dihydroperoxides on oxidation. Some of the problems of the relative knock resistances of hydrocarbons can be explained on this basis. The high anti-knock effect of lead tetraethyl can then also be explained if in the cylinder a fog of lead oxide is produced, causing rapid heterogeneous decomposition of peroxide intermediates, and thus preventing branching due to these compounds.

THE relative knock resistances of a large number of hydrocarbon fuels have been determined[1]. The higher the critical compression ratio [c.c.r.] for incipient knock under standard conditions in an internal combustion engine the smaller the tendency for knocking combustion to occur with the fuel. Many workers have attempted to correlate the wide differences in knock resistance of hydrocarbons with their combustion characteristics, e.g. minimum ignition temperature, without marked success[2,3]. However, K. C. SALOOJA[4] has recently shown that the anti-knock performance of various fuels and the change in performance with alteration in the operating conditions of the engine is related to the extent of the pre-flame reaction.

It has been known for some time that there is a general correlation between the ease of oxidation of a hydrocarbon [e.g. in a static system under standard conditions] and the c.c.r.[5]; for instance, as the length of the carbon chain in a normal paraffin or olefin is increased the oxidation rate becomes progressively higher and the c.c.r. progressively lower. Branching of the carbon backbone decreases the rate of oxidation and raises the c.c.r. Such results have been explained on the basis of the peroxide mechanism for slow combustion[6–8]. With fuels that oxidize only above 350° to 400°C under normal conditions (e.g. methane, ethane, ethylene) chain branching is due to aldehydes from the decomposition of the RO_2 radicals produced, whereas with the higher paraffins and olefins at lower temperatures hydroperoxides may be formed by the reaction

$$RO_2 + RH \longrightarrow ROOH + R$$

and these will also cause branching if they decompose homogeneously to some extent giving radicals. It is supposed that the rate of decomposition and thus the rate of oxidation depends markedly on the structure of the hydroperoxide. However, this supposition is not borne out by recent work[9,10]. Also since hydrogen abstraction at a tertiary carbon atom is more rapid than at a secondary or primary one it might be expected that, for example, *iso*octane or triptane would oxidize readily. Actually these fuels only oxidize at higher temperatures and are very knock-resistant. It has been suggested that this is due to the formation of ketones, which will not cause branching, rather than aldehydes on decomposition of the RO_2 radicals[5]. In fact oxidizability increases and knock resistance decreases with increase in the number of secondary rather than primary or tertiary carbon atoms in the molecule.

Peroxidic Products of Gas-phase Oxidation

Recently the authors have been able to identify the peroxidic components in the products of the gas-phase oxidation of a number of hydrocarbons[11]. The oxidation of propane at 327°C and of triptane at 360° to 370°C in a flow system gives traces of hydrogen peroxide [and peracetic acid with propane] only. With

n-butane between 315° and 345°C and *cyclo*hexane between 300° and 316°C appreciable quantities of the monohydroperoxides [C_4H_9OOH and $C_6H_{11}OOH$] and various of their addition compounds with aldehydes (e.g. $C_4H_9OOCH[OH]R$) are present in the products and with *n*-heptane between 240° and 310°C the peroxides formed are mainly heptane dihydroperoxide and various aldehyde addition compounds together with small amounts of what is probably trihydroperoxide. Also only when hydroperoxides were produced was the oxidation, when proceeding at an appreciable rate, very exothermic.

A. D. KIRK and J. H. KNOX[10] have shown that in fact alkylhydroperoxides do decompose in the gas phase to give free radicals [RO and OH] and thus, if formed in oxidation systems, will cause branching. It seems probable that the O—O bonds in dihydroperoxides, trihydroperoxides and aldehyde-hydroperoxide compounds will also undergo homolytic fission and with the first two types of compounds more than two radicals may be produced. Although heterogeneous decomposition also occurs this will be less important in engines owing to the higher pressures and the very short pre-ignition times. When peroxide branching occurs the extra heat liberated will also increase the tendency to knock by increasing the rate of heating of the unburnt gas.

The probable mechanism whereby the important intermediates are formed is summarized at the foot of this page.

Step *a* involves internal hydrogen abstraction. With *n*-heptane the experimental results and a scaled molecular model indicate that this occurs at the CH_2 groups β or γ with respect to the point of original attack,

e.g. $CH_3CH(O{-}O\cdot)CH_2CH_2CH_2CH_2CH_3 \longrightarrow CH_3CH(O{-}OH)CH_2\dot{C}HCH_2CH_2CH_3$

or $CH_3CH(O{-}OH)CH_2CH_2\dot{C}HCH_2CH_3$

Knock Resistance

Propane and triptane are very knock-resistant [c.c.r. 12·2 and 14·4 respectively at 600 rev/min and 212°F jacket temperature], *n*-butane and *cyclo*hexane are moderately prone to knock [c.c.r. 5·5 and 4·9 respectively] and *n*-heptane has a very low knock resistance [c.c.r. 3·0]. It is possible therefore that an increasing tendency to knock is related to an increased tendency for the fuel to form hydroperoxides and in particular dihydroperoxides or even trihydroperoxides on oxidation. It is not suggested that this is the only factor involved but such a correlation does throw a light on some of the problems of knock resistance.

Normal alkanes

The oxidation of methane, ethane and propane under normal conditions does not give hydroperoxides[10,11]. With *n*-butane, however, not only is butyl hydroperoxide produced but there is the possibility of internal hydrogen abstraction, i.e.

$$CH_3CH(O{-}O\cdot)CH_2CH_3 \longrightarrow CH_3CH(O{-}OH)CH_2CH_2\cdot$$

This will not occur readily because of the high dissociation energy of the primary C—H bond

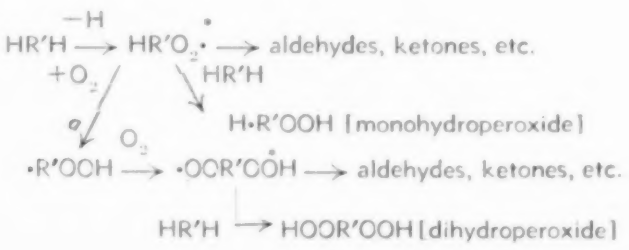

but it can account for the presence of traces of β-dicarbonyl compounds in the products[12,13], e.g.

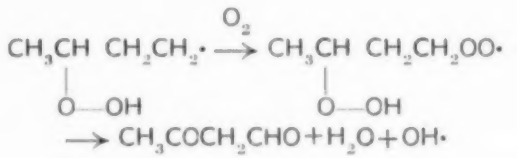

Another possible mode of decomposition of the $\cdot OOC_4H_8OOH$ radical is

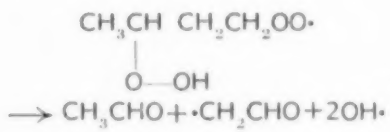

In other words internal hydrogen abstraction may lead to branching even if no dihydroperoxides are formed. Elementary reactions similar to the above are not possible with *iso*butane, and this may account for its higher c.c.r. [8·0].

With *n*-pentane internal hydrogen abstraction can occur more readily, since a secondary hydrogen atom can be removed, i.e.

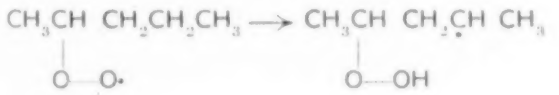

and the dissociation energy of a secondary C—H bond is less than that of a primary. As the length of the chain increases the probability of dihydroperoxide formation obviously also increases and to a marked extent. With normal alkanes above hexane double internal hydrogen abstraction eventually giving trihydroperoxides, e.g.

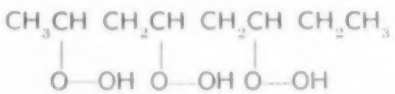

or

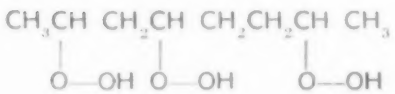

becomes possible, though it is likely that such a process is never of great importance.

It is interesting that C. WALCUTT, J. M. MASON and E. B. RIFKIN[14] found that a relatively stable pro-knock was formed when a mixture of *n*-heptane and air was passed through a heated tube at 225°C. This was presumably the dihydroperoxide.

Normal alkenes

The insertion of a double bond in the straight chain of five or more than five carbon atoms increases the knock resistance, despite the fact that the hydrogen atoms in the CH_2 group α to the double bond are more easily removed. However, the probability of internal hydrogen abstraction by the $HR'O_2$ radical, e.g.

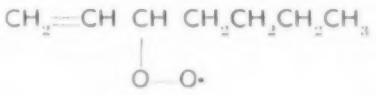

is considerably reduced. Also the c.c.r. increases as the double bond becomes more centralized, e.g. in passing from 1- to 2- to 3-heptene, again despite the presence in 3-heptene of two CH_2 groups α to the double bond. It is easy to see that, since there is no rotation about this bond, if it is in a central position internal hydrogen abstraction is greatly restricted, e.g. in the radicals

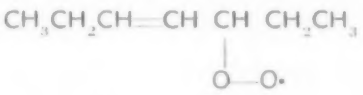

or

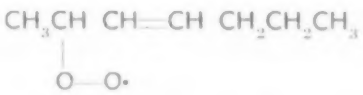

Branched alkanes

It might be expected that methyl substitution in a normal alkane such as heptane to give, say, 2-methylheptane would lead to enhanced reactivity, since initial hydrogen abstraction [at the tertiary carbon atom] is more rapid and the radical

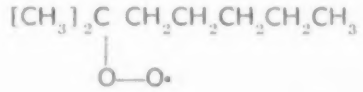

still possesses a chain of CH_2 groups so that internal hydrogen abstraction should be relatively easy. In fact the c.c.r. of 2-methyl heptane [3·3] is slightly higher than that of normal heptane. This may be partly due to the fact that branching of the carbon backbone restricts the coiling of the radical, but the main factor is probably the increased rate of decomposition of the alkylperoxy radical reducing the amount of the intramolecular hydrogen shift. With highly branched compounds, e.g. triptane, this decomposition must be very rapid since otherwise hydroperoxide formation, branching and thus appreciable oxidation could occur below 350°C, and the compounds would not be so knock-resistant. However, with many mono- and di-methyl alkanes the values of the c.c.r.s [< 6] suggest that formation of mono- and even di-hydroperoxides is still of importance, and it is interesting that of all the dimethylhexanes the one with the lowest c.c.r. [3·95] is the 2,5 isomer, which would be expected to give a dihydroperoxide most readily. In fact, 2,5-dimethylhexane-2,5-dihydroperoxide is one of the primary products of the oxidation of this hydrocarbon in solution[15].

Cyclic hydrocarbons

*cyclo*Pentane and *cyclo*hexane are both moderately knock-resistant but the c.c.r. for the latter is less than that for the former. Molecular models of the appropriate $HR'O_2$ radicals show that internal hydrogen abstraction is possible with $C_6H_{11}O_2$ but not with $C_5H_9O_2$ and in fact β-dicarbonyl compounds have been detected in the products of *cyclo*hexane but not those of *cyclo*pentane oxidation. The situation is thus comparable with that for *n*- and *iso*-butane.

However, in contrast to the effect of branching of the carbon backbone on the oxidizability of open chain paraffins, the monomethyl derivatives are less knock-resistant than the unsubstituted *cyclo*hexanes. Probably the *cyclo*alkylperoxy radicals are relatively stable and the rate of formation of monohydroperoxides is increased due to the presence of a tertiary hydrogen atom in the fuel molecule. Lengthening the side chain markedly reduces the knock resistance, the *n*-propyl and *n*-butyl derivatives having c.c.r.s about the same as those of *n*-hexane and *n*-heptane respectively. It is apparent from molecular models that if the O—O group in the $HR'O_2$ radicals is attached to one of the secondary carbon atoms of the side chain, e.g.

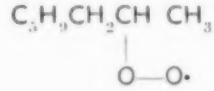

internal abstraction of any of a number of hydrogen atoms in the ring should be relatively easy, and this may account for the effect. The c.c.r. rises with the degree of branching of the side chain as might be expected and in fact *t*-butyl*cyclo*pentane or *cyclo*hexane are fairly knock-resistant [c.c.r.s 10·75 and 7·5 respectively].

The knock resistances of alkyl*cyclo*alkenes follow the same pattern. However, whereas *cyclo*pentene is more reactive than *cyclo*pentane, *cyclo*hexane and *cyclo*hexene have approximately the same c.c.r.s. The formation of monohydroperoxide will be more rapid if a double bond is present in the fuel molecule due to the four hydrogen atoms on the α CH_2 groups being more labile, but with *cyclo*hexene this effect is counteracted by the greatly reduced likelihood of internal hydrogen abstraction due to the ring being no longer 'flexible'.

Aromatic hydrocarbons

Most aromatic hydrocarbons are very knock-resistant. Even compounds like *n*-butylbenzene, where internal hydrogen abstraction appears to be possible in the peroxy radical, e.g.

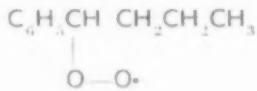

and others like '*iso*propyl- or ethyl-benzene which readily oxidize in solution to give hydroperoxides, have c.c.r.s above 10. It appears that the presence of a phenyl group causes the peroxy radical to decompose readily at higher temperatures.

Earlier work[10,16] and the recent work by the authors has shown that peroxides and especially hydroperoxides undergo heterogeneous decomposition readily. Thus, if it is true that low knock resistance is the result of the formation of mono- and/or di-hydroperoxides in the fuel–oxygen mixture ahead of the spark-ignited flame, the high anti-knock efficiency of lead tetraethyl may well be due to the presence of a fog of lead oxide particles in the cylinder as suggested by D. E. CHEANEY *et al.*[17]. The enormous surface area of the oxide will mean that branching due to homogeneous decomposition of the peroxide intermediates is almost completely suppressed. Thus the rate of oxidation in the mixture ahead of the flame is very greatly reduced, especially as branching due to the oxidation of aldehydes will also tend to be suppressed due to heterogeneous destruction of radicals[17]. With added amines, for instance, homogeneous chain termination[18], e.g.

$$X\cdot + ArNHR \longrightarrow XH + \dot{A}rNR$$

replacing a chain carrier X· by a less reactive radical, cannot be as efficient in lowering the oxidation rate.

References

1 American Petroleum Institute, Research Project 45, Eighteenth Annual *Report*, 1956
2 FRANK, C. E. and BLACKHAM, A. U. *Industr. Engng Chem.* (*Industr.*), 1952, **44**, 862
3 SWARTS, D. E. and ORCHIN, M. *Tech. Note Nat. Adv. Comm. Aero., Wash., No. 3379*, 1955
4 SALOOJA, K. C. *Combustion & Flame*, 1960, **4**, 193
5 e.g. LIVINGSTON, H. K. *Industr. Engng Chem.* (*Industr.*), 1951, **43**, 2834
6 WALSH, A. D. *Trans. Faraday Soc.* 1946, **42**, 269
7 CULLIS, C. F. and HINSHELWOOD, C. N. *Disc. Faraday Soc.* 1947, **2**, 117
8 SMALL, N. J. H. and UBBELOHDE, A. R. *J. appl. Chem.* 1953, **3**, 193
9 WILLIAMS, H. R. and MOSHER, H. S. *J. Amer. chem. Soc.* 1954, **76**, 2984
10 KIRK, A. D. and KNOX, J. H. *Proc. chem. Soc.* **1959**, 384
11 CARTLIDGE, J. and TIPPER, C. F. H. *Proc. chem. Soc.* **1959**, 190; **1960**, 219
12 THOMAS, J. R. and CRANDALL, H. W. *Industr. Engng Chem.* (*Industr.*), 1951, **43**, 2761
13 BARUSCH, M. R., NEU, J. T. PAYNE, J. Q. and THOMAS, J. R. *Industr. Engng Chem.* (*Industr.*), 1951, **43**, 2766
14 WALCUTT, C., MASON, J. M. and RIFKIN, E. B. *Industr. Engng Chem.* (*Industr.*), 1954, **46**, 1029
15 WIBAUT, J. P. and STRANG, A. *Verh. Akad. Wet. Amst. B*, 1951, **54**, 101; 1952, **55**, 207
16 HARRIS, E. J. *Proc. Roy. Soc. A*, 1939, **173**, 126
17 e.g. CHEANEY, D. E., DAVIES, D. A., DAVIS, A., HOARE, D. E., PROTHEROE, J. and WALSH, A. D. *Seventh Symposium* (*International*) *on Combustion*, p 183. Butterworths: London, 1959
18 BROWN, J. E., MARKLEY, F. X. and SHAPIRO, H. *Industr. Engng Chem.* (*Industr.*), 1955, **47**, 2141

Light Scattering Measurements on Particles Condensed from Boron-containing Flames

W. E. KASKAN

Research Laboratory, General Electric Co., Schenectady, N.Y.

(*Received June 1960*)

Light scattering measurements have been made on particles of liquid boron oxide condensing in flame gases. The method and apparatus are described, and some typical results presented. It appears that at first a relatively large number of small particles are formed, and these grow both by collision and by further condensation. The final size observed is about 0·2 micron. The errors and limitations of the experiments are discussed.

Introduction

THE problem of the condensation of a liquid hase from boron-containing flames is of terest from both theoretical and practical ints of view. Taken as a whole, this is a ite complicated problem, depending as it es not only on such obvious variables as essure, temperature, fuel/air ratio, but also the details of the high temperature chemistry such systems and on the fact that there may be (and in some cases, at least, there finitely is not[1]) chemical equilibrium in the as coming from the flame. The purpose of is communication is to describe a few experients whose purpose was simply to determine rticle numbers and sizes as a function of time ter burning, and to do this *in situ* rather than probe sampling and subsequent examination probe-treated samples[2].

e method used was to employ light ring measurements. The fundamental ptions which are made are that: (*a*) the cles are of uniform size, and (*b*) the cles are boron oxide [$B_2O_{3\,(liq)}$] and their ical properties can be computed from the al properties of boron oxide glass at room erature and from the known density of $_{(liq)}$ at elevated temperatures.

e results obtained are of limited use in the on of the overall problem, mostly because e difficulty in achieving uniformly cong clouds, but it is felt that the progress made and the interest in this problem warrant a report at this time.

Method

In section (a) below are described the details of the preparation of suitable flame gases for study and in section (b) the details of the light scattering measurements and the reduction of the data.

(*a*) Trimethyl borate–air flames were burned on annular cooled porous metal burners. The flames were flat discs, and the flow of flame gases was normal to the burner surface, and thus provided conditions suitable for optical probing as previously described[1,3].

The general arrangement of the apparatus is shown in *Figure 1*. The trimethyl borate (TMB) was supplied by a Lapp Microflow pump which both metered and pumped the liquid. A constriction was provided to ensure that the pump worked against suitable pressure, necessary to ensure seating of the ball valves. The TMB was then added to the air just upstream of a packed coil of heated ($\sim 60°C$) copper tubing which served as an evaporator. A plenum chamber served to mix further the gases before they were fed to the burner. The TMB–air flame was surrounded by a hydrogen–air flame which was adjusted to prevent a curtain of smoke which would otherwise form between the TMB–air flame gases and the surrounding air.

The optical arrangement was as previously

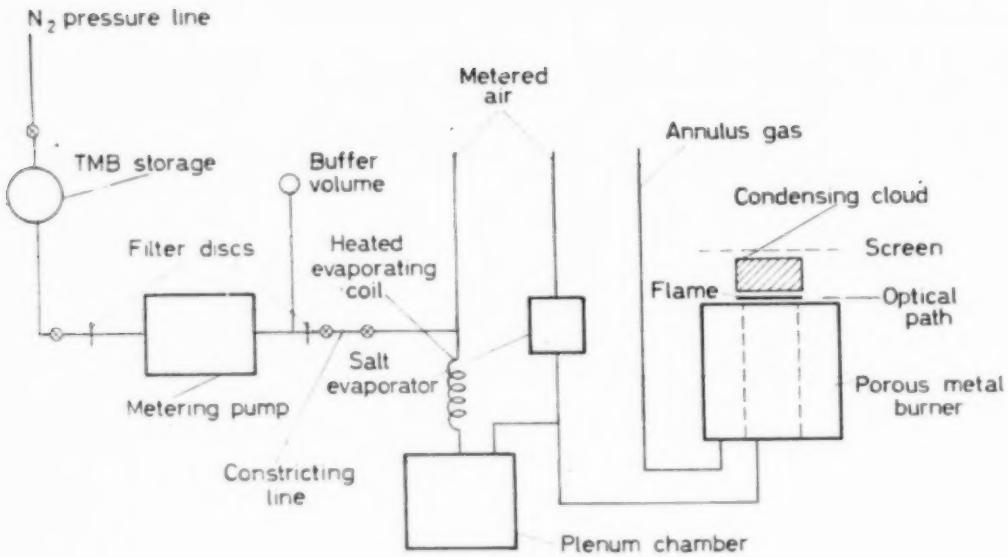

Figure 1. Arrangement of apparatus

described[3]. Measurements of the transmission at 2500, 3000, 5000 and 6000 Å were made as a function of height above the burner, using a hydrogen discharge tube as a background. It was established in separate experiments that there was no source of absorption other than the continuous absorption due to scattering; in particular, there was no absorption in the fluctuation bands[1] under conditions where there was condensation. The wavelengths were chosen to provide a large wavelength variation and to take advantage of both orders of the grating monochromator by simply switching filters to change from the visible to the ultraviolet.

Only a limited number of runs were made, principally because of the rapidity with which the burner surface became fouled with boron oxide. This fouling consisted of the precipitation of beads of boron oxide on the surface of the burner, and after this had progressed a while the cloud of condensing particles could be seen to be non-uniform; vertical streaks of relatively dense smoke would appear in the hot gas column. Even before these appeared, however, there was evidence that not all was well. If a flame were lit on a clean burner and the attenuation of a beam of light observed at a fixed distance over the burner, it would vary during the period preceding obvious non-uniformity. With TMB flames the period of burning before obvious fouling could be made a minute or so.

It was felt that what was required was a set of measurements at four wavelengths at each of five or six levels above the burner. Since this could not be accomplished in one minute, the procedure was adopted whereby, starting with a clean burner, the monochromator was set on one wavelength and readings of attenuation were taken as rapidly as possible as a function of height above the burner. The burner was then cleaned, by flushing with hot water, and this procedure repeated for each of the other wavelengths.

The most reliable results were obtained as described above. In addition some measurements were attempted with flames containing diborane, since a preliminary experiment had suggested that the smoke clouds obtained using this fuel remained uniform for longer burning times than those from TMB. Measurements using the procedure outlined above, however, were very unsatisfactory. The data showed a lot of scatter and often would not fit the theoretical curve (see below) at any point. Some, but not all, of this difficulty could be

ascribed to metering difficulties, since the diborane lines became contaminated with a whitish dust which at times plugged the orifice meter.

It was thought that some improvement might result by making all the measurements at a single level simultaneously. To accomplish this, four photocells and slits were arranged at the focal plane of the 1·5 m Bausch and Lomb Stigmatic spectrograph. These were appropriately filtered to select four wavelengths in the range 2500 to 6000 Å. The outputs were fed to a Consolidated 5–116 recording oscillograph through the 'system D' amplifier system. A fifth photocell monitored the light source. The beam was chopped in roughly a sinusoidal manner, since the recorder does not respond to direct current. The linearity of the amplifier–oscillograph system was checked directly using known test signals, and found to be adequate. Several runs were made by lighting a diborane-containing flame on a clean burner, and changing the burner level from one level to another as rapidly as possible, so that the run was complete in less than a minute. Even though at the end of this minute the smoke clouds looked uniform, the data still did not show the regularity of those obtained with TMB flames as described above.

(*b*) The scattering measurements were made entirely by determining the extinction (absorption) as a function of wavelength. The relevant theory is discussed in the book by H. C. VAN DEHULST[4]. It was found in preliminary experiments that Rayleigh scattering was nearly but not quite obeyed. For Rayleigh scattering, with refractive index, n, close to 1

$$Q = 32/27\,(n-1)^2 x^4 \qquad \ldots\ldots [1]$$

where Q is the ratio of the effective cross section for scattering to the actual cross section and

$$x = \pi D/\lambda \qquad \ldots\ldots [2]$$

where D is the diameter of the particle and λ is the wavelength of the light being scattered. The observed extinction coefficient ε is

$$\varepsilon = NQ\pi D^2/4 \qquad \ldots\ldots [3]$$

where N is the number of particles per cubic centimetre. Thus, for Rayleigh scattering a plot of $\log \varepsilon$ against $\log 1/\lambda$ would be a straight line (assuming n constant) with a slope of four. Preliminary results for the scattering by liquid boron oxide particles in flames showed approximately this behaviour, but the scattering at short wavelengths appeared relatively less efficient than at higher wavelengths. This is to be expected when the particles are a little too large for pure Rayleigh scattering[4].

It appeared that this departure from pure λ^{-4} scattering could be used to determine both particle size and number, in the following way. If a plot of $\log Q$ against $\log x$ were made using rigorous scattering theory, it would be found to be a straight line with a slope of 4 at low x, but to depart in the direction of a smaller slope at larger values of x, as in *Figure 2*. If a set of experimental data, in the form of a plot of $\log \varepsilon$ against $\log 1/\lambda$, could be made to match the theoretical plot in the curved region, then one would simultaneously have determined the two parameters x and Q. From the first, one could compute the diameter of the particles from equation 2, and from this and Q one could determine the number of particles from equation 3.

Actually Q involves the refractive index, n. However, it can be shown by numerical computation from the tables of R. B. PENNDORF[5] that, for a given x, the function

$$Q/(n-1)^2$$

is essentially independent of n over the range of refractive index and of x encountered here. Use of this function then allows use of the method provided that one knows the refractive index at the wavelengths to be employed.

The refractive indices were estimated in the following way. Refractive index data given by G. W. MOREY[6], and based on $n_D = 1{\cdot}4582$ at room temperature, where the density of $B_2O_{3(g)}$ is 1·85 g/cm³, were plotted in the form

$$\frac{1}{n-1} = -\frac{k}{\lambda^2} + \text{a constant} \qquad \ldots\ldots [4]$$

which is the form to be expected from dispersion theory[7]. The given data ranged from 4086 to 7682 Å and fell very accurately on a straight

line. From the value of the constant, it was deduced that the optical transition governing the dispersion curve was in the neighbourhood of 1 000 Å, so it was felt that it was safe to extrapolate equation 4, at least as far as 2 500 Å, in order to obtain refractive indices for $B_2O_{3(gl)}$ at room temperature below 4 086 Å. Finally, to obtain the indices at the elevated temperatures to be expected in flames, the equation for the molar refraction was used[8]

$$\frac{1}{\rho}\frac{n^2-1}{n^2+2}=\frac{R}{M} \qquad \ldots . [5]$$

where ρ is the density, M is the molecular weight, and R is the molar refraction, both independent of temperature. For simplicity, all calculations were made for $\rho = 1{\cdot}45$ g/cm³, the density[9] of $B_2O_{3(liq)}$ at *ca.* 1 500° K.

With the refractive indices so determined, the tables of Penndorf[5] were utilized to construct a theoretical scattering curve, with the ordinate $\log Q/(n-1)^2$ and the abscissa $\log x$, which is the curve shown in *Figure 2*. The straight line in *Figure 2* represents equation 1, the Rayleigh scattering expression, and is shown to illustrate the difference between the simple theory and the accurate Mie theory. The curve is a composite in the following sense. As pointed out above, $Q/(n-1)^2$ is not quite independent of n. However, preliminary experiments, using wavelengths from 2 500 to 6 000 Å, had shown on what parts of the curve the data for the different wavelengths should fall. Thus, the particular values of $Q/(n-1)^2$ used in plotting *Figure 2* were those appropriate to the wavelength involved, i.e. 2 500 Å at large x (2 to 3) and 6 000 Å at small x (up to about 0·8). A smooth curve was then made to connect all the points. Actually this last refinement is almost insignificant on the scale of the figure.

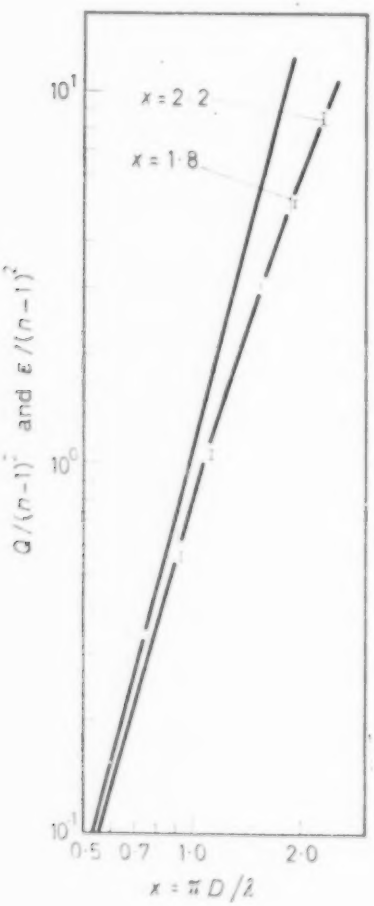

Figure 2. Theoretical scattering curves. The straight line is for Rayleigh scattering, and the curved line for $B_2O_{3(liq)}$ particles, derived as described in the text

Having constructed *Figure 2*, data were reduced by plotting the experimental $\log \varepsilon/(n-1)^2$ against $\log 1/\lambda$ on a piece of translucent graph paper and sliding it over the theoretical curve until a match was observed. Once a match was achieved, the value of $x = \pi D/\lambda$ was read off, from which D could be calculated. This value was then combined with the value of $Q/(n-1)^2$ read off the theoretical curve for that value of x, and N calculated by equation 3. The total volume and mass of $B_2O_{3(liq)}$ could then be calculated easily.

Errors

Apart from the problem of attaining a decent cloud of particles to work on, two sources of error need discussion: the assumption of uniform particle size, and our ability to make extinction measurements accurate enough to carry out the curve matching.

The first will only be discussed qualitatively. It is highly probable that the particles are not actually all the same size. The method discriminates against small particles and, in effect, measures only the larger ones since they scatter more effectively, roughly proportional to D^4. On the other hand, the mass of boron oxide per particle is proportional to D^3, so that in order to determine how much material has condensed it is only necessary in the first approximation

to count the large particles. This, in effect, is what the method does. By the same token, it is probably inappropriate for studying the very small particles that first appear out of the gas phase. This is true even if these particles do have the same diameter, since all that will be observed is Rayleigh scattering, and the experimental curve will be a straight line and could be fitted to the theoretical curve over a wide range of x.

As to the accuracy of the measurements, the extinction coefficient, ε, is given by

$$\varepsilon = (1/l) \ln (I_0/I) \quad \ldots . [6]$$

where l is the optical path, I_0 is the incident intensity, and I the transmitted intensity. If we let δ be an error in a parameter we have

$$\frac{\delta\varepsilon}{\varepsilon} = \frac{1}{\ln I_0/I}\left[\frac{\delta I_0}{I_0} + \frac{\delta I}{I}\right] \quad \ldots . [7]$$

The quantities in the brackets are essentially the noise-to-signal ratios, and were generally 0·01 to 0·02 for weak absorption ($I_0/I = 1{\cdot}1$ or so). For strong abosrption ($I_0/I = 100$) the second was as high as oil. Thus, for weak absorption $\delta\varepsilon/\varepsilon$ might be 0·2 and for strong absorption 0·02. Most of the work involved intermediate to strong absorption where the errors were ten per cent or less in ε, and since what is plotted was log ε, this is not too large. Actually, in the curve fitting it was found that at best the parameter x could only be determined to 10 to 20 per cnt, a value not inconsistent with the above conclusions.

These considerations are also illustrated in *Figure 2*. The data consist of a set of four points, and in the figure they are plotted twice; once by putting the 2 500 Å point (largest x) on the curve at $x = 2{\cdot}2$, and again at $x = 1{\cdot}8$. The vertical heights of the data points indicate the expected uncertainty, according to equation 7. The set matched at $x = 2{\cdot}2$ have horizontal marks at the top and bottom, and those matched at $x = 1{\cdot}8$ do not have marks. It can be seen that the higher wavelength points fall off the curve by a little more than the experimental uncertainty. In this particular case the best match occurred at a value of x (at $\lambda = 2\,500$ Å) of 2·0, but this could probably be equally well taken as 1·9 or 2·1.

Results

In *Table 1* are given the results for what is felt to be the most reliable run. In addition to the

Table 1

z mm	x	Q	$10^5 D$ cm	$10^{13} N$ cm^3	$10^5 \rho$ g/cm^3	t msec	% condensed
2	1·5	0·52	1·20	0·23	0·31	3·5	30
4	1·7	0·72	1·35	0·184	0·35	10·5	34
6	1·9	0·94	1·51	0·164	0·44	18·0	43
10	2·1	1·24	1·69	0·179	0·65	32·0	64
12	2·4	1·74	1·91	0·127	0·69	46·0	69
			(at equilibrium)		1·02		100

symbols defined earlier, z in *Table 1* denotes distance from burner, t is the time from the flame and ρ is measured in g $B_2O_{3(liq)}$ per cubic centimetre of gas. The last column is based on the computed equilibrium condition where there is $1{\cdot}02 \times 10^{-5}$ g $B_2O_{3(liq)}$ per 1 cm^3 of gas. This run was made with a TMB–air flame of equivalence ratio 1·10, burning on a ·7 cm diameter burner at a cold gas (25° C) velocity of 5·1 cm/sec. The time from the flame, t, was computed from z, the cold gas velocity, the temperature rise, the mole number change, and the assumption that the hot gas column cross section remained constant. The flame gas temperature, measured by sodium D line reversal about 2 or 3 mm from the burner, was 1 500° ± 50° K. *Table 2* gives in part the calcu-

Table 2

Component	*Mole fraction of the gas for* (a) *No condensation*	(b) *Equilibrium*
HBO_2	0·0415	0·0064
$B_2O_{3(g)}$	0·0007	0·0000145
H_2O	0·158	0·180

lated composition of this mixture (at 1 500° K) both for equilibrium and for the pseudo-equilibrium which would prevail if no condensation had taken place. At equilibrium both of the reactions

$$2HBO_2 \rightleftharpoons H_2O + B_2O_{3(g)}$$

$$B_2O_{3(g)} \rightleftharpoons B_2O_{3(liq)}$$

were assumed to take place, but for the no-condensation pseudo-equilibrium only the first one was taken into account. For these calculations the recent thermodynamic data of D. WHITE *et al.* were employed[10].

From *Table 1* it can be seen that although the changes from point to point are irregular, there is a definite trend in that in the early part of the process there are a relatively large number of small particles and at later times a smaller number of large particles. In addition to this, there is apparently a further increase in the amount of material condensed. This behaviour was generally observed in all of the runs made. Apparently most of the boron oxide has condensed by the time the first measurement is made, and after this the principal effect appears to be an agglomeration of small particles into larger ones.

The final size reached in all of the experiments was in the range indicated in the table, about 0·2 micron. As indicated previously, the method as used probably could not reliably measure the size of particles smaller than 0·1 micron. Thus, this method turns out to have only limited usefulness, although it has been able to throw some light on the process.

One final point should be made. The scattering measurements are entirely independent of any knowledge of the composition of the flame gases. Thus, the fact that the amounts of boron oxide condensed calculated from the scattering data agree fairly well with the amounts to be expected from thermodynamic considerations suggests that the results have some validity.

In conclusion, the author would like to thank Drs Bruno Zimm and Fraser Price for helpful discussions of scattering theory, and Mr William Crotty and Mr William Foss for aid in the experimental work.

References

[1] KASKAN, W. E. and MILLIKAN, R. C. *J. chem. Phys.* 1960, **32**, 1273; *Eighth Symposium (International) on Combustion*, to be published
[2] SETZE, P. C. *Nat. Adv. Comm. Aero., Wash., RM E55I20a*, April 1957
[3] KASKAN, W. E. *Combustion & Flame*, 1958, **2**, 229
[4] VAN DEHULST, H. C. *Light Scattering by Small Particles*. Wiley: New York, 1957; especially Chapter 7
[5] PENNDORF, R. B. *Geophys. Res. Pap. No. 45*, part 6, Air Force Cambridge Research Center; Table A1, p 53
[6] MOREY, G. W. *Properties of Glass*, p 371. Reinhold: New York, 1954
[7] See, for example, GLASSTONE, S. *Textbook of Physical Chemistry*, 2nd ed., p 533. Van Nostrand: New York, 1946
[8] See, for example, GLASSTONE, S. *Textbook of Physical Chemistry*, 2nd ed., p 528. Van Nostrand: New York, 1946
[9] MACKENZIE, J. D. *J. phys. Chem.* 1959, **63**, 1875
[10] WHITE, D., MANN, D. E., WALSH, P. N. and SOMMER, A. *J. chem. Phys.* 1960, **32**, 481 and 488

Recent Developments and Notes

Hydrogen Flame Continuum

P. J. PADLEY, Department of Physical Chemistry, University of Cambridge, has described the application of flame-photometric techniques for the measurement of concentrations of hydrogen atoms and hydroxyl radicals in flames [*Trans. Faraday Soc.* 1960, **56,** 449]. The techniques used were those developed by T. M. SUGDEN and his co-workers [*Proc. Roy. Soc. A,* 1956, **235, 89**; 1958, **248, 238**; *Trans. Faraday Soc.* 1958, **54, 1855**].

A specially designed burner was used so as to give laminar-flow flames with a flat reaction zone when premixed hydrogen–oxygen–nitrogen flames were burned above it. The particular spectral feature of these flames that was studied is the continuum that extends over the region 2200 to 6000 Å, and measurements of its intensity were made near 4900 Å. As a result it is very strongly suggested that the origin of this continuum which gives these flames their pale-blue appearance, is due to the radiative association

$$H + OH \longrightarrow H_2O + h\nu$$

The Oxidation of Propane

The general features of the low-temperature oxidation of ethane and propane were the subject of a paper about two years ago by J. H. KNOX, Department of Chemistry, University of Edinburgh [*Trans. Faraday Soc.* 1959, **55,** 937]. The work described and other earlier work on this subject concentrated mainly on the oxygenated products from the later stages of the reactions. More recently this investigator has used gas chromatography to determine with considerable precision the yields of different products from the very early stages of reaction in the oxidation of propane [*Trans. Faraday Soc.* 1960, **56,** 1225].

It was found that the initial conversion of propane at 318°C is 75 per cent to propylene, 5 per cent to ethylene and 10 to 20 per cent to carbon monoxide. These values are almost independent of oxygen pressure over a 20-fold range. The main initial reaction is regarded as being best represented by the HO_2 radical chain defined in two reactions:

$$C_3H_7 + O_2 = C_3H_6 + HO_2$$

$$C_3H_8 + HO_2 = C_3H_7 + H_2O_2$$

The yield of propylene in oxygen-rich mixtures reaches a maximum which is independent of oxygen pressure and nearly independent of added propylene pressure.

A high-temperature study of the oxidation of propane by J. W. FALCONER and J. H. KNOX [*Proc. Roy. Soc. A,* 1959, **250,** 493] showed that an important reaction in the early stages was the conversion of propane to propylene by an HO_2 radical chain. It is concluded, therefore, that an equilibrium is reached and that a change of mechanism occurs, the HO_2 radical chain giving way to a more complex multi-radical reaction in the later stages.

Trends in I.C.E. Developments

V. G. RAVIOLO, Executive Director, Engineering Staff, Ford Motor Company, Dearborn, Michigan, gave a talk last May at a meeting of the Automobile Division of the Institution of Mechanical Engineers, on automotive development trends in the U.S.A. [*Chart. mech. Engr,* 1960, **7,** 458]. In this talk the speaker considered first the likely market requirements of motor cars in the next decade and then the technical possibilities in the development of new engines, both of which must be taken into account in planning for the future and consequently give direction to research in the motor industry.

With regard to engine development, a new series of engines is coming from the speaker's own company, probably about 1965. Considerable progress has been made with a new gas turbine arrangement. This consists of a small compressor turbine combination supercharged by a low-pressure compressor, resulting in a high overall pressure machine. It includes

intercooling between compressor stages, a reheat burner between turbine stages and stationary exhaust heat exchangers. Component development is complete, the assembled engine has been on bench test for some time, and vehicle installation was expected before the end of 1960. It is believed that this turbine will be competitive in cost with low-volume, high-quality diesel engines.

There is considerable promise in the results of recent research on high-speed diesel engines. New developments in gasoline engines are likely in the use of a stratified charge. This may involve pre-combustion chambers in which a stoichiometric mixture will be spark-ignited and, in turn, fire a lean mixture in the main chamber. Another method would use a stratified charge in the main chamber by control of air and fuel flow. With either procedure fuel injection will almost certainly be used.

Coal Dust Explosions

In continuance of the investigations on the mechanism of coal dust explosions by the Safety in Mines Research Establishment, to which reference was made in these notes a few months ago [*Combustion & Flame*, 1960, **4**, 270], further work is briefly described in the latest annual report of the S.M.R.E. [*Safety in Mines Research 1959*; Her Majesty's Stationery Office: London, 1960]. Upward propagation of flame has been studied in reasonably uniform clouds of lycopodium dust falling through still air in a vertical tube of $2\frac{3}{4}$ in. diameter and the ratio of limestone to lycopodium dust necessary to give a 50 per cent probability of propagation at various lycopodium concentrations was determined. The results suggest that dust clouds, like gases, have both upper and lower limits of inflammability and the curve obtained is similar to those obtained by H. F. Coward and F. J. Hartwell in their investigation of the effect of the addition of carbon dioxide on the limits of inflammability of methane in air [*Saf.-i.-Mines Res. Bd Pap. No. 19*, 1926]. A tube of larger (6 in.) diameter has been designed for future work with coal dust, as propagation was not obtained in the $2\frac{3}{4}$ in. diameter tube previously used.

In regard to the aerodynamics of coal-dust explosions in a gallery, with ignition at the closed end, the speed of the shock wave preceding the flame has been deduced for given flame speeds and values of q, the energy released per unit mass of dust–air mixture, assuming that the explosion is fully developed so that the flame speed has reached a constant value. For each value of q there is one maximum speed at which the flame can propagate as a deflagration, but the value of q has little effect on the shock speed produced by a given flame speed. The considerable alteration of the maximum flame speed with the value of q, however, is in agreement with the observation that although stone dusting may not always stop an explosion, the explosion is less violent with stone dusting than without, corresponding to a reduced maximum flame speed.

Droplet Combustion in Turbulent Flow

The question as to whether molecular exchange or turbulent diffusion is the determining factor in the combustion of an oil droplet in a turbulent air flow has been considered by V. Ya. Basevich [*Zh. fiz. Khim., Mosk.* 1957, **31**, 7, 1619–1627; *Ref. Zh. Mekh.* 1958, **No. 8**, Rev. 8976]. By analysing the equations describing the combustion of a fuel droplet the author shows that the rate of combustion in turbulent flow is very little dependent on particle exchange. Evaluation of the ratio of the velocities of combustion of the droplet and of the fuel in the gaseous phase, in a stream of atomized liquid fuel, for different mechanisms of exchange (molecular diffusion, turbulent diffusion towards a solid wall, free turbulent diffusion), and comparing the results with experimental data, lead to the conclusion that free turbulent diffusion is qualitatively correct as a description of the process of mass exchange in the reaction zone of a burning droplet under such conditions; the postulate of molecular diffusion is not justifiable [O. V. Yakovlevskii; Courtesy *Referativnyi Zhurnal*, U.S.S.R., *Appl. mech. Rev.* 1960, **13**, 602].

A further contribution to this subject has been made by V. Ya. Basevich and S. M. Kogarko, Institute of Chemical Physics, U.S.S.R.

Academy of Sciences, Moscow, who read a paper at the Eighth Symposium (International) on Combustion, held at Pasadena, California, 28 August to 2 September 1960, on the factors influencing the probability of combustion of droplets of atomized liquid fuel in turbulent flow and determining the absolute value of the probability under different conditions.

Tetramethyl Lead Additive

In a paper presented to the Summer Meeting of the Society of Automotive Engineers in Chicago, R. H. PERRY, Jr, C. J. DIPERNA and D. J. HEATH, of the Socony Mobil Oil Company, gave an account of their investigations of the properties of tetramethyl lead (TML), a new additive for the improvement of motor gasoline anti-knock quality which was announced about a year ago [*Inst. Petroleum Rev.* 1960, **14**, 266].

It was pointed out that in the past ten years there has been a considerable increase in the proportion of catalytic reformate gasoline produced at the expense of that produced by straight-run and thermal processes. This has made possible most of the increase in motor gasoline octane numbers that has occurred during this period. It has been found, however, that gasolines containing large percentages of reformate have much lower road octane numbers than were predicted from the research and motor method ratings, especially in cars with manual transmission.

The best method of reducing the depreciation in road octane number is considered to be that of increasing the research octane number of the lower boiling fractions. For this purpose TML was found to be the most effective additive, since it has the lowest boiling point of a large number of lead alkyls tested and, in the induction manifold, is distributed with the lower octane fractions of the gasoline.

Liquid Fuel Combustion

A residential course on 'Liquid Fuel Combustion' was held in the University of Sheffield from 10 to 16 July last, under the direction of Professor M. W. THRING, head of the Department of Fuel Technology and Chemical Engineering. The attendance at the course was about 200, and a considerable number were from other countries. Discussions, demonstrations and experimental work in the laboratories of the Department formed an important part of the course and there was a comprehensive exhibition of oil burners, furnaces, boilers, ovens and accessories.

Professor THRING, in his contribution on present day views of the physics of oil burning, drew attention to the significant values in experimental investigations of industrial oil flames. These include: (*i*) flame or unburnt gas velocity distribution over the whole cross section of the combustion chamber, (*ii*) macromixing, that is the fuel/air ratio at any given point in the combustion chamber, (*iii*) micromixing, that is the degree of fuel–air mixing, achieved by very extensive atomization of the fuel and intensive turbulent mixing, (*iv*) the mean time of duration of the fuel in the combustion system, (*v*) the distribution of the actual times of duration over particular cross sections of the combustion chamber, and (*vi*) recirculation of the combustion products which plays an important part in the ignition of incoming fuel and in increasing the temperature of the fuel–air mixture.

P. J. FOSTER and I. A. MCGRATH, University of Sheffield, dealt with the emissivity of hydrocarbon flames. Soot giving rise to the continuous emission of such flames may arise in two ways, from hydrocarbons in the gas phase, or from the carbonization of liquid fuel droplets. Carbon particles of the first type are always spherical with average diameters between 400 and 550 Å, as have particles withdrawn from similar flames in the experiments carried out at IJmuiden. Cenospheres, arising from the carbonization of droplets are large and hollow, and are only formed from residual fuel oils. For small sizes of particles the emissivity appears to be dependent on the soot concentration and not on the particle size.

In a contribution by G. WHITTINGHAM, B.P. Trading Co. Ltd, London, on boiler deposits and corrosion, attention was drawn to the need for further knowledge of the behaviour of ash constituents in combustion gases, particularly

in view of the increasing use of residual fuel oil in steam raising and electricity generating plant, especially in boilers of advanced superheat and low gas exit temperatures. The fundamental solution to the deposit problem is regarded as ultimately to be found in the control of sulphur trioxide formation because of its rapid reactions in the high and low temperature zones. The temperatures concerned in these zones are respectively above 600°C and below 150°C, and deposits differ widely in physical and chemical characteristics according to the zone in which they occur.

Experimental Boiler for Fuel Oil Combustion Research

For some years The British Petroleum Co.'s research organization has been engaged on problems of high and low temperature corrosion in boilers. At the same time it has also been investigating the associated problem of air pollution from boiler stacks. The initial research into these problems was carried out at the Company's Research Centre at Sunbury-on-Thames and was followed by trials on full-scale boilers made available by industries in the U.K. and other European countries. The results of the work were reported in a paper read at the World Petroleum Congress held in 1959.

These investigations have contributed towards improvements in superheaters and superheater supports. The extensive study of low temperature corrosion problems has led to a method of controlling the effects of acid on heat exchangers by the use of ammonia gas injected into the low temperature zone of the flue gases.

It has become clear, however, that complementary to these trials experiments on a full-scale basis would have to be conducted with a boiler installation under the complete control of the research team. The Company therefore decided to install its own water-tube boiler on a site adjoining its refinery on the Isle of Grain in Kent. This location enables purified feed-water and fuel-oil of the required specification to be drawn from the refinery, and the steam produced to be piped back to the refinery system for use. The boiler, designed to BP specifications by Babcock and Wilcox, is capable of producing 20 000 lb of steam per hour at 350 lb/in² gauge and 1 200°F when operating under high temperature conditions, or 30 000 lb per hour at 175 lb/in² gauge and 480°F under low temperature conditions. It is of a specially designed two-drum water-tube type, with an economizer, air heaters and flue-gas recirculation system.

One of the most important amongst the problems to be studied in this plant is that relating to the conversion of boilers from firing with solid fuel to the use of liquid fuels. In doing this there is a change in the heat transfer characteristics within the boiler since fuel-oil flames give an increase in heat radiation and a reduction in the gas mass flow when compared with the combustion of solid fuel. The consequent increase in the evaporation rate from the radiant generator section of the boiler leads to difficulties in attaining the required superheated steam temperature. This has been found in new boilers arranged for oil firing, due to the design of boiler being based on data from solid fuel-fired plant.

Fire Resistance of Prestressed Concrete

In a paper read in October last to the Institution of Civil Engineers, L. A. ASHTON, Joint Fire Research Organization, and S. C. C. BATE, Building Research Station, presented the results of an investigation of the fire-resistance of prestressed concrete beams with post-tensioned cables [*Proc. Instn civ. Engrs*, Sep. 1960, **17**, 15]. The main object was to obtain information on the design of beams for buildings of high fire risk, where a fire-resistance of four hours would be required for structural elements.

Their results show that failure of a prestressed concrete beam carrying its design load will occur when the mean temperature of the prestressing steel reaches about 400°C. For normal forms of such beams used in floor construction, resistance is governed by the protection given to the prestressing steel. A fire-resistance of one hour is obtained when the cover of concrete to the steel is 1½ in., and for longer periods of fire-resistance, secondary reinforcement is necessary to hold the concrete cover in place, a cover of 4 in. giving a resistance of four hours.

A substantial increase in the fire-resistance of a beam is obtained by the application of some form of insulation to its exposed surfaces, provided that the adhesion of the insulation to the concrete is ensured for the whole of the fire period. Precast slabs of lightly reinforced vermiculite concrete used as a mould lining when casting the beam were found to be equivalent in insulating value to about twice their thickness of concrete.

Gas-Oil Flames for Metal Heating

An investigation has been carried out under the direction of The Gas Council, primarily to study some of the merits claimed for the combined town gas–fuel oil flame for heating ferrous metals. The results obtained have also enabled some conclusions to be drawn as to the relative merits of straightforward town gas and fuel oil for this purpose. The work was described at the Autumn Research Meeting of the Institution of Gas Engineers in November last, by E. A. K. PATRICK and N. G. PATEL, Watson House, London Research Station [*Res. Commun. No. GC67*. The Gas Council: London, 1960].

The effect of types of fuel with differing excess air and times of heating on the quantity and adherence of scale formed on mild steel and alloy steels, was examined. Decarburization of steel surfaces was also considered. A furnace was used whose size and flue outlets could be varied and the combination gas-oil burner was of the self-proportioning type.

It was found that with a 20 ft³ combustion chamber at above 1 000°C the low-pressure air blast oil burner was capable of burning 200 and 900 sec fuel oil with less than 2 per cent excess air. When the combustion chamber conditions are less satisfactory, more excess air is necessary and in such circumstances the addition of town gas to the fuel oil flame can reduce the excess air and help to stabilize the flame.

With excess air values below 10 per cent, town gas produces less scale on both carbon steels and nickel–chromium–molybdenum alloy steel than oil; above 30 and 10 per cent respectively this is reversed. With excess air below 10 per cent, town gas produces significantly less adherent scale with both types of steel. The mixed flame, however, behaves substantially as the 100 per cent fuel oil flame with carbon steels, and produces more scale on the alloy steels than either of the single fuels when the excess air is below 10 per cent. In most of the tests town gas was found to give less decarburization than fuel oil.

From the point of view of metallurgical effects, there is little evidence to support the suggestion that disproportionate advantages can be attained by the addition of up to 15 per cent of town gas to an oil flame.

International Flame Research Foundation

In 1956 research began on the combustion and heat transfer from pulverized-fuel flames by the International Flame Research Foundation on a special furnace constructed at their Research Station at IJmuiden, Holland. Four papers have now been published describing the work of the first two trials [*J. Inst. Fuel*, 1960, **33**, 366–402]. The first of these is a summary by G. G. THURLOW, of the work carried out up to 1959, and a detailed account of the first Performance Trial on Coal (P.T.C.I) and the first Combustion Mechanism Trial on Coal (C.M.C.I) is given in another paper, by E. H. HUBBARD. In P.T.C.I the variables studied were the primary air velocity, the burner nozzle diameter being constant; secondary air velocity; coal fineness; and water-cooling, in order to obtain a general picture of the relative importance of these variables. The results show that the velocity of the secondary air is only important when the primary air quantity is below a certain level. High levels of primary air quantity are accompanied by lower flame radiation, due to temperature dilution by air during the early stages. Decreasing the coal size increases the rate of combustion, particularly of the coke residue, and increases the flame radiation. The introduction of a thermal load into the combustion chamber reduces the rate of combustion and lowers the general level of flame temperature. The C.M.C.I compared the aerodynamics of a coal flame as used in a cement kiln with the present theories of free and enclosed turbulent jets, and shows that in this slow mixing flame, combustion of the

volatile matter is governed by turbulent diffusion, but that combustion of the residue is slower and probably depends on molecular diffusion of oxygen to, and removal of the products of combustion away from, the particle surface. The emissivity of a pulverized-coal flame approaches unity for over half its length and this means that any changes in flame-radiation properties must come as a result of changes in the temperature of the outer burning sheath.

After improvements had been made in flame alignment and stability C.M.C.II and P.T.C.II were carried out. In the first of these trials the secondary air velocity was studied in order to find the readings necessary to characterize a pulverized fuel flame, and in the second of these trials the volatile matter and ash content of the coal, and the primary air quantity and its velocity, were the variables studied. The secondary air velocity was low. In P.T.C.III, carried out in February 1960, the primary and secondary air velocity, the primary air quantity and its humidity were investigated, the purpose of this trial being to study the burner variables, especially where the momentum of the secondary air is higher than that of the primary air. These conditions covered some of those met with in the boiler industry.

New Laboratories at the Fire Research Station, Boreham Wood

Lord Hailsham, Minister for Science, officially opened new buildings and laboratories at the Fire Research Station, Boreham Wood, Hertfordshire, on 4 November. The new buildings include chemical engineering, hydraulic and radiation laboratories, as well as administrative offices and have cost about £300 000. These additions, together with the older buildings, some of which date back to 1935, when the Fire Testing Station was built on part of the present site by the Fire Offices' Committee, make the Fire Research Station the largest and best equipped organization of its kind in the world.

The Station is controlled by the Joint Fire Research Organization, an organization of the Department of Scientific and Industrial Research and the Fire Offices' Committee, set up in 1946, in which Government and the Fire Insurance Companies are equal partners. The Director of the Station is Mr D. I. Lawson, and there is a total staff of 136.

The work of the Station is organized in five sections. The Operational Research and Intelligence Section deals with the details of about 120 000 fires a year. The work of this section provides a background for planning the research programme as a whole and for the administration of fire protection. The Ignition and Growth of Fire Section studies the physical aspects of ignition, combustion and heat transfer, using models, and carrying out work on the development of fires in the open. The Building Materials and Structures Section studies building materials under fire conditions to obtain basic data for the design and protection of structures. The Chemistry and Chemical Engineering Section is concerned with fires and explosions involving gases, vapours, flammable liquids, dusts and the use of inhibiting agents and inert atmospheres. The Extinguishing Materials and Equipment Section deals with the methods of applying water, foam and dry powder, and testing fire-fighting equipment.

Combustion Oscillations

A. M. Brown, University of Sheffield, gave an account at the residential course on 'Liquid Fuel Combustion' held in the University of Sheffield [see page 101] of oscillations in combustion systems. Non-premixed turbulent diffusion flames are characterized by flame noise and by diffuse boundary regions. Within these flames there are often separate locations of fuel–air mixtures, consequent upon the turbulent conditions, and at these sites there may be irregular local mixing rates and sudden rapid ignition and combustion. Sound waves thus arise and can become the source of other types of oscillations in the combustion system. In industrial combustion equipment the frequency is between about 60 to 200 c/s and these oscillations may reduce the efficiency of the combustion system, and upset the effectiveness of regulating apparatus. They are often

associated with increased soot formation in boilers and may eventually lead to extinction of the flame. There may also result resonance effects between the flame and combustion space which are influenced by the fuel/air ratio, pressure difference between fuel and air at the entrance to the combustion chamber, and the geometry of the chamber. Means of prevention may be looked for in two directions: by increasing the damping of such systems, for example, by increasing the air resistance in the lead-in equipment or by enlarging the combustion chamber, and also by reduction of the ignition delay time so as to increase the oscillation frequency and the effect of the damping factor.

Combustion of Liquid Fuel Droplets

An account of investigations in the University of Sheffield on the combustion of single droplets of fuel was given by E. G. MASDIN, now of Shell Research Ltd, Thornton, Cheshire, to the residential course on 'Liquid Fuel Combustion' held in the University of Sheffield in July 1960 [see note above]. The experimental techniques used were of three kinds: (*i*) single droplets, 500 to 1 500 microns in diameter, supported from fine silica filaments; (*ii*) fuel supplied to the surface of a supporting sphere at the same rate as it is being burned; (*iii*) studying a freely moving droplet which is falling or being projected through a furnace. In all these methods the droplet diameters are greater than those met with in practice and therefore results must be extrapolated in order to apply them to the combustion of droplets in a burner spray.

The important variables which affect droplet combustion are droplet size and composition, the ambient temperature and gas composition, and the relative velocity of the droplet and the gas, and these were discussed by the author, as well as the three phases through which a droplet may pass when injected into a combustion chamber, the pre-ignition period, the combustion of the fuel vapour evolved from the droplet, and with residual oils, the combustion of carbonaceous material (cenospheres) which is formed from these fuels during the second stage.

It is shown that it is possible to use certain equations to predict values of the burning constant which are close to those determined experimentally by the suspended droplet method, even though there is uncertainty of the appropriate thermodynamic data which apply and also about the effects of natural convection on the shape of the flame. A linear relationship between the square of the droplet diameter and time is found to apply generally to the evaporation period during the combustion of liquid fuel.

Soot in Oil-fired Furnaces

P. DRAPER, Shell-Mex and B.P. Ltd, London, discussed the formation of soot flakes in oil-burning furnaces, in a contribution to the residential course on 'Liquid Fuel Combustion' held in the University of Sheffield in July 1960 [see note above]. These flakes are formed by the agglomeration of carbon particles due to the presence of acidic moisture. They vary in size from 0·8 to 25 mm, the average diameter being 3 mm. The free carbon can be formed in three different ways: (*i*) by impingement of oil drops on a heated surface, resulting in carbonization; (*ii*) by incomplete combustion; (*iii*) by thermal cracking of oil drops during the burning of heavy fractions of certain residual oils.

Unless the carbon particles formed in one or more of these ways undergo agglomeration to larger flakes they are not objectionable except as regards atmospheric pollution. The actual process of soot flake formation begins as soon as condensed constituents of the combustion gases are deposited on the carbon particles and they come into contact one with another. An important role is played in this process by the presence of sulphur trioxide in the combustion products. The author made reference to an investigation on the use of aluminium sheath for surrounding metal chimneys, whereby the emission of smuts is prevented and corrosion reduced to a very small amount [H. A. BLUM, B. LEES and L. K. RENDLE, *J. Inst. Fuel*, 1959, **32**, 165]. This investigation was carried out jointly by the British Launderers' Association and British Petroleum Company Ltd.

Kinetics of Methane Oxidation

Further work has been carried out on the kinetics of methane oxidation by E. M. MAGEE, in his studies at the Humble Oil and Refining Company, Baytown, Texas [*J. Amer. chem. Soc.* 1960, **82**, 3553]. In a previous communication the author showed that proposals of mechanisms for the slow reaction of methane with oxygen do not predict the correct dependence of the maximum formaldehyde concentration on the oxygen concentration at 815°C [*ibid*, 1959, **81**, 278; see *Combustion & Flame*, 1959, **3**, 256]. The work described in the present paper continues the attempt to find the analytical relationships of the reaction variables. The experiments were carried out by the flow method in a quartz reactor at 815°C as in the previous work, with the purpose of determining the effect of methane concentration on the course of the reaction.

The results show that the maximum in the formaldehyde/time curve is proportional to the methane only at very low concentrations, whilst at higher concentrations the formaldehyde maximum is independent of methane. The rate of reaction at the formaldehyde maximum first decreases with increasing methane and then increases. At high concentrations of methane the reaction proceeds smoothly, but at low concentrations the reaction exhibits a discontinuity, after the formaldehyde maximum has been reached, after which the methane is completely consumed. There is a discussion of the results and their relation to other work.

Aeronautical Research

Professor A. J. MURPHY, Principal of the College of Aeronautics, Cranfield, delivered a lecture early in 1960 before the Royal Aeronautical Society on the research which is being undertaken at the College and this has recently been published [*J. Roy. aero. Soc.* 1960, **64**, 579–606]. In the Department of Aircraft Propulsion research covers a wide field, ranging from piston engines through gas turbines and ram-jets to rockets of various types.

For research on rockets, a rocket motor test bed for rockets up to 3000 lb thrust was brought into operation in 1955. So far the bed has been operated with liquid propellant rockets of about 2000 lb thrust, and the type used is a small one, with the combination of hydrogen peroxide and kerosine as the propellant. Investigations have been made on the effect of combustion chamber length; the reduction in efficiency on making the chamber too short; the effect of varying the quantity of silver-plated gauzes used to decompose the hydrogen peroxide before its reaction with the kerosine; and the effect of deliberately lowering the injector efficiency. A useful pressure transducer was produced to measure fluctuating pressures. For investigating flow patterns with a rocket combustion chamber, the smear technique, using zirconia, has given useful results. Colour contours on the zirconia smear were found which were thought to indicate contours of composition of reactants within the chamber. A theoretical investigation is also being made into the problem of high frequency pressure oscillations in solid propellant rocket motors.

In the field of fuel and combustion research, the problem of local spontaneous ignition in spark-ignition piston engines, by heated surfaces, is being investigated. A surface-ignition flow rig has been constructed in an attempt to separate three superimposed effects which complicate the results of engine tests. These are the tendency of the fuel to form deposits, the tendency of the deposits to glow, and the tendency to ignition induced by these glowing deposits or by other overheated surfaces. Preliminary work is in hand on pre-ignition in engines, especially with regard to the relationship between, on the one hand, shape of the heated surfaces and the nature of the local mixture flow, and, on the other hand, the ignition delay. The effects of engine speed are also being examined.

Growth of Fire

The Chairman of the Fire Research Board, Professor A. R. J. P. UBBELOHDE, F.R.S., in his report for 1959 makes special mention of the active use that is being made of the Models Laboratory which was completed at the Fire Research Station in 1958. The wind-producing apparatus in this Laboratory is completed and provides facilities believed to be unique in the

field of fire research [*Fire Research 1959:* Report of the Fire Research Board with the Report of the Director of Fire Research. Department of Scientific and Industrial Research and Fire Offices' Committee: Her Majesty's Stationery Office; London, 1960].

In the researches on the growth of fire, a significant advance has been made in the modelling of building fires. The report shows that the rate of burning and the maximum temperature in fires is affected by the window openings for burning compartments of various sizes. The flame height and radiation from windows is shown to be amenable to scaling within the limits of the experiments that have been carried out. Eight countries abroad have combined to extend this work of compartments of various shapes and with different window openings. Some of the results are already being used in the drafting of building regulations for Scotland and it seems likely that they will provide a scientific background for the fire grading of buildings within the next few years.

The experimental work undertaken in conjunction with Colt Ventilation Ltd, to determine principles for the design of roof vent installations, has been extended to deal with the effect of roof venting on fires. Two models have been used, representing one bay of a factory separated from the rest of the building by a fire curtain, extending part of the way from the ceiling to the floor. The first experiment has given results from which a theory has been developed and enables a calculation to be made of the depth of curtain and area of vent required to prevent hot gas being discharged beneath the curtain when a factory bay contains a fire which is either localized or spreading slowly.

The second study has concerned the effect of opening a vent on the speed at which a fire progresses. The rate of burning of wooden cribs inside the model has been measured. Opening a vent increases the rate of burning if this was initially restricted by the air flow, but it also releases smoke and by increasing the efficiency of burning, improves visibility and assists fire-fighting.

Air Pollution and People

A special report on 'Air Pollution' has been published in a recent issue of *Power* [McGraw-Hill: New York and London, December 1960, 69–113]. The report is the outcome of a year's research by the editors for information from source materials, on-the-spot investigations, and interviews with authorities. There are four sections, the first of which is devoted to the effects of air movements and weather conditions. Then the ways in which pollution occurs are examined. In the third section the effects of air pollution on social and economic life are dealt with and a model approach to planning a control programme for a typical city is set out. In the final section an outline is given of the design and location necessary for new industrial plants in order to ensure the elimination of pollution, and of how problems of existing plants may be solved.

The report concludes that people are the key to the solution of the problem of air pollution, and public education is an integral part of any pollution-control programme. To this end this report contributes considerably, especially by means of a large number of effective diagrams.

Evaluating the Explosibility of Dust

A report describing the equipment and test procedures used by the U.S. Bureau of Mines in laboratory studies on the explosibility of dusts, together with a brief history of these studies, has recently been published [*Report of Investigations No. 5624*, 1960]. The authors are H. G. Dorsett, Jr, M. Jacobson, J. Nagy and R. P. Williams. Through this concise description of current methods it is hoped to facilitate the interpretation of data previously published and those proposed to be published on the numerous mineral, agricultural and industrial dusts that have been studied.

The equipments described include the Godbert–Greenwald furnace for determining the ignition temperature and relative flammability of a dust cloud, and of a dust layer by a modified form of this furnace; the Hartmann apparatus for determining the minimum electrical energy for igniting a dust cloud and also the lower explosive limit of a dust; an

apparatus for a similar determination in respect of a dust layer; a Hartmann tube for determining pressure and rates of pressure rise in a dust explosion; and an apparatus for determining ignitability of a dust cloud in a controlled atmosphere using an induction spark igniting source.

Refractories in the Iron and Steel Industry

In a review of the refractories industry during 1960, Professor J. WHITE, Department of Refractories Technology, University of Sheffield, mentions the continued increase in demand for basic refractories in the iron and steel industry, as a notable feature of the year [*Sheffield Telegraph*, 31 December 1960]. This is accounted for mainly by the trend towards higher operating temperatures, particularly where oxygen is used, to obtain higher production rates and higher efficiency in the open hearth process. All-basic construction of open hearth furnaces is increasing considerably, with roofs being made of chrome–magnesite or magnesite–chrome bricks in conjunction with basic walls, ports and uptakes. The upper structures of such furnaces are also being made with basic bricks to an increasing extent and magnesite is somewhat replacing dolomite for hearth construction in both open hearth and electric arc furnaces when oxygen is used. It appears evident that a major part of the new steelmaking capacity to be provided in the U.K. in the next few years will employ oxygen-blowing processes of one kind or another, and this will favour the trend towards the use of basic refractories. The consumption of silica bricks, however, rose appreciably during the first half of the past year and silica roofs are still used on over 80 per cent of the open hearth furnaces in the U.K.

Influence of Secondary Atmospheric Moisture upon Carbon Monoxide Flames

D. J. SEERY and H. B. PALMER wish to make it clear that line 13, column 2, page 292 of the December 1960 issue of *Combustion and Flame* should read: 'hydrogen gas. With the 150 p.p.m. gas, we'. It is regretted that this printer's error occurred in the final preparation of the Journal for machining.

The Mechanics of the Formation and Adhesion of Deposits arising from the Combustion of Liquid Fuel

On Wednesday, 8 March, five papers sponsored by the Internal Combustion Engines Group Committee will be read at the Institution of Mechanical Engineers, 1 Birdcage Walk, London, S.W.1, under the general title above. P. F. WHELAN will review the 'Mechanisms proposed to Explain Carbon Formation during Combustion of Fuels'. K. H. GRAY will discuss 'Combustion Deposits in Compression-ignition Engines'. K. CAMPBELL and S. T. GRIFFITHS will speak on 'Combustion Chamber Deposits in Spark-ignition Gasoline Engines', followed by A. LEWIS on 'Ash Deposits in the Gas Turbine'. The final paper will be 'Oil-fired Boilers' by G. WHITTINGHAM. A general discussion of these papers is planned and a small exhibition of modern types of apparatus dealt with in the papers has been arranged.

W. A. KIRKBY

FUEL

The following *Notes* were published in *Fuel* in January and may be of interest to readers of *Combustion and Flame*:

Intermittent heating and fuel saving

Russian research on coke oven heating

Measurement of heat of combustion

Working of the Clean Air Act

while the March issue of *Fuel* carries *Notes* dealing with:

Atmospheric pollution research

Accuracy of instruments for measuring air pollution

Publications

ENTHALPY–ENTROPY CHART FOR AIR AND COMBUSTION GASES

O. Lutz and F. Wolf†. 2nd ed. revised and enlarged by O. Lutz and W. Lohse. With handbook, 18 *pp.* Berlin: Springer, 1959. *DM* 7.50

The *hS* chart for dry air has been re-drawn and extended to higher temperatures and pressures on the basis of more recent experimental work. The authors have superposed a supplementary grid whereby the thermal properties of exhaust gases from normal hydrocarbon fuels can be found from the same chart. The new chart will be of importance and considerable use to specialists in the field of liquid fuel motors.

Lutz's method of correlating the heat capacities of similar gases through a characteristic B value is explained and illustrated very briefly in the handbook. It might have been considered worthwhile expanding the explanation of the method for the benefit of non-specialists. Similarly, the two illustrative examples, useful as they are, would be more helpful if they were explained more fully. The use of the chart for 'exotic' fuel additives is discussed and illustrated briefly for pentaborane. The B corrections for boron additions are set out in appendix curve 5. The authors say that similar graphs can be prepared for other additives. Here again the brevity of the discussion might be considered unfortunate by people other than specialists.

Two minor errors occur in the handbook, the gas constant R is missing from $R \ln (p_1/p)$ in equation 4 and the caption of appendix curve 1 should obviously read B_{H_2O} and not B_{N_2O}. Aside from these, however, the use of lower case letters to indicate the weight composition of fuels and upper case letters for the percentage weight composition seems incongruous. There can be no objection to the use of the upper case to represent elements and compounds, especially when a Gothic script is employed for the thermodynamic properties.

S. H. Bransom

THE CHEMISTRY OF PROPELLANTS

Edited by S. S. Penner and J. Ducarme. Oxford: Pergamon; AGARD, *xiv*+651 *pp.* 70s

This book contains a number of invited papers and prepared comments on the chemistry of propellants and is a comprehensive record of a meeting held in Paris in June 1959 under the auspices of the AGARD Combustion and Propulsion Panel. Although one section deals with propellants for air breathing engines, the majority of the work is taken up with rocket propellants and the topics discussed include availability, theoretical performance, experimental evaluation, the preparation and properties of liquid and solid propellants and the merits of high energy fuels. There are also sections dealing with nozzle flow and with deposits in jet engines and there is an edited version of a round table discussion on basic propulsion problems. In a way the book presents a snapshot of current knowledge and thought on propellants. It is not complete, however, and the information on solid propellants appears to be a little out of date because no doubt the authors were handicapped by either security or an unwillingness to divulge technical know-how. The overall view is reasonably accurate, and standing out prominently is the subject of high specific impulse which occupies much research and development effort at the present time. One paper suggests that this property may be over-emphasized and that the absolute necessity for using high energy propellants which have objectionable handling characteristics should be critically examined. Several of the papers contain excellent reviews of existing knowledge on basic problems such as chemical recombination reactions in high energy gas flow but the round table discussion which is stated to have been a highlight of the meeting is not fully reported and lacks the excitement of a verbal debate. A valuable feature of the whole work is the numerous references drawing attention to the appropriate sources in the literature.

W. G. Parker

COMPUTER ABSTRACTS AND COMPUTER NEWS

Vol. **4**, No. 6, June 1960, 19 *pp.* London: Technical Information Co. Ltd. £25 4s 0*d* p.a.

In recent years there has been a vast increase in the literature on computers and computer applications. As a contribution towards coping with the resultant confusion the Technical Information Company Ltd publishes a monthly journal, *Computer Abstracts*, which lists many of the available sources. Appearing with the abstracts, as an insert, is *Computer News* which gives information on computers and applications, and is of a more ephemeral nature.

The compilers of the abstracts have cast their nets widely and papers of Russian and Japanese origin are mentioned. The entries are indexed and collected under sub-headings such as Analogue Computers, Digital Computers and Programming. In addition there is a large section on Computer Applications with detailed sub-headings. Subjects dealt with here include Aeronautics, Chemical Processes and Mechanical Engineering. A miscellaneous section lists oddities such as the solution of church bell change ringing problems by use of a Ferranti Pegasus computer. A separate section lists information on recent books dealing with computers and applications. The main sections and sub-sections have cross references. Each monthly issue also contains a name and patent index.

Matters dealt with in *Computer News* include trade literature, exhibitions, conferences and 'news and views' of the industry, as well as book reviews. In addition there is a list of pre-prints of papers to be

presented at forthcoming conferences and where these may be obtained.

As a whole *Computer Abstracts* compares very favourably with the corresponding D.S.I.R. publication but its high price will only bring it within reach of large companies and institutions.

J. ADLER

FLUIDIZATION AND FLUID-PARTICLE SYSTEMS

F. A. ZENZ and D. F. OTHMER. New York: Reinhold; London: Chapman and Hall, 1960. $x+513$ *pp.* $15.00 or 120*s*

As given by its title, this book is not only confined to fluidization but also gives a full review of the characteristic behaviour of particles and powders. In their general treatment, the authors seek to develop, more fully than previously attempted, a fundamental description of fluidized systems. In this, the mechanics of particle systems are obviously important and it is not without value to have in addition, within the one book, a review which includes single particle behaviour even though this is seldom applicable in multi-particle systems. However, due to the present inadequacy of the understanding of fluidized systems, the authors' chosen treatment of necessity leaves a negative impression.

For anyone beginning a fundamental study of fluidized systems this volume is an invaluable starting point. The breadth of the authors' study will raise many provocative thoughts. Indeed, its very breadth will mean that the book will retain much of its value despite the spate of work which has continued to be published in this field while the book has been in production and subsequently.

The practitioner who wants only to apply current empirical knowledge will find this volume of considerable value—but elsewhere he could find simpler and more helpful reviews.

The authors make no reference to a study by S. YAGI and D. KUNII published in the *Fifth Symposium (International) on Combustion 1955* which considered the effect of a combustion reaction in which the particle size is reduced as the reaction proceeds. This necessitated a statistical consideration of the effect of the changing particle size distribution on bed behaviour which is not without promise.

In all, the volume presents a very full review of fluidization and fluid-particle systems which it is most useful to find between the covers of one book.

J. S. M. BOTTERILL

ELEMENTS OF THE KINETIC THEORY OF GASES

E. A. GUGGENHEIM. Oxford: Pergamon, 1960. 92 *pp.* 17*s* 6*d*

THIS volume is one of a series of about one hundred projected volumes of the 'International Encyclopaedia of Physical Chemistry and Chemical Physics' designed to present a comprehensive and modern account of all aspects of the domain of science between chemistry and physics to the graduate and research worker.

Starting from the assumption that molecules are spherically symmetrical and undeformable, the author of this volume develops first the kinematics of the encounter of two molecules. Then following MAXWELL'S assumption of separability of velocity components, the law of distribution of velocities in a gas at equilibrium is developed. These principles are then employed to develop the equation of state of an 'ideal' gas and expressions for the collision rate, mean speed and free path. Theories of viscosity, thermal conductivity and diffusion are then developed following the procedures evolved by MAXWELL, BOLTZMANN and CHAPMAN. The treatment of thermal conductivity is of course restricted to monatomic gases. A chapter on thermal diffusion serves mainly to indicate the complexity and theoretical difficulties of this aspect of the subject. The text concludes with a brief treatment of the influence of external fields on molecular behaviour with special reference to non-ideal gases. Present knowledge of molecular interactions in argon is discussed in some detail to illustrate these principles. It can be argued that the considerations of this chapter may well have justified at least a brief reference to current interest in the 'exponential-6' interaction equation, and perhaps a mention of repulsive field studies by fast molecular beams.

The book is clearly written and free from errors. Theoretical arguments are developed in a concise and logical manner which should present no difficulty to the reader. Mathematics is of course inevitable in a book on this subject but the standard carefully chosen by the author should present little difficulty to graduates in pure and applied sciences.

C. W. NUTT

Letters to the Editors

Letters to the Editors on points of scientific interest related to combustion and flames are invited. The Editors do not hold themselves responsible for opinions expressed in correspondence. Anonymous contributions cannot be accepted.

Comparison of Temperatures of Flames on Porous Burners

In a recent communication[1], W. E. KASKAN has compared maximum temperatures for lean, flat hydrogen–air flames on porous burners obtained by measurement with coated thermocouples with temperatures for corresponding flames deduced from the heat loss data of D. B. SPALDING and V. S. YUMLU[2]. Kaskan found that temperatures based on the data of Spalding and Yumlu were several hundred degrees higher than those obtained with his coated thermocouples, but could not account for the difference in terms of reasonable sources of heat loss.

We have used the heat abstraction method to deduce flame temperatures based on the upstream heat loss from a flame to water flowing through a coil sintered to the base of a porous copper burner 4 in. in diameter and $\frac{5}{16}$ in. thick. As a precaution before applying these temperatures, we compared them with thermocouple temperatures previously reported by W. E. KASKAN[3,4]. As shown by the examples given in *Table 1*, the correspondence is fairly good. The differences are always less than 100° K, and a reasonable allowance for the small differences in initial conditions shows that the thermocouple temperatures are usually higher.

These results suggest that in the method used by Spalding and Yumlu to determine the heat loss a significant part of the heat loss was not measured. Apparently, if the heat abstraction rate is measured with sufficient accuracy, valid temperatures can be obtained.

B. FINE

NASA Lewis Research Center,
21000 Brookpark Road,
Cleveland 35, Ohio

(Received November 1960)

Table 1. Comparison of flame temperatures obtained by thermocouple and heat abstraction methods for closely corresponding initial conditions

Pressure atm	*Equiv. ratio*	*Stream velocity of unburnt gas*	*Temp. °K*	*Source*
Heat abstraction				
1	0·80	30	1645	*This work*
1	0·80	45	1690	
0·41	0·70	13·5	1377	
0·41	0·70	30	1513	
0·25	0·50	25	1447	
Thermocouple				
1	0·80	30	1695	Ref. 3
1	0·80	45	1780	Ref. 3
0·45	0·80	13·6	1435	Ref. 4
0·45	0·60	31·1	1560	Ref. 4
0·45	0·50	20·6	1410	Ref. 4

References

[1] KASKAN, W. E. *Combustion & Flame*, 1960, **4**, 285
[2] SPALDING, D. B. and YUMLU, V. S. *Combustion & Flame*, 1959, **3**, 553
[3] KASKAN, W. E. *Sixth Symposium (International) on Combustion*, p 134. Reinhold: New York, 1957
[4] KASKAN, W. E. *Combustion & Flame*, 1958, **2**, 229

Inflammability Limits

A. L. BERLAD and C. H. YANG[1] have recently suggested that we 'showed experimentally[2] that the inflammability limit of a flame can be extended without limit by imparting heat to the flame from the hot boundary'. We wish to emphasize that in only two of our flames was the temperature of the hot plate above the adiabatic flame temperature; and that only in relatively few cases did we impart heat to the flames at all, as shown by our temperature plots. In most of the cases where heat was supplied to the flames, this was probably occasioned by the low heat release rates towards the end of the reaction zone. In general we merely reduced downstream heat losses, and by doing so extended the range of inflammability.

We feel that this distinction is important inasmuch as there is no *a priori* reason why, in the absence of other heat exchange with the surroundings, heat imparted to a flame from the hot boundary is not virtually equivalent to increasing the total gas enthalpy by preheating the gases entering the flame. Such preheat is known to widen the inflammability limits. Since most of our flames avoid this type of situation they seem to us to show more conclusively the effect of environmental factors on limits.

G. DIXON-LEWIS
G. L. ISLES

Houldsworth School of Applied Science, University of Leeds

(*Received January 1961*)

References

[1] BERLAD, A. L. and YANG, C. H. *Combustion and Flame*, **1960**, **4**, 325
[2] DIXON-LEWIS, G. and ISLES, G. L. *Seventh Symposium (International) on Combustion*, p 475 Butterworths: London, 1959

The Ignition of Gases by Electrically Heated Wires

L. E. Ashman and A. Büchler

Arthur D. Little, Inc., 15 Acorn Park, Cambridge 40, Mass.

(*Received February 1960*)

Experimental studies have been conducted on the ignition of gases with constant temperature wire ignition sources. The wire is heated to the desired temperature in a period of microseconds by means of a condenser discharge. Thereafter, its temperature is maintained constant by a unique feedback control circuit, incorporating a photomultiplier tube that monitors radiation from the centre of the wire. With this apparatus experimental studies of ignition temperature and ignition delay have been made on stoichiometric methane–air and hydrogen–air mixtures. With the methane–air mixture, an exothermic reaction occurs during the pre-ignition period. This pre-ignition reaction occurs at a velocity and for a period of time that depend upon the temperature of the wire. Near the end of this pre-ignition period, the reaction accelerates to a more rapidly propagating flame front. In the hydrogen–air mixture, on the other hand, no measurable reaction occurs during the pre-ignition period. The behaviour of the hydrogen–air ignition conforms to the theory of Semenov on the ignition of gases by small ignition sources. The methane–air ignition properties do not conform to the theory, possibly because the ignition temperature is sufficiently high in the presence of small sources for the corresponding high reaction rate to reduce significantly the concentration of reactants near the source. Some effects of wire size, wire composition and gas pressure on the ignition delay have been investigated for the hydrogen–air mixture. For a given wire temperature, the ignition delay increases when either the diameter of the wire or the gas pressure is reduced. The magnitude of this reduction in ignition delay agrees, at least to a first approximation, with theoretical considerations of the effect of wire size and gas pressure on ignition delay.

Introduction

The present paper describes experiments on ignition by means of fine wires that are suddenly brought to a high temperature and maintained there. Much recent work on gas ignition has been concerned with the determination of the minimum ignition energy, since this quantity can be measured very accurately by electric-spark-gap experiments[2]. Work with heated wires is less intensive*. Although the use of electrically heated wires to determine minimum ignition energies of gases has also been described[3], the results obtained in this manner are open to question, since a large part of the electrical energy is used up in raising the temperature of the wire. Long extrapolations are needed and little accuracy is obtained, therefore, in determining the energy that goes into the gas. B. Lewis and G. von Elbe have discussed the discrepancies between the results obtained in this manner and those obtained from spark experiments[4].

*An excellent review of earlier work on hot-wire ignition is given by W. C. F. Shepherd and R. V. Wheeler, G. B. Safety in Mines Research Board Paper No. 36 (1927).

On the other hand, hot wires provide a good method for observing the effect of the temperature of a small ignition source on the ignition of gases. N. N. Semenov[1] has derived critical conditions for thermal ignition by small sources. Assuming that critical ignition conditions occur when the temperature gradient at the surface of the heated body is zero, he derived an expression relating the dimensions of the hot source to the ignition temperature T. In the case of a wire,

$$r = [E\lambda\,(T - T_a)/2F\,(T)RT^2]^{\frac{1}{2}} \quad \ldots . [1]$$

where r is the radius of the wire, E is the activation energy for the overall reaction, R is the gas constant, T_a is the ambient temperature, and $F\,(T)$ is the rate of heat release per unit volume resulting from the reaction at temperature T. Thus the ignition temperature increases as the radius of the wire decreases. Equation 1 is similar to the Frank-Kamenetsky[5] criteria for ignition of a gas contained in a spherical vessel. It is important to note that the validity of the Semenov theory, as well as that of Frank-

Kamenetsky, requires that the reaction rate be small at the ignition temperature. Thus the concentration of reactants must remain essentially constant during the pre-ignition or induction period.

A further consequence of the Semenov theory is the relationship[6]

$$\ln \tau = E/RT - m \ln p + \text{const.} \quad \ldots\ldots [2]$$

where τ is the ignition delay, p is the pressure, and m is related to the overall reaction. Thus hot wire studies offer a means of obtaining information about the kinetics of a reaction. In this paper we give the results of a study of the effects of source temperature on ignition delay, i.e. the time needed for ignition to occur in the presence of a wire at a given temperature.

Apparatus and Method

The means of obtaining a *constant-temperature pulse* in a wire, the methods used to measure the temperature, and the cell in which the experiments are carried out have been described elsewhere[7]. In the present experiments, gases were mixed in explosion-proof tanks and introduced into the cell through an appropriate filling system. In order to determine the critical current necessary to produce a given temperature, the cell was first filled with a non-combustible mixture having the same thermal diffusivity as the explosive mixture to be tested. In the hydrogen–air experiments, for example, this mixture consisted of 30 per cent hydrogen and 70 per cent nitrogen.

The method of timing the occurrence of ignition varied somewhat with the gas mixture and temperature range involved; it is discussed, therefore, in connection with the experimental results for each mixture.

A schlieren system was used to obtain smear photographs of the ignition process. The optical system is illustrated in *Figure 1*. A point-source of light A is located at the focal point of a parabolic mirror B. Parallel light from the mirror passes through the combustion chamber C and illuminates the ignition wire D. A second parabolic mirror E focuses the light on a knife edge F. The knife edge is mounted parallel to the ignition wire and is adjusted to block out half the light focused upon it. An image of the wire is formed by the lens G on a narrow slit H, which is mounted perpendicular to the knife edge. The slit passes the light that emanates from a narrow region extending directly above and below the centre of the wire. This slit-image is then focused on the rotating drum camera K by the lens J. A shutter I synchronizes the heating of the wire with the exposure of the film. With this apparatus, either schlieren or shadowgraph streak pictures of the ignition could be obtained. For shadowgraph pictures the knife edge F was omitted.

The light from the centre of the wire and the flame are monitored by two photomultiplier tubes depicted in *Figure 1*. In each case an image of the wire is focused on a mask. For the flame monitor, the mask is so constructed that only the light from the flame reaches the

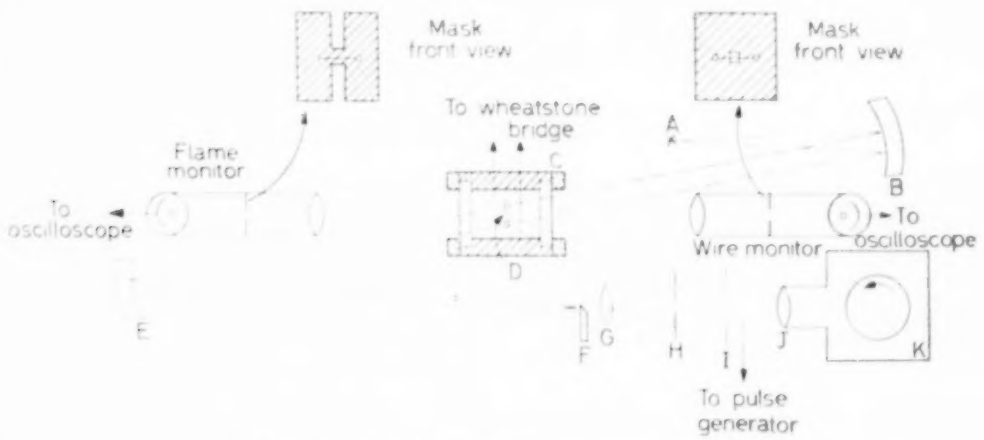

Figure 1. Optical apparatus for viewing ignition

phototube. For the wire monitor, on the other hand, the mask blocks all radiation except that which emanates from the centre of the wire. A change in the signal from the wire-monitor phototube is a very sensitive indication of a change in the temperature. Temperature changes of a few degrees can thus be detected.

Results

(A) *The hydrogen–air mixture*

In the experiments to be described, a stoichiometric mixture of hydrogen and air (30 per cent hydrogen) was used.

(1) *Schlieren streak photographs—Figures* 2(a) and 2(b) show photographs of the ignition of hydrogen–air mixtures. They indicate a well-defined preheat period in which a heat-diffusion wave proceeds from the wire with a velocity of the order of 32 cm sec^{-1}. At the end of this period a flame front suddenly appears. The ignition delay is constituted by this preheat period.

From the slope of the trace of the flame front, a flame speed of 1 460 cm sec^{-1} (with respect to laboratory-fixed coordinates) is obtained for the flame in *Figure 2*(a) and a speed of 1 150 cm sec^{-1} for that in *Figure 2*(b). Since the flame initially propagates under effectively isobaric conditions, the burning velocities S_u (with respect to the unburnt gas) can be calculated. If we take 300°K as the temperature of the unburnt gas and 2 300°K as the flame temperature, and allow for the decrease in mole number produced by the reaction, we obtain $S_u = 220$ cm sec^{-1} from *Figure 2*(a) and $S_u = 175$ cm sec^{-1} from *Figure 2*(b). At 1 atm the velocity agrees satisfactorily with published values[5].

(2) *Detection of ignition*—Since the wire temperature in these experiments ranged from 800 to 1 200°C and the flame temperature was about 2 000°C, the onset of the flame was reflected in a sudden heating of the wire, and consequently, in a sharp rise in its resistance. The oscillogram in *Figure 3* illustrates the heating effect. Simultaneously, the signal from the

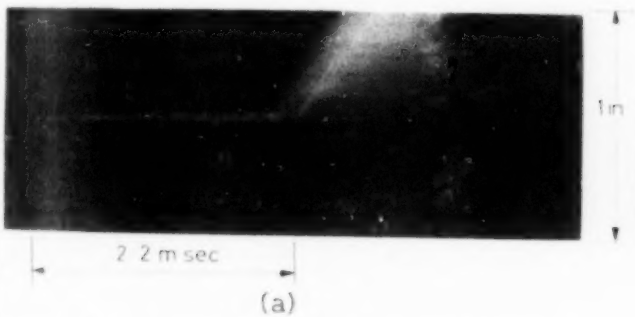

Figure 2(a). *Schlieren streak photograph of ignition of stoichiometric hydrogen–air at 1 atm. The double appearance of the flame front is due to a wide entrance slit. Temperature 800°C; 2 mil tungsten wire*

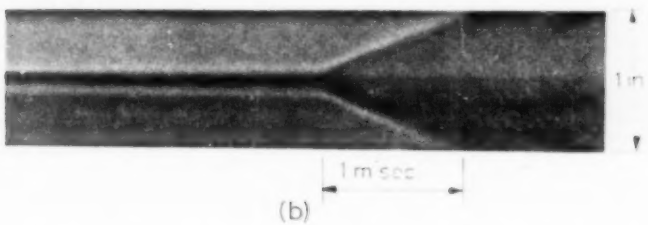

Figure 2(b). *Shadowgraph streak photograph showing ignition of stoichiometric hydrogen–air at ½ atm. Temperature 970°C; 1 mil tungsten wire*

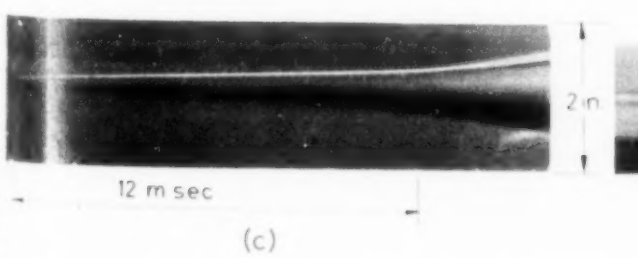

Figure 2(c). *Schlieren streak photograph of ignition of methane–air mixture. Temperature 2200°C; 2 mil tungsten wire*

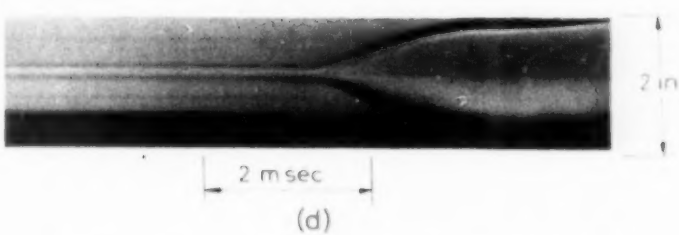

Figure 2(d). *Shadowgraph streak photograph of ignition of 10% propane–45% oxygen–45% nitrogen mixture. Temperature 1400°C; 2 mil tungsten wire*

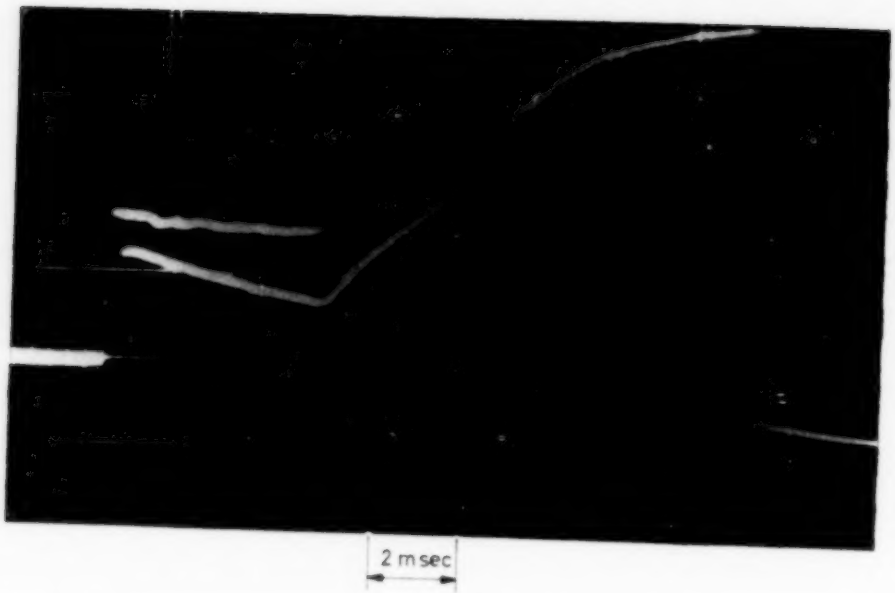

Figure 3. Oscilloscope traces showing the bridge output (lower trace) and the signal from the wire monitor (upper trace). Radiation from the wire is seen to be relatively constant during the pre-ignition time. Both signals increase rapidly when ignition occurs. When the gas ignites, the phototube signal goes abruptly off the screen, while the bridge signal (reflecting the resistance of the wire) increases steadily for about 10 msec. The initial decrease in the bridge signal results from end losses in the wire. The gas was stoichiometric hydrogen–air at ½ atm

wire-monitor photocell shown in *Figure 3* increases so sharply that the beam of the oscilloscope goes abruptly off screen. The interval between the start of the temperature pulse and the appearance of the resistance rise is taken as the experimental value of the ignition delay.

(3) *Ignition delays*—Ignition delays were measured at gas pressures of 1, ½ and ¼ atm for 0·001 in. and 0·002 in. tungsten wires, and at 1 atm for 0·0015 in. platinum wire. Preliminary plots of ignition delays against wire temperature suggested that the use of equation 2 for analysing the data was justified. Equations of the form

$$\ln \tau = A + B/RT \qquad \ldots . [3]$$

were, therefore, fitted to the data by the method of least squares. Plots of the fitted curves are shown as solid lines in *Figures 4* and *5*. The values of A and B and the standard deviations of B, S_B, are listed in *Table 1*.

To determine the effect of pressure and wire size on ignition delay, we fitted parallel straight lines to the experimental data. The slope B'/R for this 'smoothed' set of lines was obtained by taking the mean of the slopes B/R of the five lines (1) to (5) which were based on the largest number of experimental points. Parameters for the smoothed set are also given in *Table 1*, and the curves obtained are indicated as the dashed lines in *Figures 4* and *5*. The justification of this procedure is discussed below.

(B) *The methane–air mixture*

Ignition experiments on mixtures containing 9 per cent methane in air gave results that differed in two important respects from the hydrogen–air experiments. First, wire temperatures higher than about 1 470°C were necessary to ignite the methane mixture, whereas hydrogen mixtures could be ignited by temperatures as low as 800°C. Secondly, with methane mixtures, it was not possible to hold the centre of the wire at a constant temperature during the pre-ignition period with a steady current. Instead, the current required to maintain a constant wire temperature continuously decreased, at first slowly and then rapidly to

Table 1. Parameters for ignition delay temperature curves

Figure No.	Curve No. (solid line)	Number of experimental points	Ignition wire	P atm	A ln (*msec*)	B kcal	S_B kcal	Curve No. (broken line)	A' ln (*msec*) ($B'=33{\cdot}6$ kcal throughout)
1	(1)	37	0·002 *in.* W	1	−15·0	36·6	3·8	(1)	−13·8
2	(2)	23	0·002 *in.* W	½	−12·7	33·6	4·2	(2)	−12·7
3	(3)	20	0·002 *in.* W	¼	− 9·9	28·8	3·4	(3)	−11·8
4	(4)	21	0·001 *in.* W	1	− 9·4	23·8	3·6	(4)	−12·6
5	(5)	12	0·001 *in.* W	½	−15·3	43·0	3·6	(5)	−11·7
6	(6)	7	0·001 *in.* W	¼	− 4·6	17·2	5·4	(6)	−10·6
7		8	0·0015 *in.* Pt	1	− 9·4	26·0	3·2		−12·5

zero after a delay of some milliseconds. In an inert atmosphere or in hydrogen–air mixtures, on the other hand, the current demand is constant. We assume, therefore, that the decreasing current demand in the methane–air mixtures is due to pre-ignition reactions accompanied by heat release which begin at the instant the wire is brought up to temperature and which alter the usual temperature distribution in the gas near the wire.

(1) *Schlieren streak photographs*—A typical photograph is shown in *Figure 2*(c). In contrast to the hydrogen–air mixture, no definite point corresponding to the sudden appearance of a flame front can be observed. The photograph shows a slow process propagating with a velocity of 65 cm sec^{-1}, which then accelerates and reaches a final velocity of 295 cm sec^{-1}. The maximum velocity in the photograph corresponds to a burning velocity S_u of 48 cm sec^{-1} where a flame temperature of 1 800° C is assumed for calculation. Reported values give a burning velocity of 35 cm sec^{-1} for this mixture. Actually, we found that the final burning velocity tended to increase slightly with the wire temperature. This is described below.

Typical ignition data for 9 per cent methane–air mixtures at various wire temperatures are illustrated by the curves shown in *Figure 6*. These curves were obtained by measurement of

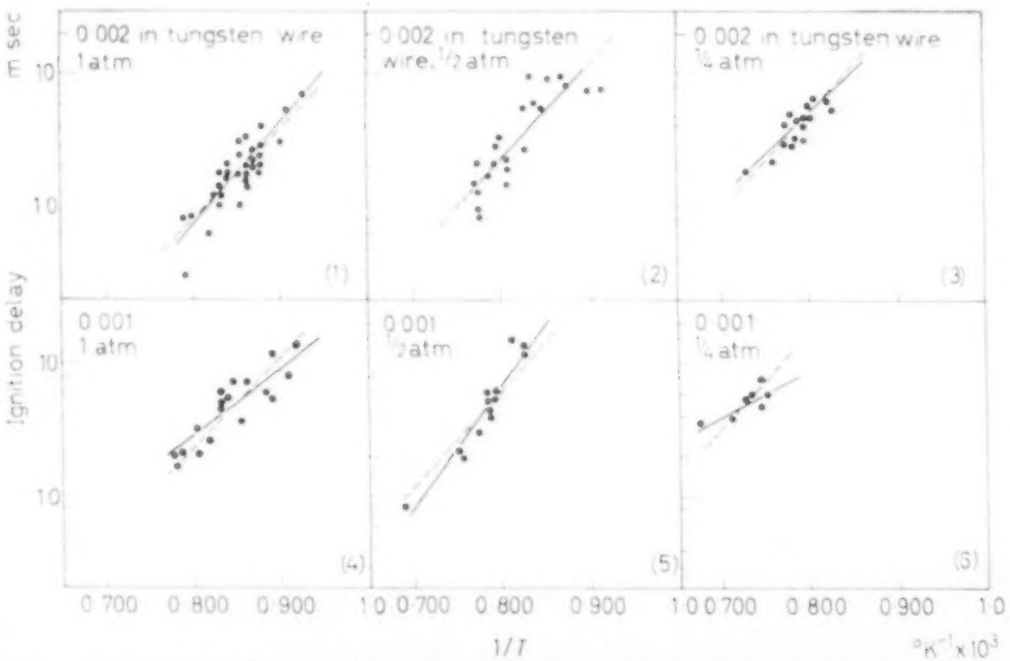

Figure 4. Ignition delays of stoichiometric hydrogen–air mixtures

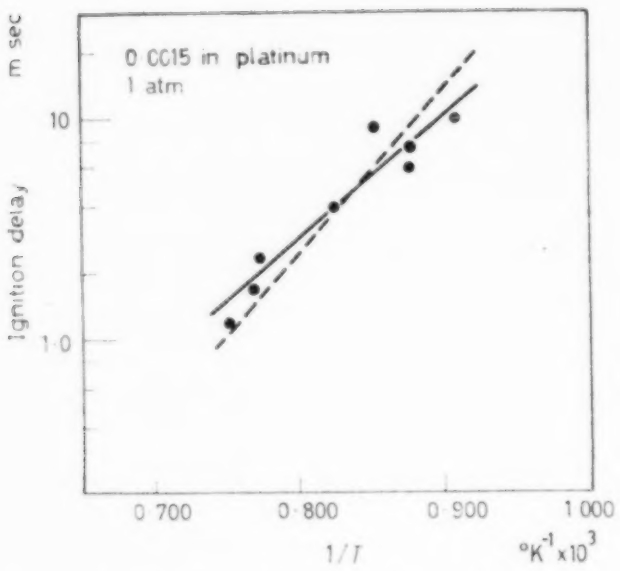

Figure 5. Ignition delays of 30% hydrogen–15% oxygen–55% nitrogen at 1 atm, with 1·5 mil platinum wire

the schlieren streak pictures and a plot of the position of the wave front on a scale that more clearly shows the acceleration of the reaction zone. The ignition phenomenon follows a similar pattern at each temperature: a period of slow propagation followed by a sudden acceleration to a flame front of about normal speed. The velocity of the slow process is strongly temperature dependent while that of the flame front is only moderately so. The distance travelled before the point of maximum acceleration appears to be significant. This distance, between 8 and 10 mm, is essentially

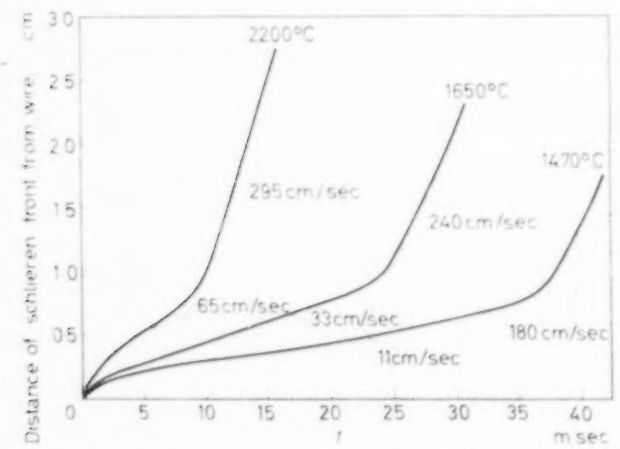

Figure 6. Development of a flame front during the ignition of 9% methane–air

independent of wire temperature. The appearance of a flame as marked by the photoelectric flame monitor very nearly coincides with the time of maximum acceleration.

The 1 470°C curve in *Figure 6* represents minimum ignition conditions. Several attempts to ignite the gas at slightly lower temperatures were unsuccessful. Schlieren streak photographs for these experiments showed a gradual deterioration of the characteristic slow front. In these cases, presumably, convective cooling is rapid enough to offset the effects of the internal heating of the gas.

Discussion

(A) *Hydrogen–air and methane–air; the ignition delay/temperature relationship*

The logarithmic temperature dependence of the ignition delay provides clear evidence that with hydrogen–air mixtures the rate-controlling factor that determines the ignition delay is provided by chemical kinetics, at least in the range of temperatures, pressures and wire sizes investigated. In this respect, therefore, the ignition delays observed are related to induction periods in the theory of homogenous explosions[5–8]. The concept of the ignition kernel[9–11]—a minimum volume of gas that must reach a certain temperature for a flame to propagate—is also valuable in this context.

The results of our experiments on the hydrogen–air system thus tend to confirm the general character of the ignition process as predicted by Frank-Kamenetsky and Semenov. The temperature and diameter of the wire define a volume of gas which reaches the ignition stage according to an exponential dependence on temperature. It has been pointed out repeatedly (e.g. ref. 6) that this behaviour of the induction period holds for both thermal and chain-branching explosions, and therefore cannot be used to distinguish between the two mechanisms. Some indication of the nature of the processes that precede ignition may, however, be obtained from the behaviour of the wire temperature. We have seen that with methane–air mixtures an exothermic reaction appears to take place the moment the wire is brought up to temperature. In the hydrogen–air mixtures, on the

other hand, the wire temperature remains steady until the flame front appears, provided that a certain critical constant current is applied—the same current value which is required to hold the temperature constant in an inert mixture. Thus very little heat is produced by the preflame reactions, a situation which implies that we are dealing essentially with a chain-explosion mechanism.

The methane–air experiments emphasize the limitations of the Frank-Kamenetsky and Semenov theories. These theories are useful only insofar as the reaction rate near the wire is so small that the reactants are not significantly depleted. Apparently this condition was satisfied in the hydrogen–air experiments but not in those with methane–air mixtures. The very high ignition temperatures of the latter may be partially explained by the relatively lower activation energy of hydrocarbons compared to hydrogen. This lower activation energy results in high reaction rates near the surface of the wire, so high in fact as to cause a substantial depletion of reactants near the wire. Thus when the wire size is sufficiently small, the rate of heat release is less dependent upon wire temperature and more and more upon the rate of diffusion of fresh reactants into the high-temperature region. In this case, an increase in the temperature of the wire does not substantially increase the likelihood of ignition since it does not increase the reaction rate by an exponential law but only by an enlargement of the reaction zone. Similarly, increases in temperature beyond the minimum ignition temperature for a given wire do not substantially reduce the ignition delay. For larger-diameter wires, which would lead to increased reaction zones, or with higher concentrations of reactants, we would expect results similar to those for the hydrogen–air system.

(B) *Hydrogen–air: temperature coefficients and delay times*

The coefficients B (*Table 1*) have the dimensions of energy and can be considered as apparent activation energies for the ignition process. At this time, however, it would be unwise to regard them as anything more than empirical parameters. The determination and interpretation of overall activation energies is difficult enough with stationary laminar flames; it is complicated here by the non-steady character of the processes leading to ignition. Furthermore, the wire temperature, which has been used to evaluate B, is certainly higher than the effective temperature in the gas surrounding the wire. Thus we shall limit ourselves to a comparison of our values with those obtained in other flame and ignition experiments.

It is difficult to decide at present to what extent the differences between the various apparent activation energies in our experiments are significant. The 'smoothed' set of lines in *Figures 4* and *5* has been drawn on the assumption that, at least for the purposes of investigating pressure and wire-size dependence, the differences are not significant. The mean value (B') is 34 kcal. The best available apparent activation energy value for laminar stoichiometric hydrogen–air flames is 47 kcal[11].

Brokaw has given a summary of ignition-delay measurements in hydrogen–air mixtures under approximately isothermal conditions (see Figure 17 of ref. 10). For a temperature range of 650° to 600°C, his compilation shows one set of values between 20 and 30 msec (B. P. Mullins's data), and another set ranging between 100 msec and a few seconds. If either the smoothed or unsmoothed lines for the 1 atm, 0·001 in. and 0·002 in. tungsten wire experiments are extrapolated to the 650° to 600°C range, ignition delays of the order of 100 to 500 msec are obtained. The somewhat tenuous nature of such an extrapolation need not be emphasized.

(C) *Hydrogen–air: pressure dependence*

From the smoothed set of lines, the pressure dependence of the ignition delay is found to be of the order of $p^{-1.5}$ for both the 0·001 in. and 0·002 in. tungsten wire experiments. For chain-branching explosions involving, at the point of ignition, chemical reactions of overall nth order, the pressure dependence of the induction time is of the form p^{-n}, i.e. $m = n$ in equation $2^{[5,6]}$. B. Lewis and G. von Elbe[12] have shown that in the reaction of hydrogen and oxygen

near atmospheric pressure and at a temperature just below the explosion limit, the overall reaction depends on the fourth power of the total pressure. Thus the high pressure exponent for the hot-wire ignition delay may be interpreted as being entirely due to reaction-kinetic effects.

A. G. GAYDON and H. G. WOLFHARD[13,14] have considered the effect of pressure on minimum ignition times for long-duration sources in terms of the minimum volume of gas to be heated. Since their argument is based on diffusion of heat as the rate-controlling process, it would appear to be valid only at temperatures somewhat higher than those involved in the present experiments.

(D) *Hydrogen–air: dependence on wire size*

Comparison of the smoothed 1, ½ and ¼ atm lines for 0·001 in. and 0·002 in. tungsten wires gives for this range a variation of ignition delay τ with wire radius a of the order of $a^{-1\cdot6}$.

This dependence on wire size is predicted by equation 1. For example, for two wires of radius r_1 and r_2 corresponding to ignition temperatures T_1 and T_2, equation 1 predicts approximately

$$\ln \frac{r_1}{r_2} = \frac{E}{2R}\left(\frac{1}{T_1} - \frac{1}{T_2}\right) \quad \ldots\ldots [4]$$

if the temperature-dependence $F(T)$ of the heat release is assumed to be of the Arrhenius type. For hydrogen–oxygen experiments, $r_1/r_2 = 2$, and $E = 34$ kcal. Thus, equation 4 predicts $T_2 - T_1 \simeq 100°C$, which is approximately the observed difference between the ignition temperature of 1 mil and 2 mil wires.

(E) *Hydrogen–air: dependence on wire material*

An increase in ignition temperatures on platinum surfaces has been reported in a number of experimental situations[15]. Some experiments were, therefore, performed with a 0·0015 in. platinum wire (see *Figure 5*). For comparison, ignition-delay values for a 0·0015 in. tungsten wire were estimated by interpolation between the smoothed 0·001 in. and 0·002 in. lines. On this basis, the temperatures for corresponding ignition delays appear to be about 50 degrees higher for the platinum wire than for a tungsten wire of the same diameter.

(F) *Propane–oxygen–nitrogen*

In conclusion, the question may be raised whether the behaviour of either the hydrogen–air or methane–air mixtures is unique. A partial answer is provided by *Figure 2*(d) which shows the ignition of a mixture of 10 per cent propane, 45 per cent oxygen and 45 per cent nitrogen at 1 atm with a 0·002 in. tungsten wire at about 1 400°C. The pattern of hydrogen–air ignition is repeated. In fact, this mixture was selected because of its having a quenching distance[2] about equal to that of the hydrogen–air mixture at 1 atm. Quenching distance by itself, however, cannot be a deciding factor in hot-wire ignition since the quenching distance of 30 per cent hydrogen–air at ½ atm [*Figure 2*(b)] is about the same as that of 9 per cent methane–air at 1 atm [*Figure 2*(c)]. It remains to be shown whether the ignition behaviour of methane–air is duplicated by other mixtures.

This work was supported by the Combustion Dynamics Division, Air Force, Office of Scientific Research, ARDC, Washington 25, D.C., under Contract No. AF18(603)–109.

References

[1a] SEMENOV, N. N. *Adv. phys. Sci., Moscow*, 1940, **24**, 251; English translation: *Tech. Memor. Nat. Adv. Comm. Aero., Wash., No. 1024*, 1942

[1b] SEMENOV, N. N. *Some Problems in Chemical Kinetics and Reactivity*, Vol. II, pp. 87–110. Princeton University Press: Princeton, N.J., 1959

[2] LEWIS, B. and VON ELBE, G. *Combustion, Flames and Explosion of Gases*, pp. 390–425. Academic Press: New York, 1951

[3] STOUT, H. P. and JONES, E. *Third Symposium (International) on Combustion*, pp. 329–336. Williams and Wilkins: Baltimore, 1949

[4] Ref. 2, pp. 444–446

[5] FRANK-KAMENETSKY, D. A. *Acta phys.-chim. U.R.S.S.* 1939, **10**, 365–370

[6] BROKAW, R. S. *Selected Combustion Problems*, Vol. II, pp. 115–138. AGARD; Butterworths: London, 1956

[7] PRESTON, J. and ASHMAN, L. E. *Rev. sci. Instrum.* 1960, **31**, 53

[8] TODES, O. M. *Acta phys.-chim. U.R.S.S.* 1936, **5**, 785–805
TODES, O. M. and MELENTJEV, P. V. *Acta phys.-chim. U.R.S.S.* 1939, **11**, 153–180
MELENTJEV, P. V. and TODES, O. M. *Acta phys.-chim. U.R.S.S.* 1941, **14**, 27–52

[9] ARNOLD, J. S. and SHERBOURNE, R. K. *Fourth Symposium (International) on Combustion*, pp 139–143. Williams and Wilkins: Baltimore, 1953
MOZER, C. F. and SHERBOURNE, R. K. *Proceedings, Gas Dynamics Symposium on Aerothermochemistry*, pp 159–165. Northwestern University: Evanston, 1956

[10] OLSEN, J. L., GAYHART, E. L. and EDMONDSON, H. B. *Fourth Symposium (International) on Combustion, pp* 144–148. Williams and Wilkins: Baltimore, 1953

[11] KASKAN, W. E. *Sixth Symposium (International) on Combustion*, pp 134–143. Reinhold: New York, 1957

[12] Ref. 2, pp 40–41

[13] GAYDON, A. G. and WOLFHARD, H. G. *Flames, Their Structure, Radiation and Temperature*, pp 328–347. Chapman and Hall: London, 1953

[14] WOLFHARD, H. G. *Selected Combustion Problems*, Vol. II, pp 328–347. AGARD; Butterworths: London, 1956

[15] See, for example, COWARD, H. F. and GUEST, P. J. *J. Amer. chem. Soc.* 1927, **49**, 2479

Flame Propagation by Non-branching Chain Reactions

J. ADLER and D. B. SPALDING

Imperial College of Science and Technology, London, S.W. 7

(Received March 1960)

Steady, one-dimensional, laminar flame propagation, proceeding by a non-branching chain reaction with negligible chain breaking is considered. Some exact analytical solutions for the temperature gradient, radical concentration and flame propagation speed are obtained for particular systems of reaction rate functions. Approximate methods are developed by means of which the flame propagation speed for any given reaction scheme may be determined.

Introduction

STEADY, one-dimensional laminar flame propagation involving a chain reaction has been considered by a number of workers. J. O. HIRSCHFELDER, C. F. CURTISS and D. E. CAMPBELL[1] consider the decomposition of ozone by a non-branching, non-propagating chain reaction. By making the 'steady-state assumption', T. VON KÁRMÁN and S. S. PENNER[2] have shown that for this flame the existence of the chain reaction doubles the rate of the main reaction. D. B. SPALDING[3] has considered chain reactions with particular reference to the hydrazine decomposition flame.

In chain reactions which either satisfy 'steady-state approximations' or proceed via 'explosive chain branching' considerable simplification is possible, c.f. D. B. SPALDING[4]. In such cases the volumetric reaction rate controlling the chemical reaction can be made temperature-explicit and the assumption of normal diffusion and constant gas enthalpy leads to a single differential equation determining the flame propagation speed. When such simplification is no longer valid, more than one differential equation has to be solved. Since these equations are non-linear and have to be solved simultaneously, some mathematical difficulty is encountered. A chemical reaction proceeding via a non-branching chain reaction can be expressed by the solution of two such equations in which the flame propagation speed occurs as an eigenvalue.

D. B. SPALDING[4] has derived a number of exact solutions of the equations defining single-step reactions. On plotting eigenvalue λ, against centroid position τ_c, of the various reaction rate functions, he obtained curves which for $\tau_c \geqslant 0{\cdot}7$ are nearly coincident regardless of function shape. A theoretical explanation of the so-called 'centroid rule' has recently been given by J. ADLER[5]. The rule makes it possible to predict approximate flame propagation speeds knowing only the area and centroid position of the reaction rate curve. In the work presented below we have obtained some exact analytical solutions of the equations defining non-branching chain reactions. Attempts have been made to find a corresponding relationship between the centroids of the reaction rate functions and the eigenvalue λ. They have been only partially successful.

Approximate methods for solving single-step reaction problems have been employed by E. N. ADAMS[6], T. VON KÁRMÁN and S. S. PENNER[2] and by K. A. WILDE[7]. They depend essentially on choosing an adjustable temperature-gradient profile, the parameters being determined by direct substitution into the eigenvalue equation. G. MILLÁN and S. SANZ[8] and L. A. LOVACHEV[9] have used similar approximate methods to obtain solutions to the non-branching chain reaction flame. In view of the success of such profile methods we have developed approximations by means of which the flame propagation speed for any given reaction scheme may readily be obtained.

Notation

The following meanings have been ascribed to the symbols listed:

- A Initial reactant
- B Intermediate radical
- c Average specific heat at constant pressure, assumed independent of composition and temperature (cal/g °C)
- D Product of reaction (combustion)
- E/RT_s Reduced activation energy
- $F(\tau)$ Function of dimensionless temperature [equation 89]
- $f_A(T)$ Function of absolute temperature for reactant A [equation 1]
- $f_B(T)$ Function of absolute temperature for radical B [equation 2]
- G Mass flow rate per unit area (g/cm² sec)
- H Standard heat of reaction of A(cal/g of A)
- k Local thermal conductivity coefficient (cal/cm sec °C)
- m_A Fractional mass concentration of fuel (g/g)
- $\dot{m}'''_A$ Mass rate of consumption of fuel per unit volume (g/cm³ sec)
- m_B Fractional mass concentration of radical (g/g)
- $\dot{m}'''_B$ Mass rate of production of radical per unit volume (g/cm³ sec)
- p Dimensionless temperature gradient [equation 17]
- q Dimensionless concentration gradient [equations 38, 39]
- R_A Normalizing function for A [equation 12]
- R_B Normalizing function for B [equation 13]
- s Scaled dimensionless radical concentration [equation 18]
- S_u Flame propagation speed (cm/sec)
- T Absolute temperature (°K)
- x Distance in stream direction (cm)
- y Dimensionless distance [equation 6]
- λ Eigenvalue [equation 11]
- λ' Scaled eigenvalue [equation 21]
- λ'' Scaled eigenvalue [equation 21]
- ρ Local density of the mixture (g/cm³)
- σ Dimensionless radical concentration [equation 10]
- τ Dimensionless temperature [equation 7]
- τ_A Temperature centroid of $\phi_A(\tau)$ [equation 31]
- τ_B Temperature centroid of $\phi_B(\tau)$ [equation 31]
- $\phi_A(\tau)$ Dimensionless rate of consumption of A [equation 8]
- $\phi_B(\tau)$ Dimensionless radical generating rate [equation 9]

Millán and Sanz

- c_p Specific heat at constant pressure
- M Molecular weight
- Y_B Mass fraction of radical
- z_1, z_2 Frequency factors for reaction rates
- γ Parameter, see equation 65ff
- ε Flux fraction of hydrazine
- ε_B Flux fraction of radical
- θ Dimensionless temperature
- θ_A Reduced activation energy for hydrazine
- θ_B Reduced activation energy for radical
- Λ_A Eigenvalue for hydrazine equation
- Λ_B Eigenvalue for radical equation

Lovachev

- c Specific heat
- D_A Diffusion coefficient of A
- D_B Diffusion coefficient of B
- h Thermal effect of reaction
- $K_A(T)$ Rate constant of reaction
- l Parameter, see equation 74
- n_A Dimensionless concentration of A
- n_B Dimensionless concentration of B
- p Temperature gradient
- $Q(T)$ Rate of consumption of initial substance A
- $R(T)$ Rate of generation of radical B
- T Temperature measured relative to the initial temperature T'_u
- δ Parameter, see equations 77, 78
- η Parameter, see equations 84

Reaction Mechanism

We consider a steady, one-dimensional laminar flame whose mode of propagation is determined by the following reaction scheme:

(*i*) $A \longrightarrow 2B$ (radical generating)

(*ii*) $A + B \longrightarrow B + D$ (chain propagating reaction)

(*iii*) $fB \longrightarrow D$ (chain breaking).

In a manner similar to that of Spalding[3], we make the following assumptions regarding the importance of the various reactions:

(*a*) Ignore (*i*) compared to (*ii*) as destroyer of A
(*b*) Ignore effect of (*i*) on temperature
(*c*) Ignore (*iii*) completely
(*d*) Assume normal diffusion coefficients (defined below).

With these assumptions $\dot{m}'''_A$ and $\dot{m}'''_B$ can be expressed as

$$\dot{m}'''_A = m_A m_B f_A(T) \quad \ldots [1]$$

$$\dot{m}'''_B = m_A f_B(T) \quad \ldots [2]$$

in which $f_A(T)$ and $f_B(T)$ are known functions of the absolute temperature T.

Derivation of Equations

Conservation equations

If the Lewis numbers of the components of the reaction are taken as unity, the energy conservation equation may be written as

$$\frac{d}{dx}\left(k\frac{dT}{dx}\right) - cG\frac{dT}{dx} = -Hm_A m_B f_A(T) \quad \ldots [3]$$

and that for the conservation of radical as

$$\frac{d}{dx}\left(\frac{k}{c}\frac{dm_B}{dx}\right) - G\frac{dm_B}{dx} = -m_A f_B(T) \quad \ldots [4]$$

The corresponding conservation equation for the fuel A may be combined with equation 3 and integrated to give

$$(T - T_u)/(T_b - T_u) = -m_A/m_{Au} \quad \ldots [5]$$

where the suffixes $_u$ and $_b$ refer to the unburnt and burnt states respectively.

Equations in dimensionless form

It is convenient to introduce the following transformations:

Dimensionless distance

$$dy = (cG/k)\,dx \quad \ldots [6]$$

Dimensionless temperature

$$\tau = (T - T_u)/(T_b - T_u) \quad \ldots [7]$$

Dimensionless rate of consumption of fuel A

$$\phi_A(\tau) = \frac{(1-\tau)\,k f_A(T)}{\int_0^1 (1-\tau)\,k f_A(T)\,d\tau} \quad \ldots [8]$$

Dimensionless radical generating rate

$$\phi_B(\tau) = \frac{(1-\tau)\,k f_B(T)}{\int_0^1 (1-\tau)\,k f_B(T)\,d\tau} \quad \ldots [9]$$

Dimensionless radical concentration

$$\sigma = m_B(\bar{R}_A/R_B m_{Au})^{\frac{1}{2}} \quad \ldots [10]$$

Eigenvalue

$$\lambda = (k_u/cG^2)(\bar{R}_A \bar{R}_B m_{Au})^{\frac{1}{2}} \quad \ldots [11]$$

where the constants $\bar{R}_A$ and $\bar{R}_B$ are defined by the equations:

$$\bar{R}_A = \frac{1}{k_u}\int_0^1 (1-\tau)\,k f_A(T)\,d\tau \quad \ldots [12]$$

$$\bar{R}_B = \frac{1}{k_u}\int_0^1 (1-\tau)\,k f_B(T)\,d\tau \quad \ldots [13]$$

With the transformations above, equations 3 and 4 become:

$$\frac{d^2\tau}{dy^2} - \frac{d\tau}{dy} = -\lambda\sigma\phi_A(\tau) \quad \ldots [14]$$

$$\frac{d^2\sigma}{dy^2} - \frac{d\sigma}{dy} = -\lambda\phi_B(\tau) \quad \ldots [15]$$

The boundary conditions are:

$$y = -\infty;\ \tau = 0,\ \sigma = 0$$
$$y = +\infty;\ \tau = 1,\ d\sigma/dy = 0 \quad \ldots [16]$$

Change of form of equation for mathematical solution

Since y is not contained explicitly in equations 14 and 15, one can reduce the order of the energy equation by the substitution

$$p = d\tau/dy \quad \ldots [17]$$

It is also mathematically convenient to introduce the following dimensionless radical concentration

$$s = \sigma/\sigma_{max.} \quad \ldots [18]$$

in which $\sigma_{max.}$ is the maximum value of σ. Evidently s is now restricted to lie in the range $0 \leqslant s \leqslant 1$. Assuming s to be a function of τ, equations 14 and 15 may be written:

$$p\frac{dp}{d\tau} - p = -\lambda' s \phi_A(\tau) \quad \ldots\ldots [19]$$

$$p\frac{d}{d\tau}\left(p\frac{ds}{d\tau}\right) - p\frac{ds}{d\tau} = -\lambda'' \phi_B(\tau) \quad \ldots\ldots [20]$$

where the constants λ' and λ'' are defined by:

$$\lambda' = \lambda \sigma_{max.}$$
$$\lambda'' = \lambda / \sigma_{max.} \quad \ldots\ldots [21]$$

The boundary conditions applicable to equations 19 and 20 are:

$$\tau = 0 : p = 0, \; s = 0$$
$$\tau = 1 : p = 0, \; s = 1 \quad \ldots\ldots [22]$$

Derivation of the flame speed

For given reaction rate functions $\phi_A(\tau)$, $\phi_B(\tau)$ it is necessary to solve equations 19 and 20 subject to the boundary conditions 22. This leads to numerical values for λ' and λ'' which, like λ, are eigenvalues. If S_u is the flame speed and ρ_u the corresponding density of the unburnt mixture, rearrangement of equation 11 gives

$$S_u = \left[\frac{k_u}{c\rho_u^2}\left(\frac{\bar{R}_A \bar{R}_B m_{Au}}{\lambda' \lambda''}\right)\right]^{\frac{1}{2}} \quad \ldots\ldots [23]$$

where use has been made of the relation

$$G = S_u \rho_u \quad \ldots\ldots [24]$$

Analytical Solutions

Analytical solutions to equations 19 and 20 for particular systems of reaction rate functions may be determined by the following alternative means:

(*i*) Assume for p and s, analytical functions of τ, satisfying the boundary conditions and containing arbitrary parameters. Hence determine the corresponding $\phi_A(\tau)$ and $\phi_B(\tau)$ by direct substitution.

(*ii*) Consider simplified functions for $\phi_A(\tau)$ and $\phi_B(\tau)$ for which analytical solution of equations 19 and 20 is possible. It will be shown below that suitable systems of functions are step function reaction rates.

Parametric system (i)

Suitable functions for the dimensionless temperature gradient and radical concentration, which satisfy the boundary conditions 22, are:

$$p = \tau - \tau^{d+1} \quad \ldots\ldots [25]$$
$$s = a\tau + (1-a)\tau^b \quad \ldots\ldots [26]$$

in which a, b, d are parameters, which satisfy

$$d > 0 \quad \ldots\ldots [25a]$$
$$0 < a \leqslant 1, \; b > 1 \quad \ldots\ldots [26a]$$

Substituting in equations 19 and 20 and normalizing the resultant functions, one obtains:

$$\phi_A(\tau) = \frac{(d+1)}{\lambda'} \frac{\tau^d (1-\tau^d)}{a + (1-a)\tau^{b-1}} \quad \ldots\ldots [27]$$

$$\phi_B(\tau) = \frac{a(d+1)}{\lambda''} \tau^{d+1}(1-\tau^d) + (1-a) \frac{b(b+d)}{\lambda''} \tau^{d+b}(1-\tau^d) - (1-a)\frac{b(b-1)}{\lambda''} \tau^b (1-\tau^d) \quad \ldots\ldots [28]$$

where the constants λ' and λ'' are given by:

$$\lambda' = (d+1)\int_0^1 \frac{\tau^d (1-\tau^d)}{a + (1-a)\tau^{b-1}} \, d\tau \quad \ldots\ldots [29]$$

$$\lambda'' = \frac{(1-a)bd}{d+b+1}\left(\frac{d+b}{2d+b+1} - \frac{b-1}{b+1}\right) + \frac{ad}{2(d+2)} \quad \ldots\ldots [30]$$

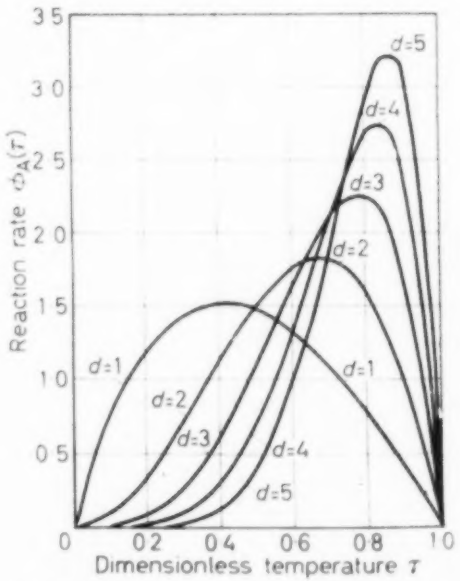

Figure 1(a). Typical reaction rate functions $\phi_A(\tau)$ of parametric system (i). Parameters: $a = d/(d+1)$; $b = d+1$

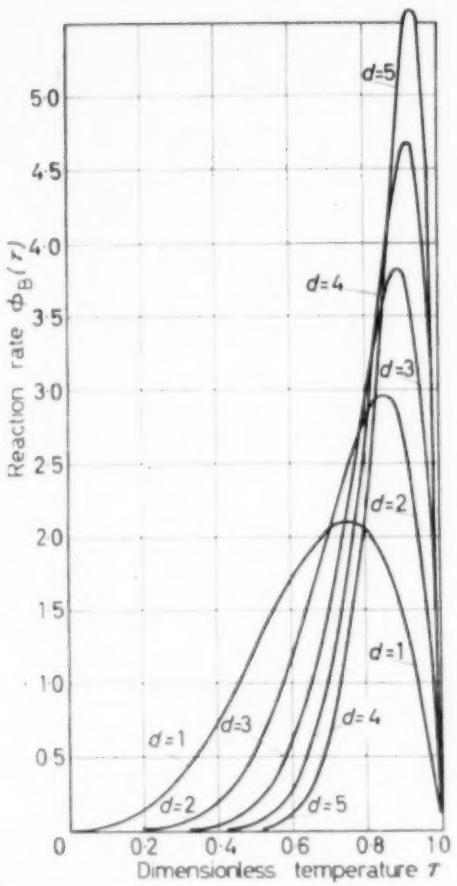

Figure 1(b). *Typical reaction rate functions* $\phi_B(\tau)$ *of parametric system* (i). *Parameters:* $a=d/(d+1)$; $b=d+1$

In *Figures 1*(a), (b) are shown typical reaction rate functions and the corresponding $p(\tau)$ and $s(\tau)$ curves belonging to this system are displayed in *Figures 2*(a), (b).

Centroids of the reaction rate functions—For single-step reactions, the centroid of the normalized reaction rate function has been found to be its most important characteristic. We have, therefore, for the case of flames propagating by non-branching chain reactions, plotted the eigenvalue λ against the centroids of $\phi_A(\tau)$ and $\phi_B(\tau)$.

If one defines centroids of the reaction rate functions by:

$$\tau_A = \int_0^1 \tau\phi_A(\tau)\,d\tau \qquad \ldots\ldots[31a]$$

$$\tau_B = \int_0^1 \tau\phi_B(\tau)\,d\tau \qquad \ldots\ldots[31b]$$

then from equations 27 and 28 one obtains:

$$\tau_A = \frac{(d+1)}{\lambda'}\int_0^1 \frac{\tau^{d+1}(1-\tau^d)\,d\tau}{a+(1-a)\tau^{b-1}} \qquad \ldots\ldots[32]$$

$$\tau_B = \frac{d}{\lambda''}\left[\frac{a(d+1)}{(d+3)(2d+3)} - \frac{(1-a)b}{d+b+2}\left(\frac{b+d}{2d+b+2} - \frac{b-1}{b+2}\right)\right] \qquad \ldots\ldots[33]$$

It is seen that $\lambda\,[\equiv(\lambda'\lambda'')^{\frac{1}{2}}]$, τ_A and τ_B are functions of the chosen parameters a, b and d. By varying these one can obtain graphical relationships between the eigenvalue and centroids. The restrictions 25a and 26a are insufficient to ensure that $\phi_A(\tau)$ and $\phi_B(\tau)$ are of realistic shape. We have thus introduced additional restrictions on the parameters so that in all cases $\phi_A(\tau) \geqslant 0$, $\phi_B(\tau) \geqslant 0$ when $0 \leqslant \tau \leqslant 1$.

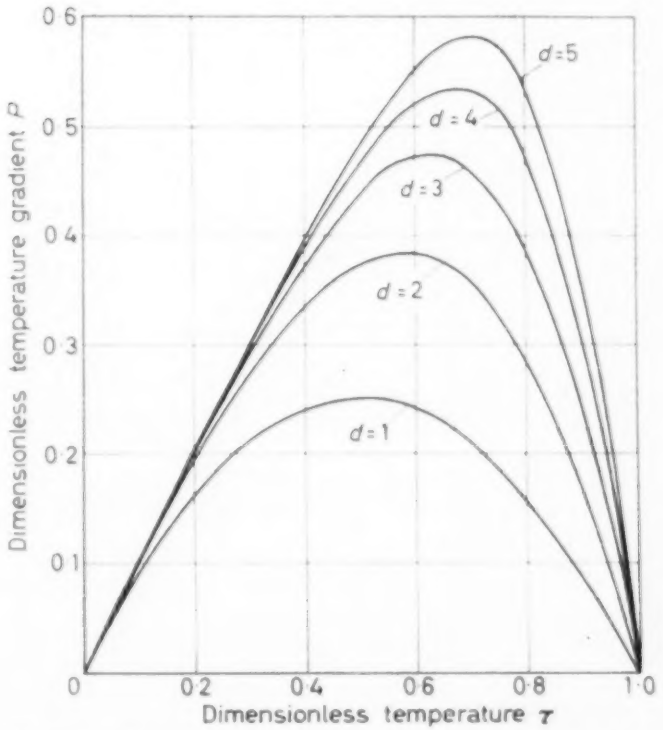

Figure 2(a). *Typical dimensionless temperature gradients of parametric system* (i). *Parameters:* $a=d/(d+1)$; $b=d+1$

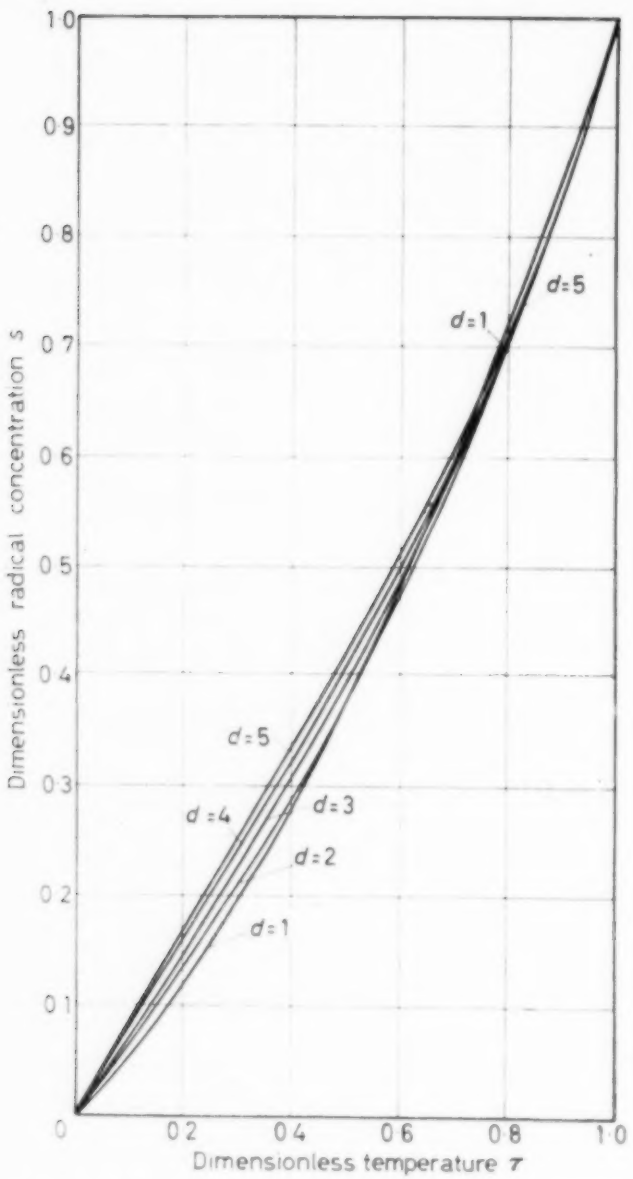

Figure 2(b). *Typical dimensionless radical concentrations of parametric system (i). Parameters:* $a=d\,(d+1)$; $b=d+1$

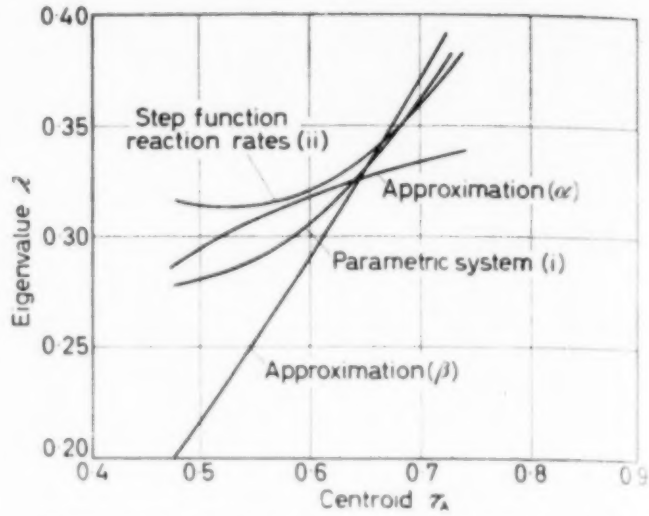

Figure 3(a). *Curves of eigenvalue* λ *versus centroid* τ_A *for centroid* $\tau_B=0{\cdot}7$

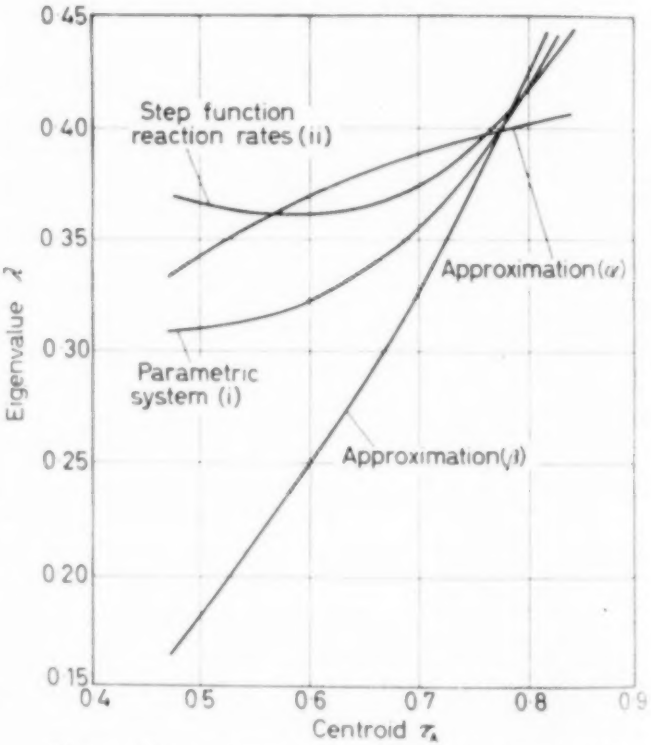

Figure 3(b). *Curves of eigenvalue* λ *versus centroid* τ_A *for centroid* $\tau_B=0{\cdot}8$

In *Figures 3*(a), (b), (c) are shown λ versus τ_A curves for $\tau_B=0{\cdot}7$, $0{\cdot}8$ and $0{\cdot}9$.

Step function reaction rates (ii)

A system of functions for which it is possible to obtain analytical solutions to equations 19 and 20 is:

$$0\leqslant\tau<\tau_i;\ \phi_A(\tau)=0$$
$$\tau_i\leqslant\tau\leqslant 1;\quad =1/(1-\tau_i) \quad \ldots\ [34]$$

$$0\leqslant\tau<\tau_j;\ \phi_B(\tau)=0$$
$$\tau_j\leqslant\tau\leqslant 1;\quad =1/(1-\tau_j) \quad \ldots\ [35]$$

with the restriction $\tau_i\leqslant\tau_j$.

It is seen that each of these functions is either zero or constant in the range $0\leqslant\tau\leqslant 1$, the

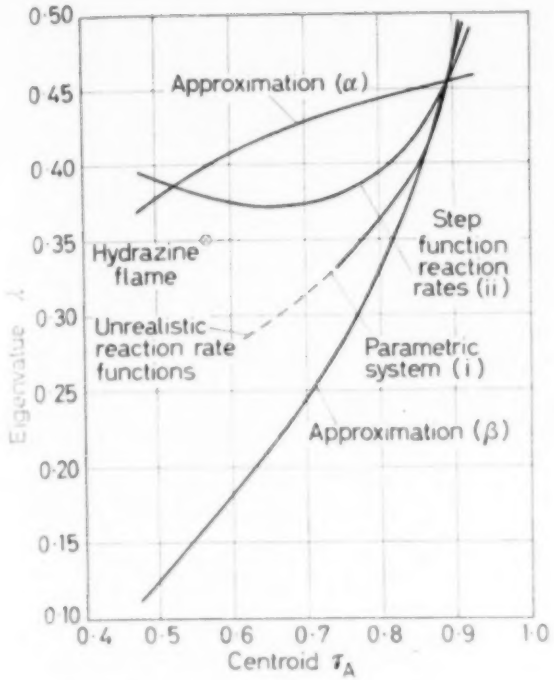

Figure 3(c). *Curves of eigenvalue* λ *versus centroid* τ_A *for centroid* $\tau_B = 0{\cdot}9$

constant being fixed by the normalization requirement. The inequality $\tau_i \leqslant \tau_j$ is necessary to ensure that s remains finite for all values of τ. To solve equations 19 and 20 for functions 34 and 35 it is necessary to consider the differential equations in the three regions $0 \leqslant \tau \leqslant \tau_i$, $\tau_i \leqslant \tau \leqslant \tau_j$ and $\tau_j \leqslant \tau \leqslant 1$.

(a) *Region* $0 \leqslant \tau \leqslant \tau_i$—In this region both $\phi_A(\tau)$ and $\phi_B(\tau)$ are zero. It is seen that the required solutions are:

$$p = \tau \qquad \ldots . [36]$$

$$s = A\tau \qquad \ldots . [37]$$

where A is a constant.

(b) *Region* $\tau_i \leqslant \tau \leqslant \tau_j$—Since for these values of τ, $\phi_B(\tau) = 0$, it is more convenient to make the substitution $q = \mathrm{d}s/\mathrm{d}y$ in equations 14 and 15, with s as defined before. If τ may be written as a function of s, one obtains:

$$q \frac{\mathrm{d}}{\mathrm{d}s}\left(q \frac{\mathrm{d}\tau}{\mathrm{d}s}\right) - q \frac{\mathrm{d}\tau}{\mathrm{d}s} = \alpha s \qquad \ldots . [38]$$

$$q \frac{\mathrm{d}q}{\mathrm{d}s} - q = 0 \qquad \ldots . [39]$$

where $\alpha = -\lambda'/(1-\tau_i)$. Equation 39 is also valid in the range $0 \leqslant \tau \leqslant \tau_j$ and hence may be integrated to give $q = s$. Substituting in equation 38 one obtains the single equation

$$\mathrm{d}^2\tau/\mathrm{d}s^2 = \alpha/s \qquad \ldots . [40]$$

Integrating this subject to the boundary conditions:

$$\tau = \tau_i : s = s_i = A\tau_i$$

one obtains:

$$\mathrm{d}\tau/\mathrm{d}s = \alpha \ln (s/s_i) + A \qquad \ldots . [41]$$

$$\tau = \alpha [s_i - s + s \ln (s/s_i)] + As \qquad \ldots . [42]$$

(c) *Region* $\tau_j \leqslant \tau \leqslant 1$—For values of τ in this range one requires simultaneous solution of equations:

$$\frac{\mathrm{d}^2\tau}{\mathrm{d}y^2} - \frac{\mathrm{d}\tau}{\mathrm{d}y} = \alpha s \qquad \ldots . [43]$$

$$\frac{\mathrm{d}^2 s}{\mathrm{d}y^2} - \frac{\mathrm{d}s}{\mathrm{d}y} = \beta \qquad \ldots . [44]$$

with constants α, β defined by $\alpha = -\lambda'/(1-\tau_i)$, $\beta = -\lambda''/(1-\tau_j)$. If, as before, $q = \mathrm{d}s/\mathrm{d}y$, equation 44 may be rewritten as

$$q\,\mathrm{d}q/\mathrm{d}s - q = \beta \qquad \ldots . [45]$$

Integrating this subject to the boundary conditions:

$$\tau = 1 : s = 1,\ q = 0$$

one obtains

$$s = q + 1 - \beta \ln (1 + q/\beta) \qquad \ldots . [46]$$

Writing equation 43 in the form

$$\frac{\mathrm{d}\tau}{\mathrm{d}y}\frac{\mathrm{d}}{\mathrm{d}q}\left(\frac{\mathrm{d}q}{\mathrm{d}y}\frac{\mathrm{d}\tau}{\mathrm{d}q}\right) - \frac{\mathrm{d}q}{\mathrm{d}y}\frac{\mathrm{d}\tau}{\mathrm{d}q} = \alpha s \qquad \ldots . [47]$$

it is seen that use of equations 45 and 46 gives

$$\frac{\mathrm{d}^2\tau}{\mathrm{d}q^2} = \frac{\alpha}{(q+\beta)\cdot}\left[q + 1 - \beta \ln\left(1 + \frac{q}{\beta}\right)\right] \qquad \ldots . [48]$$

The appropriate boundary conditions are:

$$\tau = 1 : q = 0,\ \mathrm{d}\tau/\mathrm{d}q = 0$$

Integrating, one obtains:

$$\frac{\mathrm{d}\tau}{\mathrm{d}q} = \frac{\alpha}{q+\beta}\left[(2\beta + q)\ln\left(1 + \frac{q}{\beta}\right) - \frac{(2\beta - 1)}{\beta} q\right] \qquad \ldots . [49]$$

$$\tau = 1 + \alpha\left[(q+3\beta-1)\ln\left(1+\frac{q}{\beta}\right)+\frac{\beta}{2}\left\{\ln\left(1+\frac{q}{\beta}\right)\right\}^2 - \frac{(3\beta-1)}{\beta}q\right] \quad \ldots\ldots [50]$$

Combination of equations 45 and 49 also gives

$$\frac{d\tau}{ds} = \frac{\alpha}{q}\left[(2\beta+q)\ln\left(1+\frac{q}{\beta}\right) - \frac{(2\beta-1)}{\beta}q\right] \quad \ldots\ldots [51]$$

The functions τ and $d\tau/ds$ must be continuous at all values of s. Fitting the solutions obtained in the regions $\tau_i \leqq \tau \leqq \tau_j$ and $\tau_j \leqq \tau \leqq 1$ at $\tau = \tau_j$, one has:

$$\lambda' = \alpha(As_i - 1) \quad \ldots\ldots [52]$$

$$\lambda'' = \alpha[(3\beta-2)(1-s_j)+1{\cdot}5] \quad \ldots\ldots [53]$$

where

$$A = \alpha\left[\frac{2}{\beta} - \frac{2(1-s_j)}{s_j} + \ln\left(\frac{s_i}{s_j}\right)\right] \quad \ldots\ldots [54]$$

If s_i and s_j are specified α, β are determined from:

$$1 = \beta\ln(1+s_j/\beta) \quad \ldots\ldots [55]$$

$$\alpha = 1/(1/2\beta + s_i - 1) \quad \ldots\ldots [56]$$

From the definitions of the reaction rate function it is seen that the centroid positions are:

$$\tau_A = 1 + \lambda'/2\alpha \quad \ldots\ldots [57]$$

$$\tau_B = 1 + \lambda''/2\beta \quad \ldots\ldots [58]$$

Equations 52 to 58 have been used to derive λ versus τ_A curves for various values of τ_B. The results are shown in *Figures* 3(a), (b), (c).

Approximate Solutions

For general reaction rate functions $\phi_A(\tau)$ and $\phi_B(\tau)$ it is not possible to obtain analytical solutions to equations 19 and 20 and numerical methods must be resorted to. Some difficulty is encountered here, since the equations satisfy two point boundary conditions, but an iterative method, such as used by Spalding[5] is often a suitable technique.

An alternative approach is the use of approximate methods for solving the flame equations. For single-step reactions such methods have been highly successful and have determined flame speeds to a few per cent accuracy for most reaction schemes of importance.

Approximate methods for dealing with non-branching chain reactions have been considered by Millán and Sanz[8] and Lovachev[9]. They depend essentially on choosing a suitable temperature dependent function for the radical concentration and then fixing the values of the parameters contained in the function. This must usually be done by substitution back into the differential equations and using subsidiary conditions. Below, we consider some of these approximate methods.

The Millán–Sanz approximation

Making similar approximations as we have made in the section on the reaction mechanism, Millán and Sanz were able to write the equations determining the concentrations of radical and hydrazine in the following form:

Equation for the flux fraction of radical z_B

$$\frac{dz_B}{d\theta} = \Lambda_B \frac{(1-\theta)\,e^{-\theta_B(1-\theta)/\theta}}{\theta[\theta - 1 + (1-\theta_u)(z/z_u)]} \quad \ldots\ldots [59]$$

Equation for the mass fraction of radical Y_B

$$\frac{dY_B}{d\theta} = \frac{Y_B - z_B}{\theta[\theta - 1 + (1-\theta_u)z/z_u]} \quad \ldots\ldots [60]$$

Equation for the flux fraction of hydrazine z

$$\frac{dz}{d\theta} = -\Lambda_A \frac{(1-\theta)\,Y_B \exp\{\theta_A(1-\theta)/\theta\}}{\theta[\theta - 1 + (1-\theta_u)z/z_u]} \quad \ldots\ldots [61]$$

where $\theta = T/T_b$, the dimensionless temperature; $\theta_B = E_B/RT_b$, the reduced activation energy for the radical B; and $\theta_A = E_A/RT_b$, the reduced activation energy for hydrazine A. The suffixes $_u$ and $_b$ refer to the initial and final states of the gas respectively. The constants Λ_B and Λ_A, determining the flame propagation speed, are given by:

$$\Lambda_B = z_2 \frac{k_b\theta_u z_u \exp(-\theta_B)}{S_u^2 \rho_u c_p (1-\theta_u)} \quad \ldots\ldots [62]$$

$$\Lambda_A = z_1 \frac{k_b\theta_u^2 z_u \exp(-\theta_A)}{S_u^2 \sigma_p (1-\theta_u) M} \quad \ldots\ldots [63]$$

where z_1, z_2 are frequency factors for the

reaction rates of hydrazine and radical. Integration of equation 61 results in

$$\lambda_A = \frac{\frac{1}{2}(1-\theta_u)\,\varepsilon_u - \int_0^{\varepsilon_u}(1-\theta)\,d\varepsilon}{\int_{\theta_u}^{1}\{(1-\theta)/\theta\}\,Y_B \exp(-\theta_A)\,\{(1-\theta)/\theta\}\,d\theta} \quad \ldots.[64]$$

It is seen that once this integral expression is known the flame propagation speed may be determined by rearrangement of equation 63.

To obtain approximate solution to equations 59 to 61, the temperature range $\theta_u \leqslant \theta \leqslant 1$ is divided into three regions and the following profile assumptions for the variables made:

(a) Region $\theta_t \leqslant \theta \leqslant 1$:

$$\varepsilon_B = b - \beta(1-\theta)$$
$$Y_B = b - \gamma_1(1-\theta) \quad \ldots.[65]$$

(b) Region $\theta_x \leqslant \theta \leqslant \theta_t$: $\varepsilon_B = 0$

$$Y_B = Y_{Bt}\left\{\frac{(1-\theta_t)}{1-\theta}\right\}^{1+[1-\theta_u)/(\theta_t-\theta_u)]} \quad \ldots.[66]$$

(c) Region $\theta_u \leqslant \theta \leqslant \theta_x$:

$$\varepsilon_B = 0$$
$$Y_B = \gamma_2(\theta - \theta_u) \quad \ldots.[67]$$

For the flux fraction of material A it is assumed that near $\theta = 1$

$$\varepsilon = \alpha(1-\theta) \quad \ldots.[68]$$

and this approximation is used for evaluating the integral occurring in the numerator of equation 64. Equations 65 to 68 contain the nine parameters α, β, γ_1, γ_2, b, θ_t, θ_x, Y_{Bt}, Y_{Bx} which must be determined by continuity requirements at the boundary temperatures and use of equations 59 to 61.

Millán and Sanz finally obtain the following expression

$$\lambda_B \lambda_A = \frac{\varepsilon_u(1-\theta_u)^2\,[1 - I_1^{1/2}/(1-\theta_u)]^2}{[-\exp(-\theta_B)\,\mathrm{Ei}(-\theta_B)]\,I_1^{3/2}} \quad \ldots.[69]$$

in which

$$-\mathrm{Ei}(-x) = \int_x^{\infty}(1/x)\,e^{-x}\,dx$$

is the exponential integral function and I_1 is given by

$$I_1 = 2\int_{\theta_u}^{1}\frac{(1-\theta)}{\theta}\,\frac{(\theta-\theta_u)}{1-\theta_u}\exp[(-\theta_A)(1-\theta)/\theta]\,d\theta \quad \ldots.[70]$$

this being a first approximation to a function I defined iteratively. Substitution of equations 62 and 63 into 69 gives the flame speed on rearrangement.

The Lovachev approximation

Lovachev writes equations 3 and 4 of our paper in the form

$$k\rho\frac{d\rho}{dT} - G c\rho + Q n_B = 0 \quad \ldots.[71]$$

$$D\rho\frac{d}{dT}\left(\rho\frac{dn_c}{dT}\right) - G\rho\frac{dn_B}{dT} + R = 0 \quad \ldots.[72]$$

where

$$T = T' - T'_u$$
$$\rho = dT/dx$$
$$Q(T) = hk_A(T)\,n_A(T)$$
$$D = \rho D_B$$
$$k = c\rho D_A$$
$$G = \rho_u S_u$$

It is assumed that k and c are independent of T. The final combustion temperature is determined from

$$h(n_{Au} - n_{Ab}) = cT_c$$

The assumption is made that the radical concentration n_B can be approximated by a quadratic function in T, of the form

$$n_B = n_{Bu} + (l - z_m T_b)\,T + z_m T^2 \quad \ldots.[73]$$

where

$$l = (n_{Bb} - n_{Bu})/T_b \quad \ldots.[74]$$

and z_m is determined by substituting equation 73 in 71. Assuming that the value obtained, where

$$T = T_m : \rho = \rho_m,\ d\rho/dT = 0$$

is valid for the whole range of temperature, one obtains

$$z_m = 1/\{T_m(T_b - T_m)\}\,(n_{Bu} + lT_m - Gcp_m/Q_m) \quad \ldots [75]$$

If equation 73 is substituted in 72 and the conditions at $T = T_m$ introduced, one obtains on solving for z_m

$$z_m = \frac{R_m - Glp_m}{Gp_m(2T_m - T_b) - 2D_m p_m^2} \quad \ldots [76]$$

Combining equations 75 and 76 and solving for the mass flow rate G, one obtains

$$G = (\varkappa p_m^2 + \beta) - \{(\varkappa p_m^2 + \beta)^2 - 4\varepsilon(\gamma p_m^2 + \delta)\}^{\frac{1}{2}}/2\varepsilon p_m \quad \ldots [77]$$

in which the root tending to infinity for $\varepsilon \longrightarrow 0$ has been neglected. The values of $\varkappa$, β, γ, δ, ε are given by:

$$\left.\begin{aligned} \varkappa &= 2cD_m/Q_m \\ \beta &= (2T_m - T_b)\,n_{Bu} + lT_m^2 \\ \gamma &= 2D_m(n_{Bu} + lT_m) \\ \delta &= R_m T_m (T_b - T_m) \\ \varepsilon &= (c/Q_m)(2T_m - T_b) \end{aligned}\right\} \quad \ldots [78]$$

In these definitions Q_m and R_m are the rate of consumption of A and rate of generation of B when $T = T_m$.

Considering the variables 78 as fixed, the function G is stationary with respect to p_m, where $\partial G/\partial p_m = 0$. Evaluating this one finds that

$$a_1 y^3 + a_2 y^2 + a_3 y + a_4 = 0 \quad \ldots [79]$$

where $y = p_m^2$ and the constants are related to those of 78 by the equations

$$\left.\begin{aligned} a_1 &= \varkappa^2\gamma \\ a_2 &= -\varkappa(2\beta\gamma - 3\varkappa\delta) \\ a_3 &= \beta(\beta\gamma - 2\varkappa\delta) \\ a_4 &= -\delta(\beta^2 - 4\varepsilon\delta) \end{aligned}\right\} \quad \ldots [80]$$

Lovachev now examines the functional relationship between G and p_m. It is argued that the flame will propagate with the maximum possible $p_m = (p_m)_z$ consistent with the boundary conditions:

$$\left.\begin{aligned} T = 0 &: n_B = n_{Bu},\ p = 0, \quad p\frac{d}{dT}(n_B) = 0 \\ T = T_b &: n_B = n_{Bb},\ p = 0, \quad p\frac{d}{dT}(n_B) = 0 \end{aligned}\right\} \quad \ldots [81]$$

Lovachev then shows that this value is approximately equal to the mean, between two roots of equation 79, such that

$$(p_m)_z^2 \simeq y_{mean} = \tfrac{1}{2}(y_2 + y_3) \simeq \beta/\varkappa \quad \ldots [82]$$

Substituting in expression 77 and simplifying one obtains for the flame speed

$$S_u = \frac{1}{\rho_u}\left[\frac{n_{Bb}Q_m\rho_m(D_p)_m}{2cT_b}\right]^{\frac{1}{2}} \quad \ldots [83]$$

The expression contains the maximum radical concentration n_{Bb} and the unknown temperature T_m. It appears to be assumed that n_{Bb} can be obtained otherwise. To obtain T_m the author uses the approximate expression

$$G^2 = \eta p_*^2, \quad \eta = 4k_u/cT_m \quad \ldots [84]$$

which when substituted into the equation for G, resulting on combination of expressions 75 and 76, gives

$$p_*^4(\varkappa - \varepsilon\eta) - p_*^2(\gamma - \beta\eta) - \delta = 0 \quad \ldots [85]$$

This is solved for p_* with the assumption that $T_m = \frac{1}{2}T_b$. The result is then equated with the value of $(p_m)_z$ from approximation 82, which allows T_m to be determined. It is difficult to see where approximation 84 comes from, since if T_m is considered as an ignition temperature, the expression for η should be without the multiplier 4 in the numerator.

Approximations based on the centroid rule

Below we consider a number of approximations which relate the eigenvalues λ' and λ'' to the centroids of suitable temperature explicit reaction rate functions.

Approximation (a)—Examination of exact solutions shows that the radical concentration for non-branching chain reactions is a monotonic function of the temperature and rises from

zero to an upper value as the dimensionless temperature τ increases from zero to unity. A simple profile assumption, which suggests itself for the scaled dimensionless radical concentration, is therefore $s=\tau$. Substituting this approximation in equations 19 and 20 one obtains:

$$p\,\mathrm{d}p/\mathrm{d}\tau - p = -\lambda'\tau\phi_A(\tau) \quad \ldots.[86]$$

$$p\,\mathrm{d}p/\mathrm{d}\tau - p = -\lambda''\phi_B(\tau) \quad \ldots.[87]$$

Examination shows that these equations are of a form describing single-step reactions, and therefore λ' and λ'' may be obtained by use of the 'centroid rule' of Spalding[4], namely: If

$$p\,\mathrm{d}p/\mathrm{d}\tau - p = -\lambda \mathrm{f}(\tau) \quad \ldots.[88]$$

such that

$$\int_0^1 \mathrm{f}(\tau)\,\mathrm{d}\tau = 1 \qquad \int_0^1 \tau \mathrm{f}(\tau)\,\mathrm{d}\tau = \tau_c$$

then λ is given approximately by

$$\lambda = F(\tau_c) = 0{\cdot}5 - 0{\cdot}6604(1-\tau_c) - 0{\cdot}4283(1-\tau_c)^2 \quad \ldots.[89]$$

The values of λ are found to be accurate to two per cent when the centroid lies in the range $0{\cdot}7 \leqslant \tau_c \leqslant 1$.

Application of 89 to equations 86 and 87 results in

$$\lambda' = F(\tau'_A)/\tau_A \quad \ldots.[90]$$

$$\lambda'' = F(\tau_B) \quad \ldots.[91]$$

In these equations τ_A and τ_B are defined by the integrals 31 and τ'_A is given by

$$\tau'_A = (1/\tau_A)\int_0^1 \tau^2\phi_A(\tau)\,\mathrm{d}\tau \quad \ldots.[92]$$

Examination of expression 90 and 91 shows that once the relationship between τ_A and τ'_A has been found, λ may be plotted as a function of τ_A and τ_B.

As an example, we have applied the approximation to the system of reaction rate functions:

$$\phi_A(\tau) = (n+1)(n+2)(1-\tau)\tau^n \quad \ldots[93]$$

$$\phi_B(\tau) = (m+1)(m+2)(1-\tau)\tau^m \quad \ldots[94]$$

where $m \geqslant n$. Reference to Spalding[4] shows that they are of realistic shape.

Substitution of 93 and 94 in equations 31 gives

$$\tau_A = \frac{n+1}{n+3} \qquad \tau_B = \frac{m+1}{m+3} \quad \ldots.[95]$$

and from 92 one obtains

$$\tau'_A = \frac{n+2}{n+4} = \frac{1+\tau_A}{3-\tau_A} \quad \ldots.[96]$$

Hence, on substitution,

$$\lambda = \left[\frac{1}{\tau_A}F\left(\frac{1+\tau_A}{3-\tau_A}\right)F(\tau_B)\right]^{\frac{1}{2}} \quad \ldots.[97]$$

The expression 97 has been used to determine λ versus τ_A curves for various values of τ_B. These are shown in *Figures* 3(a), (b), (c).

Approximation (β)—Dividing equation 20 by p and integrating between the limits $\tau=0$ and $\tau=1$, one has

$$\lambda'' = 1/\int_0^1 \phi_B(\tau)(1/p)\,\mathrm{d}\tau \quad \ldots.[98]$$

where the boundary conditions 22 have been used. The expression shows that once p is known as a function of τ, λ'' may be found. To determine such a function we shall assume that it may be approximated by expression 25 in which the parameter d is to be determined.

The assumption $s=\tau$ is made, which results in equation 86 for p. Integrating this between the limits $\tau=0$ and $\tau=1$ one obtains

$$\lambda'\tau_A = \int_0^1 p\,\mathrm{d}\tau \quad \ldots.[99]$$

Substituting expression 90 for λ' and 25 for p in the integral, one has on solving for d

$$d = 4F(\tau'_A)/\{1-2F(\tau'_A)\} \quad \ldots.[100]$$

Combination of equations 90 and 98 results in the expression for the eigenvalue

$$\lambda = \left[F(\tau'_A)/\tau_A \int_0^1 \frac{\phi_B(\tau)\,\mathrm{d}\tau}{(\tau-\tau^{d+1})}\right]^{\frac{1}{2}} \quad \ldots.[101]$$

where d is given by equation 100.

The approximation (β) has been applied to

the system of reaction rate functions 93 and 94 and λ versus τ_A evaluated for various values of τ_B. The results obtained are shown in *Figures* 3(a), (b), (c).

Application to the hydrazine decomposition flame

Spalding[3] has considered the hydrazine decomposition flame. By suitably scaling his reaction rate functions, these may be written

$$\omega_A(\tau) = A(1-\tau)\frac{T_u}{T}\exp\left[\frac{-7\,000}{R}\left(\frac{1}{T}-\frac{1}{T_b}\right)\right] \quad \ldots [102]$$

$$\omega_B(\tau) = B(1-\tau)\exp\left[\frac{-66\,000}{R}\left(\frac{1}{T}-\frac{1}{T_b}\right)\right] \quad \ldots [103]$$

where $R = 1{\cdot}98$, $T_u = 300°\text{K}$, $T_b = 1\,950°\text{K}$, $A = 48{\cdot}23$, $B = 253{\cdot}5$, A and B being normalization constants. Using an iterative quadrature method*, Spalding has integrated equations 14 and 15 for the rate functions defined above. He found that $\lambda = 0{\cdot}350$.

We have evaluated λ for the reaction rate functions using approximation (α). The value obtained was $\lambda = 0{\cdot}3908$, which when compared with Spalding's evaluation gives an error of six per cent in the flame speed.

Discussion

Examination of *Figures* 3(a), (b), (c) shows that the exact solutions (*i*) and (*ii*) give distinct λ versus τ_A relationships for fixed values of τ_B: agreement between the two sets of curves becoming worse as $\tau_B \longrightarrow 1$. We conclude that, for non-branching chain reactions, the centroids of the reaction rate curves are of less dominant importance than with single-step reactions.

The approximations (α) and (β), derived above, are seen to lie above and below the corresponding λ versus τ_A relationships obtained from (*i*) and (*ii*) as $\tau_B \longrightarrow 1$. They may thus be considered as giving approximate upper and lower bounds to λ versus τ_A for a given τ_B. Comparing approximation (α) with exact integration shows that in a typical case it gives an accuracy of six per cent in the flame speed.

*Unpublished

References

1. Hirschfelder, J. O., Curtiss, C. F. and Campbell, D. E. *J. phys. Chem.* 1953, **57**, 403
2. von Karman, T. and Penner, S. S. *Selected Combustion Problems*, p 5. AGARD; Butterworths: London, 1954
3. Spalding, D. B. *Phil. Trans.* 1956, **249**, 1
4. Spalding, D. B. *Combustion & Flame*, 1957, **1**, 287 and 296
5. Adler, J. *Combustion & Flame*, 1959, **3**, 389
6. Adams, E. N. Quoted by Henkel, M. J., Spaulding, W. P. and Hirschfelder, J. O. *Third Symposium (International) on Combustion*. Williams and Wilkins: Baltimore, 1949
7. Wilde, K. A. *J. chem. Phys.* 1954, **22**, 1788
8. Millan, G. and Sanz, S. Instituto Nacional de Tecnica Aeronautica, Esteban Terradas, *A.F.61 (514)–734C*. Madrid, 1956
9. Lovachev, L. A. *Dokl. Akad. Nauk. S.S.S.R.* 1958, **120**, 1287

Burning Velocity and Reaction Rates in Constant Temperature Non-adiabatic Flames

C. P. FENIMORE and G. W. JONES

General Electric Research Laboratory, Schenectady, N. Y.

(Received March 1960)

Flames with different fuel/oxygen ratios can be burnt at constant final temperatures on cooled porous burners, the constant temperature being maintained by changing burning velocity so that more heat is abstracted from the flames of greater calorific value. It is not obvious whether the required change of burning velocity is also associated with a change in the rate of fuel consumption, and this question has been investigated. In some lean hydrogen or hydrocarbon flames, the rate of fuel consumption has been found to be almost constant in constant temperature flames despite large changes in burning velocity with mixture ratio; and for such flames, the change in burning velocity is accounted for merely by the necessary change in heat abstraction. In fuel-rich hydrogen flames, however, the increased burning velocity of progressively richer mixtures is also associated with a faster reaction rate. In the course of the work, it was noted that the maximum rate of fuel consumption did not occur at a constant fraction of the final temperature or of the temperature rise, and this casts doubt on an assumption sometimes made to deduce 'activation energies' of flame reactions.

Introduction

WATER cooled, flat flame burners[1,2] possess a porous surface through which the premixed reactants pass and burn on the downstream side as a non-adiabatic flame. The flame lies closer to the cooled surface, and loses more heat to it, the smaller the burning velocity imposed; so it is possible to maintain a constant flame temperature for a range of mixture compositions by choosing smaller burning velocities for the mixtures of greater calorific value.

Although a constant final temperature obviously requires that more heat be abstracted from the flames of greater calorific value, it is not obvious that this requirement is a sufficient explanation for the variation of burning velocity with mixture strength at constant final temperatures. For example, Botha and Spalding considered that even in such non-adiabatic flames, the smallest burning velocity was associated with a minimum rate of fuel consumption, much as is predicted by adiabatic flame theories. Their interpretation was not proved, however.

We have investigated whether the variation in the non-adiabatic, constant temperature, burning velocity is accounted for by the necessary variation in heat abstraction. For fuel-rich acetylene or hydrogen flames, the required change in heat abstraction does appear to be a sufficient explanation. For rich hydrogen flames, however, it is not; the increased burning velocity of progressively richer hydrogen flames at constant temperature is also associated with an increased reaction rate in the flame.

Rich hydrocarbon flames cannot be studied over a wide enough range of variables by our technique to allow a very general conclusion.

Rate of Fuel Consumption in Very Lean Acetylene Flames

At low pressures, reaction rates can be estimated in flames by probing the reaction zone, and this was done for some acetylene–oxygen–argon flames at 6 cm of mercury pressure, and with fixed final burnt gas temperatures. The experimental arrangement of porous burner in an evacuated vessel, movable sampling probe, and movable fine quartz coated thermocouple was the same as that used previously[3]. The reactant composition is expressed as

$$\phi C_2H_2 + 2{\cdot}5\,(O_2 + 0{\cdot}14\,A)$$

An example of the data is given in *Figure 1* which displays the measurements through a flame with $\phi = 0{\cdot}202$, mass burning velocity $= (\rho v) = 1{\cdot}43 \times 10^{-3}$ g cm^{-2} sec^{-1}, where ρ is density and v is linear velocity. The final temperature of this flame was 1 200°K.

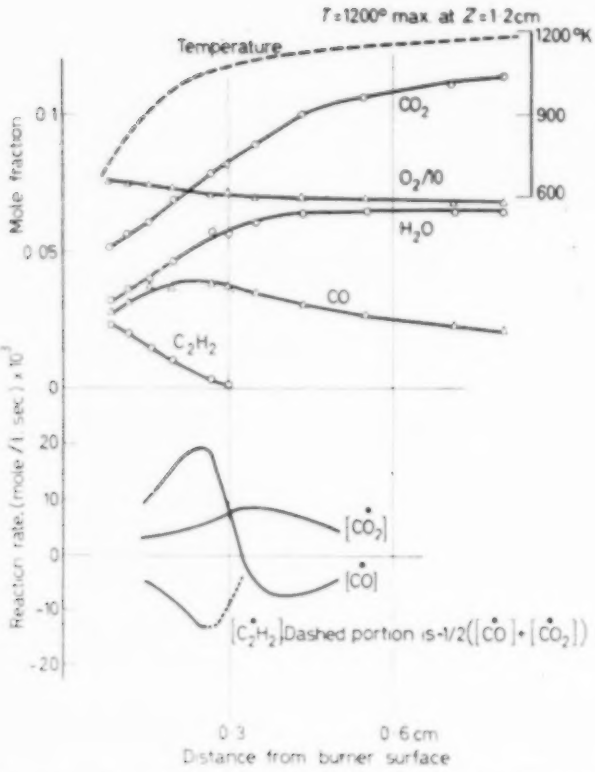

Figure 1. Temperature and composition profiles through a flame of composition 0·202 C_2H_2+2·5 (O_2+0·14 A), 1200 K *final* T, 6 cm Hg. *Reaction rates at bottom of figure:* $[\dot{C}_2H_2]$ *curve completed by assuming that* $-2[\dot{C}_2H_2]=[\dot{CO}]+[\dot{CO}_2]$

Hydrogen is not plotted because it was very small everywhere through the sampling region. By using approximate diffusion corrections, the reaction rate curves at the bottom of *Figure 1* can be derived in a way already reported[3].

Table 1 summarizes the results for all the lean acetylene flames studied. It is seen, for example, that in 1 200°K constant temperature flames (ρv) or v increases about two and a half times as ϕ decreases by about the same factor; but this is not accompanied by any considerable change in the maximum rate of $-d[C_2H_2]/dt$, which is practically constant and always occurs near 1 020°K.

The moles of fuel fed to the burner per second does not change much at each constant final flame temperature. At most, a 15 per cent increase in the flux of fuel is necessary when (ρv) is doubled. Since the flux of fuel molecules is equal to the area under the curve of $-d[C_2H_2]/dt$ versus distance, neither the area under the curve nor the maximum value changes very strikingly. Therefore, a changing (ρv) in these constant temperature flames is not associated with a marked change in the rate of fuel consumption.

If (ρv) had been proportional to the square root of the rate of fuel consumption, as is suggested by most adiabatic theories, the rate of fuel consumption should have increased by a factor of 6·5 on going from $\phi=0{\cdot}202$ to $\phi=0{\cdot}080$ in the 1 200°K flames. But no increase was observed even remotely of this value, certainly not as much as five per cent of it.

Heat Abstraction from Lean Acetylene Flames

We ask now whether the change in burning velocity is consistent with reasonable ideas about the dependence of the necessary heat abstraction from the flame on burning velocity.

Table 1. Data for flames of composition C_2H_2+2·5 (O_2+0·14A) *burnt at 6 cm of mercury*

Final T, °K	1200			1340			1540		
ϕ	0·202	0·128	0·080	0·162	0·116	0·091	0·160	0·131	0·109
$\rho v \times 10^5$, g cm^{-2} sec^{-1}	1·43	2·19	3·64	3·04	4·68	6·26	6·4	8·2	10·9
Max. rate $-d[C_2H_2]/dt$ mole l.$^{-1}$ sec^{-1}	0·013	0·015	0·014	0·032	0·035	0·031	0·085	0·075	—
T at max. rate	1030	1020	1010	1040	1070	1080	1080	1060	—
$q/(\rho v)$ *absorbed by burner*, cal g^{-1}	326	153	24	206	91	40	182	108	48

The heat absorbed by the burner can be symbolized $q/(\rho v)$ cal g^{-1}, where q is the heat flux to the burner surface in cal cm^{-2} sec^{-1}. $q/(\rho v)$ was estimated at points 0·5 cm from the burner surface from a knowledge of the reactants fed and of the analysed products at this position. The concentration of radicals was ignored, and the difference between the heat released and that required to warm the observed products to a known temperature, nearly always within 100° of the final temperature, was assumed to be absorbed by the burner, and was tabulated in *Table 1*.

How should $q/(\rho v)$ vary with (ρv)? We expect

$$q = \lambda \mathrm{d}T/\mathrm{d}Z$$

to hold approximately if λ is the thermal conductivity of oxygen at temperatures only a little above room temperature, say $\sim 7 \times 10^{-5}$ cal cm^{-1} sec^{-1} (°K)$^{-1}$, and $\mathrm{d}T/\mathrm{d}Z$ is the unknown temperature gradient at the surface of the burner. This gradient approaches zero, of course, for a near adiabatic flame, and must increase with decreasing (ρv) to a value somewhat greater than that estimated for the most strongly quenched flame which was actually studied. The most strongly quenched of the acetylene flames was that shown in *Figure 1*, and if this temperature curve is prolonged smoothly to the point 300°K at the burner surface, the gradient at the surface can be estimated to be about 9 000°K cm^{-1}. It seems reasonable to expect the gradient at the surface to be

$$\mathrm{d}T/\mathrm{d}Z \sim 9\,000\,\{1 - (\rho v)/(\rho v)_a\}$$

or perhaps somewhat larger, where $(\rho v)_a$ for a given final temperature would be the adiabatic burning velocity for the mixture having that adiabatic flame temperature.

Hence, one might expect

$$q/(\rho v) \sim 7 \times 10^{-5} \times 9\,000 \left\{\frac{1}{(\rho v)} - \frac{1}{(\rho v)_a}\right\}$$

$$\sim 0{\cdot}6 \left\{\frac{1}{(\rho v)} - \frac{1}{(\rho v)_a}\right\}$$

An expression of the form

$$q/(\rho v) = \mathrm{f}(T) \left\{\frac{1}{(\rho v)} - \frac{1}{(\rho v)_a}\right\}$$

does describe the heat loss reasonably, see *Figure 2*. $\mathrm{f}(T)$ has the empirical value 0·0038 $(T_{\mathrm{final}} - 1\,000)^\circ$ for the very lean acetylene flames; and is 0·76 for the 1 200°K series.

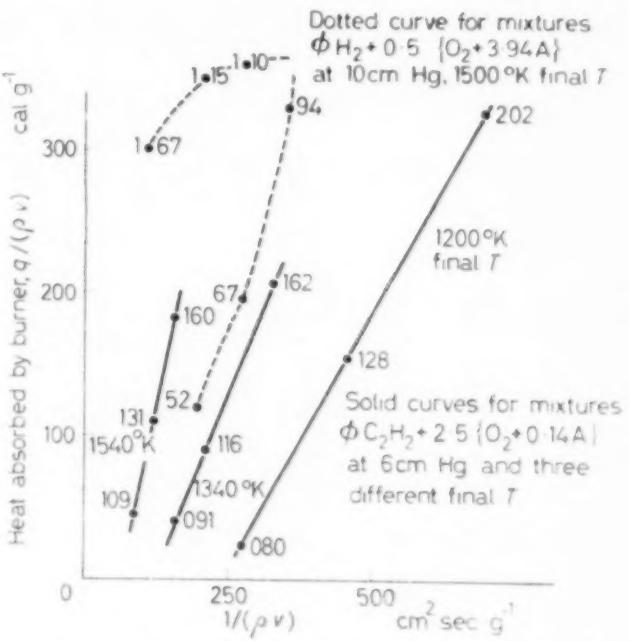

Figure 2. Heat abstracted from non-adiabatic flat flames as a function of (mass flow)$^{-1}$. The mixture strength, φ, is noted for each point and the spot locates each value.

The fact that $q/(\rho v)$ has a reasonable dependence on (ρv) and even a slope of reasonable order of magnitude suggests that the variation of (ρv) with mixture strength in these constant temperature flames is only a result of the heat abstraction required to maintain the constant temperature. The suggestion is consistent with the finding of the last section, that the maximum rate of fuel consumption does not vary with burning velocity.

Near Stoichiometric Hydrocarbon Flames

An attempt was made to study constant temperature hydrocarbon–oxygen–argon flames in the region of the stoichiometric mixture strength. Unfortunately, fuel-rich hydrocarbon flames require higher temperatures than fuel-

lean ones in order to burn at all, and our quartz coated thermocouples deteriorate rapidly in hot fuel-rich hydrocarbon flames.

Over the composition range of 0·7 to 1·2 times the stoichiometric fuel, constant temperature acetylene flames at 1 500°K, or propane flames at 1 650°K, had a 60 per cent change in (ρv) and a dependence of $q/(\rho v)$ on (ρv) much like that for very lean acetylene flames. The maximum rate of reaction was also essentially constant in either constant temperature series. The maximum rate, however, occurred at a higher temperature the richer the flame.

Flames still richer in fuel could not be studied because of the temperature limitation. This is unfortunate because we could not burn rich enough or hot enough to attain maximum $q/(\rho v)$ and minimum (ρv). At constant flame temperatures of 1 700°K or more, Kaskan found a minimum burning velocity at about the stoichiometric ratio[2]; but at lower constant flame temperatures, he too failed to find a minimum burning velocity for hydrocarbon flames. The reason is, at least in part, that at low temperatures, fuel-rich hydrocarbon flames approach equilibrium more quickly than fuel-lean ones[3], and hence the hydrocarbon flame of greatest actual calorific value is considerably richer than the stoichiometric mixture.

The data obtained are recorded in *Table 2*.

Hydrogen Flames

Fuel-rich hydrogen flames offer the only instance found in which the reaction rate increases considerably as one goes to faster burning constant temperature flames. Six compositions of $\phi H_2 + 0{\cdot}5\,(O_2 + 3{\cdot}94\,A)$ were burnt at 10 cm of mercury and 1 500°K final temperature. The $q/(\rho v)$ plot for these is given in *Figure 2*, and some of the temperature and concentration profiles are plotted in *Figure 3*.

The fuel-lean mixtures resemble very lean acetylene flames in that they possess a constant flux of fuel within five per cent and a constant maximum $-\mathrm{d}[O_2]/\mathrm{d}t$ at about 1 220°K. It is a little odd, therefore, that the lean branch of the curve in *Figure 2* does not display a strictly linear variation of $q/(\rho v)$ with $1/(\rho v)$ just as do lean acetylene flames. The curvature is of the sign expected if thermal conductivity increased with increasing hydrogen content in the gas, however, and this may explain it.

Rich hydrogen flames have a marked increase in the flux of oxygen and in $-\mathrm{d}[O_2]/\mathrm{d}t$ associated with the increased burning velocity

Table 2. Data for near stoichiometric flames, oxidant $= O_2 + 3{\cdot}94\ A$

Mixture	$\phi C_2H_2 + 2{\cdot}5$ *oxidant*			$\phi C_3H_8 + 5$ *oxidant*		
P, cm of mercury	6			10		
Final T, °K	1500			1650		
ϕ	1·17	0·93	0·75	1·29	0·98	0·69
$(\rho v) \times 10^5$ *g cm^{-2} sec^{-1}*	2·70	3·30	4·32	3·10	4·00	5·15
Moles fuel fed $\times 10^6$ *per cm^2 per sec*	6·3	6·2	6·5	4·3	3·9	3·6
*Max. reaction rate** *mole l.$^{-1}$ sec^{-1}*	0·046	0·046	0·042	0·091	0·100	0·093
T at max. reaction rate	1430	1380	1280	1620	1580	1520
q (av) absorbed by burner, cal g^{-1}	354	291	178	214	159	100

*Maximum reaction rate is $-\mathrm{d}[C_2H_2]/\mathrm{d}t$ for acetylene flames, but $-\mathrm{d}[O_2]/\mathrm{d}t$ for propane flames because the intermediate formation of C_2 hydrocarbons makes $-\mathrm{d}[C_3H_8]/\mathrm{d}t$ a false measure of the rate of fuel oxidation.

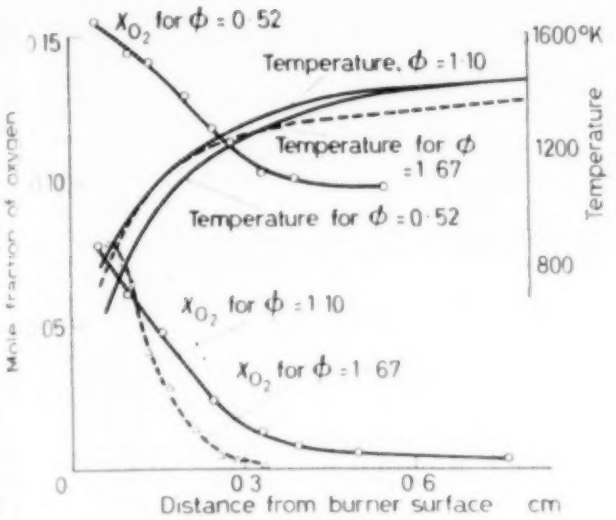

Figure 3. Profiles through three flames of composition $CH_2 + 0{\cdot}5\ (O_2 + 3{\cdot}94\ A)$, *1500°K final T, 10 cm Hg*

of progressively richer mixtures. Between $\phi = 1{\cdot}10$ and $1{\cdot}67$, (ρv) increases by a factor of $2{\cdot}7$ and v by a factor of $3{\cdot}1$, and most of this can be explained by a faster reaction rate. If all the increase were proportional to the square root of an increased ratio of reaction rates, the reaction rate should have increased about ninefold. Actually, the X_{O_2} curves of *Figure 3* imply a fivefold increase in the maximum rate of $-\mathrm{d}[O_2]/\mathrm{d}t$, after corrections have been made for diffusion. Then assuming that the average $-\mathrm{d}[O_2]/\mathrm{d}t$ is proportional to the maximum $-\mathrm{d}[O_2]/\mathrm{d}t$, we conclude that about $(5/9)^{1/2} = 3/4$ of the change in v could be accounted for by the increased reaction rate even if no change at all had occurred in the heat loss to the burner surface.

It is possible to understand why the rate of reaction in hydrogen flames should increase as one goes from stoichiometric towards richer mixtures, but not as one goes toward leaner mixtures. The rate of consumption of oxygen is the rate of $H + O_2 \longrightarrow OH + O$. This generates two free valencies per oxygen molecule consumed in either rich or lean flames and relatively large concentrations of radicals exist in the reaction zone. In rich flames the free valencies tend to exist mostly as H atoms; but the leaner the flame the more they tend to exist as OH, or O. Now our low pressure rich flames will not support large concentration gradients of H atoms, because of their easy diffusion, but do support considerable gradients of [OH] or [O][4]; and richer flames contain greater [H] in the early part of the flame. It might be thought that this would be countered by a decreased $[O_2]$ in richer flames, but the mole fraction of oxygen is about the same at the point of maximum $-\mathrm{d}[O_2]/\mathrm{d}t$ for the $\phi = 1{\cdot}67$ mixture as for $\phi = 1{\cdot}10$.

In lean flames a smaller fraction of the radicals tends to exist as readily diffusible H atoms, and the change of [H] in the reaction zone with mixture strength can also be countered more effectively by a change in $[O_2]$, for in lean flames $[O_2]$ in the reaction zone changes markedly with the oxygen concentration of the original reactants.

Perhaps it should be added that a similar increase in burning velocity in fuel-rich hydrocarbon flames is precluded by the fact that rich hydrocarbon mixtures do not generate large radical concentrations. As has been discussed elsewhere[3], the free valencies formed via $H + O_2 \longrightarrow OH + O$ in hydrocarbon flames are partly destroyed in the degradation of the fuel to carbon monoxide and hydrogen, and destroyed more completely in the mixtures richer in hydrocarbon. This can be illustrated, for example, by *Table 2* which shows that richer hydrocarbon flames require higher reaction temperatures for the same maximum rate of reaction.

Conclusion

Our results show that the change of burning velocity with mixture strength in constant temperature non-adiabatic flames is often, but not always, determined chiefly by the need for abstracting an appropriate amount of heat from the flame. One cannot, therefore, in general deduce relative reaction rates from relative burning velocities in such flames, as Botha and Spalding considered to be possible[1].

Our results are also relevant to efforts sometimes made to determine the activation energy of flame reactions from the dependence of burning velocity on final temperature. To this end it is often assumed that the reactions always

occur at some constant fraction of the final temperature, or at a constant fraction of the temperature rise[5]. The assumption is not a very good one: for in the very lean flames of *Table 1* the temperature of maximum $-\mathrm{d}[C_2H_2]/\mathrm{d}t$ is 85 per cent of T_{final} when T_{final} is 1200°K, but only 69 per cent when T_{final} is 1540°K; and in the constant temperature acetylene flames of *Table 2*, $-\mathrm{d}[C_2H_2]/\mathrm{d}t$ attains a maximum at 85 per cent of T_{final} for a moderately lean flame, but at 95 per cent for a moderately rich one. One must suspect any 'activation energy' derived under the assumption that the flame reactions occur at a constant fraction of T_{final} or of the temperature rise.

References

[1] Botha, J. P. and Spalding, D. B. *Proc. Roy. Soc. A*, 1954, **225**, 71

[2] Kaskan, W. E. *Sixth Symposium (International) on Combustion*, p 134. Reinhold: New York, 1957

[3] Fenimore, C. P. and Jones, G. W. *J. phys. Chem.* 1959, **63**, 1834

[4] Fenimore, C. P. and Jones, G. W. *J. phys. Chem.* 1959, **63**, 1154

[5] van Tiggelen, A. and Deckers, J. *Sixth Symposium (International) on Combustion*, p 61. Reinhold: New York, 1957

The Effect of Flame Configuration on Combustor Performance

C. C. MIESSE

Armour Research Foundation, Chicago 16, Illinois

(Received May 1960)

The effect of flame configuration on combustor performance is analysed theoretically by assuming that chemical conversion commences when the premixed gaseous propellants pass through the flame surface. Hence the percentage conversion, which is indicative of performance, can be determined at any point downstream of the flame surface by considering the chemical law of mass action and assuming an integral order of reaction. Integration over the cross section of the combustor then yields the theoretical performance for any selected length of combustor. As could be expected, performance increases as the flame angle increases, and flame configurations resulting from annular flameholders are more efficient than the conventional V-gutter or conical flameholders. Qualitative confirmation of the trends, predicted theoretically, is provided by experimental data obtained from a 2 in. i.d. burner.

THE combustion of premixed propellants downstream of a flame surface is determined theoretically by considering the chemical law of mass action and asserting that reaction begins at the point where the air–fuel mixture passes through the flame envelope. It is based upon a previous theory which assumes a plane flame front[2]. Under the simplifying assumptions listed below, the governing dimensionless group is identified as that established by G. DAMKÖHLER[1] and subsequently applied to the problem of scaling combustors by S. S. PENNER[3].

Basic Conversion Theory

Nomenclature

The symbols used here have the following meanings:

- A/F Air–fuel mixture ratio
- $a = kD/U_1$, Damköhler's first similarity group
- $a' = kL/U_1 = kT_g$
- c Cotangent of flame half-angle
- D Diameter or width of combustion chamber (ft)
- f Arbitrary function of transverse coordinate
- G Mass flow rate (lb sec^{-1} in^{-2})
- $\mathbf{g}$ Acceleration due to gravity
- g Arbitrary function of radial coordinate
- I_{sp} Specific impulse (sec)
- K Empirical coefficient
- k Reaction frequency (sec^{-1})
- L Characteristic length of combustor (ft)
- M Molecular weight of combustion products (lb/lb mole)
- m Empirical exponent
- n Order of reaction
- p_c Chamber pressure (lb/in^2)
- p_0 Ambient pressure (lb/in^2)
- $q = r/D$, dimensionless radial coordinate
- R Universal gas constant (1545 ft lb/lb mole °R)
- R_ρ Density ratio across the flame front
- SFC Specific fuel consumption (lb/h of fuel per lb of thrust)
- $s = y/D$, dimensionless transverse distance
- T_g Gas residence time (sec)
- T_c Combustion temperature (°R)
- t Time (sec)
- U_0 Cold gas velocity (ft/sec)
- U_1 Average axial hot gas velocity (ft/sec)
- V_f Average axial flame speed (ft/sec)
- W Percentage unreacted (available)
- W' Incremental percentage unreacted
- w Percentage conversion, combustion efficiency
- w' Incremental percentage conversion
- x Axial distance from flame anchor (ft)
- x' Axial distance downstream from flame envelope (ft)
- y Transverse distance from centreline (ft)
- z Dimensionless axial distance from flame anchor
- z_0 Dimensionless length of flame envelope
- z' Dimensionless axial distance downstream from flame envelope
- γ Ratio of specific heats
- θ Angular coordinate

Theory

The present theory is based on three assumptions regarding the chemical kinetics of the system: the propellants react only in the vapour phase and as single chemical substances; the system is isothermal; and the propellant vapours mix immediately upon formation. Thus the law of mass action is expressed as

$$dw' = k\,(W')^n\,dt \qquad \ldots . [1]$$

where dw' is incremental percentage of propellant converted in time dt; k is relative reaction rate or 'reaction frequency'[3] in fraction of propellant converted per second.

Further assumption of a uniform average velocity permits the expression of time in terms of distance

$$dz' = dx'/L = U_1(x)\,dt/L \qquad \ldots . [2]$$

For air–fuel mixtures, the available propellant can be represented by

$$W' = 1 - w' \qquad \ldots . [3]$$

and, for $n = 1$, the equation for w' becomes

$$w' = 1 - e^{-a'z'} \qquad \ldots . [4]$$

and, for $n \neq 1$ it is

$$w' = 1 - [a'(n-1)\,z' + 1]^{-1/(n-1)} \qquad \ldots . [5]$$

where

$$a' = kL/U_1 = kT_0 \qquad \ldots . [6]$$

The parameter a' can be identified as Damköhler's first similarity group[1] and is the ratio of reaction rate to rate of discharge of gases.

Effect of Flame Configuration

The combustion efficiency downstream of a non-planar flame surface can be determined by the method presented in ref. 2, except that the surface of zero conversion must now be represented by a function of the system coordinates.

The general configuration under consideration is represented schematically by *Figure 1*. The velocity of the fuel-air mixture is U_0 and that of the products of combustion U_1 (both assumed to be travelling uniformly and parallel to the walls). The 'diameter' of the duct is D, and the coordinates are represented by x (axial), y (transverse for two-dimensional flow), r (radial), and θ (angular). With D as the unit of length, the following dimensionless coordinates can be defined

$$z = x/D \quad s = y/D \quad q = r/D \qquad \ldots . [7]$$

The remainder of the analysis is dependent upon the cross sectional configuration of the duct, and will therefore be developed along two parallel avenues.

Two-dimensional duct Cylindrical duct

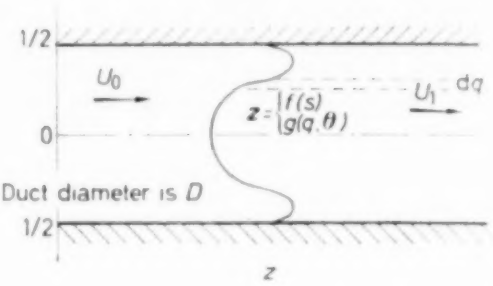

Figure 1. Schematic drawing of generalized flame configuration

The flame surface can then be represented by an equation of the form

$$z = f(s) \qquad z = g(q, \theta) \qquad \ldots . [8]$$

Under the assumption that all flow is one-dimensional and that transverse diffusion is negligible, each reaction is initiated at the flame boundary represented by equation 8 and proceeds horizontally along the stream tube. Since the total conversion at any cross section downstream requires summation of the contributions of all stream tubes in the cross section 'bundle,' it is apparent that equations 1 to 5 apply to a single stream tube only, with z' measured from the flame surface. In terms of the fixed coordinate z, measured from the upstream tip of the flame surface, it is apparent that the axial dependence must be represented by

$$z' = z - f(s) \qquad z' = z - g(q, \theta) \qquad \ldots . [9]$$

Since the total efficiency (w) at any cross section is equal to the sum of the products of

stream tube efficiency and relative area, it is apparent that the following integrals must be determined.

$$w = 2\int w'\,ds \qquad w = \frac{4}{\pi}\int_0^{2\pi}\int w'q\,dq\,d\theta \qquad \ldots [10]$$

where the integrals are evaluated from the centreline ($s = q = 0$) to the flame surface

$$s = f^{-1}(z)^* \qquad q = g^{-1}(z, \theta)^* \qquad \ldots [11]$$

where c is the cotangent of the half-angle, as depicted in *Figure 2*.

The expressions, for $n = 1$, for w' become

$$w' = 1 - e^{-a(z-cs)} \qquad w' = 1 - e^{-a(z-cq)} \qquad \ldots [13]$$

and, for $n \neq 1$,

$$w' = 1 - [1/\{1 + a(n-1)(z-cs)\}]^{1/n-1}$$
$$w' = 1 - [1/\{1 + a(n-1)(z-cq)\}]^{1/n-1} \qquad \ldots [14]$$

and the resultant expressions for w are listed in *Table 1*, for $n = 1, 2$.

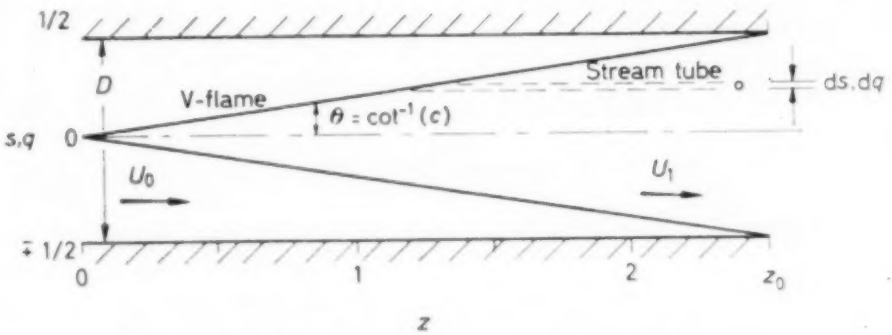

Figure 2. Schematic diagram of V-flame configuration

for $z \leqslant z_0$ (point at which flame surface touches wall), or to the duct wall ($s = q = \frac{1}{2}$) for $z \geqslant z_0$.

V-Flame

For the case of the conventional, centrally mounted bluff body flameholder, which yields the familiar V-flame surface, equation 8 becomes

$$z = cs \qquad z = cq \qquad \ldots [12]$$

* f^{-1} and g^{-1} are the inverse of functions f and g, respectively.

Representative curves for a conical flame in a cylindrical duct (for $a = 1$) are shown in *Figures 3*(a) and *3*(b), indicating the strong variation of performance with V-flame angle especially for small values of z. From the curves presented, it is apparent that efficiency decreases as the flame angle decreases, and that the character of the performance curves changes from concave to convex when the flame cone meets the wall. The influence of flame angle on performance is more graphically depicted

Table 1. Equations for propellant conversion (V-Flame)

n	z/c	*Two-dimensional duct*	*Cylindrical duct*
1	$\leqslant 1/2$	$\frac{2}{c}\left[z + \frac{1}{a}(e^{-az} - 1)\right]$	$\frac{4}{c^2}\left[z^2 - \frac{2}{a^2}(e^{-az} + az - 1)\right]$
	$\geqslant 1/2$	$1 - \frac{2e^{-az}}{ac}[e^{ac/2} - 1]$	$1 - \frac{8e^{-az}}{a^2c^2}\left[e^{ac/2}\left(\frac{ac}{2} - 1\right) + 1\right]$
2	$\leqslant 1/2$	$\frac{2}{c}\left[z - \frac{1}{a}\ln(1+az)\right]$	$\frac{4}{c^2}\left\{z^2 - \frac{2}{a^2}[(1+az)\ln(1+az) - az]\right\}$
	$\geqslant 1/2$	$1 + \frac{2}{ac}\ln\left(\frac{2+2az-ac}{2+2az}\right)$	$1 + \frac{8}{a^2c^2}\left[\frac{ac}{2} + (1+az)\ln\left(\frac{2+2az-ac}{2+2az}\right)\right]$

by the cross-plot of data shown in *Figure 3*(b). It is thus indicated that the efficiency of an air-breathing system could be increased appreciably by providing for greater flame-spreading.

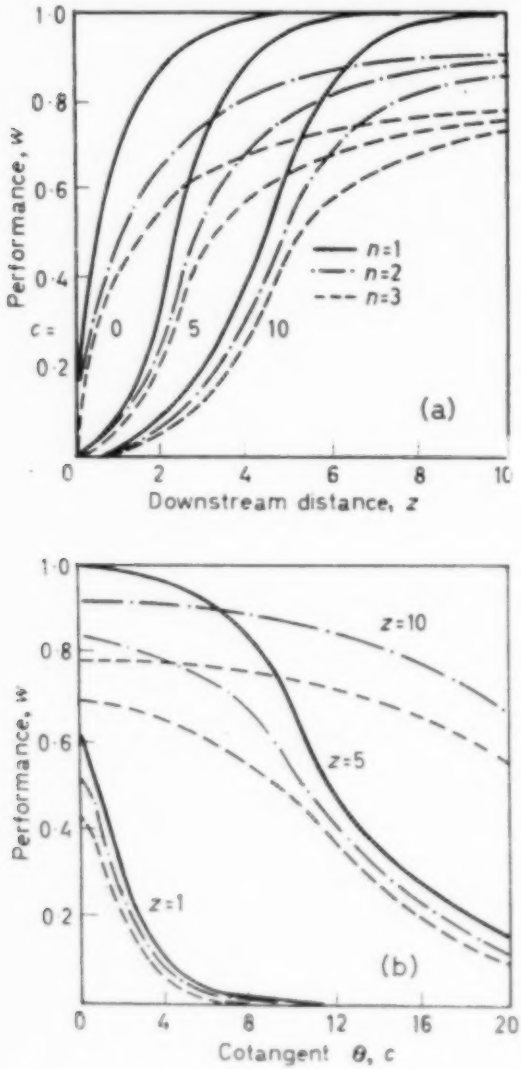

Figure 3. Effect of flame angle on performance variations

Although no apparent advantage could be gained from improved flame-spreading for $a=n=1$ and $c=z=10$, it is obvious that considerable weight saving could be achieved in that essentially complete combustion occurs for $z=6$ when $c=5$, for example.

Variation of local efficiency, as indicated by w, with transverse distance from the centreline, can be determined from equations 13 or 14. A comparison of the theoretical curve with the experimental data of R. J. PETREIN *et al.*[4] is shown in *Figure 4*, indicating the apparent validity of the analysis.

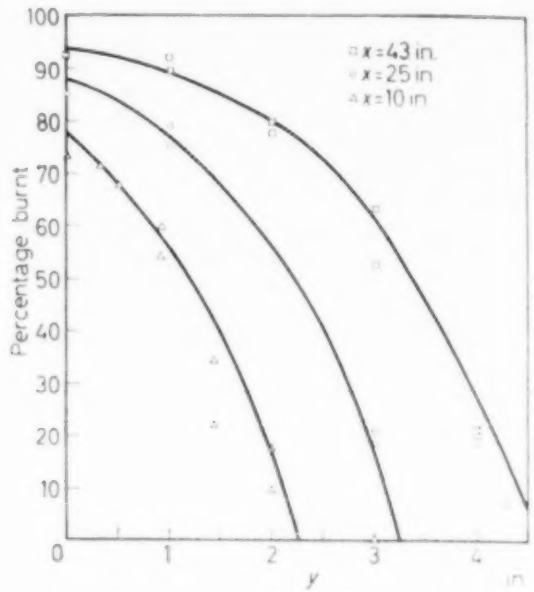

Figure 4. Comparison of efficiency data of R. J. PETREIN *et al.*[4] *with theoretical curves for* $w'=1-\exp[-0{\cdot}042\ (x+25-15{\cdot}2y)$

It is noted that a change in upstream velocity U_a will result in new values for both a and c. Under laminar flame conditions, for instance,

$$a=kD/U_1\approx kD/R_\rho\delta U_a \quad \ldots.[15]$$

and

$$c=[(U_a/V_f)^2-1]^{\frac{1}{2}} \quad \ldots.[16]$$

where R_ρ is the density ratio across the flame front, and V_f is the laminar flame speed for the combustible mixture.

Conical Flame

Since the total efficiency is dependent upon the 'average' axial distance downstream of the flame front, it follows that a flame stabilizer which provides for a larger percentage of conversion at the upstream anchor will lead to greater efficiency at any downstream position. The annular anchor provided by the recessed wall flameholder[5] exhibits the desired characteristics for premixed gaseous fuel combustion, although it is suggested that similar advantages could be achieved in liquid fuel combustion by the introduction of a circular pilot flame or a converging (impinging jet) spray from a ring of injectors.

Figure 5 depicts the conical flame produced by the recessed wall flameholder (RWF). Inspection of this figure reveals that the flame

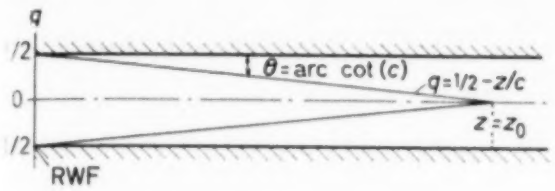

Figure 5. Conical flame configuration

front in a cylindrical duct* is represented by the equation

$$q = \tfrac{1}{2} - z/c \qquad \ldots . [17]$$

and, for $n = 1$ (first order reaction), the incremental propellant conversion can be expressed by

$$w' = 1 - \exp\{-a(z - c/2 + cq)\} \quad .. [18]$$

or, for $n \neq 1$,

$$w' = 1 - \left(\frac{1}{1 + a(n-1)(z - c/2 + cq)}\right)^{1/(n-1)} \qquad \ldots . [19]$$

Integration over the circular cross section then yields the theoretical expressions for total efficiency (w), as listed in *Table 2*.

figure, it is apparent that the conical flame exhibits as much as a 40 per cent improvement in efficiency (for $z = 0{\cdot}3\,c$) but that the margin of superiority decreases to 25 per cent at the downstream end of the flame surface and becomes negligible for $z = c$. Hence, it is concluded that substantial increases in overall performance of a combustor can be effected by substitution of a conical flame for the standard

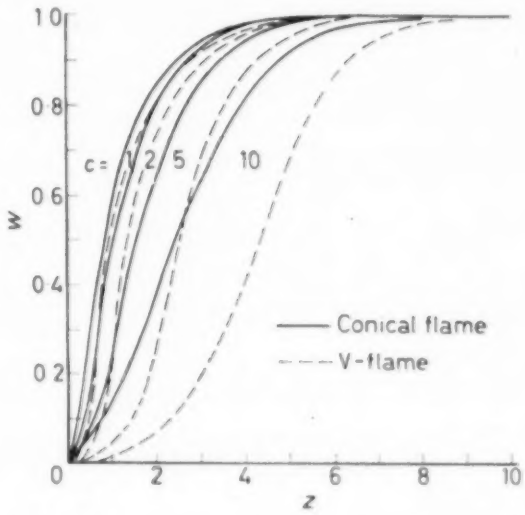

Figure 6. Comparison of performance variations for conical and V-flames when $a = n = 1$

Table 2. Equations for conical flame propellant conversion

n	z/c	w
1	$\leqslant 1/2$	$\frac{4}{c^2}\left\{cz - z^2 - \frac{2}{a^2}\left[1 + \frac{ac}{2} - az - e^{-az}\left(1 + \frac{ac}{2}\right)\right]\right\}$
	$\geqslant 1/2$	$1 - \frac{8e^{-az}}{a^2c^2}\left(e^{ac/2} - 1 - \frac{ac}{2}\right)$
2	$\leqslant 1/2$	$\frac{4}{c^2}\left\{cz - z^2 - \frac{2}{a^2}\left[az - \left(1 + az - \frac{ac}{2}\right)\ln(1 + az)\right]\right\}$
	$\geqslant 1/2$	$1 - \frac{8}{a^2c^2}\left[\frac{ac}{2} + \left(1 + az - \frac{ac}{2}\right)\ln\left(\frac{2 + 2az - ac}{2 + 2az}\right)\right]$

The superiority of the conical flame over V-flame for cylindrical ducts is indicated by *Figure 6* which compares the two curves for $a = n = 1$ and $c = 1$, 2, 5 and 10. From this V-flame if the chamber length is of the order of the length of the flame surface. For long tubular combustors, however, the improvement becomes insignificant.

Dual Flameholder

For the dual flameholder consisting of a combination of the two types of flameholders

*For a two-dimensional duct, in which the burning rate is constant across the duct, stabilization of the flame at the wall will merely translate or interchange the two surfaces of the wedge-shaped flame, so that the equations presented previously remain unchanged.

described above, the idealized flame configuration is shown in *Figure 7*. It is suggested that this type of flame configuration can provide a reasonable approximation to the more conventional arrangement of bluff-body flameholders shown in the lower half of *Figure 7*.

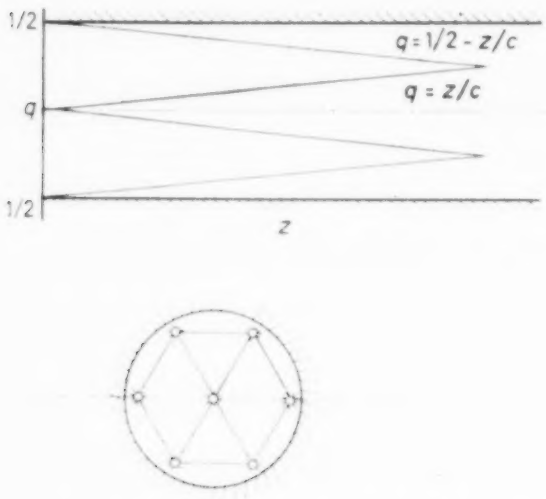

Figure 7. Schematic drawing of dual flameholder configuration with conventional flameholder counterpart

Analysis of this configuration reveals that the performance at any downstream cross section will consist of a sum of two integrals:

$$w_{\mathrm{I}} = 8\int_{0}^{z/c} (1 - e^{-a(z-cq)})\, q\, dq \quad (n=1) \quad \ldots [20]$$

and

$$w_{\mathrm{II}} = 8\int_{1/2-z/c}^{1/2} [1 - e^{-a(z-c/2+cq)}]\, q\, dq \quad (n=1) \quad [21]$$

For $z \leqslant \frac{1}{4}c$ (upstream of the intersection of the component flame surfaces), the total conversion due to the dual flameholder can be determined as the sum of the separate integrals, evaluated in the first rows of *Tables 1* and *2*, since the effects of the two component flame surfaces are separate in this region, according to the original assumptions. However, for $z > \frac{1}{4}c$, the upper limit for equation 20 and the lower limit for equation 21 equals $\frac{1}{4}$, and the corresponding expressions for w_{I} and w_{II} become:

$$w_{\mathrm{I}} = \tfrac{1}{4} - \frac{8e^{-az}}{a^2c^2}\left[(e^{ac/4} - 1)(ac/4 - 1)\right] \quad \ldots [22]$$

and

$$w_{\mathrm{II}} = \tfrac{3}{4} - \frac{8e^{-az}}{a^2c^2}\left[e^{ac/4}(ac/4 + 1) - ac/2 - 1\right] \quad \ldots [23]$$

Addition of equations 22 and 23 then yields the final expression for total conversion at any cross section downstream of the flame surface intersection

$$w = 1 - (2e^{-az}/ac)(2e^{ac/4} - 3) \quad \ldots [24]$$

Corresponding equations for performance with the dual flameholder for other values of n (order of reaction) can be determined in the same manner.

The superiority of the dual flameholder over either of the two simple configurations is adequately demonstrated in *Figure 8*, which compares the three systems for $a = n = 1$ and

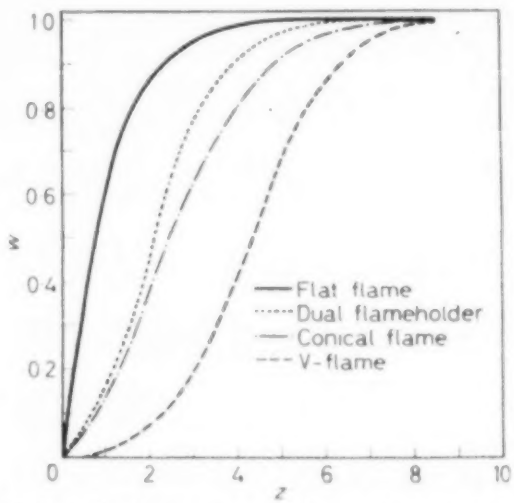

Figure 8. Performance variations for various flame configurations ($a = n = 1$, $c = 10$)

$c = 10$. Again it is noted that the difference in theoretical performance of the three systems is negligible for $z > c$.

Experimental Results

In order to obtain experimental evidence of the validity of the foregoing theory, a series of te-

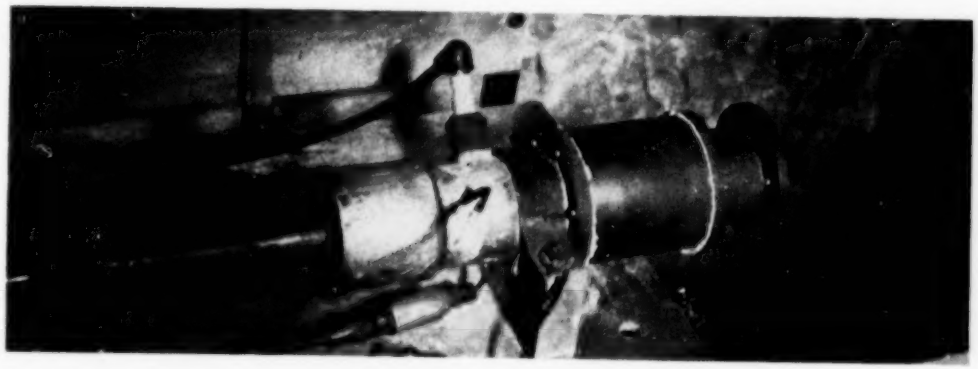

Figure 9(a). *Apparatus*

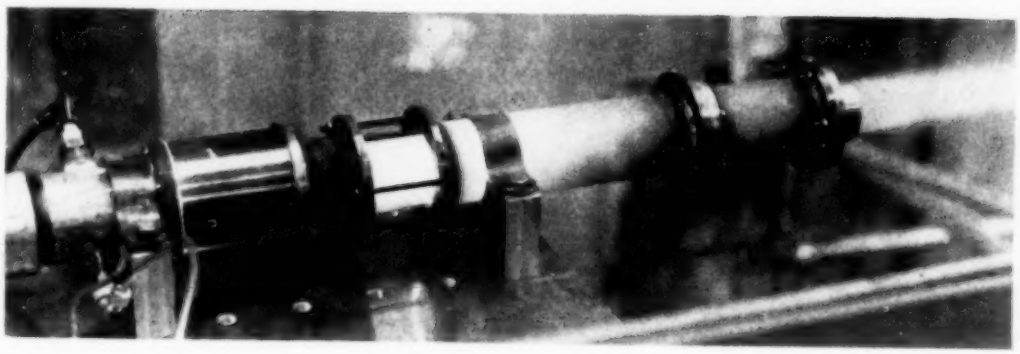

Figure 9(b). *In operation*

conducted with a propane–air mixture in the apparatus shown in *Figure 9*. The flameholder section was replaceable, and provision was made for determining the total thrust for various lengths of the extensible combustion chamber.

The performance superiority of the recessed wall flameholder over the V-gutter flameholder is demonstrated by inspection of the specific fuel consumption data obtained from a series of tests using three flow rates and two L/D ratios for each configuration. Experimental specific impulse (I_{sp}) was related to the specific fuel consumption (SFC) data by the equation

$$I_{sp} = \frac{3\,600}{(1+A/F)\ (\mathrm{SFC})} \qquad \ldots\ldots [25]$$

The theoretical specific impulse ($I_{sp\,(th.)}$) was determined from the standard rocket equation

$$I_{sp} = \left\{ \frac{2R}{\mathbf{g}} \frac{\gamma}{\gamma - 1} \frac{T_c}{M} \left[1 - \left(\frac{p_a}{p_c} \right)^{\frac{\gamma-1}{\gamma}} \right] \right\}^{\frac{1}{2}} \qquad \ldots\ldots [26]$$

Inspection of thermodynamic data[6] revealed that $k \fallingdotseq 1{\cdot}3$, $R = 1\,545$ ft lb/lb mole °R, $M = 29$ lb/lb mole, and $T_c = 4\,080$ °R. Using these thermodynamic properties, the theoretical specific impulses averaged at about 115 sec for $p_a/p_c \fallingdotseq 0{\cdot}85$ as shown in *Table 3*.

Inasmuch as C. H. TRENT[7] has demonstrated the equality of percentage conversion and ratio of experimental to theoretical specific impulse, this latter ratio was identified with the w of the foregoing theory.

Since the original plane flame-front theory[2] predicted that the percentage conversion w should be a function of $a'z' = kLz'/U_a$, and since the precise effect of flow velocity on the reaction frequency k, due to turbulence and mixing, is unknown, it is proposed to represent k by a power of the flow rate G. Hence

$$a'z' = KG^m x/U_a = K\rho g G^{m-1} x \qquad \ldots [27]$$

where ρ is the density of the gaseous mixture, and K and m are empirical constants. Plotting of w versus G, for constant values of x, on logarithmic coordinates resulted in a best-fit value of 0·35 for $m-1$, indicating

Table 3. Performance data for V-gutter and RWF flameholders

Flameholder	*L/D*	*G* *lb/sec in²*	*Thrust* *lb*	SFC *(lb/h) fuel per lb thrust*	$\bar{p}_c$ *lb/in² gauge*	$I_{sp(th.)}$ *sec*	I_{sp} *sec*	*w*
V-Gutter	3·52	0·0696	4·7	12	1·65	103·2	17·95	0·1
	3·52	0·0790	6·0	10·5	2·04	107·7	20·55	0·1
	3·52	0·0846	6·7	10·18	2·14	110·4	21·09	0·1
	4·00	0·0696	5·9	9·5	1·87	106·4	22·65	0·2
	4·00	0·0790	7·1	8·77	2·31	111·4	24·6	0·2
	4·00	0·0846	7·7	8·7	2·46	114·9	24·8	0·2
Recessed wall	4·00	0·0696	8·2	7·05	2·38	112·4	30·6	0·2
	4·00	0·0790	10·0	6·55	3·10	116·3	32·95	0·2
	4·00	0·0846	11·4	6·05	3·59	123·4	35·65	0·2
	5·96	0·0696	11·5	5·2	3·91	125·5	41·5	0·3
	5·96	0·0790	13·7	4·75	4·72	130·7	45·4	0·3
	5·96	0·0846	14·9	4·5	5·45	138·2	47·9	0·3

that the reaction frequency k varies as $G^{1.35}$. The final variations of w with $G^{0.35}$ L/D are shown in *Figure 10*, which demonstrates the superiority of the conical flame configuration. In the absence of additional data and because

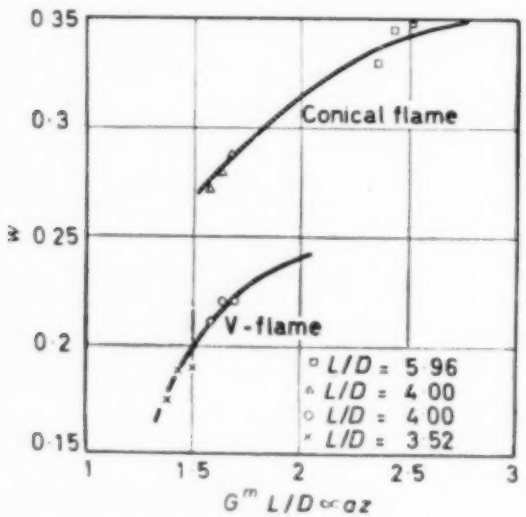

Figure 10. Experimental variation of performance with relative distances for two flame configurations

of the uncertainty of the order of reaction n, quantitative comparison of *Figures 10* and *6* is not feasible. However, the general shape and relative positions of the two curves correspond quite closely, indicating that the highly simplified theory may indeed provide a means for predicting performance of air–fuel combustors.

Conclusions

As a result of the foregoing investigation, it is concluded that the efficiency of a combustor may be improved by providing increased flameholding areas and/or additional length of combustor. The differences in the various types of flameholder configurations become negligible as the combustor length approaches twice the length of the flame envelope. Theoretical results, based on the chemical law of mass action and various one-dimensional simplifying assumptions, are verified qualitatively by experimental data.

References

[1] Damköhler, G. 'Einflüsse der Strömung, und des Wärmeüberganges auf der Leistung von Reaktionsofen'. *Z. Elektrochem.* 1936, **42**, 846; 1937, **43**, 1

[2] Miesse, C. C. 'A theory of spray combustion' *Industr. Engng Chem. (Industr.)*, 1958, **50**, 1303

[3] Penner, S. S. 'Similarity analysis for chemical reactors and the scaling of liquid fuel rocket engines', *Combustion Researches and Reviews, 1955*, p 140. AGARD; Butterworths: London, 1955

[4] Petreis, R. J., Longwell, J. P. and Weiss, M. A. 'Flame spreading from baffles'. *Jet Propulsion*, 1956, **26**, 81

[5] Ziemer, R. W., Huellmantel, L. W. and Cambel, A. B. 'Stabilization of premixed propane–air flames in recessed ducts'. *Jet Propulsion*, 1957, **27**, 31

[6] Smith, R. W., Edwards, H. E. and Brinkley, S. R. 'The thermodynamics of combustion gases' *Rep. Invest. U.S. Bur. Min. No. 4938*, 1953

[7] Trent, C. H. 'Investigation of combustion in rocket thrust chambers'. *Industr. Engng Chem. (Industr.)*, 1956, **48**, 749

*Experimental Research in Combustion Instability of Solid Propellants**

E. W. PRICE, H. B. MATHES, J. E. CRUMP and M. R. MCGIE

Research Department, U. S. Naval Ordnance Test Station, China Lake, California

(*Received May 1960*)

Experiments have been conducted on combustion instability using relatively simple propellant burners equipped with instrumentation of relatively high frequency response. By suitable control of test conditions, it was possible to establish some heretofore undetermined aspects of the behaviour of combustors during oscillatory performance and thereby to establish some new facts about the transient combustion of propellants.

Introduction

Description of the phenomenon

A FREQUENT and undesirable phenomenon encountered in the operation of rocket motors is the phenomenon of oscillatory combustion. Its usual manifestations are erratic fluctuations in pressure during operation of the motor (*Figure 1*, lower trace). This fluctuation in pressure (observed with low frequency response pressure instrumentation) is found to be accompanied by high frequency oscillations in pressure, which are seen only when high frequency response pressure detection and recording instruments are used (*Figure 1*, upper trace). The gas oscillation frequencies observed are close to the acoustic frequencies of the combustion chamber, can be of very large amplitude, and are accompanied by and driven by combustion oscillations of the same frequencies. Oscillation frequencies from 1 to 55 kc/s have been observed with a single type of propellant. Amplitudes of pressure oscillations in excess of 4000 lb/in^2 occur with power levels up to 10 per cent of the combustion enthalpy flux. Such behaviour is hard to ignore in rocket propulsion systems and is a challenging and interesting field of combustion research. Survey papers describing combustion instability phenomena in solid propellant rockets may be found in a number of sources[1–3].

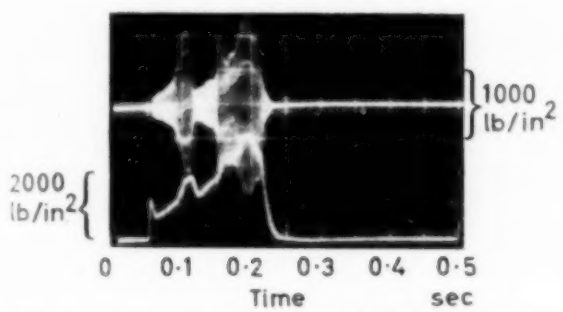

Figure 1. Pressure/time curve from a vented vessel firing yielding combustion instability. The lower trace is a low frequency response curve showing how pressure changes with the onset of oscillatory combustion. The upper trace is a high frequency response curve showing the pressure oscillations on the same compressed time scale. The propellant was a cast composite type, fired at 70°F. The frequency of the oscillations on the upper trace was 3·6 kc/s. The pressure changes (lower trace) during oscillatory combustion are an indication of the changes in propellant burning rate. The initial peak is due to the igniter

Status of the theory

The published theories of combustion instability[4–6] exhibit some aspects which must dismay the creators of more sophisticated combustion theories. The combustion models used are not derived from conservation laws, but are more nearly intuitive models. This fact dramatizes the central problem of combustion instability theory, namely, the complexity of a

*This paper was presented at the spring meeting of the Western States Section of the Combustion Institute, San Diego, California, 23 and 24 March 1959 [abstracts: *Combustion & Flame*, 1959, 3, 265].

theory which combines qualitatively accurate transient models of both the combustion processes and the gas dynamic processes involved. This problem has led theoreticians to choose very naive combustion models and to use linearized gas dynamic theory to achieve mathematical simplicity. The adequacy of the resulting theories of combustion instability is open to question, although their utility as guides to future experimental and theoretical work is unquestioned. A recent theory by R. W. HART and F. T. MCCLURE[7] presents a more sophisticated analysis of the transient response of the flame, based on an actual representation of the mass and heat transfer processes. As will be seen later, the experimental data on combustion instability seem to support the Hart–McClure theory better than the other theories. However, the presence of unevaluated parameters in the theories and the difficulty of independently controlling test variables in experiments renders conclusive evaluation of theories extremely difficult. Quantitative evaluation is neither experimentally feasible nor justified by the 'realism' of the theories. The experimental work reported here is primarily intended to reveal qualitative aspects of combustion instability. The results are then compared with the qualitative aspects of the theoretical models as a means of testing the relevance of the models to the experimental situation.

Nature of the measurement problem

In evaluating experimental approaches to combustion instability research, it is constructive to confront squarely the difficulties of measurement inherent in the nature of the phenomenon. Because of extremely high pressures, oscillation frequencies, temperatures and heat transfer rates, observations by any means are difficult. All measurements and recordings must be made at frequencies higher than those handled by instrumentation systems in the development of conventional rocket motors. Not only is the environment hostile, but the phenomenon to be studied is usually at an inaccessible location in the rocket motor, often at an uncertain and a changing location, depending on orientation of the dominant acoustic modes of the combustion chamber, and test models and operations are costly. In the face of these handicaps, very little reliable data on combustion instability became available until fifteen years after the phenomenon was first 'postulated' in about 1942.

Design of experiments in combustion instability

Although some study of combustion instability has been in progress in various agencies for many years, systematic research started only three years ago. The separation, control and measurement of variables in rocket motor firings is so difficult that the significance of most of the early testing is doubtful. Much of the recent work has been done in special burners where conditions are more easily predicted and measured. The importance of this recent trend is so great with respect to the attainment of unambiguous test data, and the importance is so little recognized, that a few words may be justified on the philosophy involved. The philosophy in the programme of work reported here is to study instability in combustion experiments which, compared to conventional rocket motor tests, (*a*) are amenable to relatively simple theoretical models, (*b*) show a high degree of susceptibility to unstable behaviour, (*c*) are small enough to be conducted in surroundings approaching laboratory conditions, and (*d*) are small enough to keep the cost of tests down and the variety of accessible test conditions up. The design of the experiment further aims to give oscillatory behaviour (*i*) in acoustic modes which are stationary (to facilitate interpretation of test results), (*ii*) in modes which place pressure antinodes in locations accessible to pressure detectors, and (*iii*) in frequencies that actually occur in rocket motors. In addition, measurements and recording are performed with instrumentation specially selected for this type of work. A number of detection methods less conventional than pressure measurement have also been adopted, such as ionization probes, photographic views through windows, and coils for detection of plasma oscillations (*Figure 2*). Some experimental studies of transient combustion phenomena are also being conducted in systems w

spontaneous instability does not occur and transient conditions are created by other means.

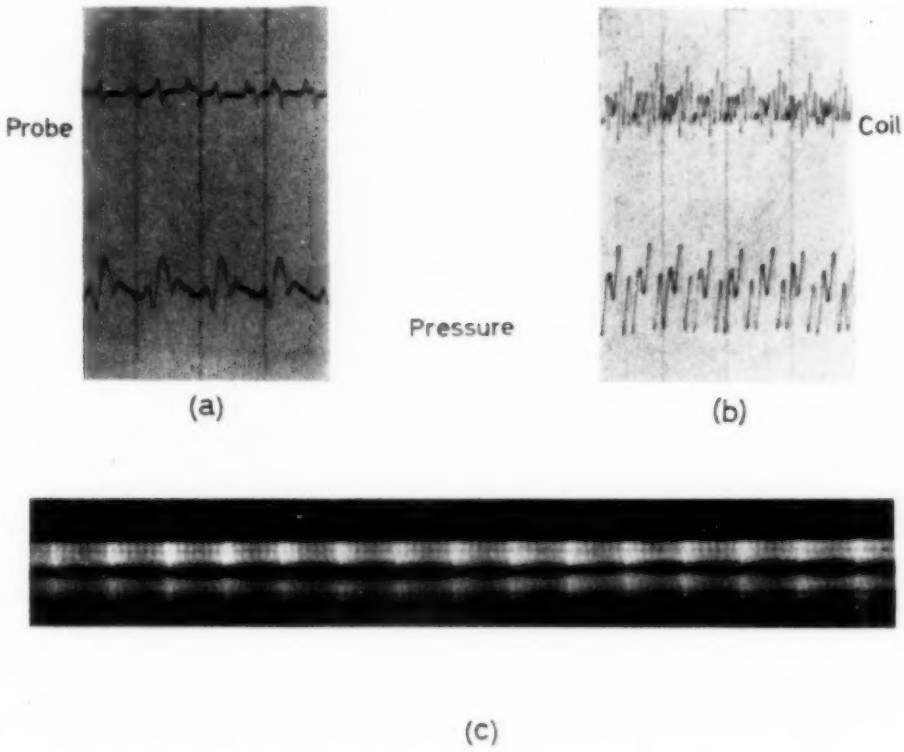

Figure 2. Records of oscillatory behaviour detected by several methods other than pressure: (a) *signal from an ionization probe extending into the combustion chamber at the pressure antinode;* (b) *signal from a toroidal coil mounted coaxially with the tubular propellant sample to show plasma oscillations during instability in longitudinal acoustic modes;* (c) *streak picture of light from a slit window across the end of the perforation of the charge (the slit is alternately light and dark as compression and rarefaction waves occur). See* Figure 4 *for details of the combustor*

These latter experiments are not discussed in this paper.

Description of the Self-excited Burner Experiment

Propellant burner

In attempting to implement the philosophy of design of experiments outlined above, a laboratory burner for small propellant charges was developed. The propellant charge for this burner is a circular cylinder (*Figure 3*), which burns only on its inner cylindrical surface. Typical dimensions are 1 in. o.d., $\frac{1}{2}$ in. i.d., 6 in. length, and 0·2 lb weight. The charge is fitted in a heavy burner designed to facilitate loading, handling and instrumentation (*Figure 4*). The propellant charge is case-bonded or expansion-fitted in the burner to minimize exposure of non-burning surfaces to propellant gases (to minimize damping of gas oscillations; this was found to be essential to attainment of reproducible behaviour). The vent from the burner is situated in the burner wall midway between the ends, in a location which minimizes

Figure 3. Photograph of a cutaway propellant sample. The end and outside surfaces are coated with non-burning plastic. Typical dimensions are 6 in. length, 1·0 in. outside diameter, and 0·5 in. inside diameter. The propellant in the figure is JPN double-base extruded propellant

damping of the fundamental longitudinal mode of oscillation of the gas in the cavity. A hole is provided in the charge web to port the gases to the vent. A high frequency response pressure gauge is used routinely in one of the burner endplates and is isolated from the hot gas by a short grease-filled hole. A burst diaphragm is used routinely in the other endplate to protect equipment against pressure excesses. A device is available for rupturing the burst diaphragm on demand when interruption of burning is desired. Variations of this typical design provide for ionization probes in the charge or the motor and closures, for coils in the charge, for windows in the end and sides, for charges made up of more than one propellant, for different lengths and diameters of the burner, for additional pressure gauges, and for various acoustic devices for suppressing instability or controlling the acoustic modes of oscillation.

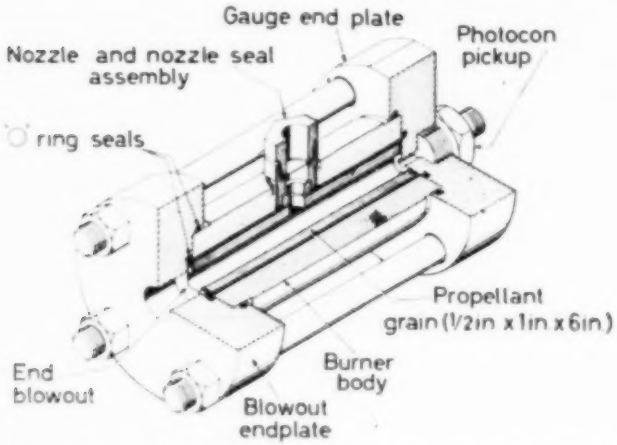

Figure 4. Diagram of the burner for combustion instability research

Recording techniques

Typical instruments used are a multi-channel magnetic tape recorder, galvanometer oscillograph, and triggered sweep dual-beam oscilloscope which simultaneously record pressure and other detector signals. *Figure 1* illustrates a two-channel oscilloscope record of the pressure/time history during a firing. The lower trace is a low frequency response record obtained by use of a low pass filter in a high frequency response pressure channel; the upper trace is a high frequency response record obtained by use of a high pass filter on the same pressure detection channel. The lower trace shows the irregular pressure/time curve, and the upper trace shows the corresponding fluctuations in amplitude of pressure oscillations. *Figure* illustrates a galvanometer oscillograph record of

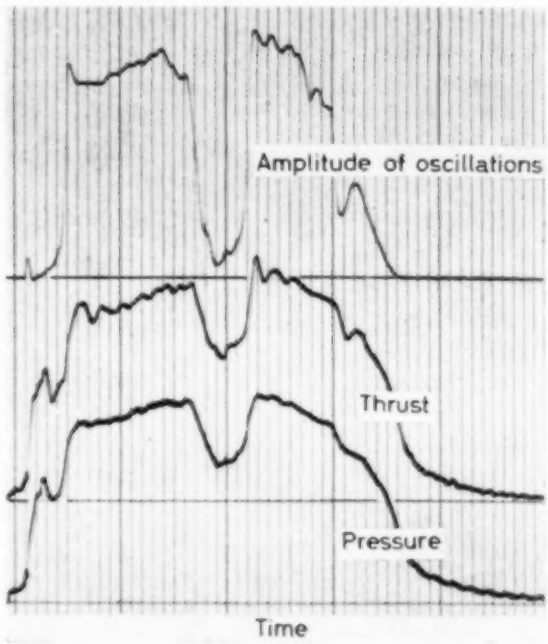

Figure 5. Galvanometer oscillograph record of pressure. Upper trace obtained from high-pass filtered, rectified output of high frequency response transducer. Lower trace obtained from low frequency response pressure transducer. Timing lines are 0·01 sec and 0·10 sec

pressure from a low frequency response, high accuracy pressure gauge (lower trace), with a corresponding record of the high frequency oscillations (upper trace) presented as a 'd.c.' record by full wave rectification of the pressure oscillation signal. *Figure 6* illustrates a section of a

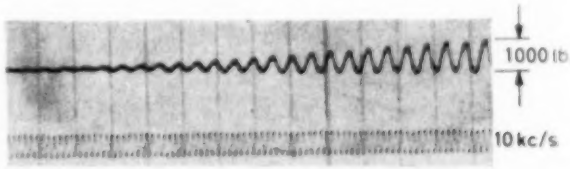

Figure 6. Pressure oscillations reproduced by high speed playback of a magnetic tape recording from the high speed pressure transducer. Upper trace is pressure oscillations. Lower trace is 10 kc/s timing signal

pressure oscillation signal recorded on a tape recorder at 30 inches per second and subsequently played back into a galvanometer oscillograph at a tape speed of $1\frac{7}{8}$ inches per second.

Observations Regarding Dynamic Instability

The most important practical question regarding combustion instability in any particular rocket motor or burner is the question of whether or not oscillatory behaviour will spontaneously develop. The theoretical works of H. GRAD[4], SIN-I CHENG[5], and R. W. HART and F. T. MCCLURE[7] are related to this question. With regard to these theories, there are two issues on which the present experimental work has bearing. The first is the representation of the combustion response to gas disturbances by some function of pressure[4,5], or by a one-dimensional flame model[7]. The second has to do with the prediction from the theory[4,5] that instability is critically dependent on frequency of oscillations with frequency intervals of stable behaviour interspersed with intervals of frequencies in which instability occurs (this attribute is not predicted in the Hart–McClure combustion theory[7]).

The flame model

In order to examine the issue of the form of the flame model in the framework of a combustion system with more than one space dimension, one must consider the fact that the gas dynamic behaviour affecting combustion at each location on the burning surface is different from that at other points on the surface. In the simplest case where standing acoustic waves occur, one can define the condition of the oscillatory gas motion in terms of the position on the acoustic mode[8]. This is illustrated in *Figure 7* for some of the longitudinal modes of a tubular burner corresponding to *Figure 4*. At any point in the flame zone, there occur oscillations in pressure, density and temperature due to the alternate compression and expansion of the adjoining gas column, and there also occurs a tangential oscillation of the gas relative to the burning surface. At pressure antinodes (*Figure 7*) the amplitudes of the pressure, density and temperature oscillations are maximum and the tangential velocity oscillations are of zero amplitude. At velocity antinodes there is no oscillation in pressure, density or temperature, but the tangential velocity oscillations have maximum amplitude. At intermediate locations, oscillations in all variables are present. From these considerations regarding the space-dependent environment in which combustion instability occurs, there arises the question as to which of the attributes of the gas oscillations is responsible for the energy coupling between the flame oscillations and the gas oscillations. Can a flame model which ignores tangential velocity oscillations explain the occurrence of instability? Is the purely one-dimensional model as used by Hart and McClure[7] qualitatively adequate? Are the models of Grad[4] and Cheng[5], which concentrate the principal

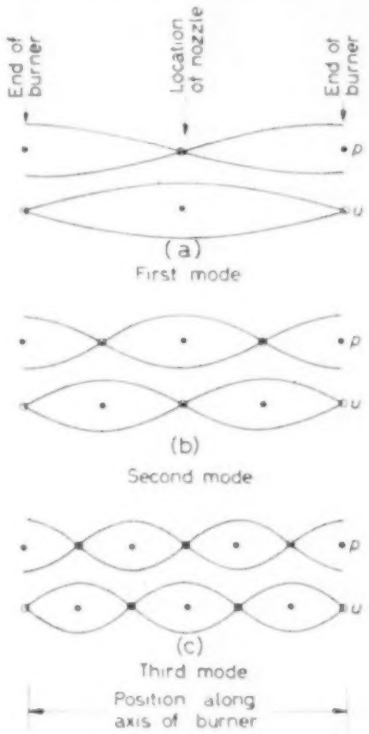

Figure 7. Envelope of standing waves of first three longitudinal acoustic modes in the combustor. The distance between envelope lines at each point indicates the amplitude of the oscillations at that point. The envelopes labelled p *may be regarded as pressure, density or temperature. The envelopes labelled* u *refer to amplitude of velocity oscillations in the axial direction. The circles designate nodal points, the dots antinodal points*

flame coupling with the gas in the region of pressure antinodes (by making the consumption rates dependent on pressure), qualitatively adequate?

Although these questions cannot be fully answered at present, one series of experiments was conducted which was related to them. Firings were made on a series of propellant charges made up partly from real propellant and partly from dummy propellant (plastic). The complete composite charge was 6 in. long with 1 in. outside diameter as described in the preceding section. In the series of tests, the amount and location of the 'live' propellant was changed to determine where, relative to location on the longitudinal acoustic modes (*Figure 7*), the propellant was most effective in producing instability and how much propellant was required. The arrangement of plastic and of live propellant in the various configurations is shown diagrammatically in *Figure 8*. Two or three tests were run with each configuration, and tests with several different propellants were conducted in the configuration in *Figures 8*(e) to 8(g). The results are typified by the test records in *Figure 9*. On an expanded time scale it was found that the pressure oscillations were roughly sinusoidal in the first longitudinal mode (similar to *Figure 6*).

The results summarized in *Figure 9* show that combustion near the pressure antinodes supports instability more effectively than combustion elsewhere on the acoustic mode, and the results of the whole study indicate that this is true for a variety of propellants (all propellants tested). From this one might be led to conclude that the aspect of the acoustic behaviour dominant in exciting combustion oscillations is the pressure oscillations (and the density and temperature oscillations whose modes are in phase and geometrically similar to the pressure mode). The argument is not as simple as this because it is well known in the theory of heat-driven acoustic systems that oscillations are most effectively driven when the oscillations in heat release occur near the pressure antinodes. Thus the present results would appear to be explainable on this basis alone. On the other hand, if one speculates that the combustion oscillations are induced primarily by the action of tangential gas oscillations, then one would expect the most severe instability to occur in tests where the propellant was at some location intermediate to the pressure antinode and the velocity antinode. In such a location the tangential velocity oscillations would be severe enough to induce significant combustion oscillations, and the combustion oscillations would

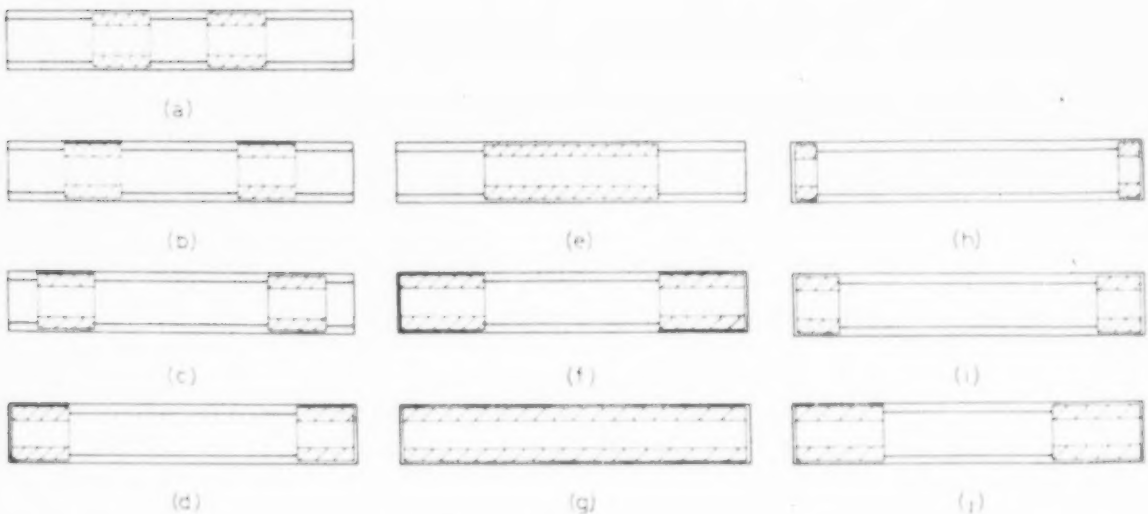

Figure 8. Configurations of propellant charges used to investigate the site of excitation of oscillatory combustion. The flame zone was localized relative to position on the acoustic mode by using dummy propellant everywhere except where the flame was desired (cross-hatched sections are propellant; external dimensions are the same as for the charges in Figures 3 *and* 4.)

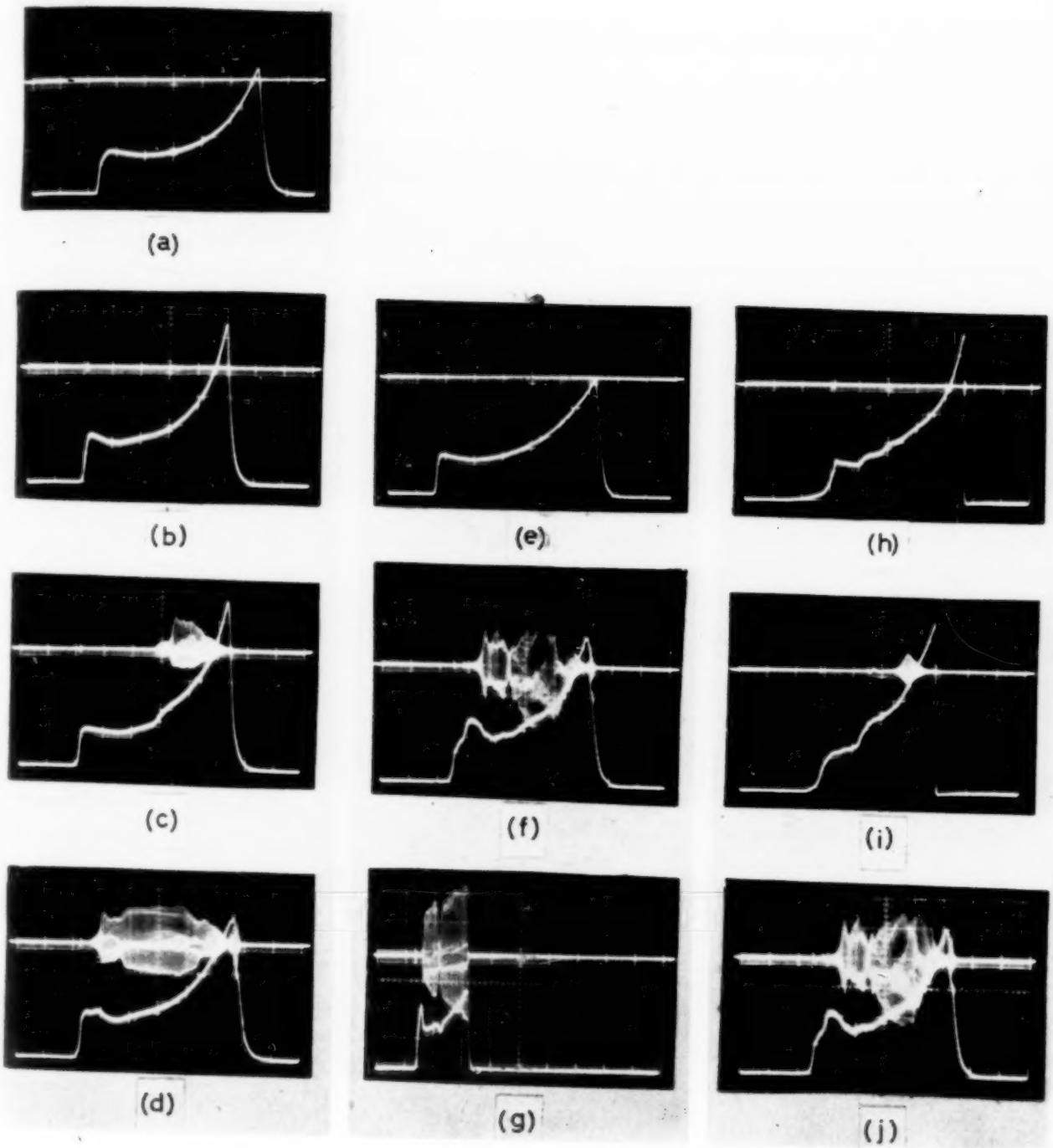

Figure 9. Typical pressure/time records obtained with the charge configurations in Figure 8 *(labels on the records indicate the corresponding configurations in* Figure 8*). The pressure scales (vertical coordinates) are 1000 (lb/in²) division for the low frequency response curve, 500 (lb/in²) division for the high frequency response curve. The time scale (horizontal) is 0·05 sec/division.*

be near enough to the pressure antinode to produce significant pressure oscillations. However, the experimental results did not support this argument, so it is tentatively concluded that the predominant factors producing combustion oscillations are connected with the pressure, density and temperature oscillations in the gas. This in turn lends some support to the models used in the papers of Grad[4], Cheng[5], and Hart and McClure[7].

A more positive verification of the adequacy of the one-dimensional flame model was sought by performing an experiment utilizing a burner like that in *Figure 4*, but with short, solid propellant 'billets' at each end, with burning surface only on the end surfaces facing into the burner (*Figure 10*). Instability in a longitudinal mode in such a system would have been convincing evidence of the adequacy of a one-dimensional flame model to describe dynamic instability. However, this end-burning system did not oscillate. It is the authors' opinion that this is not a negative result, but simply indicates that there is not sufficient energy flux in this configuration to overcome the relatively high damping. The results of firing configurations h to j (*Figure 8*) support this opinion, as do the conclusions of W. G. BROWNLEE[10] on tests in rocket motors with charges of various lengths. Recent tests[11] on the configuration shown in *Figure 11* have exhibited severe instability in the Helmholtz mode of the system, strongly supporting the use of a one-dimensional model in theoretical work. A similar conclusion was reached by Brownlee from results on burning slab-shaped charges[10].

The critical frequency phenomenon

In order to test the time-lag theories, a series of experiments was designed to demonstrate the qualitative prediction of a critical dependence of dynamic instability on the frequency of oscillation. The nature of this dependence on frequency is such that a series of tests at successively different frequencies should result in a group of tests with stable behaviour followed by a group of tests with unstable behaviour. This behaviour was sought by firing a series of tests with JPN double-base propellant[12] in configurations like *Figures 3* and *4* but with different lengths (and hence differing frequencies of the longitudinal modes). The

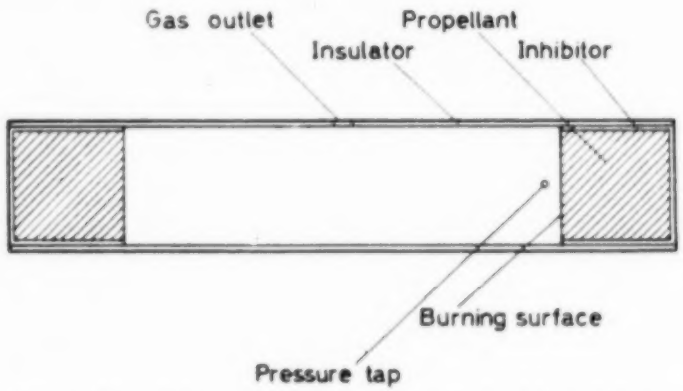

Figure 10. Internal arrangement of a double-end burner for testing the validity of a one-dimensional flame model for combustion instability theory (the sketch shows the charge and burner liner assembly; the burner was similar to that in Figure 4)

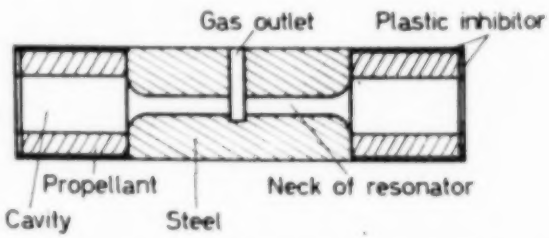

Figure 11. Internal arrangement of a 'Helmholtz' burner for testing the validity of a one-dimensional flame model for combustion instability theory (the sketch shows the charge assembly; this assembly fits tightly in a burner similar to that in Figure 4)

propellant samples ranged from 4 to 12 in. in length in 1 in. 'intervals'. Three tests were run at each length. In this series of tests, instability developed shortly after ignition in all tests, with no indication of greater stability at

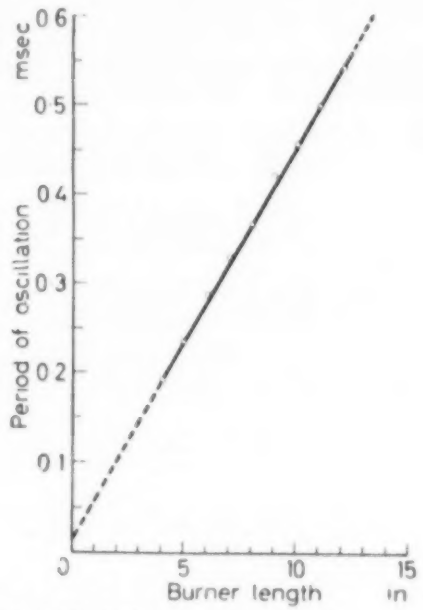

Figure 12. Variation of period of oscillation with length of the burner for JPN propellant

one length than another. The range of frequencies involved was from 1·7 kc/s to 5·35 kc/s (*Figure 12*). The initiation of oscillatory behaviour over this wide frequency range seems inconsistent with a time-lag model of combustion instability.

A further verification of the non-critical nature of instability with respect to frequency is exhibited by an evident 'indifference' to frequency exhibited in the tests on 10, 11 and 12 in. long charges. While oscillatory combustion often initiated in the fundamental longitudinal mode, it was also observed to initiate in the third or fifth longitudinal modes (*Figure 13*), representing a frequency range of 1·7 to 8·5 kc/s (initiation in the even modes rarely occurs in this system because of loss of acoustic energy of those modes through the nozzle, which is so located that it attenuates the even mode oscillations only). The random selection of modes in a non-selective system is characteristic of behaviour when the initiating turbulent fluid dynamic disturbances are random. As a matter of interest, this burner arrangement has been observed under special conditions to initiate oscillatory combustion in other modes at frequencies of up to 55 kc/s, with no indication of positive stability over any frequency range. The foregoing observations were made from tests on JPN double-base propellant. Extensive testing in 6 in. long samples with fifteen different propellants has further shown that instability is not critically sensitive to propellant characteristics. Since no evidence of large amplitude initiating disturbances is evident in these tests, it must be assumed that the results are relevant to the linearized theories of Grad[4], Cheng[5] and of Hart and McClure[7]. The absence of a critical dependence of stability on frequency, dimensional or propellant variables is consistent with the Hart–McClure[7] theory but appears to contradict the Grad[4] and Cheng[5] theories based on time-lag combustion models.

Burning Rate During Oscillatory Combustion

When oscillatory behaviour occurs in rocket motors, the operating pressure is usually observed to increase (*Figure 1*), a behaviour suggestive of increased burning rate of the propellant. The fact that burning rate does increase at such times is verified by measurements of propellant samples recovered after interruption of burning (*Figure 13*). This behaviour was investigated to determine what aspect of the gas oscillations was responsible for the increases in burning rate, and to determine in a qualitative way the degree to which the burning rate changes were dependent on the frequency of the gas oscillation. The questions answered are essentially the same as posed earlier with respect to stability of the system.

Before presenting the experimental results, a note of explanation regarding their qualitative nature is probably desirable. Evaluation of burning rate effects accompanying oscillatory burning is complicated by the absence of any method of direct measurement of rate. A qualitative evaluation of rate change at the onset and cessation of oscillatory burning is clearly demonstrated by the accompanying change in burner pressure, as in *Figure 1*.

However, the pressure/time history does not reveal *where* on the propellant charge the burning rate change occurred, only *when* it occurred and whether the 'surface averaged' effect is positive or negative. On the other hand, measurements may be made of the propellant charge after interruption of burning to determine *where* the abnormal burning rates occurred, but these measurements cannot reveal *when* the rate changes occurred. Combinations of both types of observations were used here.

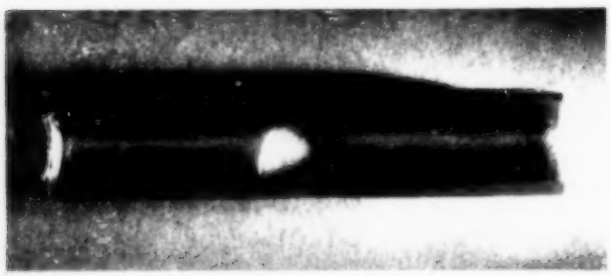

Figure 13. Photograph of a partially burnt propellant charge recovered after interruption of oscillatory burning. The charge has been sectioned lengthwise to show the effect of higher burning rate near the velocity antinode (middle). The hole in the web is the gas outlet to the nozzle

Site of burning rate change

Interrupted firings were made on a variety of propellants, both double-base and composite, using the charge configuration in *Figure 3* with 6 in. long charges. In all instances where appreciable oscillatory combustion had occurred, it was evident from visual examination of the charge remnant that the time-averaged burning rate was higher in the region of velocity antinodes than in the region of pressure antinodes of the unstable acoustic modes in which oscillations occurred (*Figure 13*). This observation was true even when tangential rather than longitudinal modes were observed. Detailed measurements were made on a number of charges of JPN double-base propellant[12], and the results are summarized in *Figure 14*. It is evident that the burning rate was higher towards the velocity antinode. The samples showing most conspicuous burning rate changes resulted from tests with most severe and sustained oscillatory behaviour. Accurate measurements of the cast composite propellant samples were not convenient because they were bonded to the inside of the burner tube and could not be removed for measurement. However, the configuration of the partially burnt samples was clearly similar to that of the JPN samples. These test results seem to support conclusively the hypothesis that the increases in total mean burning rate observed during oscillatory combustion (as indicated by pressure rises during oscillatory burning) are due to increases in linear burning rate localized in that part of the burning surface exposed to severe oscillations of the gas

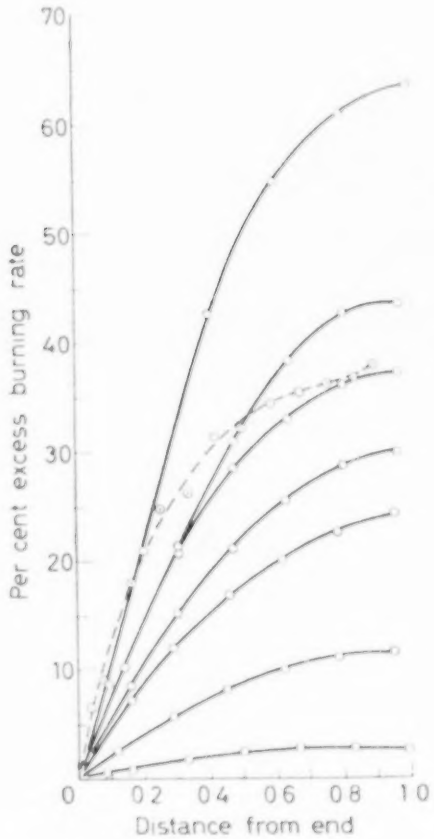

Figure 14. Variation of propellant burning rate with location on the propellant sample (compare with location on the acoustic modes shown in Figure 13). The abscissa is normalized so that 1·0 is at the head end point of the charge, the velocity antinode. The ordinate is the difference between web burnt and the average web burnt at the end of the charge, divided by the average web burnt at the end of the charge. All charges were cast as in Figures 3 and 4, with charges 6 in. long, except the uppermost curve (a 5 in. long charge) and the lowest broken-line curve (a 12 in. long charge)

tangentially to the burning surface. This in turn suggests that the mechanisms involved include enhanced shear stresses and heat transfer in the liquid boundary layer and flame zone, processes which are also reflected in the rippled burning surfaces (*Figure 15*) obtained on partially burnt samples recovered after interruption of severe oscillatory burning. This conclusion is supported by the results of Brownlee on extensive testing of a cast composite propellant. Brownlee observed[10] that in a 'slab' burner with no propellant at the velocity antinodal regions, no pressure rises accompanied oscillatory burning.

It should be emphasized that the tests reported here do not preclude the possibility that burning rates are *reduced* somewhere on the charge during oscillatory burning. The *increase* in rate is inferred from the rises in pressure during oscillatory burning, and these rises are a consequence of the change in burning rate *averaged*

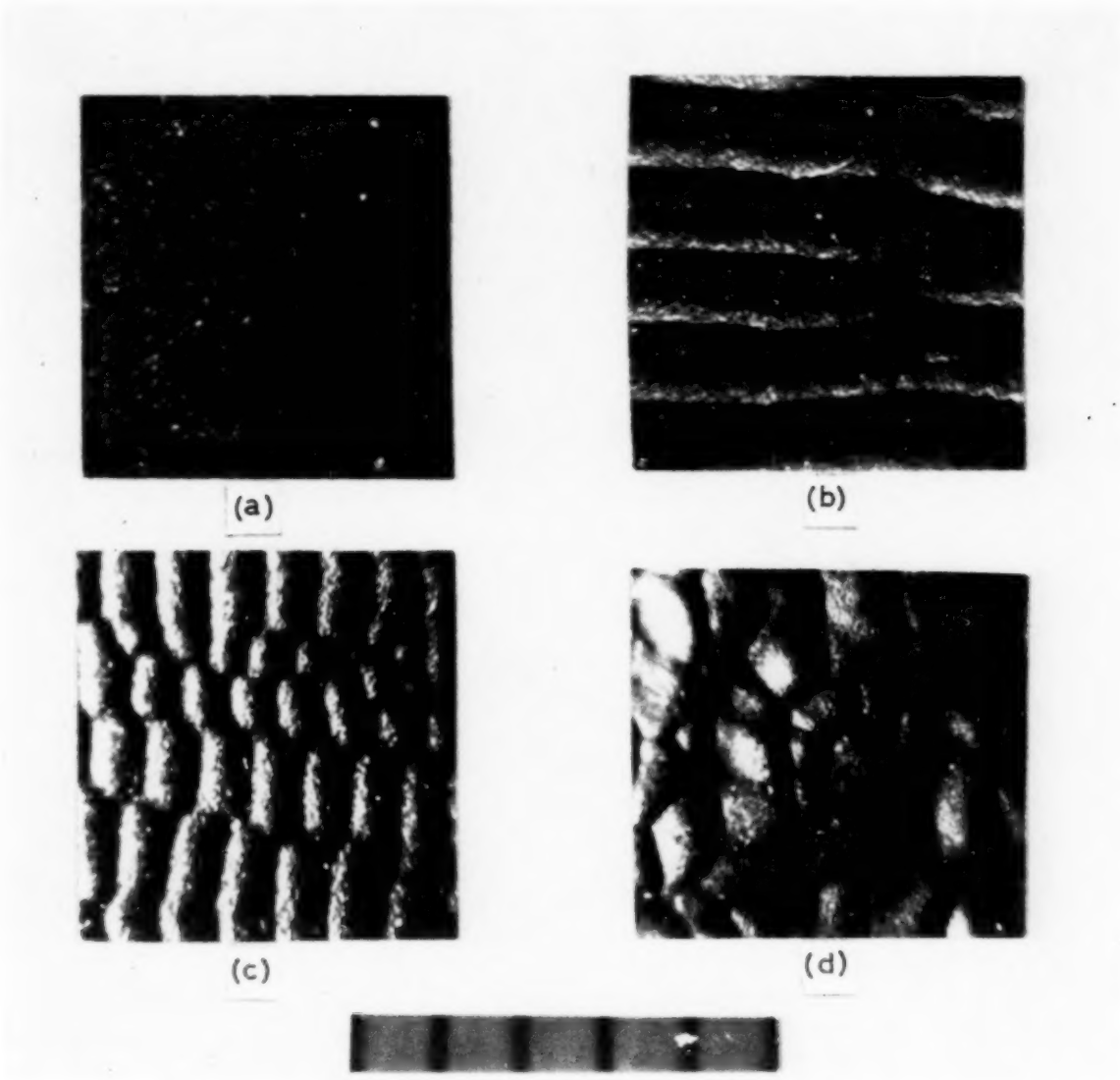

Figure 15. Photographs of the details of ripples of the burning surface of PPX propellant after interruption of oscillatory combustion. The mean gas flow was up in every case, with the oscillations in (b) *the first longitudinal mode,* (c) *the first tangential mode,* (d) *first tangential and eighth longitudinal modes, and* (a) *no oscillations. Graduations on the scale at the bottom are 0·020 in.*

over the entire charge surface. The best measurements attained to date (on JPN double-base propellant) on partially burnt charges indicate that the burning rate is *decreased* near the pressure antinodes during oscillatory burning. Thus the pressure increases during oscillatory burning reflect the combined effect of a burning rate increase in the region of the velocity antinodes and a rate decrease in the region of the pressure antinodes. It seems highly probable that the relative magnitude of these two opposing effects may differ considerably with the type of propellant and the test conditions, but only limited data are currently available. The *decrease* in burning rate is more conspicuous with the 'mesa' burning propellants*. With double-base mesa propellants the pressure actually *decreases* during oscillatory burning[2, 13], indicating that either the rate decreases are more drastic than any rate increases or that they involve a larger portion of the burning surface. The shape of the partially burnt charges indicates that these factors are involved, but only qualitatively significant data are available at present. The burning rate was consistently reduced at the pressure antinodes. Another distinctive feature of the mesa propellants with respect to combustion instability is their tendency towards rippling of the burning surfaces during oscillatory combustion (*Figure 16*). The rippling is much more severe, more widespread over the charge surface, and occurs under much less severe conditions of oscillatory combustion than with conventional double-base propellants.

Frequency dependence of rate changes

As in stability theory, so in the theory of burning rate changes, one might pose the question of whether or not the changes in burning rate observed during combustion instability are critically dependent upon the frequency of the oscillatory behaviour of the combustion-flow system. This question has been considered by L. Green, Jr. and W. Nachbar[6, 14, 15] who have developed a theory which suggests that the burning rate changes should be critically sensitive to frequency of oscillations, as well as to other test variables. An examination was made of the test results from burning propellant samples of various lengths, to determine whether any conspicuous dependence of rate change on oscillation frequency was exhibited. The examination consisted of a visual comparison

Figure 16. Photograph of a mesa propellant charge after interruption of oscillatory combustion. It shows the severely rippled burning surface and the non-uniform web thickness, reflecting a lower burning rate at the ends (pressure antinode) of the charge than near the middle (velocity antinode)

of the pressure/time histories yielded by the various firings. While such an evaluation was necessarily qualitative and subjective, it was considered adequate for an experienced observer to detect the dramatic dependence of burning rate on frequency suggested by the Green-Nachbar theory. It was found on comparison that the burning rate changes were comparable over the frequency range of 1·7 to 5·35 kc/s, and similar to the rate changes reflected by the 6 in. long samples summarized in *Figure 14*. The appearance of the limited number of partially burnt samples observed in the various lengths was similar to the appearance of the 6 in. long samples. Measurements were made on some of the longer samples because the pressure/time histories on expanded time scales indicated that the higher longitudinal acoustic modes were present concurrently with the fundamental mode, particularly on tests with longer propellant samples (lower frequencies). The geometry of the partially burnt samples qualitatively reflected the more complex mode of gas oscillation (see *Figure 14*), reflecting minimum burning rate near the ends (which

*These propellants are named after a distinctive feature of their steady-state burning characteristics, namely that their burning rates decrease with increasing pressure in some ranges of pressure.

velocity nodes for all longitudinal modes), higher than usual burning rate at locations intermediate between the end and the middle of the sample (where velocity antinodes for higher modes exist), and the highest burning rate near the middle of the charge (where velocity antinodes of the most conspicuous modes are coincident).

From the qualitative nature of these observations it is not proper to conclude that burning rate changes during oscillatory combustion are insensitive to frequency of the oscillations. However, it does seem extremely unlikely that the particular kind of frequency dependence predicted by the Green–Nachbar theory[6, 14, 15] can be reconciled with the present results without restrictions on the theory. The fact that all conventional propellants tested behaved in a qualitatively similar way seems also to be in contrast to the Green–Nachbar theory. In an unpublished note[16], Nachbar has pointed out that these alleged conflicts with the theory may, in fact, be reflections of the inadequacy of the 'linearization' in the theory, since the test results are all obtained during severe instability with pressure oscillations of several hundred pounds per square inch amplitude.

Further speculation about mechanisms of rate changes

The question has been raised[1] as to whether the burning rate changes observed during oscillatory combustion might not be similar to the erosive burning phenomenon familiar in rocket and gun internal ballistics[17–19]. Green[1] argued that the magnitude of the pressure changes (rate of change) could not be explained on this basis, and his theory predicts a more intricate behaviour, in which the burning rate changes are dependent critically on frequency of oscillations, composition of propellant and location on the propellant charge. The results of the present experiments do not reflect those 'criticalities', but do seem to support a model much like the erosive burning phenomenon. However, it seems likely that for severe instability, consideration must be given to the encroachment of turbulent tangential flow on the flame zone. In fact it is difficult to see how a linear theory can apply to the oscillatory heat transfer theory, since it seems likely that rather large amplitude flow oscillations would be necessary before the flow boundary layer could encroach on the flame zone enough to modify the heat transfer rate. (So long as the flame zone is submerged in the boundary layer, the gas immediately outside the flame zone will be at flame temperature regardless of the boundary layer, and the flame process will dominate the heat transfer process.)

In view of the rippled condition of propellant samples recovered after interruption of oscillatory burning, it is probably also desirable to consider conditions which lead to wavy boundary layers and the resultant formation of wavy burning surfaces either by direct physical action of the wavy flow or by resulting 'waviness' of the gas phase flame zone. In addition to these considerations it now seems that, during oscillatory combustion, the burning rate may be *reduced* in locations of the burning surface where the tangential gas oscillation is only slight (pressure antinodes). Since this behaviour probably obeys different 'laws' than does the rate-increasing 'erosive' behaviour, it becomes necessary to study both phenomena and their interactions in order to understand instability behaviour in rocket motors.

Conclusions

By using combustion systems designed to oscillate in acoustic modes which are particularly amenable to study, it has been possible to establish several aspects of unstable combustion which were previously undetermined. These results have direct bearing on the validity of published theories of solid propellant combustion instability. The principal facts revealed by this work are as follows:

(*1*) The response of the combustion process which is primarily responsible for driving oscillatory combustion results from oscillations of the flame zone perpendicular to the burning surface, with attendant oscillations in pressure, density and temperature. Use of either a one-dimensional model or a pressure-dependent model of transient combustion thus seems justified in instability theories.

(*2*) The response of the combustion process which is primarily responsible for increased net burning rates during oscillatory combustion is the response to the tangential oscillation of the gas (parallel to the flame zone). This result indicates that increases in burning rate are due to encroachment of the oscillating flow on the flame zone.

(*3*) In addition to the *increased* burning rate accompanying oscillations of the gas parallel to the burning surface, it is observed, with the few propellants tested, that the burning rate *decreases* in regions where severe pressure oscillations and only mild velocity oscillations occur.

(*4*) The response of the combustion zone of the solid propellant to periodic gas dynamic disturbances is not critically dependent on the frequency of the disturbances, either with regard to driving oscillations or with regard to changes in burning rate.

(*5*) Items 2 and 4 have been established for a wide variety of propellants; item 1 has been established for a wide variety of double-base propellants. Item 3 has been demonstrated for several double-base mesa propellants and one conventional double-base propellant (all propellants tested so far).

(*6*) In view of the evident capability of practically all propellants to burn unstably over an appreciable frequency range in a system with low damping, it appears that the difficulty in predicting instability in rocket motors lies in the problems of predicting damping and acoustic energy 'leakage' through the nozzle. The positively stable regions predicted by time-lag theories[20] were not evident in the present work.

References

[1] Green, L., Jr. *Jet Propulsion*, 1956, **26**, No. 8, 655

[2] Price, E. W. *Astronautica Acta*, 1959, **5**, No. 1, 63

[3] McClure, F. T., Hart, R. W. and Bird, J. F. 'Solid propellant rocket motors as acoustic oscillators'. Johns Hopkins University: Applied Physics Laboratory *Report TG335–3*, October 1959

[4] Grad, H. *Comm. pure appl. Math.* 1949, **II**, 79

[5] Sin-I Cheng. *J. Amer. Rocket Soc.* 1954, **24**, and 102

[6] Nachbar, W. and Green, L., Jr. *J. aero/space Sci.* 1959, **26**, 518

[7] Hart, R. W. and McClure, F. T. *J. chem. Phys.* 1959, **30**, 1501

[8] Wood, A. *Acoustics*, 1st ed., p 192. Interscience: New York, 1941

[9] Merk, H. J. *Analysis of Heat-Driven Oscillations of Gas Flows*, p 320. Martinus Nijhoff; Applied Scientific Research: The Hague, Netherlands, 1957

[10] Brownlee, W. G. 'An experimental investigation of unstable combustion in solid propellant rocket motors'. *Doctoral Thesis*. California Institute of Technology, Pasadena, California, 1959

[11] Mathes, H. B. *et al.* 'Combustion instability in solid propellant rocket motors' (U.S. Naval Ordnance Test Station, China Lake, California, *Seventh Progress Report* on Combustion Instability), TPR 239 (NOTS 2407). In press. Confidential

[12] Wimpress, R. N. *Internal Ballistics of Solid-Fuel Rockets*. McGraw-Hill: New York, 1950

[13] Price, E. W. and Sofferis, J. W. *Jet Propulsion*, 1958, **28**, 190

[14] Green, L., Jr. *Jet Propulsion*, 1958, **28**, 385

[15] Green, L., Jr. *Jet Propulsion*, 1958, **28**, 769

[16] Nachbar, W. Private communication to E. W. Price (Lockheed Missile Systems Division, Palo Alto, Calif., 16 November 1957)

[17] Green, L., Jr. *J. Amer. Rocket Soc.* 1954, **24**, 9

[18] Lenoir, J. M. and Robillard, G. 'A mathematical method to predict the effects of erosive burning in solid propellant rockets'. *Sixth Symposium (International) on Combustion*, p 663. Reinhold: New York, 1957

[19] Corner, J. *Theory of the Interior Ballistics of Guns*, p 74. Wiley: New York, 1950

[20] Minorsky, N. *J. appl. Mech.* 1942, **9**, A-65

Burning Velocity and the Structure of Flames near Extinction Limits

C. H. YANG

Convair Scientific Research Laboratory, San Diego, California

(Received June 1960)

Burning velocities and structures of flames are calculated near various extinction limits according to a non-adiabatic flame theory. The theory prescribes burning velocity structure, extinction limits and includes adiabatic theory as a special case. Numerical results are obtained through the use of analogue computers as illustrated.

Introduction

ALL flames lose heat to their surroundings; however, the theoretical treatment of the flame problem in the past was often based on an adiabatic model. The adiabatic idealization can be justified by the agreement of the calculated flame burning velocity with the experimental measurements for flames under ordinary conditions. Since flames ordinarily in a large tube or seated on a burner lose very little heat to their *immediate* surroundings, the mathematical model of the adiabatic theory is usually a good approximation.

The theory naturally has left unexplained the phenomena which are closely associated with heat losses. Among these are the distinctive extinction limits. As heat abstraction by the immediate surrounding of the flame increases, the structure of the flame is observed to change, and the burning velocity is noticeably lowered. An adequate flame theory should follow a mathematical model which takes heat losses into consideration. It must account for all the important flame phenomena and it must also converge to the idealization of the adiabatic theory when heat losses are very small.

Recent contributions to the theory of non-adiabatic flame theory have been made by a number of authors[1,2]. In a previous paper[3], we used the gaussian error function as an approximation to the flame profile, and obtained flame extinction limits from a one-dimensionlized mathematical model. A more general study of the flame structure and burning velocities of flames near extinction limits is made in this paper. Solutions are obtained through the use of analogue computers.

Basic Equations and Boundary Conditions

(1) *Conservation equations*

A reacting medium is assumed to flow down an infinitely long tube, with a mass flow rate, G. The tube wall is assumed to be kept at a constant temperature, T_u. A flame is assumed to be in existence in the tube, and steady state temperature and concentration profiles have been established. The temperature profile represents the average temperature at each cross section of the tube. Similarly, the concentration profile for each reactant represents the average values at each cross section of the tube. The use of average values reduces the flame system from a two-dimensional to a one-dimensional formulation. Let us consider a reaction

$$\mathrm{A} + \mathrm{B} \longrightarrow \text{Products}$$

Assume there is no change in the number of moles during the reaction. Neglecting pressure variations and kinetic energy of flow, the energy conservation and diffusion equations can be written as follows:

$$\frac{d^2T}{dx^2} - \frac{cG}{k}\frac{dT}{dx} = -\Phi(z, \beta, T) + l(T) \qquad \ldots\ldots[1]$$

$$\delta_A \frac{d^2z}{dx^2} - \frac{cG}{k}\frac{dz}{dx} = \frac{\Phi(z, \beta, T)}{T_a - T_u} \qquad \ldots\ldots[2]$$

$$\delta_B \frac{d^2\beta}{dx^2} - \frac{cG}{k}\frac{d\beta}{dx} = \frac{\Phi(z, \beta, T)}{T_a - T_u} \qquad \ldots\ldots[3]$$

where the symbols are defined as:

T Average temperature (°K) at position x
T_u Temperature at the wall of the tube (°K)
T_a Adiabatic flame temperature of the mixture (°K)
x Tube axial distance (cm)
c Average specific heat of mixture at constant pressure (cal/g °K)
G Mass flow rate (g/cm² sec), or Burning velocity × ρ_0
k Thermal conductivity (cal/cm °K sec)
Φ $=\dot{M}'''_A H/k$, the Transformed heat release rate
$\dot{M}'''_A$ Mass of reactant A consumed by chemical reaction per unit volume per unit time (g/cm³ sec)
H Standard heat of reaction of reactant A (cal/g)
z $=M_A/M_{A,u}$, the Dimensionless concentration of reactant A
M_A Mass of reactant A per unit mass of mixture
$M_{A,u}$ Mass of reactant A in unburnt mixture per unit mass of that mixture
β $=M_B/rM_{A,u}$, where r is the mass ratio of reactant A to reactant B of the unburnt mixture
σ_A $=D_A\rho c/k$, the Lewis No. for reactant A
σ_B $=D_B\rho c/k$, the Lewis No. for reactant B
D_A Diffusion coefficient for reactant A (cm²/sec)
ρ_0 Density of unburnt mixture (g/cm³)
ρ Local gas density (g/cm³)
l $=L/k$, the Transformed heat loss
L Heat loss from unit volume to surroundings (cal/cm³ sec).

(2) *Boundary conditions*

At some point upstream relative to the flame, the solution of the conservation equations must satisfy the following conditions:

$$T=T_u \begin{cases} z=1, \ \beta=1, \ dT/dx=0 \end{cases} \quad \ldots [4]$$

These conditions imply that the concentrations of reactants A and B do not change with time as long as the gas is at the temperature T_u. They exclude any heat sinks at the points where $T=T_u$, by requiring the temperature gradient at such a point to be zero. At some point downstream from the flame, the gas, of course, eventually cools to the temperature of the wall again. The solution must then satisfy the conditions:

$$T=T_u \begin{cases} \dfrac{dz}{dx}=0, \ \dfrac{d\beta}{dx}=0, \ \dfrac{dT}{dx}=0 \end{cases} \quad \ldots [5]$$

Since physically there are no mass or heat sinks placed at such a point, the temperature and concentration gradients must be zero.

The problem is to find solutions to equations 1, 2 and 3, subject to the boundary conditions 4 and 5. This will only be possible for certain particular values of G. Thus, the parameter G bears some resemblance to an eigenvalue of a linear operator. However, since the flame equations are non-linear, this can be called an 'eigenvalue problem' only in a broad sense.

For the adiabatic flame theory the 'downstream' boundary conditions change to:

$$T=T_a \begin{cases} \dfrac{dz}{dx}=0, \ \dfrac{d\beta}{dx}=0, \ \dfrac{dT}{dx}=0 \end{cases}$$

and the heat loss term in equation 1 becomes zero.

(3) *Adaptation of the flame problem to the analogue computer*

(a) *Rate function*—The propane–air system is chosen for numerical computation. The actual kinetics for a propane–oxygen reaction are very complicated. An Arrhenius type of rate function is used for simplification.

$$\Phi = k_1 H z \beta M^2_{A,u} \rho_0^2 T_u^2 \exp(-E/RT)/kT^2$$

For stoichiometric* mixtures:

$$z=\beta$$

$$\Phi = k_1 z^2 H M^2_{A,u} \rho_0^2 T_u^2 \exp(-E/RT)/kT^2$$

E is taken[4] to be 40 kcal; H is taken[5] to be $1{\cdot}11\times10^4$ cal/g for propane; k_1 is taken[5] to be 3×10^{14}; and ρ_0 is taken to be $1{\cdot}3\times10^{-3}$ for the standard one atmosphere pressure.

*Equation 3 then becomes equivalent to equation 2; therefore it can be omitted.

(b) *Specific heat and thermal conductivity*—Average values of specific heat of the gas and average value of thermal conductivity are computed[5] to be:

$$c = 0{\cdot}32 \text{ cal/g } ^\circ\text{K and}$$

$$k = 1{\cdot}6 \times 10^{-4} \text{ cal/cm } ^\circ\text{K sec}$$

(c) *Heat losses*—Following ref. 3, the heat losses are divided into two parts, conduction loss and radiation loss, viz.:

$$L_c = (gk/2d^2)(T - T_u)$$

$$L_r = \varepsilon T^4 - \varepsilon' T_u^4$$

where the symbols signify:

- L_c Conduction loss from unit volume to surroundings (cal/cm³ sec)
- L_r Radiation loss from unit volume to surroundings (cal/cm³ sec)
- g Geometric factor in channel quenching[3]. For circular tubes, $g = 32$
- d Diameter of tube in centimetres
- ε Emissivity of gas. For 5 cm tubes using data given by W. H. McAdams[6]
  $\varepsilon = 0{\cdot}75 \times 10^{-9} - 0{\cdot}30 \times 10^{-12} T$
  cal/cm³ sec °K
- ε' Emissivity of tube wall.

The term $\varepsilon' T_u^4$ is numerically very small compared to εT^4. It will be omitted in the present computation.

(d) *Initial values for computation*—As has been pointed out[7] the temperature and concentration profiles of the flame will approach the 'upstream' boundary values ($T = T_u$ and $z = 1$) asymptotically. The computer cannot start at the point, $T = T_u$, because that is located[7] at $x = -\infty$. This difficulty is avoided by choosing a point at which the temperature is slightly higher than T_u. The reaction rate and radiation loss are extremely low at temperatures near T_u if T_u is near room temperature. So heat release as well as the radiation loss can be neglected in equations 1 and 2*. Then

$$\frac{d^2T}{dx^2} - \frac{cG}{k}\frac{dT}{dx} = l_c(T) \qquad \ldots . [6]$$

and

$$\delta_A \frac{d^2z}{dx^2} - \frac{cG}{k}\frac{dz}{dx} = 0 \qquad \ldots . [7]$$

*The removal of heat release terms from the equations in the upstream part of the flame profile is also a necessary condition for the existence of a steady state solution[7].

The solutions of equations 6 and 7 are respectively:

$$T = F + D\exp\left[\frac{cG}{2k} + \left(\frac{c^2G^2}{4k^2} + \frac{g}{2d^2}\right)^{\frac{1}{2}}\right]x \qquad \ldots . [8]$$

$$z = A + B\exp(cG/\delta_A k)\,x \qquad \ldots . [9]$$

In the above, F, D, A and B are constants of integration. Since it has been shown[7] that $T = T_u$ at $x = -\infty$ then

$$F = T_u$$

From boundary condition 3 we have:

$$z = 1, \text{ at } T = T_u\,(x = -\infty)$$

$$\therefore A = 1$$

$$T = T_u + D\exp\left[\frac{cG}{2k} + \left(\frac{c^2G^2}{4k^2} + \frac{g}{2d^2}\right)^{\frac{1}{2}}\right]x$$

$$\frac{dT}{dx} = D\left[\frac{cG}{2k} + \left(\frac{c^2G^2}{4k^2} + \frac{g}{2d^2}\right)^{\frac{1}{2}}\right]\exp\left[\frac{cG}{2k} + \left(\frac{c^2G^2}{4k^2} + \frac{g}{2d^2}\right)^{\frac{1}{2}}\right]x$$

$$z = 1 + B\exp(cG/\delta_A k)\,x$$

$$\frac{dz}{dx} = B\left(\frac{cG}{\delta_A k}\right)\exp\left(\frac{cG}{\delta_A k}\right)x$$

Take $x = 0$ as the starting point of integration. Let the temperature and concentration at this point be T_1 and z_1; then:

$$T_1 = T_u + D$$

$$\left(\frac{dT}{dx}\right)_1 = \left[\frac{cG}{2k} + \left(\frac{c^2G^2}{4k^2} + \frac{g}{2d^2}\right)^{\frac{1}{2}}\right]D$$

$$z_1 = 1 + B$$

$$(dz/dx)_1 = (cG/\delta_A k)\,B$$

For the initial values for the computation we can choose D so as to make T_1 slightly higher than T_u. After D is chosen, $(dT/dx)_1$ can be computed.

Since B is an undetermined constant we cannot determine the initial values z_1 and $(dz/dx)_1$. At $x = 0$, the temperature is very close to T_u. Therefore we know z_1 is also close to unity. Since the concentration, z, cannot be larger than unity, it is obvious that B must have a small negative value.

To start the integration, we have to guess the value of the mass flow rate, and the initial value

of the concentration. The boundary condition 5 can be satisfied, of course, only when the guessed values of B and G are both exact.

However, there are two cases for which one has to guess only the mass flow rate for the calculation.

Case A. Heat losses are neglected (i.e. the adiabatic case) and the Lewis number is assumed to be unity.

Dividing equation 6 by $T_a - T_u$ and adding equation 7 we have

$$\frac{d^2}{dx^2}\left(\frac{T}{T_a - T_u} + z\right) - \frac{cG}{k}\frac{d}{dx}\left(\frac{T}{T_a - T_u} + z\right) = 0$$

Solution

$$T/(T_a - T_u) + z = F \exp(cG/k)\, x + I$$

where F and I are constants of integration. F must be zero because both T and z are bounded.

When $T = T_u$, $z = 1$:

$$\left.\begin{aligned} &I = T_u/(T_a - T_u) + 1 \\ &z + (T - T_u)/(T_a - T_u) = 1 \\ &\{1/(T_a - T_u)\}\,(dT/dx) = -(dz/dx) \end{aligned}\right\} \quad \ldots . [10]$$

Therefore in this case, whenever D is selected, all other initial values z_1, $(dT/dx)_1$ and $(dz/dx)_1$ can be calculated by equations 10. The only unknown for the subsequent computation is the mass flow rate, G.

Case B. The Lewis number is assumed to be zero. With the heat release in the flame neglected, equation 2 becomes

$$dz/dx = 0 \quad z = \text{constant}$$

The initial values z_1 and $(dz/dx)_1$ are unity and zero respectively.

In all other cases, it is necessary to make preliminary guesses of B as well as G, in order to carry out the integration.

Burning Velocities Computed According to Adiabatic and Non-adiabatic Theories

Analogue computations for the propane–air adiabatic case are shown in *Figures 1*, *2* and *3*.

It is very difficult, if not impossible, to determine the exact mass flow rate, G. Even if the correct G is programmed into the computer, one has to carry the temperature and concentration profiles to positive infinity to satisfy the boundary conditions given in equation 5. The total integration time for an analogue computer

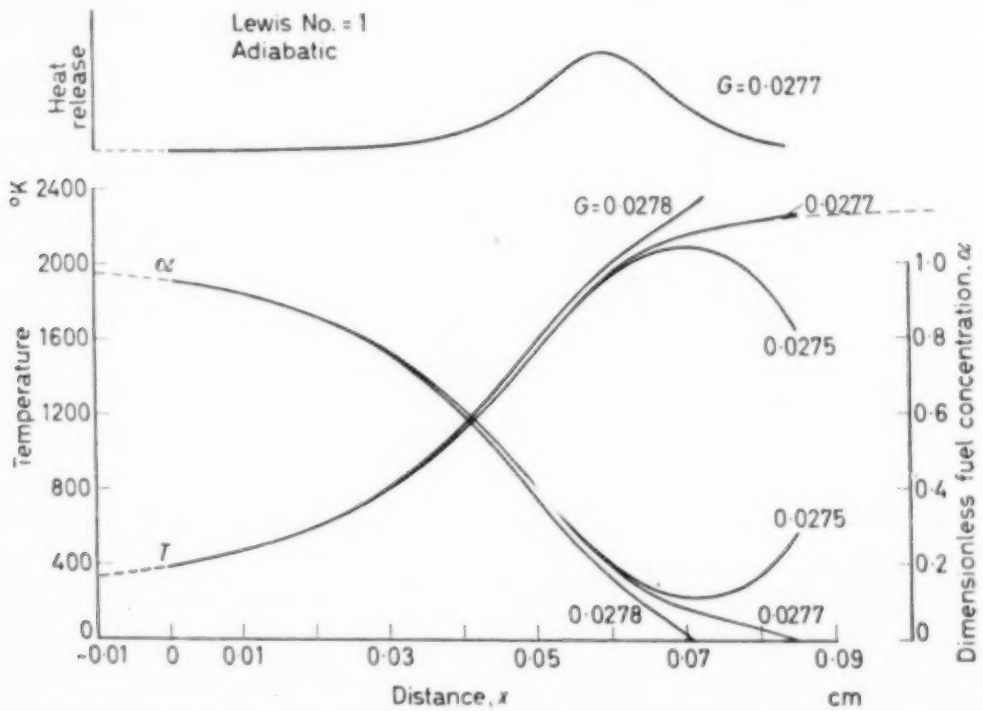

Figure 1. Temperature, concentration and heat release profiles (atmospheric pressure)

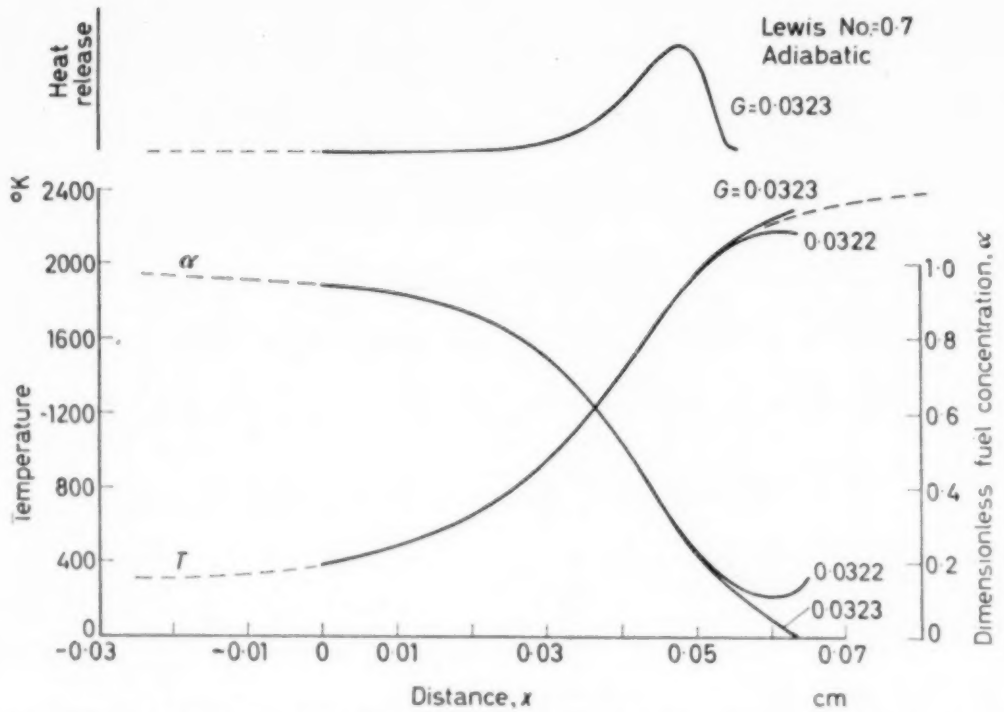

Figure 2. Temperature, concentration and heat release profiles (atmospheric pressure)

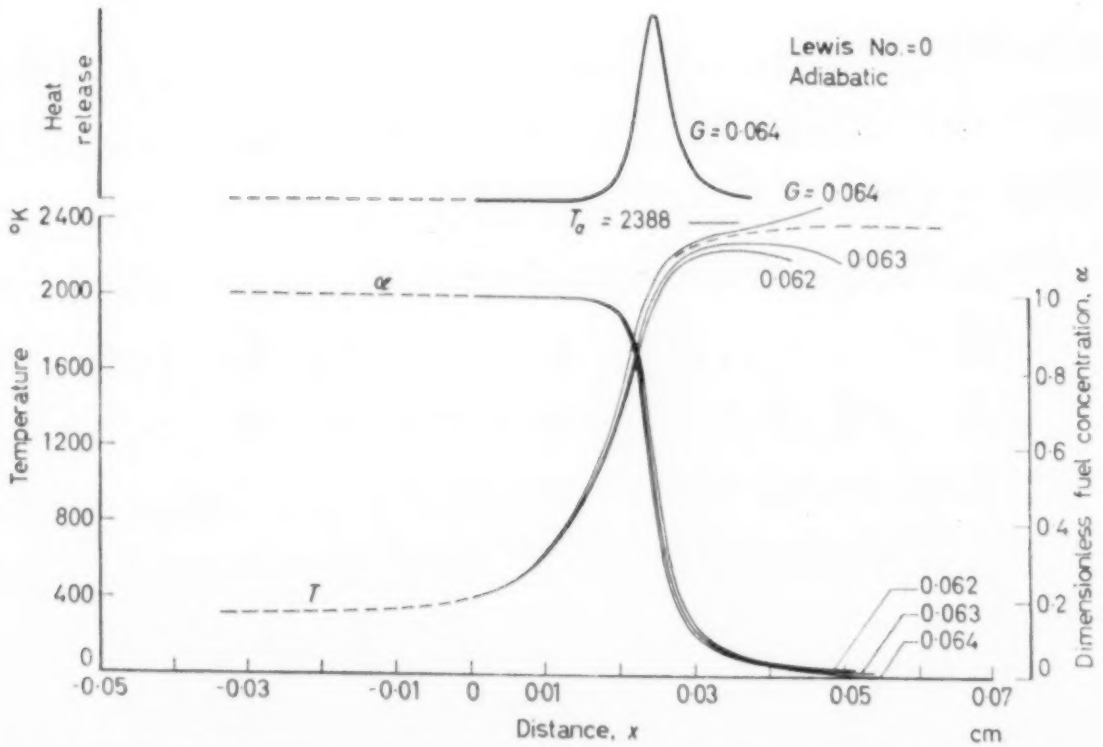

Figure 3. Temperature, concentration and heat release profiles (atmospheric pressure)

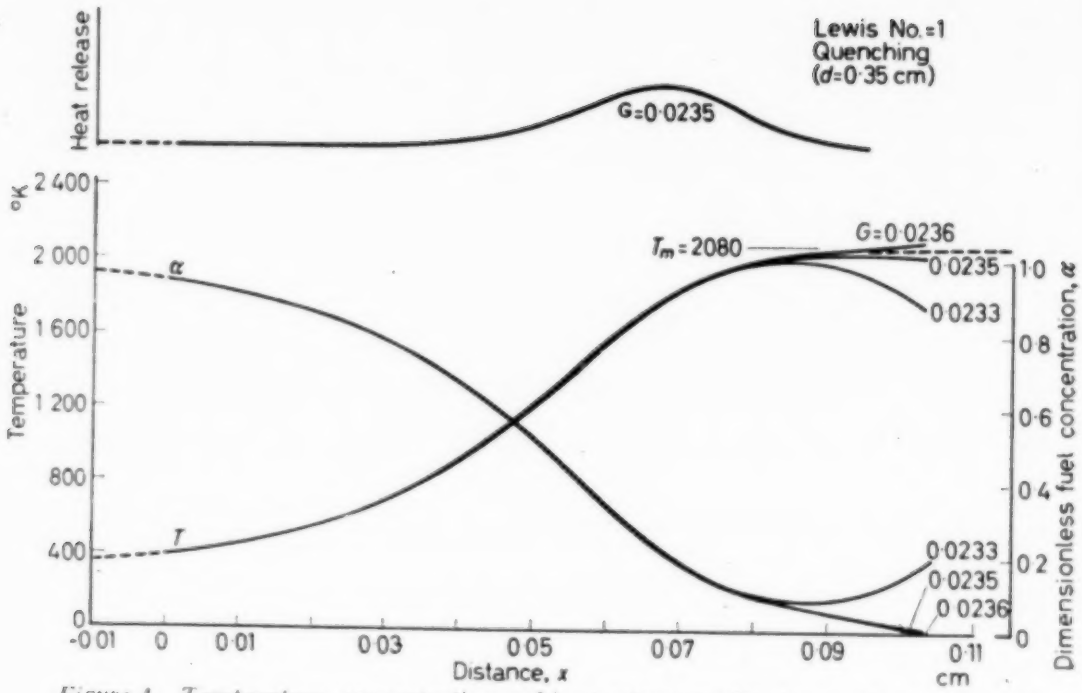

Figure 4. Temperature, concentration and heat release profiles (atmospheric pressure)

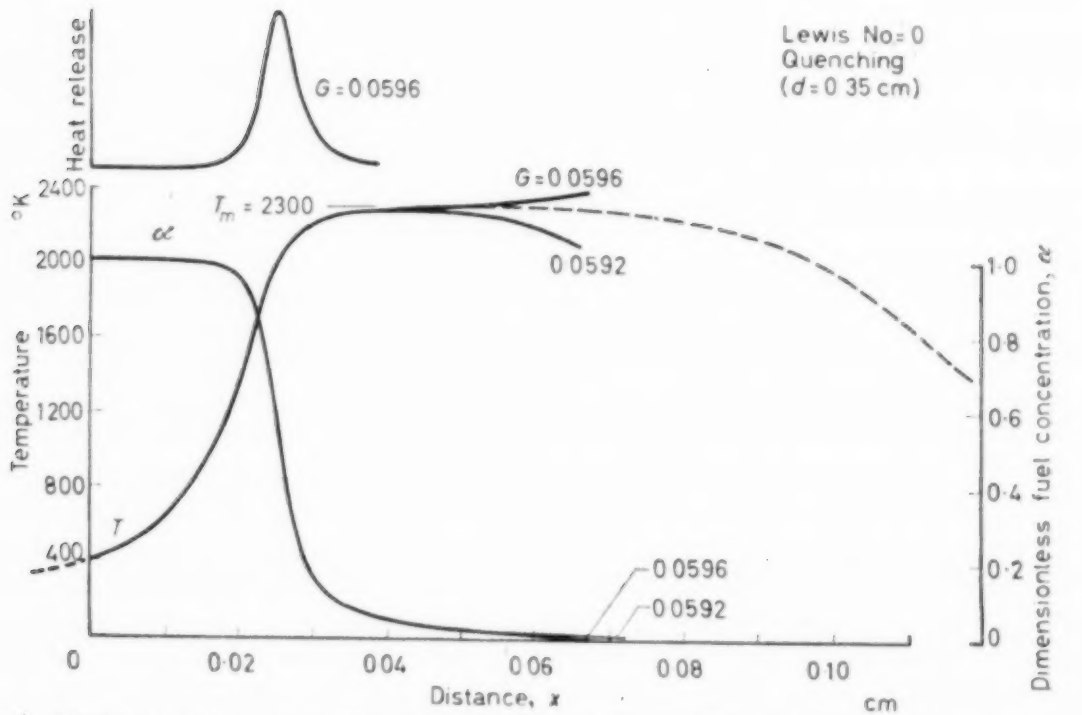

Figure 5. Temperature, concentration and heat release profiles (atmospheric pressure)

is limited by noise. So one cannot carry out the computer integration indefinitely in order to establish the boundary conditions given in equation 5. The correct mass flow for a system can only be bracketed between an upper and a lower value. Thus *Figure 1* shows that the correct mass flow for the adiabatic propane–air flame lies between $G=0{\cdot}0277$ and $0{\cdot}0275$ g/sec, if $\delta_A=1$.

The Lewis numbers were taken to be 1, 0·7 and 0 for *Figures 1*, *2* and *3* respectively. The computed burning velocities for these three cases are approximately 21·5, 25 and 49 cm/sec ($G=0{\cdot}0276$, $0{\cdot}0322$, and $0{\cdot}0635$ g/sec). The experimental value[8] is 40 cm/sec. The actual Lewis number should be between one and zero. It may be seen that the three values computed for the burning velocity bracket, the experimental value, and the difference from any one of the calculated values is small in view of the approximation used for the reaction kinetics. The use of mean values for the specific heat and thermal conductivity may have contributed a portion of error also. It should be noted in addition that the different Lewis numbers used affected the calculated burning velocity significantly.

A non-adiabatic case near the quenching limit of the flame is shown in *Figures 4* and *5*. The diameter of the tube for the quenching limit of the propane–air flame has been observed[9] to be 0·27 cm. Computations shown in *Figures 4* and *5* are for a propane–air flame in a 0·35 cm tube. From *Figure 4*, the burning velocity is 18 cm/sec ($G=0{\cdot}0234$ g/sec) and from *Figure 5*, the burning velocity is 46 cm/sec ($G=0{\cdot}0594$ g/sec).

If one tries lower values of burning velocities in the computation, the temperature profile will follow a pattern such as the one shown in *Figure 5* for $G=0{\cdot}0592$ g/sec. This profile does not satisfy the 'downstream' boundary conditions prescribed by equation 5. But when the burning velocity is reduced to a value between 4·7 and 6·2 cm/sec ($G=0{\cdot}006$ and $0{\cdot}008$ g/sec) the temperature and concentration profiles (see *Figure 6*) again satisfy the boundary conditions given in equation 5. This is obviously the often talked about 'lower eigenvalue' of the flame.

The 'upper eigenvalue' and the 'lower eigenvalue' computations are shown in *Figure 7* for a propane–air flame in a 0·20 cm tube. The burning velocities are approximately 33 and 25 cm/sec ($G=0{\cdot}043$ and $0{\cdot}033$ g/sec) respectively. These two 'eigenvalues' will approach each other (as may be seen by comparing *Figures 5*, *6* and *7*), when the diameter of the tube approaches the quenching distance. The 'lower eigenvalue' goes to zero when heat losses are neglected.

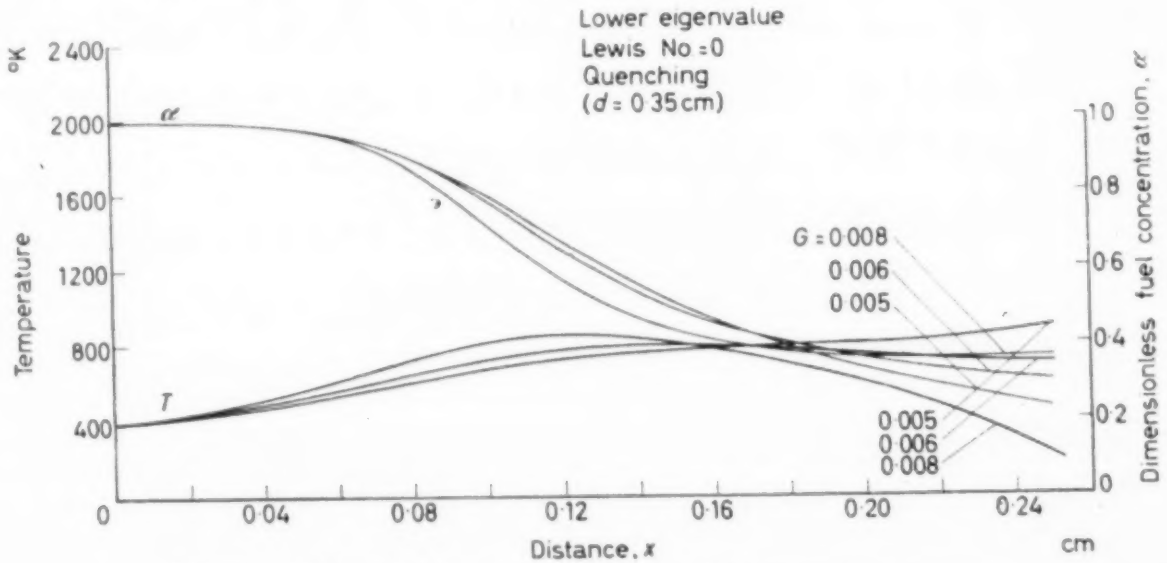

Figure 6. Temperature and concentration profiles (atmospheric pressure)

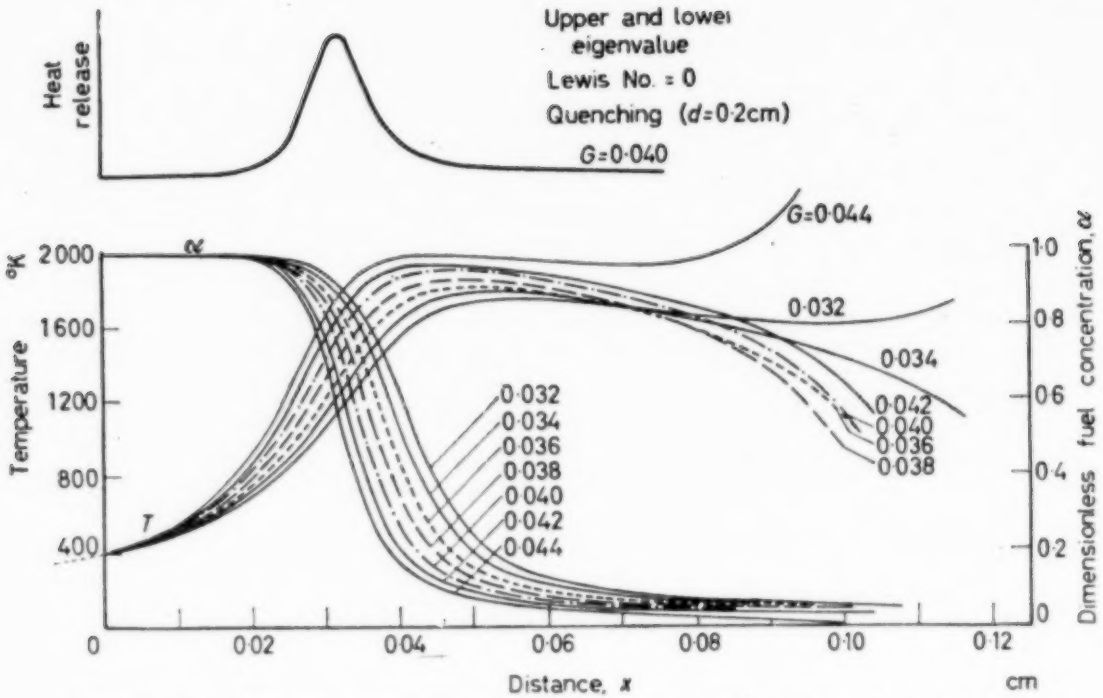

Figure 7. Temperature, concentration and heat release profiles (atmospheric pressure)

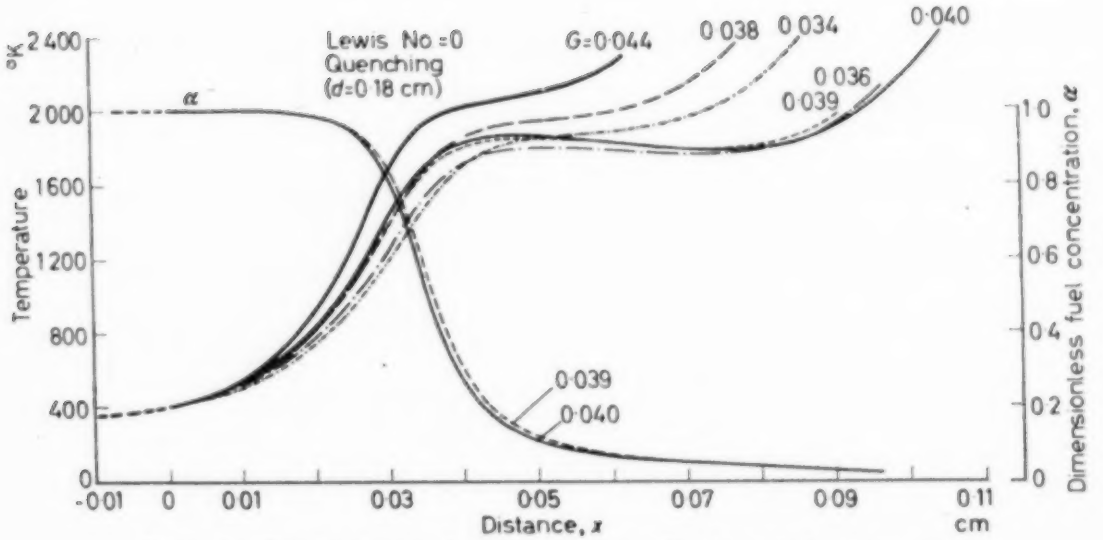

Figure 8. Temperature and concentration profiles (atmospheric pressure)

Computations for a propane–air flame in a 0·18 cm diameter tube were also attempted. Results are shown in *Figure 8*. 'Downstream' boundary conditions could never be satisfied for a spectrum of burning velocities ranging from 22 to 34 cm/sec. The computed quenching limit, which apparently lies between 0·18 and 0·20 cm, is lower than the experimental[9] value of 0·27 cm.

In a forthcoming publication entitled 'Theory of ignition' we will show that the 'lower eigenvalue' is connected with the ignition energy.

It is also interesting to note that the burning velocity of a flame which is very close to the quenching limit is lower than the burning velocity of the same flame under near-adiabatic conditions, but the effect of near-quenching is much less than that of increasing the percentage of nitrogen in air. Solutions for the stoichiometric propane–air flame under 0·7 atmosphere pressure are computed in *Figures 9* and *10*.

The experimental pressure limit observed[10] is 0·046 atmosphere for the propane–air flame. The 'upper eigenvalue' lies between 44 and 39 cm/sec ($G = 0{\cdot}004$ and $0{\cdot}0035$ g/sec). The 'lower eigenvalue' lies between 6·6 and 5·5 cm/sec ($G = 0{\cdot}0006$ and $0{\cdot}0005$ g/sec). The computed burning velocity near the pressure limit is about the same as the burning velocity of the flame under the atmospheric pressure condition.

A non-adiabatic computation was also made of the temperature and concentration profiles for a flame in a gas mixture of the following composition

$$C_3H_8 : O_2 : N_2 = 1 : 5 : 32$$

The tube diameter was 5·0 cm, and pressure was atmospheric. *Figure 11* shows the result. The burning velocity was between 12·5 and 12·7 cm/sec ($G = 0{\cdot}0155$ to $0{\cdot}0157$ g/sec). The experimental inflammability limit for propane–oxygen, as a function of dilution with nitrogen, is observed[11] at just this ratio. Since the computation shows a flame to exist under these conditions, we conclude that the prediction of the inflammability limit (namely something above 32 moles of nitrogen) is too high.

Structure of Flames Computed According to Adiabatic and Non-adiabatic Theories

The shape of the computed temperature and concentration profiles as well as the heat release curve are in agreement with the results of known experimental measurements[12]. For example, Figure 1 of ref. 12 shows a set of temperature profiles for propane–air flames, the shape of which agrees with our temperature curves, particularly *Figure 2* which employs the very reasonable Lewis number of 0·7. The experiments of R. M. FRISTROM and co-workers[12] were conducted on a burner; and hence the measured temperature profile should agree with that calculated by an adiabatic model, up to the location of the maximum

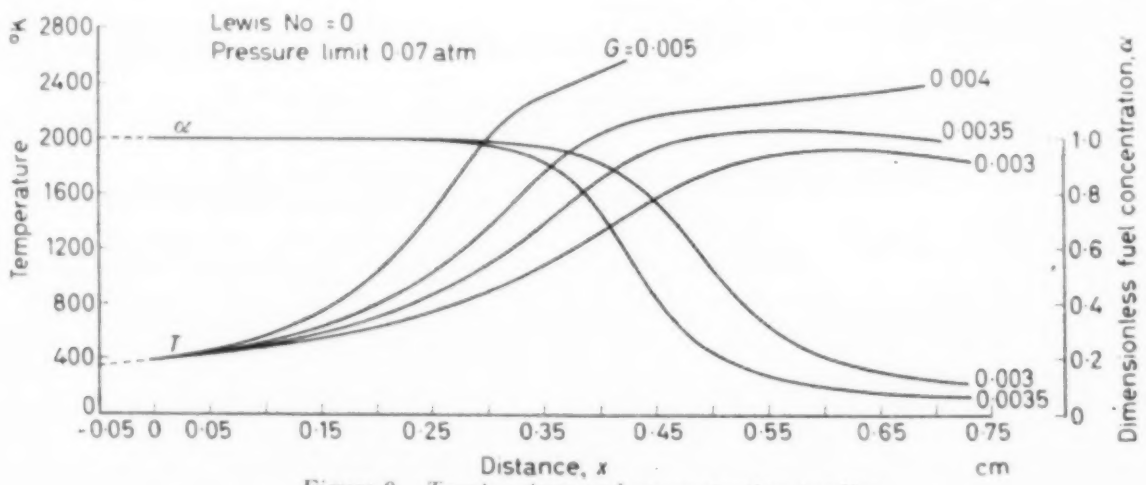

Figure 9. Temperature and concentration profiles

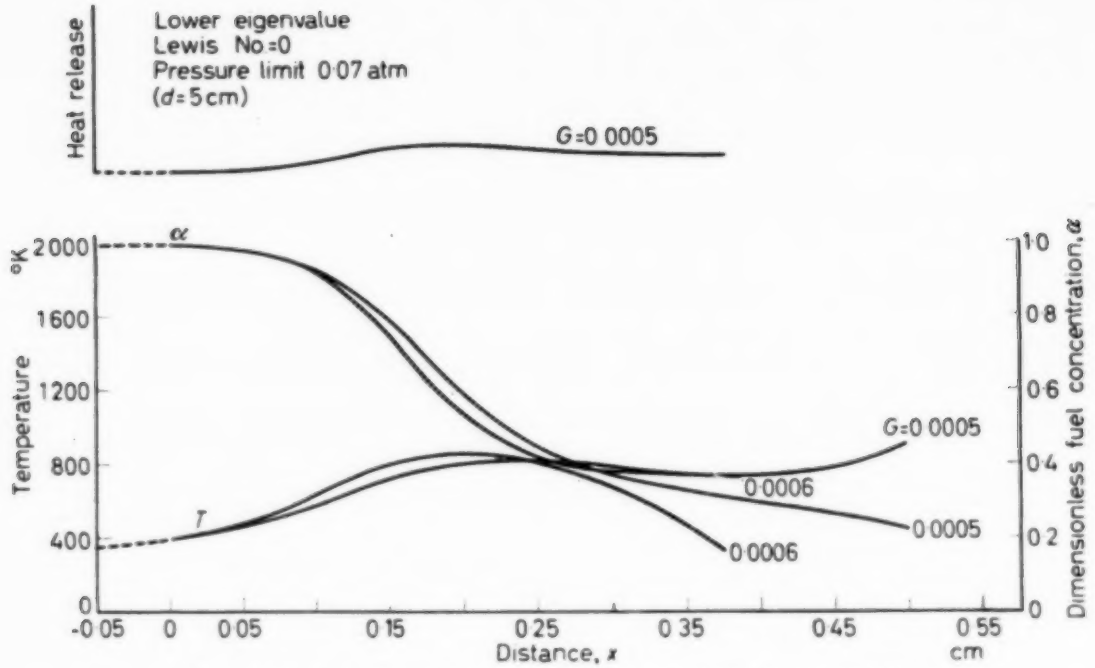

Figure 10. Temperature, concentration and heat release profiles

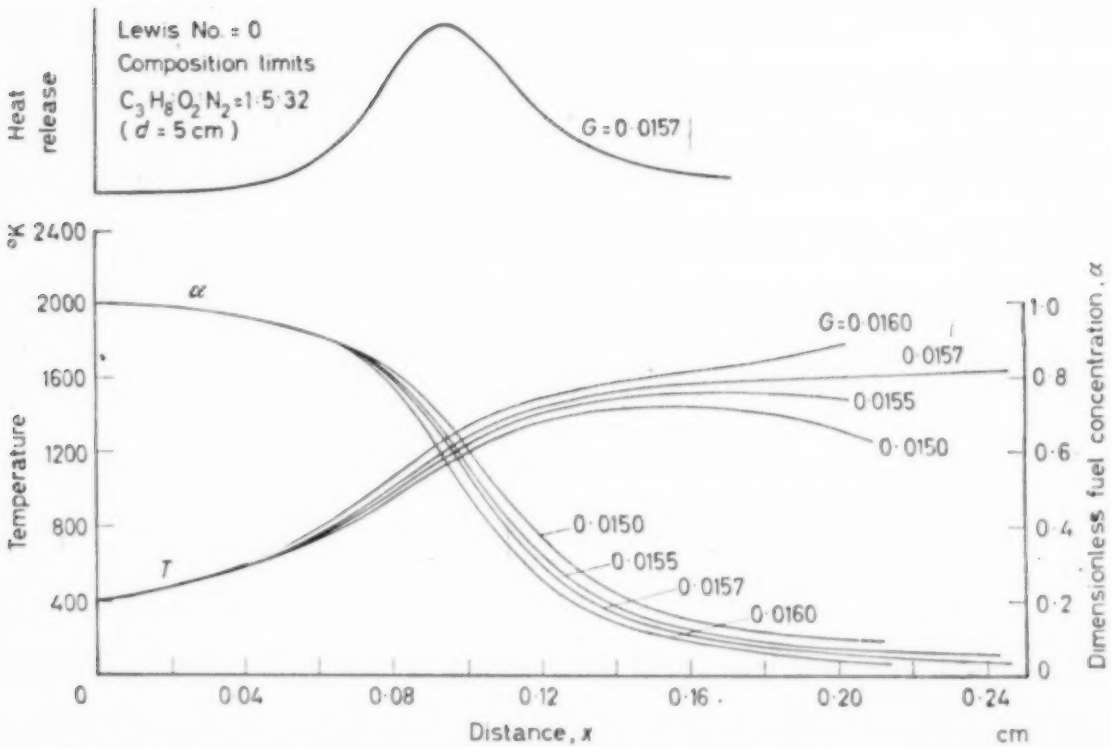

Figure 11. Temperature, concentration and heat release profiles (atmospheric pressure)

temperature. (Beyond the position of T_m, a flame on a burner expands and the temperature drops; the experiment then no longer corresponds to the adiabatic model for a flame in a tube, for which *Figure 2* was computed.) The location of the luminous zone (which probably coincides with the maximum heat release in the flame zone) was observed to be at the same position as calculated.

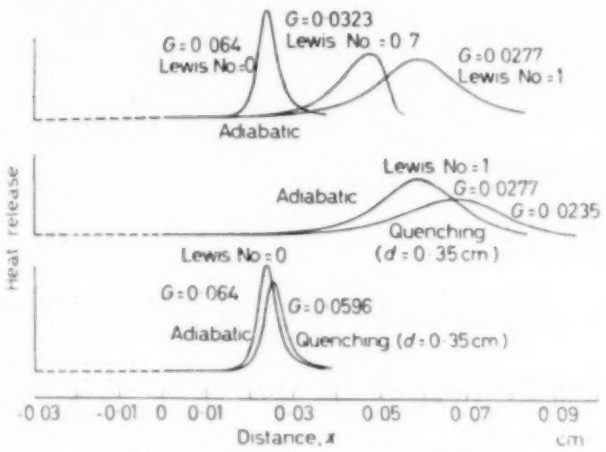

Figure 12. Heat release profiles

The structure of flames in the present theoretical model extends from $-\infty$ to $+\infty$. The term 'flame depth' has no meaning unless specific qualifications are imposed. Ordinarily when the term 'flame depth' is used, it is intended to indicate the reaction zone of the flame; and the reaction zone is indicated by the heat release curve in a flame. Heat release curves for various flames are compared in *Figure 12*. It is expected that a higher diffusivity of a fuel will result in a broader 'flame depth'; hence the effect of varying Lewis number. It is interesting to note that all the heat release curves shown in *Figures 1, 2, 3* and *4* peaked at $T = 1\,900°\mathrm{K}$ (about 80 per cent T_b). The maximum temperatures reached, as shown in *Figures 4* and *5*, are approximately 2 080° and 2 300°K respectively. Heat release curves for adiabatic flames are peaked more sharply than curves for flames near the quenching limit.

Figure 9 shows that the structure of a flame near the pressure limit differs very much from that of a flame that is near the quenching limit, the 'flame depth' being very large in the former case. The maximum temperature reached in this calculation is approximately 2 050°K. The structure of a flame near the inflammability limit lies between the structures of the flames near the quenching limit and pressure limit. However, the maximum temperature reached is almost as high as the adiabatic temperature.

Concluding Remarks

(*1*) The present non-adiabatic flame theory predicts flame structure, burning velocity and extinction limits with a single set of equations. Heat losses are considered throughout the flame. Computations have neglected only the heat release of the system at points where temperatures are low (below 400°K). The Arrhenius type of rate function as used in this paper gives:

$$\Phi = 8 \times 10^{7} z^{2} \text{ at } T = 1\,900°\mathrm{K}$$
$$\Phi = 1{\cdot}4 \times 10^{-8} z^{2} \text{ at } T = 400°\mathrm{K}$$

It is apparent that the omission of heat release at temperatures below 400°K does not introduce appreciable error.

(*2*) The calculation of flame structure, extinction limits, etc., depends upon a knowledge of the kinetics as well as of the physical properties of the system. Conversely, measurements of flame properties such as extinction limits, structure, etc., should also yield information useful to chemical kinetics, transport properties, etc., through the use of the flame theory.

(*3*) The boundary conditions **4** and **5** are sufficient to prescribe solutions to the problem. Moreover, by examining the solutions derived for the initial values, it can be deduced that the following conditions are also satisfied at the 'upstream' boundary:

$$T = T_u \left\{ x = -\infty, \frac{\mathrm{d}z}{\mathrm{d}x} = 0, \frac{\mathrm{d}\beta}{\mathrm{d}x} = 0 \right.$$

A similar consideration can be extended to the 'downstream' boundary, i.e. that the following conditions are also satisfied:

$$T = T_u \left\{ x = +\infty, \; z = 0, \; \beta = 0 \right.$$

Therefore, it can be concluded that these additional boundary conditions are implicit in equations 4 and 5.

The author wishes to express his sincere appreciation to Miss Joan Sjoblom for her expert assistance in the calculations, and to Dr Allan Wilson and Mr George Cooper of the Analog Computing Laboratory of Convair–Astronautics for their invaluable help in the analogue computing programme.

References

[1] Spalding, D. B. *Proc. Roy. Soc. A*, 1957, **240**, 83
[2] Mayer, E. *Combustion & Flame*, 1957, **1**, 438
[3] Berlad, A. L. and Yang, C. H. *Combustion & Flame*, 1960, **4**, 325
[4] Avery, W. H. *Fifth Symposium (International) on Combustion*, p 86. Reinhold: New York, 1955
[5] Rossini, F. D. *et al. Circ. Nat. Bur. Stand. No. C461*, 1947
[6] McAdams, W. H. *Heat Transmission*, pp 64–70. McGraw-Hill: New York, 1942
[7] Berlad, A. L. and Yang, C. H. *Combustion & Flame*, 1959, **4**, 447
[8] Botha, J. P. and Spalding, D. B. *Proc. Roy. Soc. A*, 1954, **225**, 71
[9] Lewis, B. and von Elbe, G. *Combustion, Flames and Explosion of Gases*, p 304. Academic Press: New York, 1951
[10] Simon, D. M., Belles, F. E. and Spakowski, A. E. *Fourth Symposium (International) on Combustion*, pp 126–158. Williams and Wilkins: Baltimore, 1953
[11] Coward, H. F. and Jones, G. W. *Bull. U.S. Bur. Min. No. 503*, 1952
[12] Fristrom, R. M., Prescott, R., Neumann, R. G. and Avery, W. H. *Fourth Symposium (International) on Combustion*, p 267. Williams and Wilkins: Baltimore, 1953

Studies of Screeching Combustion and Pressure-wave, Flamefront Interaction

A. W. Blackman

Research Laboratories, United Aircraft Corporation, East Hartford, Connecticut, U.S.A.

(*Received July 1960*)

An experimental investigation was undertaken to obtain information leading to criteria which govern the excitation of screeching combustion and to methods for its control. The screech phenomenon appears to result from a coupling between a varying energy release produced by the combustion process and standing waves produced by resonance of the combustion chamber cavity. Tests on small-scale combustors showed that screech can be eliminated by properly spacing the flameholders relative to the combustor walls or by adding sufficient damping to the combustion chamber.

Introduction

Screeching combustion, or screech, is an instability which occurs in ramjets and turbojet afterburners. It is characterized by high-frequency pressure and flamefront oscillations at a frequency corresponding to some resonant frequency of the combustion chamber cavity. These oscillations increase heat transfer and stress-repetition rates and usually cause failure of combustion chamber structural components within seconds after their onset. Understanding and control of this phenomenon are necessary for the further development of high-performance air-breathing combustors.

The screech phenomenon was first recognized in 1949 by workers at the United Aircraft Corporation Research Laboratories, and descriptions of much of the early work on the screech problem were confined to the classified literature. The general characteristics of screech, the effect of variations in flow variables on the excitation of screech, and possible mechanisms for its excitation are discussed elsewhere[1–5]. However, the existing literature does not establish criteria which can be applied to predict the excitation of screech or methods for its control. The investigation described herein was undertaken to supply information applicable to these areas.

Test Apparatus

Small-scale combustor

The small-scale combustor shown in *Figure 1* was used for all tests except those in which the locations of flameholders were varied. The combustor test section had a rectangular cross section, 3 in. wide, 4·5 in. high, and was 26·5 in. long. Vycor window sections were provided to allow observation and flame photography. A single-edge flameholder with a hydrogen–oxygen pilot located at the base was used for most test work. For some tests, two-dimensional, V-gutter flameholders were used with piloting provided at the side.

Air was supplied to the combustor from compressors having a maximum capacity of 2·4 lb/sec. A steam heater was provided which heated the air to approximately 280°F. From the steam heater, the air passed through a mixing section where fuel was injected. The fuel injectors were located 135 in. upstream of the flameholder in order to obtain a flat fuel/air distribution profile at the flameholder. From the mixing section, the air passed through the small-scale combustor into a water-cooled plenum chamber connected to a vacuum supply.

Eighty-octane gasoline (containing dye) was used as the fuel for all tests except those

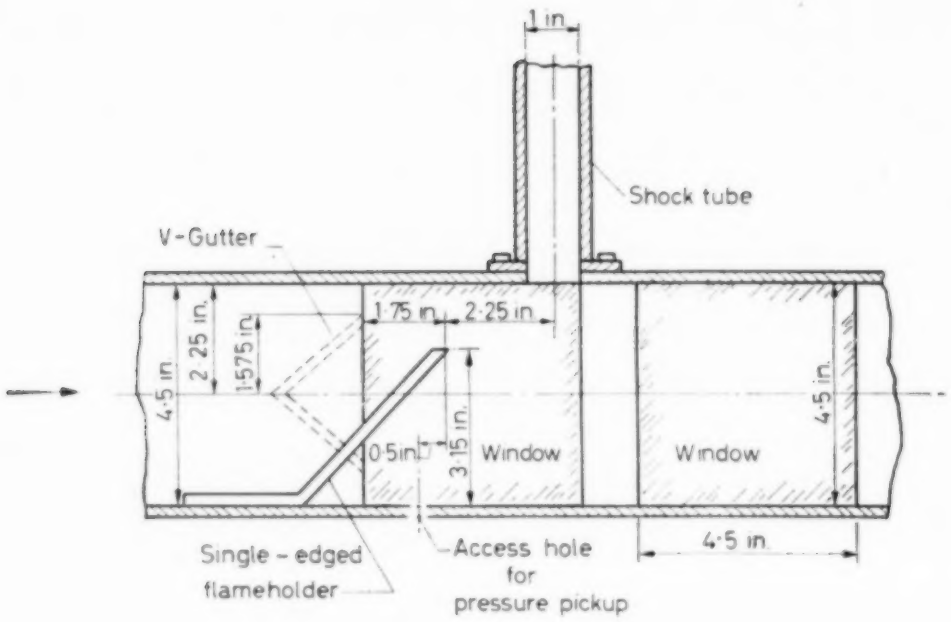

Figure 1. Small-scale combustor

involving flame photography. For these tests, a gasoline which had similar physical properties but which contained no dye was used to minimize stains on the combustion chamber windows.

A rectangular shock tube having a 1 in. by 2 in. cross section was mounted above the flameholder as shown in *Figure 1*. The high-pressure side of the shock tube was pressurized with nitrogen, and photographic film was used as a diaphragm to separate the high-pressure and low-pressure sides. The number of film layers used was increased as the pressure ratio of the shock tube was increased. Normally, three layers were used. A puncturing mechanism operated by a solenoid was used to break the diaphragm separating the high-pressure and low-pressure gases. Sufficient length was provided on the low-pressure side of the shock tube to ensure that a plane shock wave had time to develop after the diaphragm was punctured.

Large-scale combustor

The large-scale combustor used in tests in which the location of the flameholder was varied is illustrated in *Figure 2*. The combustion chamber was two-dimensional and had a cross section of 3·5 in. by 12 in. It was fabricated of stainless steel 0·5 in. thick and had twelve access holes located around the chamber to allow measurement of the screech pressure oscillations.

Airflow for the apparatus was supplied by a compressor having a maximum airflow capacity of 12 lb/sec at a pressure of 38 lb/in² absolute. The inlet of an identical compressor was attached to the exhaust ducting. This arrangement allowed testing at combustion chamber pressures above and below atmospheric pressure.

The airflow rates were measured by a standard ASME bellmouth. To simulate afterburner inlet conditions, the air was preheated to 1 000°F by burning a small amount of fuel in a J-48 burner can, thus vitiating the air slightly with combustion products. Eighty-octane gasoline for the combustor was injected far enough upstream to ensure a flat fuel-distribution profile at the flameholders. The exhaust gases passed through a water-cooled variable-area exhaust nozzle and were quenched by water sprays before entering the vacuum system.

Flameholders of various blockages were supported by a sliding bar system mounted on the duct walls, and the flameholder location was changed by moving the two bars which sup-

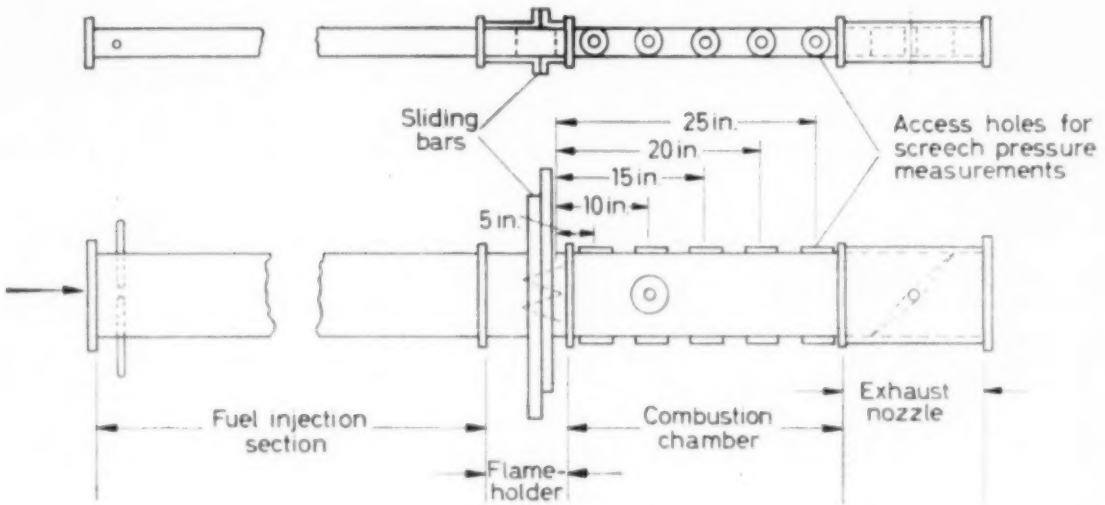

Figure 2. Large-scale combustor

ported each flameholder to a new position in the duct. Two identical V-gutter flameholders were used for each blockage. Hydrogen–oxygen pilots mounted in the sliding bar system were used for ignition. A water-cooled variable-area exhaust nozzle was used to regulate the airflow through the test section, and the pressures in the exhaust plenum chamber were always kept low enough to ensure choked flow through the exhaust nozzle.

High-speed photographic equipment

High-speed motion pictures of the interaction of a shock wave with a flamefront were obtained utilizing a Fastax camera. An Edgerton, Germeshausen, and Grier Model 501 stroboscopic light source was collimated by a 5·7 in. diameter, 36 in. focal length Dallmeyer lens and the light passed through the combustion zone of the small-scale combustor by a front-surface mirror. The light was then reflected by an identical front-surface mirror and collimating lens into the Fastax camera. A variable-reluctance pickup attached to the Fastax camera caused the stroboscopic light source to fire each time the camera shutter was opened. The light source had a maximum repetition rate of 6 000 light flashes per second with a duration which could be varied down to 1·5 microsecond.

Instrumentation for pressure measurements

A schematic representation of the instrumentation used to measure the variation of pressure with time is presented in *Figure 3*. The signal from a pressure transducer was fed into a four-channel oscilloscope. The oscilloscope trace was photographed by either a Polaroid

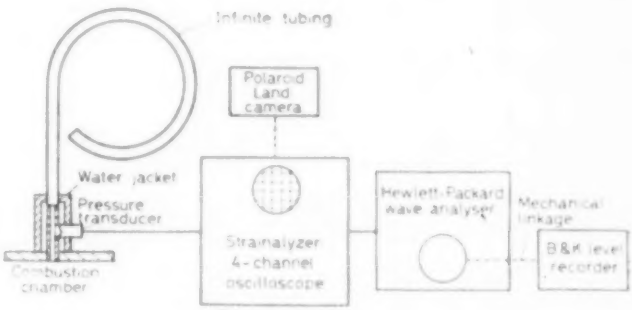

Figure 3. Pressure measurement instrumentation

Land Camera or a General Radio Strip Film Camera (Model 651–AE). A spectral analysis of the wave was obtained by feeding the signal into a Hewlett-Packard wave analyser (Model No. 300–A). A Bruel and Kjaer level recorder (Model 2304) was linked mechanically to the wave analyser in order to obtain an automatic recording of the output from the wave analyser. A typical wave analysis measured on the large-scale combustor is shown in *Figure 4*.

Strain-gauge and barium titanate transducers were used in these investigations; however, the strain-gauge transducers were used more frequently. The strain-gauge transducers were

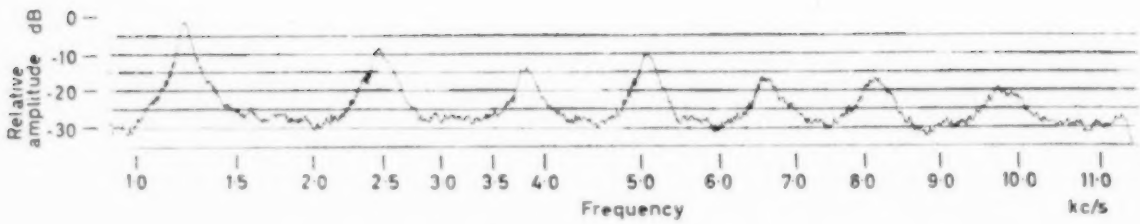

Figure 4. Typical screech pressure wave analysis

manufactured by the Control Engineering Co. and had a natural frequency of approximately 35 000 c/s, while the barium titanate transducers (manufactured by Atlantic Research Corp.) had a natural frequency of approximately 70 000 c/s.

For most tests it was possible to flush-mount the strain-gauge transducers in the combustion chamber wall if the hot combustion gases did not flow directly by the pickup diaphragm. With the barium titanate transducers, it was necessary to use the 'infinite tube' technique to eliminate the heating problem. This method consists of mounting the pickup near the entrance of a long tube which is connected to the combustion chamber (see *Figure 3*). The tube is made long enough to allow a pressure pulse originating at the tube entrance to be completely damped by the time the pulse travels to the end of the tube. Thus no resonance can occur in the tube, and the pressure felt by the pickup will be the same as that in the combustion chamber except for the losses encountered in the tube entrance and the small amount of damping that exists from the tube entrance to the point where the pickup is mounted. The pickup can be cooled by passing a small airflow through the tube into the combustion chamber. This technique is discussed more fully by P. L. BLACKSHEAR *et al.*[2].

Results and Discussion

Photographic observations

Figure 5 shows high-speed photographs taken at random and arranged sequentially to show the interaction between a shock wave and a flamefront. The time interval between the photographs is not constant. When these photographs were obtained, the small-scale combustor was operated at an inlet temperature of 280°F, a combustion chamber pressure of one atmosphere, an air weight flow of 1·1 lb/sec, and a fuel/air ratio of 0·06. These conditions produced smooth combustion which was free of screech prior to the firing of the shock tube. The stains which show up in the pictures were caused by the direct contact of the flamefront with the Vycor windows. They appeared a few seconds after combustion was initiated. The shock propagated in a cylindrical pattern. As the shock wave hit the flamefront, the burning surface became highly turbulent and moved in the direction of shock propagation. There was a resulting increase in flamefront area as the shock reached the vicinity of the flameholder lip, and a strong vortex pattern was set up. In a short time the flamefront resumed its steady-state position and no combustion chamber oscillations were maintained. For comparison, *Figure 6* shows similar photographs of the passage of a shock wave into a combustion chamber through which air is flowing but in which no combustion is occurring. The passage of the shock wave through the flamefront appears greatly to increase the turbulence and mixing between the flamefront and the surrounding unburnt fuel-air mixture. The increased mixing and turbulence would increase the local burning rate, thus causing increases in the local heat release. If the increase in the local heat release (*1*) were of sufficient magnitude to overcome the viscous damping in the system and (*2*) maintained the proper phase relationship with the pressure wave, the strength of the wave would be increased and a mechanism would be provided for the maintenance of the oscillations.

It was found that screeching combustion could not be obtained with the single-ele

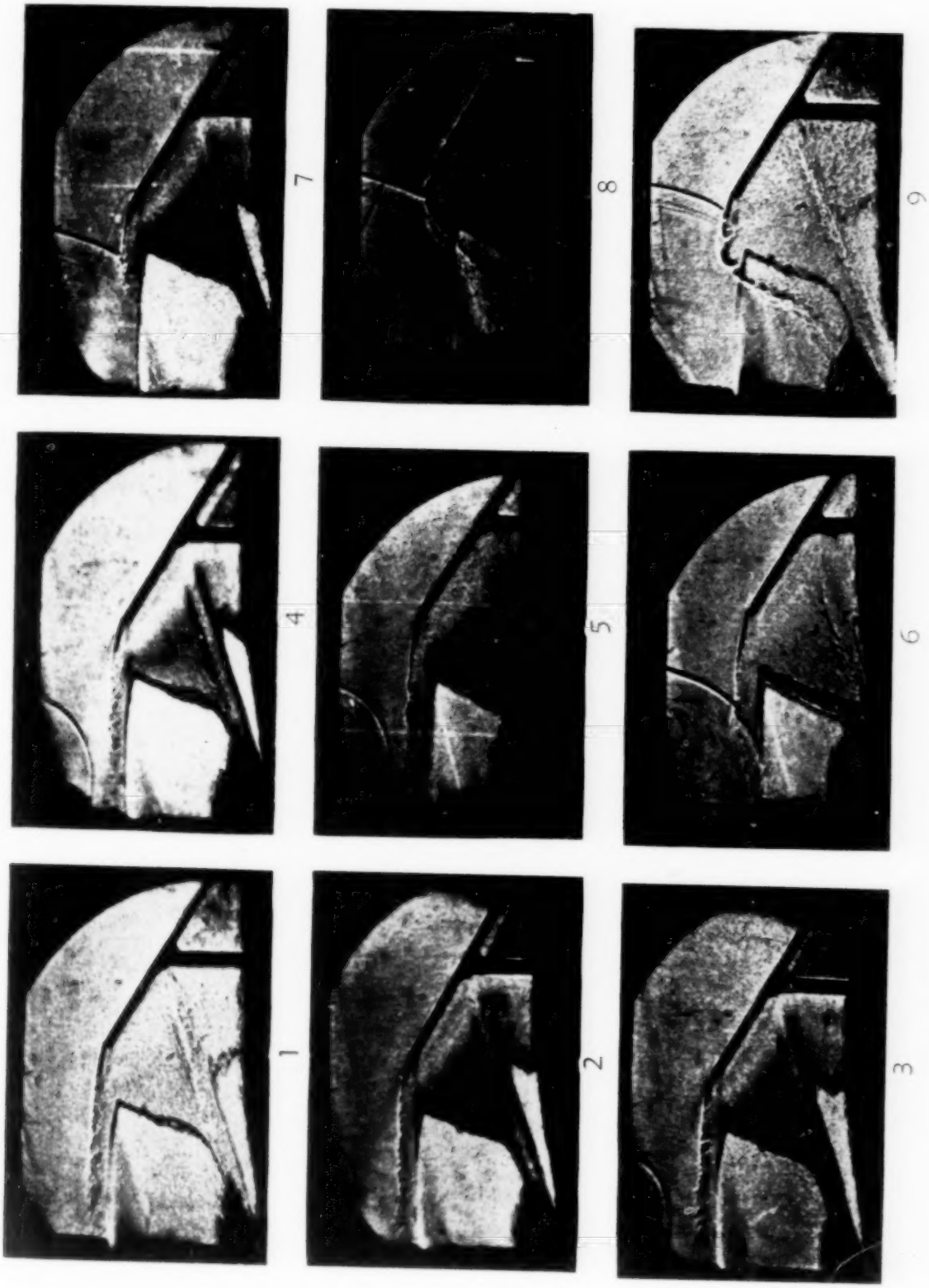

Figure 5(a). Sequence recorded

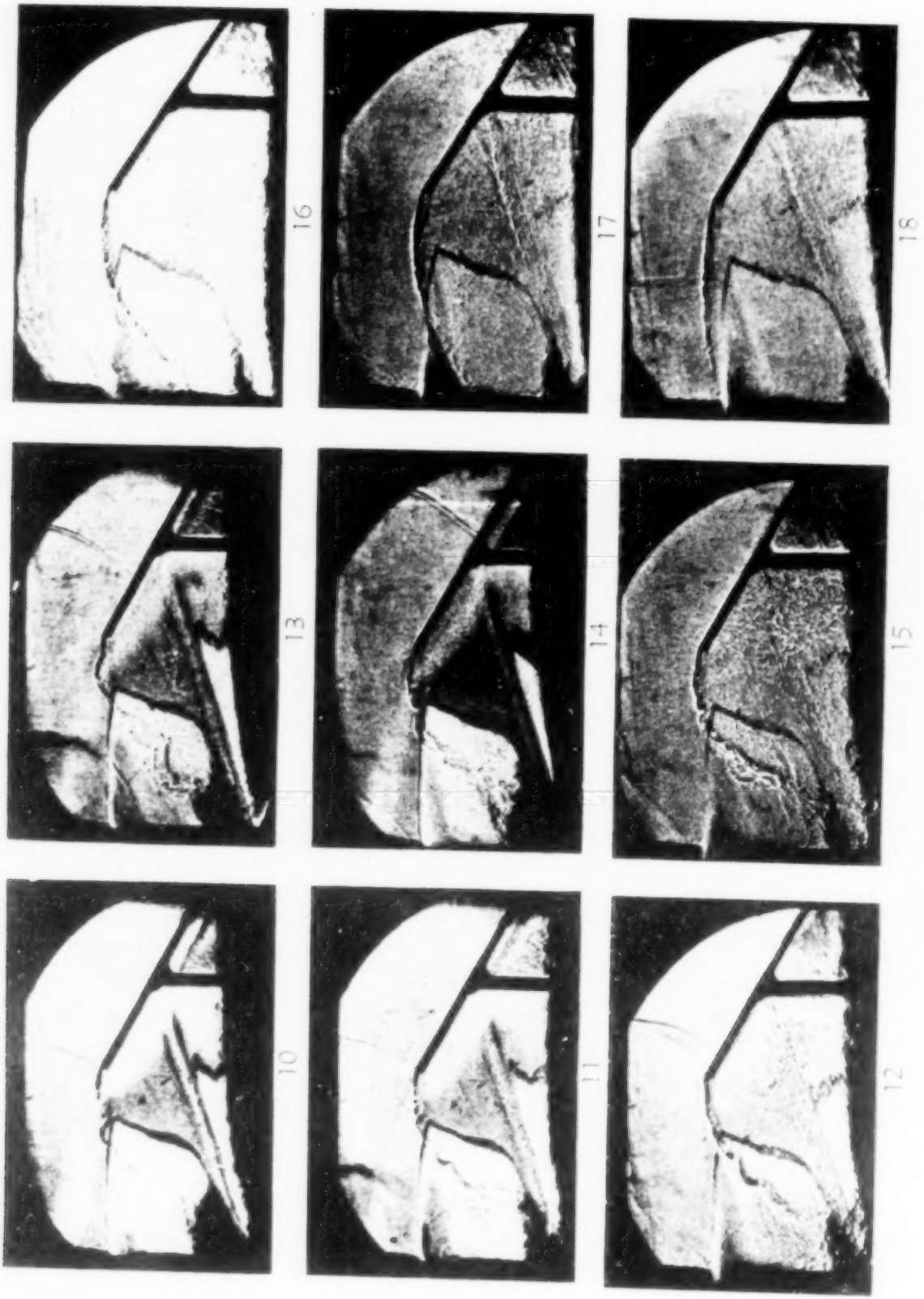
16
17
18
13
14
15
10
11
12

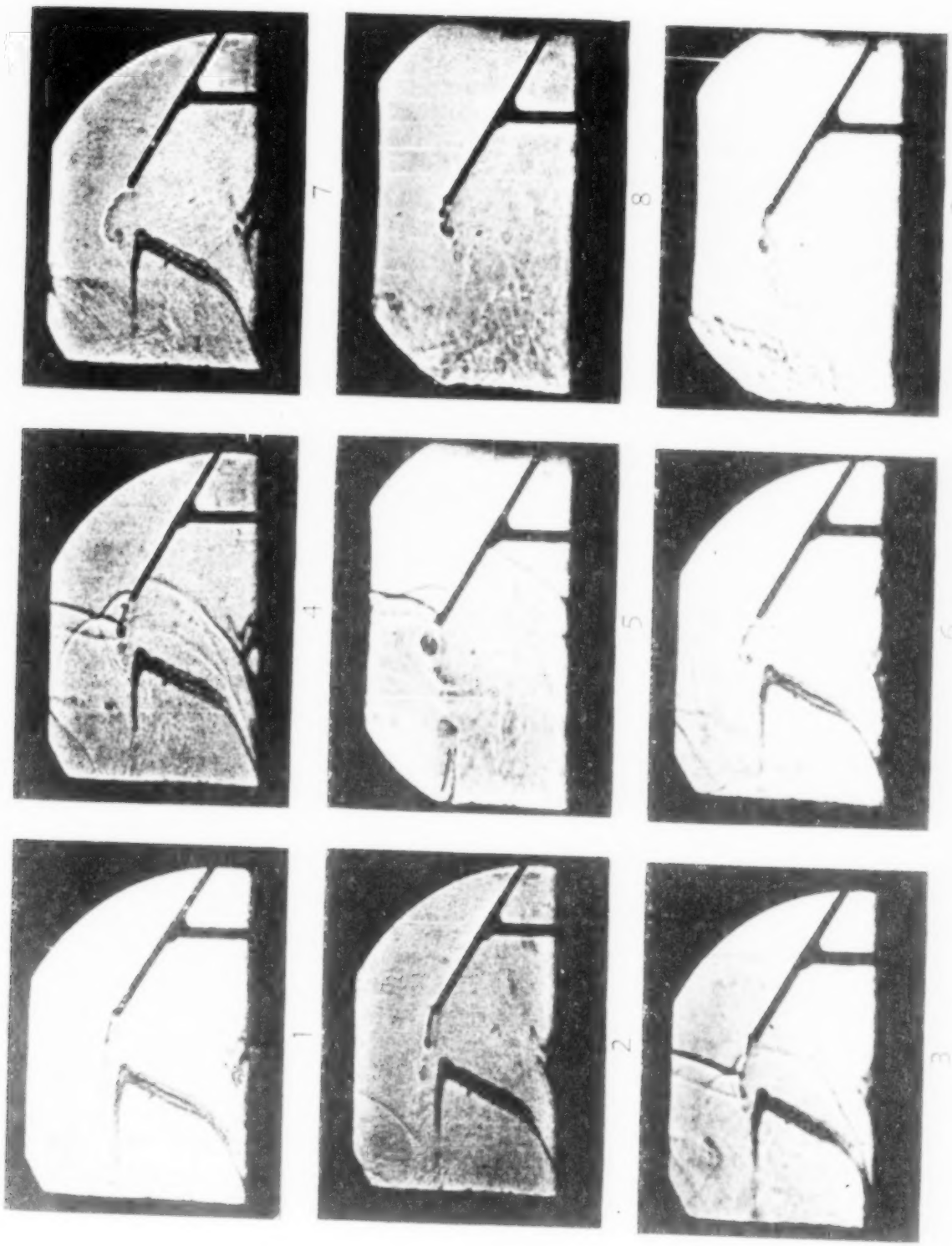
7
8
9
4
5
6
1
2
3

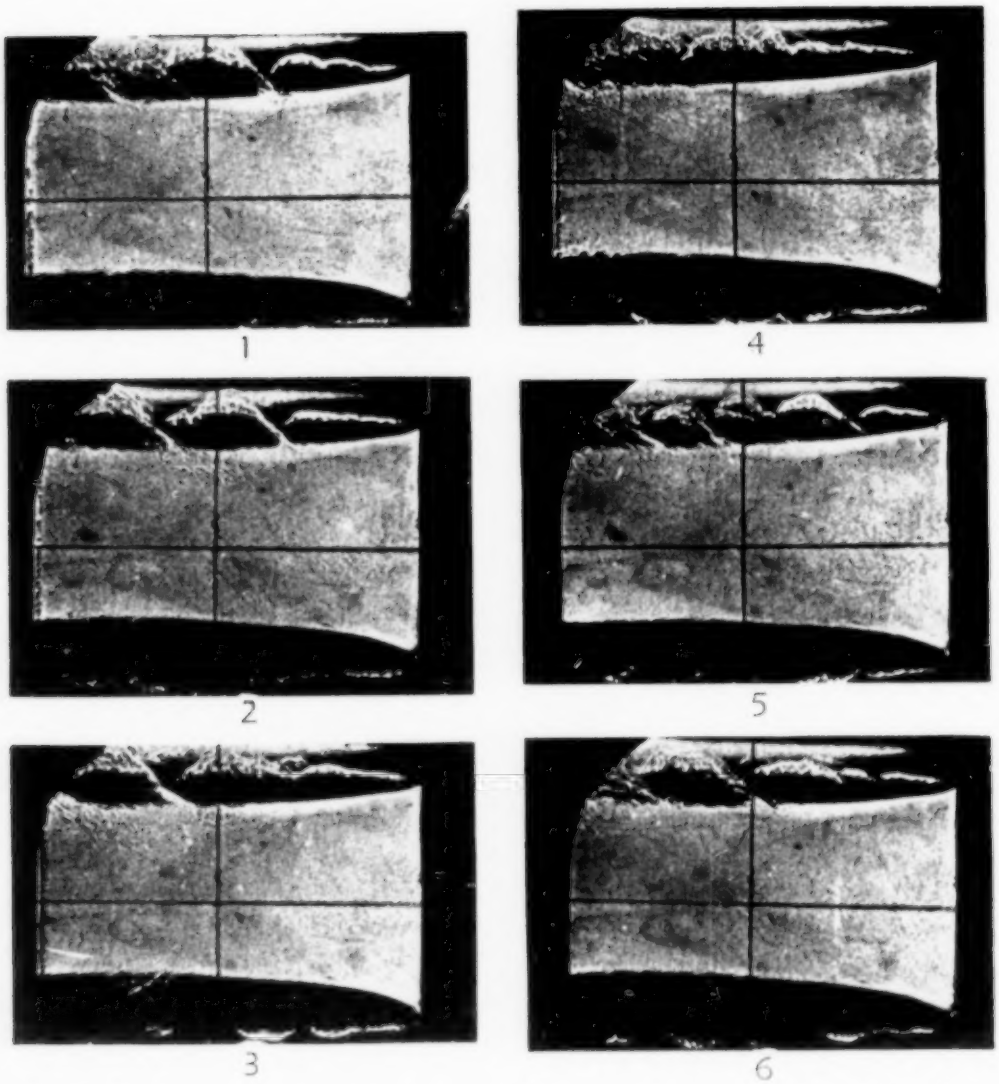

Figure 7. Photographs of screeching combustion flow from right to left. Time interval between photographs 22t microseconds; combustor pressure 14.6 lb/in² abs; inlet temperature 280 F; airflow 1.45 lb/sec; fuel-air ratio 0.072 flameholder blockage 60 per cent.

flameholder. A combustion chamber having a V-gutter flameholder, however, could be made to screech quite readily, and shadowgraph motion pictures were taken to show the flamefront motion accompanying screech. *Figure 7* presents photographs of the wake region downstream of the flameholder. Flow is from right to left and the flameholder lip is located at the right edge of the photograph. The results show that the flamefront is quite smooth at the flameholder lip but that downstream of the flameholder large-scale undulations appear. The film speed of the Fastax camera varied during a run because of camera inertia. It was found that the frequency of the flamefront movement could be determined by observing the stroboscopic effect which occurred as the film was projected. By this method it was found that the flame movement occurred at the same frequency as the screech pressure oscillations.

From the shadowgraphs of *Figure 7* it is difficult to determine definitely whether or not the vortices are shed alternately or in phase. In most cases the vortices seem to be shed alternately; this agrees with the findings of W. E. Kaskan and A. E. Noreen[1].

Oscillating pressures during screeching combustion

Oscillating pressures which occurred during screeching combustion were measured by means of a strain-gauge pressure transducer flush-mounted in the bottom of the small-scale combustor. The output of the transducer was fed into the four-channel oscilloscope which was photographed with the General Radio strip-film camera.

Figure 8 shows the variation of pressure with time for a fully developed screeching condition. The top sinusoidal trace on the film indicates timing. The high-frequency pressure variation was modulated by a low frequency. The high frequency was measured as approximately 3800 c/s, and the low frequency was measured to be approximately 318 c/s. By assuming that (*1*) the combustion chamber was a tube closed at one end and (*2*) the fundamental longitudinal acoustical frequency for the combustion chamber cavity equalled the measured frequency of 318 c/s, an average combustion gas temperature of 3560 R was calculated. Using this value for temperature, the theoretical fundamental frequency for the gases oscillating in the 'vertical' transverse plane of the combustion chamber cross section was calculated to be 3740 c/s. This checks the measured high frequency of 3800 c/s to within 1·7 per cent. The peak-to-peak amplitude of the wave had a maximum value of approximately 15 lb/in^2 at a combustion chamber pressure of 19·9 lb/in^2 absolute.

Figure 9 shows the transition from smooth to screeching combustion. It appears that a low-frequency longitudinal mode is excited initially, followed by a gradual build-up of the high-frequency 'vertical' mode at the high frequency. Although the high-frequency oscillations do not show up well in *Figure 9*, the original photographs showed weak 'vertical' oscillations superimposed on the first longitudinal pressure cycle.

Figure 10 shows the effect of passing a pressure wave into a 'weak' screeching condition. The combustion was set at a fuel/air ratio near the rich screech limit, and a shock wave was passed from the shock tube into the flamefront. The amplitude of the screech pressure fluctuations was greatly increased after the shock wave passed through the flamefront.

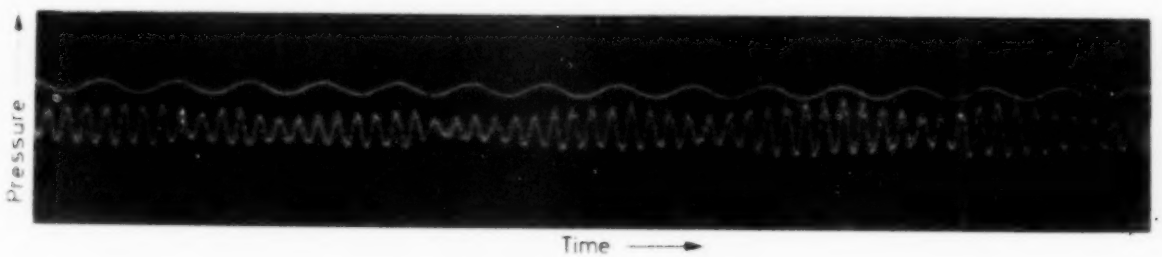

Figure 8. Pressure–time variation during screeching combustion. Combustor pressure: 19·9 lb/in^2 abs.; inlet temperature: 280° F; airflow: 1·40 lb/sec; fuel–air ratio: 0·069.

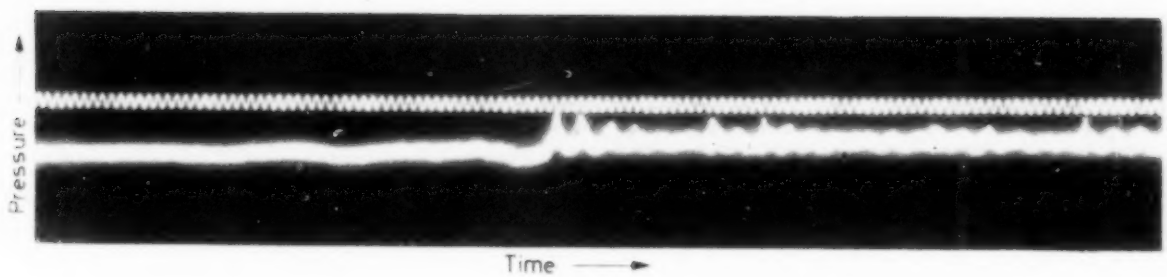

Figure 9. Pressure–time variation during transition from smooth combustion to screeching combustion. Combustor pressure: 19·9 lb/in^2 abs.; inlet temperature: 280° F; airflow: 1·40 lb/sec; fuel–air ratio: 0·045.

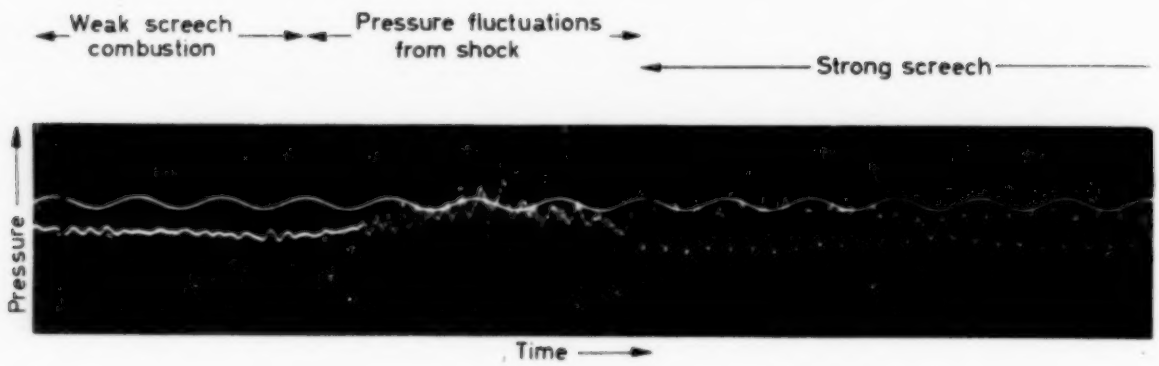

Figure 10. Weak screeching combustion going into strong screeching combustion by action of shock wave. Combustor pressure: 19·9 lb/in² abs.; inlet temperature: 280°F; airflow: 1·40 lb/sec; fuel/air ratio: 0·081

There appeared to be a very gradual decrease in the amplitude of the pulses as time increased. For relatively long periods of time, however, the pulses remained much higher after the passage of the shock than they were before the shock.

In order to investigate the energy addition supplied by the combustion process for the maintenance of combustion chamber oscillations, tests were conducted to measure the rate of decay of pressure waves generated by the passage of a shock wave into the combustion chamber. A strain-gauge pressure transducer was mounted just downstream of the shock tube diaphragm, and a barium titanate pressure transducer was mounted in an 'infinite tube' in the bottom of the small-scale combustion chamber. The output from the strain-gauge transducer was used to trigger the sweep of an oscilloscope which measured the output from the barium titanate transducer. *Figure 11* presents a semi-logarithmic plot of the envelope of the maximum value of the oscillating pressures as a function of time for burning and non-burning conditions. Airflow conditions were similar in each case. Since it was difficult to obtain a calibration of the barium titanate transducer, and the decay rates could be determined without knowing the actual magnitude of the pressure maximum, the data were plotted in arbitrary units. Data obtained using the Control Engineering strain-gauge transducer under similar conditions indicated the maximum amplitude of the pressure oscillation to be approximately 10 lb/in² at a combustor pressure of approximately 20 lb/in² absolute. It can be seen that the maximum amplitude of the wave during non-burning is slightly greater than the magnitude during burning, probably because the pressure transducer was mounted in the bottom of the combustion chamber underneath the flamefront. With a flamefront present, the pressure wave could emerge from the shock tube and be subect to partial reflection at the burning surface (caused by the temperature discontinuity) before reaching the pressure transducer. This would result in a decrease in the measured initial pressure maximum with a flamefront

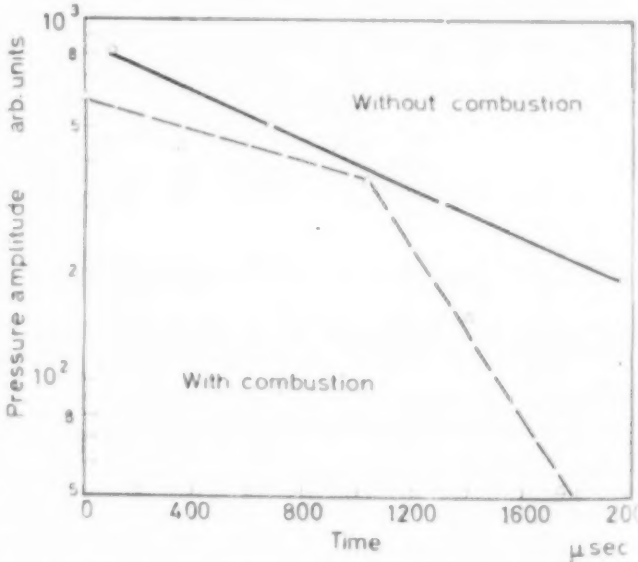

Figure 11. Envelope of maximum pressure amplitude versus time. Combustor pressure: 22·6 lb/in² abs; inlet temperature: 280°F; airflow: 1·10 lb/sec

present. The damped wave equation, derived for small signals[6], can be written as

$$\frac{\partial^2_p}{\partial t^2} + 2k\frac{\partial p}{\partial t} = c^2\frac{\partial^2_p}{\partial x^2} \qquad \ldots . [1]$$

A solution of this equation can be written as

$$p = A\sin\left[(4\pi^2\nu^2 + k^2)^{\frac{1}{2}}\frac{x}{c}\right]\exp\left[-(k + 2\pi i\nu)\,t\right] \qquad \ldots . [2]$$

where P is the pressure amplitude, A is a constant, ν is frequency, k is the damping factor, x is distance, c is the velocity of sound and t is time.

If the decay of the pressure waves is governed by this equation, i.e. if an exponential decay rate is assumed, the plot in *Figure 11* should be a straight line. This appears to be so when there is no burning present in the combustion chamber. When burning is present, there appear to be two rates of decay. For about three cycles (approximately 1 200 μsec) the decay rate was measured as approximately 401 sec^{-1}. The rate then increased to about 2 825 sec^{-1}. The transition occurred when the amplitude of the pressure oscillation was reduced to approximately 63 per cent of its maximum. This transition point was checked over a range of fuel/air ratios under similar airflow conditions and was found to be reproducible to within about 8 per cent. The decay rate was measured as approximately 741 sec^{-1} with no flamefront present in the burner. There is apparently no transition in the rate of decay when no flamefront is present. It was thought initially that the transition in the decay rate could have been caused by proper phasing between the pressure waves in the combustion chamber and emergence of the rarefaction wave from the shock tube. This supposition was checked for the test conditions used and found not to apply. It was calculated that 0·00095 sec would elapse between the emergence of the shock wave from the shock tube and the arrival of the rarefaction wave, whereas for the proper phasing to exist it was calculated that approximately 0·0014 sec would be necessary. It was concluded that the reduction was probably not caused by such an interaction. It is possible that the transition in the decay rate results from the shock tube rarefaction wave interacting with the flamefront to reduce the local heat release and hence weaken the pressure oscillations.

To obtain a general idea of the variation in the rates of damping that should be expected between flow with and without burning, it was assumed that the damping in the combustion chamber could be approximated by an expression for damping in tubes[6]. This expression was rewritten as

$$\frac{k_{\text{HOT}}}{k_{\text{COLD}}} \simeq \left[\left(\frac{\nu_{\text{HOT}}}{\nu_{\text{COLD}}}\right)\left(\frac{T_{\text{HOT}}}{T_{\text{COLD}}}\right)^{1/2}\right]^{\frac{1}{2}} \qquad \ldots . [3]$$

by assuming the gas viscosity varied as the square root of temperature, T.

With no burning present, the frequency of oscillation was measured as approximately 1 620 c/s, and with burning present the frequency was measured as approximately 2 900 c/s. By assuming that the combustion chamber gases oscillated in a vertical plane, as discussed previously, a mean temperature was calculated for each of the measured frequencies. With these temperatures the damping rates were compared, using equation 3 as shown in *Table 1*.

Table 1. Comparison of measured and calculated damping coefficients

Condition	*Meas. damping coefficients*	*Calc. ratio of* $(k_{\text{HOT}}/k_{\text{COLD}})$ *from Eq. 3*	*Meas. ratio* $(k_{\text{HOT}}/k_{\text{COLD}})$
No burning	741 sec^{-1}		
Burning (Before transition)	401 sec^{-1}	3·1	0·54
(After transition)	2825 sec^{-1}	3·1	3·81

With burning present, it appears that after transition to the high damping rate the value is the order of magnitude to be expected if no energy were being added by the combustion process. Before transition, the damping rate is lower by a factor of approximately 7; therefore, it becomes clear that the combustion process is adding energy to drive the oscillation.

To recapitulate, the following effects were observed as a pressure wave was passed through a flamefront.

(*1*) Initially, the pressure wave damped out slowly and energy was added to the wave from the combustion process until the wave was reduced to approximately 63 per cent of the maximum pressure.

(*2*) After the pressure was reduced by this amount, the wave appeared to be damped at a rate which corresponded to no energy addition from the combustion process.

(*3*) With no burning present in the combustion chamber (but with flow conditions similar to those existing during burning), the pressure wave was damped with a constant exponential decay.

From these results, it would appear that when a system undergoes the transition from smooth to screeching combustion enough energy is added to pressure waves in the combustor to change the damping coefficient, i.e. the real part of the exponential term in equation 2 from a negative to a positive value. A positive coefficient would cause the pressure oscillations to build up until they became limited by non-linearities in the system.

From a knowledge of the damping coefficients, it is possible to approximate the amplitude response of the combustion chamber for various frequencies. E. M. KERWIN[7] has developed an expression relating the steady-state response of a system to its transient behaviour. Near resonance, the steady-state response of a system is characterized by a centre frequency and a bandwidth. The bandwidth is defined as the frequency spread between half power points, i.e. where the amplitude response is 0·707 times the response at the centre frequency.

The Q of a system is defined as the ratio between the centre frequency and the bandwidth (BW). The resonant frequency of a system is very nearly equal to the centre frequency for $Q \geq 10$, and Q can be related to the damping factor as:

$$1/2Q = -k/2\pi\nu \quad \ldots [4]$$

$$\mathrm{BW}/2\nu = -k/2\pi\nu \quad \ldots [5]$$

$$\mathrm{BW} = -k/\pi \quad \ldots [6]$$

From measured values of the damping coefficient k (before transition), the approximate response curve (*Figure 12*) was determined for the small-scale combustion chamber. The curve has the characteristic shape of a system with relatively low damping.

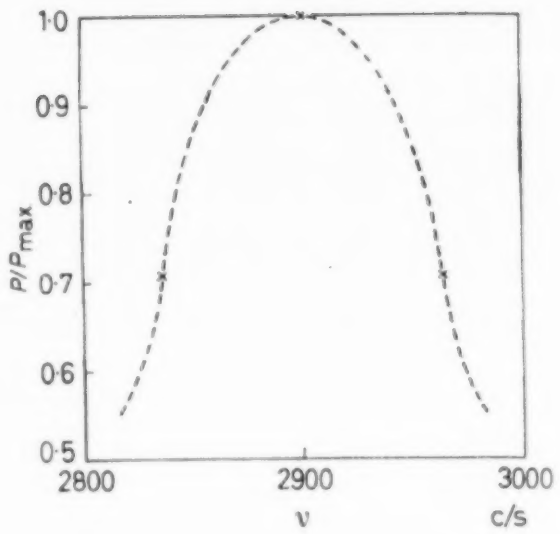

Figure 12. Amplitude response of small-scale combustor calculated from damping coefficients. P_{max} is the pressure amplitude at the resonant frequency of the combustor (2900 c/s)

Elimination of screech pressure oscillations

As previously discussed, screech oscillations would not be expected to occur if sufficient damping were present in the combustion chamber cavity. To determine the amount of absorption required on combustion chamber walls to obtain a given reduction in the amplitude of screech pressure oscillations, the top of the small-scale combustor was fitted with a perforated liner designed to have an absorption coefficient (defined as the ratio of the absorbed energy to incident energy) of approximately 0·3. The liner was 13 in. long and the liner face extended into the combustion chamber 0·5 in. The liner was designed to permit various amounts of the perforated area to be inserted into the combustion chamber, and thereby to allow the overall absorption coefficient of the combustion chamber cavity to be varied. Frequency spectrum analyses were obtained by passing the output from a Control Engineering pickup (flush-mounted in the bottom of the combustion chamber) into a Hewlett–Packard wave analyser.

An average absorption coefficient for the combustion chamber was calculated as

$$\bar{\alpha} = \frac{\alpha_{\text{LINER}} S_{\text{LINER}} + \alpha_{\text{TOP}} S_{\text{TOP}} + \alpha_{\text{SIDES}} S_{\text{SIDES}} + \dots}{S_{\text{LINER}} + S_{\text{TOP}} + S_{\text{SIDES}} + \dots} \quad \dots [7]$$

where α is the absorption coefficient of a given surface of area S. An absorption coefficient of zero was assumed to exist for walls having no perforations, a coefficient of 1·0 was assumed for open ends, and a coefficient of 0·3 for the perforated section.

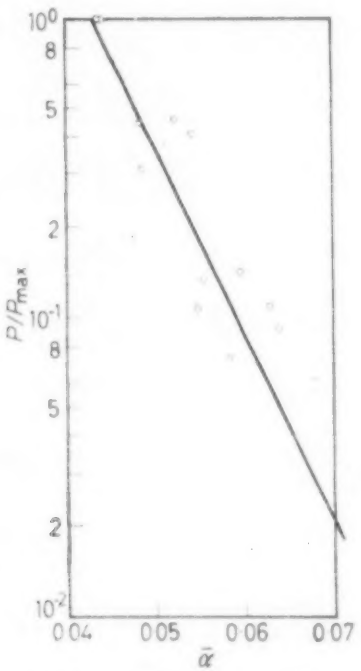

Figure 13. Effect of combustor absorption coefficient on screech pressure amplitude. P_{max} is screech pressure amplitude without the absorption liner in the combustor. Combustor pressure: 21·6 lb/in² abs.; inlet temperature: 208° F; airflow: 0·85 lb/sec; flameholder blockage: 70 per cent

Figure 13 shows the amplitude of the predominant frequency component as obtained from wave analysis plotted against the calculated average absorption coefficient. Small changes in the liner perforated area inserted into the combustion chamber caused small changes in the average absorption coefficient but reduced the pressure amplitude of screech by a large amount; e.g. increasing the average absorption coefficient from 0·05 to 0·06 reduced the pressure amplitude by 76 per cent.

From the discussions presented previously, it can be inferred that a certain minimum pressure amplitude is required before energy will be added to the pressure waves from the combustion process. This consideration, coupled with the fact that some viscous damping always exists in a combustion chamber, would indicate that the absorption coefficient required for an absorption liner to eliminate screech could be relatively small.

Effect of flameholder location and blockage on screeching combustion

Lord RAYLEIGH[5] in 1878 first pointed out the importance of the location of the energy release with respect to the nodal configuration in driving standing acoustic waves with heat addition (see also P. L. BLACKSHEAR[1] and E. M. KERWIN[7]). According to E. E. ZUKOSKI[9], chemical reaction downstream of a flameholder occurs in the mixing region between the flameholder recirculation zone and the region containing the unburnt fuel–air mixture. Hence it would be expected that the most likely place for varying heat release to occur at the onset of screech would be in a relatively thin region defined by a line drawn from the flameholder lip parallel to the combustion chamber axis.

The effects of flamefront location can be clarified through the following simplified analytical model. The actual boundary conditions which describe the mechanism by which energy is supplied from the combustion process to drive the screech oscillations are extremely complicated and unknown; if such boundary conditions could be written, it would probably be relatively simple to describe the screech phenomenon analytically. As an approximation to the boundary condition, it was assumed that the effects of periodic combustion could be represented by a periodic velocity change lagging the acoustical oscillation by some phase angle, ψ:

$$\left.\frac{\partial \xi}{\partial t}\right|_{x=b} = V_a \sin(2\pi t - \psi) \quad \dots [8]$$

where ξ is the displacement amplitude, V_a is the steady-state velocity and b is the distance from the wall to the location of the flamefront.

A solution of the one-dimensional wave equation describing the particle velocity can be written as

$$\frac{\partial \xi}{\partial t} = A \sin \frac{n\pi x}{h} \sin 2\pi\nu t \quad n = 1, 2, 3, \ldots \quad \ldots . [9]$$

where A is a constant and h is the height of the duct. Substituting,

$$\frac{A}{V_a} = \frac{\sin (2\pi\nu t - \psi)}{\sin n\pi b/h \sin 2\pi\nu t} \quad \ldots . [10]$$

The value of A indicates the amount of amplification of a given boundary condition velocity for a given flamefront location. If the phase angle ψ can be considered to be negligible, equation **10** is independent of time and the amplification factor is a function only of combustion chamber geometry. *Figure 14* presents a plot of the amplification factor as a function of flamefront location for various modes of oscillation (assuming $\psi = 0$). These amplification curves probably explain why the **70** per cent, V-gutter flameholder in the small-scale combustor tests could be made to screech while a 'single-edge' flameholder of the same blockage could not. On the basis of the flamefront locations which existed for each of the two

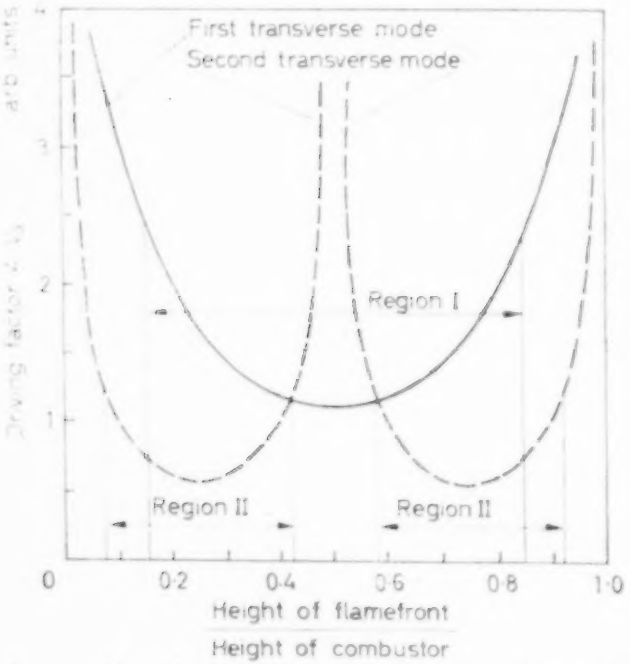

Figure 14 Amplification factor versus flamefront location

flameholders, it was calculated that the V-gutter flameholder had a driving factor almost twice as large as the 'single-edge' flameholder for the fundamental transverse mode. This would indicate that the V-gutter flameholder was about twice as prone to produce screech as the 'single-edge' flameholder.

Investigations were conducted on the large-scale combustor to determine the effects of flameholder location and blockage on the selection of the mode of screech oscillation. A sliding-bar flameholder system was used; this allowed two V-gutter flameholders to be moved independently in a vertical plane to various positions relative to the combustion chamber walls. Three sets of double V-gutter flameholders having blockages of **65**, **55** and **45** per cent were tested. Each set of flameholders was tested initially with the flameholder lips located **0·5** in. from the top and bottom of the combustor walls; the flameholders were then moved symmetrically in **0·5** in. increments toward the centreline. During these tests, the combustor inlet temperature was held constant at **1 000°F**; the fuel/air ratio, at approximately **0·065**; the flameholder Mach number, at approximately **0·55**. The mode of the excited screech oscillation was determined from measurements of the amplitude, frequency and phase relationships of pressure oscillations measured by pressure pick-ups mounted in the top, bottom and/or side of the combustion chamber.

The previously derived simplified equations for the excitation criterion were solved for conditions comparable to those existing during this investigation (see *Figure 14*) and applied to the test data. To apply this curve to data obtained from the tests of flameholder location, it was necessary to approximate the location of the varying heat release, b, relative to the combustion chamber walls. Measurements of the axial distribution of oscillating pressure indicated that the maximum screech intensity occurred approximately **10** in. downstream of the flameholder lip, and the position (during smooth non-screeching combustion) of the flamefront at this point relative to the combustion chamber walls was assumed to be the position governing excitation. It was estimated that

the flamefront would have moved roughly 1 in. in a vertical direction away from the flameholder lip at this point; this rate of spreading was used in connection with *Figure 14* to determine driving factors for the various flameholder locations relative to the combustion chamber walls. It was not possible to maintain screeching combustion during the tests and move the flameholders without also changing the mass-flow distribution around the flameholders between the centre and side walls of the combustion chamber. In determining the driving factors for the various flameholders, it was assumed that the controlling driving factor would be on the side of the flameholder which had the largest mass-flow since more energy release would be expected on that side. Mass-flow distributions were assumed to be determined by the flameholder area distributions. The results are given in *Table 2*, which shows that the predicted modes agree fairly well with the actual mode of excitation, considering the numerous simplifying assumptions which were made. This interpretation of the data would indicate that flameholder blockage *per se* would only affect the overall damping of the combustion chamber cavity and would not be as important a parameter as the location of the heat release in the wake zone downstream of the flameholder lip relative to the acoustical pressure distribution for a particular screech mode. According to *Table 2*, there appeared to be no excitation of the first transverse mode for driving factors less than about 2·4, and there appeared to be no excitation of the second transverse mode for driving factors less than about 1·2. These points constituted the no-screech region which is shown in *Figure 14*. It should be borne in mind that these limits would be expected to shift depending on flameholder blockage, combustor output, etc.; however, they do indicate the flamefront spacings which would tend to minimize screech excitation.

Concluding Remarks

In conclusion, the following general requirements appear to be necessary for the excitation and maintenance of screech.

(*1*) An excitation source must exist to produce pressure fluctuations which initiate screech. Such a source could be provided by random noise in the combustion chamber which, because of turbulence, time-variations in fuel/air ratio, etc., would be expected to be present in almost any combustor.

(*2*) Energy must be added from the combustion process in sufficient amount to strengthen the random pressure oscillations, overcome

Table 2. Comparison of predicted and measured modes

Flameholder blockage, %	*Flameholder width, in.*	*Location from wall, in.*	*% Mass-flow through centre of duct*	*% Mass-flow next to walls*	*Centre driving factor Transverse mode* 1st	2nd	*Wall driving factor Transverse mode* 1st	2nd	*Predicted transverse mode*	*Actual transverse mode*
65	3·9	0·5	60	40	1·15	1·80			*Second*	*Second*
		1·0	51	49	1·14	∞	∞	∞	*Either*	*Second*
		1·5	43	57			∞	2·20	*First*	*First*
		2·0	34	66			3·00	1·10	*First*	*First*
		2·5					*This location was not tested*			
55	3·3	0·5	65	35	1·20	1·00			*First*	*No screech*
		1·0	57	43	1·15	1·50			*Second*	*Second*
		1·5	48	52	1·14	∞	∞	2·20	*Either*	*Second*
		2·0	40	60			3·00	1·10	*First*	*First*
		2·5	32	68			2·60	0·80	*First*	*First*
45	2·7	0·5	69	31	1·24	0·80			*First*	*No screech*
		1·0	60	40	1·20	1·00			*First*	*No screech*
		1·5	53	47	1·16	1·60	∞	2·20	*Either*	*Second*
		2·0	44	56			3·00	1·10	*First*	*No screech*
		2·5	36	64			2·60	0·80	*First*	*No screech*

the damping inherent within the system, and excite one (or more) of the resonant frequencies of the combustion chamber cavity.

(3) To excite a particular mode, the energy addition must occur very nearly in phase with a pressure maximum which exists with the standing wave pattern for the mode. A varying energy release nearly in phase with the pressure maximum could be produced by the pressure waves causing (*i*) changes in flamefront area, (*ii*) changes in the chemical reaction rate, (*iii*) changes in the burning velocity of the mixture, or (*iv*) the generation of vortices at the flameholder lip which cause periodic transport of combustible material into the hot wake of the flameholder (D. E. ROGERS and F. E. MARBLE[5]). This last mechanism is considered to be the most realistic.

(4) The mode of screech which is excited should depend on the amount of energy available to drive the oscillation and the spatial position of the energy addition with respect to the pressure nodes and antinodes of a given mode of oscillation of the combustion chamber cavity. Because lower-frequency modes require less energy addition to drive them, the fundamental frequency would be preferentially excited if the phase requirements are met. The amount of energy available to drive screech oscillations would appear to be related to the overall energy release of the combustor. Therefore, the tendency to excite screech would increase as the combustor heat release increases.

Screeching combustion can be eliminated by increasing the damping within the combustion chamber cavity or by properly spacing flameholders to minimize the excitation of the lower frequency modes of oscillation. The design of absorbers which eliminate screeching combustion by increasing combustion chamber damping is discussed by A. W. BLACKMAN[10].

References

[1] BLACKSHEAR, P. L. *Tech. Note Nat. Adv. Comm. Aero., Wash., No. 2772* (1952)

[2] BLACKSHEAR, P. L., RAYLE, W. D. and TOWLE, L. K. *Res. Memo. Nat. Adv. Comm. Aero., Wash., No. RME53I28* (1953)

[3] MOORE, F. K. and MASLEN, S. K. *Tech. Note Nat. Adv. Comm. Aero., Wash., No. 3152* (1954)

[4] KASKAN, W. E. and NOREEN, A. E. *Trans. Amer. Soc. mech. Engrs*, 1955, **77**, 885

[5] ROGERS, D. E. and MARBLE, F. E. 'A mechanism for high frequency oscillation in ramjet combustors and afterburners'. *Jet Propulsion*, 1956, **26**, 456

[6] MORSE, P. M. *Vibration and Sound*, p 213. McGraw-Hill: New York, 1936

[7] KERWIN, E. M. 'A study of a class of thermoacoustic oscillations', p 75. *D.Sc.Thesis*, Massachusetts Institute of Technology, January 1954

[8] RAYLEIGH, Lord J. W. S. *Nature, Lond.* 1878, **18**, 319

[9] ZUKOSKI, E. E. *Rep. No. 20-75*. Jet Propulsion Laboratory, California Institute of Technology, 1954

[10] BLACKMAN, A. W. 'Effect of non-linear losses on the design of absorbers for combustion instabilities'. *J. Amer. Rocket Soc.* (November) **1960**, 1022

On the Inflammability Ranges of Formaldehyde and Carburetted Air* under Reduced Pressure

Miss M. P. Brunold, R. Delbourgo and P. Laffitte

Laboratoire de Chimie Générale, Sorbonne, Paris, France

(Received October 1960)

The inflammability regions of formaldehyde and air with small amounts of hydrocarbon (2·4 to 5·4 per cent) have been studied. The addition of propane or methane leads to a strong inhibition of the formaldehyde range together with the appearance of a second lobe structure of the curves described with pseudo cool flame characteristics. The influence is continuous and leads to a well laid out family of curves. Whenever hydrocarbon is present in the mixture, even in trace amounts, the properties of flames encountered are those of the hydrocarbon and not those of the formaldehyde mixture.

The important role played by formaldehyde in our understanding of combustion reactions[1], the well known fact that it is often present in the combustion products of most types of flames added to its great instability and reactivity, had previously led us to examine the flames of mixtures of air and formaldehyde vapour (in the monomer form) and to determine the inflammability range of these mixtures under reduced pressure[2]. The main conclusions of this investigation were that mixtures of formaldehyde and air at 120°C were able to ignite and propagate a flame—under the standard conditions of inflammability range determinations—in a concentration range extending from 12·5 to 80·0 per cent of formaldehyde vapour expressed as a percentage of the mixture. The limit curve obtained was classical, consisting of a single lobe, while the flames observed were mostly brilliant and white (except at the lower limit where they were bluish); propagation was noted to be irregular and rapid, and likely to become violent in some cases.

Following on from this work we have now undertaken a systematic investigation of the influence of various hydrocarbons—in variable quantities—on the type of flame observed and on the shape of the inflammability region described. This has led us to prepare ternary mixtures of formaldehyde vapour–air–hydrocarbon in which the formaldehyde was considered as the main fuel and the hydrocarbon added in trace concentrations (up to 5 per cent) to the oxidizer component of the mixture. Thus the procedure was to make up a standard mixture of hydrocarbon and air in small and definite concentrations and use these mixtures of 'carburetted air' to make up the formaldehyde mixtures at various concentrations. Propane and methane were successively studied as the hydrocarbon investigated. These mixtures, when submitted to ignition by an electric spark can either be considered as lean mixtures of hydrocarbon and air with additions of known amounts of formaldehyde vapour in steadily increasing concentration or as mixtures of formaldehyde and air (the oxidizer containing a small amount of hydrocarbon).

*Air to which small amounts of hydrocarbon have been added.

Experimental

The arrangement of the apparatus is shown in *Figure 1*. The hydrocarbon and air mixtures are made up in a 10 l. spherical mixing vessel (not shown in the drawing), each constituent being introduced under its own partial pressure. The hydrocarbons used were Philips Pure grade submitted to desiccation by passing through phosphorus pentoxide before being stored. The section of the apparatus intended for the preparation of the formaldehyde monomer vapour and the mixtures of this vapour with the hydrocarbon and air was heated to a temperature of 120°C. The vessels were immersed in an oil bath maintained thermostatically at this temperature and all the

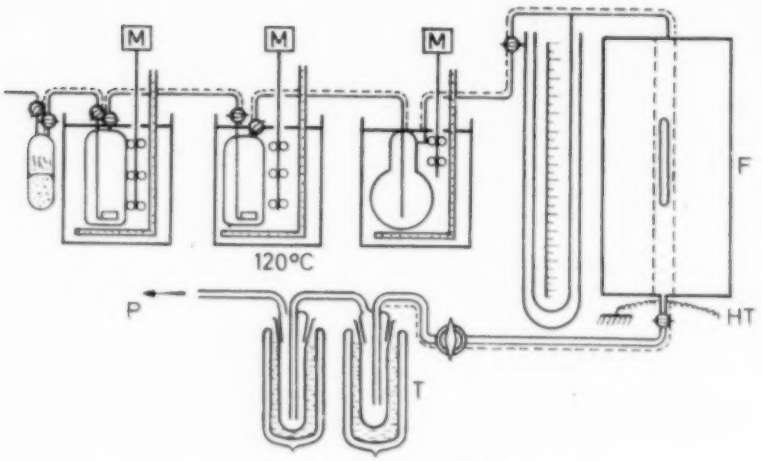

Figure 1. Apparatus

connections from this section to the ignition tube were wound with an electric heater to prevent condensation and polymerization of the formaldehyde.

The ignition tube of 4 cm diameter and 60 cm long was placed vertically inside an electrically heated and regulated furnace (120°C) with a built-in window to permit observation of the flames. Two tungsten electrodes, both 1·5 mm in diameter and 12 mm apart, are sealed at the bottom of the tube and allow the passage of an h.t. spark produced by the discharge of 120 pF air condenser charged to 15 kV. The tube is closed at both ends and, as in previous experiments of this type, propagation is upwards and the criterion for inflammability is total propagation. Classical vacuum equipment permits part or all of the apparatus to be evacuated, and two traps cooled in liquid nitrogen serve to condense the excess formaldehyde before it enters the pump. The formaldehyde vapour is prepared in a manner already described by gently heating α-polyoxymethylene (paraldehyde) to depolymerize it.

Results

Figure 2 illustrates the results obtained with mixtures of propane and air (2·4, 3·0, 4·0 and 5·4 per cent) added to formaldehyde vapour in concentrations up to 65 per cent. The comparison of any of the four curves obtained with the curve relevant to the formaldehyde mixture

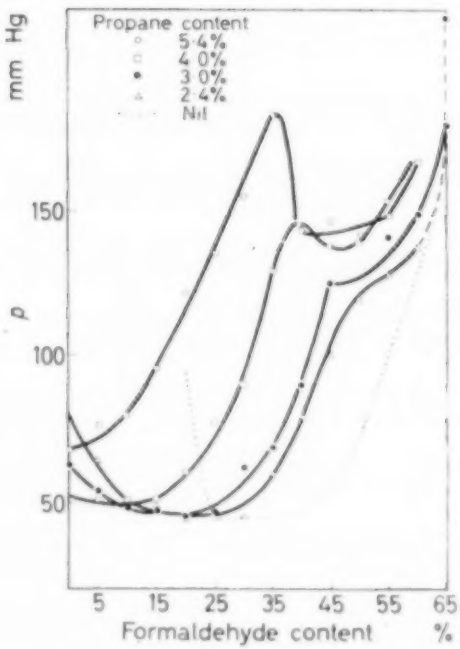

Figure 2. Effect of propane on inflammability of formaldehyde

with *pure air* (i.e. with no addition of hydrocarbon) determined under identical experimental conditions shows the striking and fundamental difference introduced by the small amount of the hydrocarbon constituent in the mixture.

The influence of the hydrocarbon trace appears to be continuous since it leads to a well laid out family of curves. The rich side of the inflammability range of formaldehyde is strongly inhibited by the addition of propane. This effect becomes more clearly defined as the

percentage of hydrocarbon is steadily increased from 2·4 to 5·4 per cent.

In addition to the inhibiting effect it was also noted that the flames observed throughout these ranges are altogether different from the flames of formaldehyde and air mixtures. Without the addition of the hydrocarbons the flames are fast and appear white. The presence of as little as 2·4 per cent of propane in the oxidizer mixture leads to a complete change of the flame type which becomes similar to the normal hydrocarbon–air flames with no formaldehyde added. The resemblance to hydrocarbon flames is in fact so great that on increasing the formaldehyde content the flames observed behave as if propane was being added to the mixture. The flames are blue along the lower limit and become green and rapid as the fuel concentration increases.

A third important observation arises from the existence for rich mixtures of a second lobe in which the flames are extremely faint and of a greyish colour. They are invisible in the normal light of the laboratory and can only be observed in complete darkness. From their appearance and from the region of the diagram covered one would be tempted to identify these flames with the well known cool flames of similar characteristics. However, one must point out that neither formaldehyde–air mixtures (without any propane added to them) nor propane–air mixtures (without any formaldehyde added to them) exhibit cool flame phenomena under the present experimental conditions. This point will be discussed later in this paper.

Figure 3 shows the results obtained when the hydrocarbon used is methane instead of propane. Two samples of carburetted air were used one with 7·2 per cent methane and the other with 9 per cent methane. Here again the inhibiting effect is well marked together with the two-lobe structure of the range obtained accompanying the fundamental difference in the flames observed in each region. It is remarkable that in no case is the formaldehyde type of flame apparent, the hydrocarbon type of flame taking over as formaldehyde is added to the mixture.

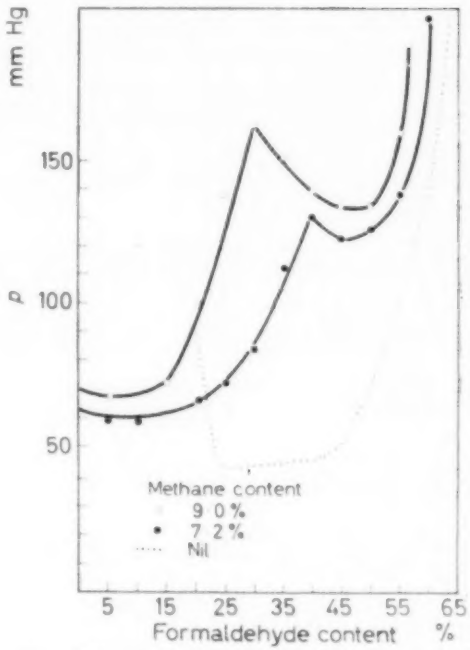

Figure 3. Effect of methane on inflammability of formaldehyde

Discussion

In spite of the important role attributed to formaldehyde in combustion reactions little experimental data can be found on the combustion of formaldehyde itself or of its mixtures with air and hydrocarbons.

M. Vanpee and his associates[3,4] have studied the thermal ignition of formaldehyde and oxygen mixtures extensively. In some cases the influence of methane on the combustion of formaldehyde together with that of formaldehyde on the combustion of methane has been examined. The conclusion is of a mutual catalysis of the two oxidation reactions depending to an important degree on thermal conditions.

Little comparison can be drawn between thermal ignition and explosion regions obtained therefrom, and artificial ignition and inflammability regions. In studying rich mixtures of formaldehyde and oxygen Vanpee has noticed the existence of a region of faint bluish luminescence. Under our experimental conditions at a lower temperature (120°C against 480°C), the electric spark may well be considered to ignite a strongly perturbed mixture through the effect of induced pyrolysis and the hydrocarbonated species present.

J. F. McKellar and R. G. W. Norrish[5] have also studied the combustion of gaseous formaldehyde, the explosive reaction being initiated by the well known flash technique. One may wonder what new experimental evidence could be obtained if mixtures of formaldehyde and oxygen were sensitized by a trace of hydrocarbon and then flash ignited.

At this stage of this work little can be said of the origin and nature of the phenomena observed. A great number of experiments on such ternary mixtures are needed and are in process of being carried out in spite of considerable experimental difficulty which is inherent in all work involving formaldehyde. The results given in this paper should be considered tentatively especially in respect of the absolute values of concentrations and critical pressures. A systematic error may well exist in the determinations of the concentrations of the mixtures and in the measurement of the critical pressures. However, the family of curves obtained is self-consistent and remains sufficiently valid to show that the luminous phenomena observed are no single accident and that they appear important enough to stimulate discussion and further work.

The question is raised as to whether the pseudo cool flames observed are hydrocarbon or formaldehyde flames. In fact they belong to a ternary system where formaldehyde, hydrocarbon and air are present and competitive. Bearing in mind the proportions of each constituent in these mixtures one is inclined to assign to formaldehyde the main fuel constituent role and to the hydrocarbon a trace-like effect. The disturbance introduced into the formaldehyde system by this trace is such that nothing remains of the formaldehyde flames: those observed are those the hydrocarbons considered are likely to exhibit under different experimental conditions of temperature and pressure.

References

[1] Klein, R. and Schoen, L. J. 'Literature of the Combustion of Petroleum'. *Advances in Chemistry Series No. 20*, p 58-68. American Chemical Society: Columbus, Ohio, 1958
Legrand, J., Delbourgo, R. and Laffitte, P. *C.R.Acad.Sci., Paris*, 1959, **249**, 1514

[3] Vanpee, M. 'Contribution à l'étude des mécanismes de combustion du méthane et du formaldéhyde'. *Thèse*. Université de Louvain: Ceuterick, Louvain 1956

[4] Vanpee, M. and Grard, F. 'Formaldehyde and the oxidation of methane'. *Fuel, Lond.* 1955, **34**, 433

[5] McKellar, J. F. and Norrish, R. G. W. 'The combustion of gaseous aldehydes studied by flash photolysis and kinetic spectroscopy'. *Proc. Roy. Soc. A*, 1960, **254**, 147

Recent Developments and Notes

Physical Properties of Gases and Liquids

DATA on the physical properties of fluids are widely scattered throughout numerous journals and reports and, in addition, they are recorded in various units and often need conversion to a convenient form. The National Engineering Laboratory (NEL) has been collecting data from all over the world and offers a service to industry in answering specific enquiries; specialist advice can be given on the selection of the most reliable results from contradictory sources.

Data are available on thermodynamic properties, for example, enthalpy, compressibility and specific heat, and transport properties, for example, viscosity and thermal conductivity. Values of the physical properties of about twenty of the commoner fluids are indexed at NEL in standard units and their accuracy has been assessed. Data can also be provided on many other organic and inorganic fluids, including refrigerants.

Some enquiries can be answered immediately from existing information on the particular fluid involved; if the required experimental data are not available, it may be possible to determine them from other properties of the fluid, from the same properties of other fluids, or from theoretical considerations. Information can also be given on methods of extrapolation and interpolation of experimental data, and on the range over which this may be done safely.

An electronic digital computer is available at NEL for calculating physical properties; it has already been used in the preparation of the British draft of the new international skeleton table for steam, covering temperatures up to 800°C and pressures up to 1 000 atmospheres.

Requests for information on thermal conductivity, viscosity or thermodynamic properties of a specific fluid should include details of the temperature and pressure range for which data on a particular property are required. No charge is made for the service unless a substantial amount of work is necessary. Communications are to be addressed to The Director, National Engineering Laboratory, East Kilbride, Glasgow. A review of *Heat Bibliography 1959* issued recently by NEL is to appear in the July issue of *Fuel*.

Fuels for Supersonic Speeds

Methods for producing two types of fuels which may allow jet aircraft to break through the heat barrier have been announced by Shell International Petroleum Company as a result of investigations at the Research Centre, Emeryville, California. The fuels, based on mixtures of naphthenes and paraffins, can be made directly from refinery streams and can withstand the high temperatures which will be encountered by jet aircraft travelling at three to five times the speed of sound.

The heat-absorbing capacity of present jet fuels is limited because certain components begin to break down into gum and carbon deposits when temperatures reach 200° to 250°C, and fuels for jet aircraft that are now being designed may be required to withstand temperatures of 430°C. It had been thought that the only fuels able to withstand these temperatures would be the more expensive pure hydrocarbons.

Fire Protection in Factory Buildings

A report entitled *Fire Protection in Factory Buildings* was published by the Building Research Station in January. It provides for factory managements and building designers an introduction and a guide to the various legal requirements.

The report also indicates the precautions that may be taken beyond those required by law to reduce the hazard of fire breaking out and spreading within a factory building. Precautions that should be adopted for the safety of personnel, in case of fire, are also considered. Technical appendices deal with common causes of fires in factories, standard fire resistance tests and the behaviour of materials and elements

J. F. McKellar and R. G. W. Norrish[5] have also studied the combustion of gaseous formaldehyde, the explosive reaction being initiated by the well known flash technique. One may wonder what new experimental evidence could be obtained if mixtures of formaldehyde and oxygen were sensitized by a trace of hydrocarbon and then flash ignited.

At this stage of this work little can be said of the origin and nature of the phenomena observed. A great number of experiments on such ternary mixtures are needed and are in process of being carried out in spite of considerable experimental difficulty which is inherent in all work involving formaldehyde. The results given in this paper should be considered tentatively especially in respect of the absolute values of concentrations and critical pressures. A systematic error may well exist in the determinations of the concentrations of the mixtures and in the measurement of the critical pressures. However, the family of curves obtained is self-consistent and remains sufficiently valid to show that the luminous phenomena observed are no single accident and that they appear important enough to stimulate discussion and further work.

The question is raised as to whether the pseudo cool flames observed are hydrocarbon or formaldehyde flames. In fact they belong to a ternary system where formaldehyde, hydrocarbon and air are present and competitive. Bearing in mind the proportions of each constituent in these mixtures one is inclined to assign to formaldehyde the main fuel constituent role and to the hydrocarbon a trace-like effect. The disturbance introduced into the formaldehyde system by this trace is such that nothing remains of the formaldehyde flames: those observed are those the hydrocarbons considered are likely to exhibit under different experimental conditions of temperature and pressure.

References

[1] Klein, R. and Schoen, L. J. 'Literature of the Combustion of Petroleum'. *Advances in Chemistry Series No. 20*, p 58-68. American Chemical Society: Columbus, Ohio, 1958
Legrand, J., Delbourgo, R. and Laffitte, P. *C.R.Acad.Sci., Paris*, 1959, **249**, 1514
[3] Vanpee, M. 'Contribution à l'étude des mécanismes de combustion du méthane et du formaldéhyde'. *Thèse*. Université de Louvain: Ceuterick, Louvain. 1956
[4] Vanpee, M. and Grard, F. 'Formaldehyde and the oxidation of methane'. *Fuel, Lond.* 1955, **34**, 433
[5] McKellar, J. F. and Norrish, R. G. W. 'The combustion of gaseous aldehydes studied by flash photolysis and kinetic spectroscopy'. *Proc. Roy. Soc. A*, 1960, **254**, 147

Recent Developments and Notes

Physical Properties of Gases and Liquids

DATA on the physical properties of fluids are widely scattered throughout numerous journals and reports and, in addition, they are recorded in various units and often need conversion to a convenient form. The National Engineering Laboratory (NEL) has been collecting data from all over the world and offers a service to industry in answering specific enquiries; specialist advice can be given on the selection of the most reliable results from contradictory sources.

Data are available on thermodynamic properties, for example, enthalpy, compressibility and specific heat, and transport properties, for example, viscosity and thermal conductivity. Values of the physical properties of about twenty of the commoner fluids are indexed at NEL in standard units and their accuracy has been assessed. Data can also be provided on many other organic and inorganic fluids, including refrigerants.

Some enquiries can be answered immediately from existing information on the particular fluid involved; if the required experimental data are not available, it may be possible to determine them from other properties of the fluid, from the same properties of other fluids, or from theoretical considerations. Information can also be given on methods of extrapolation and interpolation of experimental data, and on the range over which this may be done safely.

An electronic digital computer is available at NEL for calculating physical properties; it has already been used in the preparation of the British draft of the new international skeleton table for steam, covering temperatures up to 800°C and pressures up to 1 000 atmospheres.

Requests for information on thermal conductivity, viscosity or thermodynamic properties of a specific fluid should include details of the temperature and pressure range for which data on a particular property are required. No charge is made for the service unless a substantial amount of work is necessary. Communications are to be addressed to The Director, National Engineering Laboratory, East Kilbride, Glasgow. A review of *Heat Bibliography 1959* issued recently by NEL is to appear in the July issue of *Fuel*.

Fuels for Supersonic Speeds

Methods for producing two types of fuels which may allow jet aircraft to break through the heat barrier have been announced by Shell International Petroleum Company as a result of investigations at the Research Centre, Emeryville, California. The fuels, based on mixtures of naphthenes and paraffins, can be made directly from refinery streams and can withstand the high temperatures which will be encountered by jet aircraft travelling at three to five times the speed of sound.

The heat-absorbing capacity of present jet fuels is limited because certain components begin to break down into gum and carbon deposits when temperatures reach 200° to 250°C, and fuels for jet aircraft that are now being designed may be required to withstand temperatures of 430°C. It had been thought that the only fuels able to withstand these temperatures would be the more expensive pure hydrocarbons.

Fire Protection in Factory Buildings

A report entitled *Fire Protection in Factory Buildings* was published by the Building Research Station in January. It provides for factory managements and building designers an introduction and a guide to the various legal requirements.

The report also indicates the precautions that may be taken beyond those required by law to reduce the hazard of fire breaking out and spreading within a factory building. Precautions that should be adopted for the safety of personnel, in case of fire, are also considered. Technical appendices deal with common causes of fires in factories, standard fire resistance tests and the behaviour of materials and elements

of structure under fire conditions [Factory Building Studies No. 9; Department of Scientific and Industrial Research, Her Majesty's Stationery Office: London, 1961. 3*s* 6*d*].

In a new Factory Act which came into force on 1 December 1960, there are amendments to the Factories Acts of 1937 and 1948, relating to protection against fire and explosion. These are dealt with in sections, amongst others, on explosive dust, steam boilers, prevention of fire, fire fighting, and safety provisions in case of fire [Factories Act, 1959, 7 and 8 Eliz. 2, Ch. 67].

Measuring Metal Temperature in Engines

A simple method for measuring the operating temperatures of engine parts has been developed at the Thornton Research Centre, 'Shell' Research Ltd, Cheshire. The usual temperature measuring devices cannot easily be attached to rapidly moving parts inside the engine block, but the new technique enables the maximum temperature to which any component has been exposed, to be determined when the engine is taken apart.

The technique, known as the 'hardness relaxation' method, depends on the well-established fact that when certain alloys are heated and then cooled, their original hardness is changed, the extent of the change depending on the maximum temperature reached. Usually it is only necessary to compare the original hardness of an engine component with its hardness after running to determine with accuracy the maximum temperature reached in the range of 100°C to 1 000°C. When the metal of a particular engine component is not suitable for recording accurately the maximum temperature reached, small amounts of a suitable alloy can be inserted in the part under study. A wide range of alloys of suitable sizes and shapes for this purpose has been developed. The method is obviously of considerable value in pin-pointing causes of engine failure due to hot spots in pistons, rings, bearings, gaskets and valves.

History of the Fuel Research Station, D.S.I.R.

One of the most striking events in the development of national scientific policy in the U.K. during the past half century was the creation by the Government in 1916, as an outcome of the 1914–18 war, of the Department of Scientific and Industrial Research. One of the earliest acts of the Department was the appointment in 1917 of a Fuel Research Board, with Sir GEORGE BEILBY as its first Chairman and Director of Research, 'to investigate in the broad national interest the nature, preparation, utilization and treatment of coals and other fuels, and of products derived from fuels'. In the following year the Fuel Research Station was established at Greenwich. Some forty years later, in 1958, the Research Council considered that, in view of many developments in the fuel world, the Fuel Research Station had completed its work and should be closed down. An account has now been published of the work of the Board, under the title *Fuel Research 1917–1958* (D.S.I.R., Her Majesty's Stationery Office: London, 1960, 120 pp. 15*s*).

The main sections deal with basic aspects of fuel research including fuel analysis, carbonization, preparation of coal for the market, gasification of coal and coke, coal constitution, combustion and steam raising, hydrogenation of coal and coal tar, the Fischer–Tropsch synthesis, atmospheric pollution, and domestic heating. There is an important section on the coal survey laboratories.

These subjects provided the main basis of the Station's research throughout its existence but priorities altered continuously to meet changing needs. During the 1939–45 war the emphasis naturally changed radically and the Station became deeply involved in such activities as camouflage by smoke and coal dust, production of flame thrower fuels and other incendiaries, mobile producer gas units, and the use of liquid methane as a fuel for motor vehicles. Postwar investigations included studies on orchard heating, the combustion of flax shives, the flow properties of residual fuel oils, and the pollution of the sea by oil.

There is a list of 151 references to publications covering the work of the Station's staff. The review was edited by Dr A. C. MONKHOUSE, formerly Deputy Director, and Sir HAROLD HARTLEY, F.R.S., refers in a foreword to the

Coal Survey as the outstanding achievement of the Fuel Research Organization. The Coal Survey organization was transferred to the National Coal Board in 1947 on terms that provided for its identity to be maintained and its basic task of evaluating the national coal resources to be continued.

Automation in Industrial Gas Appliances

Some interesting gas appliances incorporating push-button control were on show for the first time on the Gas Council's stand at the Engineering, Marine, Welding and Nuclear Energy Exhibition held recently at Olympia, London.

A packaged conversion burner for central heating boilers, process air heaters, and other applications was shown, designed at the North Western Gas Board's industrial gas development centre at Manchester. It is the first gas unit made in Britain complete with fan, automatic ignition and all control equipment. Forced draught is used to obtain maximum thermal efficiency with the minimum of site work and to be independent of flue conditions. Electronic flame-failure equipment is built in and there is negligible pilot gas rate.

The South Western Gas Board is responsible for a brass billet heating furnace of entirely new design which handles billets three inches long and up to two inches in diameter and is for hot brass stamping. The furnace can be set to discharge billets automatically at a predetermined rate or singly by the operator pushing a button. This plant is expected to show great improvements in operation and efficiency.

The prototype of a flash melting machine was on view. This is due to the North Eastern Gas Board's work on the design of a furnace for melting non-ferrous metals more rapidly and economically. The unit has a melting capacity of 100 lb per charge and incorporates load recuperation in addition to combustion air preheating. The hourly capacity is from 5 to 5½ cwt. On production trials the unit proved very successful as regards improved quality of metal cast, reduction in metal loss, and fuel consumption per lb of metal.

Burning of Solid Propellants

A critical review of the present state of theories of the burning rate of solid propellants has been published by V. R. GUTMAN, United Technology Corporation, California [*Aircr. Engng*, 1960, **32**, 255]. Attempts to base a theory on the reaction rate of the combustion processes as the controlling factor, have not been successful. The idea of control of burning rate by downstream reaction rates must be rejected if, as is believed, there is a transpiration zone between the exothermic flame zone and the endothermic surface decomposition.

For some time past attention has been given to the importance of the feedback of energy from the flame to the surface of the dissipating solid as the direct link between the production of energy and the rate of consumption of the fuel. In the past two or three years a quantitative analysis has been made by L. GREEN, based on energy feedback, but a number of assumptions of doubtful validity are made [*Jet Propulsion*, 1956, **26**, 655; 1958, **28**, 386].

Another contribution to the problem is the theory postulating two different temperatures at which two components undergo pyrolysis in the surface of a propellant. The importance of this view, according to the author, is that it explains the heterogeneity observed in motion pictures.

A serious defect in existing theories is their failure to explain the action of burning rate additives. A possible explanation of their effect put forward in the paper is that they may be involved in heat transfer by radiation. It is suggested that chemiluminescence may supply energy for photolytic decomposition of propellant binders at rates beyond those associated with pyrolysis at the surface temperature.

French Combustion Pot Experiments

A considerable programme of research on the burning of sized coals in a combustion pot has been carried through by CERCHAR and a detailed account has now been published by P. DUMOUTET, Chef du Groupe Combustion, and J. DESSEINE, Ingénieur au Groupe Combustion [*Flamme et Thermique*, 1960, No. 143, 13–26, 31–37]. The objective of the work has been to make a complete analysis, as precisely as possible, of the physicochemical features of the burning of charges of sized coals under

rigorously controlled conditions. The results obtained, particularly in regard to the behaviour of different types of fuels, should be of practical value. The combustion pot was constructed and operated so as to simulate the conditions of combustion in small central heating boilers using *maigres* coal. The pot, of a dismountable type, consists essentially of four double-walled cylindrical hoops, each 100 mm in depth and 300 mm wide, fitted one above the other, and these rest on an ash-pan in which is the air distributor. Between the ash-pan and the first hoop is fixed a Nichral grate. Surmounting the four hoops is a double-walled truncated cone, forming the top of the pot, and this contains a charging door, side-chimney, from which gas samples can be taken, and provision for thermocouples. Provision is made for ensuring the same rate of flow of cooling water in the walls of the different sections of the pot, and for taking the temperature of the water at appropriate places. All joints in the pot are sealed so that the combustion takes place without any secondary air.

Two different types of experiments were made, those under normal method of working with constant rate of air flow, and those with the air flow very much reduced. The latter type of experiments is suggested as a means for assessing the 'reactivity' of fuels.

It is shown that the quantity of coal burnt per hour increases a little more rapidly than the rate of flow of air, due to an increased proportion of carbon gasified to carbon monoxide as the flow of air is increased. The speed of combustion only depends on the rate of flow of air, except that any factor, such as increase in air flow or reduction in size of fuel, which tends to increase the proportion of carbon which is transformed to carbon monoxide, increases slightly the speed of combustion.

The regularity of combustion was examined by determining the *instantaneous dissipation of calorific power* of the fuel. For a given coal the curves showing the variations of this value with time preserve similar profiles for changes in rate of air flow and size range. The type of the fuel, however, decidedly affects the regularity of combustion. Anthracites, *maigres* coal, metallurgical coke and low temperature coke were examined.

Determinations were also made of the relative importance of the latent heat of the flue gases in the dissipation of the calorific power of the fuel; of the temperatures in the fuel bed at different heights above the grate; and of the heat transmitted laterally to the pot walls.

Forge Furnace Design

The Plant Engineering and Energy Division of the British Iron and Steel Research Association has made a preliminary study of forge furnace design problems by carrying out tests on an oil-fired bogie-hearth forge furnace, capable of heating ingots up to 65 tons in weight, at the works of Walter Somers Ltd, Shotton, Cheshire. Batch-type heating is a very inefficient process and as a result of this work basic improvements are suggested, as regards both furnace design and operation.

As regards design, this should be such that there is high convective heat transfer in the early stages of heating and uniform heating by radiation in the later stages. Hot-face insulating brickwork should be used so that the furnace should have the minimum practicable heat capacity. High velocity jet burners are recommended, combined gas and oil burners being possible. There should be a waste heat recovery unit.

As regards furnace operation, the heating cycle should be kept as short as possible. Maximum heating rates should be established by numerical analysis of the distribution of internal temperature in an ingot, and the soaking times needed for close uniformity of temperature can be estimated. Furnace loading must be such as will produce maximum thermal efficiency. The suggested instruments are temperature controllers, possibly programme controllers, temperature recorders, pressure controller, and mechanical proportioning device for fuel/air ratio at each burner or a proportioning controller for the whole furnace. A detailed account of the tests and a numerical method of evaluating temperature distribution is contained in BISRA report *PE/A/44/59*.

Clean Air Congresses

L'Association pour la Prévention de la Pollution atmospherique held its first congress in Paris from 24 to 26 November last. Some twenty papers were presented on general information, industrial problems, and methods already in use to reduce atmospheric pollution, and about two dozen papers on technical problems and scientific researches. The address of the Association is 62 rue de Courcelles, Paris [for list of papers see *J. Ind. du Gaz*, 1960, **84**, 506].

The Verein Deutscher Ingenieure in 1957 formed a Kommission Reinhaltung der Luft and from 21 to 23 September last year its first general conference was held in Wiesbaden. About twenty seven papers were read, mostly dealing with technical problems and researches [for list of papers see *Gas- u. Wasserfach*, 1960, **101**, 1226].

Waverley Gold Medal Essay Competion

The Waverley Gold Medal Essay Competition is being sponsored by *Research* again this year. It is intended as a means of encouragement to scientists in the laboratory and engineers on production plant to write clearly about their work in such a way as to be readily understood by other scientists, directors of industrial firms and others interested in science and technology.

The Medal together with £100 will be awarded for the best essay of about 3 000 words describing a new project or practical development in pure or applied science. Entry forms, which should accompany all essays, can be obtained with full particulars, from the Editor, *Research*, 38 Kingsway, London, W.C.2, and essays should reach the Editor not later than 31 July 1961.

Improved Method of High Speed Photography

At the Fifth International Congress on High Speed Photography held in Washington in October last, an account was given of an important improvement in the Schardin system of high speed photography and has now been published by L. Deffet and R. Vanden Berghe, Centre de Recherches pour l'Industrie des Produits Explosifs [*Explosifs*, 1960, **13**, 119].

In a study of the detonation of explosives it was found that in the shadowgraph method of visualization of the rapid phenomena, using an explosive flash lamp, it was impossible to overcome the difficulty due to intense luminosity occurring with some explosives. To obviate this a system of the Cranz–Schardin type, with explosive lamps free of argon, instead of the use of sparks, has been developed, and used in conjunction with ultra-rapid cinematography. Synchronization between the phenomenon to be studied and the flash is achieved by a 10 g charge of tetryl which is detonated in a suitable housing. The photographic arrangements are such that there is almost total extinction of the luminosity due to the passage of the wave front from the extremity of the tetryl charge up to where it meets the edge of the shock wave. Only the luminosity produced at the moment of impact is photographically recorded. With the argon explosive flash lamp the intense luminosity produced by the passage of the front of the wave intervenes during the flash period. It is possible to record 10^6 images per second with a precision of $0{\cdot}2 \times 10^{-6}$ sec and photographs of excellent quality of very luminous explosives can be obtained.

New Thermionic Generator

A thermionic device for converting heat directly into electric current, which appears to have considerable promise for practical use, has recently been described in some detail by Professor D. Gabor, F.R.S., of the Department of Electrical Engineering, Imperial College of Science and Technology, London [*Nature, Lond.* 1961, **189**, 868]. The research of which this is the outcome has been supported by the National Research Development Corporation. Essentially the device is a diode valve constructed in the form of a cellular metal structure and contains a small amount of either argon or a mixture of argon and mercury vapour. An experimental cost rating of 0·05 to 0·1 W/A has been achieved with argon, and if caesium were used the cost could be reduced by a factor of 3 to 4. Owing to its chemical activity, however, caesium might shorten the useful life of the generator.

Efficiencies up to about 30 per cent in the generation of direct current are regarded as being possible, and 22 per cent for alternating current, at a working temperature of 1800°C. There are problems to be solved in connection with materials. A cathode material is required with 2·0 to 2·5 V work function, with small radiation emissivity, capable of supplying 4 A/cm² or more at 1200° to 1800°C. A suitable collector is necessary, with high reflectivity and low work function. The most difficult problem is the provision of a ceramic envelope which will be impervious at 1400° to 1800°C, to operate for long periods when exposed to flame gases and with high thermal shock resistance.

A New Type of Internal Combustion Engine

A new form of internal combustion engine has been described by E. SCHMIDT [*Z. Ver. dtsch. Ing.* 1960, **102**, 293] in which gas spaces varying in volume are formed between a continuously rotating shaped runner and a cylinder of epitrochoid cross section. The cylinder may be either stationary or rotating. The preferred form has a three-cornered runner rotating in a cylinder which approximates a figure 8. The configuration is not necessarily limited to this form, but can be made with runners of 2,3,4 or 5 corners. With the higher numbers of corners, the epitrochoid becomes more sharply cusped. No analysis is given of the forms of these figures, but some results of relative speeds of eccentric and runner, and the maximum pressure ratios obtainable are stated.

Thermodynamic testing of this four-cycle rotary engine and development work on it have been described by E. W. HUBER [*Z. Ver. dtsch. Ing.* 1960, **102**, 298] and by W. FROEDE [*Z. Ver. dtsch. Ing.* 1960, **102**, 322]. Indicator diagrams and performance data are given for various speeds. The first machine tested had rather serious leakage losses, but this was improved in a later machine and it is thought that development will proceed rapidly [M. A. MAYERS, *Appl. Mech. Rev.* 1960, 13, 935].

Oil Burner Performance

An experimental programme on the performance of commercial oil burners has been carried out at Warren Spring Laboratory, D.S.I.R., Stevenage, particularly from the point of view of the formation of carbonaceous material and the emission of acid smuts. This work has recently been described by L. E. REED and S. C. WALLIN [*J. Inst. Fuel*, 1961, 34, 26].

Five different types of natural-draught burners were investigated, a mechanical rotary burner, a medium-pressure and a low-pressure air burner, a pressure-jet burner and a steam-atomizing burner. The test rig simulated the furnace tube of an economic boiler. Heavy fuel oil with a viscosity of 950 sec Redwood No. 1 at 100°F was used. The quantities of primary and secondary air and the oil temperature at the burner were varied.

The results show that for the purpose of steam raising there is little to choose between any of the burners. They all produced solid material some of which would be emitted from the chimney with the flue gases. The quantity produced varied with the type of atomization used and with the quantity of excess air supplied to the burner. In general, the minimum quantity of solids was produced when about 30 to 40 per cent of excess air was used. This solid material was acidic.

Fuel Distribution and Reaction Rates

M. V. HERBERT, National Gas Turbine Establishment, has published a paper containing an attempt to calculate the reaction rate for liquid fuel systems in which there is non-uniform fuel distribution due, for example, to incomplete vaporization, incomplete mixing, or both [*Aeronaut. Quarterly*, 1961, **12**, 41]. Applications of particular interest are reheat systems and ram-jet pilot burners, in which there may be insufficient distance between fuel injection and stabilizer for fuel diffusion.

The arrangement considered is a circular duct containing a single central point-source fuel injector upstream of the flameholder. Turbulent and uniform conditions in the duct are assumed, both for velocity and temperature. Reaction rates are arbitrarily computed for unvitiated air at 500°K. It is assumed that diffusion and evaporation of liquid fuel take place simultaneously after injection, and the

turbulent diffusivity is taken to be an effective one for the state of the fuel at the station considered.

The reaction rate was calculated for a number of cases with an overall stoichiometric mixture, and the 'loss' due to uneven distribution was found to be 75 per cent in the worst conditions considered.

Jet Combustion of Pulverized Coal

The combustion process of a jet using pulverized coal has been examined by A. B. REZNYAKOV [Issled. Fiz. Osnov Rabochego Protesessa Topol i Pechei, Alma-Ata, Akad. Nauk Kaz.S.S.R., 1957, 361-379; *Ref. Zh. Mekh.* No. 5, 1959, rev. 4768].

An approximate theory is worked out applicable to the conditions prevailing in reverberatory (smelting) furnaces. For these conditions the pulverized coal–air jet travels in a rectilinear horizontal channel of constant section while the solid dispersion phase of the jet burns in the gaseous medium with a rapidly decreasing concentration of oxygen. The flow is considered to be one-dimensional, isobaric and steady. In order to calculate the velocity of motion of the jet, known principles for free isothermal turbulent flows are employed. From the available experimental data the author concludes that the combustion of an individual particle of coal is practically the same as the surface combustion of a particle of pure carbon. This, together with some supplementary assumptions, enables an approximate formula to be evolved for computing the time required for the combustion of an individual coal particle. A relation was thus obtained giving the amount of incomplete combustion, treating the jet as a polydisperse system and assuming the principle of distribution of particles in the jet according to their dimensions. The equation obtained for complete combustion of a jet was tested in a pilot-plant scale furnace by determining the composition of the gases over the furnace length and the temperature of the jet, thus enabling an estimate to be made of the amount of incomplete combustion. Changes in the coefficient of excess air were made within the range 1·15 to 2·0. The approximate analytical correlations obtained are said to have shown satisfactory agreement with the experimental results of other investigators and with the results of the above test [O. V. YAKOVLEVSKII, *Ref. Zh. U.S.S.R.; Appl. Mech. Rev.* 1961, **14**, 63].

Ignition Delay in the Diesel Engine

In the series of papers on preflame reactions in diesel engines published during the past few years by Professor F. H. GARNER, O.B.E., and his colleagues in the Department of Chemical Engineering, University of Birmingham, a further paper (Part V) was presented to the Institute of Petroleum in London in January by F. H. GARNER, F. MORTON, and J. B. SAUNBY. This describes an analysis of the pressure and temperature variations occurring during the cycle in order to establish the energy released during the preflame period. Temperatures were determined by means of an electro-optical pyrometer and simultaneous pressure/time records were obtained by the use of a capacitance-type pressure pickup. The effect of variations in compression ratio, injection-timing and fuel characteristics was studied. The standard CFR–ASTM diesel testing unit was used.

Two temperature peaks were observed, their magnitude depending on the conditions of compression ratio and injection timing. The temperature which was being measured, was that of carbon particles present at the onset of visible radiation. The first peak occurs immediately after ignition and after the second maximum the temperature falls as the expansion stroke is entered. The intermediate fall in temperature is not accompanied by measurable change in the rate of pressure rise and varies markedly with variations in the operating conditions.

Thermodynamic analysis of the pressure measurements shows that the preflame energy release is constant for a given fuel, and at high compression ratios this energy is derived mainly from the compression of the charge. With optimum injection settings and appropriate compression ratios, preflame reactions are of little importance as the spontaneous ignition temperature of the fuel is achieved by the heat of compression in the course of a few degrees

crank angle. With early injection it is otherwise, since there is time for the production of large concentrations of intermediate oxidation products and for the accumulation of unburnt fuel which may undergo pyrolysis.

Liquid Fuel Combustion Deposits

The mechanics of the formation and adhesion of deposits arising from the combustion of liquid fuel formed the subject of five papers presented to the Institution of Mechanical Engineers in London in March. The papers were sponsored by the Committee of the Internal Combustion Engines Group.

A review of the mechanisms proposed to explain the formation of carbon during the combustion of fuels, was given by P. F. Whelan, Principal Research Engineer, British Internal Combustion Engine Research Association. Summarizing the present position, the author classifies the theories into four groups: I. Hydrocarbon→carbon atoms or molecules (C, C_2, C_3) or the free radical CH→carbon: II. Hydrocarbon→acetylene and benzene (possibly through CH radical)→carbon; III. Hydrocarbon→polycyclic compounds (which possibly pass through the liquid phase)→carbon; IV. Hydrocarbon→oxidized polycyclic compounds→carbon.

K. H. Gray, Principal Research Engineer, B.I.C.E.R.A., gave a review of information collected from various sources of the mechanics of the formation and adhesion of deposits of carbon in compression ignition engines. Deposits of soot and hard carbon do not constitute a serious problem, chiefly being symptomatic of some abnormal condition which can be corrected. The relation between these deposits and the nature of the fuel is discussed.

A paper by A. Lewis, 'Shell' Research Ltd, Thornton Research Centre, Chester, dealt with deposits in gas turbines. In distillate fuel units the chief component of deposits is carbon, but the percentage of free carbon may differ considerably in deposits according to whether they are around the atomizer, on the combustion chamber walls, or on heat exchanger surfaces. With the exception of the latter instances the effect upon operation of the units is not generally very serious. On the other hand deposits of ash in residual fuel units are of major importance and the problem they present is a main stumbling block to the wider adoption of industrial and marine gas turbine sets. Ash deposits on turbine blades soon lower their aerodynamic efficiency. Of the large number of elements concerned sodium and vanadium are the most important. The additives which can best modify the nature of the deposits are compounds of aluminium, calcium, magnesium, silicon and zinc.

The mode of combustion of droplets of fuel is a direct factor in the manner of release of ash from the fuel, influencing the degree of coking of the fuel droplet residues and the speed of combustion of the metallo-organic compounds. Under the effect of fairly strong adhesive forces both ash vapour and small particles can yield appreciable deposits on turbine blades. The mechanisms of deposition involved may be molecular diffusion, brownian movement, turbulent diffusion and inertial impaction.

Light-scattering Measurements on Particles Condensed from Boron-containing Flames

W. E. Kaskan, author of the article with the above title [this journal, **1961**, **5**, 93], wishes to make it clear that the fifth line below equation 7 on page 97 should read: 'second was as high as 0·1. Thus, for weak', while the unit for column 5 of *Table 1* on the same page should read: 'cm^{-3}'. It is regretted if confusion has been caused by either of these errors to which attention was drawn when the proofs were corrected.

W. A. Kirkby

FUEL

Readers of *Combustion and Flame* may like to know that the May issue of *Fuel* contained *Notes* dealing with the D.S.I.R. cooperative investigation of atmospheric pollution, coal burning appliances, and mineral processing.

Publications

PROGRESS IN COMBUSTION SCIENCE AND TECHNOLOGY

Volume I

Edited by J. DUCARME, Université de Liège, M. GERSTEIN, National Aeronautics and Space Administration, Ohio, and A. H. LEFEBVRE, Rolls-Royce Ltd, Derby. Oxford: Pergamon, 1960. *viii*+226 *pp.* 70s or $10.00

THIS is the second publication in the 'International Series of Monographs in Aeronautics and Astronautics'. The objective of this ambitious project is to provide a complete source of study and reference in the various regions of these two fields of science and technology. There are to be nine divisions in the series and the present volume is in Division III: Propulsion systems including fuels, the editors of this division being A. D. BAXTER and E. R. SHARP. The volume now being considered consists of six review articles which are primarily concerned with the aeronautical aspects of combustion. In future volumes, to be issued annually, advances in other branches of combustion science and technology will be reviewed.

The authors of the articles in this volume are, with perhaps one exception, recognized by their previous publications in the past few years as authorities in their particular fields. As might be expected from the trend of recent research much the larger part of this book deals with the physics of combustion and physical techniques of study. In the chapter on flow visualization techniques, E. F. WINTER, 'Shell' Research Ltd, Thornton Research Centre, Chester, gets to grips with what is probably the most important approach to solving the problems of the practical operation of combustion equipment whether as industrial furnaces or engines. Great strides have been taken on this approach to the subject since the pioneering work of W. E. GROUME-GRJIMAILO in Russia about forty years ago and the important studies of P. O. ROSIN in this country about twenty five years ago on aerodynamics in fuel practice. In the present chapter there is a well developed account of the progress in the use of models as a necessary stage between fundamental combustion research and the application of its results in practical combustion systems. In two- or three-dimensional models, using air or water, flow phenomena can be studied for a variety of combustion systems in which the paramount factors relate to flame stabilization and rapid gas mixing. The models of interest here are those in which all the essential variables, including time, are repeated on a suitable scale.

M. V. HERBERT, National Gas Turbine Establishment, Farnborough, in writing on aerodynamic influences on flame stability, has reviewed in the light of more recent data, some of his conclusions published in 1957, and a more comprehensive argument has been developed for the characteristics of baffle and 'can' stabilizers. A general connection is put forward between chemical reaction and Reynolds number, even for fully turbulent flow conditions, to explain the aerodynamic factors in flame stabilization. The relation is probably similar for all forms of stabilizer, 'cans' with both large- and small-scale recirculating internal flow patterns, and both three- and properly two-dimensional baffles. In addition the relation is probably not dependent on the level of pressure loss for a system with forced injection.

An aspect of combustion research which has not previously received anything in the way of full descriptive treatment is that of measurements depending on the changes in refractive index in flames and their associated gases. This defect is now remedied by a comprehensive account, with a considerable number of excellent illustrations, of geometric-optical techniques in combustion research, by F. J. WEINBERG, Department of Chemical Engineering, Imperial College of Science and Technology, London. The methods described are based on the change of direction which the light beam undergoes when 'transluminating' each part of the particular phenomenon under investigation. The sections of the review are: the geometric optics of flames; 'schlieren' methods; shadowgraphs; deflection mapping. Apart from the methods of physical optics, the background of the optics and combustion theory involved has been assumed.

The major portion of the chapter on flame quenching is devoted to a discussion of the measurement, variation with factors, and interpretation of the quenching distance. This has been written by A. E. POTTER Jr, National Aeronautics and Space Administration, Lewis Research Center, Cleveland, Ohio, and he takes the work of J. M. HOLM in 1932 and 1933 as his starting point. The importance of Holm's work is that he defined the quenching distance, an easily measured, reproducible quantity related to the ease whereby flames could be quenched. In discussing theories of flame quenching the author appears to have overlooked the interesting work of E. AUDIBERT published in 1948, on the inhibition, under appropriate conditions, of a chain-branching mechanism when the inflammable mixture is in contact with a solid of appropriate surface area. The important work of P. J. DANIELL in 1930, resulting in the first solution for the energy balance equation in flames, including heat losses but not diffusion, is noted in the chapter. This work has largely been ignored, but some of the predictions arising from it have been found to agree with experimental results of recent years.

Perhaps the most formidable task of any of the authors of these chapters is that of discussing within the available space the subject of ignition in liquid propellant engines. A very good survey of work done in the past eight years or so has been given by E. A. FLETCHER and G. MORRELL, Department of Mechanical Engineering, University of Minnesota, dealing with the delay period before ignition takes place, which is the important parameter in rocketry, rather than the phenomenon of ignition itself.

The chapter on chemical analysis in combustion chamber development, by B. TOONE, Rolls-Royce Ltd, Derby, is the same to a very large extent as his paper presented to the Seventh Symposium (International) on Combustion in 1958. The descriptions of methods of analysis would not be expected in a book of this character; they can be found in textbooks and catalogues. The whole treatment is in a rather naive fashion and is not on a par with the high standard of the other chapters. 'Katharometer' is the correct spelling, not with 'e' for the second 'a'.

For much the greater part this volume gives a first class critical review of recent advances in the selected fields, and, of considerable importance, there are many pointers to where further research is needed. References are adequate, about 370 of them, and the indexes are good. If future volumes achieve the same standard as this one, there will be a valuable series of publications, providing the specialist reader in particular with a reasoned survey.

W. A. KIRKBY

COAL TAR FUELS

Edited by W. H. HUXTABLE. 2nd ed. London: Association of Tar Distillers, 1961, *vi*+111 *pp*. 21s

THE total amount of coal tar produced in Britain is some three million tons per annum and although this is the source of valuable aromatic compounds, about a million tons of it is disposed of after refining in the form of coal tar fuels.

The designation of a fuel derived from coal tar as C.T.F. 50, C.T.F. 100, C.T.F. 200 etc. indicates the temperature (°F) at which it has a suitable viscosity for successful atomization at the burner.

In the earlier part of the book the chemical composition and physical properties of these fuels are reviewed and a brief discussion of their combustion is presented. Coal tar fuels are characterized by a high ratio of carbon to hydrogen and although this may lead to difficulties because of a tendency to form carbonaceous deposits at the burner tip it is advantageous in giving the flame a high emissivity. The low sulphur and vanadium contents of coal tar fuels are cited as advantages.

A chapter is devoted to the design of equipment for the storage and handling of coal tar fuels and graphs and nomograms are provided to simplify the evaluation of heat losses from tanks and the design of steam heating coils for storage tanks.

Liquid fuel burners and associated equipment are illustrated and discussed and the final chapter summarizes information on the use of coal tar fuels in various types of furnace and boiler plant.

This second edition is virtually a new book: it is essentially practical in outlook and will prove of value to engineers and fuel technologists concerned with the combustion of liquid fuels in industrial plant.

R. LONG

ADVANCES IN POLAROGRAPHY

Edited by I. S. LONGMUIR. Three volumes: *xv*+407, *ix*+409–803, and *vii*+805–1204 *pp*. Oxford: Pergamon Press, 1960. £15 or $45.00 per set of three volumes

THE first polarographic measurements were made by JAROSLAV HEYROVSKY in 1921 and within three decades, polarography had become one of the most widely used techniques of instrumental analysis. It serves for the identification and determination of trace constituents and its application to problems of physical, inorganic and organic chemistry have been numerous and fruitful.

Advances in Polarography contains the authoritative proceedings of the Second International Congress of Polarography held at Cambridge in 1959 to honour the 70th birthday of Professor HEYROVSKY and it consists of one hundred and three papers, occupying about twelve hundred pages, on the many different aspects of polarography.

Thus there is a group of about two dozen papers on theoretical aspects; among these are valuable surveys by such well known experts as DELAHAY and BRDICKA, and a group of about a dozen papers on the newer oscillographic, derivative and alternating current polarography. Other papers are about the hanging mercury drop electrode, solid microelectrodes, carbon paste electrodes and other techniques, while most of the remaining papers, about half the total, deal with the analytical aspects, particularly biological, medical and industrial applications.

The papers in this three volume work were not arranged in sections dealing with specific aspects but are in the same order as they appeared in the collection of abstracts of the conference. However, these volumes offer a valuable and up to date account of the state of polarography and will be welcome to those interested in this important field.

G. R. NEWNS

A DICTIONARY OF NAMED EFFECTS AND LAWS

D. W. G. BALLENTYNE and L. E. Q. WALKER. *v*+234 *pp*. London: Chapman and Hall, 1961,. 30s

THIS dictionary is the second edition and refers primarily to chemistry, physics and mathematics. This field is reasonably well covered particularly in chemistry. The definitions where necessary include an illustration and are precise and concise.

It is always possible to criticize a book of this kind for omissions but possibly in future editions, some attention might be given to including definitions of various forms of expressing experimental errors together with some expansion of the treatment of heat transfer which is an important field of physics. The range of information given and the number of references is very large indeed and undoubtedly this book is of value to readers interested in these subjects

Letters to the Editors

Letters to the Editors on points of scientific interest related to combustion and flames are invited. The Editors do not hold themselves responsible for opinions expressed in correspondence. Anonymous contributions cannot be accepted.

An Estimate of the Rate of Growth of Lead Oxide Particles in Engine Gases

THERE has been some dispute as to whether in the anti-knock action of lead tetraethyl the active agent is lead monoxide vapour[1] or a cloud of small solid particles of lead monoxide[2]. No numerical estimate of the rate of formation of solid particles has appeared, although the related problem of the rate of destruction of active chemical species at the surface of solid particles was treated twenty years ago by L. J. OOSTERHOFF[3], who showed that if all the lead present were converted to solid particles of radius 100Å or less, then their total surface area would be sufficient to destroy the gaseous radicals responsible for knock. (This result assumes the surface to destroy the radicals with great efficiency, which is known[2, 4] to apply for a surface of solid lead monoxide.) It has been asserted[1] that the presence of the engine gases would greatly impede the growth of solid particles of lead monoxide. It is shown below that this is not so, because of the small size of even the largest particles which could be formed.

Experimental work on engine processes[2, 5–7] shows that lead tetraethyl is oxidized at about 700°K and 10 atm, and that about 1 msec later the products are acting as an anti-knock. The mole fraction of lead tetraethyl before combustion is about 10^{-5}; it follows that a reasonable estimate of n_2, the number of gaseous lead monoxide molecules (species 2) in unit volume, is 10^{15} cm^{-3}. An upper limit to the rate of growth of a solid particle may be obtained by applying the Hertz–Knudsen equation with a condensation coefficient α equal to unity, giving

$$da/dt = n_2\bar{c}_2/4n_{2s} \quad . \quad . \quad . \quad . \quad [1]$$

where a is the radius of the particle (supposed for simplicity to be spherical), n_{2s} is the number of 'molecules' in unit volume of the solid, and $\bar{c}_2$ is the mean molecular velocity of species 2. Substituting numerical values ($n_{2s} \doteqdot 0{\cdot}25 \times 10^{23}$ cm^{-3}, $\bar{c}_2 = 2{\cdot}58 \times 10^4$ cm sec^{-1}) appropriate to the case considered, it is found that $da/dt \doteqdot 25$Å (msec)$^{-1}$. Growth for the period (1 msec) which is available would thus form particles of radius not exceeding 25Å.

While the assumption of a condensation coefficient equal to unity could lead to an over-estimate of the rate of growth, the available evidence on the evaporation of solids and their growth from the vapour (summarized in general terms[8] and with special reference to the present problem[9]) suggests that the rate has not been grossly over-estimated. For when the evaporation of solids and their growth from the vapour can be represented simply by the Hertz–Knudsen equation with a condensation coefficient α, the value of α is never very much less than unity, except for a few covalent macromolecular solids such as violet phosphorus. Moreover, J. P. HIRTH and G. M. POUND[8] have presented a theoretical argument which indicates that even when α takes the relatively low value 0·3 for a moderately supersaturated system or for evaporation, it will become almost equal to unity at extreme supersaturations.

It is readily shown by applying well-established theories[10–12] of evaporation and condensation that any particles formed are so small that their growth (and by a like argument, the destruction of active free radicals at their surface*) cannot be appreciably impeded by diffusion in the gaseous phase. The retarding effect of the gaseous phase may be represented[10–12] (in the case of quasi-stationary

*L. J. OOSTERHOFF's[3] estimate of the value of the radius necessary for solid particles to be effective in anti-knock is thus correct, as it was derived from an equation of the Hertz–Knudsen type (with an approximate correction for any diffusional retardation). N. N. SEMENOV's[13] estimate, assuming the surface destruction of active intermediates to be diffusion controlled, would apply only to particles of a size much greater than that to which they can actually grow in the present case.

diffusion: in other cases the effect is less) by dividing the Hertz–Knudsen value of the rate of growth by the quantity

$$1 + \frac{z}{2}\,\frac{a}{2D_{12}/\bar{c}_2}\,\frac{a}{a+\Delta} \quad \ldots \quad [2]$$

where D_{12} is the mutual diffusion coefficient of the gas (species 1) and the vapour (species 2), Δ is a length which may[12] be equal to $2D_{12}/\bar{c}_2$ or (for a mass ratio appropriate to the case where species 1 is N_2 or CO_2 and species 2 is PbO) perhaps only half this value. Estimating D_{12} to be 0·05 cm^2 sec^{-1} at 10 atm (by analogy with known values[14] for the interdiffusion of mercury vapour and air) it follows that the two possible values of Δ are (at 10 atm) *ca.* 400Å and *ca.* 200Å. Thus the correcting denominator becomes (at the most) $1 + \frac{1}{2}(25/400)(25/225) = 1{\cdot}0035$. The closeness of this value to unity shows that any diffusional retardation is negligible.

If lead monoxide molecules numbering 10^{15} cm^{-3} were all to condense to solid particles of radius 25Å, each would contain 1600 'molecules', and the number of solid particles in unit volume would be 6×10^{11} cm^{-3}. It has been calculated[2] that such a cloud of particles would not become appreciably coagulated during 1 msec.

The decisive point in the theory of the formation of solid particles is whether so large a number of particles could in fact be formed by self-nucleation of lead monoxide vapour (at about 709° K and, temporarily, highly supersaturated: partial pressure about 10^{-1} mm of mercury, saturated vapour pressure[15] $< 10^{-7}$ mm of mercury). The necessary rate of formation of nuclei is about 10^{15} cm^{-3} sec^{-1}. It appears to be impossible to carry out a really decisive calculation.

The experimental evidence on the formation of solid lead monoxide is as follows. In an engine running with a lead anti-knock there is far more scattering of light than in an engine with no anti-knock[17], which indicates that solid particles are formed when lead tetraethyl is introduced. In a flash photolysis apparatus no solid particles are formed[1]. In burner experiments[18] solid particles are detectable, but above the flame. The solid particles of lead compounds which emerge in the exhaust of a motored engine have been shown[19] to consist of crystals of dimensions varying from 15 to 500Å. It has been shown in the present communication that particles of similar dimensions would be formed, and previously[3] that such dimensions are those appropriate to an effective inhibitor.

Spectroscopic examination[18] of cool flames in a burner shows that atomic lead is present, but the oxide spectrum is very weak. This observation suggests that any solid particles might perhaps be formed by the condensation of the vapour of the metal and not of the oxide. If, in engine gases, such were to occur, numerical estimates of the rate of nucleation and the rate of growth (calculated as above) would not be greatly altered. Assuming the surface of such particles to be oxidized, the estimated rates of destruction of active intermediates would thus likewise be almost unaltered.

I wish to thank Professor A. D. Walsh, Dr C. R. Allen, Dr R. S. Bradley and Dr D. E. Hoare for helpful discussion.

P. G. Wright

Chemistry Department,
Queen's College,
Dundee

(Received December 1960)

References

1 Norrish, R. G. W. *Proc. Roy. Soc. A*, 1935, **150**, 36
Erhard, K. H. L. and Norrish, R. G. W. *Proc. Roy. Soc. A*, 1956, **234**, 178
Norrish, R. G. W. *Seventh Symposium (International) on Combustion*, p. 203. Butterworths: London, 1959

2 Downs, D., Walsh, A. D. and Wheeler, R. W. *Phil. Trans. A*, 1951, **243**, 463
Chamberlain, G. H. N. and Walsh, A. D. *Proc. Roy. Soc. A*, 1952, **215**, 175
Hoare, D. E. and Walsh, A. D. *Proc. Roy. Soc. A*, 1952, **215**, 454
Chamberlain, G. H. N., Hoare, D. E. and Walsh, A. D. *Disc. Faraday Soc.* 1953, **14**, 89
Cheaney, D. E., Davies, D. A., Davis, A., Hoare, D. E., Protheroe, J. and Walsh, A. D. *Seventh Symposium (International) on Combustion*, p. 186. Butterworths: London, 1959

3 Oosterhoff, L. J. *Rec. Trav. chim. Pays-Bas*, 1940, **59**, 811

4 Cherneskey, M. and Bardwell, J. *Canad. J. Chem.* 1960, **38**, 482

[5] Taylor, C. F., Taylor, E. S. Livengood, J. C., Russell, W. A. and Leary, W. A. *S.A.E. quart. Trans.*, 1960, **4**, 232
[6] Rifkin, E. B., Walcutt, C. and Betker, G. W. *S.A.E. quart. Trans.* 1952, **6**, 472
[7] Mason, J. M. and Hesselberg, H. E. *Trans. Soc. automot. Engrs, N.Y.* 1954, **62**, 141
[8] Hirth, J. P. and Pound, G. M. *J. phys. Chem.* 1960, **64**, 619
[9] Wright, P. G. *Proc. Leeds phil. lit. Soc.* In press
[10] Fuchs, N. A. *Phys. Z. Sowjet.* 1934, **6**, 225
Fuchs, N. A. *Trans. Faraday Soc.* 1936, **32**, 1067
Fuchs, N. A. *Evaporation and Droplet Growth in Gaseous Media*. Pergamon: London, 1960
[11] Bradley, R. S., Evans, M. G. and Whytlaw-Gray, R. W. *Proc. Roy. Soc. A*, 1946, **186**, 368
[12] Wright, P. G. *Disc. Faraday Soc.*, 1960, **30**, 100
[13] Semenov, N. N. *Acta phys.-chim. U.R.S.S.* 1943, **18**, 93
[14] Reid, R. C. and Sherwood, T. K. *The Properties of Gases and Liquids*, p. 274. McGraw-Hill: New York, 1958
[15] Kelley, K. K. *Bull. U.S. Bur. Min No. 383*, 1935
[16] Volmer, M. *Kinetik der Phasenbildung*. Theodor Steinkopff: Dresden and Leipzig, 1939
[17] Downs, D., Griffiths, S. T. and Wheeler, R. W. Paper presented before the Institute of Petroleum, 1960
[18] Agnew, W. G. *Combustion & Flame*, 1960, **4**, 29
[19] Rifkin, E. B. Paper presented before the American Petroleum Institute, Los Angeles, 1958

On the Burning Rate of a Fuel Droplet in an Oxidizing Atmosphere

It is well known that theories which assume spherically symmetrical, quasi-steady-state flow, neglect radiation, thermal diffusion and natural convection, and hypothesize a single (overall) rate-controlling reaction step, have met with considerable success in predicting the burning rates of fuel droplets in oxidizing atmospheres[1-4]. The predicted burning rate is, in essence, given by the expression

$$\dot{m} = 4\pi r_l \, (\bar{\lambda}/\bar{c}_p) \ln\left\{1 + \frac{\bar{c}_p \, (T_\infty - T_l) + QY_{o,\infty}}{L}\right\} \quad [1]$$

where $\dot{m}$ denotes mass per second of fuel leaving the droplet, r_l is the radius of the liquid droplet, $\bar{\lambda}$ is the average thermal conductivity of the gas mixture surrounding the droplet, $\bar{c}_p$ is the average specific heat at constant pressure for the gas mixture, T_∞ is the temperature of the oxidizing atmosphere far from the droplet, T_l is the temperature at the surface of the droplet, Q is the heat of reaction per unit mass of *oxidizer* consumed, $Y_{o,\infty}$ is the mass fraction of oxidizer in the oxidizing atmosphere, and L is the heat of vaporization per unit mass of fuel evaporating. Equation 1 relates the unknown burning rate to known quantities, e.g. the liquid temperature and the temperature and mass fraction of oxidizer at infinity. In deriving equation 1, in addition to the usual mass and energy conservation conditions it is assumed that the mass fraction of fuel at infinity is zero and the mass fraction of oxidizer at the droplet surface is zero. These last two criteria cause $\dot{m}$ to be independent of the chemical reaction rate and to be determined by diffusion rates alone.

The fact that all of the fuel will burn before reaching infinity is hardly questionable; and in any event the composition of the surrounding atmosphere must be specified to determine the burning rate. However, the mass fraction of oxidizer at the droplet surface is determined by the solution of the equation for the conservation of mass of oxidizer, involving both diffusion and chemical reaction rates. It is physically apparent that, unless the chemical reaction rate somewhere approaches infinity (as occurs in the flame surface approximation, for example), some of the oxidizer will diffuse to the droplet surface*. The mass fraction of oxidizer at the surface $Y_{o,l}$ will therefore be greater than zero for realistic reaction rates. The Shvab–Zeldovich procedure[1-6] is easily extended to provide an expression for $\dot{m}$ when $Y_{o,l} \neq 0$. The result, which apparently has not been given in the literature, is

$$\dot{m} = 4\pi r_l \, (\bar{\lambda}/\bar{c}_p) \ln\left\{\frac{L + \bar{c}_p \, (T_\infty - T_l) + QY_{o,\infty}}{L + QY_{o,l}}\right\} \quad [2]$$

Equation 2 enables us to compute $\dot{m}$ when the reaction rate is finite, provided $Y_{o,l}$ can be found. It is seen from equation 2 that increasing $Y_{o,l}$ (decreasing the chemical reaction rate) decreases the burning rate $\dot{m}$. If typical numbers are inserted in equation 2, it is found that $\dot{m}$ is decreased by about 10 per cent if $Y_{o,l}$ is increased from zero to 0·01. Numerical solutions[7] of the conservation equations with an

*According to W. Nachbar, there exists a uniqueness theorem for the non-homogeneous diffusion equation which proves this assertion.

Arrhenius reaction rate have shown that in some reasonable cases $Y_{0,l}$ is approximately 10^{-8}. In such cases the decrease in $\dot{m}$ is unobservable. This result implies that, in all cases of practical interest, it will probably be valid to expand equation 2 in powers of the small parameter $Y_{0,l}$ and keep only the first term in the expansion. The resulting equation for $\dot{m}$, which exhibits explicitly an additive correction for $Y_{0,l} \neq 0$, is

$$\dot{m} = 4\pi r_l (\bar{\lambda}/\bar{c}_p) \ln\left\{1 + \frac{\bar{c}_p (T_\infty - T_l) + QY_{0,\infty}}{L}\right\} - \frac{4\pi r_l \bar{\lambda} Q}{\bar{c}_p L} Y_{0,l} \quad . \quad . \quad . \quad . \quad [3]$$

F. A. Williams

Harvard University,
Cambridge 38, Mass.

(Received February 1961)

References

[1] Godsave, G. A. E. *Fourth International Symposium on Combustion*, pp 818–830. Williams and Wilkins: Baltimore, 1953

[2] Spalding, D. B. *Fourth International Symposium on Combustion*, pp 847–864. Williams and Wilkins: Baltimore, 1953

[3] Goldsmith, M. and Penner, S. S. *Jet Propulsion*, 1954, **24**, 245

[4] Penner, S. S. and Williams, F. *Tech. Rep. No. 19*, Office of Ordnance Research, U.S. Army, Contract DA 04–495–Ord–446, California Institute of Technology: Pasadena, 1959

[5] Shvab, V. A. *Gos. Energ. izd.* M-L, 1948

[6] Zeldovich, Y. B. *Zh. tekh. Fiz., Mosk.* 1949, **19**, No. 10; translation *Tech. Memor. Nat. Adv. Comm. Aero., Wash., No. 1296*, 1951

[7] Lorell, J., Wise, H. and Carr, R. E. *J. chem. Phys.* 1956, **25**, 325

The Pressure Dependence of Laminar Burning Velocity by the Spherical Bomb Method

J. T. AGNEW and L. B. GRAIFF

Department of Mechanical Engineering, Purdue University, West Lafayette, Indiana

(*Received May 1960*)

The effect of pressure on the burning velocity of four fuel–air and three fuel–oxygen mixtures, all in stoichiometric proportions, was determined using the constant-volume bomb method. Ionization gaps were employed to obtain the flame radius/time data. The pressure range investigated was from 0·2 to 20 atmospheres. Burning velocity values were calculated from flame speed measurements using the recently developed equations of Eschenbach and Agnew. Possible sources of errors which are peculiar to the ionization gap technique of measuring flame speeds are discussed along with the precautions taken to minimize their effects.

Introduction

THE normal burning velocity, S_u, of a combustible mixture is the velocity relative to the unburnt gas at which a plane flame front propagates into the mixture. It is thought to be a function of the thermodynamic properties of a combustible homogeneous gas mixture.

The methods of measuring burning velocity employ either stationary or moving flames. In the first category come such methods as the bunsen burner, slot burner, particle track, and flat-flame burner. The flame tube, soap bubble (constant-pressure bomb) and constant-volume bomb methods come under the classification of moving flames. Of the above methods measurements from the flat-flame burner and the Mache–Hebra slot burner are taken from planar combustion waves. Consequently, most experimentally determined values of the burning velocity deviate somewhat from the true value as a result of flame curvature and other effects peculiar to the particular apparatus.

It is thought, however, that a spherical combustion wave which has grown to such a size that curvature effects are negligible is the ideal surface to use for measuring burning velocities[1]. Such a flame surface is used for flame speed measurements in the constant-volume bomb technique. However, the constant-volume bomb method, which was employed to obtain measurements discussed in this paper, has not been too widely used because of the relatively expensive and specialized equipment needed, and because of the complicated analysis required to obtain burning velocity values from the flame speed measurements.

In order to compare data obtained by this method with those from other techniques, the pressure dependence of burning velocity for stoichiometric methane–air mixtures was determined. Having confirmed that the method gave satisfactory results for this mixture, other mixtures were chosen to include variation in fuel type and oxidant. All mixtures investigated were in stoichiometric proportions. Fuel–air mixtures studied, in addition to methane–air, were propane–air, ethylene–air, and acetylene–air.

Considerable controversy has existed in the past concerning the pressure dependency of burning velocity for fast burning mixtures. Three such mixtures were chosen for investigation: hydrogen–oxygen, methane–oxygen, and ethylene–oxygen.

Description of Apparatus

A schematic diagram of the experimental apparatus is shown in *Figure 1*. The 10 in. spherical combustion bomb used in the experimental work was machined from 410 stainless steel. The vessel consists of two hemispheres which were locked into an outer metal rim by two threaded rings. One hemisphere has two wells tapped for 18 mm spark plugs; the other hemisphere has three openings to which $\frac{1}{4}$ in. high pressure tubing could be fitted and two drilled passages for insulated electrodes. Each

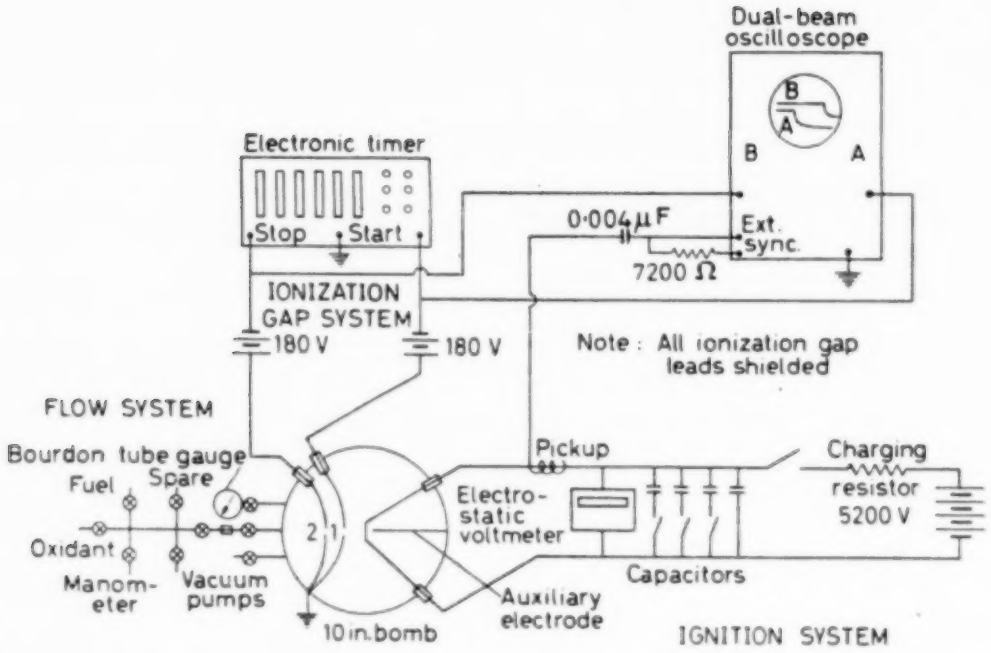

Figure 1. Schematic arrangement of experimental apparatus

half of the vessel has provision for two cylindrically shaped window inserts. The windows were replaced with steel plugs under severe operating conditions. The bomb was hydrostatically tested to 7 500 lb/in^2 and burning velocity determinations have been made with initial mixture pressures as high as 20 atmospheres. To facilitate handling of the bomb and to provide for a means of mixing fuel and oxidant, the bomb was supported on two steel rollers one of which was driven by a variable speed electric motor.

The fuel and oxidant tanks, a mercury manometer, and vacuum pumps were attached to the bomb through a manifold-type flow system. A mercury manometer was used to measure pressures up to two atmospheres, and a Bourdon tube gauge was employed for higher pressures. All of the gases used including the air were obtained from commercial gas cylinders.

A capacitance-type ignition system was employed to permit calculation of the spark energy since it was desirable to determine its effect, if any, on the flame speed. The power supply which consisted of sixty 90 V radio batteries in series was connected through a knife switch and charging resistor to the condenser bus bar. The ignition energy was varied by changing the number of condensers in the system. When the knife switch was closed, the capacitors charged slowly and then discharged across the spark gap when the breakdown voltage, which was read from an electrostatic voltmeter, was reached.

The two ignition electrodes were pointed 0·060 in. diameter molybdenum wires each of which was silver soldered to the centre electrode of a spark plug. In most test runs the spark gap which was accurately centred in the bomb was 0·010 in.; however, because of the limited supply voltage it was necessary to use a smaller gap at high initial reactant pressures. The use of a spark plug with each spark gap electrode insulated the ignition system from the test apparatus and resulted in a floating earth for the ignition system. It was observed that when the voltage across the spark gap was a maximum for the system ($\sim$ 5 400 V), the low voltage side of the ignition system had a potential of about 600 V above that of the bomb wall which was earthed. The problem encountered with a floating earth is discussed later.

The ionization gap system consisted basically of two identical ionization gap circuits, a dual-

beam oscilloscope, and an electronic timer which employed a temperature-regulated crystal megacycle oscillator as the time base. Each ionization gap was formed from two 0·060 in. diameter pointed molybdenum electrodes. The gap width was approximately $\frac{3}{16}$ in. for all the tests. Two of the electrodes were earthed to the bomb wall while the other two were inserted through insulated passages of the bomb and sealed in place with Epon resin to prevent leakage at high pressures. When the bomb was assembled, the spark gap and ionization gaps were in the central plane of the sphere with both ionization gaps on the same side of the centred spark gap. As shown in *Figure 1*, ionization gap 1 was connected through a 180 V battery to the start input of the timer and to the Y axis of one beam of the oscilloscope; ionization gap 2 with identical circuitry was attached to the stop input of the timer and the Y axis of the other oscilloscope beam.

The ionization gap system functioned in the following manner. When the combustible mixture in the bomb was ignited by a spark, the resultant voltage collapse in the spark circuit triggered the oscilloscope traces through the magnetic pickup. The potential across each ionization gap was 180 V. When the flame front reached the first gap, the hot ionized gases reduced the resistance appreciably; the resulting current flow started the timer and caused trace A on the oscilloscope to deflect. On arrival of the flame front at the second gap, the electronic timer stopped and trace B on the oscilloscope deflected. The data obtained were used to calculate the speed of the flame front.

Because the ignition system, as previously mentioned, was operated with a floating earth, it had a relatively high potential with respect to the bomb wall. Consequently, the inflamed sphere of gas suspended on the ignition electrodes was likewise charged relative to the bomb wall. Photographs of preliminary test runs with the floating earth circuitry showed that the oscilloscope trace for the first ionization gap circuit did not deflect sharply as did the trace for the second ionization gap circuit, but curved downwards relatively slowly. This indicated diffusion of electrons or other charged particles between the first gap electrodes and the flame front as it approached. The problem was rectified by placing an auxiliary electrode from the bomb wall to the vicinity of the spark gap such that the flame front would intercept this electrode before reaching the first ionization gap. With this arrangement, sharp deflection of both oscilloscope traces was obtained. Earthing the low voltage side of the ignition system to the bomb wall did not serve the same purpose, but rather resulted in poorly defined oscilloscope traces and usually in premature starting of the timer when the ignition switch was closed.

Experimental Procedure

Prior to a test run the bomb was taken apart and the spark gap was repositioned in the centre of the bomb, if necessary. To assist positioning of the ionization gaps, an alignment sight consisting of cross wires on a steel ring was used which not only aided in locating the ionization gaps in the central plane of the bomb but also helped to position them on a diameter of the sphere. A cathetometer, which could be read to 0·005 cm, was used to measure the distances from the bomb centre to each ionization gap.

After the cathetometer readings were taken, the bomb halves were assembled and connected to the valve system and vacuum pumps. The bomb, which had a very good seal both at high pressures and with a vacuum, was then evacuated to a pressure less than 0·5 mm of mercury absolute. The vessel was filled with the desired mixture, the fuel being introduced before the oxidizer. To eliminate possible stratification of the fuel and oxidant, the bomb was then rotated on the motor driven assembly for about 15 minutes. To further accelerate the mixing process, a small cylindrical piece of stainless steel ($\frac{1}{2}$ in. by $\frac{1}{2}$ in.) was placed in the bomb to make use of the turbulence created by its rolling on the bottom of the spherical cavity.

After the mixing process a period of about five minutes was allowed for turbulence in the vessel to subside. During this time, the instruments were adjusted for the test run. The oscilloscope was set to obtain the entire trace pattern on the tube face during a single sweep. After all equipment was readied, the oscilloscope

camera shutter was held open and the ignition switch closed. After the explosion the shutter was released. The electrostatic voltmeter reading at spark discharge was recorded along with the timer reading. The Polaroid photographs of the oscilloscope traces were used to determine if the ionization gap circuitry was functioning properly. Dissimilar trace deflections indicated an erroneous timer reading. The bomb was then evacuated and taken apart to make necessary adjustments for the next run.

The standard test technique used consisted of positioning the first ionization gap about $\frac{1}{4}$ in. from the spark gap and using this as the base point; that is, for a given gas mixture at a given pressure the first gap was always set at the same distance from the centre. The second gap was then set at various distances from $\frac{1}{4}$ in. to 2 in. from the centre for successive runs of the same mixture at a given pressure. Generally, four or five tests were conducted for a given mixture–pressure combination using this technique. The timer and cathetometer readings for a series of runs with the same mixture at a given pressure were used to plot points on a flame radius/time (r_b/t) diagram. Using the method of least squares, a straight line was fitted to the points. The slope of the line, dr_b/dt, is a quantity used in determining the burning velocity of a combustible mixture.

Factors Affecting the Measurements

Since the constant-volume bomb ionization gap technique of measuring burning velocities is a relatively new method[2], problems uncommon to the usual photographic methods of measuring flame speeds were encountered during the investigation. These problems and other likely causes of experimental errors are now discussed along with the precautions taken to minimize their effects.

Variation of flame speed with radius

Photographs of the combustion process[3] in spherical bombs and soap bubbles show a period of acceleration of the flame front after ignition of the mixture by a spark. After the acceleration period, the flame speed, S_u, is constant until the bomb walls exert an influence. *Figure 2* shows a theoretical flame radius/time (r_b/t) diagram for a combustion wave ignited from the centre of a bomb (solid line) and from the centre of a soap bubble (dotted line). For accurate values of burning velocity by the constant-volume bomb method wherein ionization gaps are used to detect flame position, measurements of the flame speed must be taken within the region where it is constant.

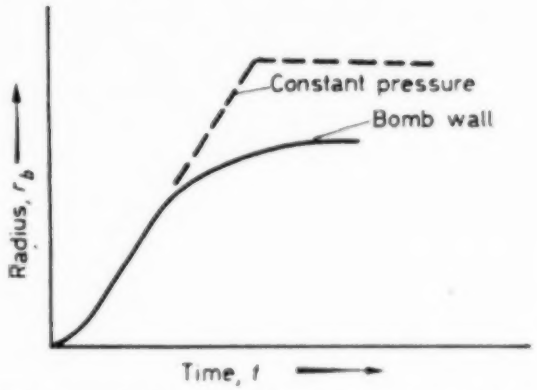

Figure 2. Theoretical flame radius/time diagram

The acceleration period was easily detected for slow burning mixtures but was not so apparent for the rapid reacting mixtures. In accordance with the work of E. F. Fiock *et al.*[4], it was found that the duration of the initial acceleration period lengthens as the mixture pressure is reduced. After the period of uniform flame speed, the value of S_u for slow burning mixtures decreases as the flame front approaches the

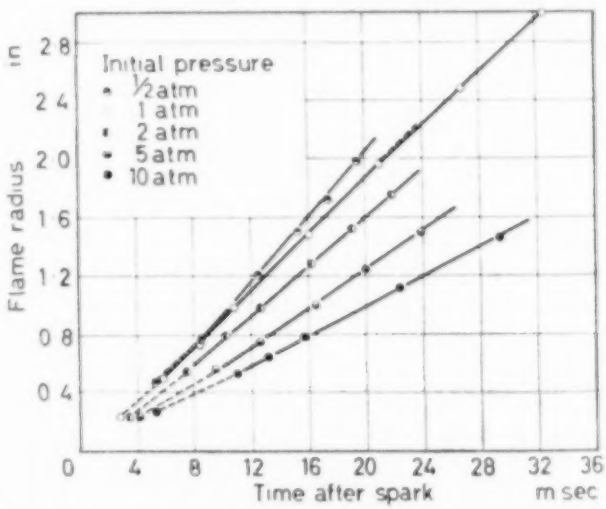

Figure 3. Flame radius/time data for stoichiometric methane–air

bomb wall. Measurement of r_b/t data out to a radius of 3·5 in. for methane–air at one atmosphere pressure shows the decrease in S_u, *Figure 3*. It was also found that some of the more rapid burning mixtures accelerated after a short period of constant speed deflagration, *Figure 4*.

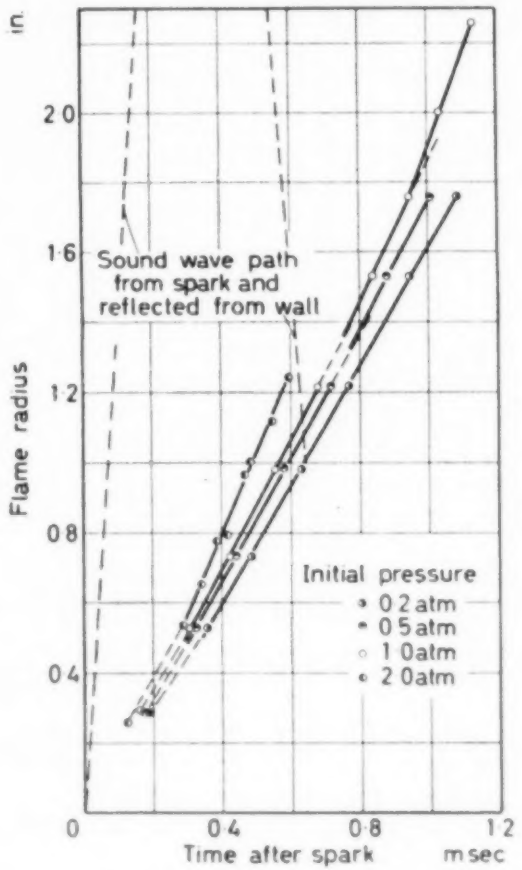

Figure 4. Flame radius/time data for stoichiometric methane–oxygen

Other investigators have noticed this same phenomenon with soap bubble and with flame tube experiments. D. M. SIMON and E. L. WONG[5] using high speed photography with soap bubble experiments found that for fast flames the combustion wave developed a rough surface causing the acceleration. The distorted flame surface was thought to be a type of Taylor surface instability. Other investigators attributed the acceleration to a disturbance of the flame front by pressure waves produced by the spark[6,7] or by the initially accelerating flame front[8,9] and reflected from the vessel walls.

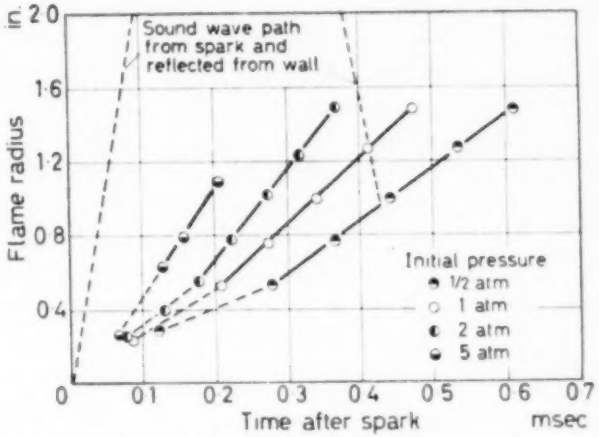

Figure 5. Flame radius/time data for stoichiometric hydrogen–oxygen

In this investigation it was found that the time of the flame front acceleration could not be predicted by calculating the time a reflected pressure wave (travelling at acoustic velocity) originating from the spark would intersect the combustion wave. This is shown in *Figures 4* and *5*.

Effect of ignition energy

Preliminary test runs indicated that precautions must be taken to control the spark energy if the ionization gap technique of measuring flame speeds is employed. The effect of spark energy on the flame speed of stoichiometric methane–air mixtures at low pressures was determined. The results are given in *Tables 1* and *2*.

It is to be noted that the method used to calculate the flame speeds listed in the tables was not that employed to obtain the burning velocity data. The flame speed values in the tables are distances between the two ionization gaps divided by the elapsed times.

Table 1. Effect of spark energy on S_u of methane–air initially at half atmospheric pressure

Spark gap to gap No. 1 (SG to No. 1): 0·946 in.
Gap No. 1 to gap No. 2 (No. 1 to No. 2): 0·792 in.

Spark energy, mJ	*Flame speed in./sec*	*Time, msec*	
		SG to No. 1	*No. 1 to No. 2*
62	104·5	9·850	7·575
51	105·7	10·140	7·490
21	109·2	10·460	7·251

As shown in the tables, the apparent flame speed decreased as the spark energy was increased. Although the time to reach the first gap was shorter for the flame fronts initiated by the higher energy sparks, the time to travel between the two ionization gaps was longer, accounting for the decrease in the flame speed.

Table 2. Effect of spark energy on S_u of methane–air initially at atmospheric pressure

Spark gap to gap No. 1 (SG to No. 1): 0·506 in. Gap No. 1 to gap No. 2 (No. 1 to No. 2): 1·287 in.

Spark energy, mJ	*Flame speed in./sec*	*Time, msec*	
		SG to No. 1	*No. 1 to No. 2*
684	87·3	4·990	8·988
462	90·0	4·550	8·720
275	91·2	4·520	8·620
16	94·8	7·490	8·280

During the initial test runs in which the flame speeds were calculated as in the tables, it was found that spark energy variation had the greatest effect upon the low-pressure fuel–air mixtures. In general, it was observed that the magnitude of the spark energy had little apparent effect upon the fast burning mixtures except at very low pressures ($P < 0{\cdot}5$ atm).

The following explanation is thought to account for the observed spark energy effect. A high-energy spark encompasses and ignites a larger volume of gas than a weak spark; but both volumes of inflamed gas start out with the same initial velocity and have essentially the same velocity/time history during the entire course of the deflagration process. On a flame radius/time diagram, the high spark energy initiated flame trace would be similar to the one in *Figure 2* but starting a short distance from the origin, that is, displaced upwards a distance equivalent to the spark radius. This model would explain the earlier arrival of the higher energy initiated flame fronts at the first gap and also the longer time between gaps. The latter is because a larger part of the initial accelerating period is located between gaps for the higher energy ignited flames.

Fiock and Marvin[9], who photographically recorded the combustion process in a constant-volume bomb, also found that the stages of the combustion process after ignition were not reproducible from run to run but the straight line portions of the traces were parallel indicating consistent values of the flame speed. Simon and Wong[5], using the soap-bubble method of measuring burning velocities, found that changing the spark energy by a factor of 100 did not affect the flame speed. The findings of these investigators support the explanation in the preceding paragraph that the ignition energy does not affect the flame speed (provided it is measured within the constant speed region) but only alters the combustion process immediately after ignition.

The test technique employed along with the use of a nearly constant low-energy spark for a given mixture and pressure rendered negligible possible errors in the flame speed determinations from the above-mentioned effects. For most of the flame speed determinations the ignition energy was from about one to five millijoules except for the low-pressure air–fuel mixtures which had higher minimum ignition energies at the spark gap width used.

Effect of ionization gap electrodes

Although the most likely way to eliminate any effect of the ionization gap electrodes on the flame speed would be to place the gaps on opposite sides of the spark gap, this method would introduce errors in the measurements from at least several possible sources. Slightly non-spherical propagation of the combustion wave would cause a sizable error in the measurements. Aspherical flame fronts were reported by other investigators[10] to result if the ignition energy and spark gap width were not properly chosen; however, it is reasonable to expect that some asphericity would not greatly affect the flame speed if it is measured by tracing the progress of the same point on the combustion wave. Since the ignition electrodes were located in one hemisphere of the bomb and the ionization gap electrodes in the other, the distance from the spark gap to each ionization gap could not be measured directly, and consequently another error would have been introduced into the flame speed determination by placing the ionization gap electrodes on opposite sides of

the ignition gap. For the reasons given the above-mentioned technique was not used in determining flame speeds.

An indirect test procedure was used to determine if the ionization gap electrodes had any effect upon the flame speed. Flame speed data were obtained for individual test runs with both ionization gaps located in the region where the standard test technique, described in the section on experimental procedure, showed the flame speed to be constant. It was found that, in general, the flame speeds of some low-pressure fuel–air and fuel–oxygen mixtures were somewhat lower than the values obtained by the standard test method. This apparently indicated that the first ionization gap electrodes could affect the flame speed measurements for some mixture conditions.

It is thought that the low flame speeds which were indicated by the flame radius/time diagrams (*Figures 3* and *5*) to result immediately after the location of the first ionization gap for some mixtures were caused primarily by the gap electrodes. In some manner, possibly by quenching and disrupting the flame surface, the first ionization gap probes retarded the flame front only momentarily since S_u soon attained a constant value. This is shown particularly by the hydrogen–oxygen mixtures, *Figure 5*. The r_b/t diagrams also indicate that the electrode effect was approximately constant from run-to-run for a given mixture and pressure, and that the experimental technique used to obtain S_u eliminated this effect from the calculations.

Mixture composition

Since the bomb was charged by introducing the fuel and oxidant separately, there existed the possibility of a heterogeneous mixture in the bomb. Experimentation indicated that fuel and oxidant at initial pressures greater than five atmospheres remained stratified for a considerable length of time unless the vessel was rotated as described in the section on procedure. This would be expected since the diffusion rate is inversely proportional to the pressure.

Small variations in the initial mixture composition from run-to-run probably caused negligible errors since the burning velocity of a mixture does not change rapidly with the equivalence ratio near the stoichiometric composition. It is thought that the relatively small scatter in the test data indicated nearly constant composition and uniform mixtures between test runs.

The initial mixture pressures measured with the mercury manometer were adjusted to values at standard density, while the initial mixture temperature for most runs was maintained between 25°C and 27°C.

Burning Velocity Results

The normal burning velocity pressure dependence of seven stoichiometric fuel–oxidant mixtures initially at room temperature was determined. The flame speeds for all mixtures except methane–air at 20 atm were found from the slope of the best straight line fitted to the flame radius/time data which were obtained by the test method previously described. The flame speed of methane–air at 20 atm was taken as the average of three individual test runs.

For illustrative purposes the flame radius/time diagrams of only three fuel–oxidant mixtures are given in this paper, *Figures 3*, *4* and *5*. All the r_b/t diagrams along with the individual test data used to plot them are given in ref. 11. Although the r_b/t diagrams are plotted with the abscissa as 'time after spark', the spark time was found to be a very poor base point as indicated by the large variation in the flame front arrival times. Several factors may have contributed to this large arrival time variation. The time from the spark to the first ionization gap was scaled from the oscilloscope trace photographs, and any late or premature triggering of the trace yielded incorrect values. It is likely that ignition delay and small changes in ignition energy from run-to-run also contributed to the time variation. Since the time to the first ionization gap did not enter into the calculation of the flame speed but only served to locate the flame trace curve on the r_b/t diagrams, the value plotted was the average for the set of runs. Each of the other points on these diagrams, however, was determined from a single test run.

Since the test technique employed was specially designed to indicate where the flame radius/time data for any mixture deviated significantly from linearity, either in the early burning stages after ignition or at larger flame radii where abnormal pressure effects may exist, data points located in such regions were disregarded in the calculations. Experimental values which were apparently in the constant flame speed region but not lying on the curve were, of course, considered. As a measure of the reliability of the experimental data, bars which represent plus and minus twice the standard error of the calculated burning velocity are plotted above and below each burning velocity value on the graph.

The equations which were used to calculate the burning velocities from the flame speed measurements were taken from the analysis of R. C. Eschenbach and J. T. Agnew[7], which presents the theory for computing burning velocity from constant-volume bomb measurements. $S_u = S_s/E_i$ was the equation used to calculate the burning velocities of the fuel–air mixtures;

$$S_u(P_u, T_i) = (S_s/E_i)(T_i/T_u)(1+\gamma_u\beta^2 T_i/T_u)$$

was employed for the fuel–oxygen mixtures. In these equations, S_u is the burning velocity, S_s the flame speed, E the expansion ratio, γ the ratio of specific heats, P and T are the pressure and temperature, and $\beta = (S_s - S_u)/c_i$ where c is the acoustic velocity. The subscripts $_i$ and $_u$ represent, respectively, the initial condition and the conditions in the unburnt gas immediately ahead of the combustion wave. The method of finding the correction factors in the second equation is given in ref. 7.

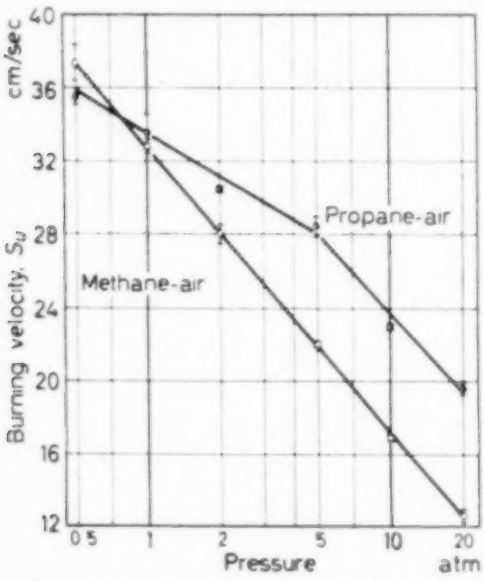

Figure 6. Effect of pressure on the burning velocity of stoichiometric methane–air and propane–air

The experimental flame radius/time curves for methane–air are given in *Figure 3*. The calculated burning velocity values for both methane–air and propane–air are plotted against the logarithm of the pressure in *Figure 6*. The pressure dependence of stoichiometric methane–air within the pressure range of $\frac{1}{2}$ to 20 atm is given quite accurately by the equation

$$S_u = -6{\cdot}78 \ln P_i + 32{\cdot}9 \ \text{(cm/sec)}$$

The effect of pressure on S_u of stoichiometric ethylene–air is shown in *Figure 7*. Within the interval $\frac{1}{2}$ to 10 atm pressure, the burning velocity of ethylene–air is given by

$$S_u = -4{\cdot}34 \ln P_i + 59{\cdot}8 \ \text{(cm/sec)}$$

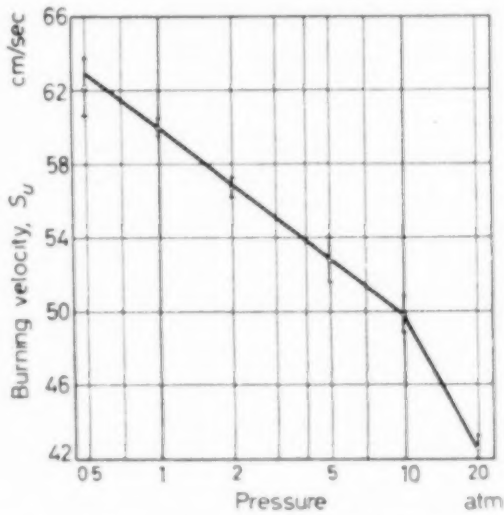

Figure 7. Effect of pressure on the burning velocity of stoichiometric ethylene–air

Figure 8 indicates that the burning velocity of acetylene–air is relatively insensitive to pressure. At pressures above 2 atm the burning velocity seems to increase with pressure, but the two sigma limits are sufficiently large to mask a definite trend.

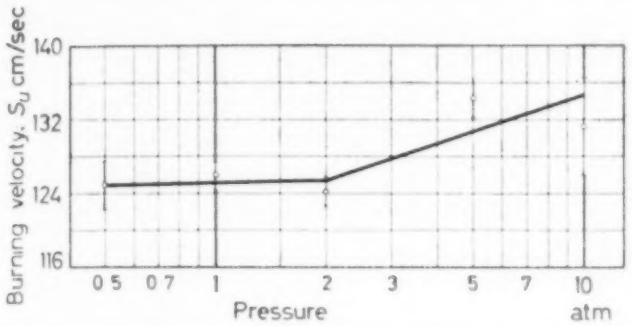

Figure 8. Effect of pressure on the burning velocity of stoichiometric acetylene–air

The flame front/time traces for the stoichiometric methane–oxygen mixtures are given in *Figure 4*. Scatter in the experimental data points at a pressure of 2 atm possibly indicates a rough-surfaced flame front as reported by Simon and Wong[5]. *Figure 9* gives the burning

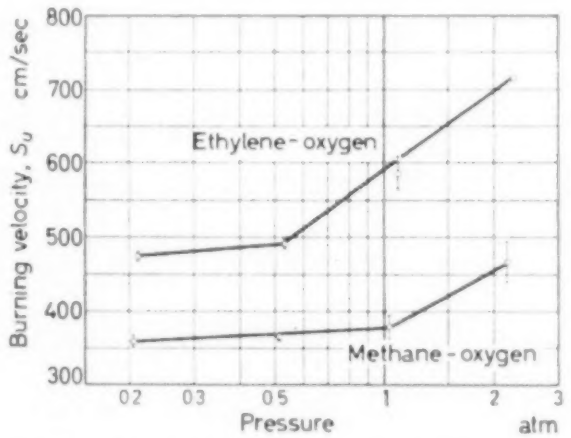

Figure 9. Effect of pressure on the burning velocity of stoichiometric methane–oxygen and ethylene–oxygen

velocity pressure dependence of stoichiometric methane–oxygen and ethylene–oxygen. Only one test run with ethylene–oxygen at 2 atm was conducted since the high temperature and possibly a detonation wave in the last part of the charge to burn shattered the ceramic in both spark plugs. The molybdenum electrodes were badly bent and the pointed tips were melted. The reliability of the run at 2 atm is thought to be about ± 5 per cent.

The burning velocity of hydrogen–oxygen approximately doubled over the pressure range for which determinations were made, *Figure 10*.

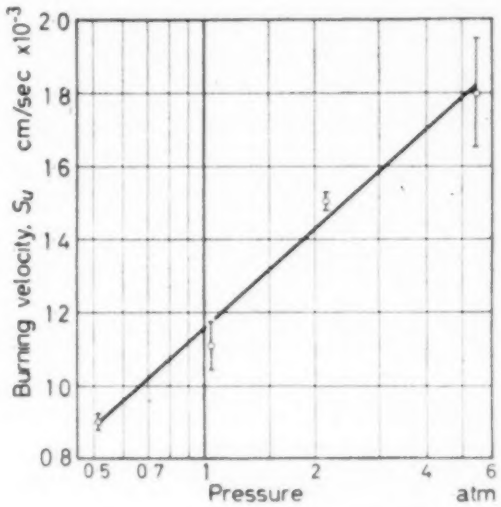

Figure 10. Effect of pressure on the burning velocity of stoichiometric hydrogen–oxygen

Between $\frac{1}{2}$ and 5 atm pressure, the burning velocity of stoichiometric hydrogen–oxygen is represented fairly accurately by

$$S_u = 98 \ln P_i + 1150 \text{ (cm/sec)}$$

Precautions should be taken in extrapolating the pressure dependence curves of this investigation for the fuel–air mixtures (acetylene–air not considered) since they indicate that at a finite high pressure, the burning velocities become zero. This is quite unlikely. Undoubtedly, a change in reaction mechanism occurs at very high pressures, e.g. W. A. Strauss and R. Edse[12] found that S_u for carbon monoxide–oxygen mixtures increased with pressure until about 52 atm after which it decreased.

Discussion

With the exception of methane–air mixtures, very little data are available on the pressure dependence of burning velocity at pressures above atmospheric. Most literature burning velocity values have been determined using the stationary flame (burner) method, and the pressure dependence analyses were concerned primarily with the sub-atmospheric range.

All burning velocity measuring techniques are subject to certain possible errors. The burner method is particularly susceptible to many sources of errors which are discussed by J. M. Singer, J. Grumer and E. B. Cook[13]. The

bomb method is handicapped by the possibility of incomplete combustion[7], that is, the equilibrium expansion ratio may not be attained during the burning period of interest. This may be particularly true at very low pressures where the flame thickness may be quite large. Under such conditions, the calculated burning velocity would be lower than the true value.

From an experimental standpoint, the effect of pressure on the laminar burning velocity has been in considerable dispute but at present there seems to be better agreement at least on whether increasing the initial pressure of a given mixture increases or decreases S_u. Literature data for the burning velocity pressure dependence of methane–air is shown in *Figure 11*. At high pressures, the burner technique appears to give somewhat lower values of S_u than those determined by the bomb method. The very small burner tubes necessary at high pressures may introduce large measurement errors, for it is unlikely that the burning velocities determined by the bomb method are high since incomplete expansion would yield low values. There is good agreement between values of this work and those obtained by Strauss and Edse[12] using the soap-bubble technique. From *Figure 11* it appears that at pressures above 50 atm S_u may increase or approach a constant value.

There is general concordance that the burning velocity of propane–air and ethylene–air mixtures increases with a decrease in mixture pressure. R. E. Cullen[14] found that the burner diameter had a large effect on the measured value of S_u, and from his measurements at pressures less than 2 atm showed that the burning velocities of propane–air and ethylene–air were inversely proportional to the logarithm of the pressure. Cullen is the only other investigator known to the authors to have found this type of pressure dependency. There is also good agreement that the burning velocity of chemically correct acetylene–air is essentially independent of pressure in the sub-atmospheric range[15]. The results of this investigation tend to indicate that S_u for acetylene–air may increase somewhat with pressure above 2 atm.

J. Diederichsen and H. G. Wolfhard[16], using the bunsen burner method, have also shown that the burning velocity of stoichiometric methane–oxygen is essentially independent of pressure in the sub-atmospheric range. It is thought that the data of R. C. Eschenbach and J. T. Agnew[7] at 0·1 and 0·2 atm were affected by the ionization gap electrodes and by measurements taken too near the spark gap. W. A. Strauss and R. Edse[12,17] who used both the burner and bubble methods at atmospheric pressure and up to 90 atm, found that the burning velocity of methane–oxygen increased rapidly with pressure. The results of this investigation and those of Strauss and Edse show conclusively that the burning velocity of

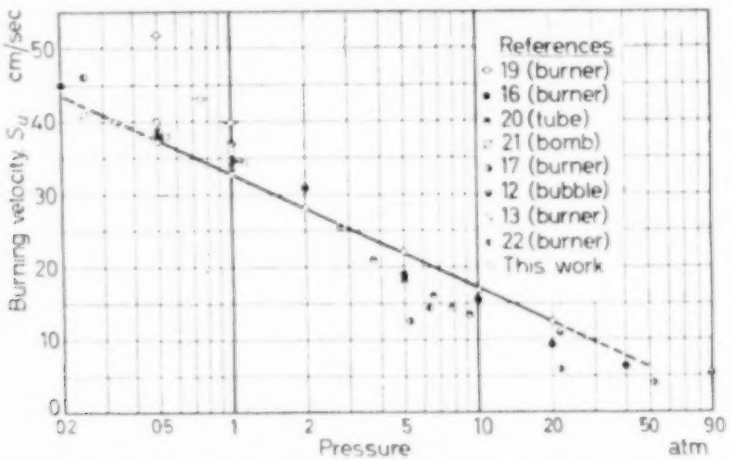

Figure 11. Literature values of S_u against ln P *for stoichiometric methane–air*

hydrogen–oxygen mixtures increases very rapidly with initial pressure.

Both the diffusion and thermal theories of flame propagation predict the following type of pressure dependency: $S_u \sim P^n$. In the diffusion theory proposed by Tanford and Pease, n can vary from zero for very hot flames to $-0{\cdot}25$ for slow burning mixtures, while for the thermal theory of Semenov $n=0$ for a bimolecular reaction and n is $-0{\cdot}5$ for a monomolecular reaction[18]. Because of the possibility of differentiating between the diffusion and thermal theories of flame propagation by comparing predicted with experimentally determined pressure dependencies, most of the early investigations on the effect of pressure were concerned with determining the value of the exponent, n, for a given mixture. It is apparent from the results of this investigation that the simplified theories of flame propagation break down for the rapid burning mixtures, since neither accounts for an increase in burning velocity with pressure. Furthermore, due to the known complexity of the reaction mechanisms of hydrocarbon oxidation, there does not appear to be any justification for relating the pressure coefficient of burning velocity to the order of the reactions. The order of a hydrocarbon oxidation reaction probably would have little significance in the conventional sense.

For their financial support during the course of this investigation, one of the authors (L.B.G.) is grateful to the Shell Companies Foundation, Inc., the Standard Oil Company of Indiana, and the Purdue Research Foundation.

References

[1] Lewis, B. *Selected Combustion Problems*, p 176. A.G.A.R.D.; Butterworths: London, 1954

[2] Smith, D. and Agnew, J. T. *Sixth Symposium (International) on Combustion*, p 83. Reinhold: New York, 1956

[3] Fiock, E. F. and Marvin, C. F. *Chem. Rev.* 1937, **21**, 367

[4] Fiock, E. F., Marvin, C. F., Caldwell, F. R. and Roeder, C. H. *Nat. Adv. Comm. Aero., Wash., Rep. No. 682* (1940)

[5] Simon, D. M. and Wong, E. L. *Nat. Adv. Comm. Aero., Wash., Rep. No. 3106* (1954)

[6] Burke, E. *Fourth Symposium (International) on Combustion*, p 406. Williams and Wilkins: Baltimore, 1953

[7] Eschenbach, R. C. and Agnew, J. T. *Combustion & Flame*, 1958, **2**, 273

[8] Everett, A. J. and Minkoff, G. J. *Fuel, Lond.* 1954, **33**, 66

[9] Egerton, A. C., Saunders, O. A., Lefebvre, A. H. and Moore, N. P. W. *Fourth Symposium (International) on Combustion*, p 396. Williams & Wilkins: Baltimore, 1953

[10] Manton, J., von Elbe, G. and Lewis, B. *Fourth Symposium (International) on Combustion*, p 358. Williams & Wilkins: Baltimore, 1953

[11] Graiff, L. B. 'The pressure dependence of laminar burning velocity'. *Ph.D. Thesis*. Purdue University: Lafayette, Indiana, 1959

[12] Strauss, W. A. and Edse, R. *Seventh Symposium (International) on Combustion*, p 377. Butterworths: London, 1959

[13] Singer, J. M., Grumer, J. and Cook, E. B. *Gas Dynamics Symposium on Aerothermochemistry*, p 139. Northwestern University: Evanston, 1956

[14] Cullen, R. E. *Trans. Amer. Soc. mech. Engrs*, 1953, **75**, 43

[15] Wheatley, P. J. and Linnett, J. W. *Trans. Faraday Soc.* 1952, **48**, 338

[16] Diederichsen, J. and Wolfhard, H. G. *Trans. Faraday Soc.* 1956, **52**, 1102

[17] Strauss, W. A. and Edse, R. *Wright Air Development Center, Report No. 56–49* (1956)

[18] Simon, D. M. *Selected Combustion Problems*, p 59. A.G.A.R.D.; Butterworths: London, 1954

[19] Clingman, W. H. and Pease, R. N. *J. Amer. chem. Soc.* 1956, **78**, 1775

[20] Egerton, A. C. and Lefebvre, A. H. *Proc. Roy. Soc. A*, 1954, **222**, 206

[21] Manton, J. and Milliken, B. B. *Gas Dynamics Symposium on Aerothermochemistry*, p 151. Northwestern University: Evanston, 1956

[22] Wohl, L. and Kapp, N. M. *Project Meteor Rep. No. UAC–42* (1949)

A Theoretical Study of Interactions Between Two Parallel Burning Fuel Plates

TAU-YI TOONG

Massachusetts Institute of Technology, Cambridge 39, Mass., U.S.A.

(Received May 1960)

This is the first of a series of papers, intended to discuss the basic causes and mechanisms of the interactions among burning fuel droplets and their effects on the performance of a combustor employing fuel sprays, with respect to both overall burning rate and combustion roughness and stability. The interactions between two parallel fuel plates burning in an oxidizer stream are studied by the use of an integral method. Within the region of validity of this method, where the flames adjacent to the plates are separated from each other, the evaporation or sublimation rate at the fuel surface increases with decreasing spacing between the plates, while, in the meantime, the combustion rate at the flame front decreases. These interactions become less important with decreasing value of the heat ratio. Applying the results obtained in this work to the case of two fuel droplets burning side by side, one would predict an increase in both the burning rate and the flame length with decreasing droplet spacing, as long as the flames surrounding the droplets are separated from each other. These predictions are found to agree well with the experimental results, which will be presented in another publication.

Introduction

DURING recent years, much progress has been achieved in the study of the combustion of a single fuel droplet in an oxidizer medium. However, in order to apply the knowledge so acquired to the understanding and the prediction of the performance of a combustor employing fuel sprays, with respect to both overall burning rate and combustion roughness and stability, it is essential to seek first (among other things) a thorough understanding of the basic causes and mechanisms of the interactions among burning fuel droplets.

Interactions between two burning fuel droplets placed side by side with the line joining their centres normal to the flow direction of an oxidizer stream are illustrated schematically in *Figure 1*. As the droplets are brought closer together, both the flame shapes and the burning rates are affected. When the distance between the droplets is relatively large, the two flames surrounding the droplets remain separated, although their shapes are distorted due to an increase in the stream velocity between the droplets and in the evaporation rate at the droplet surface. When the droplets are closer together, as shown in the lower part of *Figure 1*, the flames bcome merged together and the two

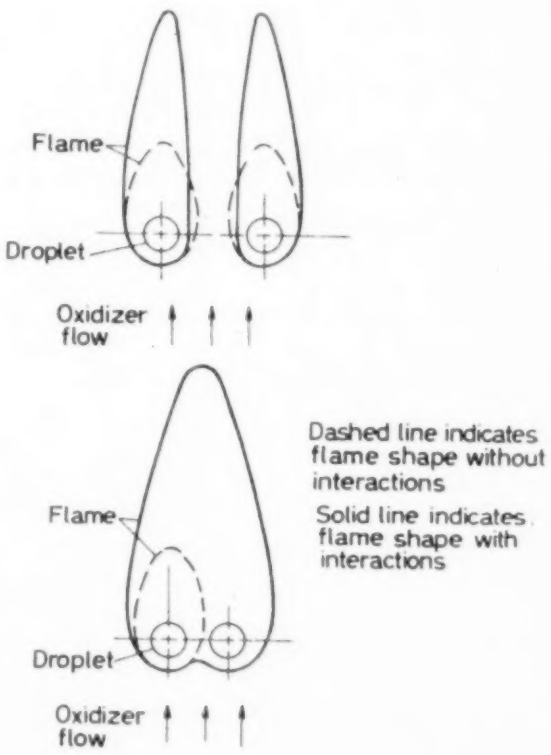

Figure 1. Schematic drawing showing interactions between two fuel droplets burning side by side in an oxidizer stream

droplets would then burn like one larger droplet and thus at a smaller rate.

J. F. Rex, A. E. Fuhs and S. S. Penner[1] studied experimentally the interactions between two fuel droplets burning side by side in a natural-convective field. It was found that as the distance between the droplets decreased, the burning rate of each droplet first increased and then decreased. N. Nishiwaki and M. Hirata[2] investigated the burning of two fuel droplets, one of which was placed upstream of the other. In this case, as the distance between the droplets decreased, the burning rate first decreased and then increased. It is to be noted that these observations are just contrary to those for the case where the two droplets are placed side by side in an oxidizer atmosphere.

In the experiments of J. N. Kanevsky[3], the burning rate of the centre droplet of a three-dimensional body-centred cubic array of nine fuel droplets in still air was investigated. The results in this case are quite similar to those observed by Rex *et al.*

Since the flames can be regarded as the sources of energy and of hot products as well as the sinks for the fuel and the oxidizer, the above observations indicate that there is a change in the spatial distribution and the intensity of these sources and sinks as the distance between the droplets varies. Thus, the interactions mentioned above are important in determining not only the overall burning rate of a fuel spray in a given combustor but also the combustion stability and roughness. It is conceivable that, under certain circumstances, some oscillations which might be present in a combustion chamber could alternately induce the separation and the merging of the flames surrounding the droplets, thus changing the spatial distribution and the intensity of the sources of energy and of hot products in the combustor. New oscillations resulting from such changes might possibly amplify or damp the initial oscillations, thus resulting in an unstable, rough or steady burning.

The present series of papers is intended to discuss the basic causes and mechanisms of the interactions among burning fuel droplets and their effects on overall burning rate, combustion stability and roughness. In this first paper, the interactions between two parallel fuel plates burning in a steady oxidizer stream are studied by means of an integral method. These flat plates, covered with fuel, are used to simulate two droplets burning side by side in a forced-convective field. The method presented here, however, is valid only in a region where the boundary-layer thickness is small as compared with the spacing between the plates. Under such conditions, the flames adjacent to the plates are separated from each other.

The results presented in this paper include the effects of the spacing between the plates on the evaporation (or sublimation, should the fuel at the plate surface be in a solid phase) rate at the fuel surface as well as the combustion rate at the flame front. Also included are the effects of the heat ratio on interactions. These results are then used to interpret and predict the interactions between two fuel droplets burning side by side in an oxidizer stream.

Theoretical Model

Figure 2 shows a theoretical model used in the study of interactions between two steadily burning parallel fuel plates. A gas stream, in which the mass fraction of the oxidizer is c_{0_∞} and of which the temperature is T_∞, flows steadily between these two flat plates covered with fuel. Fuel vapour, evaporating or subliming at the fuel surface at temperature T_s, convects along the plates and diffuses away from them until it is mixed with a sufficient amount of the oxidizer and starts to burn. As

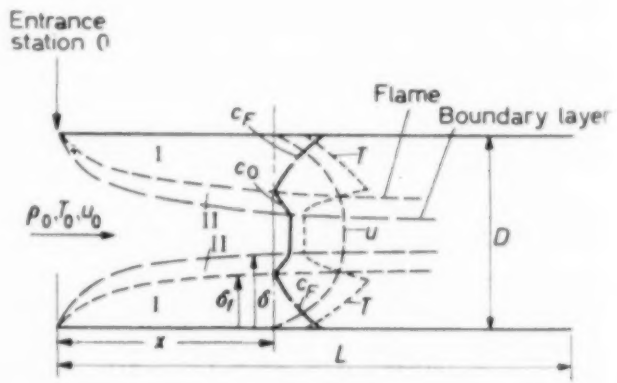

Figure 2. Theoretical model

in the study of the steady burning of a single fuel plate presented in ref. 4, burning is assumed to occur and be completed in a very thin flame front, which is treated as a discontinuity. Thus, the boundary layers developing from the leading edges of the plates are divided into two regions, I and II—region I consisting of fuel vapour and product of combustion, and region II consisting of oxidizer and product of combustion. (All the inert gases are here assumed to have the same properties as the product of combustion and are lumped together with the latter as one species.)

Due to the growth of boundary layers from the entrance station, the free-stream velocity u_∞ increases from u_0 as the gas flows downstream. It will be shown later that one of the interactions between two burning fuel plates is due to this increase in the free-stream velocity.

Method of Analysis

In this paper, an integral method is used to investigate some of the possible interactions between two burning plates. The integral method chosen here follows exactly the one used by TAU-YI TOONG and A. H. SHAPIRO[3] in the investigation of the frictional effects in the entrance region of a tube flow. It is assumed that, when the boundary layer is thin, its growth along the duct formed by the two plates can be approximated by that for flow over a single flat plate. In other words, the local velocity, temperature and concentration profiles in the boundary layers of two burning plates are assumed to be identical with those in the boundary layer of a single burning plate having the same free-stream conditions and at the same distance from the leading edge. The longitudinal variations of the free-stream velocity, evaporation or sublimation rate at the fuel surface and combustion rate at the flame front can then be computed by the use of the continuity equations as shown in the following sections.

One main limitation of this method is that the error introduced by the use of the profiles for flow over a single plate becomes large as the ratio of the boundary-layer thickness to the distance between the plates increases. In other words, the results become inaccurate when the two plates of given length are close to each other.

Continuity Equations

For a control volume between the entrance station 0 and any other station at a distance x therefrom, as shown in *Figure 2*, the continuity equation may be written as follows

$$\rho_0 u_0 D + 2\int_0^x \rho_w v_w \, dx = \rho_\infty u_\infty (D - 2\delta) + 2\int_0^{\delta_f} \rho_I u_I \, dy + 2\int_{\delta_f}^{\delta} \rho_{II} u_{II} \, dy \quad \ldots . [1]$$

where ρ is the mass density, u is the velocity (in x direction) along the fuel surface, v is the velocity (in y direction) normal to the fuel surface, D is the spacing between fuel surfaces, δ is the boundary-layer thickness and δ_f is the flame position. The subscripts $_0$, $_w$, $_\infty$, $_I$ and $_{II}$ refer to conditions at the entrance station, fuel surface, local free stream, and in regions I and II, respectively.

Dividing throughout by $\rho_\infty u_\infty D$, one obtains from equation 1

$$\frac{\rho_0 u_0}{\rho_\infty u_\infty} + \frac{2}{\rho_\infty u_\infty D}\int_0^x \rho_w v_w \, dx = 1 - 2\left(\frac{\delta_I^* + \delta_{II}^*}{D}\right) \quad \ldots . [2]$$

where

$$\delta_I^* \equiv \int_0^{\delta_f} (1 - \rho_I u_I / \rho_\infty u_\infty) \, dy \quad \ldots . [3]$$

and

$$\delta_{II}^* \equiv \int_{\delta_f}^{\delta} (1 - \rho_{II} u_{II} / \rho_\infty u_\infty) \, dy \quad \ldots . [4]$$

Note that the values of δ_I^* and δ_{II}^* depend only on the velocity and density distributions inside the boundary layers. Thus, according to the assumption on boundary-layer profiles stated in the previous section, under Method of Analysis, these values can be computed as follows, by the use of the velocity and density profiles in the boundary layer of a single burning plate.

In the solution of the boundary-layer flow over a single burning plate[4], one introduces a new independent variable η, such that

$$\eta \equiv \frac{1}{2x}\left(\frac{u_\infty x}{\nu_\infty}\right)^{1/2} \int_0^y \frac{\rho}{\rho_\infty} \, dy \quad \ldots . [5]$$

It can then be shown that

$$\frac{\delta_{\mathrm{I}}^*}{x}\left(\frac{u_\infty x}{\nu_\infty}\right)^{1/2}=2\int_0^{\eta_f}\left(\frac{\rho_\infty}{\rho_{\mathrm{I}}}-\frac{u_{\mathrm{I}}}{u_\infty}\right)\mathrm{d}\eta\equiv C_{\mathrm{I}} \quad \ldots.[6]$$

and

$$\frac{\delta_{\mathrm{II}}^*}{x}\left(\frac{u_\infty x}{\nu_\infty}\right)^{1/2}=2\int_{\eta_f}^{\eta_\delta}\left(\frac{\rho_\infty}{\rho_{\mathrm{II}}}-\frac{u_{\mathrm{II}}}{u_\infty}\right)\mathrm{d}\eta\equiv C_{\mathrm{II}} \quad \ldots.[7]$$

where ν is the kinematic viscosity, η_f and η_δ denote the values of η at δ_f and δ, respectively, and C_{I} and C_{II} are constants (being always positive) for a given problem.

With $\rho_\infty/\rho_{\mathrm{I}}=T_{\mathrm{I}}/T_\infty$, $\rho_\infty/\rho_{\mathrm{II}}=T_{\mathrm{II}}/T_\infty$ (for mixtures of perfect gases with constant molecular mass) and the velocity and temperature profiles derived for a single burning plate[4], one further obtains that:

$$C_{\mathrm{I}}=2\eta_f\left(\frac{T_w}{T_\infty}\right)+(f_f-f_w)\left(\frac{q\phi c_{O\infty}}{c_p T_\infty}-\frac{T_w}{T_\infty}\right) \quad \ldots.[8]$$

$$C_{\mathrm{II}}=(C_3+f_f-2\eta_f)\left(\frac{T_w}{T_\infty}+\frac{qc_{fw}}{c_p T_\infty}\right) \quad \ldots.[9]$$

where the newly introduced symbols are defined as follows:

- c mass fraction
- c_p specific heat at constant pressure
- C_3 a constant to be computed from equation 10
- f a function of η and a solution to equation 13 of ref. 4
- q heat of reaction per unit mass of fuel vapour
- q_f heat transfer required to evaporate or sublime one unit mass of fuel
- ϕ stoichiometric fuel/oxidizer ratio.

The subscript $_f$ refers to flame front, $_F$ refers to fuel vapour, and $_O$ refers to oxidizer.

It is to be noted that the quantities η_f, f_f, f_w, T_w/T_∞ and c_{fw} can be readily obtained by the use of equations 32 to 35 in ref. 4 and of solutions of f as a function of η tabulated, for example, in ref. 6. Furthermore, since the boundary condition for the function f is such that $\mathrm{d}f/\mathrm{d}\eta\longrightarrow 2$ as $\eta\longrightarrow\eta_\delta$, one obtains

$$f_\delta\longrightarrow 2\eta_\delta-C_3 \text{ as } \eta\longrightarrow\eta_\delta \quad \ldots.[10]$$

wherefrom C_3 is easily calculated with the use of tabulated values of $f(\eta)$. Thus, for a given problem, C_{I} and C_{II} can be evaluated from equations 8 and 9, and accordingly δ_{I}^* and δ_{I}^* from equations 6 and 7.

Within the aforementioned assumption on boundary-layer profiles, the second term on the LHS of equation 2 can also be evaluated by the use of the following expression derived in ref. 4 for the case of a single burning plate; viz.

$$\rho_w v_w=-\tfrac{1}{2}\rho_\infty u_\infty(\nu_\infty/u_\infty x)^{1/2}f_w \quad \ldots.[11]$$

For flow at low velocities, one may further assume that

$$\rho_o=\rho_\infty,\ T_o=T_\infty,\ \nu_o=\nu_\infty \quad \ldots.[12]$$

Thus, with equations 6, 7 and 11, equation 2 becomes

$$\frac{u_o}{u_\infty}\left[1-f_w R_{Do}^{-1/2}\int_0^{x/D}\left(\frac{u_o}{u_\infty}\frac{x}{D}\right)^{-1/2}\mathrm{d}\left(\frac{x}{D}\right)\right]=1-2(C_{\mathrm{I}}+C_{\mathrm{II}})\left(\frac{x}{DR_{Do}}\right)^{1/2}\left(\frac{u_o}{u_\infty}\right)^{1/2} \quad \ldots.[13]$$

where $R_{Do}\equiv u_o D/\nu_w$.

Equation 13 gives a relationship between u_∞/u_o and x/D. To solve this equation, one can differentiate this expression with respect to x/D and obtain*

$$\frac{\mathrm{d}(u_\infty/u_o)}{\mathrm{d}(x/D)}=\frac{(C_{\mathrm{I}}+C_{\mathrm{II}}-f_w)R_{Do}^{-1/2}\left(\frac{u_\infty}{u_o}\right)^{1/2}\left(\frac{x}{D}\right)^{-1/2}}{1-(C_{\mathrm{I}}+C_{\mathrm{II}})\left(\frac{x}{DR_{Do}}\right)^{1/2}\left(\frac{u_\infty}{u_o}\right)^{-1/2}} \quad \ldots.[14]$$

Within the assumption of thin boundary layers, the denominator of the right-hand member of equation 14 is roughly equal to one. With this approximation, equation 14 can be integrated readily to give

$$\left(\frac{u_\infty}{u_o}\right)^{1/2}\approx 1+(C_{\mathrm{I}}+C_{\mathrm{II}}-f_w)\left(\frac{x}{DR_{Do}}\right)^{1/2} \quad \ldots.[15]$$

A better approximation for (u_∞/u_o) can be obtained, if necessary, by substituting equation 15 into the denominator of the RHS of equation 14 and then graphically integrating the resulting expression.

*One can of course get the same expression by applying the continuity equation to a control volume of $\mathrm{d}x$ in length. The present approach is taken so that it runs parallel to that used in ref. 5.

As C_{I} and C_{II} are always positive due to boundary-layer growth and f_w is negative for the case with evaporation or sublimation, it is obvious from equation 15 that the free-stream velocity u_∞ increases from u_0 with increasing distance downstream of the entrance station.

Evaporation or Sublimation Rate

From equations 11 and 15, one gets

$$\frac{\rho_w v_w}{\rho_0 u_0} = -\frac{f_w}{2}\left(\frac{\nu_0}{u_0 x}\right)^{1/2}\left(\frac{u_\infty}{u_0}\right)^{1/2} = -\frac{f_w}{2R_{D_0}}\left[\left(\frac{x}{2D_{D_0}}\right)^{-1/2} + (C_{\mathrm{I}} + C_{\mathrm{II}} - f_w)\right] \quad \ldots . [16]$$

For a single burning plate with a free-stream velocity of u_0, equation 11 gives

$$\left(\frac{\rho_w v_w}{\rho_0 u_0}\right)_{\text{single plate}} = -\frac{f_w}{2}\left(\frac{\nu_0}{u_0 x}\right)^{1/2} \quad \ldots . [11a]$$

Thus

$$\frac{\rho_w v_w}{(\rho_w v_w)_{\text{single plate}}} = \left(\frac{u_\infty}{u_0}\right)^{1/2} \approx 1 + (C_{\mathrm{I}} + C_{\mathrm{II}} - f_w)\left(\frac{x}{DR_{D_0}}\right)^{1/2} \quad \ldots . [17]$$

In other words, due to an increase in the free-stream velocity, the local evaporation or sublimation rate per unit area at the fuel surface for the case of two burning plates is greater than the corresponding value for the case of a single burning plate, the excess becoming greater as the distance from the entrance station increases. For the first approximation, the excess evaporation or sublimation rate per unit plate area varies directly with the square root of the distance parameter (x/DR_{D_0}).

The mean evaporation or sublimation rate per unit plate area, $\bar{M}_w$, over a distance L at the fuel surface of one of the two burning plates is obtained by integrating equation 16 over dx. Thus

$$\frac{\bar{M}_w}{\rho_0 u_0} \equiv \int_0^1 \frac{\rho_w v_w}{\rho_0 u_0}\, \mathrm{d}\left(\frac{x}{L}\right) = -\frac{f_w}{R_{D_0}}\left[\left(\frac{L}{DR_{D_0}}\right)^{-1/2} + \left(\frac{C_{\mathrm{I}} + C_{\mathrm{II}} - f_w}{2}\right)\right] = -\frac{f_w}{R_{L_0}^{1/2}}\left[1 + \left(\frac{C_{\mathrm{I}} + C_{\mathrm{II}} - f_w}{2}\right)\left(\frac{L}{DR_{L_0}^{1/2}}\right)\right] \quad \ldots . [18]$$

where $R_{L_0} \equiv u_0 L/\nu_0$.

For plates of a given length L separated at large distances from each other, equation 18 is reduced to the following expression, which can also be obtained directly by integrating equation 11a for the burning of a single plate, viz.

$$\left(\frac{\bar{M}_w}{\rho_0 u_0}\right)_{\text{single plate}} = -\frac{f_w}{R_{L_0}^{1/2}} \quad \ldots . [19]$$

Thus

$$\frac{\bar{M}_w}{(M_w)_{\text{single plate}}} = 1 + \left(\frac{C_{\mathrm{I}} + C_{\mathrm{II}} - f_w}{2}\right)\left(\frac{L}{DR_{L_0}^{1/2}}\right) . [20]$$

Combustion Rate

For a control volume between the entrance station 0 and any other station at a distance L therefrom, the continuity equation for the fuel vapour may be written

$$\int_0^L M_f\, \mathrm{d}x = \int_0^L M_w\, \mathrm{d}x - \left(\int_0^{y_f} \rho_1 u_1 c_F\, \mathrm{d}y\right)_L \quad . . [21]$$

where M_f and M_w are, respectively, the local combustion rate at the flame front and the local evaporation or sublimation rate the fuel surface per unit plate area and the last integral is evaluated at $x = L$. By use of the expressions derived above and in the study of the burning of a single plate[4], it can be shown that

$$\frac{M_f}{M_w} = (1 - c_{Fw})\left(\frac{f_f''}{f_w''}\right) - \left[1 - (1 - c_{Fw})\left(\frac{f_f''}{f_w''}\right)\right] \times \frac{[(C_{\mathrm{I}} + C_{\mathrm{II}} - f_w)\,(L/2DR_{L_0}^{1/2})]}{[1 + (C_{\mathrm{I}} + C_{\mathrm{II}} - f_w)\,(L/2DR_{L_0}^{1/2})]} \quad \ldots . [22]$$

Again, when two plates of a given length L are separated at a large distance D, equation 22 is identical with the expression derived for the burning of a single plate. Thus

$$\frac{(M_f/M_w)}{(M_f/\bar{M}_w)_{\text{single plate}}} = 1 - \left[\left(\frac{1}{1 - c_{Fw}}\right)\left(\frac{f_w''}{f_f''}\right) - 1\right] \times \frac{[(C_{\mathrm{I}} + C_{\mathrm{II}} - f_w)\,(L/2DR_{L_0}^{1/2})]}{[1 + (C_{\mathrm{I}} + C_{\mathrm{II}} - f_w)\,(L/2DR_{L_0}^{1/2})]} \quad \ldots . [23]$$

Results

In ref. 4, the profiles of the velocity, temperature and composition in the boundary layer of a single benzene plate burning in an air stream were presented for a specific set of conditions; in particular, $f_w = -0{\cdot}90$ and $B = 7{\cdot}91$, where B is the heat ratio and is equal to

$$(c_p T_\infty + q\phi c_{O_\infty} - c_p T_w)\, q_L$$

Under these conditions, the values of C_{I} and C_{II}, given by equations 8 and 9, are 25·8 and 5·61, respectively. Assuming, as in the work of TAU-YI TOONG and A. H. SHAPIRO[5], that the present analysis is valid only in a region where the boundary-layer thickness is less than three tenths of the half-distance between the two plates, one finds that the limiting value of $(x/DR_{D_0})^{1/2}$ is 0·005 for the example chosen. At this latter value, the local evaporation rate at the benzene surface of one of the two plates is predicted from equation 17 to be sixteen per cent higher than that for a single plate.

Figure 3 shows the variation of the ratio of the *mean* evaporation rate per unit area at the surface of one of the two benzene plates to that for a single plate versus the dimensionless distance between the plates. Within the region of validity of the present work shown in *Figure 3*, the mean evaporation rate increases as the plates of a given length are brought closer together at constant conditions

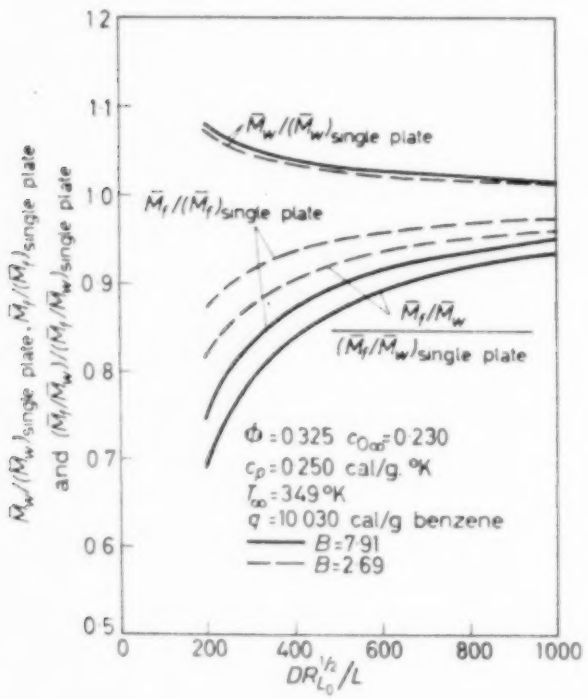

Figure 3. Variation of mean evaporation and combustion rates for one of two burning benzene plates versus distance between them

at the entrance station. Assuming that the mean evaporation rate represents in some manner the burning rate of fuel droplets, the variation shown in *Figure 3* agrees qualitatively with the experimental observations of Rex *et al.*[1], when the distance between the droplets is relatively large. These theoretical predictions are also found to agree quantitatively with the experimental results, which are to be reported in another publication.

Figure 3 also shows the effect of the heat ratio B on the ratio of the mean evaporation rates as the distance between the two plates varies. The curves shown are for two different values of B; viz. 7·91 and 2·69, which correspond to 94·7 and 279 cal/g for the values of heat transfer required to evaporate one unit mass of benzene. (Other conditions specified here are given in the legend of *Figure 3*.) Although such a decrease in B results in a 28 per cent decrease in the mean evaporation rate for a single plate, the ratio of the mean evaporation rates remains within one per cent.

Figure 3 further shows that both M_f and (M_f/M_w) decrease as the two plates are brought closer to each other. This drop in the combustion rate at the flame front, coupled with an increase in the evaporation rate, indicates that, when the spacing between two droplets burning side by side in an oxidizer stream decreases, there would be an increase in the length of the over-ventilated portion of the flames at the wake region of the droplets. (Note, however, that the upstream portion of the flames is under-ventilated.) This prediction is again found to agree well with the experimental results obtained at the M.I.T.

The effect of the heat ratio on the ratio of the combustion rates is also demonstrated in *Figure 3*. As expected, the interaction becomes less important with decreasing value of B.

Figure 4 shows the variation of the mean evaporation and combustion rates versus the distance between two benzene plates at three different values of the heat ratio. It is interesting to note that the combustion rate is less affected by a variation in B (in the range illustrated) than the evaporation rate. Thus, as the value of B increases, there is an

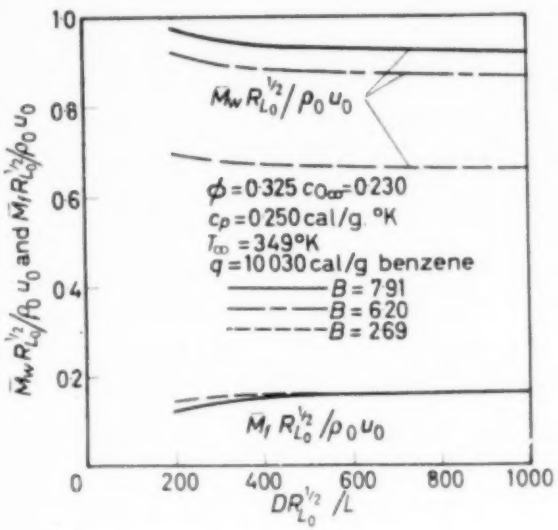

Figure 4. Variation of mean evaporation and combustion rates for one of two burning benzene plates versus distance between them

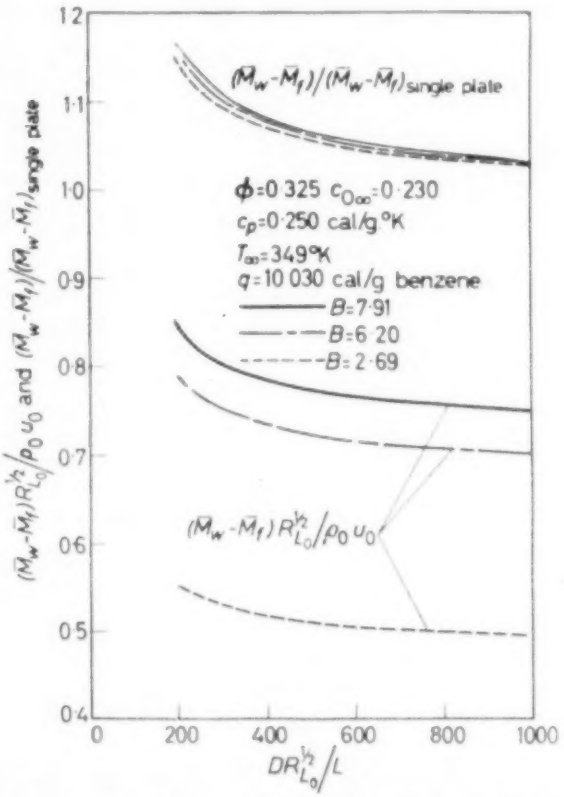
$(\bar{M}_w - \bar{M}_f)/(\bar{M}_w - \bar{M}_f)_{\text{single plate}}$
$\phi = 0.325\ c_{O\infty} = 0.230$
$c_p = 0.250$ cal/g °K
$T_\infty = 349$°K
$q = 10\,030$ cal/g benzene
$B = 7.91$
$B = 6.20$
$B = 2.69$
$(\bar{M}_w - \bar{M}_f) R_{L_0}^{1/2}/\rho_0 u_0$
$(\bar{M}_w - \bar{M}_f) R_{L_0}^{1/2}/\rho_0 u_0$ and $(\bar{M}_w - \bar{M}_f)/(\bar{M}_w - \bar{M}_f)_{\text{single plate}}$
$DR_{L_0}^{1/2}/L$

Figure 5. Variation of excess of mean evaporation rate over combustion rate for one of two burning benzene plates versus distance between them

increasing difference between the evaporation and the combustion rates, as shown in the lower part of *Figure 5*. This fact accounts for the observation in the case of burning fuel droplets that the length of the over-ventilated portion of the flames at the wake region is greatly increased with increasing value of the heat ratio. This fact further demonstrates the importance of the control and measurement of B in actual experimentation.

The upper portion of *Figure 5* shows that the relative change in the difference between the mean evaporation and combustion rates at constant values of B is rather insensitive to the variation in B. As the benzene plates are brought closer together at constant values of B, there is an increase of approximately 15 per cent in the excess of mean evaporation rate over and above the mean combustion rate at the limit of validity of the present method. However, should the value of B increase as the distance between the plates decreases, there should be a larger percentage increase in this excess.

The work reported here was partially supported by the Shell Oil Company and by the Air Force Office of Scientific Research of the Air Research and Development Command, under Contract AF49(638)-629.

References

[1] Rex, J. F., Fuhs, A. E. and Penner, S. S. *Jet Propulsion*, 1956, **26**, 179

[2] Nishiwaki, N. and Hirata, M. 'Some phenomena on the combustion of fuel droplets.' Unpublished report, 1957

[3] Kanevsky, J. N. *Tech. Rep. No. 15*, Guggenheim Jet Propulsion Center, California Institute of Technology, June 1956

[4] Toong, T. Y. *Tech. Rep. No. 8227-1*, Mechanical Engineering Department, Massachusetts Institute of Technology, 1960 or *Tech. Note No. 60-516*, Air Force Office of Scientific Research, 1960

[5] Toong, T. Y. and Shapiro, A. H. *Anniversary Volume on Fifty Years of Boundary-Layer Theory*, pp 181–192. Vieweg: Braunschweig, 1955

[6] Emmons, H. W. and Leigh, D. *Interim tech. Rep. No. 9*, Combustion Aerodynamics Laboratory, Harvard University, November 1953

A Technique for Sampling Reaction Intermediates in a Rapid Compression Machine

L. H. S. ROBLEE, Jr

Esso Research and Engineering Company, Products Research Division, Linden, New Jersey

(*Received August 1960*)

A technique devised for rapidly quenching reactions occurring in a rapid compression machine during the ignition delay period is described and the results of preliminary studies made with it are presented. The quenching device was designed and adapted to the machine to extend its utility and provide a means of studying the chemical reactions preceding autoignition. With this device preflame reactions can be arrested at any predetermined point during compression or ignition delay. Suitable techniques may then be employed to analyse the partial oxidation products. An initial investigation with the device was conducted on the stoichiometric benzene–air system. These studies confirmed the previously known fact that only a negligible amount of benzene or oxygen is consumed during the early stages of the ignition delay. Based on this finding and ignition delay time measurements, a global activation energy of ca. 11 kcal/gmole was calculated for the benzene–air reaction which may apply to the initiating steps of the reaction mechanism. The device described shows promise of being a powerful tool for following the chemical course of preflame reactions which occur at high pressure and temperature.

THE effect of various chemical and physical parameters on knock phenomena in spark-ignited engines has been studied extensively for several years. One of the most important conclusions deriving from these studies is that knock is intimately connected with reactions which occur in the combustion chamber 'end gases'. To obtain a better understanding of this phenomenon, a number of studies have been made with both motored and spark-ignited engines. Important among these studies were those in which (*a*) pressure and temperature variations during the engine cycle were measured[1–3], (*b*) chemical analyses were made of partial and complete combustion reaction products[4, 5] and (*c*) cool flames were detected in motored engines[6–8]. In all of these studies, however, the continuously changing engine conditions greatly complicate interpretation of the measurements obtained. To provide a more controllable and constant environment for the study of precombustion reactions, a number of rapid compression machines have been designed and built[9–13]. With this type of device, a combustible mixture can be rapidly compressed to a preselected and essentially constant pressure and temperature. Following compression, the fuel–air mixture undergoes reactions at constant volume which usually culminate in autoignition of the entire charge.

Previously, these machines have been used principally to record the pressure/time histories and the burning characteristics of various fuel–air mixtures. Comprehensive studies along these lines have been made by C. F. TAYLOR *et al.*[10], by J. C. LIVENGOOD and W. A. LEARY[14], and by H. RÖGENER[15]. These studies, concerned primarily with the physical aspects of autoignition, have considerably increased our knowledge of combustion phenomena. Their full significance, however, will not be realized until far more is known about the mechanism of the precombustion reactions. Although research into the chemistry of these reactions at low pressures and fairly high temperatures has been extensive, only a limited number of studies have been made at conditions of both high pressure and temperature.

Recently, a device has been designed and adapted to a rapid compression machine which provides a means of following the chemical history of the high pressure and temperature preflame reactions which occur prior to autoignition. This device and initial studies with it on the benzene–air system are described in this paper.

Experimental Procedure

Apparatus

A comprehensive description of the type of rapid compression machine used in the present work has been given in earlier papers[10, 16, 17]. With this machine, a premixed combustible mixture is adiabatically compressed to and maintained at a preselected pressure and temperature until spontaneous ignition occurs. This is accomplished by the motion of a piston in a closed-end cylinder of variable compression ratio. Through the use of high-speed strip film cameras and a rapid-response pressure transducer, traces reflecting piston motion during compression and combustion chamber pressure during and after compression are obtained. From these traces, the ignition delay time, defined as the time from the end of compression to autoignition (peak pressure), is determined.

A means of rapidly cooling (freezing) the fast gas-phase reactions which occur during the ignition delay is provided by a stainless steel expansion chamber separated from the combustion chamber by a rupturable diaphragm. A diagram and a photograph of the device are shown in *Figures 1* and *2*, respectively. In the initial studies, aluminium diaphragms have been used exclusively. The diaphragm is ruptured either through pressure buildup or by a mechanical probe. Neoprene O-rings are used for seals between the probe and expansion chamber walls. To minimize flow resistance during expansion, the probe support was machined to a thin aerofoil cross section. The catch mechanism on the spring-loaded probe is released by a solenoid which, in turn, is fired through an electronic circuit. This circuit can be preset to actuate the solenoid over a broad time range in intervals of about 0·1 msec. The end of the expansion chamber is threaded into the head of the combustion chamber and seals against an O-ring. The inside face of the combustion chamber head is recessed for the rupture diaphragm which is held in place by a metal washer and set-screw. This arrangement provides a vacuum-tight seal and facilitates diaphragm replacement. A miniature SLM Kistler pressure pickup, flush with the inside face of the combustion chamber head, is located next to the diaphragm recess.

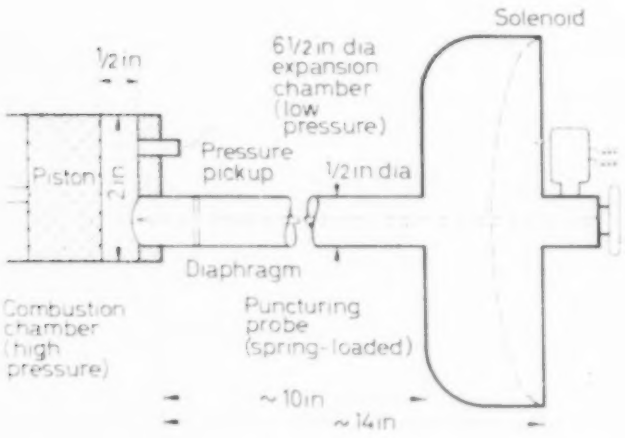

Figure 1. Pictorial diagram of quick-quench and diaphragm-rupturing apparatus

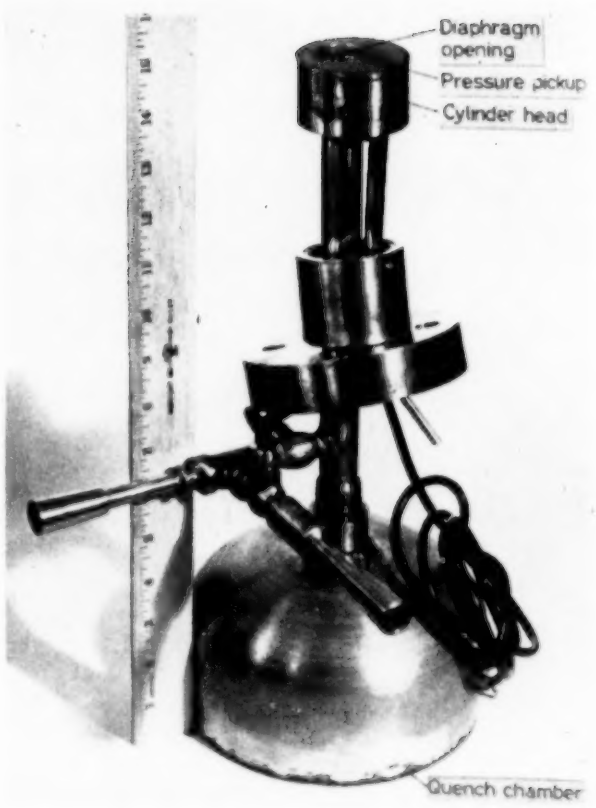

Figure 2. Quench chamber attached to rapid compression machine cylinder head

Basically, the quenching device operates on the principle of shock cooling. At the moment of diaphragm rupture, the pressure differential between the two chambers (diaphragm pressure

ratio) causes a flow of high pressure gas from the combustion chamber into the relatively low pressure gas in the expansion chamber. Within a few chamber diameters, a shock wave develops which propagates through the expansion chamber at a velocity greater than sound relative to the gases at rest in this chamber. Simultaneously, and in the opposite direction, a rarefaction wave propagates into the combustion chamber. This wave rapidly expands the reacting gases from the high pressure and temperature developed on compression to a much lower pressure and temperature. Because the expansion chamber is long relative to the combustion chamber, interaction of the rarefaction wave with the reflected shock wave occurs well into the expansion tube. This geometry provides ample time for the expansion of the high pressure, hot reacting gases. At the end of a run, the quenched reaction products are transferred from both the combustion and expansion chambers to a stainless steel coil immersed in liquid nitrogen (−196°C) where the condensate and non-condensables are stored prior to analysis.

Analytical procedure

The amount of fuel charged to the combustion chamber per run is quite small; $\sim 10^{-3}$ g depending upon the particular fuel used and fuel/air ratio. Since the combustion reactions are halted well before completion, the amount of an intermediate present in the quenched reaction products may range from 10^{-4} to 10^{-6} g or less. Using gas chromatographic techniques quite extensive qualitative analysis can be made of quenched mixtures containing a large number of intermediates in small amounts. To date, trapped reaction products have been analysed exclusively on a Perkin–Elmer Model 154-C Vapor Fractometer equipped with a thermal conductivity cell. A second, powerful technique is currently being perfected to analyse these complex mixtures. This technique combines a gas chromatographic unit with a Time-Of-Flight mass spectrometer. As a fraction elutes from the chromatographic column at a particular retention time, a mass spectrogram of the eluted material is simultaneously recorded. Thus, two analytical identifications are obtained for the same particular fraction.

Results and Discussion

Preliminary tests

The strength of the shock and rarefaction waves is determined, other factors equal, by the pressure differential across the diaphragm at the time of rupture. An increase in this ratio increases the strength of the rarefaction wave with the result that greater cooling rates can be realized during expansion. However, increasing this ratio increases the strength of the shock wave such that for sufficiently large ratios the reflected shock wave will induce further reaction in the previously quenched gases. This phenomenon is shown in *Figure 3*. This pressure/time trace was obtained when a stoichiometric benzene–air mixture reacting at 33 atm and *ca.* 1580°F (860°C) was expanded into an evacuated (4 mm of mercury, absolute) cylindrical chamber of uniform cross section rather than an expansion chamber of the type shown in *Figure 1*. For these studies and those described later in this paper, reagent grade

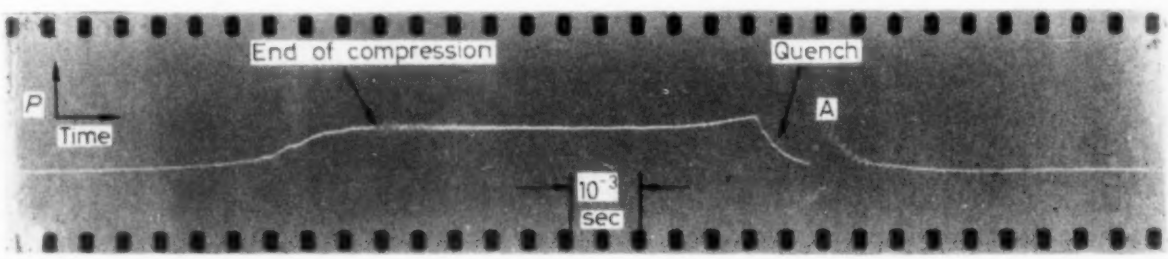

Figure 3. Pressure/time trace for stoichiometric benzene–air mixture shows additional reaction at point A after quench

benzene having a boiling range of 0·2°C including the temperature 80·1°C was used. The pressure rise marked A on the trace reflects additional reaction in the quenched mixture following the initial expansion. Three sets of experiments were made which established that the reflected shock wave caused the additional reaction after quench. In the first set of experiments, runs were made at three different diaphragm pressure ratios and the time from initial rupture to the pressure rise measured. In *Table 1*, these times are compared with those calculated[18] for the shock wave to travel the length of the expansion chamber, reflect and interact with the expanding gases.

Table 1. Time from rupture to onset of additional reaction

Run No.	*Expl time, msec*	*Calc. time, msec*	*Ratio: Calc./Exp.*
34–A	0·62	0·40	0·65
33–A	0·78	0·54	0·69
35–A	0·94	0·65	0·69

Operating conditions

Combustion chamber:
System — Stoichiometric benzene–air mixture Comp. Ratio—8·7/1; Initial pressure, 0·82 atm; Initial temp., 150°F. Specific heat ratio, 1·35.

Expansion chamber:
Helium; initial temp., 72°F; Specific heat ratio, 1·67.

Run No.	*34–A*	*33–A*	*35–A*
Initial pressure (atm.)	0·066	0·399	0·820

The close proportionality and the trend of the measured and calculated values indicates that the reflected shock wave induces further reaction after quench. Further verification is also provided by the fact that the pressure rise actually observed is much greater than the pressure which is caused by the reflected shock wave alone based on calculations. In the second set of experiments, the end of the expansion chamber was partially filled with glass wool which attenuated both the incident and reflected shock waves. In these experiments, the pressure rise following quench was observed to be considerably reduced thus providing further evidence that the reflected shock wave causes additional reaction. In the third and last set of experiments, a benzene–air mixture was slowly compressed over a two minute interval to eliminate the possibility of reaction. Then, in one case, this mixture was slowly expanded through a small hole punched in the diaphragm and, in the second case, rapidly expanded by complete rupturing of the diaphragm. In the second case, that of rapid expansion, conditions based on calculations were selected so that reaction could not be caused by the *incident* shock wave but could be by the *reflected* wave. Chromatographic analysis of each system established that reaction occurred only in the mixture which had been rapidly expanded when 25 to 30 per cent of the benzene was decomposed.

In the light of these results, experiments were conducted at lower diaphragm pressure ratios and the geometry and size of the expansion chamber modified to that illustrated in *Figure 1*. Several pure hydrocarbons including heptane, hexane and *iso*octane were tested under these conditions and fast, permanent quenches were obtained which established that preflame reactions could be arrested at any point in the ignition delay. A typical pressure/time trace, recorded for a benzene–air mixture reacting at 33·8 atm and *ca.* 2580°F (1415°C), is shown in *Figure 4*. For this run, the expansion chamber was filled with helium at 2·04 atm and 72°F (22°C). It may also be noted that although extensive studies have not been made to establish the point, it is felt that the concaved end of the expansion chamber (*Figure 1*) plays an important role in the quench process by causing divergence of the reflected shock wave and, hence, weakening the wave.

Since, to a good approximation, the rarefaction wave is isentropic, the average cooling rate during the expansion can be calculated from the pressures recorded on the pressure/time traces. For the run shown in *Figure 4*, the average cooling rate during the first 0·8 msec after rupture is *ca.* 10⁵F/sec. In the initial stage of the expansion, this rate is even greater as reflected by the larger, almost instantaneous, pressure drop at the start of rupture.

Benzene studies

Various researches[9,15,19] have measured the effect of temperature on ignition delay at a

constant pressure level. A summary of this work has recently been made by L. S. ECHOLS *et al.*[20]. Based on these measurements global activation energies, E, have been determined using the relationship

$$\delta_0 = A \exp(E/RT) \quad \ldots . [1]$$

where δ_0 is the delay measured from the end of compression to the first detectable pressure rise, A is a constant, E is the global activation energy, R is the universal gas constant and T is the absolute temperature. In the development of this equation, several assumptions are made and these have been discussed in detail by A. BECKERS and W. J. LEVEDAHL[21,22]. One important assumption of this equation is that the extent of fuel and oxidant consumption during δ_0 are negligible. Studies recently made with the device described here have shown that many hydrocarbons, e.g. heptane, hexane and *iso*octane, are extensively oxidized very early in the ignition delay period. For such systems, an activation energy computed from equation 1 would appear to be of doubtful significance. Previous studies have indicated, however, that benzene–air mixtures are quite resistant to oxidation and, therefore, would constitute a system to which equation 1 would apply. Accordingly, two series of experiments were conducted: (*1*) quench of a reacting stoichiometric benzene–air mixture at the end of δ_0 followed by analysis to determine the extent of preflame reaction, and (*2*) measurement of delay, δ_0, for the same system as a function of temperature. These studies are described below.

Benzene quenching studies

To establish the extent of benzene preflame reaction during δ_0 and thereby determine the applicability of equation 1 to this system, various experiments were made in which reacting stoichiometric benzene–air mixtures were quenched at the end of δ_0. The quenched reaction products were collected in the cold trap and subsequently analysed on the vapour fractometer. Within the analytical accuracy of the fractometer ($\sim$3 per cent), no fuel or oxygen consumption could be detected. Thus, since the concentration of fuel and oxidant are essentially constant during δ_0, the major assumption made in developing equation 1 is satisfied. Consequently, the applicability of equation 1 to the benzene system is reasonably assured.

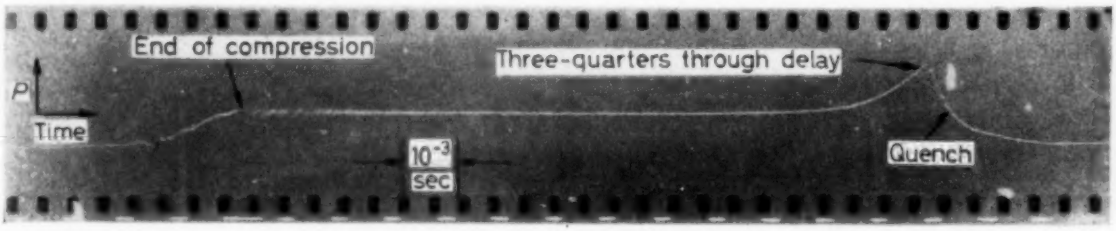

Figure 4. Pressure/time trace shows quench of reacting stoichiometric benzene–air mixture at point three-quarters through delay

Benzene delays

Operating at conditions giving a peak compression pressure of 19 atm, a set of runs was made over the temperature range 800°F (427°C) to 900°F (482°C) from which delays, δ_0, to the first detectable pressure rise were measured. These conditions were essentially the same as those used in the quenching studies. Using equation 1, an Arrhenius plot was made of the logarithm of delay against the reciprocal temperature. The slope of the straight line obtained from this plot is equal to E/R and was determined to be *ca.* 5 500°K. This value corresponds to a global activation energy of 11·0 kcal/gmole and agrees well with previously reported values of 11·6 and 12·4 kcal/gmole[19,21]. Photographs of the benzene system made at the MIT[19] using a rapid compression machine equipped with a quartz window have shown that inflammation appears as a series of bright spots distributed at random throughout the combustion chamber from which flame propagation spreads. Because these ignition centres first

appear near the end of δ_0, the activation energy calculated in this investigation may well apply to those reactions which initiate the first ignition centres.

Concluding Remarks

Preliminary tests have been satisfactory with a device which provides a means of rapidly cooling the high pressure and temperature reactions occurring in a rapid compression machine during the ignition delay period. The device promises to be a powerful tool for studying the kinetics and especially the mechanism of fast gas-phase reactions under severe pressure and temperature conditions. An initial investigation with this equipment on the benzene–air system has confirmed the previously known fact that during the early stages of the ignition delay, a negligible amount of benzene or oxygen is consumed. Based on this finding and ignition delay time measurements, a global activation energy of *ca.* 11 kcal/gmole was calculated for the benzene–air reaction which may apply to the initiating steps of the reaction mechanism.

The author wishes to thank Esso Research and Engineering Company for permission to publish this paper. He also expresses his appreciation to J. F. Kunc and H. L. Yowell for their help and valuable suggestions in the preparation of this manuscript.

References

[1] Livengood, J. C., Taylor, C. F. and Wu, P. C. *S.A.E. quart. Trans.* 1958, **66**, 683
[2] Pastell, D. L. *S.A.E. quart. Trans.* 1950, **4**, 571
[3] Rifkin, E. B., Walcutt, C. and Betker, G. W. *S.A.E. Jl.* 1952, **60**, 50
[4] Downs, D., Walsh, A. D. and Wheeler, R. V. *Proc. Roy. Soc. A*, 1951, **243**, 463
[5] Pahnke, A. J., Cohen, P. M. and Sturgis, B. M. *Industr. Engng Chem. (Industr.)*, 1954, **46**, 1024
[6] Agnew, W. G., Agnew, J. T. and Wark, W. *Fifth Symposium (International) on Combustion*, p 766. Reinhold: New York, 1955
[7] Downs, D., Street, J. C. and Wheeler, R. W. *Fuel, Lond.* 1953, **32**, 279
[8] Wentworth, J. T. and Daniel, W. A. *S.A.E. Jl*, August 1955, **63**, 55
[9] Jost, W. *Third Symposium on Combustion*, p 423. Williams and Wilkins: Baltimore, 1949
[10] Taylor, C. F. *et al.* 'The ignition of fuels by rapid compression'. *S.A.E. quart. Trans. April* 1950, **4**, No. 2, 232
[11] Teichmann, von H. *Z. Elektrochem.* 1941, **47**, No. 4, 297
[12] Tizard, H. T. and Pye, D. R. *Phil. Mag.* 1922, **44**, Ser. VI, No. 259, 79 and 121
[13] Tizard, H. T. and Pye, D. R. *Phil. Mag.* 1926, **1**, Ser. VII, No. 5, 1094
[14] Livengood, J. C. and Leary, W. A. 'Autoignition by rapid compression'. *Industr. Engng Chem. (Industr.)*, 1951, **43**, 2797
[15] Rögener, H. 'The ignition of a hydrocarbon–air mixture through adiabatic compression'. *Z. Elektrochem.* 1949, **53**, 389
[16] Draper, C. S. and Li, Y. T. *J. Inst. aeronaut. Sci.* 1949, **16**, No. 10
[17] Jovellanos, J. V., Taylor, E. S., Taylor, C. F. and Leary, W. A. *Tech. Note Nat. Adv. Comm. Aero., Wash., No. 2127*, June 1950
[18] Shapiro, A. H. *The Dynamics and Thermodynamics of Compressible Fluid Flow*, Vol. I. Roland: New York, 1954
[19] Rifkin, E. B. *The Role of Physical Factors in Knock*. A.P.I. Division of Refining, Los Angeles, California, 12 May 1958
[20] Echols, L. S., Yust, V. E. and Bame, J. L. 'A review of research on abnormal combustion phenomena in internal combustion engines'. *1959 Fifth World Petroleum Congress*, New York, 30 May 1959
[21] Beckers, A. and Levedahl, W. J. 'Mechanism of autoignition in benzene–air mixtures'. *Industr. Engng Chem. (Industr.)*, 1956, **48**, 411
[22] Levedahl, W. J. *Fifth Symposium (International) on Combustion*, p 372. Reinhold: New York, 1955

Chronology and Topography of Sparks at Minimum Energy for Ignition

E. L. LITCHFIELD

Explosives Research Laboratory, Bureau of Mines, U.S. Department of the Interior, Pittsburgh, Pa

(Received August 1960)

Microsecond exposure schlieren observations of ignition kernels and developing flames are reported for a set of minimum energy conditions holding for electrostatic spark ignition of 8·5 per cent methane–air mixtures at 0·1 atmosphere initial pressure. Time of appearance of a flame and the extent of influence of the shock wave generated by the electric discharge were determined experimentally. A time of appearance investigation has also been reported by Lintin and Wooding; their mixtures were at one atmosphere initial pressure. Comparison of the two results then gives an estimate of the effect of pressure upon time of appearance. This investigation indicates that the time of appearance of the flame varies inversely with initial pressure and also indicates that only a small portion of the original stored energy is caused to be dissipated outside the ignition kernel as a consequence of the shock wave.

Introduction

THE purposes of this investigation were (*1*) to estimate the time (and size) at which the developing ignition kernel could reasonably be considered to have the attributes of a self-propagating flame, (*2*) to estimate the wasteful dissipation of energy by the shock wave resulting from the spark discharge. Additional knowledge in these two areas should be helpful in delineating the individual processes involved in spark ignition.

Experimental Procedures and Techniques

The basic experimental observation was a single-frame microsecond-exposure schlieren photograph of the developing ignition kernel. The schlieren system was a conventional one which used a single pass of a light beam through the mixture. A long-focal-length mirror was the objective for an *f*2 Biotar that recorded schlieren formed from a knife edge. Recording was on 35 mm Microfile film, used because of its fine grain characteristics and the limited image size obtainable with the available equipment. The photographs show both the spark in the bomb and selected subsequent schlieren activity.

Photographic exposure time was controlled by the backlighting source. Several different lighting sources were used, including air sparks in capillary tubes. In those instances where exposure time was a critical consideration, the light source was an E.G. and G. type FX-11 flash tube operated from 0·0075μF at 11 kV through a 5C22 switch. The light duration has not been adequately established for this source, but it certainly does not exceed 0·8μsec. There is some evidence that the effective duration does not exceed 0·1 μsec under the operating conditions.

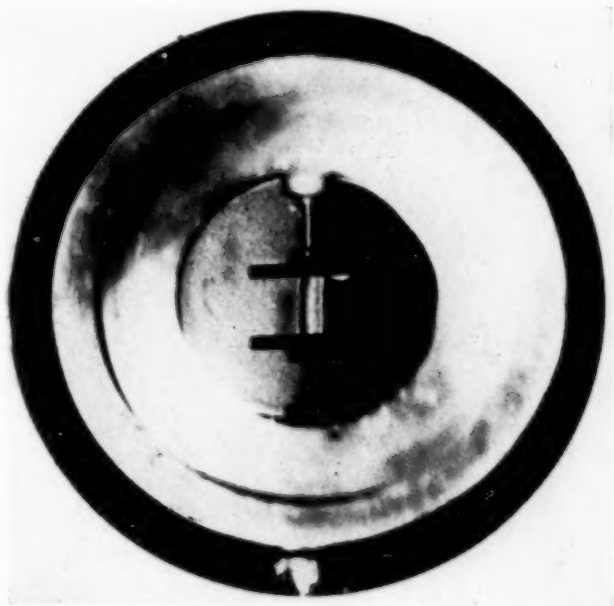

Figure 1. Photograph of bomb showing location of pressure 76 mm Hg. Spark energy 40 mJ

The combustible mixtures were 8·5 per cent methane in air contained in a brass bomb at a pressure of 76 mm of mercury absolute (*Figure 1*). The electrodes were of the conventional glass flanged type[1, 2]; the flanges were 1 in. in diameter in this investigation. The electrode gap in the bomb was set at either slightly more (0·63 in.) or slightly less (0·60 in.) than the quenching distance, depending upon whether or not the flame was intended to propagate throughout the bomb. The results justify this procedure; kernel sizes from sparks in air alone, from quenched ignitions, and from ignitions that failed at gaps greater than the quenching gap are indistinguishable at early stages of the ignition processes.

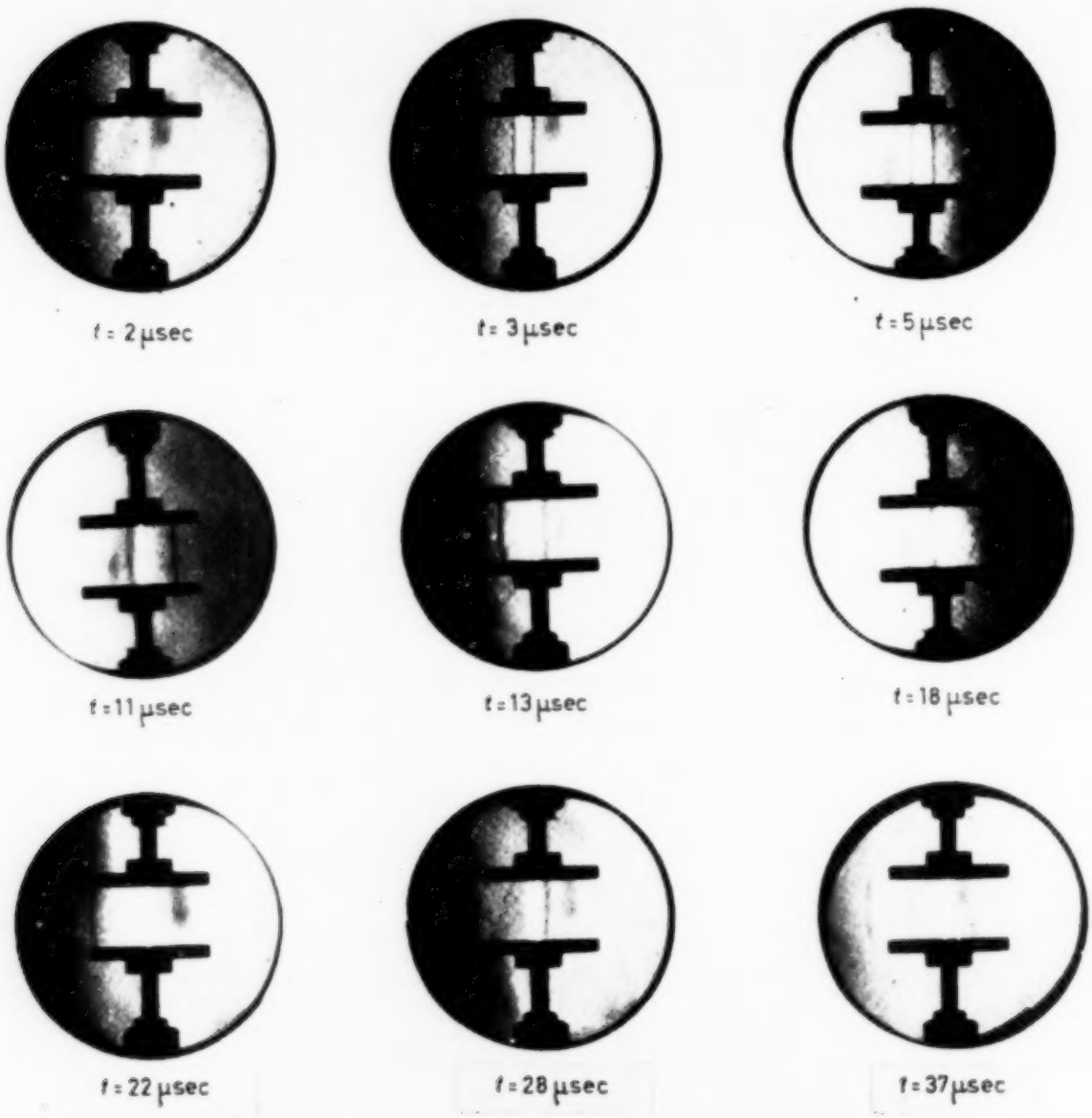

Figure 2. Early time phenomena associated with sparks and showing the development of the compression wave. 8½ per cent methane–air at 0·1 atm. Electrode separation approximately 2 in. Stored energy approximately 40 mJ. Numbers represent delay in microseconds between spark in mixture and backlight framing spark

The spark in the bomb was produced from a condenser charged to an appropriate voltage and discharged through a hydrogen thyratron. This system[3,4] produces ignitions at the same energy level as the older static breakdown technique[1,2] and offers considerable simplification through synchronization techniques. For intervals of 50 μsec or less, the time interval between triggering of the bomb spark and triggering of the backlight was monitored with a photocell and oscilloscope. At separations in excess of 50 μsec, the time interval was generated by a Tektronix 162 Waveform Generator with 161 and 163 pulse generators and was not monitored. For time intervals of less than 10 μsec, the error in interval determination is not more than 0·3 μsec. For time intervals between 10 and 50 μsec, the error is not in excess of 3 μsec. For intervals in excess of 50 μsec, the time error is less than 10 per cent.

Experimental Results and Discussion

A typical sequence of photographs is shown in *Figure 2*. It may be noted that 2 μsec after initiation of the spark there is no schlieren indication of any sort of activity. However, 3 μsec after passage of the spark, the original spark channel is surrounded by a strong schlieren outline, the diameter of which is approximately four to five times that of the original spark. These observations regarding time of appearance of schlieren phenomena need some qualification. At times between 2 and 3 μsec, very faint outlines can be perceived around the spark; it is even possible that the size of the outline is growing with a velocity of approximately Mach 2. These outlines are at the extreme limit of sensitivity of the schlieren system, whereas the outlines appearing at 3 μsec are very well defined when observed with the same schlieren system. The photographs published by K. R. Allen and K. Phillips[5] suggest that this very early behaviour may be due to an electron-range phenomenon but there is no conclusive evidence.

In the interval from 3 to 8 μsec after the spark, the schlieren outline thickens and expands rather rapidly. After about 8 μsec it becomes clear that a compression wave is propagating outward and that a contact surface remains behind. The diameter of the contact surface is approximately the diameter of the original schlieren outline.

The expansion velocity of the outer portion of the schlieren outline appears to be constant at about Mach 1·4 within the period of 3 to 8 μsec. The maximum indicated velocity is the Mach 2 already mentioned. The velocity then degrades rapidly to about Mach 1 at 10 μsec and later. Estimates of this latter velocity lie between the reasonable extremes of 350 and 405 m/sec, with a best estimate of about 385 m/sec. Sonic velocity is about 350 m/sec. The agreement between this best estimate and the anticipated value is within expectations from the data set and the claimed accuracy. The fact that there is no velocity decay over the region of observation indicates that the wave was almost certainly Mach 1.

The shock trajectory permits an estimate of thermodynamic conditions immediately behind the shock and of the pressure driving the shock. Approximate calculations, treating methane as air, indicate driving pressures of about twice the ambient pressure for the period of 3 to 8 μsec. (Even with a Mach 2 condition the driving pressure ratio would not exceed 5.) The corresponding temperatures behind the compression wave (due to the compression) would be less than 60°C above ambient. (For the extreme case of Mach 2 the temperature would be 200°C.) There is little to be concluded directly regarding the state enclosed within the contact surface except that the pressure here is compatible with the driving pressure and becomes approximately the ambient pressure after 10 μsec. On the other hand, the original stored energy would produce a uniform temperature of 300° to 400°C within the quenching volume usually considered (which is considerably larger than either the contact surface volume or the volume influenced by the supersonic wave).

Figure 3 shows a sequence of photographs from one combustible mixture which was prevented from igniting by deliberately using a reduced energy until the last exposure. Although the hour-glass shape of the developing kernel is not necessarily typical, non-cylindrical out-

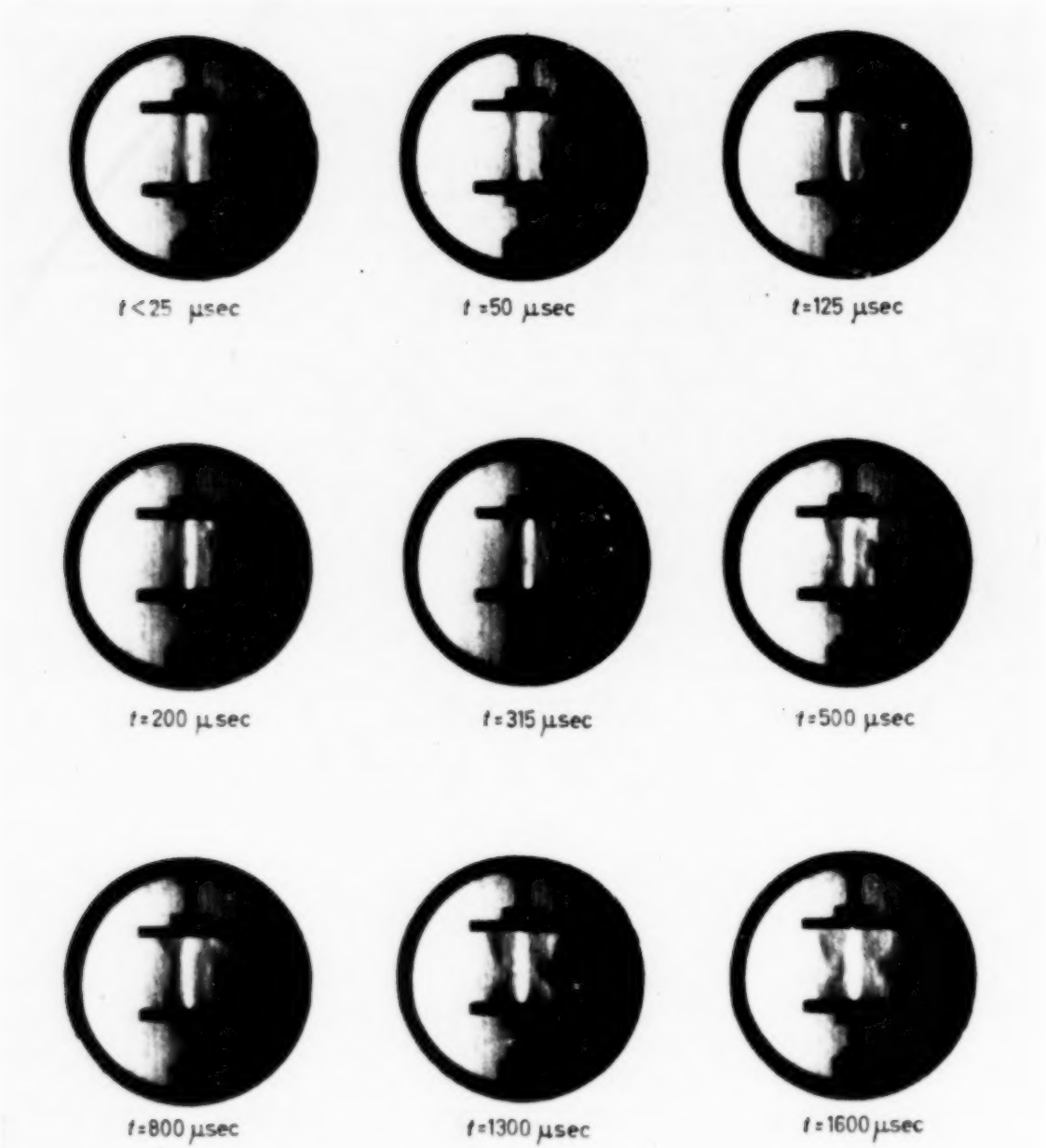

Figure 3. Phenomena associated with sparks in a combustible gas mixture. 8½ per cent methane–air at 0·1 atm. Electrode separation approximately $\frac{1}{8}$ in. Stored energy approximately 30 mJ. Numbers represent delay in microseconds between spark in mixture and backlight framing spark

lines do appear rather frequently and *Figure 3* shows one form that they may assume. It also shows the reproducibility of such non-cylindrical forms, as each of the photographs is from a different spark within the mixture. Outlines such as these may well be associated with certain electrode imperfections such as roughness and pitting.

Figure 4 is a plot of measurements from the photographs that have been obtained. Measurements resulting from sparks in air only, and from both ignitions and non-ignitions of the combustible methane–air mixtures, are included. There is no clear delineation of the data points at times of 1 msec or less. Extrapolation of the data might suggest that the

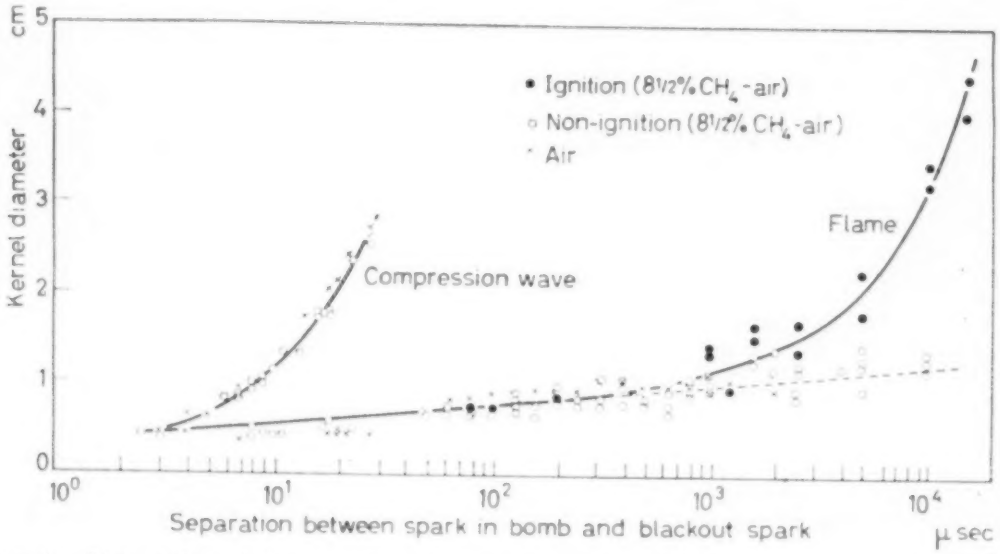

Figure 4. Plot of kernel diameter versus time for 8½ per cent methane–air mixtures. Initial pressure 76 mm Hg. *Spark energy 40 mJ*

ignition and non-ignition points begin to separate at times of 0·5 to 0·7 msec, but the clear physical separation is not apparent until times of about 1 msec.

Two other observations are of some interest. The kernel size at which appearance of the flame can be detected is effectively the size of the region affected by the original Mach 1·4 wave. Typically, the volume at this time is about four times the original volume of the contact surface.

In *Figure 4* the kernel radius is satisfactorily represented as a linear function of the logarithm of the time for a considerable range of times. These times extend effectively from the instant of separation of the shock wave to the instant where there is a recognizable flame, or to even longer times in the cases where ignition does not occur. The exponential variation is not particularly surprising as it must be a representation of thermal diffusivity, but the range of applicability of the representation and the particular value of the slope are perhaps unexpected.

Assuming the indicated straight line to be a satisfactory representation of the data, it is easy to compute bubble expansion velocity as a function of time. It is then noted that a propagating flame is not observed at least until the bubble expansion velocity has fallen to the normal flame speed. This is an interesting result and raises the rather thorny question of whether, under these circumstances, one observes a time of ignition or only a time of emergence of the flame front from the decelerating ignition kernel.

There are other possible criteria for ignition beyond the one of physical size discussed in preceding paragraphs. In the interval from about 30 μsec to about 100 μsec after the spark, the schlieren outlines tend to lose their initial sharpness. This is probably due in part to dissolution of the contact surface (i.e. thermal diffusivity). At about 100 μsec, rather sharp outlines again appear which are similar to the outlines typical for a combustion wave. However, these gradients appear irrespective of whether ignition occurs or even of whether there is a combustible mixture in the bomb. This behaviour is almost certainly an expression of thermal diffusion, and the persistence of these outlines is rather surprising. They have been observed for as long as a second after passage of the spark.

At about 0·7 msec after the spark, a quantitative difference in this wave structure distinguishes the ignitions from the non-ignitions. With sufficient space resolution, the schlieren boundary of the kernel exhibits a wavelike characteristic. For non-ignitions this wave tends to flatten as though heat conduction outward

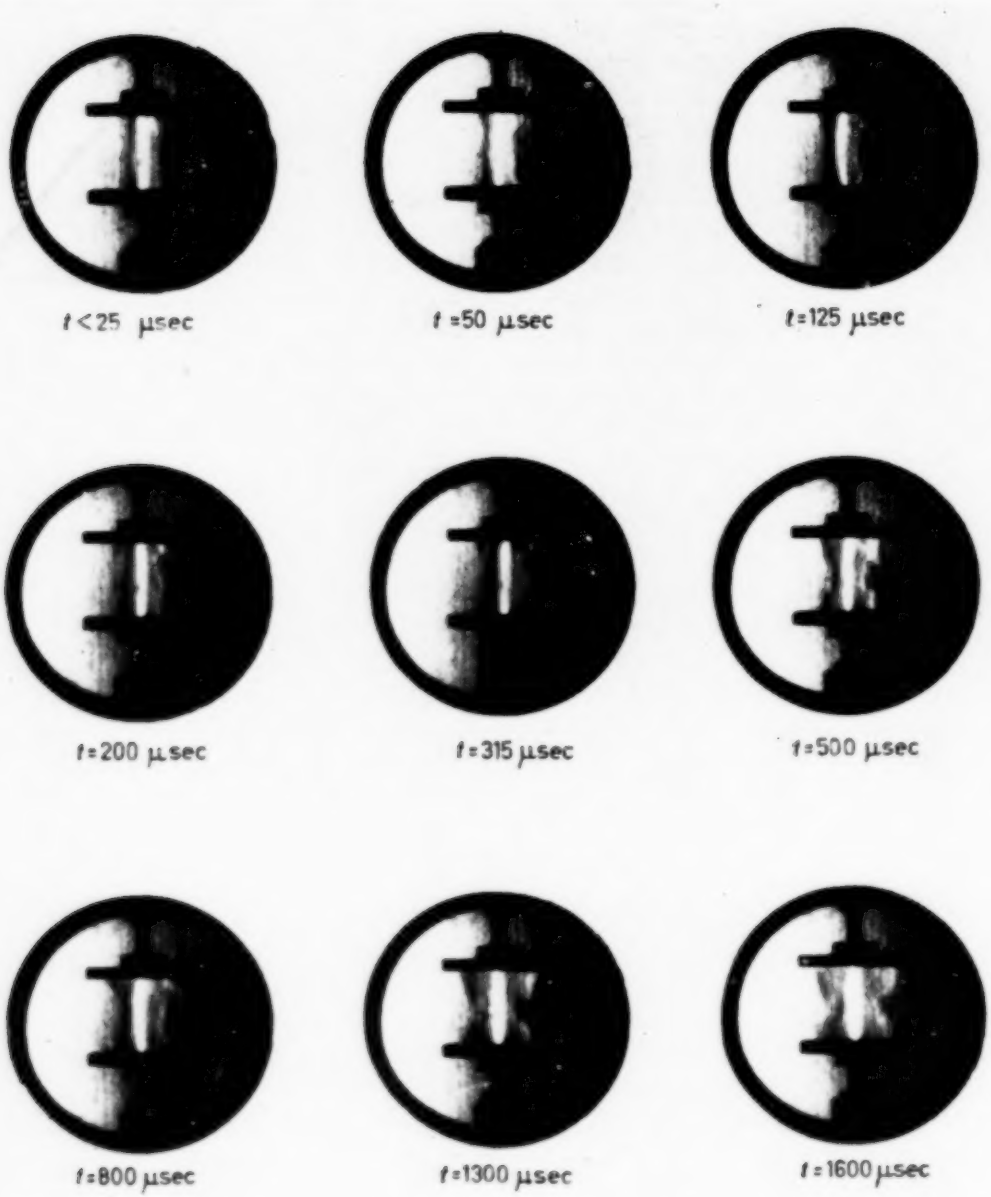

Figure 3. Phenomena associated with sparks in a combustible gas mixture, 8½ per cent methane-air at 0·1 atm. Electrode separation approximately ¾ in. Stored energy approximately 30 mJ. Numbers represent delay in microseconds between spark in mixture and backlight framing spark

lines do appear rather frequently and *Figure 3* shows one form that they may assume. It also shows the reproducibility of such non-cylindrical forms, as each of the photographs is from a different spark within the mixture. Outlines such as these may well be associated with certain electrode imperfections such as roughness and pitting.

Figure 4 is a plot of measurements from the photographs that have been obtained. Measurements resulting from sparks in air only, and from both ignitions and non-ignitions of the combustible methane-air mixtures, are included. There is no clear delineation of the data points at times of 1 msec or less. Extrapolation of the data might suggest that the

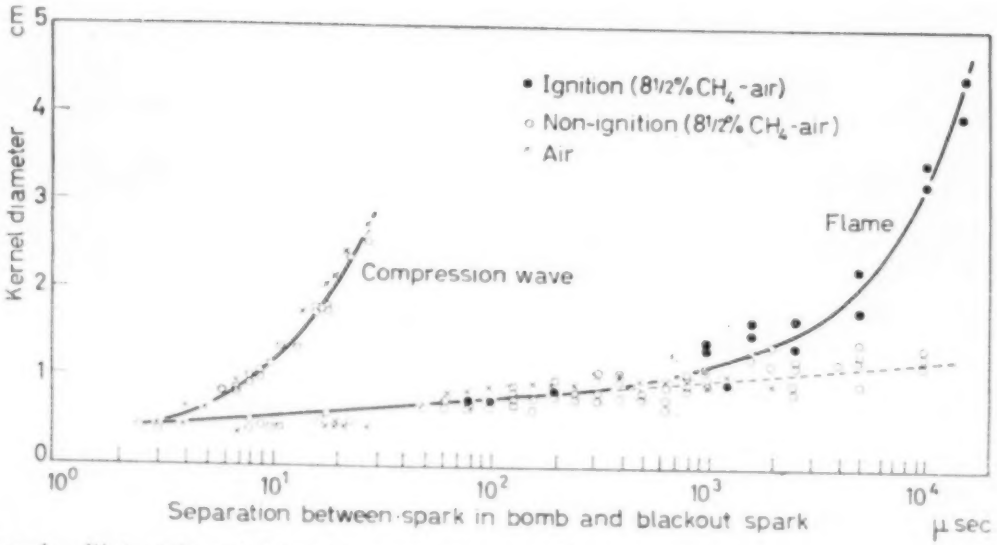

Figure 4. Plot of kernel diameter versus time for 8½ per cent methane–air mixtures. Initial pressure 76 mm Hg. *Spark energy 40 mJ*

ignition and non-ignition points begin to separate at times of 0·5 to 0·7 msec, but the clear physical separation is not apparent until times of about 1 msec.

Two other observations are of some interest. The kernel size at which appearance of the flame can be detected is effectively the size of the region affected by the original Mach 1·4 wave. Typically, the volume at this time is about four times the original volume of the contact surface.

In *Figure 4* the kernel radius is satisfactorily represented as a linear function of the logarithm of the time for a considerable range of times. These times extend effectively from the instant of separation of the shock wave to the instant where there is a recognizable flame, or to even longer times in the cases where ignition does not occur. The exponential variation is not particularly surprising and must be a representation of thermal diffusivity, but the range of applicability of the representation and the particular value of the slope are perhaps unexpected.

Assuming the indicated straight line to be a satisfactory representation of the data, it is easy to compute bubble expansion velocity as a function of time. It is then noted that a propagating flame is not observed at least until the bubble expansion velocity has fallen to the normal flame speed. This is an interesting result and raises the rather thorny question of whether, under these circumstances, one observes a time of ignition or only a time of emergence of the flame front from the decelerating ignition kernel.

There are other possible criteria for ignition beyond the one of physical size discussed in preceding paragraphs. In the interval from about 30 μsec to about 100 μsec after the spark, the schlieren outlines tend to lose their initial sharpness. This is probably due in part to dissolution of the contact surface (i.e. thermal diffusivity). At about 100 μsec, rather sharp outlines again appear which are similar to the outlines typical for a combustion wave. However, these gradients appear irrespective of whether ignition occurs or even of whether there is a combustible mixture in the bomb. This behaviour is almost certainly an expression of thermal diffusion, and the persistence of these outlines is rather surprising. They have been observed for as long as a second after passage of the spark.

At about 0·7 msec after the spark, a quantitative difference in this wave structure distinguishes the ignitions from the non-ignitions. With sufficient space resolution, the schlieren boundary of the kernel exhibits a wavelike characteristic. For non-ignitions this wave tends to flatten as though heat conduction outward

from the boundary were ending. However, for ignitions the wave sharpens as though a new heat source were operating to enhance conduction. This attribute encourages a belief that the kernel actually becomes a flame at about this time. Because of reproduction difficulties, these particular characteristics have not been illustrated with photographs.

The observed time of appearance of schlieren phenomena is 2 to 3 μsec after the spark and may be compared with the 0·25 to 0·50 μsec given by H. L. Olsen *et al.*[6] for sparks in air at atmospheric pressure. These times compare inversely as the pressures, as would be anticipated if this is a representation of a vibrational or thermal relaxation mechanism.

Comparison of the times required for separation of the shock waves is not necessarily significant since the stored energies used by Olsen *et al.* were many times greater than the appropriate minimum energy. However, such a comparison is between 2 μsec from Olsen *et al.*[6] and something between 3 and 8 μsec from this work. The ratio of these times is not a good approximation to the inverse ratio of initial pressures. The failure of the time ratio to correspond to the pressure ratio may reasonably be attributed to the relative excess of ignition energy in the work of Olsen.

Comparative times for clear appearance of the flame are 1 msec from this work and 100 μsec in the work of D. R. Lintin and E. R. Wooding[7]. Since Lintin and Wooding worked at atmospheric pressure, the times compare inversely as the initial pressures.

Assuming a similarity between the spark ignition processes for the various straight-chain hydrocarbons, it is significant that the time for the clear appearance of the flame in this investigation is definitely in excess of the upper limit estimated by J. S. Arnold and R. K. Sherburne[5]. (Their estimated critical time is about the same for all straight-chain hydrocarbons and is about twice the value obtained by Lintin and Wooding.) This is another indication that the time of appearance of the self-propagating flame is indeed pressure-dependent.

In the experimental situation discussed here it is possible to obtain adequate estimates of the shock trajectory. This shock trajectory permits a simple calculation of an upper limit on the amount of pressure energy transferred from the initial discharge channel to the kernel considered. An upper limit results because the driving energy of this decaying shock must be derived in part from the elements that have been shocked earlier. If we take the kernel size to be that of the region where the velocity is greater than Mach 1, the energy involved in the compression is less than 30 per cent of the original stored energy*. Since an appreciable portion of this energy is external to the contact surface, practically all of this energy might be considered as lost to the significant aspects of ignition. This is not necessarily correct, as the situation would always be favourable to later reduction of thermal diffusion; if all of this compression energy is lost (or if only 30 per cent[8, 9] to 80 per cent[10] is lost) the total energy involved in this aspect of the phenomena is only a small fraction of the original stored energy. (It must be admitted that there is at present no clear evidence that an amount of energy greater than that represented in the pressure energy is made available under these circumstances through conversion of the stored energy. The experimental work showing high utilization efficiencies was accomplished with noble gases. Extension of this work to argon, or the extension of the work of others to this combustible mixture, would be required to establish this. However, the time distribution of the derivation of the pressure energy and the rather extensive evidence of thermal diffusion provide some basis for belief that the overall efficiency of energy conversion certainly exceeds the 30 per cent or 5 per cent cited in earlier paragraphs for pressure equilibration processes.)

Conclusions

The significant aspect of this work is that one observes a rather weak shock which propagates at an effectively constant velocity over most of the affected region and which dissipates a

*Thirty per cent is computed on the basis of an assumed constant Mach 2 velocity and an assumed kernel size greater than that size actually occurring—a more reasonable value is 5 per cent, which is still ample.

relatively small portion of the original stored energy. Rather than an instantaneous source of heat and pressure energy, as assumed by Olsen[6,9] and by Edmonson *et al.*[10], a time distribution of the source energy is indicated. This time distribution of the energy source almost certainly arises from relaxation phenomena.

It is impossible at present to associate an energy with the sonic wave in a fashion that will be satisfactory to all. It might be anticipated that the energy associated with the sonic wave would not exceed the energy available from pressure equilibration. This, of course, is the estimate given above.

The determinations of time, size and shape of the flame in its initial stages, together with the time/pressure dependence of such appearance, have considerable practical potential value. However, additional work with other mixtures and geometries is required to demonstrate ability to interpret such results properly.

There is no actual discrepancy between the results discussed in this paper and those of Olsen[6,9] and of Edmonson *et al.*[10]. Differences are entirely attributable to differences in energy in the initial assumptions, and to the gases used. It is quite possible that the relatively great differences in spark energy levels have a significant bearing upon the results.

References

[1] Blanc, M. V., Guest, P. G., von Elbe, G. and Lewis, B. *J. chem Phys.* **1947**, **15**, 798

[2] Lewis, B. and von Elbe, G. *Combustion, Flames and Explosions of Gases.* Academic Press: New York, **1951**

[3] Litchfield, E. *Rep. Invest. U.S. Bur. Min. No. 5671*, **1960**

[4] Litchfield, E. L. *Rev. sci. Instrum.* **1960**, **31**, 572

[5] Allen, K. R. and Phillips, K. *Rev. sci. Instrum.* **1959**, **30**, 230

[6] Olsen, H. L., Edmonson, R. B. and Gayhart, E. L. *J. appl. Phys.* **1952**, **23**, 1157

[7] Lintin, D. R. and Wooding, E. R. *Brit. J. appl. Phys.* **1959**, **10**, 159

[8] Arnold, J. S. and Sherburne, R. K. *Fourth Symposium (International) on Combustion*, pp 139–43. Williams & Wilkins: Baltimore, **1953**

[9] Olsen, H. L., Gayhart, E. L. and Edmonson, R. B. *Fourth Symposium (International) on Combustion*, pp 144–48. Williams & Wilkins: Baltimore, **1953**

[10] Edmonson, R. B., Olsen, H. L. and Gayhart, E. L. *J. appl. Phys.* **1954**, **25**, 1008

Effect of Temperature on the Ignition Characteristics of Hydrocarbons

K. C. SALOOJA

'Shell' Research Ltd, Thornton Research Centre, P.O. Box 1, Chester

(Received August 1960)

The ignition lag/temperature relationship and the effect of fuel–air composition on this relationship have been investigated for n*-heptane, methylcyclohexane,* isooctane*, diisobutylene, benzene and ethylbenzene, from temperatures near their minimum ignition points to 800°C. Marked changes in the ignition characteristics have been shown to occur with increasing temperature. In general, as the temperature is increased* (i) *ignition lag decreases,* (ii) *the slope of ignition lag/temperature relationship becomes less steep, and* (iii) *the marked effect of fuel–air composition observed near the minimum ignition point decreases and eventually tends to disappear. Although the general trend of behaviour of different hydrocarbons with increasing temperature is similar, there are usually marked differences amongst them with respect to the above characteristics at all temperature levels. This often results in a change in the order of relative susceptibility to ignition of the different fuels at higher temperatures. The results obtained, while indicating the general pattern of transition in ignition characteristics from lower temperatures to higher temperatures, help in coordinating some of the diverse observations of early investigators.*

Introduction

STUDIES of the chemical reaction rates in flames are of both practical and theoretical interest. Considering that chemical factors were rate-controlling in continuous flow engines, such as gas turbines and jet engines, B. P. MULLINS[1], R. E. MILLER[2], and R. S. BROKAW *et al.*[3] have carried out fundamental investigations on the ignition lags of fuels; the ignition lag being regarded as a convenient index of the overall reaction rate responsible for ignition.

Among the early investigators Mullins has made the most extensive study of the ignition characteristics. Moreover, he alone has so far investigated the ignition lags of liquid hydrocarbons which typify the constituents of practical fuels.

Mullins measured the ignition lags in a 6 in. metal duct in which fuel was injected into a high velocity air stream heated by burning a small quantity of fuel in an upstream slave combustor. The ignition lag was measured from the distance between the fuel injector and the position at which a stable flame front was formed in the duct, together with the known air velocity.

In such a system lags can be affected by the presence of the flame front. Furthermore, temperature and oxygen concentration cannot be varied independently; at the higher temperature the oxygen mole fraction is lower while carbon dioxide and water concentrations are increased. Finally, the fuel/air ratios may vary across the duct and in the preflame region, so that the exact composition at the moment of ignition is unknown.

The ignition lag measurements of Mullins extended from *ca.* 750°C to *ca.* 1 100°C. One of the surprising results of his studies was that fuel concentration had no effect on the ignition lag. Brokaw *et al.*, who determined the ignition lags of propane from 524° to 738°C in an apparatus where most of the shortcomings of Mullins's techniques were overcome, found, however, that increasing fuel concentration markedly decreased the ignition lag. A similar effect of fuel concentration on the ignition lag/temperature relationship has been observed by the author[4] for a variety of hydrocarbons near their minimum ignition points.

The object of the present studies was to investigate the ignition characteristics of fuels from temperatures near their minimum ignition points upwards. The method used was in some ways similar to that of Brokaw *et al.* The hydrocarbons examined were selected from

different structural categories and included *n*-heptane, methyl*cyclo*hexane, *iso*octane, di*iso*-butylene, benzene and ethylbenzene. In this paper the results are presented on their ignition characteristics up to 800°C.

Experimental

The details of the equipment will be described elsewhere. Briefly, the studies were carried out in a silica tube which was 3 cm in diameter and 25 cm in length. A nitrogen stream carrying the fuel vapour and an oxygen stream were separately pre-heated to the temperature of the reaction tube. The two streams were allowed to mix together in a small mixer before their entry into the reaction chamber. The size of the mixing section was such that the residence time of the reactants in it was only about two per cent of the residence time in the reaction tube. The furnace was fitted with a window through which the onset of ignition could be viewed. Nitrogen, oxygen and the fuel under study were metered into the rig at constant flow rates. The flow of gases through the reaction tube was induced by means of a suction pump, the flow rate being adjusted with a coarse and a fine control valve. The composition of the gases and their flow through the reaction chamber was so uniform that the flame always passed through the tube as a flat disc. For determining the ignition lag at any well-controlled temperature the rate of flow of the gases, which had been kept too fast for ignition to occur, was reduced till ignition took place. The limiting ignition pressure was measured and thence the ignition lag (the residence time of the fuel–air mixture at the instant of ignition) was calculated. Although, at any given temperature, the limiting ignition pressure was perforce different for different fuels, the comparisons in all cases were made under identical mass flow conditions.

Results

The values of ignition lag were determined at different temperature levels about 50°C apart. At each temperature level ignition lags were obtained over a narrow temperature range (±5°C) and from these results the value of the ignition lag at the desired temperature was obtained. Such values of ignition lag for the different hydrocarbons at temperatures ranging from about 500° to 800°C are presented in *Figure 1*.

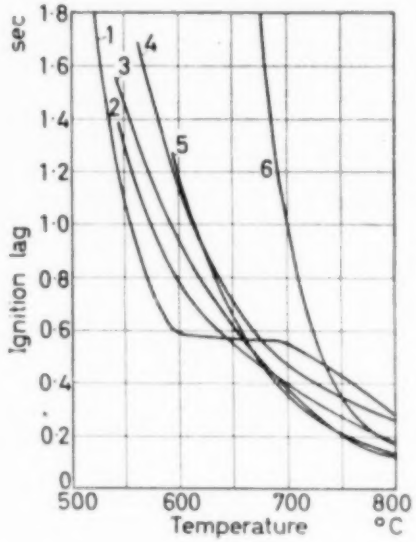

Figure 1. Influence of temperature on ignition lag: 1 diisobutylene, 2 methylcyclohexane, 3 n-heptane, 4 isooctane, 5 ethylbenzene, 6 benzene

These results show that although, in general, the ignition lag decreases with temperature, there are marked differences in the lag versus temperature relationship for the different hydrocarbons. The curves displaying this relationship often cross over. Thus, the relative order of the ease with which different hydrocarbons ignite is not the same at all temperatures. Methyl-*cyclo*hexane and di*iso*butylene have shorter lags than *n*-heptane till about 670°C, but the reverse applies at higher temperatures. Ethylbenzene, which has a much longer lag than *n*-heptane at 600°C, has nearly the same lag as the latter at temperatures above 650°C. The decrease in ignition lag with temperature is highest for benzene. Its ignition lag, while being longer than that for any other hydrocarbon up to 730°C, falls at higher temperatures below those for di*iso*butylene and *iso*octane, and finally below that for methyl*cyclo*hexane. Di*iso*-butylene has the most unusual combustion behaviour. It has the shortest lag up to 650°C

and the longest above *ca.* 730°C. Furthermore, its ignition lag remains virtually constant between 600° and 700°C.

Mullins has also observed a change in the relative order of ignition lags with increasing temperature. Some of his observations, particularly those with regard to benzene, ethylbenzene and *iso*octane, are similar to the results presented here. However, it is difficult to draw a direct comparison between the two sets of results since the temperature ranges investigated and also the experimental conditions are widely different.

Overall activation energy

The values of overall activation energy for the data for *Figure 1* were obtained). The values of overall activation energies are presented in *Table 1*. The fuel–air composition was approximately stoichiometric in all cases; the exact composition is tabulated in parentheses under each value of activation energy.

The results in *Table 1* indicate that the overall activation energy is different for different hydrocarbons, and for any given hydrocarbon it changes with temperature. With *n*-heptane and methyl*cyclo*hexane the energy of activation tends to increase with temperature, while for benzene it tends to fall. The activation energy for ethylbenzene falls with temperature up to 750°C but rises again around 800°C. With

Table 1. Overall activation energies at different temperature levels

Temperature °C	Overall activation energy, kcal					
	n-*Heptane*	*Methylcyclo-hexane*	iso*Octane*	*Diisobutylene*	*Benzene*	*Ethylbenzene*
550	11·3 (1·18)	13·8 (0·94)	—	20·7 (1·03)	—	—
562·5	—	—	20·0 (1·11)	—	—	—
575	—	—	—	18·8 (0·91)	—	—
600	13·5 (1·03)	14·5 (0·99)	14·3 (1·12)	9·2 (0·93)	—	20·2 (1·10)
650	17·6 (1·00)	10·2 (1·07)	14·9 (1·00)	0 (0·91)	—	18·1 (1·17)
700	17·4 (0·91)	10·2 (1·10)	10·7 (1·07)	5·6 (0·96)	40·8 (1·03)	18·7 (1·02)
750	22·8 (1·16)	17·7 (0·94)	12·3 (1·16)	15·0 (1·08)	27·4 (1·02)	14·4 (1·10)
800	22·2 (1·14)	31·0 (0·95)	16·5 (1·12)	16·5 (1·06)	20·6 (1·00)	20·4 (1·00)

N.B.—The figure in parentheses under each value of activation energy represents the stoichiometric composition of the fuel–air mixture investigated.

ignition, for whatever they are worth in such a complex process, were calculated for different hydrocarbons at different temperature levels from the data in *Figure 1*. In cases where the slope of the ignition lag/temperature curve could not be determined satisfactorily the values of activation energy were calculated from the ignition lag/temperature relationship extending over ±5°C (the results from which

*iso*octane it tends to decrease around 700°C and then rises. With di*iso*butylene there is a marked decrease in the value between 600° and 700°C, the activation energy being nil at 650°C.

Effect of fuel concentration

The effect of increasing fuel concentration from *ca.* 0·5 to 2·0 times stoichiometric was observed, usually at every 50°C interval (*Figure 2*). In

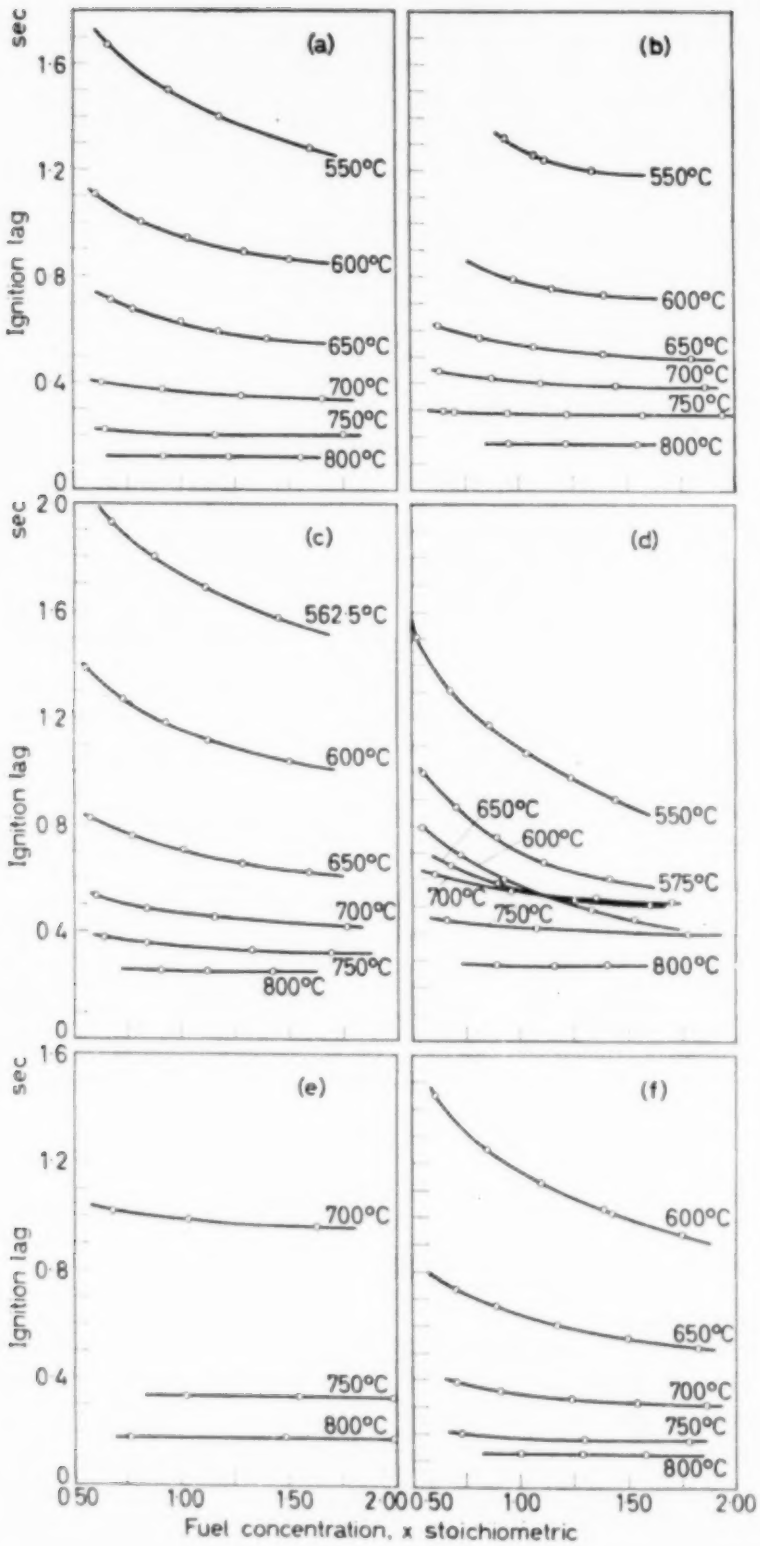

Figures 2. Effect of fuel concentration at different temperature levels: (a) n-*heptane*, (b) *methylcyclohexane*, (c) isooctane, (d) *diisobutylene*, (e) *benzene*, (f) *ethylbenzene*

all cases increasing the fuel concentration markedly shortened the ignition lags near their minimum ignition points. The effect gradually decreased at higher temperatures till eventually, at about 800°C, the variation in fuel concentration had virtually no effect on the ignition lag.

Discussion

The present investigation fills the gap in our knowledge between ignition around minimum ignition point and at 'high' temperatures (above 750°C). The results show that whereas, in general, the ignition lag decreases with increasing temperature, there are marked differences in the lag versus temperature relationship for the different hydrocarbons. As a consequence the relative ease of ignition of different hydrocarbons often changes with temperature.

The results on the effect of fuel concentration at different temperature levels are of particular interest. They help in resolving the controversy that has existed so far between those who worked at 'high' temperatures and showed that variations in fuel concentration produced no discernible effect on the lag and those who observed that at 'low' temperatures lag is markedly affected by changes in fuel concentration. The present results have shown clearly that in all fuels increasing fuel concentration markedly reduces the lag around their minimum ignition points, and the effect gradually decreases as temperature is raised till eventually, above *ca.* 750°C, variations in fuel concentration have hardly any effect.

The changes in the effect of fuel concentration, and also in activation energy, suggest that the mechanism of combustion changes with temperature. It is naturally of great interest to explore the mechanism of the processes that underlie the present observations on the ignition phenomenon. We are carrying out detailed analyses of the combustion products formed at different temperatures; these results will form the subject of a subsequent paper.

The permission of the Directors of 'Shell' Research Ltd to publish this work is gratefully acknowledged. The author also wishes to thank Mr W. N. Sailes for his able assistance in experimental work, and Dr A. Thomas for valuable discussions.

References

1 MULLINS, B. P. *Fuel, Lond.* 1953, **32**, 218, 234, 327, 343, 363, 451, 467 and 481
2 MILLER, R. E. *Seventh Symposium (International) on Combustion*, p 417. Butterworths: London, 1959
3 BROKAW, R. S., JACKSON, J. L., WEAST, R. C. and GERSTEIN, M. *Industr. Engng Chem. (Industr.)*, 1954, **46**, 2547
4 SALOOJA, K. C. *Combustion & Flame*, 1960, **4**, 117

The Gaseous Oxidation of Para*Xylene*

J. A. BARNARD and P. HAWTIN

Department of Chemical Engineering, University College, London, W.C.1

(*Received December 1960*)

The gaseous oxidation of para*xylene has been investigated in a static system at temperatures between 460° and 512°C. The reaction has been followed by pressure change and by chemical analysis of the reactants and products. The reaction is autocatalytic and it has been shown that formaldehyde is the degenerate branching intermediate. The order of the reaction varies somewhat with mixture composition, but for a fuel/oxygen ratio of 1/2·5, the order with respect to oxygen is about 2·0 and with respect to* para*xylene about 1·0. A mechanism is suggested, based upon the generally accepted scheme for the oxidation of methane, which accounts satisfactorily for the principal kinetic features of the reaction.*

Introduction

GASEOUS combustion reactions have been extensively studied over the past 60 years, principally with aliphatic hydrocarbons, and relatively little work has been done on aromatic hydrocarbon oxidation. Early work was concerned mainly with the oxidation of benzene[1–3] but J. H. BURGOYNE and his collaborators[4–9] extended this to include other simple aromatic compounds. Monoalkyl benzenes were found to possess both high and low temperature zones of oxidation as is normal with aliphatic hydrocarbons, and the progressive formation of products during slow combustion at 270° to 480°C was studied.

More recently R. G. W. NORRISH and G. W. TAYLOR[10] examined the oxidation of benzene in a flow system at atmospheric pressure and at a temperature of 685°C. Their findings confirmed the results of earlier workers that benzene possesses no low temperature oxidation mechanism. Complete material balances were drawn up at all stages of the reaction and it was suggested that the reaction proceeded by successive hydroxylation of the ring which then broke to give fragments which in turn were rapidly degraded to C_2 products. R. G. W. NORRISH and G. W. TAYLOR[11] have also made less complete studies of the oxidation of toluene and ethylbenzene in a static system at temperatures between 300° and 500°C. Cool flames were observed for both hydrocarbons and a semi-quantitative estimate was made of the reaction products of the ethylbenzene oxidation.

The present work was designed to study the low pressure gaseous oxidation of *para*xylene and especially to elucidate the principal features of the reaction mechanism.

Experimental

Materials

B.D.H. laboratory grade *para*xylene was fractionally distilled using a 1 m column packed with glass helices. The product collected had a boiling point at 139·25°C (760 mm of mercury), and was further purified by repeated fractional crystallization. After some four or five recrystallizations the melting point of the purified *para*xylene was 13·25°C, and was unaltered by further purification. The most reliable value[12] of the melting point is 13·263°C and J. TIMMERMANNS[13] states that the best criterion of purity is the constancy of the melting point.

Oxygen was prepared by heating degassed potassium permanganate. Carbon dioxide and water vapour were removed by passage through suitable absorbents.

Formaldehyde was prepared by gentle heating of *para*formaldehyde.

Apparatus and procedure

The apparatus was of the usual static type. Because of the low volatility of *para*xylene and some of the products, special precautions were taken to ensure that all parts of the apparatus in contact with reactants and products were heated electrically to at least 100°C. Mixtures of *para*xylene and oxygen in known proportions

were stored in a heated 2 l. flask and admitted to the reaction vessel via a doser maintained at constant temperature. Knowledge of the 'sharing factor' between the reaction vessel and the doser enabled the initial pressure of reactants to be determined precisely.

The cylindrical reaction vessel, volume 300 ml and surface : volume ratio 0·85 cm^{-1}, was of Pyrex glass and surrounded by an electric furnace whose temperature was maintained constant to within ±1°C by an electronic controller.

The reaction was followed by pressure change on a mercury manometer, and by periodical chemical analysis. Samples were condensed by passage through a trap cooled in liquid air and the condensate analysed by gas chromatography on a 2 m dinonyl phthalate/celite column at 90°C. This column resolved *para*xylene, water, benzene and toluene. C_4 and C_5 hydrocarbons would also have been detected had they been present. The condensates from a number of runs were also analysed on a polyethylene glycol (mol. wt 400)/celite column at 52°C: this confirmed the identity of the peaks already observed—with the exception of water which is very strongly bound on such a column—and also revealed the presence of traces of methanol and glyoxal. The identity of the toluene peak was further confirmed by condensing out the substance responsible for this peak as it was eluted from the dinonyl phthalate column and subjecting it to infra-red analysis.

The gas analyses were performed separately. Samples withdrawn from the reaction vessel were again passed through a trap cooled in liquid air. The uncondensed gas was measured and then pumped away for chromatographic analysis on a 2 m activated charcoal column at 25°C which resolved hydrogen, oxygen, carbon monoxide and methane. After the permanent gas had been pumped away, the trap was allowed to warm up to the temperature of solid carbon dioxide–acetone (−85°C); the gas evolved was measured and pumped away for analysis on a 100 cm activated carbon column at 100°C. This column resolved carbon dioxide, ethylene, ethane, acetylene, propane and propylene. Only carbon dioxide was detected and the correlation between peak area and sample volume showed that only small amounts of any other gases could have been present.

Formaldehyde was analysed in a separate series of runs. Samples were condensed at −183°C in a trap containing ice. The trap was isolated, removed from the apparatus and the condensate allowed to warm up. The trap was shaken to ensure that the formaldehyde dissolved in the water and the concentration of the formaldehyde solution determined by the chromotropic acid method[14].

The aqueous solution of the products obtained by this means was also tested for peroxyacids, hydrogen peroxide and organic peroxides[15]: none was detected. Tests for acetaldehyde and for aromatic aldehydes were negative, but Millon's test for the presence of phenols was weakly positive[16].

Results

Pressure/time curves

In order to obtain reproducible results it was necessary to age the reaction vessel by performing in it a large number of runs carried to a high degree of completion. This ageing had to be repeated whenever the temperature or mixture composition was changed, when air or pure oxygen was admitted to the vessel, or when an ignition occurred.

The rate of reaction in an unaged vessel was less than in an aged one and somewhat irreproducible, but once the ageing had been satisfactorily carried out, the pressure/time curves were very reproducible.

Some typical pressure/time curves are shown in *Figure 1*, where it can be seen that they are of the S-shaped type frequently observed in oxidation studies. The maximum rate of pressure increase ($r_{max.}$) was obtained by drawing a tangent to the pressure/time curve at the point of maximum gradient.

For a given mixture composition and temperature $r_{max.}$ increased up to the ignition point approximately according to the equation

$$r_{max.} = kp_0^n$$

where k and n are constants, and p_0 is the initial pressure. Some five mixture compositions

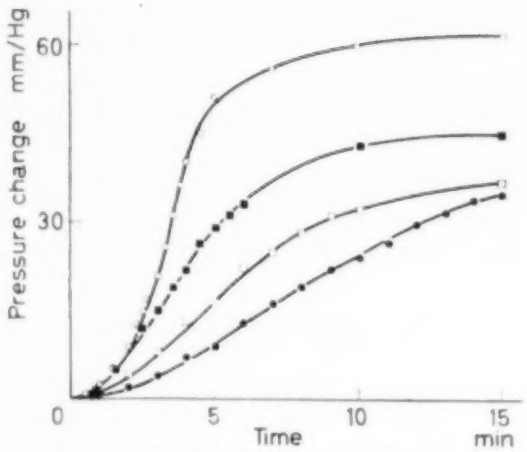

Figure 1. Some typical pressure/time curves for the 2·5: 1 mole mixture of oxygen and paraxylene. *Initial pressure 200 mm* Hg. ⊙ *512°C,* ■ *485°C,* ⊡ *469°C,* ● *460°C*

were studied and the results are summarized in *Table 1*.

Table 1

Mixture composition, moles oxygen: moles paraxylene	*n*	*Ignition pressure mm* Hg
1 : 1	3·32	560
2·5 : 1	2·68	395
5·0 : 1	3·50	395
7·5 : 1	3·60	360
10·0 : 1	2·60	270

The effect of oxygen and *para*xylene pressure on $r_{max.}$ was calculated from these results and it was found that

$$r_{max.} \propto [O_2]^{2\cdot0}\,[\textit{para}\text{xylene}]^{1\cdot0}$$

for oxygen pressures between 50 and 375 mm of mercury and *para*xylene pressures from 20 to 60 mm of mercury.

The 2·5 : 1 mixture was chosen for the most detailed study as this was the richest mixture which could be examined without excessive deposition of polymer and consequent blocking of the tubing leading from the reaction vessel. Using this mixture the effect of temperature on $r_{max.}$ was studied and it was found that between 460° and 512°C the rate could be expressed in the form already quoted, viz.

$$r_{max.} = kp_0^{2\cdot68}$$

where $k = 10^{8\cdot47} \exp(-48\,000/RT)$, $r_{max.}$ denotes maximum rate in mm/min and p_0 is the initial pressure of reactants in mm of mercury.

Analytical results

These were confined to the 2·5 : 1 mixture at 460° and 512°C. Initial pressures from 100 mm to 250 mm of mercury were employed.

(a) *Reactant consumption*—At both temperatures and over the whole range of pressures studied, the disappearance of oxygen and of *para*xylene was proportional to the pressure change, at least for the first 25 per cent of the reaction. This is shown in *Figure 2*.

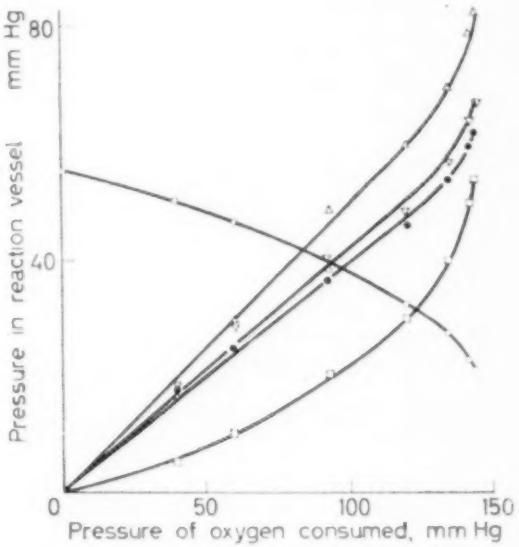

Figure 2. para*Xylene consumption* ⊙. *Formation of carbon monoxide,* ▽ *carbon dioxide* △, *and water* ●. *Overall pressure change* ⊡. *2·5: 1 mole mixture of oxygen and* paraxylene. *Initial pressure 200 mm* Hg. *Temperature 460°C*

(b) *Product formation*—The major products were carbon monoxide, carbon dioxide and water. Some typical results are shown in *Figure 2*. These results show that it is possible to represent the overall reaction, as far as the three major products are concerned, by the approximate equations:

at 460°C

$$1C_8H_{10} + 5O_2 = 2{\cdot}0H_2O + 2{\cdot}5CO_2 + 2{\cdot}1CO$$

and at 512°C

$$1C_8H_{10} + 4O_2 = 2{\cdot}0H_2O + 1{\cdot}4CO_2 + 2{\cdot}3CO$$

The formation of the minor products hydrogen, methane and toluene is shown in *Figure 3*. There were also traces of benzene, glyoxal and methanol present.

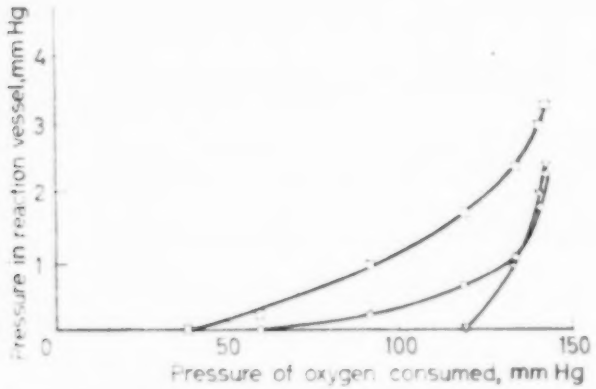

Figure 3. Minor product analyses. Toluene ⊡, *hydrogen* ⊙, *methane* ▽. *Conditions as Figure 2*

Formaldehyde concentration built up to a maximum at the time at which the rate of pressure change was greatest, and then fell off to zero at the completion of the reaction (cf. *Figure 6*).

(c) ***Pressure and element balances***—Pressure balances were drawn up. These were substantially complete within experimental error, although towards the end of the reaction a deficit of about five per cent of the total pressure appeared.

The element balances showed appreciable carbon and hydrogen deficits (cf. *Figure 4*) as

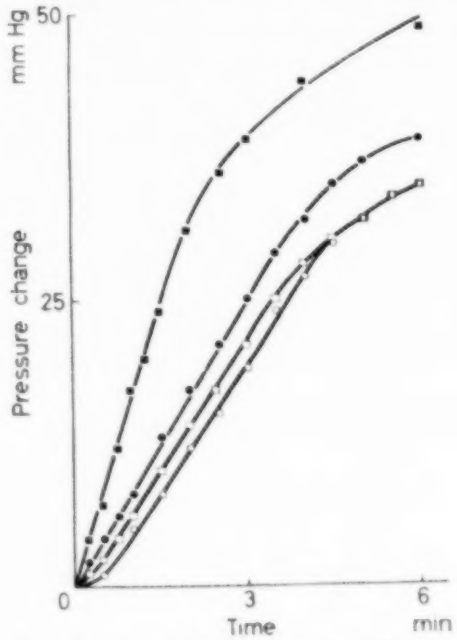

Figure 5. Effect of added formaldehyde. ⊙ *Nil,* ⊡ *1·0 mm,* ● *2·0 mm,* ■ *17·5 mm* HCHO. *Conditions as Figure 2*

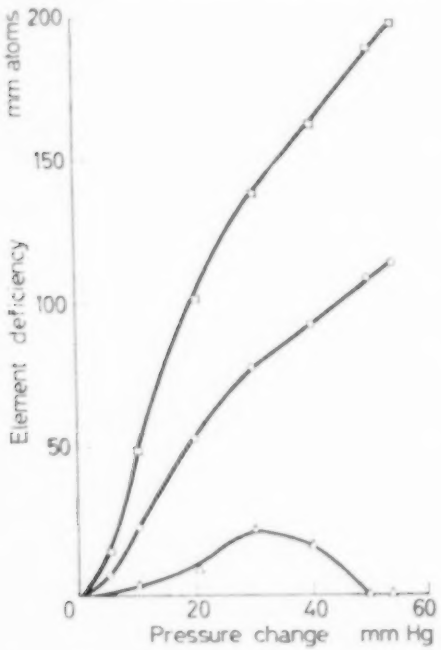

Figure 4. Element deficiencies. Hydrogen ⊡, *carbon* ⊙, *oxygen* △. *Conditions as Figure 2*

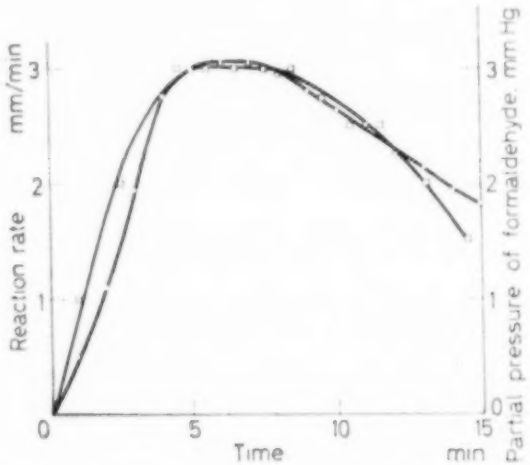

Figure 6. Comparison between the reaction rate and formaldehyde partial pressure in the reaction vessel. ⊙ HCHO *pressure.* ⊡ *reaction rate. Conditions as Figure 2*

was to be expected from the large amount of blackish solid deposited in the reaction vessel and connecting tubing.

(d) *Examination of the polymer*—At the completion of a lengthy series of runs the reaction vessel was removed from the apparatus and some of the polymer scraped out. Conventional spot tests described by F. FIEGL[16] showed the presence of oxalic acid, *p*-methyl phenol and a quinone; phenols with a free para position were absent, as were aromatic aldehydes and acids.

Microanalysis of the polymer showed its empirical formula to be approximately $C_{5.9}H_{6.3}O$.

(e) *Effect of added formaldehyde*—In view of the importance of formaldehyde in the suggested mechanism (see Discussion), the effect of added formaldehyde on the rate of reaction was investigated. It was found that although small additions of formaldehyde reduced the time for the reaction to accelerate to maximum rate, they did not alter $r_{max.}$. Larger amounts of formaldehyde did increase the rate, however (cf. *Figure 5*).

Discussion

Hydrocarbon oxidations frequently involve degenerate branching[17] and this is apparent in the present reaction. Thus both graphs of $d(\Delta p)/dt$ versus Δp and of $\log \Delta p$ versus t are found to be linear over that part of the reaction where the rate is increasing; the value of the acceleration constant, ϕ, is approximately 0·9 min^{-1}. The compound responsible for the branching is formaldehyde; this is shown by:

(*i*) the concomitant rise in the reaction rate with increase in formaldehyde concentration (cf. *Figure 6*);

(*ii*) the effect on the reaction rate of small additions of formaldehyde (cf. *Figure 5*), which is identical with the behaviour normally associated with degenerate branching intermediates[18].

Furthermore, no other likely compounds were detected which could act as degenerate branching intermediates: in particular peroxides and higher aldehydes were absent.

The mechanism proposed involves the formation and subsequent breakdown of formaldehyde by a linear chain process, with occasional branching on these chains. The initiating step which is most probable on thermochemical grounds [19,20] is

$$CH_3C_6H_4CH_3 + O_2 = CH_3C_6H_4CH_2 + HO_2 \qquad \Delta H = 33 \text{ kcal} \quad \ldots . [1]$$

The *para*xylyl radical is believed to be quite stable and its most likely fate is reaction with oxygen

$$CH_3C_6H_4CH_2 + O_2 = CH_3C_6H_4CH_2O_2 \quad \ldots . [2a]$$

The reactions of the *para*xylylperoxy radical are not known with certainty, but by analogy with the decomposition of the methylperoxy radical[18]

$$CH_3O_2 = HCHO + OH$$

it is suggested that it may react either by

$$RCH_2O_2 = HCHO + OR \qquad (\text{where } R = CH_3C_6H_4) \quad \ldots . [2b]$$

or

$$RCH_2O_2 = RCHO + OH \quad \ldots . [2c]$$

the *para*xylylperoxy radical behaving in each case simply as a substituted methylperoxy radical.

Since formaldehyde, but no *para*tolualdehyde, was observed in the reaction products equation 2b appears to represent the major path. However, since *para*tolualdehyde is easily oxidized, it may have been formed, but oxidized further so rapidly that it escaped detection. This seems a plausible source of the small quantities of toluene observed, via side reactions such as:

$$RCHO + X = RCO + XH$$

where $X = O_2$ or a radical

$$RCO = R + CO$$

$$R + RCH_3 = RH + RCH_2 \qquad (RH = CH_3C_6H_5)$$

If we assume that equation 2b is the major reaction path, then we have to include reactions for the oxidation of formaldehyde, especially the reaction which gives rise to occasional chain-branching. Following N. S. ENIKOLOPYAN[18] we write these reactions:

$$\left.\begin{aligned} R + HCHO &= RH + CHO \\ CHO + O_2 &= CO + HO_2 \\ HO_2 + RH &= R + H_2O_2 \end{aligned}\right\} \text{Linear chain oxidation of formaldehyde}$$

and branching by

$$HCHO + O_2 = HO_2 + CHO$$

The other product in equation 2b is the aryloxy radical, $CH_3C_6H_4O$. Now traces of para-substituted phenols were observed in the products, and infra-red analysis of the polymer showed peaks tentatively assigned to CH_3, OH and the benzene nucleus. Thus, it appears that this radical may react by H abstraction

$$CH_3C_6H_4O + YH = CH_3C_6H_4OH + Y$$

Alternatively, the radical may be oxidized further or reach the wall and be deactivated. The absence of large carbon-containing fragments in the gaseous products makes the interpretation of these results difficult and we therefore write

$CH_3C_6H_4O\cdot + O_2$ = products + a radical to continue the chain

and

$CH_3C_6H_4O\cdot$ = deactivated at the wall

The manner in which the benzene ring is broken down is not clear, but Norrish and Taylor[19] concluded from their work on benzene that oxidation of the nucleus takes place in a stepwise fashion to the dihydroxy stage and that the ring then ruptures to products which are rapidly degraded to the C_2 state.

There is further evidence to support the view that disruption of the benzene ring occurs, since C. F. Cullis and J. W. Ladbury[21] have shown that in the much milder conditions of oxidation with acid potassium permanganate, considerable amounts of carbon dioxide are evolved. This proves that, although oxidation is confined mainly to the methyl group which is converted to a carboxyl group, disintegration of the benzene nucleus also takes place. The only isolatable products were *para*tolualdehyde, *para*toluic acid and terephthalic acid, but phenols may also be formed. Since more ring-rupture occurred with *para*xylene than with *para*toluic acid, the authors concluded that fission of the ring took place before the mono-carboxylic acid was formed, and this was in agreement with the earlier conclusion reached with toluene, where it was shown that breaking of the ring occurred at the alcohol or aldehyde stage.

The product analyses of the present work clearly show that from the beginning of the reaction more than two moles of oxides of carbon are being obtained from one mole of *para*xylene; thus ring fission is an important reaction from the beginning of the oxidation.

So the major steps in the reaction sequence are initiation by

$$CH_3C_6H_4CH_3 + O_2 = CH_3C_6H_4CH_2 + HO_2 \quad \ldots [3]$$

followed by

$$CH_3C_6H_4CH_2 + O_2 = CH_3C_6H_4CH_2O_2 = CH_3C_6H_4O + HCHO \quad \ldots [4]$$

$$HO_2 + CH_3C_6H_4CH_3 = CH_3C_6H_4CH_2 + H_2O_2 \quad \ldots [5]$$

$$CH_3C_6H_4O + CH_3C_6H_4CH_3 = CH_3C_6H_4OH + CH_3C_6H_4CH_2 \quad \ldots [6]$$

and

$$CH_3C_6H_4O + HCHO = CH_3C_6H_4OH + CHO \quad \ldots [7]$$

Also we include further oxidation of the toluoxy radical

$$CH_3C_6H_4O + O_2 = \text{products} + HO_2 \quad \ldots [8]$$

and the degenerate branching reaction

$$HCHO + O_2 = HO_2 + CHO \quad \ldots [9]$$

The oxidation of formaldehyde proceeds by

$$CHO + O_2 = CO + HO_2 \quad \ldots [10]$$

$$HCHO + HO_2 = CHO + H_2O_2 \quad \ldots [11]$$

The suggested chain-ending reaction is

$$CH_3C_6H_4O = \text{inactive products at wall} \quad \ldots [12]$$

If the assumption is made that the toluoxy radical is an efficient H abstractor, then clearly reactions 6 and 7 will predominate, and 8 may be neglected. In this case the usual steady-

state analysis leads to the conclusion that

rate of reaction

$$= -\mathrm{d}[\textit{para}\text{xylene}]/\mathrm{d}t$$

$$= A[\textit{para}\text{xylene}][\mathrm{O_2}](1 + B[\textit{para}\text{xylene}])$$

where

$$A = k_3 + k_9(k_5k_6/k_7k_{11})^{\frac{1}{2}}$$

and

$$B = \{k_7(k_5k_6/k_7k_{11})^{\frac{1}{2}} + k_6\}/k_{12}$$

At high pressures, k_{12} is small since diffusion to the wall is hindered, and thus

$$B[\textit{para}\text{xylene}] \gg 1$$

$$\therefore -\mathrm{d}[\textit{para}\text{xylene}]/\mathrm{d}t \sim AB[\textit{para}\text{xylene}]^2[\mathrm{O_2}]$$

and

$$\mathrm{d}p/\mathrm{d}t \sim k'[\textit{para}\text{xylene}]^2[\mathrm{O_2}]$$

where k' includes the constant of proportionality between *para*xylene disappearance and pressure change.

Since this result is contrary to experimental findings concerning the order of reaction, we conclude that the assumption that reaction 8 can be neglected in comparison with 6 and 7 is incorrect. Accordingly, we now assume that reactions 6 and 7 are negligible and that 8 is the principal path by which the toluoxy radical disappears. The steady-state analysis then shows that

rate of reaction $= -\mathrm{d}[\textit{para}\text{xylene}]/\mathrm{d}t$

$$= D(1 + E[\mathrm{O_2}])[\mathrm{O_2}][\textit{para}\text{xylene}]$$

where

$$D = 2(k_3k_{11} + k_5k_9)/k_{11}$$

and

$$E = k_8/k_{12}$$

At high pressures k_{12} is small, and hence E will be large.

$$\therefore -\mathrm{d}[\textit{para}\text{xylene}]/\mathrm{d}t \sim DE[\mathrm{O_2}]^2[\textit{para}\text{xylene}]$$

and

$$\mathrm{d}p/\mathrm{d}t \sim k''[\mathrm{O_2}]^2[\textit{para}\text{xylene}]$$

which is in agreement with the experimental findings concerning the effects of the concentrations of oxygen and *para*xylene. The observed power of the overall pressure dependence of the reaction was about 2·7 for the 2·5 : 1 oxygen–*para*xylene mixture and this suggests that the overall rate expression should include a term for the total pressure.

The reactions of the toluoxy radical do not seem to have been studied. Such evidence as is available is conflicting. Thus K. U. INGOLD and F. P. LOSSING have reported[22] that the pyrolysis of dibenzyl ether yields initially benzyl and benzyloxy radicals; the latter decompose

$$\mathrm{C_6H_5CH_2O} = \mathrm{C_6H_5CHO} + \mathrm{H}$$

rather than abstract hydrogen from any suitable donor, for no benzyl alcohol was detected in the products. At lower temperatures (*ca.* 100°C), however, benzyloxy radicals produced in the pyrolysis of benzyl nitrite do abstract hydrogen[23].

The mechanism suggests hydrogen peroxide and formaldehyde as major products, together with the fragments resulting from disruption of the benzene ring, and polymer. No hydrogen peroxide was detected, although the tests employed[15] would have readily detected 0·1 mm or less of hydrogen peroxide in the reaction vessel; this absence of peroxidic products seems to be typical of aromatic oxidations (cf. Burgoyne[3–9], Norrish and Taylor[10, 11]) and it must be concluded here that the hydrogen peroxide rapidly decomposes, without building up a stationary concentration large enough to be detected, or to contribute significantly to the degenerate branching.

Once the reaction is proceeding steadily, the majority of the *para*xylene is removed by reactions 4, 5 and 8, and the formaldehyde by reactions 10 and 11. According to these steps, destruction of one mole of *para*xylene leads to one mole of hydrogen peroxide and one mole of formaldehyde, which in turn leads to one mole of carbon monoxide and a second mole of hydrogen peroxide. Now, presumably the hydrogen peroxide is quantitatively converted to water and thus the destruction of one mole of *para*xylene leads to one mole of carbon monoxide and two moles of water. Unfortunately, reaction 8 yields ill-defined 'products' which could include carbon monoxide and water. Thus the only conclusion that can be drawn is that the mechanism requires that at least one mole of carbon monoxide and two moles of water are produced for every mole of *para*xylene oxidized; this is in agreement with

the overall product equations, as shown above.

The polymer formula indicated by the mechanism is $(C_7H_7O)_n$; the formula found by microanalysis is in tolerable agreement with this.

The minor products are easily accounted for. A suggested route by which toluene could arise has already been outlined, and clearly this is capable of extension to yield the trace amounts of benzene observed. Hydrogen has been noted as one of the products of benzene oxidation[10], and glyoxal and oxalic acid are obvious two-carbon fragments resulting from ring-fission, while methane[24] and methanol[18] have both been observed in formaldehyde oxidation.

The mechanism proposed is based on that suggested by Enikolopyan[18] and others[25,26] for the oxidation of methane. This mechanism gives an excellent quantitative account of the methane–oxygen reaction but in view of the complexity of the *para*xylene oxidation and the fact that little is known of the kinetic parameters of some of the individual steps such detailed agreement is not to be expected here. However, a reasonably satisfactory account is given of:

(*a*) the dependence of the rate on the oxygen and *para*xylene pressures;

(*b*) the variation of the formaldehyde concentration throughout the course of the reaction, and

(*c*) the amounts of carbon monoxide and water formed and polymer deposited.

There are, however, a number of features of the reaction which are still obscure, and it is hoped that these will be elucidated by further work.

The authors wish to thank Dr R. Chayen for considerable help and advice, especially with the infra-red analyses, and the Gas Council for a grant to P.H.

References

1 Fort, R. and Hinshelwood, C. N. *Proc. Roy. Soc. A*, 1930, **127**, 218

2 Amiel, J. *C.R. Acad. Sci., Paris*, 1933, **196**, 1 22 and 1896; **197**, 984; 1936, **202**, 946

3 Amiel, J. *Ann. Chim.* 1937, **7**, 70

4 Newitt, D. M. and Burgoyne, J. H. *Proc. Roy. Soc. A*, 1936, **153**, 448

5 Burgoyne, J. H. *Proc. Roy. Soc. A*, 1937, **161**, 48

6 Burgoyne, J. H. *Proc. Roy. Soc. A*, 1939, **171**, 421

7 Burgoyne, J. H., Tang, T. L. and Newitt, D. M. *Proc. Roy. Soc. A*, 1940, **174**, 379

8 Burgoyne, J. H. *Proc. Roy. Soc. A*, 1940, **174**, 394

9 Burgoyne, J. H. *Proc. Roy. Soc. A*, 1940, **175**, 539

10 Norrish, R. G. W. and Taylor, G. W. *Proc. Roy. Soc. A*, 1956, **234**, 160

11 Norrish, R. G. W. and Taylor, G. W. *Proc. Roy. Soc. A*, 1956, **238**, 143

12 Fortziati, A. F., Glasgow, A. R., Jr, Willingham, C. B. and Rossini, F. D. *J. Res. Nat. Bur. Stand.* 1945, **35**, 219

13 Timmermanns, J. *Physico-Chemical Constants of Organic Compounds*. Elsevier: Amsterdam, 1950

14 Bricker, C. E. and Johnson, H. R. *Analyt. Chem.* 1945, **17**, 400

15 Cullis, C. F. and Newitt, E. J. *Proc. Roy. Soc. A*, 1956, **237**, 530

16 Fiegl, F. *Spot Tests in Organic Analysis*. Elsevier: Amsterdam, 1956

17 Semenov, N. *Chemical Kinetics and Chain Reactions*. Oxford University Press: London, 1935

18 Enikolopyan, N. S. *Seventh Symposium (International) on Combustion*, p 157. Butterworths: London, 1959

19 Gray, P. *Trans. Faraday Soc.* 1959, **55**, 408

20 Szwarc, M. and Williams, D. J. *J. chem. Phys.* 1952, **20**, 1171

21 Cullis, C. F. and Ladbury, J. W. *J. chem. Soc.* **1959**, 1407

22 Ingold, K. U. and Lossing, F. P. *Canad. J. Chem.* 1953, **31**, 30

23 Gray, P., Rathbone, P. and Williams, A. *J. chem. Soc.* **1960**, 3932

24 Bone, W. A. and Gardner, J. B. *Proc. Roy. Soc. A*, 1936, **154**, 297

25 Hoare, D. E. and Walsh, A. D. *Proc. Roy. Soc. A*, 1952, **215**, 454

26 Egerton, Sir A., Minkoff, G. J. and Salooja, K. C. *Proc. Roy. Soc. A*, 1956, **235**, 158

Thermochemical Equilibrium in Hydrocarbon–Oxygen Reactions Involving Polyatomic Forms of Carbon

N. R. Gay, J. T. Agnew, O. W. Witzell and C. E. Karabell

Purdue University, W. Lafayette, Indiana

(*Received October 1960*)

Equilibrium composition and flame temperatures have been calculated for the reaction of acetylene and ethylene with oxygen over a range of mixture ratios. Emphasis has been placed on the determination of conditions necessary for the formation of solid carbon in the products. The influence of the presence of long-chain carbon molecules on the mixture ratio and temperature required for carbon deposition has been investigated. Premixed flames of acetylene and ethylene with oxygen have been studied experimentally to determine the correlation between theoretical calculations and actual combustion reactions. Calculations indicate that, for acetylene, carbon begins to appear in the condensed form at an equivalence ratio (actual fuel/oxygen ratio divided by the stoichiometric ratio) of approximately 2·7 when the only forms of carbon vapour considered are monatomic and diatomic. The equilibrium flame temperature is 3 275°K. If longer chain forms of carbon vapour are considered (consistent with a triple point pressure of about 100 atm at 4 000°K) then carbon formation begins at an equivalence ratio of 3·37 and the flame temperature would be 3 095°K. This difference is not so pronounced with the other hydrocarbons considered. Experimentally, conclusive evidence of carbon formation was apparent at an equivalence ratio of 2·9. Based upon the property data used, the experimental evidence would indicate the presence of carbon molecules containing up to five atoms of carbon. Of these forms the odd number species probably predominate.

Introduction

The computations necessary to predict the equilibrium characteristics of chemically reacting thermodynamic systems, involving a large number of constituents, have become more feasible with the advent of digital computers as an aid to solution. This is also true with respect to the calculation of the thermodynamic properties of the system components, which must be obtained before a reaction equation can be analysed. Such calculations have been made for the relatively few hydrocarbon molecules for which fundamental molecular constants are known, e.g. CH_4, C_2H_2, C_2H_4, C_2H_6 and C_3H_4. Emphasis has been placed on the compilation of consistent thermodynamic data for all species considered, either by calculation or adaptation from the best available sources.

In considering the reaction of the above-mentioned hydrocarbon fuels with oxygen, it would seem reasonable to predict that some of these fuels, and in particular acetylene (C_2H_2), should appear as stable equilibrium products. Acetylene is unique among these fuels in that the reaction involving its formation from solid carbon and molecular hydrogen is highly endothermic. In addition, evidence has recently been found for the existence of polyatomic forms of carbon molecules and some predictions have been made regarding the thermodynamic properties of these linear polyatomic carbon molecules.

Both of the above considerations have been combined for the first time in calculations designed to determine the equilibrium composition of acetylene–oxygen, and ethylene–oxygen, systems as a function of mixture ratio; and in each case to ascertain the critical mixture ratio for the formation of solid carbon as an equilibrium product. This critical mixture ratio is defined as the leanest oxygen/fuel ratio at which solid carbon appears as an equilibrium product. The composition of combustion products and the condensation conditions for solid phases are of major importance in calculating the thrust obtainable from propulsion devices and in determining the tendency towards carbon formation in heat engines which burn rich hydrocarbon–oxidant mixtures.

Experimental work was also undertaken in which acetylene–oxygen and ethylene–oxygen premixed flames were studied and photographed

in an attempt to correlate actual combustion reactions with the results predicted by theoretical calculations.

Determination of Thermodynamic Properties

The calculation of the equilibrium composition for a fuel–oxidant reaction according to the method mentioned in the next section requires use of the following thermodynamic properties or relations:

(*1*) Specific heat at constant pressure
(*2*) Enthalpy
(*3*) Equilibrium constant, and
(*4*) Enthalpy change for formation of a substance from its gaseous monatomic elements divided by the product of the gas constant and absolute temperature.

These quantities have been obtained either by calculation from partition functions or compiled from various sources making whatever corrections might be necessary to form a consistent set of tables.

Inherent in the compilation of such a consistent set of properties is the selection of a standard state enthalpy for the substance at zero degrees absolute (H_0°) and a heat of formation under the same conditions (ΔH_f°). *Table 1* is a compilation of these values for all elements and compounds involved in this work. The H_0° values are all positive due to the fact that, in their derivation, the H_0° values for certain compounds were arbitrarily assigned a value of zero. The compounds assigned a zero value of H_0° were $CF_{4(gas)}$, $HF_{(gas)}$, $H_2O_{(crystal)}$ and $O_{2(crystal)}$. The heat of sublimation of graphite was a rounded value intermediate between the value of 170·39 as given by F. D. Rossini *et al.*[1] and the value 169·58 as quoted by K. S. Pitzer and E. Clementi[2]. Values for CH_4, C_2H_2, C_2H_4, C_2H_6, CO_2, H_2, O_2 and H_2O were derived by making use of heats of formation from solid carbon and/or molecular gaseous species from ref. 1. Similar data were taken from: ref. 3 for CH and CO; ref. 2 for C_2; ref. 4 for C_3H_4; and ref. 5 for OH.

Table 1. Enthalpies and heats of formation based on formation from gaseous atomic species

Substance	H_0°, kcal/mole	ΔH_f°, kcal/mole
C	282·088	
H	85·329	
O	59·604	
C_{solid}	112·088	−170·000
C_2	424·176	−140·000
CH	287·388	−80·029
CH_4	230·937	−392·467
C_2H_2	345·923	−388·911
C_2H_4	373·534	−531·958
C_2H_6	409·913	−666·237
C_3H_4	517·117	−670·463
CO	85·462	−256·230
CO_2	20·155	−381·141
H_2	67·418	−103·240
H_2O	11·329	−218·933
O_2	2·036	−117·172
OH	43·453	−101·480

The data in *Table 1* then form the basis for the calculation of the required thermodynamic properties. Complete tables of values of the thermodynamic properties used have been given by N. R. Gay[6]. The properties of $C_{(gas)}$ were taken directly from the report of L. V. Feigenbutz *et al.*[7], by simply rounding the values to three decimal places. The specific heat and enthalpy of $C_{(graphite)}$ were taken from the same reference but the equilibrium constants were determined from information reported by L. Brewer *et al.*[8] regarding the vapour pressure of carbon and using 170 kcal/mole as the heat of formation. The equation for $\log P$ and consequently $\log K$ for the sublimation of carbon in the monatomic form is

$$\log K = -37\,156/T + \text{constant}$$

If the temperature at which the vapour pressure of carbon is one atmosphere is taken as 4 640° K, then the constant in the above equation becomes 8·0078. Thus the equilibrium constant for the reaction $C_{(gas)} \longrightarrow C_{solid}$ can be evaluated by the relation

$$\log K = -37\,156/T + 8{\cdot}0078$$

The thermodynamic properties of C_2 were calculated using data furnished by J. S. Gordon[9]. The heat of formation of C_2 was taken to be 140 kcal/mole, a value near that

suggested by G. GLOCKLER[10] derived from bond-energy and bond-distance considerations. This in turn yields a heat of sublimation of C_2 of 200 kcal/mole which agrees with the value used by Pitzer and Clementi[2]. The calculations by Gordon[9] made use of the molecular constants given by G. HERZBERG[3] plus information from E. A. BALLIK and D. A. RAMSAY[11] in which the authors unequivocally give the $^1\Sigma_u^+$ state as the ground state of the C_2 molecule. This is contrary to the assumption that the ground state is the lowest triplet $^3\pi_u$ state which corresponds to the Swan bands easily observable in absorption. The $^1\Sigma_g^+$ state lies below the zero vibrational level of the $^3\pi_u$ state by 610 cm^{-1} and this value was used by Gordon in his calculations.

The thermodynamic properties of the hydrocarbons were calculated from partition functions using molecular and numerical constants taken mainly from G. HERZBERG[12]. The equations used in the calculations were based on the rigid-rotator, harmonic-oscillator molecular model. The maximum error using this simplified model is in the neighbourhood of five per cent. Complete tables of original calculations of the thermodynamic properties of methane, ethylene, acetylene and methyl acetylene are given by Gay[6].

The specific heat of OH was taken directly from Feigenbutz *et al.*[7], but the enthalpy was adjusted to a datum consistent with those for the monatomic constituents and the heat of formation. The change in the dissociation energy from the value cited in the reference necessitated an adjustment of the equilibrium constants therein. Feigenbutz *et al.* used a value of $-106{\cdot}759$ kcal/mole for $(\Delta H_0^0)_{OH}$ and a value of $-101{\cdot}480$ was used in this work. The values for $\log K$ were obtained by subtracting an amount equal to $1\,153{\cdot}82/T$ from the values listed in ref. 7.

The resulting tables of properties enable the calculation of equilibrium products of reaction when these products include carbon vapour species C_1 and C_2. For the polyatomic forms of carbon vapour which are to be considered, similar properties must be obtained. Such data have been derived from a recent paper by Pitzer and Clementi[2]. *Tables 2, 3* and *4* are taken directly from this reference and can be used to formulate the enthalpy and equilibrium constant as will be shown.

Table 2. Calculated values for ΔH_0^0 of formation (kcal/mole) for carbon

C_1	169·58	C_{10}	263·3
C_2	200·0	C_{11}	249·2
C_3	186·5	C_{12}	282·4
C_4	224·5	C_{13}	271·7
C_5	193·3	C_{14}	302·9
C_6	232·9	C_{15}	294·1
C_7	208·8	C_{16}	324·8
C_8	246·3	C_{17}	318·1
C_9	228·0	For the infinite chain 12·7 kcal/g atom of carbon	

The values in *Table 2* were those given by the so-called $(L-F)$ series which, according to the authors, have the best theoretical basis. This involves a semi-empirical method of calculation described by A. LOFTHUS[13] using self-consistent field atomic orbital overlap integrals.

Table 3. The free energy function, $-(F^0-H_0^0)/T$, cal/mole deg. for carbon

Substance	*Temperature, °K* 2000	2500	3000	3500	4000
Graphite	5·37	6·39	7·28	8·07	8·78
C_1	42·215	43·334	44·251	45·029	45·707
C_2	56·39	58·27	59·82	61·22	63·35
C_3	61·82	64·59	66·93	68·95	70·73
Increment per C atom	8·32	9·35	10·24	10·99	11·66

The values in *Table 3* were calculated with the increment per carbon atom adjusted to the triple point pressure of about 100 atm at 4 000° K. Also a term equal to 3·56 cal/mole deg. is to be added to the values for even number of carbon atom species (except for C_2). This was due to the assumption by the authors that the electronic contribution to the partition function based on a multiplicity of 6 for the

ground state would add $R \ln 6$ to the even species values.

Table 4. The heat content function, $(H^\circ - H^\circ_0)/T$, cal/mole deg. for carbon

Substance	2000	2500	3000	3500	4000
Graphite	4·39	4·74	5·01	5·22	5·40
C_1	5·014	5·019	5·036	5·062	5·092
C_2	8·14	8·20	8·33	8·35	8·41
C_3	12·21	12·66	12·95	13·23	13·41
Increment		*Temperature, °K*			
per C atom	4·55	4·77	4·90	5·01	5·08

Enthalpy values for the polyatomic forms of carbon were calculated using *Tables 2* and *4*. The general formula for such a calculation would be of the form

$$H^\circ_0]\,C_{n(gas)} - nH^\circ_0]\,C_{solid} = \Delta H^\circ_0]\,C_n$$

where n is the number of carbon atoms in the molecule. Thus one obtains the datum enthalpy or H°_0 for the polyatomic carbon forms which together with the enthalpy function listed gives the enthalpy values at the temperature indicated. As specific examples we might consider finding the H°_T value for C_1 and C_{20} at 2 500° K. For the C graphite a datum enthalpy of 112·0876 was used for consistency with the previously calculated tables, as well as a rounded value of heat of formation for C_1 of 170 kcal/mole. Then the calculation becomes

$$H^\circ_0]_{C_1} = 170 + 112{\cdot}0876 = 282{\cdot}0876 \text{ kcal/mole}$$

and since

$$(H^\circ_T - H^\circ_0)/T = 5{\cdot}019$$

then

$$H^\circ_{2500} = 294{\cdot}6351 \text{ kcal/mole}$$

The calculation for C_{20} at 2 500° K gives

$$H^\circ_0]_{C_{20}} = 375{\cdot}6 + 20\,(112{\cdot}0876)$$
$$= 2617{\cdot}352 \text{ kcal/mole}$$

and

$$H^\circ_{2500} = 2617{\cdot}352 + 93{\cdot}75\,(2500/1000)$$
$$= 2851{\cdot}727 \text{ kcal/mole}$$

It should be noted in the calculation of heats of formation from *Table 2* that 25·4 kcal should be added alternately to even and odd species starting with C_{16} and C_{17} and progressing to the higher forms.

A complete table of enthalpies, at the temperatures indicated, for the polyatomic carbon forms up to C_{27} inclusive are given in *Table 5*.

Values of the equilibrium constant can be determined from the free energy functions and heats of formation. If the equilibrium constant is to be based on the reaction of monatomic gaseous carbon to polyatomic carbon, the heats of formation of *Table 2* must be changed since these are based on formation from carbon-graphite. For C_3 the heat of formation becomes $-656{\cdot}7$ kcal/mole and using the definition of equilibrium constant, i.e.

$$K = \exp\,(-\Delta F^\circ_T/RT)$$

then $\ln K = -\Delta F^\circ_T/RT$ and at 3 000° K using values from *Table 3* we obtain

$$-\frac{\Delta F^\circ}{T} = -\left[\frac{F^\circ - H^\circ_0}{T}\right]_{C_3} - 5\left[-\frac{(F^\circ - H^\circ_0)}{T}\right]_{C_1} - \frac{\Delta H^\circ_0}{T}$$

$$-\frac{\Delta F^\circ}{T} = 87{\cdot}41 - 221{\cdot}255 - (-656{\cdot}7)\,(1000)/3000$$
$$= 85{\cdot}055$$

$$\therefore \log K = \frac{85{\cdot}055}{1{\cdot}987\,(2{\cdot}30259)} = 18{\cdot}590$$

A similar calculation would enable finding the equilibrium constants for each individual species and the specific heats could be estimated from enthalpy data. Actually, because of the method of calculation used, such individual quantities were not necessary, and an average polymer of carbon was used in the equilibrium composition depending on the flame temperature.

It was necessary to determine the total pressure of the many forms of carbon considered and the mean formula weight and enthalpy at each of the temperatures for which data were obtainable and then to interpolate for the required temperature. From the total pressure

Table 5. Enthalpies of the polyatomic forms of carbon, H_T^0, kcal/mole

No. of carbon atoms	*Temperature, °K*				
	2000	2500	3000	3500	4000
$1_{(graphite)}$	120·868	123·938	127·118	130·358	133·688
$1_{(gas)}$	292·116	294·635	297·196	299·805	302·456
2	440·455	444·675	449·165	453·400	457·815
3	547·183	554·413	561·613	569·068	576·403
4	706·370	716·425	726·400	736·690	746·810
5	796·358	809·238	821·988	835·113	848·018
6	957·146	972·851	988·376	1004·336	1020·026
7	1054·233	1072·763	1091·063	1109·858	1128·333
8	1212·921	1234·276	1255·351	1276·981	1298·241
9	1315·808	1339·988	1363·838	1388·303	1412·348
10	1472·296	1499·301	1525·926	1553·226	1580·056
11	1579·384	1609·214	1638·614	1668·749	1698·364
12	1733·771	1766·426	1798·601	1831·571	1863·971
13	1844·259	1879·739	1914·689	1950·494	1985·679
14	1996·646	2034·951	2072·676	2111 316	2149·286
15	2109·034	2150·164	2190·664	2232·139	2272·894
16	2260·922	2304·877	2348·152	2392·462	2436·002
17	2375·409	2422·189	2468·239	2515·384	2561·709
18	2528·697	2578·302	2627·127	2677·107	2726·217
19	2643·184	2695·614	2747·214	2800·029	2851·924
20	2796·472	2851·727	2906·102	2961·752	3016·432
21	2910·960	2969·040	3026·190	3084·675	3142·140
22	3064·247	3125·152	3185·077	3246·397	3306·647
23	3178·735	3242·465	3305·165	3369·320	3432·355
24	3332·022	3398·577	3464·052	3531·042	3596·862
25	3446·510	3515·890	3584·140	3653·965	3722·570
26	3599·798	3672·003	3743·028	3815·688	3887·078
27	3714·285	3789·315	3863·115	3938·610	4012·785

of the vapour over carbon-graphite, the equilibrium constant could be calculated as shown later.

As a sample calculation consider C_{10} at 2 500° K: from *Table 3* the free energy function for C_{10} is 64·59 + 7 (9·35) + 3·56 or 133·6 cal/mole deg.; the free energy function for $C_{graphite}$ is 10 (6·39) = 63·90 cal/mole deg.; the change in this function is therefore 69·70 cal/mole deg. and combining this with the ΔH_0^0 value from *Table 2* we obtain

$$69{\cdot}70 - 263{\cdot}3(1000)/2500 = -35{\cdot}62 \text{ cal/mole deg.}$$

This is equivalent to $-\Delta F/T$ and thus we obtain log P as

$$\log P = -\frac{\Delta F}{T}\left(\frac{1}{R}\right)\frac{1}{2{\cdot}30259} = -7{\cdot}784$$

or the pressure in atmospheres is $0{\cdot}0164 \times 10^{-6}$. Summing these pressures we have the total pressure of the mixture from which the equilibrium constant can be calculated. Also the ratio of the partial pressure of each species to the total pressure gives the mole fraction or concentration. This is used to calculate the equivalent molecular weight of the many carbon forms.

The values of log P, mean number of carbon atoms and enthalpy of the polyatomic carbon vapour in equilibrium with graphite are shown in *Figure 1* as a function of temperature. These values were taken directly from Pitzer and Clementi[2]. Using a ratio of partial pressure of each carbon species to total pressure as a criterion, the relative abundance of each carbon molecular species in the equilibrium vapour can be shown at any particular temperature. Thus, we have the prediction that certainly C_3, C_7 and C_9 can be important in addition to the well established C_1 and C_2 molecules. *Table 6* shows these proportions.

ground state would add $R \ln 6$ to the even species values.

Table 4. The heat content function, $(H^\circ - H^\circ_0)/T$, cal/mole deg. for carbon

Substance	2000	2500	3000	3500	4000
Graphite	4·39	4·74	5·01	5·22	5·40
C_1	5·014	5·019	5·036	5·062	5·092
C_2	8·14	8·20	8·33	8·35	8·41
C_3	12·21	12·66	12·95	13·23	13·41
Increment		*Temperature, °K*			
per C atom	4·55	4·77	4·90	5·01	5·08

Enthalpy values for the polyatomic forms of carbon were calculated using *Tables 2* and *4*. The general formula for such a calculation would be of the form

$$H^\circ_n]\, C_{n(gas)} - nH^\circ_0]\, C_{solid} = \Delta H^\circ_0]\, C_n$$

where n is the number of carbon atoms in the molecule. Thus one obtains the datum enthalpy or H°_0 for the polyatomic carbon forms which together with the enthalpy function listed gives the enthalpy values at the temperature indicated. As specific examples we might consider finding the H°_T value for C_1 and C_{20} at 2 500°K. For the C graphite a datum enthalpy of 112·0876 was used for consistency with the previously calculated tables, as well as a rounded value of heat of formation for C_1 of 170 kcal/mole. Then the calculation becomes

$$H^\circ_0]_{C_1} = 170 + 112{\cdot}0876 = 282{\cdot}0876 \text{ kcal/mole}$$

and since

$$(H^\circ_T - H^\circ_0)/T = 5{\cdot}019$$

then

$$H^\circ_{2500} = 294{\cdot}6351 \text{ kcal/mole}$$

The calculation for C_{20} at 2 500°K gives

$$H^\circ_0]_{C_{20}} = 375{\cdot}6 + 20\,(112{\cdot}0876)$$

$$= 2617{\cdot}352 \text{ kcal/mole}$$

and

$$H^\circ_{2500} = 2617{\cdot}352 + 93{\cdot}75\,(2500/1000)$$

$$= 2851{\cdot}727 \text{ kcal/mole}$$

It should be noted in the calculation of heats of formation from *Table 2* that 25·4 kcal should be added alternately to even and odd species starting with C_{16} and C_{17} and progressing to the higher forms.

A complete table of enthalpies, at the temperatures indicated, for the polyatomic carbon forms up to C_{27} inclusive are given in *Table 5*.

Values of the equilibrium constant can be determined from the free energy functions and heats of formation. If the equilibrium constant is to be based on the reaction of monatomic gaseous carbon to polyatomic carbon, the heats of formation of *Table 2* must be changed since these are based on formation from carbon-graphite. For C_5 the heat of formation becomes $-656{\cdot}7$ kcal/mole and using the definition of equilibrium constant, i.e.

$$K = \exp\,(-\Delta F^\circ_T/RT)$$

then $\ln K = -\Delta F^\circ_T/RT$ and at 3 000°K using values from *Table 3* we obtain

$$-\frac{\Delta F^\circ}{T} = -\left[\frac{F^\circ - H^\circ_0}{T}\right]_{C_5} - 5\left[-\frac{(F^\circ - H^\circ_0)}{T}\right]_{C_1} - \frac{\Delta H^\circ_0}{T}$$

$$-\frac{\Delta F^\circ}{T} = 87{\cdot}41 - 221{\cdot}255 - (-656{\cdot}7)\,(1000)/3000$$

$$= 85{\cdot}055$$

$$\therefore \log K = \frac{85{\cdot}055}{1{\cdot}987\,(2{\cdot}30259)} = 18{\cdot}590$$

A similar calculation would enable finding the equilibrium constants for each individual species and the specific heats could be estimated from enthalpy data. Actually, because of the method of calculation used, such individual quantities were not necessary, and an average polymer of carbon was used in the equilibrium composition depending on the flame temperature.

It was necessary to determine the total pressure of the many forms of carbon considered and the mean formula weight and enthalpy at each of the temperatures for which data were obtainable and then to interpolate for the required temperature. From the total pressure

Table 5. Enthalpies of the polyatomic forms of carbon, H_T°, kcal/mole

No. of carbon atoms	*Temperature, °K*				
	2000	2500	3000	3500	4000
$1_{(graphite)}$	120·868	123·938	127·118	130·358	133·688
$1_{(gas)}$	292·116	294·635	297·196	299·805	302·456
2	440·455	444·675	449·165	453·400	457·815
3	547·183	554·413	561·613	569·068	576·403
4	706·370	716·425	726·400	736·690	746·810
5	796·358	809·238	821·988	835·113	848·018
6	957·146	972·851	988·376	1004·336	1020·026
7	1054·233	1072·763	1091·063	1109·858	1128·333
8	1212·921	1234·276	1255·351	1276·981	1298·241
9	1315·808	1339·988	1363·838	1388·303	1412·348
10	1472·296	1499·301	1525·926	1553·226	1580·056
11	1579·384	1609·214	1638·614	1668·749	1698·364
12	1733·771	1766·426	1798·601	1831·571	1863·971
13	1844·259	1879·739	1914·689	1950·494	1985·679
14	1996·646	2034·951	2072·676	2111·316	2149·286
15	2109·034	2150·164	2190·664	2232·139	2272·894
16	2260·922	2304·877	2348·152	2392·462	2436·002
17	2375·409	2422·189	2468·239	2515·384	2561·709
18	2528·697	2578·302	2627·127	2677·107	2726·217
19	2643·184	2695·614	2747·214	2800·029	2851·924
20	2796·472	2851·727	2906·102	2961·752	3016·432
21	2910·960	2969·040	3026·190	3084·675	3142·140
22	3064·247	3125·152	3185·077	3246·397	3306·647
23	3178·735	3242·465	3305·165	3369·320	3432·355
24	3332·022	3398·577	3464·052	3531·042	3596·862
25	3446·510	3515·890	3584·140	3653·965	3722·570
26	3599·798	3672·003	3743·028	3815·688	3887·078
27	3714·285	3789·315	3863·115	3938·610	4012·785

of the vapour over carbon-graphite, the equilibrium constant could be calculated as shown later.

As a sample calculation consider C_{10} at 2 500° K: from *Table 3* the free energy function for C_{10} is $64{\cdot}59 + 7\,(9{\cdot}35) + 3{\cdot}56$ or 133·6 cal/mole deg.; the free energy function for $C_{graphite}$ is $10\,(6{\cdot}39) = 63{\cdot}90$ cal/mole deg.; the change in this function is therefore 69·70 cal/mole deg. and combining this with the ΔH_0° value from *Table 2* we obtain

$$69{\cdot}70 - 263{\cdot}3\,(1000)/2500 = -35{\cdot}62 \text{ cal/mole deg.}$$

This is equivalent to $-\Delta F/T$ and thus we obtain $\log P$ as

$$\log P = -\frac{\Delta F}{T}\left(\frac{1}{R}\right)\frac{1}{2{\cdot}30259} = -7{\cdot}784$$

or the pressure in atmospheres is $0{\cdot}0164 \times 10^{-6}$. Summing these pressures we have the total pressure of the mixture from which the equilibrium constant can be calculated. Also the ratio of the partial pressure of each species to the total pressure gives the mole fraction or concentration. This is used to calculate the equivalent molecular weight of the many carbon forms.

The values of $\log P$, mean number of carbon atoms and enthalpy of the polyatomic carbon vapour in equilibrium with graphite are shown in *Figure 1* as a function of temperature. These values were taken directly from Pitzer and Clementi[2]. Using a ratio of partial pressure of each carbon species to total pressure as a criterion, the relative abundance of each carbon molecular species in the equilibrium vapour can be shown at any particular temperature. Thus, we have the prediction that certainly C_5, C_7 and C_9 can be important in addition to the well established C_1 and C_3 molecules. *Table 6* shows these proportions.

Determination of Equilibrium Composition and Flame Temperature with Monatomic and Diatomic Forms of Carbon Vapour

Calculations of the equilibrium composition and flame temperature for the combustion of acetylene and oxygen were made using essentially the technique described by V. N. HUFF *et al.*[14].

For this and succeeding calculations the combustion was assumed to take place at a constant total pressure of one atmosphere and with no external transfer of heat.

Various assumptions are made in the analysis

Table 6. Relative abundance of carbon species in equilibrium vapour

Temperature °K				
2000	2500	3000	3500	4000
C_5 0·5023	C_5 0·3780	C_7 0·2759	C_9 0·1674	C_{15} 0·0938
C_7 0·1980	C_7 0·3210	C_9 0·2167	C_{11} 0·1499	C_{13} 0·0875
C_3 0·1428	C_9 0·1324	C_5 0·1891	C_7 0·1395	C_{17} 0·0840
C_1 0·1169	C_3 0·0738	C_{11} 0·1215	C_{13} 0·1113	C_{11} 0·0817
C_9 0·0307	C_{11} 0·0365	C_{13} 0·0549	C_{15} 0·0839	C_9 0·0649
C_2 0·0046	C_1 0·0313	C_3 0·0300	C_5 0·0686	C_{19} 0·0620
C_{11} 0·0029	C_{13} 0·0078	C_{15} 0·0253	C_{17} 0·0502	C_{16} 0·0511
C_6 0·0006	C_2 0·0050	C_{10} 0·0154	C_{12} 0·0329	C_{21} 0·0464
C_8 0·0004	C_8 0·0045	C_8 0·0136	C_{14} 0·0328	C_{14} 0·0441
C_4 0·0003	C_6 0·0034	C_{12} 0·0124	C_{10} 0·0272	C_7 0·0401
C_{13} 0·0002	C_{10} 0·0029	C_{17} 0·0089	C_{16} 0·0265	C_{18} 0·0380
C_{15} 0·0001	C_{15} 0·0017	C_1 0·0086	C_{19} 0·0247	C_{23} 0·0345
C_{10} 0·00002	C_{12} 0·0012	C_{14} 0·0078	C_8 0·0166	C_{12} 0·0322
	C_4 0·0009	C_6 0·0066	C_{18} 0·0130	C_{20} 0·0282
	C_{14} 0·0004	C_{16} 0·0039	C_{21} 0·0121	C_{25} 0·0256
	C_{17} 0·0003	C_2 0·0034	C_3 0·0097	C_{22} 0·0210
	C_{16} 0·0001	C_{19} 0·0025	C_{20} 0·0064	C_{10} 0·0195
		C_4 0·0014	C_6 0·0060	C_{27} 0·0190
		C_{18} 0·0011	C_{23} 0·0059	C_{24} 0·0156
		C_{21} 0·0007	C_{22} 0·0031	C_5 0·0155
		C_{20} 0·0003	C_{25} 0·0029	C_{29} 0·0141
		C_{23} 0·0002	C_1 0·0022	C_{26} 0·0115
		C_{22} 0·0001	C_2 0·0017	C_{31} 0·0105
			C_{24} 0·0015	C_8 0·0091
			C_{27} 0·0014	C_{28} 0·0086
			C_4 0·0011	C_{33} 0·0079
			C_{26} 0·0007	C_{30} 0·0064
			C_{29} 0·0007	C_{35} 0·0058
			C_{28} 0·0004	C_{32} 0·0047
				C_{37} 0·0043
				C_{34} 0·0035
				C_6 0·0027
				C_{35} 0·0026
				C_3 0·0020
				C_2 0·0007
				C_4 0·0004
				C_1 0·0004

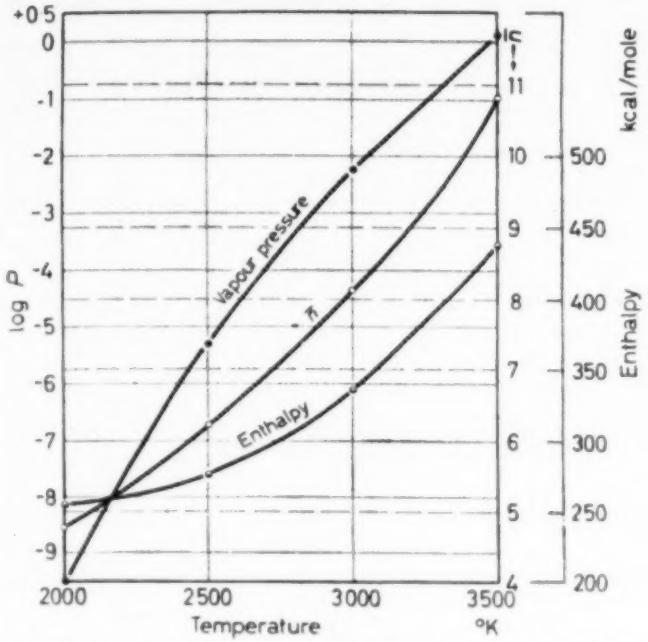

Figure 1. Equilibrium vapour pressure, mean number of carbon atoms, and enthalpy of polyatomic carbon vapour

of the combustion reaction as follows:

(*1*) Reactants and products in the gas phase are assumed to behave as ideal gases which form ideal gas mixtures.

(*2*) The solid phase is defined to have a partial pressure of zero and a fugacity of one atmosphere; its volume is negligible compared with the gas volume, and the temperature is the same as the gas temperature.

As an example consider the constant pressure, adiabatic combustion of one mole of acetylene with 0·9 mole of oxygen according to the following general reaction equation

$$A\,[C_2H_2 + 0{\cdot}9O_2] \longrightarrow \Sigma n_{i\ (\text{products})}$$

where the products were assumed to consist of the following molecules, radicals, and atoms:

$$CO,\ CO_2,\ O_2,\ H_2,\ H_2O,\ OH,\ C_2,\ CH,\ CH_4,\ C_2H_2,\ C_2H_4,\ O,\ H,\ C_{gas},\ C_{solid}$$

Machine computations were made for mixtures of one mole of acetylene with, respectively,

Table 7. Equilibrium composition and flame temperature results—I

Moles fuel	*One mole of acetylene*					
Moles oxygen	2·5	2·0	1·5	1·2	1·1	1·0
Flame temp. °K	3345	3398	3435	3415	3383	3325
CO	0·33400	0·40701	0·49771	0·56129	0·58396	0·60687
H_2	0·03619	0·05430	0·09194	0·14235	0·17159	0·21380
H	0·07747	0·10797	0·15367	0·18205	0·18539	0·17924
C_2H_2	$1{\cdot}92\times10^{-15}$	$1{\cdot}07\times10^{-14}$	$1{\cdot}22\times10^{-13}$	$1{\cdot}64\times10^{-12}$	$9{\cdot}00\times10^{-12}$	$1{\cdot}64\times10^{-}$
CH	$2{\cdot}52\times10^{-11}$	$7{\cdot}76\times10^{-11}$	$3{\cdot}15\times10^{-10}$	$1{\cdot}05\times10^{-9}$	$2{\cdot}10\times10^{-9}$	$2{\cdot}11\times10^{-}$
CH_4	$3{\cdot}31\times10^{-14}$	$1{\cdot}29\times10^{-13}$	$8{\cdot}91\times10^{-13}$	$6{\cdot}56\times10^{-12}$	$2{\cdot}17\times10^{-11}$	$4{\cdot}60\times10^{-}$
C_2H_4	$6{\cdot}39\times10^{-21}$	$4{\cdot}87\times10^{-20}$	$8{\cdot}81\times10^{-19}$	$1{\cdot}90\times10^{-17}$	$1{\cdot}34\times10^{-16}$	$3{\cdot}38\times10^{-}$
$C_{1\,(g)}$	$5{\cdot}55\times10^{-10}$	$1{\cdot}50\times10^{-9}$	$4{\cdot}93\times10^{-9}$	$1{\cdot}28\times10^{-8}$	$2{\cdot}23\times10^{-8}$	$1{\cdot}86\times10^{-}$
$C_{1\,(g)\ (sat.)}$	$8{\cdot}30\times10^{-4}$	$1{\cdot}95\times10^{-3}$	$1{\cdot}64\times10^{-3}$	$1{\cdot}41\times10^{-3}$	$1{\cdot}11\times10^{-3}$	$7{\cdot}18\times10^{-}$
$C_{2\,(g)}$	$1{\cdot}52\times10^{-16}$	$7{\cdot}92\times10^{-16}$	$6{\cdot}77\times10^{-15}$	$5{\cdot}17\times10^{-14}$	$1{\cdot}92\times10^{-13}$	$1{\cdot}94\times10^{-}$
C_{solid}*	0	0	0	0	0	0
O	0·11963	0·09958	0·05675	0·01955	0·00811	$5{\cdot}01\times10^{-}$
O_2	0·12049	0·06274	0·01671	0·00221	0·00045	$2{\cdot}47\times10^{-}$
OH	0·09662	0·08702	0·05913	0·02668	0·01302	$1{\cdot}06\times10^{-}$
H_2O	0·10105	0·09493	0·07504	0·04456	0·02651	$2{\cdot}85\times10^{-}$
CO_2	0·11455	0·08644	0·04905	0·02133	0·01097	$9{\cdot}99\times10^{-}$
p (*atm*)	1·00000	0·99999	1·00000	1·00002	1·00001	1·00000
A	0·22428	0·24673	0·27338	0·29118	0·29743	0·30347

*Moles per mole of gaseous products.

Continued overleaf

Table 7. Equilibrium composition and flame temperature results—I (continued)

Moles fuel	*One mole of acetylene*				
Moles oxygen	0·97	0·93	0·9	0·8	0·5
Flame temp. °K	3304	3275	3266	3233	3122
CO	0·60318	0·59692	0·59139	0·56749	0·46559
H_2	0·21636	0·22092	0·22651	0·25426	0·37119
H	0·17097	0·15989	0·15887	0·15433	0·13735
C_2H_2	0·00905	0·02154	0·02257	0·02338	0·02572
CH	$4·45\times10^{-5}$	$6·11\times10^{-5}$	$5·77\times10^{-5}$	$4·91\times10^{-5}$	$2·75\times10^{-5}$
CH_4	$1·15\times10^{-6}$	$1·75\times10^{-6}$	$2·14\times10^{-6}$	$2·76\times10^{-6}$	$6·63\times10^{-6}$
C_2H_4	$1·96\times10^{-7}$	$5·19\times10^{-7}$	$5·51\times10^{-7}$	$6·85\times10^{-7}$	$1·39\times10^{-6}$
$C_{1(g)}$	$3·77\times10^{-4}$	$4·84\times10^{-4}$	$4·52\times10^{-4}$	$3·46\times10^{-4}$	$1·34\times10^{-4}$
$C_{1(g)(sat.)}$	$6·09\times10^{-4}$	$4·84\times10^{-4}$	$4·52\times10^{-4}$	$3·46\times10^{-4}$	$1·34\times10^{-4}$
$C_{2(g)}$	$9·17\times10^{-5}$	$1·89\times10^{-4}$	$1·70\times10^{-4}$	$1·24\times10^{-4}$	$4·18\times10^{-5}$
C_{solid}*	0	0·00091	0·01973	0·09447	0·41389
O	$1·95\times10^{-7}$	$1·06\times10^{-7}$	$1·01\times10^{-7}$	$8·36\times10^{-8}$	$4·11\times10^{-8}$
O_2	$4·02\times10^{-13}$	$1·39\times10^{-13}$	$1·33\times10^{-13}$	$1·11\times10^{-13}$	$5·28\times10^{-14}$
OH	$4·30\times10^{-7}$	$2·49\times10^{-7}$	$2·47\times10^{-7}$	$2·36\times10^{-7}$	$1·88\times10^{-7}$
H_2O	$1·23\times10^{-6}$	$7·99\times10^{-7}$	$8·27\times10^{-7}$	$9·34\times10^{-7}$	$1·32\times10^{-6}$
CO_2	$4·27\times10^{-7}$	$2·71\times10^{-7}$	$2·70\times10^{-7}$	$2·62\times10^{-7}$	$2·13\times10^{-7}$
p (atm)	1·00008	1·00001	1·00002	0·99998	1·00005
A	0·31092	0·32092	0·32854	0·35468	0·46559

*Moles per mole of gaseous products.

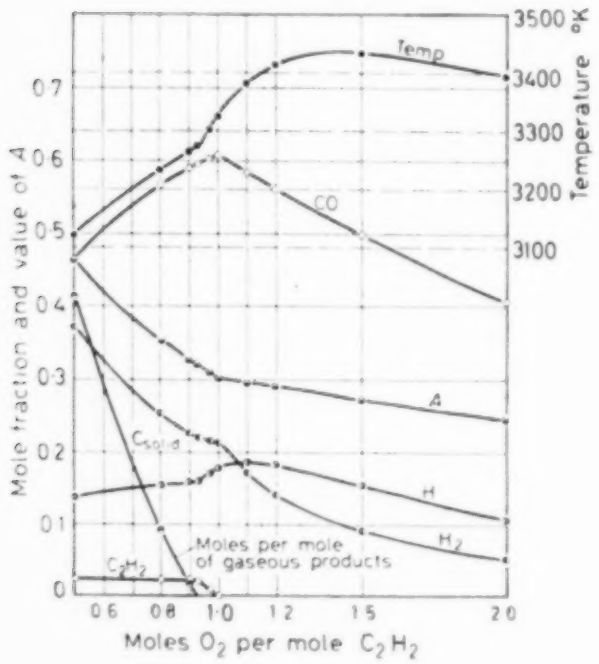

Figure 2. Equilibrium concentration of main combustion products, flame temperature, and value of A

2·5, 2·0, 1·5, 1·2, 1·1, 1·0, 0·97, 0·93, 0·9, 0·8 and 0·5 moles of oxygen. The results of these calculations are compiled in *Table 7*. For the study of comparisons and trends, various of these results are plotted in the figures following. A mixture of 2·5 moles of oxygen to one mole of acetylene represents the stoichiometric mixture so that all the calculations were for rich mixtures except for this chemically correct one.

Figure 2 shows the mole fraction of the principal products of combustion and the variation of the parameter *A* and flame temperature with changes in the mixture ratio. The flame temperature reaches a maximum of approximately 3 435° K at a mixture ratio of 1·4 mole of oxygen per mole of acetylene and decreases rapidly for richer mixtures. There is a definite change in trend for the temperature occurring at the point where C_{solid} appears as a product, i.e. at approximately 0·93 mole of oxygen per mole of fuel. This pronounced change is also evident in the acetylene and hydrogen (H) curves. Abrupt changes in slope for the carbon mon-

oxide and hydrogen (H_2) curves occur at the 1:1 mixture ratio; the former reaching a maximum at this ratio, as might be expected, and the latter showing a change in trend toward generally increasing amounts as the mixture is made richer. The value of A changes continuously in the way that would be expected from the fact that the total pressure is held constant but more and more moles of products must be formed from the leaner mixtures. Acetylene itself becomes an appreciable product as the mixtures are enriched beyond 1:1 and the amount of C_{solid} formed is shown to increase rapidly. It is to be noted that the C_{solid} curve is plotted in terms of moles per mole of gaseous products since the solid carbon was assumed to have a partial pressure of zero.

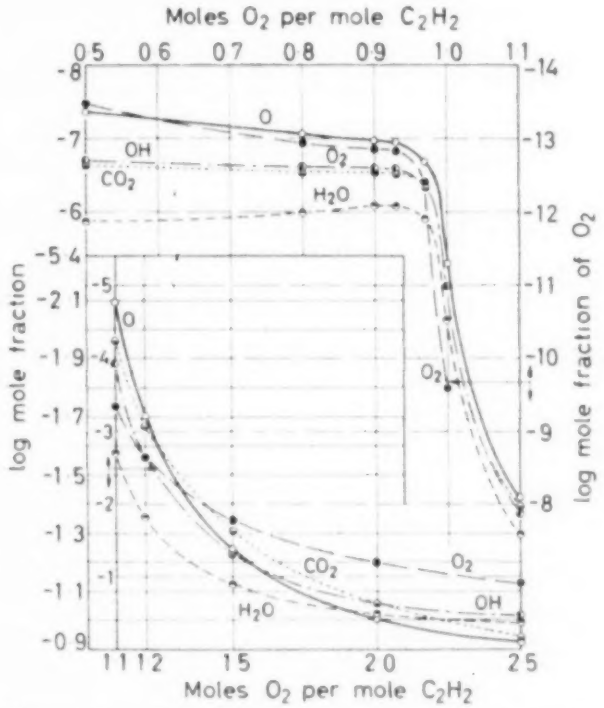

Figure 3. Equilibrium concentration of oxygen-containing species (except CO)

Figure 3 shows the concentration of monatomic and diatomic oxygen and the other species containing oxygen except for CO which is shown in *Figure 2*. All of these substances exhibit a marked change in concentration between narrow limits of oxygen/fuel ratios in the vicinity of the 1:1 mixture and the curves in *Figure 3* are broken in that region. All of them change by about five or six orders of magnitude in this region, becoming significant only on the lean side of the 1:1 ratio. The curve for O_2 is drawn to a separate vertical scale because it differs in concentration at all mixture ratios by several orders of magnitude from the other components.

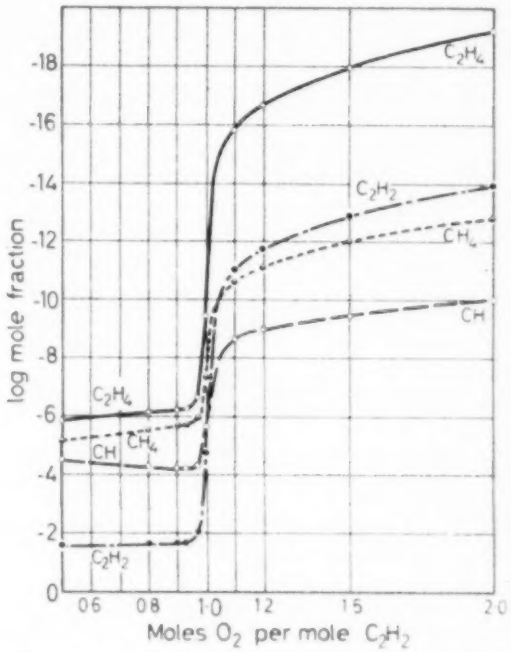

Figure 4. Equilibrium concentration of the hydrocarbons

Figure 4 indicates the concentration of the hydrocarbon compounds as a function of mixture ratio. As in the oxygen-containing components there is a marked change in concentration around the mixture ratio 1:1, but in the opposite direction. A decrease of concentration of six to twelve orders of magnitude is noted as the mixtures become leaner. Acetylene is also plotted in this figure over the complete range of mixture ratios shown.

Figure 5 shows the concentration of diatomic and monatomic carbon gas as well as the concentration of monatomic carbon gas which would be required in order for it to be in equilibrium with solid carbon at the corresponding calculated adiabatic flame temperature.

The results of these calculations may be compared with those of other workers[15] at mixture ratios of 2·5 and 0·5 moles oxygen per

Table 7. Equilibrium composition and flame temperature results—I (continued)

Moles fuel	*One mole of acetylene*				
Moles oxygen	0·97	0·93	0·9	0·8	0·5
Flame temp. °K	3304	3275	3266	3233	3122
CO	0·60318	0·59692	0·59139	0·56749	0·46559
H_2	0·21636	0·22092	0·22651	0·25426	0·37119
H	0·17097	0·15989	0·15887	0·15433	0·13735
C_2H_2	0·00905	0·02154	0·02257	0·02338	0·02572
CH	$4·45\times10^{-5}$	$6·11\times10^{-5}$	$5·77\times10^{-5}$	$4·91\times10^{-5}$	$2·75\times10^{-5}$
CH_4	$1·15\times10^{-6}$	$1·75\times10^{-6}$	$2·14\times10^{-6}$	$2·76\times10^{-6}$	$6·63\times10^{-6}$
C_2H_4	$1·96\times10^{-7}$	$5·19\times10^{-7}$	$5·51\times10^{-7}$	$6·85\times10^{-7}$	$1·39\times10^{-6}$
$C_{1(g)}$	$3·77\times10^{-4}$	$4·84\times10^{-4}$	$4·52\times10^{-4}$	$3·46\times10^{-4}$	$1·34\times10^{-4}$
$C_{1(g)(sat.)}$	$6·09\times10^{-4}$	$4·84\times10^{-4}$	$4·52\times10^{-4}$	$3·46\times10^{-4}$	$1·34\times10^{-4}$
$C_{2(g)}$	$9·17\times10^{-5}$	$1·89\times10^{-4}$	$1·70\times10^{-4}$	$1·24\times10^{-4}$	$4·18\times10^{-5}$
C_{solid}*	0	0·00091	0·01973	0·09447	0·41389
O	$1·95\times10^{-7}$	$1·06\times10^{-7}$	$1·01\times10^{-7}$	$8·36\times10^{-8}$	$4·11\times10^{-8}$
O_2	$4·02\times10^{-13}$	$1·39\times10^{-13}$	$1·33\times10^{-13}$	$1·11\times10^{-13}$	$5·28\times10^{-14}$
OH	$4·30\times10^{-7}$	$2·49\times10^{-7}$	$2·47\times10^{-7}$	$2·36\times10^{-7}$	$1·88\times10^{-7}$
H_2O	$1·23\times10^{-6}$	$7·99\times10^{-7}$	$8·27\times10^{-7}$	$9·34\times10^{-7}$	$1·32\times10^{-6}$
CO_2	$4·27\times10^{-7}$	$2·71\times10^{-7}$	$2·70\times10^{-7}$	$2·62\times10^{-7}$	$2·13\times10^{-7}$
p (atm)	1·00008	1·00001	1·00002	0·99998	1·00005
A	0·31092	0·32092	0·32854	0·35468	0·46559

*Moles per mole of gaseous products.

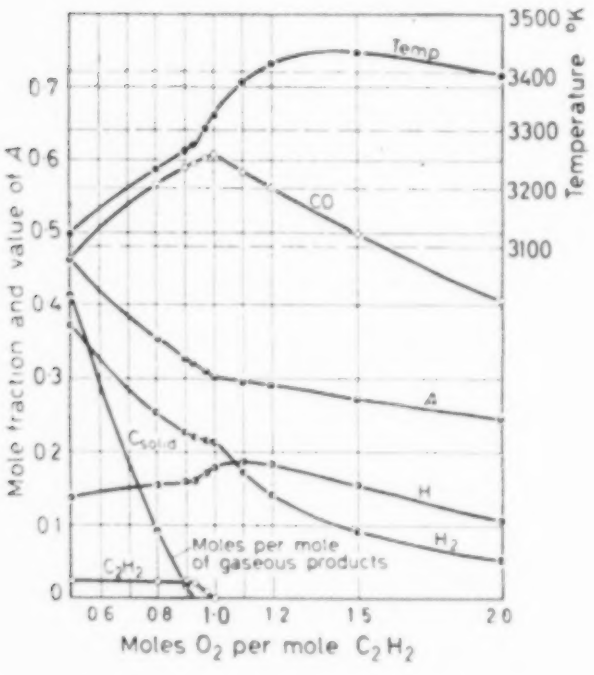

Figure 2. Equilibrium concentration of main combustion products, flame temperature, and value of A

2·5, 2·0, 1·5, 1·2, 1·1, 1·0, 0·97, 0·93, 0·9, 0·8 and 0·5 moles of oxygen. The results of these calculations are compiled in *Table 7*. For the study of comparisons and trends, various of these results are plotted in the figures following. A mixture of 2·5 moles of oxygen to one mole of acetylene represents the stoichiometric mixture so that all the calculations were for rich mixtures except for this chemically correct one.

Figure 2 shows the mole fraction of the principal products of combustion and the variation of the parameter *A* and flame temperature with changes in the mixture ratio. The flame temperature reaches a maximum of approximately 3 435 °K at a mixture ratio of 1·4 mole of oxygen per mole of acetylene and decreases rapidly for richer mixtures. There is a definite change in trend for the temperature occurring at the point where C_{solid} appears as a product, i.e. at approximately 0·93 mole of oxygen per mole of fuel. This pronounced change is also evident in the acetylene and hydrogen (H) curves. Abrupt changes in slope for the carbon mon-

oxide and hydrogen (H_2) curves occur at the 1:1 mixture ratio; the former reaching a maximum at this ratio, as might be expected, and the latter showing a change in trend toward generally increasing amounts as the mixture is made richer. The value of A changes continuously in the way that would be expected from the fact that the total pressure is held constant but more and more moles of products must be formed from the leaner mixtures. Acetylene itself becomes an appreciable product as the mixtures are enriched beyond 1:1 and the amount of C_{solid} formed is shown to increase rapidly. It is to be noted that the C_{solid} curve is plotted in terms of moles per mole of gaseous products since the solid carbon was assumed to have a partial pressure of zero.

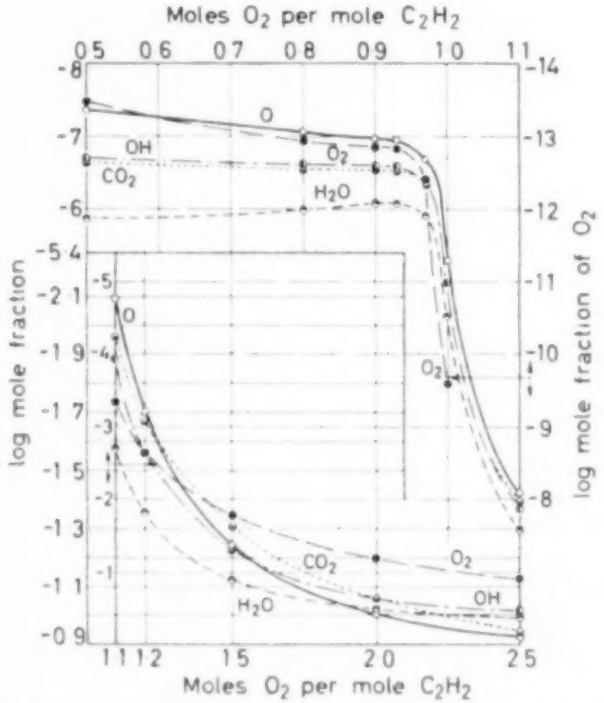

Figure 3. Equilibrium concentration of oxygen-containing species (except CO)

Figure 3 shows the concentration of monatomic and diatomic oxygen and the other species containing oxygen except for CO which is shown in *Figure 2*. All of these substances exhibit a marked change in concentration between narrow limits of oxygen/fuel ratios in the vicinity of the 1:1 mixture and the curves in *Figure 3* are broken in that region. All of them change by about five or six orders of magnitude in this region, becoming significant only on the lean side of the 1:1 ratio. The curve for O_2 is drawn to a separate vertical scale because it differs in concentration at all mixture ratios by several orders of magnitude from the other components.

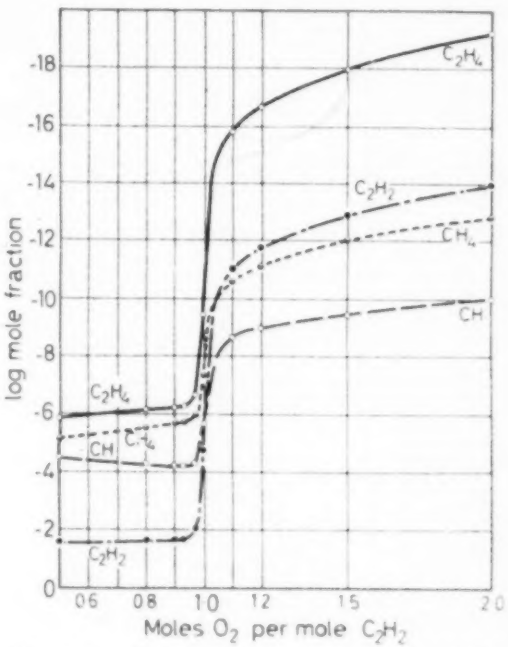

Figure 4. Equilibrium concentration of the hydrocarbons

Figure 4 indicates the concentration of the hydrocarbon compounds as a function of mixture ratio. As in the oxygen-containing components there is a marked change in concentration around the mixture ratio 1:1, but in the opposite direction. A decrease of concentration of six to twelve orders of magnitude is noted as the mixtures become leaner. Acetylene is also plotted in this figure over the complete range of mixture ratios shown.

Figure 5 shows the concentration of diatomic and monatomic carbon gas as well as the concentration of monatomic carbon gas which would be required in order for it to be in equilibrium with solid carbon at the corresponding calculated adiabatic flame temperature.

The results of these calculations may be compared with those of other workers[15] at mixture ratios of 2·5 and 0·5 moles oxygen per

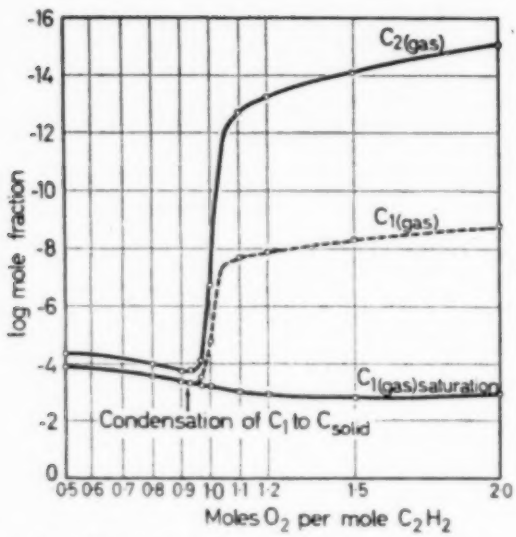

Figure 5. Equilibrium concentration of C_1, C_2 and $C_{1\,(sat.)}$

mole of acetylene. The comparison is shown in *Table 8* where the values given are mole fractions for the gaseous components and moles/mole of gaseous products for solid carbon. The comparison is quite reasonable at the 2·5/1 ratio when it is considered that a different value for the dissociation energy of OH was used in this work. Comparison of the results at the mixture ratio of 0·5/1 shows the importance of including acetylene as a product. The temperature is significantly different as is also the amount of solid carbon in the products.

Table 8. Comparison with reference of the concentration of the combustion products of oxyacetylene mixtures

Species	*Ref. 4*	*This work*
Mixture ratio: 2·5 moles O_2/mole C_2H_2		
CO	0·33453	0·33400
CO_2	0·10940	0·11455
O_2	0·12346	0·12049
H_2	0·03926	0·03619
H_2O	0·09784	0·10105
OH	0·08596	0·09662
O	0·12577	0·11963
H	0·08376	0·07747
CH_4	0	$3·31 \times 10^{-11}$
C_2H_2	*Not included*	$1·92 \times 10^{-11}$
C_{solid}	0	0
T, °K	3358·5	3345
Mixture ratio: 0·5 mole of O_2/mole C_2H_2		
CO	0·45589	0·46559
CO_2	0	$2·13 \times 10^{-7}$
O_2	0	$5·28 \times 10^{-14}$
H_2	0·36765	0·37119
H_2O	0	$1·32 \times 10^{-6}$
OH	0	$1·88 \times 10^{-7}$
O	0	$4·11 \times 10^{-8}$
H	0·17645	0·13735
CH_4	0·00001	$6·63 \times 10^{-6}$
C_2H_2	*Not included*	0·02572
C_{solid}	0·49999	0·41389
T, °K	3213·6	3122

Determination of Mixture Ratio and Flame Temperature for the Formation of Solid Carbon, considering Polyatomic Carbon Vapour Species

Since the main objective of this research was to determine the leanest mixture ratio for which solid carbon would appear as an equilibrium product, it became evident from the preceding work on acetylene that a simplified procedure might be used before attempting calculations involving the polyatomic forms of carbon. It can be seen in *Table 7* that the equilibrium products of combustion for fuel–oxygen mixtures rich enough to allow solid carbon as a product of the reaction consist essentially of: CO, H_2, H, C_2H_2, C_n, and C_{solid}. In this case C_n represents the vapour phase of carbon which may contain polyatomic molecular species. The simplified procedure evolved from a number of attempts to find a system of equations, containing these products, which were adaptable to solution by other than successive approximation methods. This procedure was then used to pinpoint the leanest oxygen/fuel ratio and flame temperature for the condensation of carbon when considering only C_1 and C_2 as the possible carbon vapour constituents.

In order to test the validity of the simplified calculation procedure, a calculation was made of the equilibrium composition and flame temperature for the mixture of one mole of C_2H_2 and 0·9 mole of O_2. The second column in

Table 9. Equilibrium composition and flame temperature results—II

Mole fuel	1 C_2H_2	1 C_2H_2	1 C_2H_2	1 C_2H_2	1 C_2H_4
Mole oxygen	0·928	0·900	0·865	0·743	0·990
Flame temp. °K	3275	3266·5	3197	3095	2345
CO	0·59745	0·59138	0·58316	0·55316	0·49529
H_2	0·21958	0·22651	0·24728	0·29632	0·49355
H	0·15995	0·15890	0·13807	0·11362	0·00885
C_2H_2	0·02235	0·02258	0·02078	0·01912	0·00232
CH	$6·00\times10^{-5}$	$5·76\times10^{-5}$	$3·79\times10^{-5}$	$1·94\times10^{-5}$	$1·97\times10^{-8}$
CH_4	$1·97\times10^{-6}$	$2·12\times10^{-6}$	$2·71\times10^{-6}$	$1·30\times10^{-7}$	$4·52\times10^{-5}$
C_2H_4	$5·21\times10^{-7}$	$5·52\times10^{-7}$	$6·38\times10^{-7}$	$7·92\times10^{-9}$	$1·92\times10^{-6}$
$C_{1\,(gas)}$	0·00048	0·00045	$C_n=0·01072$	$C_n=0·01778$	$1·53\times10^{-8}$
$C_{2\,(gas)}$	0·00018	0·00017	$n=4·57$	$n=8·58$	$1·16\times10^{-9}$
C_{solid}*	0·00081	0·01975	0·0049	0·00052	0·00037
O	$1·06\times10^{-7}$	$1·01\times10^{-7}$	$7·30\times10^{-8}$	$1·77\times10^{-8}$	$3·29\times10^{-10}$
O_2	$1·39\times10^{-13}$	$1·33\times10^{-13}$	$1·05\times10^{-13}$	$1·16\times10^{-14}$	$2·26\times10^{-15}$
OH	$2·49\times10^{-7}$	$2·47\times10^{-7}$	$2·24\times10^{-7}$	$3·10\times10^{-8}$	$3·05\times10^{-8}$
H_2O	$8·01\times10^{-7}$	$8·27\times10^{-7}$	$9·86\times10^{-7}$	$5·37\times10^{-7}$	$1·01\times10^{-5}$
CO_2	$2·71\times10^{-7}$	$2·70\times10^{-7}$	$2·94\times10^{-7}$	$5·29\times10^{-8}$	$1·59\times10^{-6}$
Σp *(atm)*	1·00005	1·00005	1·00005	1·00002	1·00007
A	0·32190	0·32854	0·33709	0·37225	0·25015

*Moles per mole of gaseous products.

Table 9 shows the results of these calculations, wherein the concentrations of the minor components were obtained simply by use of the equilibrium constants of formation for these compounds. Comparison of these results with those in *Table 7* for the same mixture shows that the results are essentially the same. The first column in *Table 9* contains the results of a calculation, using the simplified procedure, of the equilibrium composition and flame temperature at the point of carbon condensation, considering only C_1 and C_2 as the possible carbon vapour species. Again the results agree very well with the matrix solution results.

When considering all reasonably possible forms of carbon vapour, the above procedure was used but a number of trial and error solutions were necessary when both amount of oxygen and temperature were not known, even approximately. Calculations were made for the following fuels: acetylene (C_2H_2); ethylene (C_2H_4); methane (CH_4); ethane (C_2H_6); and methyl acetylene (C_3H_4).

Acetylene

The reaction equation for acetylene was considered to be

$$A\,(C_2H_2 + xO_2) \longrightarrow 2Ax\,[CO] + n_2\,[H_2] + 2\,(A - n_2 - n_5)\,[H] + n_4\,[C_n^-] + n_5\,[C_2H_2] + n_6\,[C_{solid}]$$

Beginning with an assumed number of moles of oxygen for combustion and a flame temperature, calculations would proceed until it was evident that no solid carbon could be formed, or if solid carbon existed then the procedure would be carried until a final enthalpy balance of the products formed, at the assumed temperature, could be made. In addition, even supposing the satisfaction of the above two requirements, calculations were continued until the amount of solid carbon formed was so small that the moles of oxygen required was affected only in the third decimal place. The required values of n_4 and n for the polyatomic carbon were taken from *Figure 1*. In the final solution for acetylene, these values were:

$$n_4 = P = \text{antilog}\,(-1{\cdot}75) = 0{\cdot}017783$$

and

$$n = 8{\cdot}58$$

The enthalpy for $C_n^=$ was determined from the same figure and since these enthalpies were calculated above graphite at 0° K for the datum, the actual enthalpy, to be consistent with the other thermodynamic properties, must be calculated as

$$H\,[C_n] = H\,[C_n]_{\text{(Figure 1)}} + n\,[H_n^0]_{C_{\text{solid}}}$$

$$= 354 + 8{\cdot}58\,(112{\cdot}088) = \mathbf{1\,315{\cdot}715}\ \text{kcal/mole}$$

The final result was concluded to occur when the amount of carbon-solid was 0·00052 mole/mole of gaseous products, and at this time, the amount of oxygen was 0·743 mole/mole of C_2H_2 and the equilibrium flame temperature was 3 095° K. The final equilibrium composition of the products is given in *Table 9*.

Ethylene

The reaction equation for ethylene was written as

$$A\,[C_2H_4 + xO_2] \longrightarrow 2Ax\,[CO] + n_2\,[H_2] + 2\,(2A - n_2 - n_5)\,[H] + n_4\,[C_n^=] + n_5\,[C_2H_2] + n_6\,[C_{\text{solid}}]$$

Assuming various combinations of x and temperature, the calculations were carried out until final results of 0·990 mole of O_2 per mole of C_2H_4 and a temperature of 2 345° K were obtained. At this point the amount of carbon-solid was 0·000365 mole per mole of gaseous products and all final results are tabulated in *Table 9* as for acetylene. Unlike acetylene, however, the difference in the ethylene calculations using either C_4 and C_2 or values of $C_n^=$ with $n = 5{\cdot}7$ were negligibly small because of the low partial pressure of the carbon vapour at the temperature of 2 345° K and its consequent insignificant contribution to the total.

Methane, ethane, methyl acetylene

Simplified calculations for these three fuels showed that the flame temperatures for mixtures sufficiently rich to form solid carbon were well below 1 000° K, and that the mixtures were beyond the rich inflammability limits. Therefore these fuels were excluded in the experimental work discussed in the next section.

Experimental Determination of the Mixture Ratio for the Formation of Solid Carbon

Experiments were performed in the laboratory whereby premixed flames of oxygen–acetylene and oxygen–ethylene were studied and photographed. A diagrammatic sketch of the apparatus used is shown in *Figure 6*. One of the first steps was to calibrate the rotameters used against a wet-test meter in order to be certain of the fuel/air mixture ratio to be studied. Recalibration runs were made frequently to assure continued accuracy. The fuels and oxygen were thoroughly mixed before issuing from the burner orifice tip and the fuels used were chemically pure. To eliminate the influence of the air surrounding the open flame several experiments were run using an 80 mm glass tube in various heights over the burner plate. The same effect was also accomplished by blowing a blanket of nitrogen through an annular space surrounding the burner tip. In both cases, the only observable effect of this precaution was to eliminate the secondary diffusion flame and no effect was discernible regarding the inner flame cones which were of primary interest to the study.

A small water-cooled plate held just over the tip of the flame proved to be the best method for determining the existence or non-existence of solid carbon in the products of combustion. Simple visualization of the yellow-orange streaks generally assumed to be incandescent carbon proved a faulty measure of actual carbon formation. Many runs were made varying the water flow rate and consequently the plate temperature over a wide range, and there was no apparent influence of plate temperature on the critical mixture ratio. Runs were made also for various lengths of time in order to verify that the results were a function only of mixture ratio and not of time.

With ethylene as the fuel no carbon was deposited on the cooled plate, with a volumetric oxygen/ethylene ratio of 1·02. When this ratio was changed to 0·994, carbon deposition was

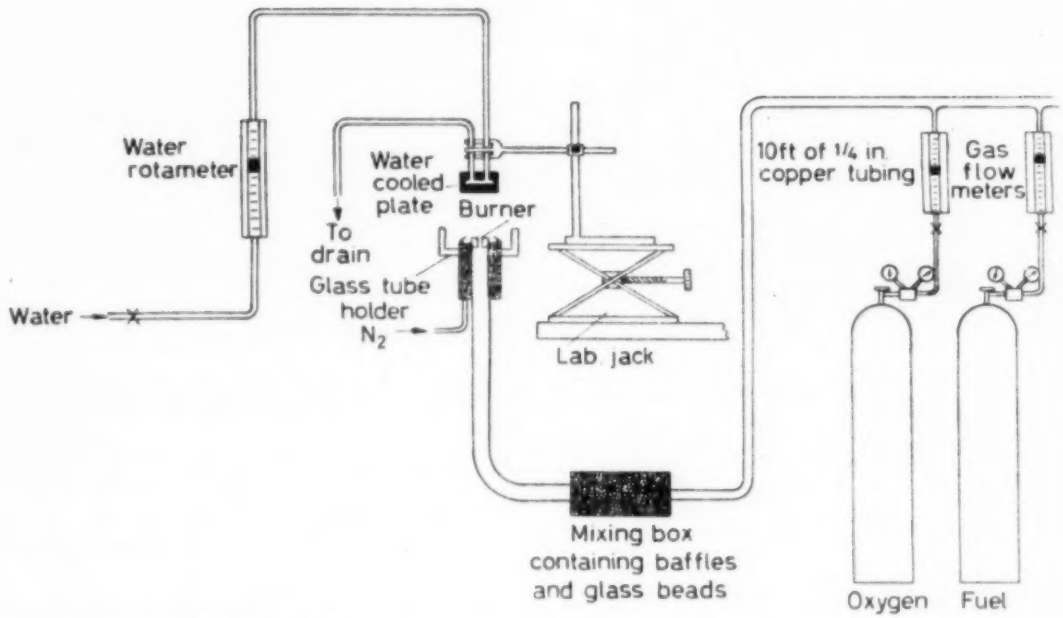

Figure 6. Schematic diagram of experimental apparatus

obtained even though the appearance of the flame was not noticeably different. Several combinations of mixture flow rate and burner orifice diameter were tried in order to produce the most stable flame, without pulsations or a tendency to blow off. An orifice diameter of $\frac{3}{32}$ in. was used and the flow rate of ethylene was maintained constant while the oxygen flow was varied. The presence of the cooled plate had no noticeable effect on the flame structure, as evidenced both by visual inspection with filters, and by coloured photographs of the flame structure.

Photographs of the oxyacetylene flame are shown in *Figures 7* and *8*. A burner tip diameter of $\frac{1}{16}$ in. was used with this much faster burning, hotter flame as compared with ethylene. A striking and abrupt change occurred when the transition was made from an oxygen/fuel ratio exhibiting no carbon formation tendency to one wherein carbon was deposited. Evidence of the presence of carbon deposits was obtained with the plate held at various heights over the flame cone and in every case when the deposition of carbon was observed it was possible to adjust the plate to such a height over the flame as to cause the instantaneous appearance of the brilliant inverted cone shown in *Figure 8*. At mixture ratios leaner than some critical ratio, no such inverted cone could be made to appear nor could any evidence of the formation of solid carbon on the cooled plate be obtained. A typical flame without carbon formation is shown in *Figure 7*. As with ethylene, the acetylene flow was maintained at a constant value and the oxygen flow was adjusted to vary the mixture ratio. The formation of carbon was first noted to appear at an oxygen/fuel ratio of approximately 0·865 to 1. This result lies between the value predicted from the calculations using C_1 and C_2 forms of carbon vapour only and that value predicted on the possibility of longer carbon vapour molecules. Therefore, calculations were made using these results in an attempt to predict the number of possible polymers of carbon present in the actual flame. These calculations and further diagnosis of the flame structure are discussed in the next section.

Results and Conclusions

Results of the calculations of equilibrium composition and flame temperature for the various mixture ratios and fuels are compiled and presented in *Table 9*.

As stated previously, the results for ethylene, calculated considering either a large number of

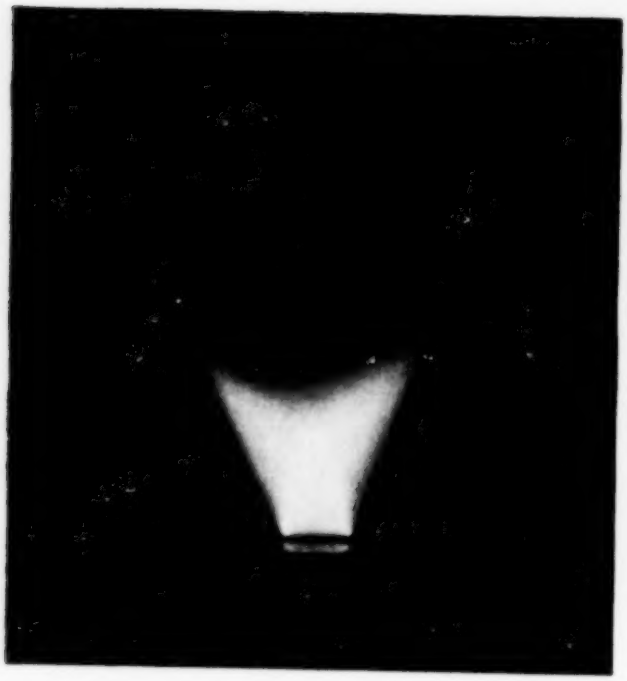

Figure 7. Acetylene–oxygen flame, 0·87 mole O_2/mole C_2H_2

Figure 8. Acetylene–oxygen flame, 0·86 mole O_2/mole C_2H_2

molecular carbon species in the products or only monatomic and diatomic forms of carbon yield almost identical results. The experimental results indicated the formation of carbon at an oxygen/fuel ratio by volume of slightly under 1·0 and both these results are in reasonable agreement with the theoretical carbon point, i.e. where the O/C ratio is 1·0.

For acetylene, however, with its considerably higher flame temperatures, the results in all cases deviate from the theoretical carbon point of 1·0. Calculations based on the assumed presence of only monatomic and diatomic forms of carbon in the products yielded an O/C ratio of 0·928 and a flame temperature of 3 275°K, whereas calculations based on the theory of indefinite carbon chains with correspondingly increased vapour pressures yielded a value of 0·743 for this ratio and a flame temperature of 3 095°K. Neither of these predictions was verified by the flame studies wherein an O/C ratio of 0·865 intermediate to the calculated values was obtained.

Using this experimentally determined ratio, calculations were then made in a manner similar to that described above. In this case, however, the O/C ratio, instead of being considered an unknown parameter, was taken at the 0·865 value, and various values of the number of carbon atoms per equivalent molecule were assumed until a solution was obtained. A reaction equation of the form

$$A\,[C_2H_2 + 0{\cdot}865O_2] \longrightarrow 1{\cdot}73\,[CO] + n_2\,[H_2] + 2\,(A - n_2 - n_5)\,[H] + n_4\,[C_n] + n_5\,[C_2H_2] + n_6\,[C_{solid}]$$

was considered where n and n_4 were calculated over a range of temperatures for carbon vapour made up of the species $C_1 + C_2$, $C_1 + C_2 + C_3$, $C_1 + C_2 + C_3 + C_4$, etc. The necessary values of $\log P$, n and enthalpy for each aggregation were calculated and a typical example of the results of such calculations is shown in *Figure 9*. This figure is for a mixture consisting of C_1, C_2, C_3, C_4 and C_5 molecules which proved in fact to be the necessary vapour composition to give a solution to the above reaction equation. Simultaneous solution of the mass balance, dissociation, pressure and energy equations yielded the equilibrium composition and flame temperature results given in *Table 9* for this

experimentally determined O/C ratio. Taken at face value, these results indicate the existence of carbon molecules containing up to five atoms in the flame. Spectroscopically, carbon molecules up to three atoms per molecule have been observed. It can be postulated that the lack of proof of higher order species may be due to a reaction rate phenomenon not considered in equilibrium state calculations.

Referring again to *Figures 7* and *8*, it is emphasized that these photographs are considerably enlarged. *Figure 7* shows the appearance of the flame slightly leaner, and *Figure 8* slightly richer than a volumetric O_2/C_2H_2 ratio of 0·865 : 1. In *Figure 8* the bright spots at the outer edges of the inverted (yellow) cone are due to glowing carbon deposits on the water-cooled brass plate suspended approximately $\frac{1}{4}$ in. above the tip of the burner. The flame structure shown in *Figure 7* was as pictured in the photograph even when the water-cooled plate was removed, and whether or not a glass cylinder was placed around the burner tip to exclude atmospheric air from the combustion zone. However, as the mixture was made slightly richer, i.e. when the mixture was changed from that producing the flame shown in *Figure 7* to that producing the flame shown in *Figure 8*, the inverted cone of carbon did not appear unless the water-cooled plate was in place. Furthermore, the appearance of the carbon cone was critically dependent on a certain minimum distance of the cooled plate from the burner tip. Movement of the cooled plate less than $\frac{1}{32}$ in. beyond this minimum distance caused the yellow cone to disappear suddenly. All of the above remarks concerning the flame behaviour are relevant to oxygen–acetylene mixtures near the leanest mixture for which the carbon cone could be observed, i.e. at a volumetric oxygen/acetylene ratio of 0·865. It is rather doubtful that it is only coincidental that actual carbon deposition could be observed on the water-cooled plate only at this same ratio of 0·865 or lower. When the plate was suspended below the minimum distance required for the carbon cone to appear at a ratio of 0·865, and the ratio was changed to 0·87, not only did the carbon cone disappear but no carbon was collected on the cooled plate after as long as fifteen minutes of operation.

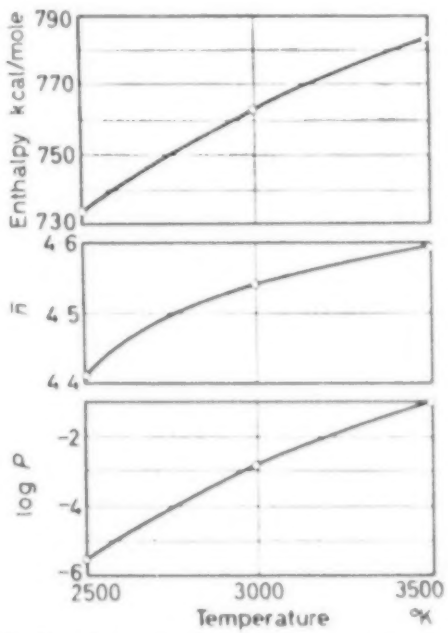

Figure 9. Equilibrium vapour pressure, mean number of carbon atoms, and enthalpy of carbon vapour consisting of a mixture of the species C_1, C_2, C_3, C_4 and C_5

The most interesting fact, when considered in the light of the above evidence, is that when the carbon cone is made to appear by means of the cooled plate, the point of initiation of the condensed carbon must be immediately above the tip of the inner cone, i.e. the lowest point of the inverted carbon cone. This point is only 0·015 in. above the tip of the inner cone and should correspond to the region of highest temperature of the product gases.

A further observation, which may be significant and which is evident in the photographs, is the fact that the inverted cone exhibits a cellular structure which is generally attributed to a preferential diffusion mechanism. Since it is difficult to believe that the temperature at a point 0·015 in. above the tip of the inner cone is any different with or without the cooled plate present, a logical conclusion would appear to be that condensed carbon is there when the plate is not present, but moves away so quickly that it is not evident visually. Although not visible in *Figure 8*, a swirling action was observed on

the surface of the inverted carbon cone. Thus, it is possible that with the cooled plate present, a more-or-less stagnant or recirculation zone is formed whose boundaries are essentially the hydrodynamically induced surface of the inverted carbon cone, and there is more time available for condensation and agglomeration of the carbon trapped in this stagnant zone. *Figure 8* makes it apparent that agglomeration certainly takes place on the plate itself, which would form the upper boundary of the recirculation zone. Consideration was given to the possibility tnat the inverted cone was an isothermal surface, but no reasonable argument was forthcoming to support such a view.

When ethylene was the fuel there was no evidence of an inverted carbon cone. Considering the product gases as a mixture in chemical equilibrium, the much lower temperature and correspondingly lower carbon vapour pressure in the ethylene–oxygen flame must be considered. In the ethylene–oxygen calculations, the equilibrium between carbon vapour and solid carbon was not included since the mole fraction of carbon vapour was of the order of 10^{-7}. Solid carbon was included in the calculations by means of the reaction

$$2C_{solid} + H_2 \longrightarrow C_2H_2$$

Since the equilibrium constant for this reaction, considering acetylene as a product, decreases with decreasing temperature, and since there is a significant concentration of acetylene as an equilibrium product of the ethylene–oxygen reaction, it is possible that the amount of solid carbon calculated as an equilibrium product is dictated entirely by this reaction. It is true that the solid carbon present must still be in equilibrium with its vapour in order for condensation to occur, but the calculations show that the order of magnitude of the moles of solid carbon per mole of product was the same for both the ethylene–oxygen flame and the acetylene–oxygen flame at the critical fuel/oxygen ratio, whereas the corresponding equilibrium carbon vapour pressures in the two cases were several orders of magnitude apart.

It may be postulated that in the acetylene–oxygen flame the carbon deposition is due to condensation of carbon vapour, of either the monatomic or polyatomic form, and that in the ethylene–oxygen flame the carbon formation is due to the overall reaction

$$C_2H_2 \longrightarrow H_2 + 2C_{solid}$$

It is possible that from kinetic considerations the reaction mechanism for the latter reaction involves elementary reactions whose rate constants are much lower and that insufficient time is available in the case of the lower temperature ethylene–oxygen flame for carbon deposition to occur immediately above the tip of the inner cone.

Regardless of the actual chemical mechanism by which solid carbon is formed in the two flames, the fact remains that the cooled plate technique confirmed the calculations for ethylene, as regards the mixture ratio at which solid carbon appears. For acetylene, the experimental results with the cooled plate must be regarded as satisfactory, in view of the remaining uncertainty as to the existence of polyatomic carbon vapour species at the high temperature levels encountered in acetylene–oxygen flames.

References

[1] Rossini, F. D. *et al. Circ. U.S. Bur. Stand. No. 500*. Washington, 1952
[2] Pitzer, K. S. and Clementi, E. *J. Amer. chem. Soc.* 1959, **81**, 4477
[3] Herzberg, G. *Spectra of Diatomic Molecules*, 2nd ed. Van Nostrand: New York, 1950
[4] Rossini, F. D. *et al. Circ. U.S. Bur. Stand. No. 461*. Washington, 1947
[5] Sehon, A. H. and Szwarc, M. *Annu. Rev. phys. Chem.* 1957, **8**, 441
[6] Gay, N. R. *Ph.D. Thesis*. Purdue University, 1960
[7] Feigenbutz, L. V., Stiehl, G. L. and Katz, E. L. Convair *Rep. No. ZR-600-00 1* (1958)
[8] Brewer, L., Gilles, P. W. and Jenkins, F. A. *J. chem. Phys.* 1958, **16**, 797
[9] Gordon, J. S. Private communication, 1959
[10] Glockler, G. *J. chem. Phys.* 1954, **22**, 159
[11] Ballik, E. A. and Ramsay, D. A. *J. chem. Phys.* 1934, **31**, 1128
[12] Herzberg, G. *Infra-red and Raman Spectra*, 1st ed. Van Nostrand: New York, 1945
[13] Loethus, A. *J. Amer. chem. Soc.* 1957, **79**, 24
[14] Huff, V. N., Gordon, S. and Morrell, V. E. *Nat. Adv. Comm. Aero. Rep. No. 1037*, 1951
[15] Edwards, H. E., Smith, Jr, R. W. and Berkley, Jr, S. R. *Rep. Invest. U.S. Bur. Min. No. 4958*, 1953

Burning Velocities of the Hydrogen Peroxide Decomposition Flame

C. N. SATTERFIELD and E. KEHAT*

Department of Chemical Engineering, Massachusetts Institute of Technology, Cambridge, Mass.

(*Received October 1960*)

Burning velocities of the hydrogen peroxide decomposition flame have been measured by the bunsen burner method at pressures between 0·5 and 1 atmosphere. The flame reaction follows approximately first order kinetics with an activation energy of 35 kcal/mole, and shows general agreement with the mechanism and kinetics of the homogeneous non-flame reaction. A single plot of the logarithm of the product of the square of the burning velocity and the pressure versus the reciprocal flame temperature correlated the data obtained here at all pressures and also burning velocities above liquid solutions of hydrogen peroxide. This covers a 200-fold range of burning velocity. The burning velocity was also correlated with quenching distance.

THE object of this investigation was to measure burning velocities of decomposition flames of hydrogen peroxide–water vapour mixtures, as a function of concentration and pressure, as a means of studying the mechanism of this reaction in the flame and comparing it to the mechanism of the non-flame reaction. The homogeneous decomposition reaction has become much better understood recently[1, 2] and it was hoped that because of the relative simplicity of this reaction compared to those occurring in almost any other flame, it would be possible to relate burning velocity theories to the homogeneous reaction mechanism and actual burning velocity measurements.

The burning rates and other characteristics of the decomposition flame above aqueous hydrogen peroxide solutions have been recently published[3]. The only other study of flame velocities in hydrogen peroxide vapour was that reported by W. CECKLER[4] who did the pioneering work and obtained some preliminary data.

Procedure

Flame velocities were determined by the bunsen burner method, using shadow photography. Since hydrogen peroxide solutions and vapour decompose to some extent on all surfaces, particular care must be taken to choose proper materials of construction and methods of cleaning[5, 6]. At one atmosphere pressure, spontaneous ignition of a flame in vapour or above a solution can readily occur at temperatures of 130° to 150°C and above and concentrations above about 70 weight per cent for the liquid and over 26 mole per cent for the vapour.

In the present apparatus the hydrogen peroxide solution and vapour were allowed to come in contact only with specially treated Pyrex surfaces. The equipment was soaked in boiling detergent solution for an hour or more, rinsed with tap water and then with distilled water and then soaked in a hot solution of concentrated 3:1 sulphuric acid and nitric acid mixture for 24 hours. This treatment is believed to leach most of the traces of heavy metals from the surface. The equipment was then rinsed in conductivity water; great care being taken to exclude dust and dirt in this stage. All openings were securely covered with aluminium foil and the equipment was then placed in an annealing oven. The temperature of the oven was raised to 510°C and kept there for five minutes. The furnace was then shut off and the equipment was allowed to cool slowly in it for three hours. Five minutes was considered an optimal period at 510°C, long enough to allow some closing

*Present address: Air Products, Inc., P.O. Box 538, Allentown, Pa.

of the pores created in the leaching process, and yet not long enough for appreciable diffusion of heavy metals from the interior of the glass to the surface.

The equipment thus cleaned could be used for two or three runs. If a flame occurred in the equipment, it had to be retreated before re-use, because the flame temperatures of about 1 000°C change the nature of the surface. After 15 or 20 treatments, the glassware had to be replaced because of over-etching of the treated surfaces or partial devitrification from the many annealings.

revolving tray. After equilibrium was established, the connecting tube was removed and a hot wire was positioned over the burner tube to ignite the vapour. The last two or three samples, obtained after equilibrium had been achieved, were weighed and analysed. The flow rate and composition were calculated from the analysis and knowledge of the time during which each beaker's contents were collected.

The concentration of the vapour increased 0·1 to 0·2 weight per cent per minute as the vaporization proceeded. Only a few minutes

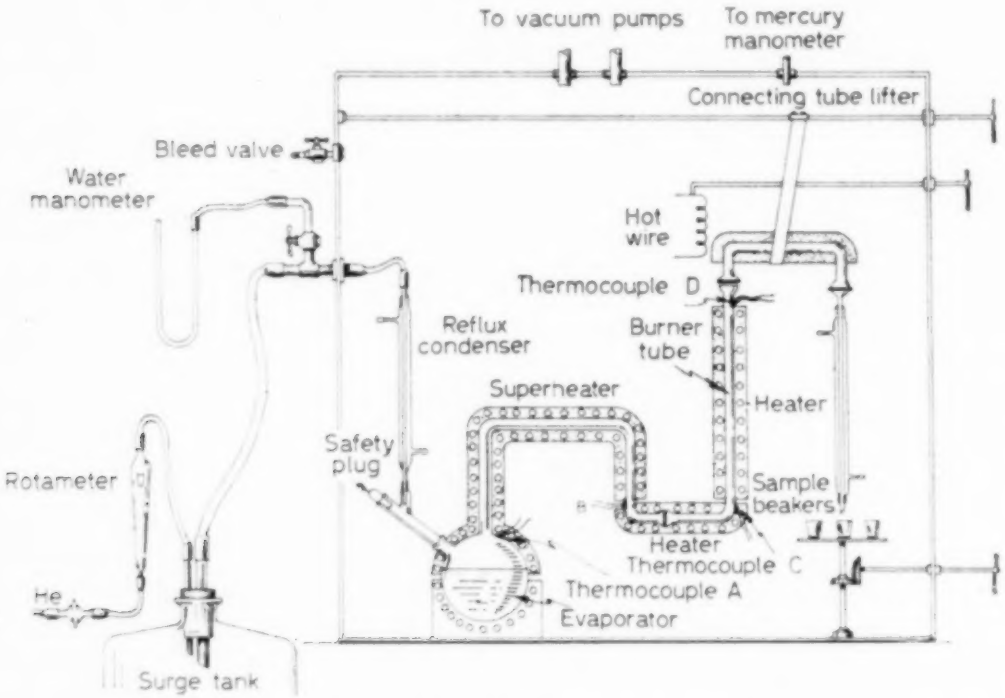

Figure 1. Schematic diagram of apparatus

The apparatus is shown in *Figure 1*. The hydrogen peroxide vapour was generated from a batch evaporator, initially containing 750 cm³ of concentrated hydrogen peroxide solution. Boiling rates were 2 to 4·5 g/min, and were controlled by the heat input to the evaporator flask. The vapour was superheated by 2° or 3° Centigrade and then passed into a 5 mm i.d., 30 cm long Pyrex burner tube that was kept at a constant temperature. During start-up, the top of the burner tube was connected to a condenser and samples of the vapour were taken by condensing all the generated vapour into a series of sample beakers placed on a

elapsed in most runs from the last sample to the blowing out of the flame. Therefore extrapolation of the concentration from the last sample to the time the pictures were taken involved only a small correction.

Four thermocouples were used for temperature control, located as shown in *Figure 1*. In a number of calibrating runs, temporary thermocouples were placed in 1 in. long Pyrex inserts inside the bottom and top of the burner tube, in order to establish the proper heating rates and permanent thermocouple settings to ensure that the vapour was kept at the same temperature at the bottom and top of the burner tube.

The evaporator flask was heated by a 400 W Thermowell shell heater, the superheaters by Electrothermal heating tapes. The burner tube was heated by surrounding it with a copper tube wound with Chromel A resistance wire. All connections were made with ball and socket clamped joints. The top of the burner tube was also a ball joint ground down to eliminate the lip originally present.

The evaporator was connected through a reflux condenser to a manometer and surge tank, both of which were used only at atmospheric pressure. Helium was fed into the evaporator and the rest of the system during warm-up to help distribute heat to the Pyrex walls more evenly, and at the end of a run to blow off the flame. No helium was used during sampling or establishment of the flame.

The whole assembly was contained in a large pressure-tight box, equipped with windows and a detachable back plate, in which a partial vacuum could be maintained. The optical system was a 2 W concentrated arc lamp, a lens that changed the light into a parallel, slightly divergent beam, and a ground glass plate on which the image was cast. This was photographed by a reflex camera with a close-up lens attachment. The best usable pictures were obtained with under-exposed fine grain film and high contrast developing.

Results

Studies were made at 1, 0·72 and 0·5 atm. The burning velocities are shown as a function of vapour concentration in *Figure 2*, together with some earlier data obtained by Ceckler[4].

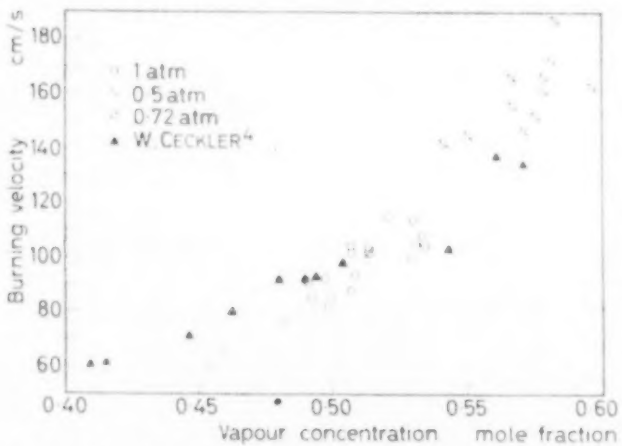

Figure 2. Effect of vapour concentration on burning velocity

The vapour temperature in each case was 2° to 3°C above the boiling temperature of the solution in equilibrium with the vapour concentration. The flame temperature was taken to be equal to the adiabatic decomposition temperature. As a test of this assumption M. A. T. MENDES[7] found with a thermocouple probe only a 10°C difference between calculated and measured flame temperatures in one of her runs. The decomposition temperature was calculated from molal heat capacities of the products (ref. 8, p 222), and the heat of decomposition of hydrogen peroxide (ref. 6, p 251).

The vapour velocity was calculated from the mass evaporating rate measured by the last three samples in each run and the concentration of the vapour, assuming ideal gas behaviour at these temperatures. Average vapour velocities ranged from 245 to 613 cm/sec.

The burning velocity is defined at the inner boundary of the flame, which is represented by the outer boundary of the flame shadow[9,10]. The burning velocity was calculated from measurements of the outer boundaries of the flame shadow by the method of W. CLINGMAN and R. N. PEASE[11]. This method gives a single average value for the burning velocity over most of the flame front by taking into consideration the laminar distribution of vapour velocity. A careful check of each point in *Figure 2* showed no correlation whatsoever between vapour velocity and burning velocity. This is consistent with the general behaviour of bunsen burner flames[12–14].

Because of the fuzzy definition of the outer edge of the shadow, it was necessary occasionally to make more than one tracing of the edge of the shadow from the same picture. Each point in *Figure 2* represents the average of measurements of three to six pictures from the same run. The scatter in the data is due mostly to the subjective inaccuracies in tracing the outer outline of the shadow, inherent in the shadow method. Only 2/5 to 2/3 of the flame periphery was used in each picture, as the shape of the flame is distorted at its base due to the quenching effect of the burner tube rim. The

shape of the flame tip is also distorted by the thermal effects from the increased ratio of flame area to vapour volume in that region, and by minute fluctuations of the vapour flow, which are exaggerated at the tip.

Runs were discarded when the vapour flow was found not to have reached steady state, where analysis of subsequent samples showed a decrease instead of a slight increase in concentration and where the pictures showed the arc lamp was not in the same horizontal plane as the top of the tube. In some low pressure runs the flames were not stable because of slight pressure variations. The flame passed through a cycle lasting from ten seconds to five minutes. At the lowest vapour velocity the flame stabilized, then it increased slightly in size and fluctuated mildly for most of the cycle. Finally it increased greatly in size and blew off. Only pictures from the middle of the cycle were used in such cases.

The ratio of length to diameter of the burner tubes was sixty. The temperature of the vapour flowing in the tube was kept constant within 1°C and the Reynolds numbers ranged between 700 and 1 400. It seems reasonable to assume that a laminar flow pattern was established at the exit of the burner tube. In the flame cone the flow pattern is distorted and local vapour velocities are changed by 5 to 15 per cent[15]. However, R. M. Fristrom[13] and B. Lewis and G. von Elbe[16] have shown that this does not appreciably affect the measured burning velocity. This is also indicated by the straight lines which were usually obtained in this work by the Clingman and Pease correlation. This correlation assumes a laminar flow distribution and would have been affected by a change in the flow pattern.

The lower limit of concentration that could be studied at each pressure was dictated by quenching effects and by the narrow range of velocities between flashback and blow-off. The upper limit of concentrations was enforced by the invariable adventitious ignition of the solution in the evaporator flask at liquid concentrations of about 90 weight per cent or above. Physical properties were calculated from the following sources.

Thermal conductivity

Only properties of the final products, water vapour and oxygen, were used in the correlations. For water, the equation of F. G. Keyes[17] is valid up to at least 823°K. It checked with the Bureau of Standards value[18] at 800°K and was used up to 1 600°K. For oxygen, the equation of F. G. Keyes[19] is valid up to at least 375°K. It checked within two per cent at 1 000°K and within eight per cent at 2 000°K with the values calculated by C. Baulknight[20] and was used up to 1 600°K. The method of Bromley as outlined in R. C. Reid and T. K. Sherwood[21] was used for the calculation of thermal conductivity of mixtures.

Molal heat capacity

Molal heat capacities were taken from the National Bureau of Standards tables[18] and the values for mixtures were combined on a molar basis.

Viscosity

Viscosity data for water vapour and oxygen were taken from the National Bureau of Standards tables[18]. Viscosities of mixtures of hydrogen peroxide and water vapour were calculated from the experimental results of C. N. Satterfield, R. L. Wentworth and S. T. Demetriades[22].

The Homogeneous Decomposition Reaction

The decomposition of hydrogen peroxide vapour is catalysed by most surfaces. Even in the most inert reactors, it is necessary to go to substantially elevated temperatures (above 400°C) before the rate of the homogeneous reaction exceeds that on the reactor surface at partial pressures of the order of 1 to 10 mm of mercury.

In the past eleven years five studies have been published on the homogeneous, non-flame, decomposition of hydrogen peroxide vapour[1,2,23–25]. Early uncertainties over the mechanism of the reaction seem to have been resolved by the similar results of the two recent extensive independent studies by D. E. Hoare and co-workers[2] and by W. Forst[1]. At concentrations of the order of 0·1 to 22 mm of mercury

and temperatures of 400° to 600°C, the mechanism is apparently as follows:

Initiation

$$H_2O_2 + M' \longrightarrow 2OH + M' \quad \ldots . [1]$$

Propagation

$$OH + H_2O_2 \longrightarrow H_2O + HO_2 \quad \ldots . [2]$$

Termination

$$HO_2 + HO_2 \longrightarrow H_2O_2 + O_2 \quad \ldots . [3]$$

or

$$HO_2 + OH \longrightarrow H_2O + O_2 \quad \ldots . [4]$$

The overall rate expression fits the form

$$-d[H_2O_2]/d\theta = k[H_2O_2][M'] \quad .. [5]$$

Here [M'] is a combination of concentrations and efficiencies of collision in the initiating step for all species present. The collision efficiencies reported by Hoare and co-workers[2], relative to a collision efficiency of unity for hydrogen peroxide, are 0·73 for water vapour and 0·12 for oxygen. Dr S. C. Yeung of these laboratories has recently recalculated the data from all the reported studies of the homogeneous decomposition of hydrogen peroxide and found that the best value for the activation energy from all the results is 44 kcal/mole.

To illustrate the significance of the M' term, *Table 1* shows how the value of [M'] is calculated to change as the decomposition reaction proceeds. This is based on [M'] = 1 for $y_0 = 1$, and shows values for initial hydrogen peroxide mole fractions of 0·45 and 0·60.

Table 1. Change in [M'] *with degree of decomposition*

Initial mole fraction of H_2O_2 (y_0)	*Degree of decomposition*	*Moles* H_2O_2 *present per one mole of initial mixture*	[M']
0·45	*Initial*	0·45	0·852
	Half reacted	0·225	0·723
	Fully reacted	0·0	0·618
0·60	*Initial*	0·60	0·892
	Half reacted	0·30	0·721
	Fully reacted	0·0	0·590

Table 1 shows that for a 100 per cent change in concentration of hydrogen peroxide, i.e. over the complete reaction, [M'] changes by less than 35 per cent and the percent change is slight over the initial concentration range of 0·45 mole fraction hydrogen peroxide to 0·60. This in effect means that the overall reaction rate is more nearly first order than second order with respect to hydrogen peroxide concentration.

Flame Propagation Theories

Nomenclature

The symbols used have the following meanings:

$C\bar{p}$	Heat capacity of species or mixture (cal/mole °K)
$C\bar{p}$	Average heat capacity of mixture for $T_0 - T_f$ (cal/mole °K)
d_t	Internal tube diameter (cm)
d_q	Quenching distance (cm)
E	Apparent activation energy (kcal)
k, k'	Constant
n	Order of reaction
P	Pressure (atm)
R	Gas constant
S	Burning velocity (cm/s)
T	Temperature (°K)
T_f	Flame temperature
V	Average vapour velocity (cm/s)
y	Mole fraction of hydrogen peroxide
λ	Thermal conductivity (cal/s cm °K)
θ	Time (sec)
$_0$	Initial
$_f$	Final

Formulations

From the formulation of the equations of flame propagation by T. von Kármán and S. S. Penner[26] for similar boundary conditions, the following relationship can be obtained

$$\frac{S^2 P^2 \overline{C\bar{p}}}{T_0^2 \lambda_f} \propto \left(\frac{P}{T_f}\right)^n \quad \ldots . [6]$$

The derivation of equation 6 is based on an eigenvalue which is constant if the preflame conditions are not varied. This condition is not met by the present studies and the correlation, as expected, was not successful.

For systems where concentrations and temperatures are held constant equation 6 can be simplified to

$$S \propto P^{(n/2)-1} \quad \ldots . [7]$$

However, since most flame reactions cannot be expressed by a precise first or second order relationship, attempts to use this expression to predict the order of flame reactions, with the notable exception of the hydrazine decomposition flame[27], have not been successful. In general, the pressure exponent has been found to vary between +0·2 and −0·5. J. MANTON and B. B. MILLIKEN[28] in their study of a large variety of hydrocarbons, found that the pressure exponent was a function of the burning velocity. For a first order reaction the term S^2P will be independent of pressure.

The most widely used of the flame propagation theories is Semenov's thermal theory[29], principally because of the integrated form of his equations which is easy to apply in the correlation of burning velocity data with any other property of the combustible system. The Semenov equations for a flame reaction of first or second order can be written in the forms:

First order

$$\frac{S^2P}{T_f^2 T_u^2 \lambda_f C_{p_f} (2+y)} = k' \exp - \frac{E}{RT_f} \quad \ldots [8]$$

Second order

$$\frac{S^2}{T_f^2 T_u^2 \lambda_f C_{p_f}^2 (2+y)^2} = k' \exp - \frac{E}{RT_f} \quad \ldots [9]$$

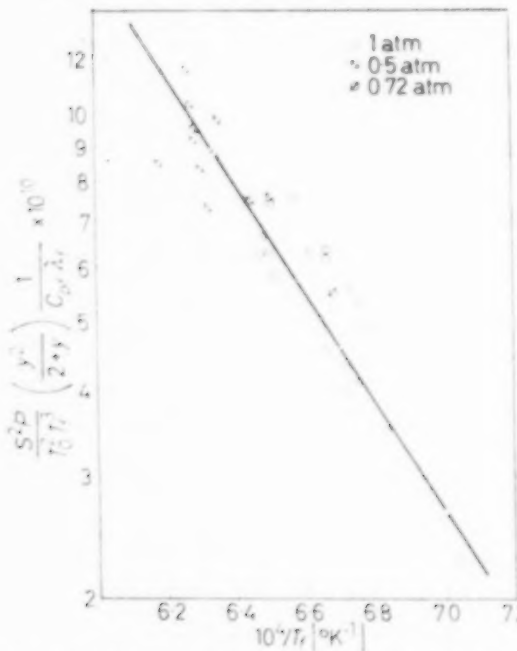

Figure 3. Correlation of data by Semenov's first order order expression

The present data were calculated in the form of equations 8 and 9 and are presented in *Figures 3* and *4*. It can be easily seen that the

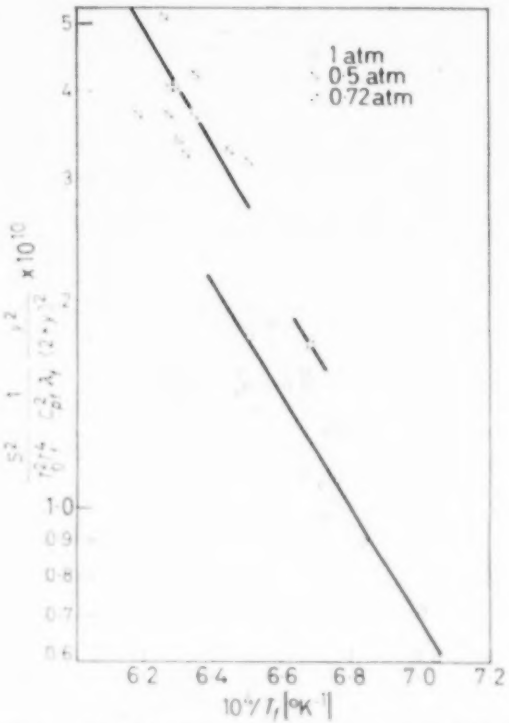

Figure 4. Correlation of data by Semenov's second order expression

first order form correlates the data well, whereas the second order form shows a distinct trend to form a different line for each pressure. These facts strongly support the conclusion that the reaction is effectively first order and that the pressure effect is that predicted for a first order reaction. The activation energy calculated from *Figure 3* is 35 kcal/mole as compared with 44 kcal/mole for the homogeneous reaction at lower temperature.

A simplified approximation of equation 8 can also be written by neglecting the small variations in transport and thermal properties with concentration and temperature over the present set of experiments, and assuming that the exponential term varies greatly compared with the variation in the flame temperature. The resulting expression is

$$S^2P = k \exp(-E/RT_f) \quad \ldots [10]$$

Figure 5 is a plot of S^2P against the reciprocal of the flame temperature. This shows greater

scatter than *Figure 3*, but an 'apparent' activation energy calculated from the slope is also 35 kcal/mole.

Activation energies for all types of flame reactions have been observed to have lower values than activation energies reported for the same reactions, believed to be taking place in the flames, when studied at much lower temperatures. This has been reported for a large variety of hydrocarbon–oxygen–nitrogen flames[30, 31], for hydrogen–nitric acid flames[32], for the ethylene oxide decomposition flame[33] and

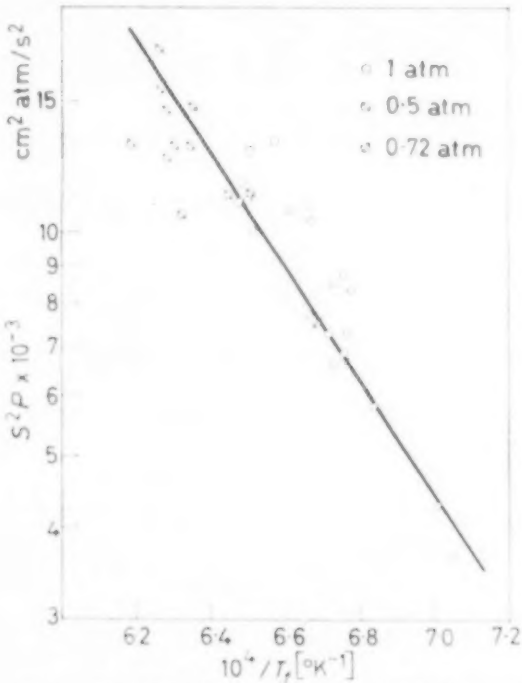

Figure 5. Simplified first order correlation of data

for the hydrazine decomposition flame[27]. There are also theoretical reasons why the activation energy should decrease with increase in reaction temperature. For example, K. E. SHULER[34] in his summary on gas phase reactions at high temperatures discusses the effect of the non-equilibrium distribution of energy for exothermic high temperature reactions. Arrhenius type rate expressions assume an equilibrium distribution of energy. At high temperature and high rates of generation of energy, this equilibrium is not obtained, i.e. some molecules have more energy than predicted by the Arrhenius theory and consequently require less 'activation' energy in order to react.

The change of [M′] as the reaction proceeds, for different initial concentrations, follows parallel curves. The correction factor [M′], based on initial conditions, should apply throughout the reaction in the flame for the effect of changes in initial concentration of hydrogen peroxide. The Semenov first order equation 8 as corrected by [M′] is replotted in *Figure 6*. The spread of the data is slightly less

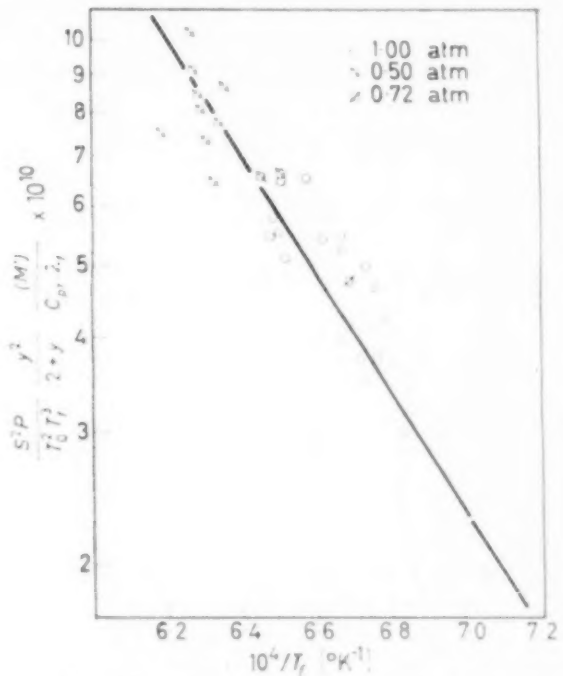

Figure 6. Semenov's first order correlation of data corrected for effect of [M′]

than that in *Figure 3* and the calculated activation energy is 36 kcal/mole, only slightly changed. It is evident that burning velocity is not a sensitive enough parameter for a study of the finer points of reaction mechanism in the flame.

Correlation of Burning Velocities above Liquid and Those in Vapour

Mendes[3, 7] studied the burning rates of hydrogen peroxide solutions in tubes of 1·5 and 3·0 cm i.d. at concentrations of 71 to 97 weight per cent and at 0·13 to 1 atm. She measured the rate of drop of liquid level under the flame and calculated burning velocities from the mass burning rates by assuming that the liquid vaporizes at the liquid temperature and then

burns, and that the flame front is essentially flat.

Mendes's data were recalculated here in the form of Semenov's first order equation (equation 8) and in the S^2P form. A plot of the logarithm of the product of the square of the burning velocity and the pressure against the reciprocal flame temperature for these data is shown in *Figure 7*. The continuation of the line from the similar plot of the data of this work (*Figure 5*), which is replotted in this figure, also correlates the data for burning velocities above liquid hydrogen peroxide solutions.

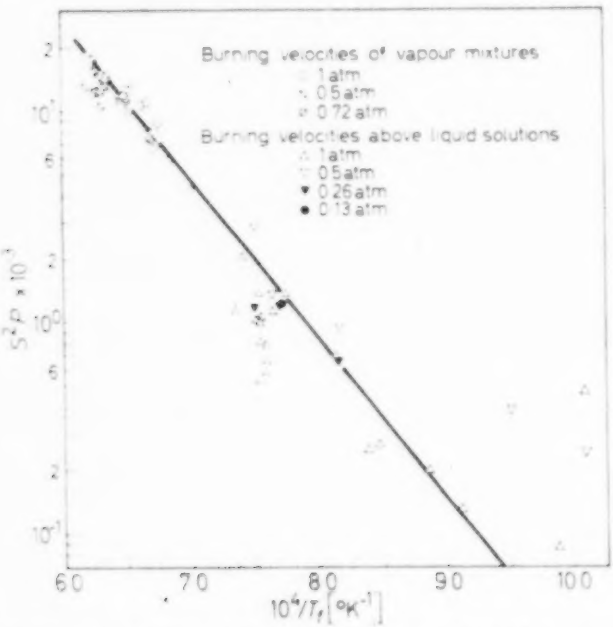

Figure 7. Correlation of burning velocities of vapour mixtures and liquid solutions of hydrogen peroxide

This is remarkable in view of the quenching effects and the heat losses typical of flames above liquid solutions[37]. However, such studies have usually used small diameter tubes in which the flame and the hot liquid are enclosed by, and close to, the tube walls all the time. Heat losses and quenching of radicals at the walls are thus considerable whereas in bunsen burner type flames for gaseous systems, only a small area at the base of the flame comes into contact with a wall. However, Mendes used large diameter tubes in her study and heated the tubes on the outside, thereby minimizing the quenching effects and heat losses.

The data for all pressures are also correlated by the line in *Figure 7*. Two groups of points deviate from the average line. One group is at concentrations of 0·95 mole fraction and higher and appears at values of $10^4/T$ of about 7·5 in *Figure 7*. It has been shown previously[3] that the scatter of these results was associated with variations in the circulation pattern of the liquid hydrogen peroxide solution. For runs at liquid temperatures the farthest below the boiling point, a sharp interface was observed about 3 mm below the surface. The top layer presumably consisted of less dense solution and probably lower concentration than that reported which was based on a sample removed from the bottom of the tube.

The second deviating group consists of four points at the lower right hand portion in which hydrogen peroxide concentration was substantially lower than that for other runs at the corresponding pressure and very close to the limiting hydrogen peroxide concentrations at which flames above the liquid extinguish themselves. Here liquid temperatures were low and the burning rate was accelerated by heat transfer from the hotter walls to the liquid. The actual flame temperatures for these runs were presumably higher than that calculated from assumption of adiabaticity, so the points should properly be displaced to the left. The overall correlation encourages belief that extrapolation of the correlating line is likely to be valid beyond the range of present studies.

The similar plot of Semenov's first order expression (equation 8) has a slope similar to that of *Figure 7*. Separate lines are obtained from the liquid and from the vapour data, as the liquid data are displaced greatly by the effect in the expression of the third power of the flame temperature.

The only reported attempt found in the literature to correlate liquid with vapour decomposition data was that made by G. K. Adams and G. W. Stocks[35] for the hydrazine decomposition flame. They obtained a curve from a Semenov first order expression for the vapour data and their liquid data fitted on an extension of this curve. This flame reaction was shown

later[27] to have a controlling second order mechanism, which may have contributed to the curved shape of the correlation they obtained.

The hydrogen peroxide flame velocities reported by Ceckler[1] which were obtained by the same general method agree fairly closely with the results in this work, although his burning velocities are slightly higher at lower concentrations and slightly lower at higher concentrations. It is believed that the present, subsequent, results are more accurate. Particular care was taken here to maintain an isothermal temperature along the burner tube to ensure that the usual laminar velocity distribution was obtained at the burner tip. The fact that the burning velocity values were generally constant over most of the flame periphery is evidence that this was achieved, whereas in the earlier work the burning velocities as reported varied considerably with position along the periphery. One possible cause was that the earlier burner tubes also served as superheaters and vaporizers of any entrained liquid drops in the vapour. Consequently some turbulence was probably present although laminar distribution of vapour velocity was assumed in calculating the burning velocity. The fact that the calculated burning velocity usually increased in the direction of the tip of the flame strongly suggests that some turbulence was actually present, which would cause a flatter velocity profile than that assumed.

Ceckler was able to propagate flames at the tip of the same size of tubes as were used in this work, at concentrations below those where quenching at the tube top prevented propagation here. This indicates that the true temperature of the walls of the tube was higher than that recorded, which made it possible to overcome the quenching effect at those low concentrations.

Correlation with Quenching Distance

A. E. Potter and A. L. Berlad[36] derived a relationship between quenching distance and burning velocity based on Semenov's equations. They found that the product of the burning velocity and the quenching distance is a complicated function of transport properties but they also found empirically that the above product term could be expressed as a simple function of initial gas temperature, flame temperature and pressure as follows

$$Sd_q \propto T_0 T_f / P \qquad \ldots . [11]$$

This correlation, for a number of hydrocarbon–oxygen–nitrogen flames, is shown in *Figure 8*.

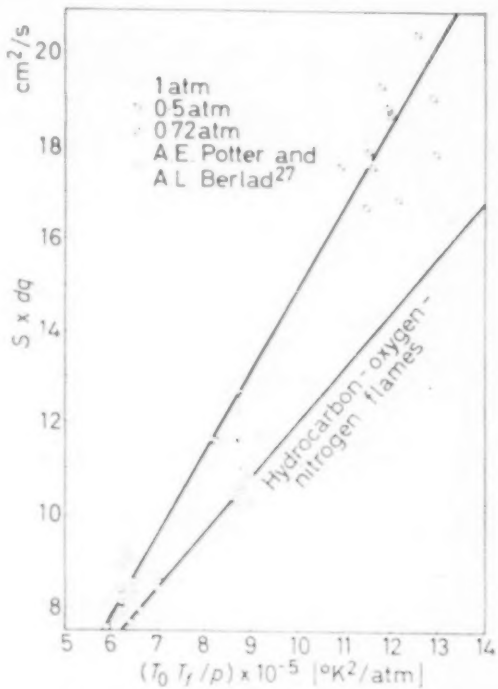

Figure 8. Correlation of burning velocity and quenching distances

J. G. Marshall[37] studied the quenching distance of hydrogen peroxide–water vapour mixtures, containing between 35 and 50 mole per cent hydrogen peroxide, at pressures between 25 and 200 mm of mercury. He correlated the values he found for quenching distance by the equation

$$\log d_q = 4{\cdot}362 - 9{\cdot}360\,y + 6{\cdot}80\,y^2 - 0{\cdot}835 \log P \qquad \ldots . [12]$$

where P is in mm of mercury. Values of quenching distance for hydrogen peroxide vapour mixtures were extrapolated by means of equation 12 to one atmosphere pressure and were combined with burning velocities obtained here to yield the correlation shown in *Figure 8*. The correlating line does not go through the

origin. A similar plot for hydrogen–air flames[38] had to introduce a modification in the form of a concentration term to allow for the large effect of hydrogen concentration on the transport properties of that system. Similarly for hydrogen peroxide–water vapour the different effect of concentration on transport properties is likely to exclude this system from a correlation for hydrocarbons.

The authors wish to acknowledge the financial support of the U.S. Office of Naval Research, under Contract Nonr 1841 (11), NR–092–008. Reproduction in full or in part is permitted for any purpose by the United States Government.

Based on the Sc.D. thesis of E. Kehat, Department of Chemical Engineering, Massachusetts Institute of Technology, 1960.

References

[1] Forst, W. *Canad. J. Chem.* 1958, **36**, 1308
[2] Hoare, D. E., Protheroe, J. B. and Walsh, A. D. *Trans. Faraday Soc.* 1959, **55**, 548
[3] Satterfield, C. N., Kehat, E. and Mendes, M. A. T. *Combustion & Flame*, 1960, **4**, 99
[4] Eckler, W. 'The decomposition flame of hydrogen peroxide vapor'. *Sc. D. Thesis*, Massachusetts Institute of Technology: Cambridge, Mass., 1960
[5] Satterfield, C. N. and Stein, T. W. *Industr. Engng Chem. (Industr.)*, 1957, **49**, 1173
[6] Schumb, W. C., Satterfield, C. N. and Wentworth, R. L. *Hydrogen Peroxide*, Reinhold: New York, 1955
[7] Mendes, M. A. T. 'Decomposition flame above liquid hydrogen peroxide'. *M.S. Thesis*, Massachusetts Institute of Technology: Cambridge, Mass., 1957
[8] Perry, J. H. *Chemical Engineering Handbook*, (3rd ed.) McGraw-Hill: New York, 1950
[9] Gerstein, M. *Fourth Symposium (International) on Combustion*, p 35. Williams and Wilkins: Baltimore, 1953
[10] Grove, J. R., Hoare, M. F. and Linnett, J. W. *Trans. Faraday Soc.* 1950, **46**, 745
[11] Clingman, W. H. and Pease, R. N. *J. Amer. chem. Soc.* 1956, **78**, 1775
[12] Culshaw, G. W. and Garside, J. E. *Third Symposium (International) on Combustion*, p 204. Williams and Wilkins: Baltimore, 1949
[13] Fristrom, R. M. *J. chem. Phys.* 1956, **24**, 888
[14] Gibbs, G. J. and Calcote, H. F. *J. Chem. Engng Data*, 1959, **4**, 226
[15] Singer, J., Grumer, J. and Cook, E. B. *Proceedings of the Gas Dynamics Symposium on Aerothermochemistry*, p 139. Northwestern University: Evanston, Ill., 1956
[16] Lewis, B. and von Elbe, G. *J. chem. Phys.* 1943, **11**, 75
[17] Keyes, F. G. *Trans. Amer. Soc. mech. Engrs*, 1951, **73**, 589
[18] Hilsenrath, J. (Ed.). 'Tables of thermal properties of gases'. *Circ. U.S. Nat. Bur. Stand. No. 564*, 1955
[19] Keyes, F. G. *Trans. Amer. Soc. mech. Engrs*, 1955, **77**, 1395
[20] Baulknight, C. 'The calculation of transport properties at elevated temperatures'. *General Electric Rep. No. R 58 SD 223*, 1957
[21] Reid, R. C. and Sherwood, T. K. *The Properties of Gases and Liquids*. McGraw-Hill: New York, 1958
[22] Satterfield, C. N., Wentworth, R. L. and Demetriades, S. T. *J. Amer. chem. Soc.* 1954, **76**, 2633
[23] Giguére, P. A. and Liu, I. D. *Canad. J. Chem.* 1957, **35**, 283
[24] McLane, C. K. *J. chem. Phys.* 1949, **17**, 379
[25] Satterfield, C. N. and Stein, T. W. *J. phys. Chem.* 1957, **61**, 537
[26] von Kármán, T. and Penner, S. S. 'Fundamental approach to laminar flame propagation' in *Selected Combustion Problems*, p 1. Butterworths: London, 1954
[27] Gray, P. and Lee, J. C. *Sixth Symposium (International) on Combustion*, p 255. Reinhold: New York, 1957
[28] Manton, J. and Milliken, B. B. *Proceedings of the Gas Dynamics Symposium on Aerothermochemistry*, p 151. Northwestern University: Evanston, Ill., 1956
[29] Semenov, N. *Theory of Normal Flame Propagation*. Translated in *Tech. Memor. Nat. Adv. Comm. Aero., Wash., No. 1026*, 1942
[30] Fenn, J. B. and Calcote, H. F. *Fourth Symposium (International) on Combustion*, p 231. Williams and Wilkins: Baltimore, 1953
[31] Penner, S. S. and Crowe, T. H. *Proceedings of the Gas Dynamics Symposium on Aerothermochemistry*, p 113. Northwestern University: Evanston, Ill., 1956
[32] Strauss, W. F. and Edse, R. *Seventh Symposium (International) on Combustion*, p 377. Butterworths: London, 1959
[33] Friedman, R. and Burke, E. *Fifth Symposium (International) on Combustion*, p 596. Reinhold: New York, 1955
[34] Shuler, K. E. *Fifth Symposium (International) on Combustion*, p 56. Reinhold: New York, 1955
[35] Adams, G. K. and Stocks, G. W. *Fourth Symposium (International) on Combustion*, p 239. Williams and Wilkins: Baltimore, 1953
[36] Potter, A. E. and Berlad, A. L. 'A relation between burning velocity and quenching distance'. *Tech. Note Nat. Adv. Comm. Aero., Wash., No. 3882*, 1956
[37] Marshall, J. G. *Trans. Faraday Soc.* 1959, **55**, 28
[38] Drell, I. L. and Belles, F. E. 'Survey of hydrogen combustion properties'. *Nat. Adv. Comm. Aero., Wash., Rep. Memor. No. E57D24*, 1957

Rate of Combustion from Free Surfaces of Liquid Hydrocarbons

W. L. Fons*

Pacific Southwest Forest and Range Experiment Station, Forest Service, U.S. Department of Agriculture, Berkeley 1, California

(*Received January 1961*)

The burning velocity of n-hexane and cyclohexane as related to the area of the burning fuel surface was studied using 10 open pans ranging from 0·22 to 11·94 in. in diameter. On the four larger pans fuel temperatures were also measured during the burning period at two depths below the surface. For small pans less than 5 in. in diameter burning velocity decreased with increasing pan size. For pans greater than 5 in. in diameter burning velocity increased with increasing pan size. Thus, there appear to be two burning régimes in the range of pan diameters tested, a laminar flow régime on small pans, and a transition flow régime on larger pans. This observation is in agreement with the experimental results reported by others for equivalent pan sizes burning less volatile hydrocarbon fuels.

Introduction

This paper presents the results of a series of laboratory experiments in which liquid hydrocarbons were burned in circular pans to learn the influence of the diameter of the fuel surface on the rate of combustion.

The study is one of several planned to help design a model combustion system to represent the complex fuel and weather conditions in forest fires. The variables which govern the spread of forest fires are numerous, and the effect of each variable on the behaviour of a forest fire is still rather vaguely defined. The development of an adequate model requires quantitative information on these effects. Therefore, the Forest Service is studying various combustion systems, each having a limited number of variables. The present study, using a combustion system with a homogeneous fuel of known physical properties, measured the rate of combustion of liquid hydrocarbons under free convection from surfaces exposed to still air.

The theory of combustion of liquid fuels in a free atmosphere has been presented by H. W. Emmons[1]. Combustion of solid and liquid fuel surfaces was considered by D. B. Spalding[2–4]. D. J. Rasbash, Z. W. Rogowski and G. W. V. Stark studied the properties of alcohol, benzene, gasoline and kerosine fires[5]. V. I. Blinov and G. N. Khudiakov[6] burned gasoline, kerosine, diesel fuel, and heavier oils in cylindrical pans of diameter from 0·37 cm to 22·9 m, measuring burning rates and flame heights. H. C. Hottel[7] summarized the data of Blinov and Khudiakov in the form of a figure in which the liquid burning velocity is plotted against pan diameter, revealing three burning régimes: laminar, transition, and turbulent flow.

Both Emmons and Spalding made mass and heat balances with the usual restrictive conditions, namely constant diffusion coefficient and thermal diffusivity, no reaction at the interface, and equality of the molecular and thermal diffusivity. Emmons arrived at the following ratio[1] of dimensionless quantities for evaluating and explaining the rate of release of vapour from a liquid surface under conditions in which the vapour burns in natural convection

$$B = \frac{h_{\infty} - h_{s} + Hm_{a}/r}{\lambda + h_{a} - h} \qquad \ldots [1]$$

where the symbols have the meanings listed under Nomenclature below. In equation 1, B is the ratio between: (*i*) the thermal energy of a unit mass of the main stream relative to the combustion surface and (*ii*) the thermal energy at the combustion surface required to drive a unit mass of fuel into the combustion zone. Spalding's analysis resulted in a somewhat

*Now at the Southern Forest Fire Laboratory, Post Office Box 1421, Macon, Georgia.

similar heat ratio. Both Emmons's and Spalding's theory pertain to the laminar flow régime.

For the combustion system reported here, the heat transfer–mass transfer analogy yields the relation

$$\frac{Md}{\nu_\infty \rho_\infty g} = KB^m \left(\frac{gd^3}{\nu_\infty^2}\right)^n \quad \ldots . [2]$$

which holds for all régimes depending on the value of the exponent n. Rasbash employed the same equation with 0·25 for the value of n.

The liquids burnt in these tests were *n*-hexane and *cyclo*hexane. *Table 1* presents the values of their physical properties. Also included in this table are the values of B calculated by equation 1.

Table 1. Physical properties of fuels[a]

Fuel	*Formula*	H^* *B.t.u./lb*	$\lambda+(h_v-h)^*$ *B.t.u./lb*	t_v °*F*	B
n-*Hexane*	C_6H_{14}	19391	193·6	156	6·25
cyclo-*Hexane*	C_6H_{12}	18846	215·5	176	5·65

[a] $H_2O_{(g)}$ and $CO_{2(g)}$.
[b] λ and h_v for boiling point, h for 68 °F.

Experimental

A diagram of the combustion burner apparatus is shown in *Figure 1*. The burner (A) is a circular pan of 19-gauge sheet copper, the upper half of which is provided with a water jacket (B) serving as a heat sink to prevent heat conduction down the metal to the fuel. Around the burner is a copper plate (K, K) to guide the flow of air horizontally into the base of the flame. The incoming water is regulated by a flowmeter (C). Thermometers (D, D) measure the temperatures of the cooling water at the inlet and outlet of the water jacket. Burners of ten sizes were used in the tests: 0·220, 0·358, 0·512, 0·661, 1·090, 1·924, 2·98, 6·00, 7·92 and 11·94 in. in diameter.

The liquid fuel was supplied continuously from a burette (E) during the burning period. The rate of fuel flowing to the burner was

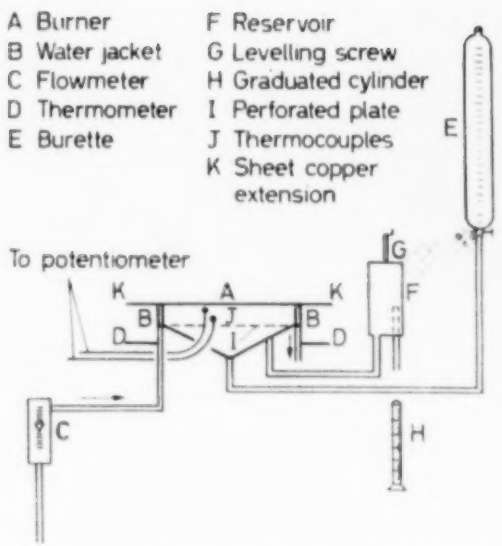

Figure 1. Schematic diagram of apparatus

adjusted by a cock on the burette, so that the quantity flowing was slightly greater than the amount being consumed. The fuel surface in the burner was maintained at a predetermined level by adjusting the height of the levelling reservoir (F) with levelling screw (G). The difference between the quantity of fuel being supplied and that being consumed was measured by a graduated cylinder (H) placed below the overflow of the reservoir. To ensure that burning took place without rippling or bubbling at the surface of the fuel, a perforated plate (I) was placed in the lower part of the burner to retard the fuel jet entering the bottom of the burner and to help maintain an undisturbed surface in the burner. Additional precautions were taken to eliminate points where disturbances might be initiated; for example, neither a thermocouple nor a point gauge was at the fuel surface.

With the four largest burners, the fuel temperature was measured by 30-gauge chromel–alumel thermocouples (J) with junctions 0·687 and 0·0625 in. below the surface of the liquid. The heat loss from the junctions by conduction was minimized by coiling the thermocouple wires horizontally immediately below each junction.

Procedure

The following standard procedure, established

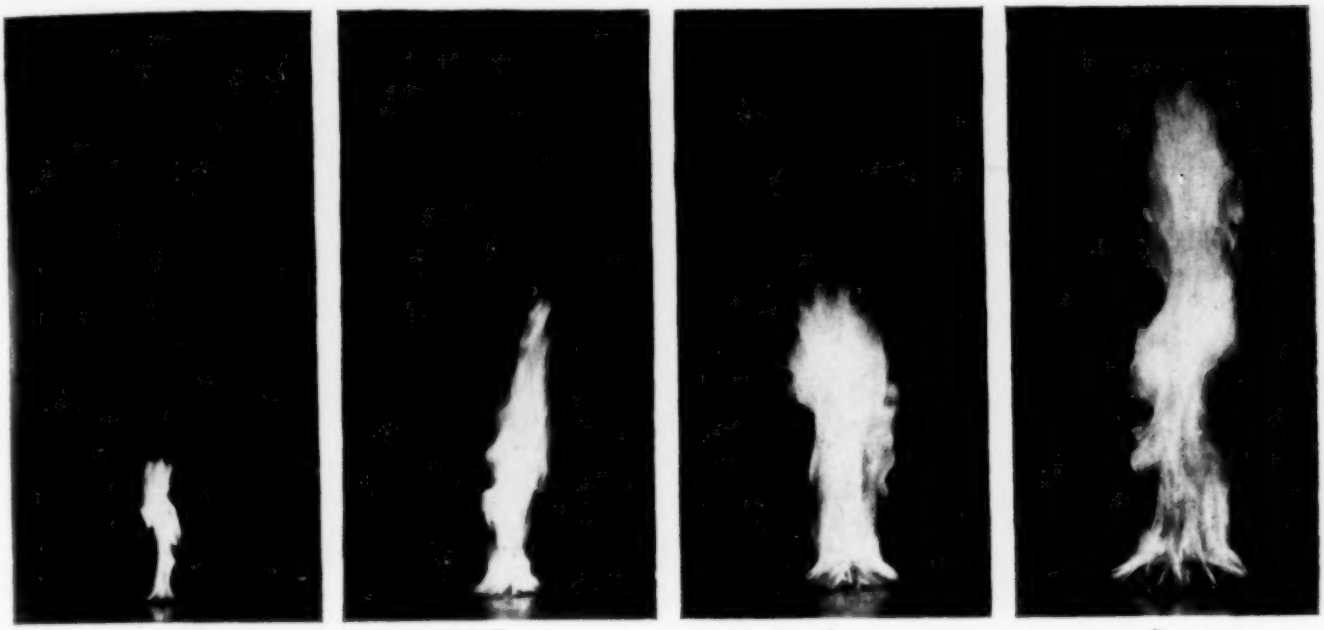

A B C D

Figure 2. Photograph of flames of cyclohexane at 5 minutes in different diameter burners: A, 2·98 in.; B, 6·00 in.; C, 7·92 in.; D, 11·94 in.

by considerable preliminary experimentation, was used on all tests:

(*1*) The wet and dry bulb room temperatures and the initial fuel temperature in the burner were measured. (*2*) The fuel level in the burner, measured by a depth gauge, was brought to within 0·220 in. of the lip by adjusting the height of the levelling reservoir while the fuel was flowing. (*3*) The rate of flow of the cooling water to and from the water jacket was adjusted so that the difference between the inlet and outlet temperatures was less than 5°. (*4*) The fuel was ignited and allowed to burn for one minute, during which time the flow of fuel was readjusted at the burette so that the overflow was about 10 per cent of the amount being consumed by burning. (*5*) After one minute of burning, the liquid level in the burette was recorded and an empty graduated cylinder was placed under the overflow of the reservoir. (*6*) Potentiometer readings of the thermocouples and the temperature of the inlet and outlet cooling water were recorded at 1-minute intervals. (*7*) At the end of each 5-minute period the quantity of fuel consumed by the fire was calculated by subtracting the volume collected at the overflow from the volume measured by the burette.

With all but one burner, the fires were allowed to burn for 15 minutes after the initial 1-minute adjustment period; fires in the 12 in. burner were burned for only ten minutes. At the end of each test the fuel level was again measured for assurance that the initial level was maintained during the test. During each of the tests the surface of the fuel was watched constantly for bubbling or rippling which would indicate that the temperature was approaching the boiling point.

Results and Discussion

Figure 2 presents photographs, taken at the end of five minutes, of the flames of *cyclo*hexane burning in the four largest pans. Observations made during the burning period and examination of the photographs taken at various times revealed no significant difference in characteristics of the flame from the two fuels in the different pans.

Figure 3 presents the average temperature/time curves obtained at the two positions below the fuel surface of the *cyclo*hexane. Similar temperature/time curves (not shown) were obtained for *n*-hexane. For the three largest pans, the curves for *n*-hexane were on an average about 10° lower after four minutes of burn-

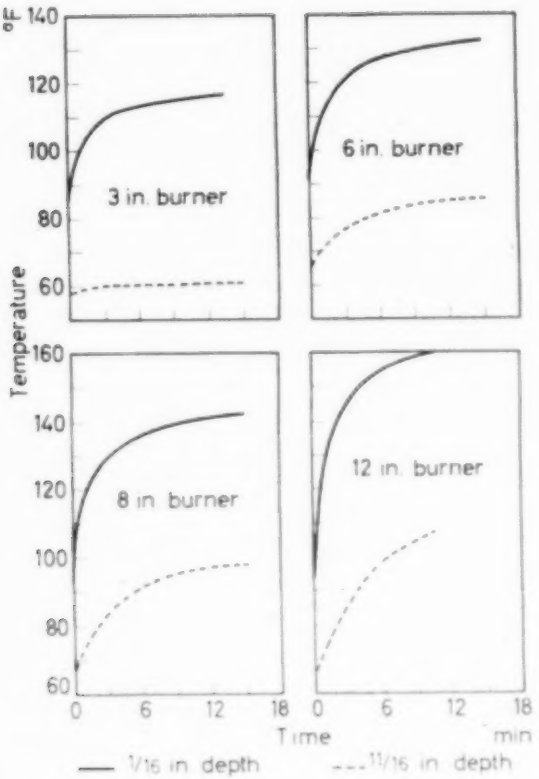

Figure 3. Effect of time of burning on temperature below surface of cyclohexane

ing than the curves for *cyclo*hexane. Temperature–time curves indicated that in calculating the B ratio serious error would not be introduced by using the values of the heat of evaporation, λ, and the enthalpy, h_{v_b}, at the boiling point of the fuels.

In the pans less than 6 in. in diameter, the fuel consumed during each consecutive 5-minute period remained substantially constant with time. The burning rates for the two larger pans showed a slight increase with time; this increase, however, was less than 10 per cent. Consequently, the rate of fuel burning was calculated for all the tests on the basis of total fuel consumed during the entire period of burning. In *Figure 4* the calculated values of $Md/\nu_\infty\rho_\infty g$ are plotted as a function of gd^3/ν_∞^2 for the four largest pans. The latter is a modified Grashof number. Each point is an average of two or more fires. The values of ν_∞ and ρ_∞ were those appropriate to the room temperature (68° F).

An examination of the experimental results

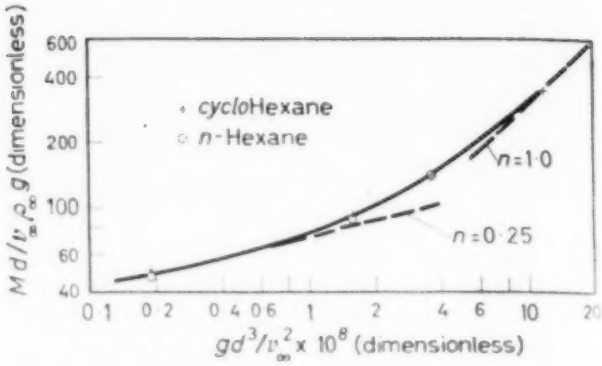

Figure 4. Dimensionless correlation of mass transfer with heat transfer in the burning of n-hexane and cyclohexane from circular pans

shown in *Figure 4* indicates that the exponent n for the modified Grashof number in equation 2 increases with diameter of the burner from about 0·25 for the 3 in. pan to about 1·0 for the 12 in. diameter pan. Spalding[3] used the value of 0·25 for n to correlate the burning rates in natural convection flames of several liquid fuels burning from spherical surfaces 1½ in. in diameter. Rasbash[5] found the rate at which alcohol burned from a pan 11·8 in. in diameter to be in good agreement with equation 2 taking a value of 0·25 for n, but he did not make the calculations for the hydrocarbon flames of greater emissivity.

Because neither rippling nor boiling of the liquid surface was observed in any of the tests, the increase of the exponent n with pan diameter probably cannot be attributed to a change in roughness of the evaporating surface. Equation 2 is based on the theory that heat transfer is by conduction and convection only through the vapour zone[1, 2]. Heat transfer by radiation from the flame to the liquid surface for small diameters may be relatively unimportant, because of the small value of the flame emissivity. However, as burner diameter increases, the height of the flame and the emissivity increase, particularly for fuels that burn with sooty flames. Under such conditions, radiation can be expected to influence the temperature of the surface and therefore the magnitude of n. This influence may account for the observed increase in n from 0·25 to 1·0 with increase in pan diameter (*Figure 4*).

Hottel's analysis[7] shows that the rate of burning does not change with pan diameters greater than about 3 ft. In this case the value of n in equation 2 would be $\frac{1}{3}$. However, our experiments did not go beyond a pan diameter of 12 in.

The velocity of burning of *cyclo*hexane in natural convection in air is plotted against the diameter of the pan in *Figure 5*. The shape of

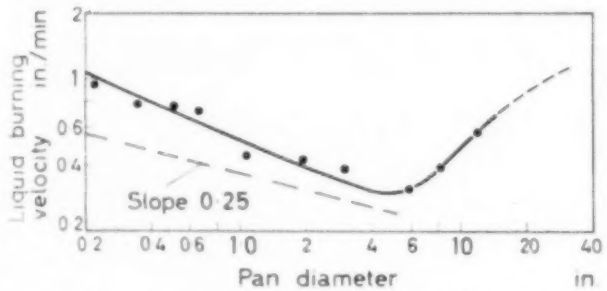

Figure 5. Burning velocity of cyclohexane as a function of pan diameter

the curve is generally similar to the curves plotted by Hottel[7] from the Blinov and Khudiakov data[8], decreasing with pan diameter when the pans are small (the laminar flow régime) but increasing with pan diameters greater than about 5 in. (the transition régime). Our experiments were not extended to the large pans of Blinov and Khudiakov's turbulent flow régime.

In designing a model for a forest-fire combustion system, it will be necessary to learn if the area of the fuel bed is as important to the rate of burning of solid fuels as it is with liquid fuels.

Nomenclature

The following meanings are attributed to the symbols listed:

- B Heat ratio, dimensionless
- d Diameter of combustion surface, ft
- g Gravitational acceleration, 32·2 ft/sec^2
- h Enthalpy of fuel, B.t.u./lb
- h_0 Enthalpy of fuel at evaporation temperature, B.t.u./lb
- h_∞ Enthalpy of air, B.t.u./lb
- $h_{\infty,0}$ Enthalpy of air at fuel evaporation temperature, B.t.u./lb
- H Heat of combustion of fuel, B.t.u./lb
- K Constant
- m Exponent
- m_0 Oxygen concentration of environment, lb/lb
- M Combustion rate, lb/sec ft^2
- n Exponent
- r Stoichiometric ratio, lb oxygen per lb of fuel
- t_0 Boiling point of fuel at atmospheric pressure, °F
- λ Heat of vaporization of fuel at evaporation temperature, B.t.u./lb
- ν_∞ Kinematic viscosity of air, ft^2/sec
- ρ_∞ Mass density of air, lb sec^2/ft^4

The author wishes to express thanks to S. S. Richards, A. R. Pirsko, H. D. Bruce, A. W. McMasters and W. Y. Pong, who assisted in the experimental work and in the reduction of data.

References

1. Emmons, H. W. 'The film combustion of liquid fuels'. Combustion Aerodynamics Lab. *Interim Tech. Report* 6, 22 pp. Harvard University, 1953
2. Spalding, D. B. 'Experiments on the burning and extinction of liquid fuel spheres'. *Fuel, Lond.* 1953, **32**, 169
3. Spalding, D. B. 'The combustion of liquid fuels'. *Fourth Symposium (International) on Combustion*, p 847. Williams and Wilkins: Baltimore, 1953
4. Spalding, D. B. *Some Fundamentals of Combustion*, p 122. Gas Turbine Services, Vol. II. Butterworths: London, 1955
5. Rasbash, D. J., Rogowski, Z. W. and Stark, G. W. V. 'Properties of fires of liquids'. *Fuel, Lond.* 1956, **35**, 94
6. Blinov, V. I. and Khudiakov, G. N. 'Certain law governing diffusive burning of liquids'. *Dokl. Akad. Nauk S.S.S.R.* 1957, **113**, 5 pp
7. Hottel, H. C. Review of Ref. 6, *Fire Research Abstracts and Reviews*, 1959, **1**, No. 2
8. Rossini, F. D. *et al.* 'Selected values of properties of hydrocarbons'. *Circ. Nat. Bur. Stand. No. C461*, 483 pp. Washington, 1947

Combustion Institute Meetings

Ninth International Symposium on Combustion, 1962

THE NINTH INTERNATIONAL SYMPOSIUM ON COMBUSTION will be held at Cornell University, Ithaca, New York, during 27 to 31 August 1962, inclusive. It will be the fourth symposium organized under the auspices of The Combustion Institute. The local arrangements are being made by the Department of Thermal Engineering at Cornell. The Institute and the local sponsors welcome the participation of all members of the organization, together with all scientists and engineers interested in combustion.

Symposium agenda—The technical programme of the Ninth International Combustion Symposium is planned to include two *Discussions*, three *Colloquia* and *Contributed Papers*. The Discussions and Colloquia are intended to lead to interchange of information in specific areas where an intensive review of the known theoretical and experimental facts is desirable. Contributed Papers will be accepted in all areas of the combustion field. When parallel sessions are unavoidable, an effort will be made to schedule papers in the same general area of interest at such times as to make attendance at all of them possible.

Discussions—The Discussion topics are: (*a*) *Fundamental Flame Processes* (with emphasis on the structure of flames) and (*b*) *Detonations*. The Discussions will revolve around *invited preprinted* papers, available for distribution several weeks before the Symposium.

Combustion Symposium participants are urged to take an active part in the Discussions. Their value and success depends to a large measure on the quality of the contributions from the audience. A brief summary by the authors of the highlights of their papers will be followed by extended discussions from the floor. It is particularly desirable to present unpublished material that is germane to the topics of the Discussions. Participants are requested to procure preprints and to prepare their comments prior to the meeting. The papers and relevant comments will be published in the Symposium Proceedings. Further information will be given in the Second Announcement.

Colloquia—The Colloquia topics are: (*a*) *Modelling Techniques* (*Engines, Furnaces, Fires*), (*b*) *Chemical Reactions and Phase Changes in Supersonic Flow* (*with emphasis on nozzle flow*), (*c*) *Reciprocating Engine Combustion Research*. The Colloquia papers will be presented in full, followed by comments from the floor. The papers will not be preprinted but will be published in the Symposium Proceedings.

The Chairmen organizing the Discussions and Colloquia are:

Dr W. H. AVERY, Applied Physics Laboratory, Johns Hopkins University—*Fundamental Flame Processes*.

Dr D. R. WHITE, General Electric Research Laboratory—*Detonations*.

Professor D. B. SPALDING, Imperial College of Science and Technology—*Modelling Techniques*.

Professor P. P. WEGENER, Yale University—*Chemical Reactions and Phase Changes in Supersonic Flow*.

Professor E. S. STARKMAN, University of California—*Reciprocating Engine Combustion Research*.

The Abstracts of the Contributed Papers will be made available to them in planning their programmes. With the authors' concurrence suitable Contributed Papers will be considered for inclusion in the Discussions and Colloquia.

Contributed papers—The Papers Subcommittee will select Contributed Papers on the *basis of 800–1 000 word Abstracts*, with a view to technical content and suitability for public presentation. Three copies of the Abstracts are to be submitted to The Combustion Institute, 936-B Union Trust Building, Pittsburgh 19, Pennsylvania, not later than 1 February 1962.

Three copies of the manuscripts of the

complete Contributed Papers are due at The Combustion Institute on or before 1 May 1962, and will be reveiwed prior to publication in the Symposium Proceedings. It is requested to restrict the length of the papers to 4 000 words or less.

Time allotted to individual Contributed Papers is 15 to 20 minutes, with 5 to 10 minutes for comments. Abstracts (revisable up to 1 May 1962) of all accepted papers will be bound together for distribution at the Symposium.

Local arrangements for the meeting—Headquarters for the meeting will be Upson Hall of the Sibley School of Mechanical Engineering, which is situated on the engineering campus of the university. This is located at the south end of the main campus, within walking distance of the dormitories and the eating facilities on the campus.

Dormitory rooms will be available, mainly in the recently built student dormitory block. Some rooms will be available for single women and couples can be accommodated. The surrounding district contains a number of hotels and motels for which information will be provided in the next announcement. Meals will be available by special arrangement with the University Department of Residential Halls and there are many nearby restaurants.

If you plan to attend the 1962 Symposium, kindly write as soon as possible to

Combustion Symposium Office, Upson Hall,
Sibley School of Mechanical Engineering,
Cornell University, Ithaca, New York.

Awards—In 1958 The Combustion Institute established three awards. Recipients of these awards at the Eighth International Combustion Symposium were: Professor H. C. HOTTEL—The Sir Alfred Egerton Medal—'For distinguished service in research and education in the field of combustion'; Dr A. G. GAYDON—The Bernard Lewis Medal—'For brilliant research in the field of flame spectroscopy'; Drs P. F. KNEWSTUBB and T. M. SUGDEN—The Silver Combustion Medal—'For an outstanding paper presented at the Seventh (International) Symposium on Combustion, Oxford University 1958'. These biennial awards are a feature of each combustion symposium.

Publications—The Third, Fourth, Fifth, Sixth, Seventh and Eighth Symposium papers have been published in single volumes of 750 to 950 pages. They have become an essential reference work in the field of combustion. The price has been kept low by the underwriting of the publications by funds generously supplied by industry. Consequently, wide dissemination of these important volumes among individual scientists and engineers has been possible.

The proceedings of the Eighth Symposium are available to members of the Institute at a pre-publication price (prepaid) of $10. Probable publication date is September 1961.

The proceedings of the Ninth Symposium will be published in like manner at approximately the same price. Informative Abstracts of Contributed Papers and Preprints of Invited Discussion Papers will be available, on order, in advance of the meeting.

The Journal of The Combustion Institute *Combustion and Flame* is published quarterly by Butterworths, London, at a price to members of $13 a year. Subscriptions from United States members should be directed to Butterworth Inc., 7235 Wisconsin Avenue, Washington 14, D.C.; from Canadian members, to Butterworths & Co., 1367 Danforth Avenue, Toronto 6, Ontario; from all other countries, to Butterworths, 4-5 Bell Yard, London, W.C.2, England.

Members may purchase through the Institute office the proceedings of the 1959 Fall Meeting of the Western States Section 'Kinetics, Equilibria and Performance of High Temperature Systems' at a special price of $10 (prepaid).

1962 Symposium Subcommittees

Papers Subcommittee: DR WALTER G. BERL, *Chairman*
Applied Physics Laboratory
The Johns Hopkins University
8621 Georgia Avenue
Silver Spring, Maryland

DR W. G. AGNEW
DR W. H. AVERY
DR C. BECKETT
MR W. J. BENNETT
DR A. L. BERLAD
PROF. M. BOUDART
PROF. F. P. BOWDEN
MR S. L. BRAGG
DR S. R. BRINKLEY, JR
DR H. P. BROIDA
DR J. H. BURGOYNE
DR H. F. CALCOTE
PROF. A. B. CAMBEL
DR H. M. CASSEL
DR J. S. CLARKE
PROF. M. A. COOK
DR R. E. DUFF
DR G. L. DUGGER
PROF. H. W. EMMONS
DR MARJORIE W. EVANS
PROF. J. A. FAY
DR J. FENN
DR S. N. FONER
MR W. L. FONS
DR R. FRIEDMAN
DR R. M. FRISTROM
PROF. D. GARVIN
DR A. G. GAYDON
DR R. D. GECKLER
PROF. I. GLASSMAN

Dr A. S. Gordon
Prof. P. Gray
Prof. A. V. Grosse
Dr F. Hill
Prof. H. C. Hottel
Dr W. H. Jones
Mr B. Karlovitz
Dr W. E. Kaskan
Dr F. Kaufman
Prof. L. N. Khitrin
Prof. T. Kinbara
Dr P. H. Kydd
Prof. P. Laffitte
Dr R. S. Levine
Dr B. Lewis (ex officio)
Prof. J. W. Linnett
Dr J. P. Longwell
Dr F. T. McClure
Prof. F. E. Marble
Dr G. H. Markstein
Prof. C. J. Marsel
Dr F. J. Martin
Dr J. F. Masi
Dr C. C. Miesse
Prof. P. S. Myers
Mr A. J. Nerad
Prof. J. A. Nicholls
Dr P. Nichols
Dr W. T. Olson
Prof. A. K. Oppenheim
Prof. H. B. Palmer
Prof. W. G. Parker
Prof. S. S. Penner
Prof. G. Porter
Mr E. W. Price
Dr D. J. Rasbash
Dr R. Roberts
Mr A. Rothrock
Prof. N. W. Ryan
Dr A. C. Scurlock
Dr E. H. Seymour
Prof. K. I. Shchelkin
Dr K. E. Shuler
Prof. D. B. Spalding
Prof. E. Starkman
Prof. T. M. Sugden
Prof. M. Summerfield
Dr C. P. Talley
Dr P. H. Thomas
Dr R. Thompson
Prof. M. W. Thring
Prof. A. R. Ubbelohde
Dr R. W. van Dolah
Dr G. von Elbe
Dr H. Gg. Wagner
Prof. A. D. Walsh
Dr S. Way
Prof. P. P. Wegener
Dr F. J. Weinberg
Dr A. A. Westenberg
Prof. F. A. Williams
Prof. G. C. Williams
Dr H. Wise
Dr H. G. Wolfhard
Prof. M. J. Zucrow
Prof. E. E. Zukoski

Finance Subcommittee
Chairman: Mr M. P. L. Love, Shell Oil Company, 50 West 50th Street, New York 20, New York

Subcommittee on Lecture Tours for Visiting Scientists
Chairman: Dr B. M. Sturgis, E. I. du Pont de Nemours & Company, Post Office Box 1671, Wilmington 99, Delaware

Cornell University Subcommittee
Chairman: Prof. D. G. Shepherd
Vice-Chairman: Prof. H. N. McManus, Jr

Ladies Programme
Co-Chairmen: Mrs H. J. Loberg
Mrs D. G. Shepherd

Belgian Combustion Meeting

The Belgian Section of the Combustion Institute is organizing a one-day Symposium on Saturday 14 October 1961. This Symposium will be held at the 'Centre de Recherches pour l'Industrie des Produits Explosifs', Val du Bois, Sterrebeek (Brabant). It will be based on contributions from Belgian specialists on combustion and detonation, who will report on the most recent work made under their direction in these fields of research.

This Meeting will be followed by some demonstrative experiments made by the staff of the above centre. Intending visitors are invited to write to Dr L. Deffet, at the Centre.

British Combustion Meeting

A one-day Symposium on Carbon Formation will be held on Wednesday 27 September 1961 in the Department of Mechanical Engineering, City and Guilds College, South Kensington, London S.W.7. There will be discussions of the mechanism of carbon formation in flames and the application of fundamental data on carbon formation to practical combustion systems. There will be brief prepared contributions; the aim, however, will be to allow as much time as possible for discussion.

A business meeting for members of the British Section of the Combustion Institute will be arranged at a convenient time on the same day.

The Symposium will be open to all members of the British Section and to others interested in the subject. If you wish to attend, please write to N. P. W. Moore at the address given.

Italian Combustion Meeting

On 25 September next the Italian Section of the Combustion Institute is organizing a Meeting in Turin in conjunction with the National Committee for Fuels and Combustion, the Italian Association of Heat Technology and the Italian Rocket Association, which will be attended by scientists and engineers in the combustion field. The purpose of this conference is an exchange of ideas about combustion and its problems, under the title 'An Italian programme of basic research on combustion—Relations with foreign study and research centres'.

A round-table Discussion will also be arranged on 'Combustion in internal and external reaction systems'.

Those desirous of attending the above Meeting should apply to the Italian Section of the Combustion Institute, at the Stazione Sperimentale per i Combustibili, Piazza L. Da Vinci, 32, Milan.

Recent Developments and Notes

Thermophysical Properties

The Second Symposium on Thermophysical Properties is now being organized by the Heat Transfer Division of the American Society of Mechanical Engineers. It is to be held at Princeton University from 24 to 26 January 1962. Those engaged in research in this field are invited to submit papers which can be reviews of the current status of theory, experimental techniques, and available data, or original papers reporting new theoretical or experimental work, or dealing with documentation methods. There will be four main sections as regards thermal properties: (*i*) thermodynamic properties and equations of state, (*ii*) molecular properties, (*iii*) transport properties, (*iv*) radiation properties, both heat and sound.

It is planned to publish the papers prior to the symposium. Further information may be obtained from E. F. LYPE, Chairman, Committee on Thermophysical Properties, c/o Thompson Ramo Wooldridge, Inc., 23 555 Euclid Avenue, Cleveland 17, Ohio, U.S.A.

Chimney Height Problem

The height of a chimney of one of the generating stations of the Pennsylvania Electric Company has recently been increased in effect in a novel way. Since there were objections to extending directly the existing 214 ft stack by 100 ft, an alternative method was adopted which consisted essentially of attaching a 10-ton stainless steel nozzle to the top of the chimney. By reducing the stack diameter in this way the velocity of the flue gases was increased by an amount equivalent to an effective increase of 50 per cent in the height of the chimney.

The main problem was presented by the dual brick–concrete construction of the chimney. The outer concrete shell is separated from the inner brick lining by a 6 in. air space which permits the chimney to sway under wind loads while the brick lining remains stationary, except for thermal expansion. The solution to the problem was a double shell skirt on the nozzle, the inner skirt being attached to the brick liner by a flexible diaphragm woven from TFE-fluorocarbon fibre impregnated with fluorelastomer, and the outer skirt was fastened to external supports on the concrete stack. In this way the annular sway-clearance space was kept unobstructed and the gas-bearing inner shell of the nozzle was effectively sealed by a material which was flexible, of good mechanical strength and resistant to corrosive gases at 200°C.

Indian Symposium on Heat Transfer

A symposium on heat transfer organized by the Mechanical Engineering Department of the Indian Institute of Science, Bangalore, was held in November 1959, in connection with the golden jubilee of the Institute. It was the first occasion on which a symposium on this subject was held in India. A review of the twenty papers presented, with a list of their titles and authors, has recently been published by A. RAMACHANDRAN, of the Indian Institute of Science [*Internat. J. Heat Mass Transfer*, 1961, **2**, 262].

Fluorescent Pigments for Stack Gases

In Sweden, where steps are now being taken by the government for concentrated action on the problems of air pollution, a team of investigators is making measurements of pollution in the atmosphere in two industrial areas in the centre of the country. An account of these has been given by Dr BERTIL WEDIN, Director, Research Institute of National Defence, Stockholm [*Smokeless Air*, Spring 1961, No. 117, 193].

The immediate purpose of the investigation is to study the horizontal and vertical extension of drifting air pollutants from different types of smoke stacks, under different weather conditions, and to determine concentrations of sulphur compounds. A method developed by R. R. BRAHAM, B. K. SEELY and W. D. CROZIER [*Trans. Amer. geophys. Union*, 1952, **33**, 825]

was modified for studying the movement of aerosol plumes. This is based on the use of a fluorescent pigment, synthetic crystalline zinc–cadmium sulphide, dispersed in aerosol form in the stack gases. The particles are collected by impactors into which a jet of air to be examined is sucked through a small fissure against a sticky strip on a rotatable cylinder. Aircraft, motorcars or boats survey the testing area by drawing the impactors at right angles across the drifting plume. Ultra-violet light is used for illuminating the impactor collections, and the concentrations of aerosol can be determined by counting the fluorescent particles by means of a microscope.

Meldola Medal Award

It is announced by the Royal Institute of Chemistry that the Meldola Medal for 1960 has been awarded to JOHN NEWTON BRADLEY, for his work in the field of physical chemistry, with special reference to the kinetics of reactions involving free radicals and reactions in shock waves studied by mass spectrometry.

The Meldola Medal, which is the gift of the Society of Maccabaeans, is awarded each year to the chemist who, being a British subject and under 30 years of age at 31 December in that year, shows the most promise as indicated by his or her published work.

Dr Bradley graduated in the University of Birmingham in 1952 and was appointed in 1959 lecturer in inorganic and physical chemistry in the University of Liverpool. His researches have included the development of a time-of-flight mass spectrometer for studying reactions in shock waves, in particular, the kinetics of nitrous oxide decomposition; the study of the pyrolysis and oxidation of acetylene; the thermal decomposition of nitroparaffins; emission from shock-heated gases; the mechanism of thermal ionization in shock waves; the combination of flash photolysis and shock tube techniques [*J. Roy. Inst. Chem.* 1961, **85**, 182].

U.S.A. Progress in Fire Protection

The annual Conference of the National Fire Protection Association was held this year in Detroit from 15 to 19 May, the chief business being the consideration of the reports and proposals presented by the thirty eight technical committees in regard to revisions of existing standards, codes and manuals, and the issue of new ones for tentative adoption.

Amongst the proposals which may be noted was a new guide for smoke and heat venting and this was adopted by the meeting. A complete revision of the manual on hazardous chemicals data was also approved. This is a comprehensive publication and for each substance information is given as to the usual shipping containers, fire and explosion hazards, life hazard, storage, and fire-fighting phases. A system for the identification of the fire hazards of materials which was adopted is intended for the protection of those concerned with fires in places where dangerous materials may not otherwise be readily recognized. A complete revision of the manual on static electricity is to be published and this will be of a very comprehensive character.

Interferometric Measurements in Flames

Following the general methods used by F. J. WEINBERG and his colleagues [see, in particular, J. H. BURGOYNE and F. J. WEINBERG, *Proc. Roy. Soc. A*, 1954, **224**, 286; A. LEVY and F. J. WEINBERG, *Seventh Symposium (International) on Combustion*, p 296. Butterworths: London, 1959], based on the optical properties of flat premixed flames for examining some of the important concepts relating to the theory of flame propagation, F. SCHULTZ-GRUNOW and G. WORTBERG, Institut für Mechanik der Technischen Hochschule, Aachen, have carried out interferometric measurements of a flat flame to determine temperature profiles from which to assess the energy transformations [*Internat. J. Heat Mass Transfer*, 1961, **2**, 56].

The interferometric temperature measurement is shown to be very simple and exact. The authors consider that by this method, using a Mach–Zehnder interferometer for direct measurement of refractive index, the difficulties of obtaining significant refractive index gradients as in Weinberg's experiments, are avoided. The error caused by the deflection of the light beams through regions of different density in the flame is negligible. Through a

flame front of approximately 4 mm thickness 60 measuring points could be obtained. The density of the measuring points was highest where the temperature gradient was large.

Energy flux was calculated from the temperature profiles. No definite point of ignition or inauguration of the reaction was observed when 80 per cent of the total increase in temperature is attained, as has often been assumed. The reaction is already completed up to an extent of 10 per cent when the increase of temperature has reached 37 per cent of its final value. The temperature corresponding to that of theoretical ignition, when 80 per cent of the total increase in temperature has been achieved, is located in the middle of the reaction zone where the chemical reaction has been 40 per cent completed and the rate of heat release has its maximum value. The specific *excess enthalpy* was determined. It has a maximum value amounting to 41 per cent of the heat of reaction, at the position where the sum of the heat conducted and radiated is a maximum.

Waste Heat Recovery Conference

The Second Conference on Waste Heat Recovery, organized by the Institute of Fuel, was held in Bournemouth, 15 to 19 May 1961, under the chairmanship of Dr W. A. MACFARLANE, C.B.E., President of the Institute and Managing Director of the National Industrial Fuel Efficiency Service. About twenty papers were presented, which fall into three groups; the first deals with the principles underlying methods of recovering waste heat, the second with the actual equipment employed for recovery, and the third with the experience of various industries in this field.

In two comprehensive papers the fundamental principles were reviewed. The subject of Dr P. O. ROSIN's paper was the total, available, returnable and recoverable heat in combustion gases. The paper by Dr M. FISHENDEN, Professor O. A. SAUNDERS, F.R.S., and Professor D. B. SPALDING, on heat transfer, was provided as a convenient source of data and methods for heat-transfer calculation.

In a paper by C. HULSE, Department of Fuel Technology and Chemical Engineering, University of Sheffield, an account was given of a recent enquiry into the effects of some aerodynamic conditions on the performance of heat exchange plant, in particular non-uniform flow distribution of fluids. It is suggested that this might commonly be found in much conventional equipment. The possibility of this is often ignored or overlooked by designers. Such conditions are to be found, for example, in the smoke tubes of Economic boilers, waste heat boilers and economizers, in regenerator settings and recuperators. It is shown in the paper that where there is bad distribution considerable loss of performance can result. In open hearth furnace regenerators the air preheat may be reduced in this way by more than 200°C. The use of baffle walls suitably placed can give at least 100° to 150°C more air preheat, with consequent saving of fuel oil up to 2·3 gal/ton steel. The effects on overall rates of heat transfer of these conditions are discussed, industrial examples are given, and suitable remedial action is indicated. Deductions have been made from cold trials of plant itself, the use of models and inferential methods.

Progress in Industrial Waste Heat Recovery

At the Second Conference on Waste Heat Recovery, held in Bournemouth, 15 to 19 May 1961 (see note above), several papers were read on the progress made in waste heat recovery in different industries since the last conference in 1946.

In the glass industry improvements in regeneration efficiency have been only on a limited scale. 'Box' type regenerators, developed to give better integration of furnace and regenerator design, have been successful on oil and clean gas-fired furnaces. Horizontal regenerators have been used to overcome the slagging problem, and the use of basic refractories may be the means of reducing the overall size of regenerators. Unit melters for glass-melting, which have no recuperation or regeneration, are now being used fairly extensively, so that waste heat recovery from their high-temperature gases is of considerable importance. A suitable metallic recuperator is described which may result in 35 per cent saving in fuel. A water-tube boiler

of very high efficiency is now being used in Germany for waste heat recovery.

In the gas industry improvement in the efficiency of waste-heat recovery is due to the concentration of production in large carburetted water gas plants whereby the integration of the steam and power requirements of the plant is easier in relation to waste heat available.

Waste heat recovery has been well-established in the chemical industries for a long time, and is practised wherever it is an economic proposition. In the very large units now used it has become possible to discriminate between high-grade heat for conversion into energy and low-grade heat for heating process materials.

The technique of coke dry-cooling, conjoined with the use of a waste-heat boiler, has developed little in the past 15 years. In this period 18 dry-cooling plants have been installed, 11 of them in Switzerland, none in Britain.

In open-hearth furnaces now using tonnage oxygen the role played by regeneration in promoting furnace performance is affected. There has come about a change in emphasis in the important properties required of the regenerator. The design must be such as to withstand the considerable fume carried over by the furnace gases. The regular cleaning programme which must be carried out requires appropriate access for this purpose. Cleaning of the regenerator becomes as important as adequate furnace-charging and correct combustion in the furnace.

High Temperature Aerodynamics

A review of this subject, supported by the National Science Foundation of the U.S.A., has recently been published by R. GOULARD, Professor of Aeronautical and Engineering Sciences, Purdue University, Lafayette, Indiana [*Appl. Mech. Rev.* 1961, **14**, 257]. There is given a useful list of about 70 references to the latest information on the subject.

The thesis of the writer is that the field of gas dynamics, previously shared by applied mathematicians and flow experimentalists, now requires more of the work of physical chemists. It is unlikely, however, that simplified models or configurations will be found that can comprise the essential concepts of both fluid dynamics and physical chemistry. The author considers that analytical work in chemical aerodynamics may reduce to two main functions, first, extensive experimental runs, supported by heavy numerical computer operations, and secondly a large number of very simple configurations that can be studied, such as in shock tubes, and this would enable the elementary processes to be properly identified as they present themselves in the complex context of actual engineering flows.

Thermodynamic properties of air in chemical equilibrium have now been tabulated up to 24 000°K so that results for enthalpy, specific heat and velocity of sound, based on methods of statistical physics together with spectrographic measurements can be confidently used. Confidence in molecular transport properties does not exist to the same extent; even for relatively low temperatures theoretical predictions are necessary and more realistic models than so far produced are required, taking into account the detailed structure of particles. Progress in the determination of radiation transfer properties of high temperature air has been notably swifter. In this connection, as in others, there has been remarkable success in shock tube experiments in which the results from normal shocks in equilibrium have now been extended for use in connection with oblique shocks and conical flows in dissociation equilibrium.

The hundred or more possible reactions of the twenty or so chemical components of air have been reduced to five thermally significant reactions for the evaluation of the chemical kinetics. The shock tube method and the experimental study of reacting particles in ion and molecular beams, in which considerable interest is now being shown, should together provide a powerful combination of complementary tools in high-temperature chemistry research. The use of simplified chemical kinetics models in work on nozzle flow is an outstanding feature of current investigations, to replace the five-reaction model referred to above.

Testing for Corrosive Tendencies of Flue Gases

One of the objectives of the Boiler Availability

Committee since its inception has been that of establishing suitable techniques to give relative indications of potential fouling or corrosion tendencies of boiler flue gases or to assess the effect of modified conditions of boiler operation on these tendencies. The value and limitations, however, of different techniques which have been described in recent years are not widely known and the Committee felt, therefore, that guidance on the subject should be given. This has now been done in a publication entitled *Testing Techniques for Determining the Corrosive and Fouling Tendencies of Boiler Flue Gases* which provides details of suitable methods in a concise form [*Bulletin XI:* MC/316; March 1961; 68 pp.].

Testing methods are divided into two main groups. In the first group there are techniques for investigating low-temperature corrosion and its causes; these include meters for measuring *acid dewpoint* temperature, corrosion probes, instruments for determining sulphur dioxide and sulphur trioxide, also *acid-deposition* probes. The second group comprises techniques designed for the determination of the nature and extent of high-temperature fouling, including probes for measuring the rates of deposition of various constituents of fuel ash.

All the methods are necessarily based on the insertion of at least one probe into the gas stream and possess the limitations inherent in this technique. The bulletin does contain, however, hints on correct sampling techniques to achieve the maximum degree of accuracy at reasonable cost in time and equipment.

Most of the techniques described are intended for tests of short duration, being designed to yield results within an hour and so are ideal for the investigation of rapid changes in boiler conditions. They are thus better suited for the comparison of different methods of boiler operation, or of variations in fuel characteristics, than the precise prediction of the period of trouble-free service likely to be obtained from a given component. Some of the tests listed are suitable for use over longer periods. For example, a liquid-cooled corrosion probe is described which can operate without attention for a period of 100 hours or more. Once optimum conditions have been established, long-term testing offers a means of determining the average corrosion to be expected under these conditions.

Attention is given in the bulletin to the safeguards essential to ensure the correct operation of instrumentation in a boiler room. Details are also given of methods for obtaining the highest possible accuracy in each test even under adverse conditions. Assessment of test results is facilitated by an indication, wherever practicable, of the errors inherent in the methods described.

Solid Propellant Rocket Motors

A survey of current developments in propellants and of motor performance in connection with solid propellant rocket motors, was given in a recent lecture to the Astronautics and Guided Flight Section of the Royal Aeronautical Society, by W. R. MAXWELL, of the Rocket Propulsion Establishment, Westcott, and G. H. S. YOUNG, of the Explosives Research and Development Establishment, Waltham Abbey [*J.R. aero. Soc.* 1961, **65**, 252].

The principal solid propellants under current investigation in this country are those of the double-base type, either in an extruded or cast form; plastic propellant, and more recently, polyurethane propellant, which is an elastomeric composite. The addition of light elements or hydrides is being given attention for improving performance. Some success has been achieved by adding aluminium to composite propellants. This has enabled the performance of both plastic and polyurethane types to be raised to about 235 lb sec/lb without noticeably increasing burning rates. The combustion temperature, however, is greatly increased and causes severe practical problems in nozzle design. The chief interest at the present time is increasing the size of solid propellant rockets. In the large Polaris and Minuteman American rockets extrusion processes for the solid propellants used in them would be uneconomical and attention is now being given to propellants that can be slurry cast and are case-bondable. The two most favoured systems are those based on

the thiokol polysulphide synthetic rubber and on the polyurethane rubber.

In connection with motor design, the problem of prime importance is to associate the maximum mass of propellant with the minimum of motor hardware. Volumetric loading density and propellant density, important in this connection, are discussed. In trying to reduce the weight of the hardware, materials are needed with high mechanical strength, low density and good thermal insulating properties. Alloy steels are now available giving ultimate tensile strengths of more than 100 ton/in². Molybdenum is most widely used as nozzle material, but for the very hottest propellants tungsten and alloys of it with molybdenum and tantalum, are being used.

The F-1 Rocket Engine

The National Aeronautics and Space Administration announced at the end of April that the largest of the rocket engine test stands, designated I-B, at the Edwards Rocket Site, Leuhman Ridge, California, is nearing completion and is to be used in early summer for full-scale testing of the F-1 engine which is being developed by Rocketdyne, a division of North American Aviation, Inc. This stand is 250 ft high, and on the top are two propellant pressure vessels. The vacuum-jacketed liquid oxygen tank has a capacity of 75 000 gallons, and the single-walled tank for fuel will hold 60 000 gallons.

Some particulars of the F-1 engine were given by S. K. HOFFMANN, president, Rocketdyne Division, in the Fifth Sir Henry Royce Memorial Lecture which he delivered to the Royal Aeronautical Society in November last, outlining the history of his organization's activity in the field of large liquid-propellant rocket engines [*J.R. aero. Soc.* 1961, **65**, 321].

The F-1 is the largest single-thrust-chamber engine known to be under development. It is designed to produce $1{\cdot}5 \times 10^6$ lb of thrust and is being developed under the technical direction of the N.A.S.A. Marshall Space Flight Center, Huntsville, Alabama. The engine is designed for operation with liquid oxygen–kerosine propellants. It uses a conventional bell-shaped nozzle design, but of very large size, which has regeneratively-cooled tubular walls. The turbopump is side-mounted on the thrust chamber and the entire unit can be gimbal-mounted. In a single-engine application, the F-1 will provide the maximum performance and ultimate reliability for an advanced second-generation space booster.

New Measuring Technique in Gases

At the XVIIIth International Congress of Pure and Applied Chemistry, held in Montreal, 6 to 12 August, a paper was read by P. L. BLACKSHEAR and L. M. FINGERSON describing a new measuring technique that has been developed recently in the Combustion Laboratory of the Mechanical Engineering Department of the University of Minnesota.

A heat flux probe has been devised which is, in effect, a constant temperature hot wire anemometer that can be operated in flames up to about 2 750°C, at atmospheric pressures and subsonic velocities. It consists of a hollow, internally cooled, non-conductor which has on its surface a thin film resistance element. The surface of the film is kept at constant temperature by a compensating power supply and the resulting power requirement represents the heat flux from the heated surface to the surroundings and to the internal coolant. The heat flux depends, *inter alia*, on the mass flow per unit area approaching the sensing element, and the probe has been used to study the effects of laminar transport properties in the mixing of a turbulent jet and also to detect the flame temperature in a burning globule of flame generated by a spark intermittently igniting a flow stream.

A similar instrument was described a short time ago by S. C. LING, particularly for use in turbulent liquid flows [*Trans. Amer. Soc. mech. Engrs* (*J. basic Engng*), 1960, **82D**, 3, 629].

The Controlled Mixing History Flame

A critical review of the progress of research on the combustion of pulverized coal has recently been published by J. M. BEÉR, Head of Research Station, International Flame Foundation, IJmuiden [*J. Sheffield Univ. Fuel Soc.* 1961, **12**, 29]. The subject is discussed from

three aspects, (*i*) flame propagation in dust clouds, (*ii*) the burning of single particles, (*iii*) the combustion of dust clouds.

In connection with flame propagation, reference is made to a theory recently put forward by J. CSABA, working in the University of Sheffield. He has measured flame speeds in a vertical conical furnace, using a stationary horizontal flame. In recent work the importance of the phenomena of recirculation of hot combustion products has become recognized for theoretical studies of propagation. In earlier work radiation alone was regarded as the important mode of heat transfer.

In studies on the burning of single particles, diffusion is generally found to be the controlling factor at flame temperatures and for relatively large particles with diameters greater than 300 microns.

Attempts to extend calculations from the combustion of single particles to the rates of combustion of dust clouds in industrial type jet flames have not been very successful. One of the most recent developments in this direction is in the study of a simplified experimental model by J. M. BEÉR and Professor M. W. THRING. The apparatus used to obtain what is called a *controlled mixing history flame* is a vertical reactor, 15 ft high and 1·5 ft i.d. The coal dust, premixed with a small fraction of the combustion air, is uniformly distributed in the cooled top part of the reactor and the remainder of the air is mixed in behind the flame front at several points down the flame so as to vary the concentration of the oxidant stepwise. Study of the physicochemical aspects of the combustion of dust clouds by this means, coupled with the results of aerodynamic investigations, may lead to a new interpretation of the experimental data of pulverized fuel flames.

Quantitative Spectroscopy and Radiative Transfer

An announcement has recently been made of the publication by the Pergamon Press during the present summer of a new international journal, *Quantitative Spectroscopy and Radiative Transfer*. The editor-in-chief is Professor S. S. PENNER, Division of Engineering, California Institute of Technology, and the editorial advisory board includes W. S. BENEDICT, A. G. GAYDON, F.R.S., J. H. JAFFE, J. LECOMTE, R. MECKE, R. W. NICHOLLS and W. M. VAIDYA.

The subjects of papers to be published will include emissivities of heated gases, liquids and solids; flame temperatures and flame emissivities; shock-tube studies in which the emphasis is on quantitative spectroscopy; radiant energy emission from plasmas.

Further particulars may be obtained from Pergamon Press, Headington Hill Hall, Oxford.

Vibrational Combustion

V. V. SOLOVEV has described an analysis of vibrational combustion in high pressure combustion chambers using pulverized coal and lignite [*Inzh-Fiz. Zh.* **1959,** No. 1, 25; *Ref. Zh. Mekh.* **1959,** No. 9, Rev. 9964]. The frequency of the vibrations was found to be close to the natural frequency of a column of gas in a tube with one end closed and it is concluded that the phenomenon under observation is that of acoustical longitudinal vibrations of a column of gas. The pressure fluctuations in the combustion chamber are said to result in rapid alterations in the composition of the fuel mixture and, in consequence, there are fluctuations in the liberation of heat. When there is a favourable phase correlation between the pulsations of heat liberation and of pressure, effected by delaying the firing of the fuel mixture, the vibrational system may be stimulated [A. B. EZROKHI; Courtesy *Referativnyi Zhurnal, U.S.S.R.; Appl. Mech. Rev.* 1961, **14,** 396].

Radiative Transfer in Combustion Chambers

The Melchett Lecture for 1960 was delivered by H. C. HOTTEL, Professor of Fuel Engineering, Department of Chemical Engineering, Massachusetts Institute of Technology, to a meeting of the Institute of Fuel, in London, in April. The lecture has now been published [*J. Inst. Fuel,* 1961, **34,** 220].

The subject of radiation from furnace gases is reviewed and an account is then given of developments in the simulation of real gases by grey-gas mixtures, together with observations on shape factors. A simplified furnace equation

is presented using a mathematical model of combustion chamber performance which, although departing seriously in many ways from reality, succeeds to a large extent in preserving the substantially correct relation amongst the dominant variables. The idealized furnace used as a basis for the calculations is referred to by the author as the *well-stirred speckled-walled grey-gas combustion chamber*. This simplification is shown to be of value in the thermal classification of furnaces. The performances of well-stirred and plug-flow furnaces are compared and an approximate method of correlating them is suggested. Finally, a review is given of the complications associated with carrying out a rigorous treatment of furnace chamber performance.

Nozzle Convergence and Combustor Performance

An investigation of the effect of nozzle convergence length on the performance of a combustor has been described by M. C. BURROWS, National Aeronautics and Space Administration [*NASA TN D-579*, 22 pp, December 1960]. The reaction chosen was that of heptane with oxygen under the conditions of a combustor with a nominal 200 lb thrust. Various lengths of the nozzle convergence section between the chamber and throat were used, as well as various cylindrical-chamber lengths to provide different combustor gas velocity profiles. Characteristic velocity as a function of the characteristic length and of the total combustor length was obtained for three lengths of the nozzle convergence section. Two injectors of different performance characteristics were used, a single contraction ratio, and one propellant-flow condition.

It was found that total combustor length provided the closest correlation of combustor performance when using short combustor lengths and a relatively low-performance injector. When the performance was increased by using a longer combustor length or injector with higher performance, the combustor performance was a function of characteristic length. The experimental effect of nozzle convergence length, expressed as equivalent chamber length, when compared with the analytical data in the literature, was found to be considerably less than the effect predicted analytically from these data.

New Chairman: Fire Research Board

Professor F. H. GARNER, O.B.E., has recently been appointed Chairman of the Fire Research Board for the next five years, succeeding Professor A. R. J. P. UBBELOHDE, F.R.S. The Fire Research Board, nominated jointly by the Department of Scientific and Industrial Research and the Fire Offices' Committee, advises the Joint Fire Research Organization on its research programme. Professor GARNER, Emeritus Professor of Chemical Engineering in the University of Birmingham, is a Past President of The Institute of Petroleum. He has recently completed a term of office as chairman of the Water Pollution Research Board.

Rate Constants of Flame Processes

In a paper presented to the Eighth Symposium (International) on Combustion, at Pasadena, in September 1960, L. A. LOVACHEV, Institute of Chemical Physics, U.S.S.R. Academy of Sciences, Moscow, dealt with laminar flame features as a function of chain reaction mechanism. From experimental flame properties the type of reaction occurring may be deduced and from the dependence of the burning velocity on the temperature, pressure and heat transfer coefficient the reaction constants of the elementary processes may be obtained. This subject is developed in a more recent paper by the author given to the XVIIIth International Congress of Pure and Applied Chemistry, in Montreal, in August.

The argument developed here is that analytical relations obtained from models using a number of experimental data of chain reactions make it possible to calculate flame velocities by thermal theory equations, which are actually empirical or semi-empirical. The overall reaction orders with respect to the initial substances determined in this way appear to be zero fractions, or variables, and this does not correspond to actual reaction orders. It is accounted for by certain relationships between constants of elementary processes and concentrations of initial, intermediary and final products, as well

as by temperature and molecular transfer coefficients. For example, with flames involving unbranched chains activation energies and heats of formation of active centres will be important. Thus, the *effective* activation energy obtained from thermal theory equations will not be a characteristic of the burning mixture since it depends mainly on the heats of formation of active centres. For flames involving branched chains the *effective* activation energy will depend mainly on the activation energy for branching which in turn depends on the temperature with which the rate function of heat emission is associated. The dependence, differing according to the type of chain reaction, of flame velocities on heat conduction and on active centre diffusion coefficients, is not consistent with functions obtained according to thermal theories. In other words, wrong allowances are made for molecular transfer coefficients when using thermal theory equations.

Stability of Turbulent Flames

Professor D. B. SPALDING and D. VORTMEYER, Imperial College of Science and Technology, London, have now published an expanded version of their contribution on the stability of turbulent flames in combustion chambers which they made to the 2nd Colloquium on Flow and Combustion, organized by the Verein Deutscher Ingenieure, and held in March 1960, at Bad Kreuznach [*Brennst.-Wärmekr.* 1961, **13**, 259; see also *Combustion & Flame*, 1960, **4**, 379].

In their analysis of the problems of the stabilization of turbulent flames by recirculation of hot gas in cylindrical combustion chambers, the authors have shown that information on the range of stability and on the efficiency can be obtained by two different quantitative methods. One of these methods depends on an integration of the energy equation. The other method is of more general applicability, when the flow pattern is too complicated for analytical description. In this method, assuming that the presence of flames does not affect the turbulent flow process, experimental results from cold models can be used in the form of *influence coefficients* for the solution of the equations for the combustion process. The influence coefficients represent the interactions as regards flow conditions between the separate volume-elements of the reaction space. The coefficients usually have to be determined experimentally. From the equations obtained the connection is established between two dimensionless numbers, the efficiency η and a chemical coefficient L. The calculations are based on the assumption that the speed of chemical reaction should be regarded purely as a function of the temperature. The graphical representation of values of η as a function of L, calculated from numerical solution of the equations, gives a set of stability curves which, with a recirculation factor as a parameter, show satisfactory agreement with the few existing stability measurements made on cylindrical combustion chambers. The results obtained by this method are applicable only to combustion chambers operating with premixed fuel, which may be gas or very finely dispersed liquid, and air, fully turbulent flow and adiabatic conditions.

Forge Furnace Design

With reference to the *Note* on this subject on page 198 of the June issue of this Journal, line 7 of the first paragraph should read: 'works of Walter Somers Ltd, Halesowen, Birmingham'.

W. A. KIRKBY

FUEL

Readers of *Combustion & Flame* may like to know that the July issue of *Fuel* contained *Notes* dealing with:

Oxygen in open hearth furnaces
Auxiliary fuels in the blast furnace
Gas in the domestic market
Reactivity of coke

and further *Notes* appear in *Fuel* for September on:

Technical communication
Electricity generation in the future
B.C.U.R.A. research

Letters to the Editors

Letters to the Editors on points of scientific interest related to combustion and flames are invited. The Editors do not hold themselves responsible for opinions expressed in correspondence. Anonymous contributions cannot be accepted.

The Influence of Coal Rank and Fineness on the Inflammability Index of Coal Dusts

THE Inflammability Index of any dust is an empirical parameter, defined by some arbitrary experimental test, that is reasonably believed to provide some relative measure of the liability of that dust to be inflamed or to explode. One such method of test, that has been widely used for assessing the inflammability of coal dusts, is the large-scale explosion gallery. This explosion gallery method requires the determination of the minimum percentage of stonedust (S) known as the stonedust or inert limit that, when intimately mixed with the coal dust, is required to prevent propagation of flame through an air-dispersed coal-dust cloud of maximum inflammability. The mechanism of flame suppression is not specified. The explosion galleries used at present in this country are typically: 4 ft diameter and 325 ft long, made up of boiler shells bolted together and with one end blanked off. The intimate mixture of coal dust and stonedust to be tested is spread uniformly on the floor of the gallery, and the mixture is then raised into a cloud and fired by some appropriate ignition source placed at the closed end of the gallery. By this method a number of important empirical relations between the inert limit, the coal rank, and the coal fineness, have been found by T. N. MASON and R. V. WHEELER[1-3], and substantiated by others, notably W. B. CYBULSKI[4]; but rather surprisingly, neither these authors, nor any others (so far as the present writer is aware), generalized the results they obtained. The purpose of this note is to show that, if these results can be taken at least at their face value, then some useful generalization can be made.

Mason and Wheeler established three particularly important results:

(*i*) that for a set of 11 coals chosen at random and ground to a common superficial fineness, the inert limit (S) was related to the volatile percentage in the coals by the expression[1]

$$Z = 100/(100 - S) = V/V_i \quad \ldots . [1]$$

where V_i was a constant that took the value of 12·5 per cent at $S = 0$; and the parameter $[100/(100 - S)]$ was defined as the Inflammability Index (written later by Cybulski[4] as Z).

(*ii*) that with change of stonedust type[2] the proportionality between Z and V remained; but since V_i (at $Z = 1$) was unchanged, the line then had an intercept. This was shown[2] graphically, but the authors did not explicitly correct their equation.

(*iii*) that with variation of fineness[3] (or specific surface) for a given coal, Z was found to be proportional also to a fineness factor F that was an estimate of specific surface. The fitted equation had the linear intercept form

$$Z = aF + b \quad \ldots . [2]$$

where a and b are constants for a given coal, but they change with coal rank. This equation was later substantiated by Cybulski[4].

In generalizing these results it is clear first from point (ii) above that the Z/V relation must also be of the linear-intercept form of equation 2; and it is entirely fortuitous that in the experiments from which equation 1 was derived, the intercept happened to be very close to zero. We have, therefore, that Z is proportional to: (*1*) V at constant F; and to (*2*) F at constant V. It is obvious, therefore, that these algebraic requirements can only be satisfied simultaneously by a general empirical equation of the form

$$Z - Z_0 = m\,(V - V_0)\,(F - F_0) \quad \ldots . [3]$$

where Z_0, V_0, F_0 and m are empirical constants having values 0·95, 12·5, 0·15 and 0·04 respectively. These values have been determined from the experimental results of the data avail-

able, and a plot of Z against $(\Delta V.\Delta F)$ is shown in *Figure 1*.

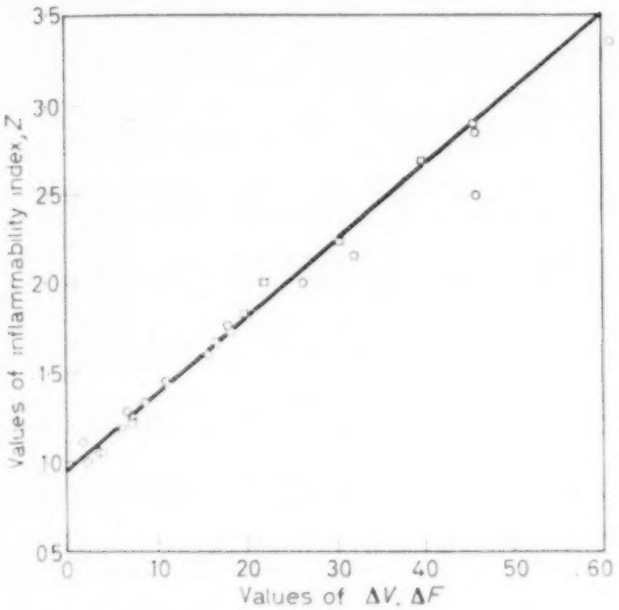

○ *Set of 11 coals at nominally the same fineness*[1]
□ *Silkstone coal: variation with fineness*[3]
◇ *Red Vein coal: variation with fineness*[3]

Figure 1. Plot of Inflammability Index Z against the product of volatile and fineness difference $(\Delta V . \Delta F)$. *Data of* T. N. MASON *and* R. V. WHEELER[1–3]

A full qualitative, and partly quantitative, analysis of these and other results has now been developed that is to be presented in due course elsewhere. In the light of this new analysis it is now clear that the experimental system involved is so complex that the probability of drawing any valid inferences about the combustion behaviour from equation 3 is small; indeed it would now seem that we should also treat with reserve the conclusion, drawn by Mason and Wheeler[1], that 'Under conditions of ignition no more severe than those obtaining in our experiments, therefore, coal dusts containing 12·5 per cent or less of volatile matter are incapable of propagating flame'. It is also possible, therefore, that this new interpretation may now require the revision of the Mines and Quarries Act which provides the regulations governing the use of stonedusting in coal mines.

R. H. ESSENHIGH

Department of Fuel Technology and Chemical Engineering, University of Sheffield

(*Received February 1961*)

References

[1] MASON, T. N. and WHEELER, R. V. *Saf.-i.-Mines Res. Pap. No. 64*, 1931
[2] MASON, T. N. and WHEELER, R. V. *Saf.-i.-Mines Res. Pap. No. 79*, 1933
[3] MASON, T. N. and WHEELER, R. V. *Saf.-i.-Mines Res. Pap. No. 95*, 1936
[4] CYBULSKI, W. B. *Paper No. 36* to Seventh International Conference of Directors of Safety in Mines Research, Buxton, 1952

Radiative Features of Ozone-Oxygen Mixture Decomposition Flames and Non-adiabatic Flame Theory

DECOMPOSITION flames of ozone–oxygen mixtures display the same phenomenological properties that are observed for other flame systems, i.e. characteristic burning velocities and extinction limits. However, a particularly interesting feature of any given ozone–oxygen flame is the spatial structure of the infra-red radiation losses of the flame to the environment.

It is well known[1] that ozone *is* infra-red active and that oxygen *is not* infra-red active. Consequently, the volumetric rate of radiative energy loss sustained by any ozone–oxygen decomposition flame is quite significant *in the upstream portion of the flame* (*in the 'reaction zone'*), *and quite insignificant downstream of the peak temperature of the wave*. This is a consequence, of course, of the fact that the ozone concentration is virtually zero, downstream of the peak temperature of the wave. In the following discussion, the peak temperature of the deflagration is taken to be at $x = 0$, with $x < 0$ 'upstream', and $x > 0$ 'downstream'.

This property of the ozone–oxygen decomposition flame (i.e. the reactant radiates in the infra-red, the product does not) provides us with an effective test of two different approaches to the formulation of a non-adiabatic flame theory. One approach is that employed at this laboratory[2,3] which differs critically from that employed by D. B. SPALDING[4]. An essential difference is the following:

(*a*) In this laboratory, we take the view that radiative and conductive heat losses from the 'reaction zone' ($x \leqslant 0$) *dominate* the description of flame extinction limits[2,3]; consequently, the energy conservation equation descriptive of this régime is written[2,3]

$$\frac{d^2\tau}{dx^2} - \frac{cG}{k}\frac{d\tau}{dx} = -\Phi(\alpha, \beta, \tau) + l(\tau)$$

It is the presence of the heat loss rate term, $l(\tau)$, *in the 'reaction zone'* which is the key element in the prediction of extinction limits presented in refs. 2 and 3.

(*b*) Ref. 4 takes the view that the 'reaction zone' heat losses may be ignored and that inclusion of heat losses in the description of the downstream 'cooling portion' ($x > 0$) is the key element in the description of extinction limits. Consequently, the limits presented in ref. 4 are deduced from a model which omits the loss term, $l(\tau)$ for $x < 0$, considering heat losses only for the régime $x > 0$.

Strictly speaking, physical reality requires that $l(\tau)$ be considered throughout the flame, for any flame. However, for any given flame, the question remains of whether or not serious 'practical difficulties' arise from neglect of $l(\tau)$ for values of $x < 0$. Here, the ozone–oxygen decomposition flame provides an answer. Quite aside from the various objections to the theoretical aspects of the flame formulation of ref. 4, there is the practical fact that neglect of losses in the reaction zone implies that the formulation cannot be employed to predict ozone–oxygen decomposition flame inflammability limits (lower limit of ozone concentration in oxygen). This follows, of course, from the fact that existence of inflammability limits rests heavily[2] on *radiation* losses. It is clear also that related difficulties are present in any application of the formulation of ref. 4 (or to unmodified extensions[5] of ref. 4) to other flame systems.

Measurements of ozone–oxygen decomposition flame inflammability limits and radiative losses are in progress at this laboratory. These results are being treated by the methods of refs. 2 and 3 and will be reported.

A. L. Berlad

Convair Scientific Research Dept, San Diego, California

(*Received May 196*)

References

[1] Herzberg, G. *Infrared and Raman Spectra of Polyatomic Molecules*. Van Nostrand: New York, 1945
[2] Berlad, A. L. and Yang, C. H. *Combustion & Flame*, 1960, **4**, 325
[3] Yang, C. H. *Combustion & Flame*, 1961, **5**, 163
[4] Spalding, D. B. *Proc. Roy. Soc. A*, 1957, **240**, 83
[5] Adler, J. and Spalding, D. B. *Proc. Roy. Soc. A*, 1961, **261**, 53

Laminar Flame Propagation Velocities in Terms of Flame Parameters in a Hydrogen–Oxygen Flame

L. A. Lovachev[1] has recently proposed some approximate methods for deriving information on high temperature kinetics in chain reaction systems from burning velocity measurements, for cases when the flame is controlled by low activation energy reactions. The first step was the approximate solution of the energy conservation equation 1.

$$\lambda\frac{d^2T}{dx^2} - Mc\frac{dT}{dx} + \phi(T) = 0 \quad \ldots [1]$$

Here T is the temperature rise from that of the unburnt starting material, λ and c are the thermal conductivity and specific heat respectively (both assumed constant throughout), M is the mass burning velocity, and $\phi(T)$ is the heat release rate. Putting $p = dT/dx$ we obtain from equation 1

$$\lambda p\,dp/dT - Mcp + \phi(T) = 0 \quad \ldots [2]$$

Equation 2 is subject to the boundary conditions

$$T = 0\ , \quad p = 0 \quad \ldots [3]$$

$$T = T_b, \quad p = 0 \quad \ldots [4]$$

where T_b is the final flame temperature.

For a low activation energy of the heat release process $\phi(T)$ is approximated by

$$\phi(T) = aT \quad \ldots [5]$$

in the interval $0 \leqslant T \leqslant T_b$, where the constant $a = \phi(T_m)/T_m$ and $T_m = \frac{1}{2}T_b$.

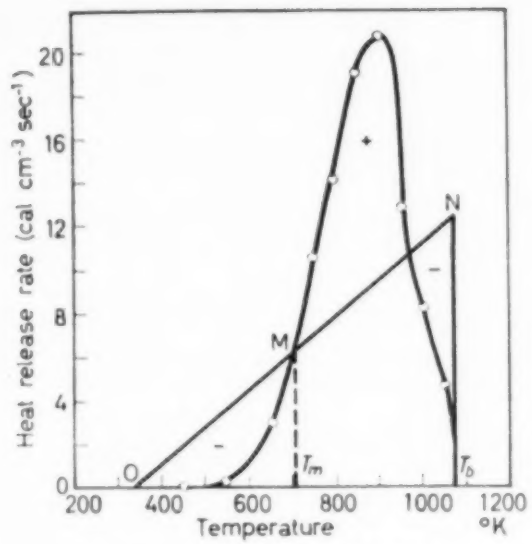

Figure 1. Linear approximation of the curve of heat release rate versus temperature

Figure 1 shows that this represents a close approximation to reality as regards the area enclosed beneath the $\phi(T)$ curve in the case of a typical slow burning hydrogen–oxygen–nitrogen flame. This flame is one of a series whose temperature distributions we have measured experimentally by means of a fine thermocouple[2]. The thermal conductivities used in deriving the experimental $\phi(T)$ curve were computed using measured composition and temperature profiles[2] in conjunction with thermal conductivity data for the pure components. Equation 2 now becomes

$$\lambda p \, \mathrm{d}p/\mathrm{d}T - Mcp + aT = 0 \qquad \ldots . [6]$$

and L. A. LOVACHEV[1] uses a solution obtained by A. N. KOLMOGOROV, I. G. PETROVSKY and N. S. PISKUNOV[3], which is

$$Mc = 2(\lambda a)^{\frac{1}{2}} = 2[\lambda\phi(T_m)/T_m]^{\frac{1}{2}} \qquad \ldots . [7]$$

If now it is assumed as a further approximation that $\mathrm{d}p/\mathrm{d}T = 0$ at T_m, then from equation 2

$$\phi(T_m) = Mcp_m \qquad \ldots . [8]$$

and substituting equation 8 into 7

$$M = (4\lambda/cT_m)\, p_m \qquad \ldots . [9]$$

An alternative approximate solution may be obtained by applying D. B. SPALDING'S centroid formula[4] to the triangle $OMNT_b$ formed by approximating the function $R(T) = (\lambda/\lambda_u)\,\phi(T)$ in a similar manner, as shown in *Figure 2*. The

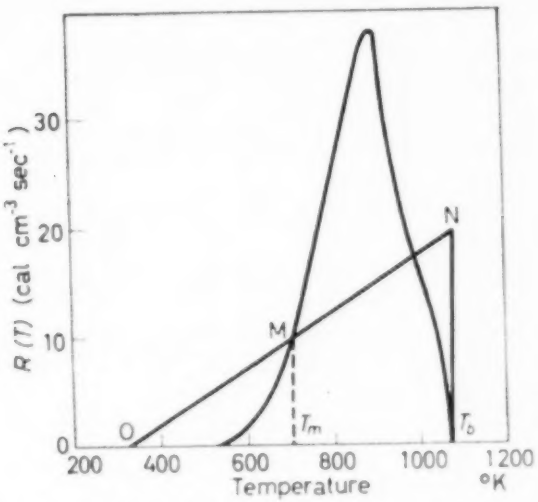

Figure 2. Linear approximation of the curve of $R(T)$ versus temperature

thermal conductivity is here no longer constant, and λ_u refers to the unburnt gas. For this linear approximation for $R(T)$ the eigenvalue in the burning velocity expression becomes 0·23, and since, for the triangle, the mean value of $R(T)$ over the interval $0 \leqslant T \leqslant T_b$ is $R(T_m)$, the solutions 10 and 11 are obtained instead of 7 and 9:

$$Mc = \left[\frac{\lambda_u R(T_m)}{0{\cdot}23 \times 2T_m}\right]^{\frac{1}{2}} \approx \sqrt{2}\left[\frac{\lambda_u R(T_m)}{T_m}\right]^{\frac{1}{2}}$$
$$= \sqrt{2}\,[\lambda_m \phi(T_m)/T_m]^{\frac{1}{2}} \qquad \ldots . [10]$$

$$M = (2\lambda_m/cT_m)\, p_m \qquad \ldots . [11]$$

In *Table 1* the experimental linear burning velocity S_u (referred to gas at 18°C and 760 mm of mercury) is compared with values calculated using the centroid formula in conjunction with the experimental $R(T)$ curve (no linear approximation involved), and with values calculated from equations 7, 9, 10 and 11. In using equations 7 and 9 it was assumed that $\lambda = \lambda_m$. It is seen that the unmodified centroid treatment gives a value within two per cent of the experimental burning velocity, whilst the linear approximation equation 10 gives a value some 10 per cent too low. Equation 11, involving the

approximation $d(\lambda p_m)/dT = 0$ in this actual case where λ is not constant, is clearly not strictly valid here. For this flame (with $T_u = 336°K$, $T_m = 707°K$), $d(\lambda p)/dT = 0$ at about 800°K.

Table 1

Method of calculation	S_u (*cm sec*$^{-1}$)
Experimental	9·2
Unmodified centroid	9·0
Equation 7	11·6 (±0·6)
Equation 9	32·5
Equation 10	8·2 (±0·4)
Equation 11	16·3

The reason for the poor agreement of the formula 7 becomes clear if we consider its derivation. The solution of equation 6, subject to boundary condition 3, is

$$p = (Mc/\lambda + b)\,T \qquad \ldots\ldots [12]$$

where

$$b = [-Mc + (M^2c^2 - 4a\lambda)^{\frac{1}{2}}]/2\lambda \qquad \ldots [13]$$

For $a > 0$, p cannot have real values unless $Mc \geqslant 2(a\lambda)^{\frac{1}{2}}$, and this is the origin of formula 7. However, solution 12 means that dp/dT must be constant throughout the interval $0 \leqslant T \leqslant T_b$. Hence, for both boundary conditions 3 and 4 to be satisfied it is necessary that $dp/dT = 0$ throughout the interval, which is impossible. The approximation 5 is therefore unrealistic in the manner in which it is used. For constant M and c it is merely equivalent to increasing the thermal conductivity of the mixture.

The centroid formula, on the other hand, does not depend in the same way on the detailed solution to equation 6, so that it provides a better approximation than the Kolmogorov formula.

G. Dixon-Lewis
A. Williams

Houldsworth School of Applied Science, University of Leeds

(*Received June 1961*)

References

[1] Lovachev, L. A. *Combustion & Flame*, 1960, **4**, 357
[2] Dixon-Lewis, G. and Williams, A. To be published
[3] Kolmogorov, A. N., Petrovsky, I. G. and Piskunov, N. S. *Bulleten Moskovskogo Gosudarstvennogo Universiteta*, Razdel A, **1937**, No. 6, 1
[4] Spalding, D. B. *Combustion & Flame*, 1957, **1**, 287, 296

Propagation Velocity and Structure of Single Step Reaction Flames

J. M. DE SENDAGORTA

Calle San Ignacio 'Eguzkiena', Neguri, Vizcaya, Spain

(*Received October 1960*)

A new analytical procedure is proposed for the calculation of propagation velocities of premixed laminar flames supported by single step chemical reactions. Simple rules or equations for predicting the propagation velocity and flame structure have been achieved through a postulated exponential approximation for the flux fraction of species, and an additional analytical approximation for concentrations. The proposed method covers also the case of second order reaction flames with Lewis–Semenov number differing from unity, to which case previous existing approximate methods were not extended with success. Evaluation of the available approximate methods is made by comparing the results with the exact results obtained by numerical integration. This evaluation shows that the method proposed by the author is superior to the others analysed because of its higher accuracy and its general applicability.

Introduction

A PRESENTATION of the analytical theory and of the equations which govern the process in a flame can be found in refs. 1 to 3. It is agreed that the essential problem of laminar flame theory lies in finding the solution of the system formed by the equations of state, diffusion and conservation. The propagation velocity and the flame structure are determined by the eigenvalue of the system of equations.

The exact solution of this system requires computing machines or an arduous numerical integration, which could be applicable to particular problems, but with the result that the theory misses the adequate mathematical instrument for its development. As a consequence, the achievement of solutions through approximate methods has received considerable attention in recent years.

The approximate methods by Y. B. ZELDOVICH and N. SEMENOV[4], S. F. BOYS and J. CORNER[5], E. N. ADAMS[6], TH. VON KÁRMÁN and S. S. PENNER[2], K. A. WILDE[7], D. B. SPALDING[8], and that proposed by the author[9, 10] have appeared in this way.

A fairly complete evaluation of these approximate methods has been realized in refs. 11 and 12, which unfortunately were not known to the author of ref. 13, where that previous work was partially repeated. J. O. HIRSCHFELDER has also proposed[13] a new approximate method, which will be considered here with the conclusion that it does not improve some of the previous methods. We present in this paper:

(*i*) The complete development of a new approximate procedure for obtaining the propagation velocity and the distribution of species in a single step reaction flame;

(*ii*) A more complete evaluation than previously carried out of the available approximate methods of predicting propagation velocity.

From this evaluation, it appears that the new approximate method introduces deviations of only a few parts per thousand from the exact propagation velocity; it is shown to be superior to the others in every case considered. Our approximate method seems to be the only applicable one in some cases, particularly when the Lewis–Semenov number differs much from unity.

Notation

$a = 1/\Lambda$
A Reactants
B Products
c_p Specific heat at constant pressure
D Diffusion coefficient
E Activation energy

h^0 Formation enthalpy
H_i $\int_0^t z^i e^{-\theta_a/\theta} dz$
k Reaction rate constant
$\mathcal{L}$ Lewis–Semenov number
M Molar mass
m Mass flow per unit surface parallel to flame
p Pressure
q_r $(h_a^0 - h^0)/c\ T_{a,f}$
R Gas constant
S_u Flame propagation velocity
T Absolute temperature
Y Mass concentration
x Abscissa (propagation direction)
$z = 1 - \theta$
ε Flux fraction of species
Λ Eigenvalue
λ Thermal conductivity coefficient
θ Reduced temperature $= T/T_{a,f}$
χ $(1-\theta)/\theta$
θ_a Reduced activation temperature
ρ Mixture density
ξ Volumetric reaction rate (mol cm^{-3} sec^{-1})

Subscripts

a Reactants
b Products
f Final state
o Initial state
i Ignition
w Wall

Equations of Flame Supported by Single Chemical Reaction

In order to introduce the notation, the equations governing flat flame steady propagation will be written as follows. The reactions of higher molecularity are not of interest here, therefore we will consider only flames supported by reactions of the type:

$$A \longrightarrow B \quad \text{first order} \quad ; \quad \ldots . [1]$$

$$A + A \longrightarrow B \quad \text{second order} \quad \ldots . [2]$$

The molar mass and specific heat of the mixture are assumed constant. The thermal conductivity is taken proportional to the temperature of the mixture and independent of its composition.

Mass conservation

The continuity equation for reactants is written

$$\frac{m}{M}\frac{d\varepsilon_a}{dx} = -\xi \qquad \ldots . [3]$$

where ξ is the volumetric rate of the reaction considered and ε_a the mass flux fraction of reactants. The condition $m = \rho v = \text{constant}$ completes the mass conservation equation.

Motion and energy equations

Viscosity and kinetic energy may be neglected under the conditions named in ref. 9. The equation of motion is then reduced to $p = \text{constant}$.

The energy equation, if the process is assumed to be adiabatic, may be written in the form

$$\frac{\lambda}{mc_p}\frac{dT}{dx} = T + \frac{h_a^0 - h_b^0}{c_p}(\varepsilon_a - \varepsilon_{a,f}) + \text{const.} \quad . [4]$$

where h_a^0 and h_b^0 are the formation enthalpies of A and B. The adiabatic flame temperature is reached when the reaction is completed $\varepsilon_{a,f} = 0$. Then

$$T_{a,f} - T_a = (h_a^0 - h_b^0)/c_p \qquad \ldots . [5]$$

where $(h_a^0 - h_b^0)$ is the heat of combustion, assumed constant. Equation 3 divided by $T_{a,f}$ can be reduced to

$$z_a = q_r \qquad \ldots . [6]$$

Similarly equation 2, for an adiabatic flame in which the reaction is completed, can be reduced to

$$\frac{\lambda}{mc_a}\frac{dz}{dx} = z - z_a\varepsilon_a \qquad \ldots . [7]$$

Cold boundary

If the process is assumed to extend from $-\infty$ to $+\infty$, a boundary condition at the unburnt side would be

$$d\varepsilon/dx \longrightarrow 0 \text{ when } x \longrightarrow -\infty$$

which is not met if ξ follows the Arrhenius law, because then (although it is very small) $\xi_o \neq 0$. This difficulty has been obviated in the ignition temperature model by TH. VON KÁRMÁN and G. MILLÁN[15], by the flameholder of J. O. HIRSCHFELDER *et al.*[1], and by our recently proposed model of ignition reaction rate[16]. These models differ only in the way they introduce boundary conditions to the reaction zone.

These approaches are justified if the propagation, structure and other flame properties remain unaffected by an arbitrary selection of ignition temperature, heat transfer to the flameholder or ignition reaction rate, respectively. This has been shown to occur with regard to propagation and flame structure in refs. 15 and 1. Therefore the selection of the model will not affect the calculations of the propagation velocity and structure of flame, which are the main objects of the present paper.

Diffusion

The diffusion of species is taken to be governed by Fick's law.

$$\rho D \frac{dY_a}{dx} = m (Y_a - \varepsilon_a) \quad \ldots . [8]$$

System of equations

Dividing equations 3 and 8 by equation 7, we obtain the system:

$$\frac{m^2 c_p}{\lambda M} \frac{d\varepsilon_a}{dz} = \frac{\xi}{z_a \varepsilon_a - z} \quad \ldots . [9]$$

$$\frac{dY_a}{dz} = \frac{\xi}{z_a} \frac{Y_a - \varepsilon_a}{z/z_a - \varepsilon_a} \quad \ldots . [10]$$

Boundary conditions

The system formed by equations 9 and 10 should satisfy the following boundary conditions:

$$\begin{array}{lll} z = 0\,, & \varepsilon_a = 0, & Y_a = 0 \\ z = z_a, & \varepsilon_a = 1, & Y_a = 1 \\ z = z_i, & \varepsilon_a = 1, & Y_a = Y_{a,i} \end{array}$$

where the subscript $_i$ refers to the state in which the reaction starts, whatever cold boundary model has been adopted. The values of m making these conditions compatible will determine the flame velocity and, by direct integration, the structure of the flame.

Prediction of Flame Propagation Velocity

There are several analytical procedures available which lead to equations or methods to determine approximately the eigenvalue of the system of equations for the flame, so obviating the numerical step-by-step method of integration.

We propose here a new procedure, which follows the development of our previous work[9,10], and presents considerable advantages over other methods, in some cases because of the shorter time required for obtaining results, and in every case for its higher accuracy and general applicability. The cases of first and second order supporting reactions are considered separately below.

Method for first order reaction flames

Eigenvalue equation—By introducing the equation of state into the Arrhenius law expression the rate of a first order reaction may be expressed as follows

$$\xi = k e^{-\nu_a} (Y_a/\theta) e^{-\nu_a \lambda} \quad \ldots . [11]$$

The thermal conductivity has been assumed to be

$$\lambda = \lambda_i \theta \quad \ldots . [12]$$

Then the flame equation 9 can be reduced to

$$\frac{d\varepsilon_a}{dz} = \Lambda \frac{Y_a e^{-\nu_a \lambda}}{\varepsilon_a - z/z_a} \quad \ldots . [13]$$

where $\Lambda = \lambda_i k e^{-\nu_a}/m^2 c_p z_a$ is the eigenvalue to be determined. Once integrated between boundaries equation 13 can be reduced to the usual form

$$\tfrac{1}{2} z_a - \int_0^{z_a} \varepsilon_b \, dz = \Lambda I_1 \quad \ldots . [14]$$

where

$$I_1 = z_a \int_0^{z_a} Y_a e^{-\nu_a \lambda} \, dz$$

Adequate approximation of ε_b against z and Y_a against z would permit calculation of the integrals on both sides of equation 14, and then from this, the finding of the eigenvalue and flame propagation velocity.

Approximation of ε_b against z—For the flux fraction of product ε_b, we adopt the following approximated form

$$\varepsilon_b = P e^{-\nu_a \lambda} \quad \ldots . [15]$$

where P is a polynomial

$$P = 1 + a_1 z + a_2 z^2 + \ldots + a_n z^n \quad \ldots . [16]$$

the coefficients a_i being determined through the analysis of the exact differential equations near the hot boundary.

When the approximated expression **15** is introduced into equation **14**, the following is obtained

$$\Lambda I_1 = \tfrac{1}{2} z_o - \sum_0^n a_i H_i \qquad \ldots . [17]$$

The integrals H_i could easily be written as functions of the exponential integral $E_i(-\theta_a)$, but for ease of computation a log diagram is provided in *Figure 1*.

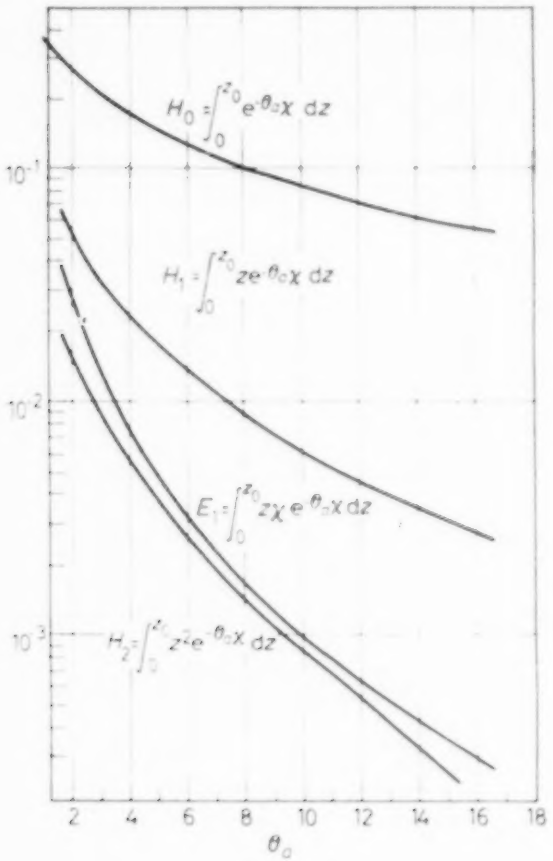
$H_0 = \int_0^{z_0} e^{-\theta_a \chi}\, dz$
$H_1 = \int_0^{z_0} z e^{-\theta_a \chi}\, dz$
$E_1 = \int_0^{z_0} z\chi\, e^{-\theta_a \chi}\, dz$
$H_2 = \int_0^{z_0} z^2 e^{-\theta_a \chi}\, dz$
10^{-1}
10^{-2}
10^{-3}
2 4 6 8 10 12 14 16 18
θ_a

Figure 1

It has been verified that it is sufficient to take the first two terms of P in order to obtain satisfactory values of the flame velocity. Then the eigenvalue equation **14** becomes

$$\Lambda I_1 = \tfrac{1}{2} z_o - H_o - a_1 H_1 \qquad \ldots . [18]$$

where the coefficient a_1 is determined by the condition that $(d\xi/dz)_{z=0}$ obtained from equation **15** would coincide with the value α deduced from the analysis of equations **10** and **13** at $z = 0$. The result is

$$a_1 = \theta_a - \alpha \qquad \ldots . [19]$$

If α and β are the slopes of curves ε_a against z and Y_a against z respectively at the point $z = 0$, then their values will be given by equations **10** and **13**, particularized for $z = 0$. By elimination of β, the following relationship results between Λ and α

$$\Lambda = (z_o \alpha - 1)(z_o \alpha + \mathcal{L} - 1)/z_o \mathcal{L} \qquad \ldots . [20]$$

An independent relationship for α will be obtained from equations **18** and **19**, once we have calculated the integral I_1, on the LHS of equation **18**.

Approximation of Y_a against z—For the general case when $\mathcal{L}$ differs from unity, the parabolic approximation of Y_b against z, in the form

$$Y_b = (1 - z/z_o)^{\mathcal{L}} \qquad \ldots . [21]$$

maintains the behaviour of equation **10** at the point $z = z_o$, but disregards it near $z = 0$. Therefore the approximation

$$Y_a = \left[1 - \left(1 - \frac{z}{z_o}\right)^{\mathcal{L}}\right]\left[n\left(1 - \frac{z}{z_o}\right) + \frac{z}{z_o}\right] . [22]$$

which coincides with equation **21** when $n = 1$, and where the parameter n is determined from the condition that $(dY_a/dz)_{z=z_o} = \beta$ must necessarily be a better approximation, especially in the neighbourhood of $z = 0$. The resulting value for n is

$$n = \beta z_o / \mathcal{L} \qquad \ldots . [23]$$

By substitution of this value into equation **22**, and taking only the first two terms on the RHS of it, the following approximation to be adopted results

$$Y_a = \beta z + \left[\frac{\mathcal{L}}{z_o} - \beta\left(1 + \frac{\mathcal{L} - 1}{2}\right)\right]\frac{z^2}{z_o^2} \ldots [24]$$

Then the required integral becomes

$$I_1 = z_o \beta H_1 + \left[\frac{\mathcal{L}}{z_o} - \beta\left(1 + \frac{\mathcal{L} - 1}{2}\right)\right] H_2 \quad . [25]$$

Eigenvalue and propagation velocity—Substituting equations **25** and **19** into equation **18** and eliminating β and Λ, the following equation is obtained for α

$$z_o \alpha^2 \left(1 - \frac{\mu}{2}\frac{H_2}{H_1}\right) - 2\alpha\left(1 - \frac{3\mu}{4}\frac{H_2}{H_1}\right) = \frac{1}{z_o}\left(J - 1 + \mu\frac{H_2}{H_1}\right) \qquad \ldots . [26]$$

where for convenience we have written:

$$\mu = (\mathcal{L} - 1)/z_a \qquad \ldots . [27]$$

and

$$J = 1 + z_a \left(\frac{z_a}{2H_1} - \frac{H_a}{H_1} - \theta_a \right) \quad [28]$$

Equation 26, which solves the problem in the general case when $\mathcal{L} \neq 1$, is a simple second order equation for z. Substituting the values found for z into equation 20, the required eigenvalue can be found explicitly. The flame propagation velocity is given by

$$S_a = \left(\frac{\lambda_f k e^{-\theta_a}}{\rho_a^2 c_p z_a} \right)^{\frac{1}{2}} \left(\frac{z_a \mathcal{L}}{(z_a z - 1)(z_a z + \mathcal{L} - 1)} \right)^{\frac{1}{2}} . [29]$$

For the case when normal diffusion prevails, $\mathcal{L} = 1$, $\mu = 0$ and the solution of equation 26 is

$$z_a z = 1 + J^{\frac{1}{2}}$$

which, substituted into equation 27, gives

$$\Lambda^{-\frac{1}{2}}_{\mathcal{L}=1} = \left(\frac{z_a}{J + J^{\frac{1}{2}}} \right)^{\frac{1}{2}} \qquad \ldots . [30]$$

Method for second order reaction flames

Eigenvalue equation—Following the same reasoning as previously with flames supported by a first order chemical reaction, we obtain: Volumetric reaction rate

$$\xi = k (Y_a/\theta)^2 e^{-\theta_a} e^{-\theta_a \chi} \qquad \ldots . [31]$$

Flame equation

$$\frac{d\varepsilon_a}{dz} = \Lambda \frac{Y_a^2 e^{-\theta_a \chi}}{\theta (z_a \varepsilon_a - z)} \qquad \ldots . [32]$$

where

$$\Lambda = \frac{\lambda_f k e^{-\theta_a}}{m^2 c_p z_a^2} \qquad \ldots . [33]$$

By integrating equation 32 in the usual form, the following eigenvalue equation results

$$\frac{z_a}{2} - \int_0^{z_a} \varepsilon_b dz = \Lambda I_2 \qquad \ldots . [34]$$

where

$$I_2 = z_a^2 \int_0^{z_a} \frac{Y_a^2}{\theta} e^{-\theta_a \chi} dz \qquad \ldots [35]$$

Approximation of ε_b against z—The integral on the LHS of equation 34 is calculated by applying the same approximation for ε_b against z that was used for first order reactions

$$\varepsilon_b = (1 + a_1 z) e^{-\theta_a \chi} \qquad \ldots . [36]$$

Here a_1 is determined by equation 19, where z should be replaced by $1/z_a$. Then the approximation to the LHS integral in equation 34 is

$$\int_0^{z_a} \varepsilon_b dz = \frac{z_a}{2} - \frac{H_1}{z_a} J \qquad \ldots . [37]$$

If this is substituted into equation 34, it can be reduced to the form

$$\Lambda I_2 = (H_1/z_a) J \qquad \ldots . [38]$$

Approximation of Y_a against z—With normal diffusion $\mathcal{L} = 1$ and the integral I_2 may be calculated exactly. Substituting $Y_a = z/z_a$ into equation 35, the following is obtained:

$$I_2 = \int_0^{z_a} z \chi e^{-\theta_a \chi} dz$$

$$\simeq \int_0^{z_a} z \chi e^{-\theta_a \chi} dz = E_1$$

where E_1 is a simple function of the exponential integral $E_1(-\theta_a)$, but for ready calculation, it has also been included in the log diagram shown in *Figure 1*. Then, when $\mathcal{L} = 1$, the eigenvalue is given by the simple approximate equation

$$\Lambda_{\mathcal{L}=1} = H_1 J / z_a E_1 \qquad \ldots . [39]$$

Propagation velocity is related to it through equation 33, and its value is proportional to

$$\Lambda^{-\frac{1}{2}}_{\mathcal{L}=1} = (z_a E_1 / H_1 J)^{\frac{1}{2}} \qquad \ldots . [40]$$

When $\mathcal{L} \neq 1$, the problem of finding an adequate approximation to the integral I_2 is apparently more involved than for the case of first order reaction studied. The difficulty lies in the fact that the progress of the second order reaction near the hot boundary is controlled by the frequency of the chemically active double collisions between the reactant molecules whose concentration, however, must be small within the same zone. As a result, the advancement of

the reaction through a zone very close to the final state is relatively slow and the mechanism is such that the energy released by the reaction is equal to that transferred through convection.

Due to this fact the point corresponding to the hot boundary appears in the flame equation as a singular point which does not characterize the zone where the major part of the reaction takes place. Therefore the number of terms which need to be taken in the expansion of Y_a against z for approximating the integral I_2 is very large, and this is the reason why other approximate analytical methods based on this expansion have failed to give a good approximation when applied to cases where the Lewis–Semenov number differs from unity. Our previous work[19] proposed the following approach.

In order to calculate integral I_2 in equation 34, we take a linear approximation of Y_a against z

$$Y_a \simeq \beta z \qquad \ldots . [41]$$

with the result that

$$I_2 = z_o^2 \beta^2 E_1$$

The following expression is then found for the eigenvalue Λ

$$\Lambda = \frac{H_1 J}{z_o E_1} \frac{1}{z_o^2 \beta^2} \qquad \ldots . [42]$$

where for the above mentioned reasons β may not be replaced by the slope corresponding to the hot boundary but by that corresponding to a somewhat lower temperature, such as that given by

$$\chi = 1/\theta_a$$

which corresponds approximately to the inflection point of the actual curve ε_a against z. On the other hand, the slope β at any point, as given by the diffusion equation 10, is

$$\beta = \frac{\mathcal{L}}{z_a} \frac{\varepsilon_a - Y_a}{\varepsilon_a - z/z_a} \qquad \ldots . [43]$$

If, in this equation, Y_a is approximated by equation 41, and $\varepsilon_a = 1 - \varepsilon_b$ by equation 36, and the result is particularized for $\chi = 1/\theta_a$ or $z = 1/(1+\theta_a)$, the following value is obtained for β

$$\beta = \frac{\mathcal{L}}{z_o} \frac{z_o n_a + 1}{z_o n_a + 1 + e\,(\mathcal{L} - 1)} \qquad \ldots . [44]$$

where n_a is a function of θ_a and

$$n_a = e\,(1+\theta_a) - (2\theta_a + 1)$$

Propagation velocity—Finally, bringing equation 44 into equation 42, the following expression is found for Λ^{-1}

$$\Lambda^{-1} = \Lambda_{\mathcal{L}=1}^{-1} \frac{\mathcal{L}(z_o n_a + 1)}{(z_o n_a + 1) + e\,(\mathcal{L} - 1)} \qquad \ldots . [45]$$

Propagation velocity is related to Λ^{-1} through equation 33. For $\mathcal{L} = 1$, Λ^{-1} is given by equation 40.

Evaluation of Analytical Methods

First order reaction

Among the available approximate analytical procedures, only those giving explicitly the eigenvalue or propagation velocity are considered.

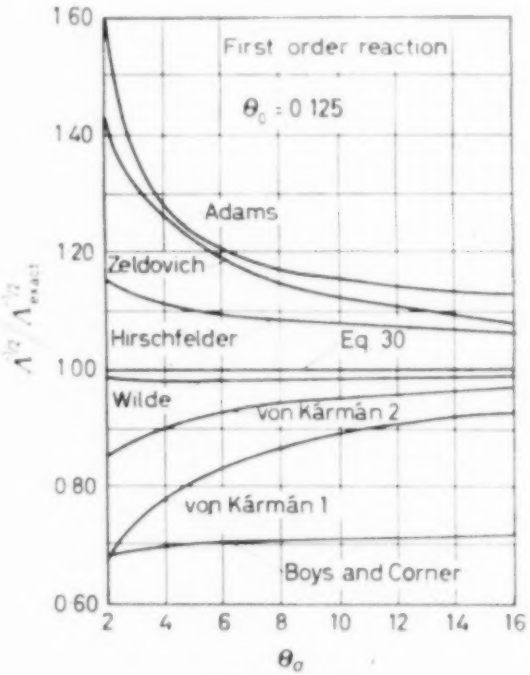

Figure 2.

When $\mathcal{L} = 1$—The relative deviations furnished by the various approximate methods are shown as a function of reduced activation temperature θ_a, when $\mathcal{L} = 1$, in *Figures 2* and *3*.

These curves have been plotted with the values obtained in ref. 11, applying the methods of Zeldovich, Boys and Corner, von Kármán 1, von Kármán 2, Wilde and equation 30, to the same flame model.

The exact values used as reference have also been extracted from ref. 11, where a numerical step by step integration was performed to find them. To these values we have now added the

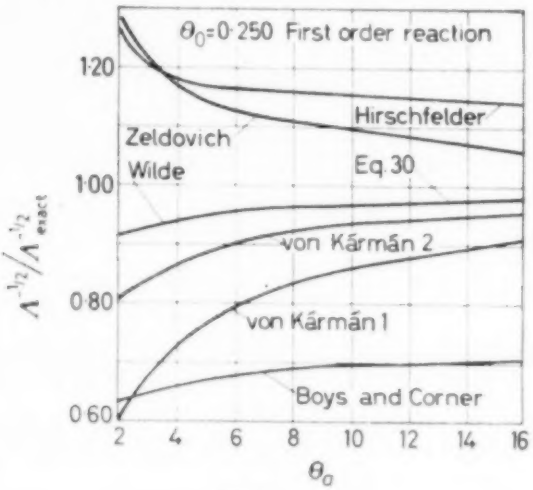

Figure 3

results obtained by Adams's and Hirschfelder's approximate procedures, applied to the same cases, through the following equations:

Adams: $\Lambda^{-1} = \{2/(z_a\theta_a - 1)(z_a\theta_a + 2)\}^{\frac{1}{2}}$

Hirschfelder: $\Lambda^{-1} = \{1/b^1(b^1 - 1)\}^{\frac{1}{2}}$

where

$$b^1 = -\tfrac{1}{2} + \tfrac{1}{2}\{1 + 2z_a^2/H_1\}^{\frac{1}{2}}$$

When $\mathcal{L} \neq 1$—Comparatively few approximate methods have been extended to the case when the Lewis-Semenov number differs from unity. Taking as reference the exact values obtained in ref. 11 by numerical integration for a reduced activation energy $\theta_a = 4$, *Figure 4* shows the relative deviations resulting from the available approximate methods.

Conclusions—The conclusions are as follows:

(*1*) Equation 30 for $\mathcal{L} = 1$ is superior to the others analysed, and gives deviations of only a few parts per thousand for reduced activation temperatures over 2.

(*2*) In contradiction of the statement made in ref. 13, Wilde's and also von Kármán's methods give higher accuracy than that recently proposed by Hirschfelder.

(*3*) Wilde's method due to the arbitrary or empirical assumption made for approximating the mass flow fraction does not lend itself to be generalized to other cases.

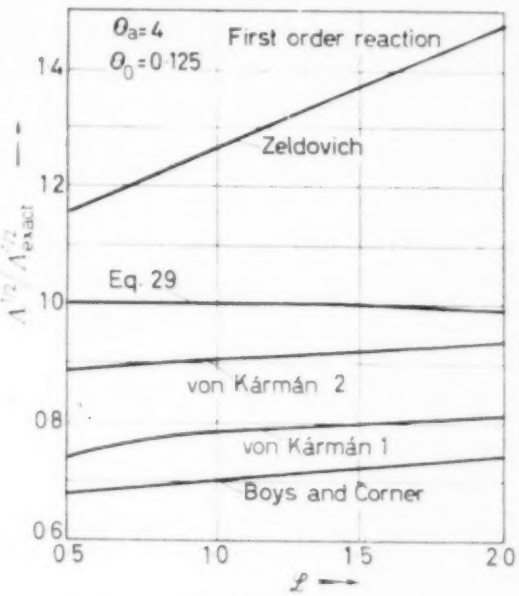

Figure 4

(*4*) *Figures 2* and *3* show results for $\theta_a = 0{\cdot}125$ and $0{\cdot}250$. It may be noted from these figures that the Hirschfelder and Wilde results, in relation to the exact ones, are sensitive to the initial reduced temperatures, the deviations being increased for higher values of θ_a.

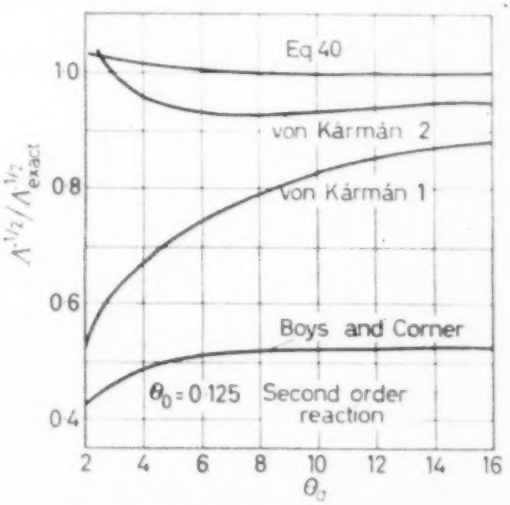

Figure 5

(5) When $\mathcal{L} \neq 1$, the application of equations 29 and 26 leads to relative errors under one per cent, and appears to be superior to the procedures of Zeldovich, Boys and Corner, and of von Kármán.

Second order reactions

When $\mathcal{L} = 1$—Before equation 40 was proposed in ref. 9, there were extensions of the Zeldovich, Boys and Corner, and von Kármán approximate methods applicable when $\mathcal{L} = 1$. *Figure 5* gathers the comparative results obtained with these methods.

When $\mathcal{L} \neq 1$—The case of second order reaction flames when the Lewis–Semenov number differs from unity has been covered by

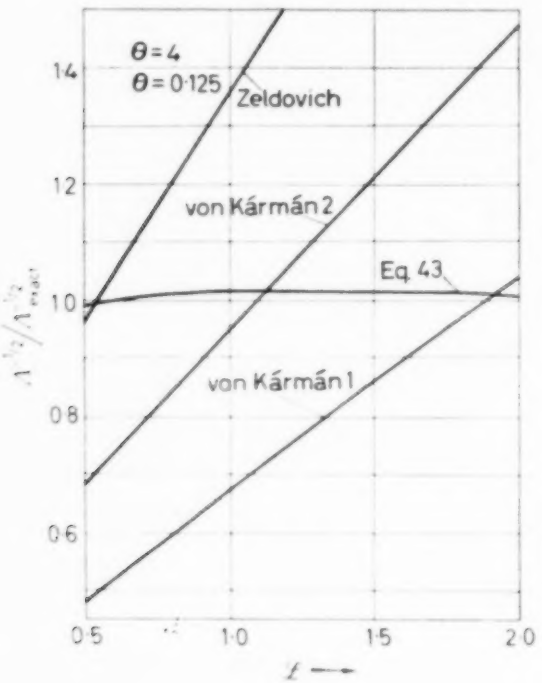

Figure 6

Zeldovich and by our own approximate procedure. More recently Millán extended the von Kármán procedure to flames where $\mathcal{L} \neq 1$. The results are shown in *Figure 6*. The exact values taken as reference have been obtained by numerical integration in ref. 12.

Conclusions—The conclusions are:

(1) Equation 40 applicable when $\mathcal{L} = 1$ leads to deviations below one per cent for $\theta_a > 4$.

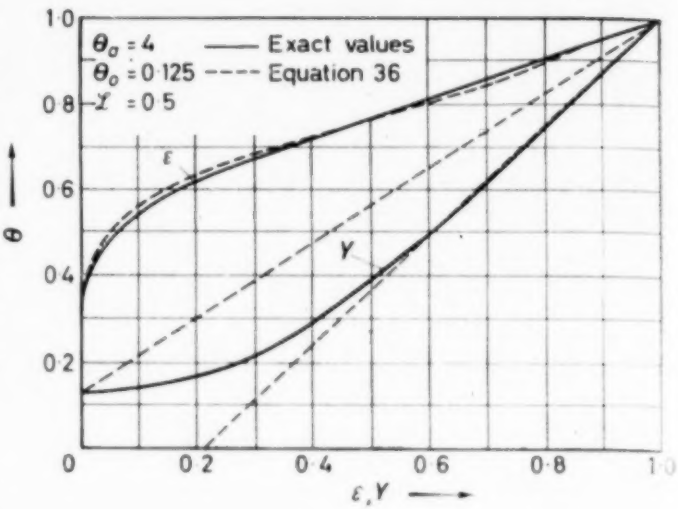

Figure 7

(2) From the results shown in *Figure 6*, it is concluded that only equation 45 could be recommended for use when $\mathcal{L} \neq 1$.

(3) Equation 36 gives an accurate approximation of the flux fraction against the temperature (*Figures 7* and *8*). Consequently the direct application of equation

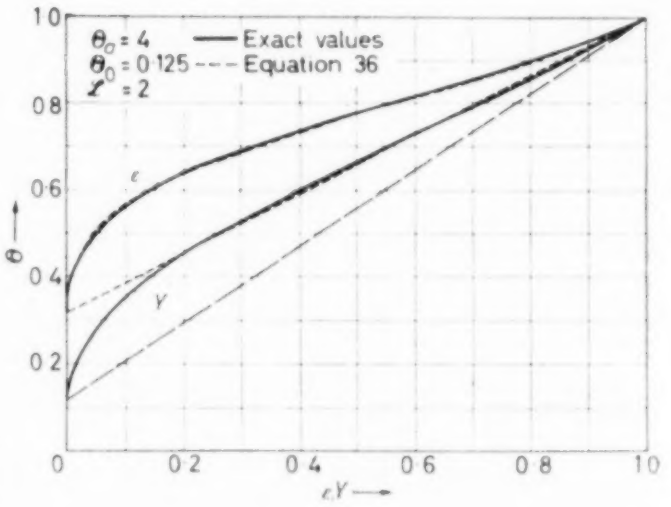

Figure 8

36 reduces further the additional problem of determining the concentration and temperature distribution along the flame, which may be readily determined with high accuracy by the same equation.

References

[1] HIRSCHFELDER, J. O., CURTISS, C. F. and BIRD, R. B. *Molecular Theory of Gases and Liquids*. Wiley: New York, 1954

[2] VON KÁRMÁN, TH. and PENNER, S. S. 'Fundamental approach to laminar flame propagation'. *Selected Combustion Problems*. AGARD; Butterworths: London, 1954

[3] HIRSCHFELDER, J. O. and MCCONE, A. 'Theory of flames produced by unimolecular reactions'. *Physics of Fluids*, 1959, **2**, 551

[4] ZELDOVICH, Y. B. and SEMENOV, N. 'Kinetics of chemical reactions in flames'. *Tech. Memor. Nat. Adv. Comm. Aero., Wash., No. 1084*

[5] BOYS, S. F. and CORNER, J. 'The structure of the reaction zone in a flame'. *Proc. Roy. Soc. A*, 1949, **197**, 90

[6] ADAMS, E. N. *Univ. Wis. Naval Res. Lab. Rep. No. CF–957*, quoted by HENKEL, M. H., SPAULDING, W. P. and HIRSCHFELDER, J. O. *Third Symposium (International) on Combustion*. Williams and Wilkins: Baltimore, 1949

[7] WILDE, K. A. *J. chem. Phys.* 1954, **22**, 1788

[8] SPALDING, D. B. *Combustion & Flame*, 1957, **1**, 296

[9] DE SENDAGORTA, J. M. 'Calculation of the propagation velocity of a plane laminar flame'. Air Research and Development Command. U.S.A.F. *AF-61(514)–997*, June 1957

[10] DE SENDAGORTA, J. M. 'Prediction of the propagation velocity of a laminar flame supported by a second order reaction'. Air Research and Development Command, U.S.A.F. *AF–61(514)–997*, April 1958

[11] MILLÁN, G., DE SENDAGORTA, J. M. and DA RIVA, I. 'Comparison of analytical methods for the calculation of laminar flame velocity'. Air Research and Development Command, U.S.A.F. *AF–61(514)–997*, August 1958

[12] MILLÁN, G. and DA RIVA, I. 'Comparison of analytical methods for the calculation of laminar flame velocity'. Air Research and Development Command, U.S.A.F. *AF–61(514)–997*, June 1958

[13] HIRSCHFELDER, J. O. 'Theory of flames produced by unimolecular reactions'. *Physics of Fluids*, 1959, **2**, 565

[14] SPALDING, D. B. *Proc. Roy. Soc. A*, 1957, **240**, 83

[15] VON KÁRMÁN, TH. and MILLÁN, G. 'The thermal theory of constant pressure deflagration'. *Biezeno's Anniversary Volume*. Delft, Holland, 1953

[16] DE SENDAGORTA, J. M. 'Theory of laminar flame extinction'. Unpublished

Supersonic Combustion

P. H. KYDD and G. J. MULLANEY

General Electric Research Laboratory, P.O. Box 1088, Schenectady, N.Y.

(*Received October 1960*)

A device is described in which diffusion flames of acetylene, hydrogen and preheated propane have been stabilized in a free jet at Mach 2·7. It consists of a hollow truncated cone through which flows a small part of the high velocity air stream in which it is submerged. The internal flow, which has been decelerated by a normal shock wave, is mixed with hydrogen and ignited. The high temperature combustion products, expanding through a nozzle in the downstream part of the cone, are used to ignite the main fuel jets surrounding this hot core. Experiments with acetylene have demonstrated that the combustion is extremely rapid and takes place at constant static pressure. The combustion efficiency 9 in. downstream from the fuel injector is 91 per cent, and the heat release rate 2·7 × 10^8 B.t.u./h-ft³-atm².

Introduction

IN the design of ramjet engines for flight at velocities higher than Mach 5, substantial advantages result from carrying out the combustion process in air that has been diffused to a lower supersonic velocity, instead of to subsonic velocity as is usually done. Both the diffuser and nozzle are shorter and simpler, and because the temperature and pressure of the incoming air do not reach the extreme values encountered in subsonic diffusion, more energy can be added to the gas by combuston, and the engine can be made lighter.

While these advantages have been recognized for some time, few experiments have been done to demonstrate how they may be achieved[1–5].

In a useful supersonic combustor, the air flow should be disturbed as little as possible, since this leads to shock wave formation and losses in total pressure, as well as increased drag. From this point of view the most efficient method of injection is to introduce the fuel in the downstream direction at high velocity. This, however, is likely to result in very poor mixing of the fuel with the air[6], unless special precautions are taken to improve it.

In the present experiments, the approach has been to inject very reactive fuels downstream with a pilot flame for ignition and a sufficiently large wake region to allow some recirculation. The use of a reactive fuel is the most important single factor in these experiments, because if the fuel burns almost immediately upon contact with the air, the fuel injector itself can function as a small flameholder, and the expansion of the hot products serves to spread the remaining fuel into the air stream.

Apparatus

The fuel injector which has been used in these experiments is a hollow cone mounted on a wedge-shaped strut (*Figure 1*). It faces a free jet from the nozzle shown at the left. This simulates air diffused from Mach 6 to Mach 2·7 at an altitude of 100 000 ft, except for the temperature which is 750°F too low. We are limited in this respect by our air preheater.

The fuel injector scoops in about 4 per cent of the air flow and brings it nearly to rest at 6 atm. Two thirds of the stoichiometric amount of hydrogen is introduced, and the mixture is lit with a spark. The hot gas then flows out through the nozzle in the back and serves to preheat, ignite, and disperse the main fuel, which is injected through a ring of holes surrounding the jet. Gaseous acetylene has been used most often as a main fuel and enough could be supplied to consume 10 per cent of the whole air stream.

To obtain larger flames and demonstrate the spreading of the flame from one injector to another, a wedge-shaped strut has been placed in contact with the cone and 90° from its mounting strut. It has a $\frac{1}{8}$ in. × 1 in. slot in

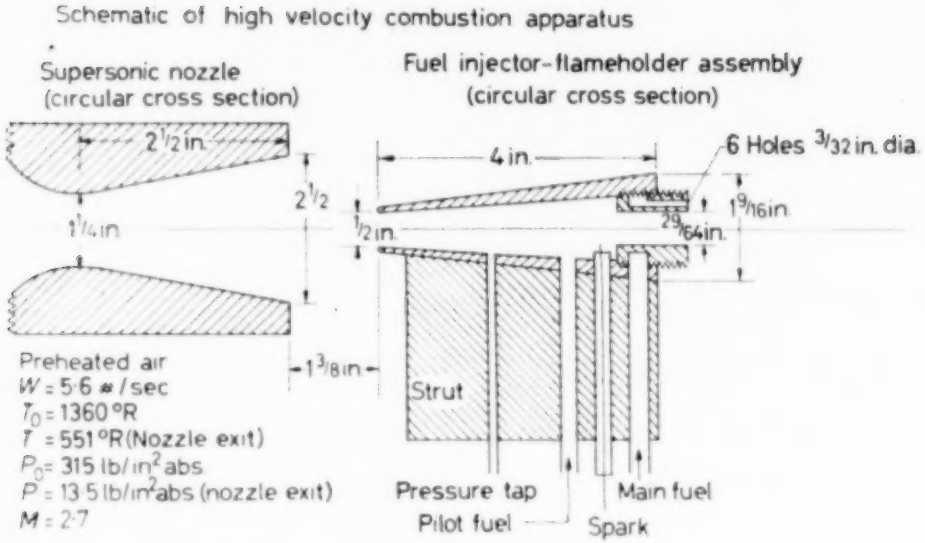

Figure 1. The fuel injector and air nozzle

its rear surface which supplies enough acetylene to burn another 10 per cent of the air.

To make quantitative measurements a probe was constructed to cover the horizontal plane from the centreline of the jet to its outer edge and from the rear of the fuel injector to a point 12 in. downstream. With interchangeable tips measurements were made of impact pressure and of surface pressure on cones of 10° to 20° half angle and these were used to determine the Mach number[7]. Gas samples could be withdrawn through the impact tube and analysed gas chromatographically to measure the spreading of the combustion products in the air stream and the combustion efficiency.

Results

Pilot flame

Preliminary experiments with this apparatus demonstrated that the pilot burner worked as expected using hydrogen as a fuel, but that it would not work using ethylene or mixtures of hydrogen with more than 30 per cent ethylene. Even under the relatively favourable conditions inside the pilot duct, only the most reactive fuels will burn effectively. The same behaviour was found in combustion of the main fuel stream. Acetylene and hydrogen burned well when ignited by the pilot flame, and both continued to burn even with the pilot turned off. Propane, on the other hand, hardly burned at all even with a very hot pilot flame running continuously.

Auxiliary strut injector

A stream of acetylene injected from the auxiliary strut, which provided very little wake for flame stabilization, could be ignited by a stable acetylene flame burning on the main injector and appeared to burn to completion in a short distance in the free stream.

Propane could be ignited in a similar fashion when injected from the strut, if it had been preheated to more than 2 300° R. At this temperature it was certainly cracked to a considerable extent[8] with hydrogen and acetylene as major products, and the high temperature of the remaining propane undoubtedly helped to complete the burning rapidly. That temperature is an important variable was demonstrated when it proved impossible to ignite even acetylene when the air supply was not preheated and the static temperature in the jet therefore dropped to less than 300° R.

Quantitative measurements

To determine the combustion efficiency and the effect of the combustion on the initially supersonic jet, a flame of 7·5 per cent of the stoichiometric amount of acetylene burning

from the main injector without the auxiliary strut was chosen as a standard. Impact pressures and cone surface pressures were measured throughout the region downstream of the injector without combustion, and a Mach number contour plot was constructed which is

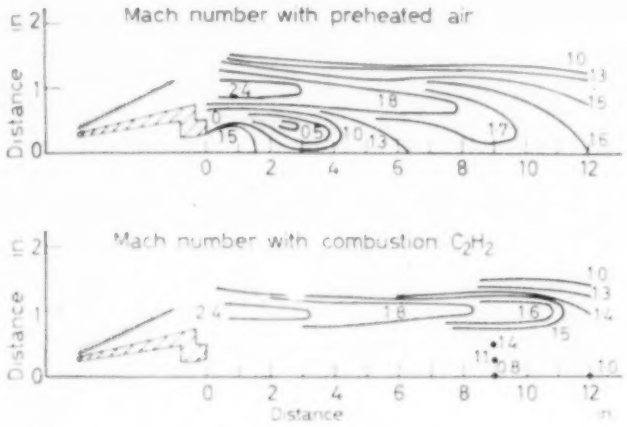

Figure 2. Mach number plots as a function of distance downstream from the fuel injection point (abscissa) and distance from the centreline of the jet (ordinate)

shown in *Figure 2*. The jet has expanded slightly from the nozzle exit and has been decelerated from Mach 2·7 to 2·4 by an oblique shock wave at the front of the injector, shown as a cross-hatched line. As it proceeds downstream, it loses its momentum to the surrounding air and the Mach number drops. Along the centreline, the supersonic jet issuing from the pilot burner may be seen, and between this and the main jet there is an annular subsonic region. In the supersonic regions, the shock wave angle from the cone probes confirmed these Mach number measurements within 10 per cent.

With combustion the flow field is rather different. Because of the temperature rise the entire central core of the jet is now subsonic, and the supersonic portions have been forced outward. The oblique shock wave at the front of the cone is unchanged. This is the type of behaviour to be expected for heat addition to a supersonic stream at constant static pressure, and measurements of the static pressure 9 in. downstream from the injector show that it is approximately uniform across the jet and does not change appreciably with combustion.

The results of the gas sampling measurements are shown in *Figure 3*. The absolute concentrations of combustion products near the

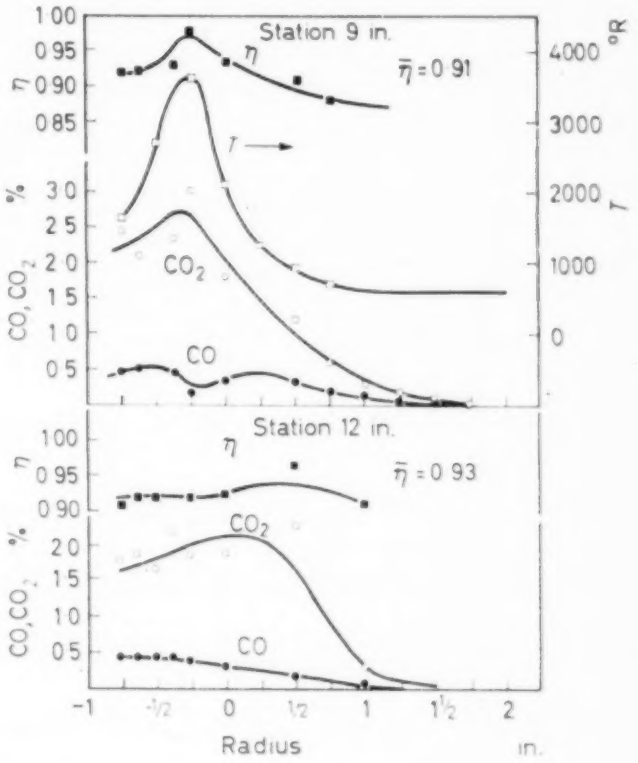

Figure 3. Composition and combustion efficiency profile at 9 in. and 12 in. behind the injector. Temperature profile computed from the Mach number change

centreline are somewhat in doubt, but we believe that the ratio of CO to CO_2 and the extent of mixing of the products with the air stream have been reliably established. No hydrocarbon products were found within the limits of the gas analysis (approximately 0·05 per cent). No hydrogen was found, either, although the sensitivity for hydrogen is considerably less (approximately 2 per cent). Consequently, the combustion efficiency was computed on the basis of the $CO/(CO+CO_2)$ ratio measured as a function of distance from the centreline at stations 9 in. and 12 in. downstream from the injector. These ratios were multiplied by 0·433 (the fraction of the heat of combustion of acetylene due to oxidation of

carbon monoxide), and the result was subtracted from unity to give the combustion efficiencies.

Average values of the combustion efficiency were arrived at by assuming cylindrical symmetry around the peak of the CO_2 distribution. The efficiencies measured at various points could then be related to the fraction of the whole fuel stream burning with that efficiency, and from these the overall efficiency for the whole fuel stream was found. Comparing the results at 9 in. and 12 in., it appears that the combustion is essentially complete at the former station. This corresponds to a reaction time of approximately 0·25 msec. Fragmentary results at 7 in. gave CO/CO_2 ratios similar to those observed farther on, so that the actual reaction time with acetylene under these conditions may be somewhat less than this.

For heat addition at constant pressure, the velocity of the stream does not change. The calculation of temperature change from Mach number change is therefore straightforward for portions of the jet in which the velocity gradient is small. A temperature profile computed on this basis is shown in *Figure 3* for comparison with the composition profiles at 9 in.

The space heat release rate of this flame has been calculated from its visible dimensions, the fuel flow rate, and the combustion efficiency at the 9 in. station. It is equal to $2{\cdot}7 \times 10^6$ B.t.u./h-ft^3-atm^2, a very high value compared to the usual range of $1\text{–}2 \times 10^7$ for turbojet combustors. Longwell's well-stirred reactor[9], which was designed to serve as a standard of maximum heat release rate, gave a value of 3×10^8 burning stoichiometric mixtures of less reactive fuels, namely solvent naphtha and *iso*-octane.

The authors wish to acknowledge the help of C. W. Moon who assisted in all the experimental work.

References

[1] Nicholls, J. A., Dabora, E. K. and Gealer, R. L. *Seventh Symposium (International) on Combustion*, p 766. Butterworths: London, 1959

[2] Gross, R. A. *J. Amer. Rocket Soc.* 1959, **29**, 63; *Research, Lond.* 1959, **12**, 381

[3] Fletcher, E. A., Dorsch, R. G. and Gerstein, M. *Nat. Adv. Comm. Aero., Wash., Rep. Memor. No. E55D07A* (1955)

[4] Dorsch, R. G., Serafini, J. S., Fletcher, E. A. and Pinkel, I. I. *Nat. Aero. Space Admin. Memo. No. 1-11-59E* (1959)

[5] Allen, Jr, H. and Fletcher, E. A. *Nat. Aero. Space Admin. Memo. No. 1-15-59E* (1959)

[6] Wilder, Jr, J. G. and Hindersinn, K. *Aeronaut. Engng Rev.* **1953** (October), p 54

[7] Shapiro, A. H. *The Dynamics and Thermodynamics of Compressible Fluid Flow*, Vol. II, Ch. 17. Ronald: New York, 1954

[8] Tropsch, H. and Egloff, G. *Industr. Engng Chem. (Industr.)*, 1935, **27**, 1063

[9] Longwell, J. and Weiss, M. *Industr. Engng Chem. (Industr.)*, 1955, **47**, 1634

The Effect of Reduced Pressure and Airflow on Liquid Surface Diffusion Flames

R. HIRST* and D. SUTTON

Rocket Propulsion Establishment, Westcott, Aylesbury, Bucks.

(Received February 1961)

A general investigation into diffusion flames burning from a liquid surface at low pressure has been made, as this type of problem is relevant to the question of the persistence of fires in aircraft flying at high altitudes. The fuels used were isododecane *and aviation kerosine. Temperatures in the carbon-free parts of the flame and in the fuel were measured in various sizes of burner. The rate of consumption of fuel was measured and the effects of air velocity around the flame and of air vitiation were noted. Evidence was found of recirculation within the vapour space of the flame. The minimum air velocities required to extinguish flames from the fuel surface at low pressures were determined in a 16 in. diameter variable density wind tunnel. The effect on the extinction velocities of the fuel temperature, the presence of flameholders, and the presence of a metal plate above the flame was investigated. It is concluded that the probability of the persistence of fire in an aircraft remains high up to 40 000 ft, is much less at 50 000 ft, and may be negligible at 60 000 ft. The probability of its persistence at the higher altitudes may be greater in a damaged aircraft.*

Introduction

EXPERIENCE has shown that fires can be initiated and can persist in aircraft flying at altitudes up to at least 20 000 ft. Above this height flight information is meagre and it is not known to what extent the hazard diminishes at greater altitudes. This investigation was made to obtain some information on the persistence of fires at high altitudes, and was in fact concerned with the behaviour of liquid surface diffusion flames at low pressures.

Fires occur much more frequently in the engine nacelle than in any other part of an aircraft. This is due mainly to the proximity of a pressurized fuel system to highly stressed mechanical parts and both thermal and electrical ignition sources. On military aircraft, fires may also result from incendiary attacks on the fuel tanks.

Three modes of combustion can exist in an engine fire, each supported by the cooling air that passes through the nacelle: a 'spray' fire, supported by fuel escaping from a fractured pipeline; a 'wick' fire, burning from fuel streaming over a hot metal surface; and a 'puddle' fire established above the surface of a pool of fuel. Flameholding in the airstream can occur in the wake of any of the obstructions and protrusions that are inevitably present within a nacelle. In a damaged tank bay, the spray fire that may exist momentarily following a strike must pass over to a puddle fire burning from the spilled fuel (unless the tank is destroyed by a vapour–air explosion).

The experiments reported here are concerned only with puddle fires, which were expected to be the most difficult to extinguish on an aircraft. It was assumed that a liquid surface diffusion flame burning in the wake of a bluff body represents the most stable mode of combustion in this environment, but further testing is needed to establish this point fully. An investigation of combustion in spray fires and wick fires will be reported later.

A considerable amount of work has been reported on the effect of reduced pressure on premixed flames and, more recently, on gaseous diffusion flames, but there is little information about diffusion flames burning from a liquid surface under these conditions. G. N. KHUDIAKOV[1] has reported an investigation into liquid surface diffusion flames in which he recorded flame temperatures, temperature profiles within the liquid, and gas composition inside the flame, but the effect of reduced pressure was not discussed. Measurements of the fuel temperature and its rate of consumption in large burners have been made by J. H.

*Present address: Group Research, Wilkinson Sword Ltd, Colnbrook, Slough, Bucks.

BURGOYNE and L. L. KATAN[2], and by D. J. RASBASH, Z. W. ROGOWSKI and G. W. V. STARK[3]. In the work reported here, measurements were made of temperatures in the carbon-free part of the flame, temperature profiles in the liquid, the rate of consumption of fuel, and flame dimensions, with respect to such variables as pressure, burner diameter, air flow around the burner, and vitiation index. In a second series of experiments, measurements were made of the minimum air velocity required to sweep the flame from the fuel surface at low pressures. The experiment was then repeated in the presence of simple flameholders, and of a metal plate above the fuel surface. The results indicate some of the critical ambient conditions for the persistence of flames at reduced pressures.

This study was primarily concerned with the behaviour of flames at high altitudes, and many of the results are therefore expressed in terms of altitude. The pressures at which tests were made, and the corresponding altitudes, are indicated in *Table 1*. Graphs in the figures have been scaled in both pressure and altitude.

Table 1. Pressures at which tests were made

Approximate pressure *atm*	*Altitude* *ft*
0·50	18 000
0·30	30 000
0·19	40 000
0·11	50 000
0·07	60 000
0·04	70 000

Effect of Reduced Pressure on Liquid Surface Diffusion Flames

Apparatus and technique

The experiments were made in a cylindrical decompression chamber of 200 ft³ capacity which could be pumped out to a low pressure limit of about 0·04 atm, corresponding to an altitude of 70 000 ft. A window was fitted at one end of the chamber and along its centre axis, through which the flame could be seen directly. A cathetometer was placed in line with this window to facilitate the accurate alignment of the burner. The burners used were 28, 41, 66 and 96 mm in diameter, about 50 mm in depth and with a wall thickness of 1 mm. The burner was supplied with a laminar airflow from a 16 cm diameter tube, the air being metered through a rotameter. The arrangement of the burner and air supply is illustrated in *Figure 1*.

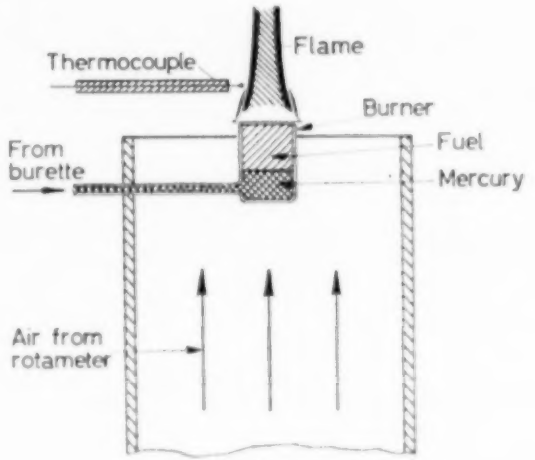

Figure 1. Diagram of burner

During the course of an experiment it was necessary to keep the fuel level with the rim of the burner, and this was done by running in mercury at the same rate as the fuel was consumed, from a burette located outside the chamber. Mercury was used instead of fuel as experience showed that bubbles formed in the supply tube when it contained fuel, which caused troublesome splashing in the burner.

Temperature measurements were made with a platinum/platinum–rhodium thermocouple, which could be moved to any position within the flame or liquid by operating three handles fixed outside the chamber, a complete turn of any one handle resulting in a movement of 1 mm along a cartesian coordinate.

Since kerosine is a mixture of hydrocarbons, it seemed probable that fractionation of the fuel would occur at low pressures, with a consequent change in properties. For this reason most of the experiments were made with *iso*dodecane as the test fuel. Sufficient tests were made with kerosine (DERD/2482) to show that differences between the two fuels were only slight.

Effect of air flow on burning rate

The effect of air flow on the rate of consumption of *iso*dodecane was studied using the 28, 41

and 66 mm burners at the pressures shown in *Table 1*. The maximum air flow used was 100 l./min. Considerable turbulence of the flame occurred in this flow, which corresponded to a linear velocity of 80 cm/sec at 0·1 atm. On the other hand, for very small air flows (e.g. 1 to 5 l./min with the 66 mm burner) insufficient oxygen was being supplied to maintain combustion, and general vitiation of the chamber atmosphere then played a part in extinguishing the flame after a certain time of burning.

In general it was found that the rate of consumption of fuel was independent of air flow above a certain lower flow limit. Flow rates well above this limit were used in all subsequent experiments.

Temperature measurements in the flame

The procedure was to traverse a diameter of the flame with the thermocouple from a position 10 or 20 mm outside the burner edge to a corresponding position at the other side of the burner. Measurements were started at a distance of 1 mm above the burner rim, and the procedure repeated at increasing distances above the burner until the carbon zone was reached. Measurements were then discontinued because deposition of solid carbon particles on the thermocouple made the temperature readings inaccurate. In this way the temperature field in the carbon-free zone of the flame was obtained using kerosine and *iso*dodecane in the 28 mm burner at atmospheric pressure and at all the pressures listed in *Table 1*.

Isothermals at 200°C intervals were then drawn and superimposed on outline drawings of the visible region of the flame that had been copied from photographs. The results obtained from the two fuels were almost identical. Measurements made in *iso*dodecane flames at four pressures are shown in *Figure 2*.

During these experiments the mass air flow was so adjusted that the linear flow around the flame was roughly the same at the different pressures.

Temperature measurements in the liquid

Temperatures below the liquid surface were measured at 1 mm intervals in *iso*dodecane in the four burners and over the pressure range previously mentioned. It was found in practice that the liquid quickly attained thermal equilibrium, and also that the temperature gradient at the edge was the same as in the centre. Readings were taken in the centre down to the depth where the temperature was constant, which was usually at between 10 and 20 mm. The results for the 41 mm burner are typical and are shown in *Figure 3*.

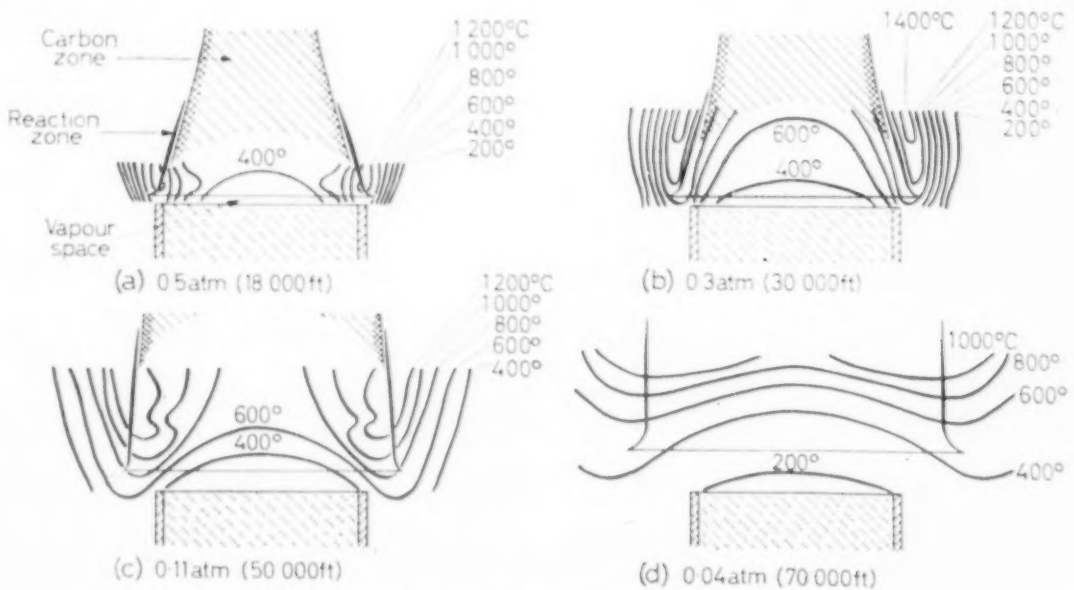

Figure 2. Isothermals in isododecane, 41 mm burner

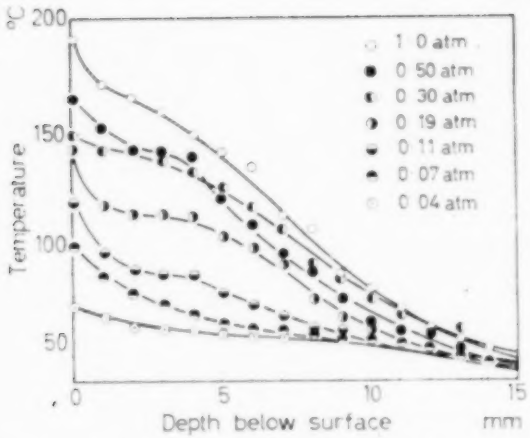

Figure 3. Temperature profiles in isododecane, 41 mm burner

Rate of fuel consumption

This was measured by observing the volume of mercury let in from the burette to replace the fuel consumed in a given time, usually 5 or 10 minutes. Values were obtained from the four burners at pressures down to 0·04 atm (70 000 ft).

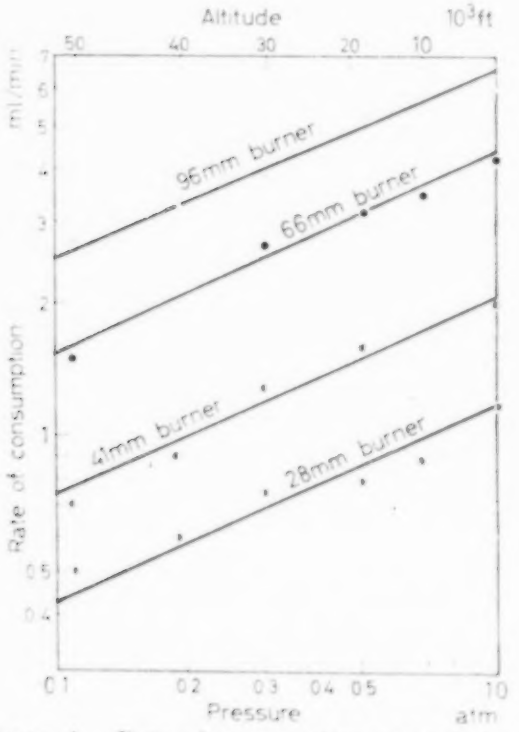

Figure 4. Rate of consumption of isododecane

The results are plotted in *Figure 4* on a log-log scale. They show that the relationship between the rate of consumption and the pressure was approximately the same for each burner, and can be expressed by $C \propto p^{0.48}$, where C denotes consumption and p the pressure.

When the relationship between the rate of consumption and the radius of the burner, r, was examined, it was found that at each pressure the result was approximately the same: the rate of consumption was proportional to $r^{1.5}$.

Effect of vitiation on burning rate

Vitiation experiments were made by measuring the rate of consumption of fuel when the incoming air was mixed with nitrogen in increasing proportions, the total gas flow being kept constant. The fuel consumption was found to fall off rapidly with an increasing admixture of nitrogen, until a point was reached where the flame was extinguished. Using the 28 mm burner, the limiting oxygen concentrations were found to vary between 12·5 per cent at 0·5 atm and 18 per cent at 0·07 atm. For the largest burner the corresponding values were 15 and 18 per cent. These results may be compared with R. F. Simmons and H. G. Wolfhard's values for liquid surface diffusion flames at atmospheric pressure[4]. Their flames were burning beneath an inverted sintered metal hemisphere. The limiting oxygen concentrations for *n*-hexane, *n*-octane and *n*-decane were all about 13·4 per cent.

Flame dimensions

The flame height was measured by means of a scale fixed by the side of the flame. Results for both fuels in the 25 mm burner are shown in *Figure 5*.

The height of the vapour space between the top of the burner and the lowest visible part of the flame was also measured. The results were the same for both fuels: the height varied inversely as the pressure, from 0·50 mm at 0·5 atm to 5·5 mm at 0·04 atm.

General character of the flame

A diffusion flame burning from a liquid surface is similar in appearance to that of a gaseous fuel burning from the top of a circular pipe, and can be divided into three distinct regions:

(*i*) A vapour space directly above the liquid surface which includes a pyrolysis zone

(*ii*) A blue reaction zone forming a sheath around the flame at the base and extending well up its side

(*iii*) A carbon zone starting some way up and inside the reaction zone and extending to the top of the flame, this zone being characterized by the emission of yellow or orange light.

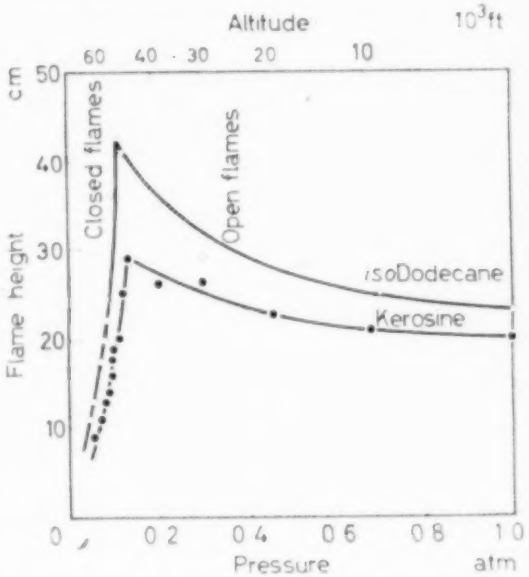

Figure 5. Flame height, 28 mm burner

In addition there is a thin sheath of weak blue radiation surrounding most of the flame. This is difficult to distinguish except near the base of the flame where it merges with the reaction zone. The flame is hollow, and may be either open at the top, with the production of grey soot particles, or closed, depending on the nature of the fuel and the size of the burner. In this investigation all the flames were open at the top at pressures down to about 0·12 atm (see *Figure 5*). In general, the effect of decreasing pressure was as follows:

(*a*) The depth of the vapour space was extended, i.e. the flame moved away from the surface

(*b*) The diameter of the reaction zone increased until it was outside the edge of the burner

(*c*) At pressures down to 0·1 atm the height of the reaction zone increased and the luminosity of the carbon zone was also extended. Below this pressure the top closed and the flame height decreased rapidly at the expense of the carbon zone.

At about 0·05 atm the flame changes its general shape to become more of a hemisphere than a cone, the carbon zone then being quite

Figure 6(a). *isododecane flame at 0·5 atm showing condensate*

Figure 6(b). *isododecane flame at 0·11 atm*

Figure 6(c). *isododecane flame at 0·04 atm*

Figure 6(d). *isododecane flame at 0·11 atm in air containing 16·2 per cent oxygen*

small. At the lowest pressures the carbon zone contracted to a yellow patch within the reaction zone.

The size of the flame was found to decrease with increasing vitiation, the whole flame contracting towards the centre of the burner, with an increase in the depth of the vapour space. The general shape of the flame remained the same, but there was considerable diminution in brightness with increasing vitiation. As the limiting conditions for a low pressure vitiated flame were approached, the flame became a small faintly-luminous cusp that tilted slowly from side to side at some distance above the burner.

Three photographs of flames burning at different pressures, and one showing the effect of vitiation, are shown in *Figure 6*. Outline drawings of the flames can be seen in *Figure 2*.

Gas flow within the flame

The accidental use of a sample of 'leaded' isododecane in these experiments provided interesting evidence of the gas flow within the flame. A white condensate, apparently solid, was observed inside the vapour space of the flame at pressures between 1·0 and 0·1 atm. This can be seen in *Figure 6*(a), and is sketched in *Figure 7*. The condensate formed a toroidal vortex which rolled slowly (as shown in *Figure 7*) at about one revolution a second. Small flocculent particles continuously formed and attached themselves to the main stream, made two or three revolutions, and finally escaped up into the carbon zone of the flame. The condensation was most marked at about 0·4 atm, and then decreased with decreasing pressure, though traces were sometimes seen at 0·07 atm. A small amount of the condensate was collected on a probe for analysis. It was found to contain a high proportion of lead.

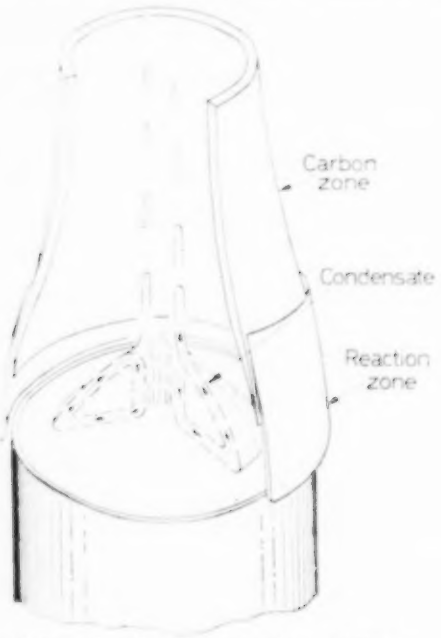

Figure 7. Condensate flow pattern

Limiting Air Velocities for Liquid Surface Diffusion Flames at Low Pressures

Apparatus and technique

The effect of airflow on low-pressure liquid-surface diffusion flames was studied in a small variable-density wind tunnel. This was connected to the vacuum main of a very large high-altitude test facility. The incoming air passed through an orifice plate flowmeter and a gate valve into a cylindrical settling tank. From this it passed through a converging bell-mouth section into a 16 in. diameter pipe. A second gate valve controlled the flow into the vacuum main. By suitable adjustment of the two valves a wide range of airflows could be obtained at pressures down to about 0·07 atm.

The 16 in. pipe formed the working section and was fitted with observation windows. An aerofoil-section model containing a tray of fuel

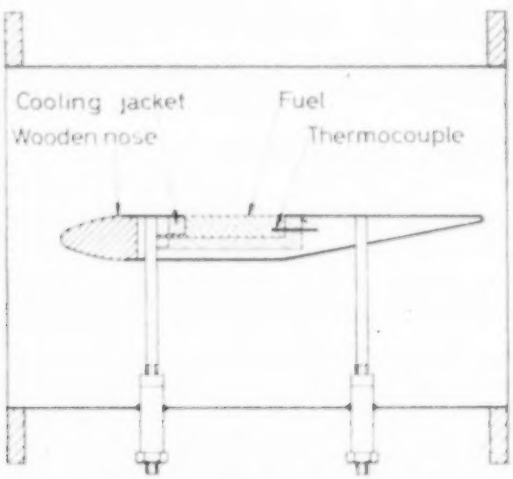

Figure 8. Section of model and working section of wind tunnel

was mounted at the axis of this pipe: this is shown in section in *Figure 8*. The fuel tray was 5 in. × 5 in. × 0·8 in. deep (12·7 cm × 12·7 cm × 2·2 cm) and was surrounded by a cooling jacket. The model was supported in the tunnel by two vertical tubes passing through the underside. These legs were threaded and permitted adjustment to be made to the height of the model. They also acted as conduits, for tubes supplying fuel and coolant, and for the leads of a thermocouple located $\frac{1}{2}$ in. below the surface of the fuel.

The velocity profile within the working section was examined by Pitot traverses and found to be very uniform. Checks with cotton tufts showed that the airflow was substantially laminar and free from any major turbulence.

Both kerosine (DERD/2482) and *iso*dodecane were tried as fuels, but no differences in behaviour could be detected. There was little evidence of fractionation of the kerosine and it was therefore used for most of the experiments.

The fuel was drawn into the tray by reducing the pressure in the tunnel. The surface was then ignited in a small airflow with the aid of a hydrogen pilot flame, which was then turned off. The pressure in the tunnel was adjusted to the desired value and the airflow gradually increased at constant pressure until the flame was extinguished. The fuel temperature, working pressure, and flowmeter manometer were read at the time of blowout, and the test then repeated at different pressure levels. In each test care was taken to maintain the fuel surface level with the surface of the model.

General nature of the flame

At low values of airflow the flame had the structure illustrated in *Figure 9*. It began near the leading edge of the fuel tray and lay nearly parallel to the surface of the model. It was very luminous over most of its surface, except for a blue reaction zone near the edge of the tray. A gap or vapour space existed between this blue zone and the edge, and the length of the gap increased as the ambient pressure decreased, in the same manner as the corresponding zone described in relation to *Figure 5*.

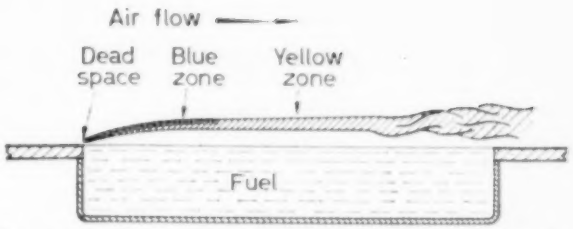

Figure 9. Flame structure in a low airflow at 0·1 atm

As the air velocity was raised the front of the flame became ragged; it then broke away suddenly from the edge of the tray and was extinguished. When obstructions to the airflow were placed at the front of the fuel tray the character of the flame was changed, particularly at the higher air velocities required for extinction. Recirculation over the fuel surface occurred, and conditions were established similar to those behind the flameholders of jet and ramjet engines. The flame was then no longer of the simple diffusion type, and the air and fuel vapour were to some extent premixed. The flame became more ragged, and less luminous.

Effect of model nose length

Since the stability of a diffusion flame depends very much on the conditions at its base (i.e. the blue zone and vapour space at the leading edge

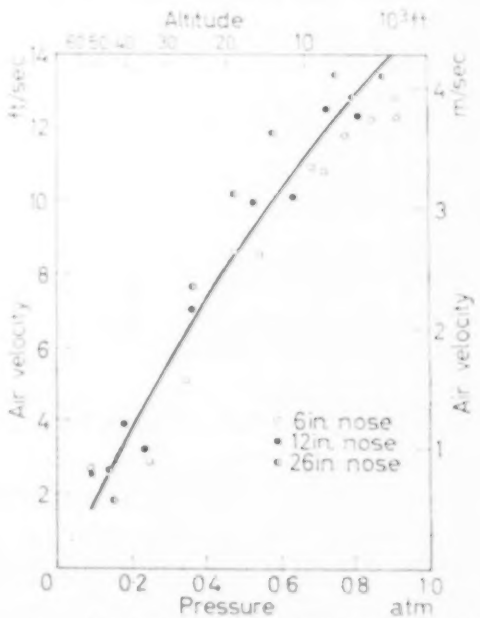

Figure 10. Variation of extinction velocity with pressure (kerosine)

of the laminar flame in *Figure 9*), it was thought that the boundary layer thickness might be important. To test this point, the elliptical-section nose of the model was made in three different lengths, measuring 6, 12 and 26 in. respectively from the leading edge to the front of the fuel tray. The observed extinction velocities for each nose at different pressures are plotted in *Figure 10*, and it is evident that within the experimental range studied the boundary layer thickness is not an important factor.

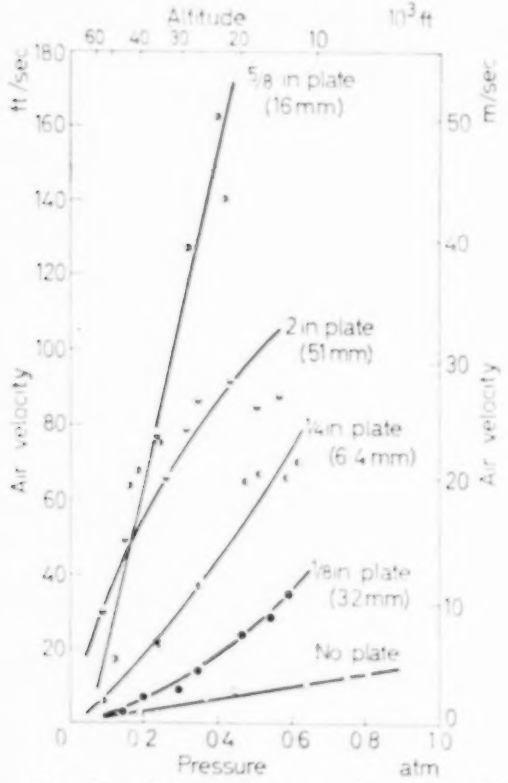

Figure 11. The effect of plates at the front of the fuel tank (kerosine)

At the low Reynolds number of the flow used in this part of the investigation the boundary layer would normally be laminar. An attempt was made to find the effect of a turbulent boundary layer by creating turbulence with a 20 s.w.g. wire stretched across the nose of the model. The results indicated that a small reduction in extinction velocity was produced in this way.

Effect of obstructions

In the experiments reported above, measurements were made of the air velocities needed to sweep the flame off the liquid surface at various pressures. The tests were now repeated with simple obstructions located at the upstream edge of the fuel tray. Metal plates, each the full width of the tray, were arranged to project $\frac{1}{8}$, $\frac{1}{4}$, $\frac{5}{8}$ and 2 in. (3·2, 6·4, 16 and 51 mm) above the surface of the fuel. Limiting airflows were determined at pressures down to about 0·1 atm. *Figure 11* shows that the extinction velocities increased with increasing height of projection up to an optimum size of plate, and then decreased. This is understandable as the flame was seen to burn from the top edge of the plate down to the fuel surface, and obviously the heat transfer became an important factor with the taller plates, where part of the flame was at a considerable distance from the fuel surface.

The effect of obstructions in the form of plates and rods in the centre of the fuel surface was also tried. It was found that the flame burned in the wake of the obstructions after it had been extinguished from the rest of the fuel surface. With increased width of obstruction the flame had higher values of extinction velocity for any given pressure.

Effect of metal plate above the fuel surface

The effect on the extinction velocities was examined of bringing a horizontal metal plate down above the fuel surface. The plate measured 9 in. × 12 in. (22 cm × 31 cm) and was placed at distances of $\frac{1}{2}$, $\frac{3}{4}$, 1, $1\frac{1}{2}$ and 2 in. (1·3, 1·9, 2·5, 3·9 and 5·1 cm) above the model. This had surprisingly little effect even when the plate was only $\frac{1}{2}$ in. from the fuel surface, although in this case the nature of the flame was radically changed: the flame burned only near the front of the fuel tray where the air entered and was used up, and again behind the back of the plate where fresh air could be obtained.

No other obstruction was present in these tests, and when the experimental results were plotted it was found that the curve drawn in *Figure 10* could be fitted to them, although the scatter was slightly greater than that in the figure.

Effect of fuel temperature

In the normal tests the fuel was cooled by forcing water through the cooling jacket, the temperature of the bulk of the fuel being maintained at between 30° and 40°C. The thermocouple, which was $\frac{1}{2}$ in. below the fuel surface, was in the region of approximately constant temperature found in the earlier experiments (page 321). Tests were conducted at lower temperatures by pumping methanol at −70°C through the cooling jacket, the fuel temperature obtained with two different rates of flow of methanol being in the ranges −5° to 0°C and 2° to 8°C. The tests were made with the $\frac{1}{8}$ in. obstruction at the front edge of the tank as this had been found to give the most reproducible results in the previous experiments.

The effect on extinction velocity was found to be negligible except at pressures below about 0·4 atm. At 0·2 atm (30 000 ft) the limiting velocities were these: fuel temperature 37° to 40°C, 12 ft/sec; 2° to 8°C, 8 ft/sec; −3° to 0°C, 4 ft/sec (3·7, 2·4 and 1·2 m/sec respectively). A further experiment conducted without any cooling, when the final fuel temperatures were between 55° and 70°C, again showed little change in extinction velocities, except at the lowest pressures.

Discussion

Simple diffusion flames

The temperature measurements made in the simple diffusion flames were not corrected for radiation and conduction losses and should therefore be regarded as purely relative, the true temperature in the hottest part of the flame being possibly about 200°C higher than those given. They correspond closely to similarly uncorrected measurements in a candle flame reported by A. G. GAYDON and H. G. WOLFHARD[2]. The effect of lowering pressure was to reduce the temperature gradients, but the maximum temperature was not greatly affected. The presence of the thermocouple appeared to make little difference to the flame except at 0·04 atm, when the whole flame tilted away from the incoming probe. The flames became very unstable at pressures below 0·04 atm, which appeared to be near the limiting pressure for these flames. Unfortunately the apparatus was incapable of producing sufficiently low pressures to prove this point.

Temperature measurements in various liquid fuels burning at atmospheric pressure have been made by G. N. KHUDIAKOV[1]. He found an exponential fall in temperature with depth below the surface. Assuming that heat penetrates the liquid by conduction alone, the heat conduction equation when thermal equilibrium has been attained is of the form

$$\lambda \frac{d^2T}{dx^2} + c\sigma \frac{R\,dT}{dx} = 0$$

where λ, c, σ and R are the thermal conductivity, heat capacity, specific gravity and rate of burning of the liquid respectively, and T is the temperature at distance x below the surface. The solution of this equation is of the form

$$(T - T_0) = (T_{max.} - T_0) \exp(-\beta x)$$

where $\beta = c\sigma R/\lambda$, $T_{max.}$ is the temperature at the surface, and T_0 is the temperature in the bulk of the liquid. A graph of $\ln(T - T_0)$ against x should therefore be a straight line. Plots of the results in the present investigation showed that the relationship was indeed linear, except for a region near the surface of the fuel. This disparity near the surface was due to a convection layer in the liquid, which is reflected in the shape of the temperature profiles in *Figure 3*. The movement in this convection layer could be observed through the window by watching the schlieren pattern in the liquid. The layer was most marked in the 28 mm burner at pressures between 0·5 and 0·1 atm, being about 5 mm deep. Very little convection was seen at other pressures, and at atmospheric pressure the layer was too thin to have been detected in Khudiakov's experiments. The layer was thinner in the larger burners, the maximum observed depth in the 96 mm burner being about 2 mm.

The rate of consumption of fuel over the range of pressures was found to be proportional to $r^{1.5}$. This means that the evaporation of fuel lies between the two extremes of:

(*1*) evaporation from the perimeter of the

burner only, when the rate of consumption would be proportional to r, and

(2) evaporation equally from the whole liquid surface, when the rate of consumption would be proportional to r^2.

This is a reasonable result and implies that the rate of evaporation at the edge of the burner, adjacent to the hot reaction zone, is higher than at the centre. There was some indication from the experimental results that the rate of consumption became more nearly proportional to r for the larger burners. V. I. BLINOV and G. N. KHUDIAKOV[6], and W. L. FONS[7], have already reported that the burning velocity of a number of liquid fuels decreases with increasing burner diameter up to about 5 in. It then increases with increasing diameter up to about 40 in., and finally becomes independent of diameter in larger burners.

The flames illustrated in *Figure 6* are markedly similar to those already reported for gaseous diffusion flames on circular tubes. The reduction of the carbon zone at reduced pressure, and its final withdrawal to within the reaction zone has been illustrated for an acetylene–air flame by A. G. GAYDON and H. G. WOLFHARD[8]. The flames of *Figures 6*(a) and (b) are similar to the 'laminar diffusion flames' described by J. BARR[9]. *Figures 6*(c) and (d) bear a close resemblance to the illustrations of vitiated flames in a paper by B. P. MULLINS[10]. Barr's flames show the effect of different air and fuel flow rates, Mullins's the effect of vitiation, and Gaydon and Wolfhard's the effect of pressure. In the present work both pressure and the degree of vitiation were varied, but the fuel flow rate varied with them (as was shown by variations in the rate of fuel consumption). A. G. GAYDON and H. G. WOLFHARD[11] have already pointed out this similarity that exists between the effects of pressure and vitiation on a diffusion flame.

The observation of an indication of the movement of fuel vapour within the flame has not been previously reported. The laminar flow that has previously been assumed in this zone is incorrect, at least for flames burning in the conditions reported here, and the actual transit time of the molecules in this zone may be many times greater than has been calculated on this basis. The toroidal movement is probably a result of the steeper temperature gradients, and hence flow velocities, near the edge of the burner. It is reflected in the displacement toward the centre of some of the isothermals in *Figure 2*. These flow conditions are in contrast to those existing in a gaseous diffusion flame where the highest velocity is at the centre of the burner. Particle track studies in gaseous diffusion flames have in fact revealed no evidence of circuitous movement[12] (although A. LEVY and F. J. WEINBERG[13] did observe the presence of a toroidal vortex, but this was located outside the edge of a flat flame burner).

Flame in airstreams

The extinction velocities in the absence of any obstruction were found to be quite small, 15 ft/sec being sufficient to sweep the flame off the surface at pressures a little below atmospheric. A higher value was obtained by G. PALMER[14] in a full-scale test at atmospheric pressure. He found that a petrol fire could not persist on the surface of an aircraft wing in air flows above about 25 ft/sec. The difference between these results is explained by Palmer's observation that some flameholding occurred at the trailing edge of the wing.

It was found that at lower pressures the flame was even easier to dislodge, and as the limiting pressures for these flames were approached, the extinction velocity diminished rapidly. Thus at pressures of 0·1 atm or less (corresponding to altitudes of more than 50 000 ft) the extinction velocity was less than 2 ft/sec.

The presence of obstructions had a marked effect on the extinction velocities, a projection only $\frac{1}{8}$ in. high being sufficient to double the values previously obtained in its absence. Still greater increases were observed with higher obstructions. The flameholding properties of these simple obstructions were so marked that it was not considered necessary to make more elaborate experiments with many varied shapes.

The effect of varying the length of the fuel tray was not examined in these experiments and this could have influenced the stability of the flame. Recirculation over the fuel surface

would create some degree of premixing in the wake of the flameholder, and the stability of the flame would be affected by the composition of the mixture. The proportion of fuel vapour would be dependent on the length of travel of the reversed airflow over the fuel surface. Hence the length of the fuel tray would affect the mixture ratio and therefore the persistence of the flame.

The length of the recirculation zone behind a simple gutter baffle has been measured by J. P. LONGWELL[15], and it was found to be between 4 and 5 baffle heights for both 1 in. and $2\frac{1}{4}$ in. gutters. These results were obtained in a premixed gas stream, but the length of the recirculation zones in the present experiments might be expected to show a similar relationship to the baffle height. Hence a 5 in. tray should contain the whole of the recirculation zone existing behind a 1 in. plate. It has recently been shown[16] that this assumption is correct: liquid surface diffusion flames burning in a similar wind tunnel at atmospheric pressure were found to have maximum stability behind a 1 in. baffle when the tray length was between 4 and 6 in. Thus the choice of tray length in these experiments was correct for baffles up to about 1 in. high, but it is possible that a longer tray might have resulted in higher extinction velocities for the 2 in. plate.

At pressures above about 0·4 atm the temperature of the bulk of the fuel had no measurable effect on the extinction velocities, but at lower pressures the increased abstraction of heat from the surface layers of the chilled fuel was sufficient to decrease the extinction velocities, presumably by decreasing the rate of fuel vaporization. The depth of fuel in these experiments was 0·8 in., well in excess of the depth of steep temperature gradients shown in *Figure 3*. The conditions did not therefore cover the case of a relatively thin layer of fuel on a metal surface at low temperature, as might well occur in an aircraft.

Conclusions

The greatly enhanced stability of flames anchored to simple obstructions as small as $\frac{1}{8}$ in. high serves to emphasize the importance of the effect of flameholders on the aircraft fire hazard. If it was possible to make an aerodynamically clean nacelle, the limiting conditions for the persistence of flight fires would be narrowed, and the fire protection problem greatly simplified. (The reduction in the quantity of chemical extinguishant required in such conditions has been demonstrated by C. A. HUGHES in a number of trials in modified engine nacelles[17].)

This work has shown quite definitely that it is possible for aircraft fuel to burn at altitudes up to 70 000 ft. The maximum temperatures in the reaction zone of the flame change very little with increasing altitude, and the flame still remains a dangerous source of heat even at the highest altitudes studied. However, as the altitude increases, the flame becomes more susceptible to the effects of vitiation and cooling, and at 70 000 ft it is unstable and readily extinguished. The conditions in an aircraft are not as favourable as those in the laboratory and the persistence of fire at this altitude is therefore improbable.

At pressures corresponding to 20 000 ft the laboratory flames were very stable and persisted in quite fast airstreams provided that some obstruction was present to act as a flameholder. At this altitude too we know from operational experience that fire can be readily started and will persist in an aircraft. The reason no doubt lies in the wide variation of conditions that a flame will tolerate at this pressure and in the fact that an aircraft structure can provide the necessary obstructions for flameholding.

Between the altitudes of 20 000 and 70 000 ft therefore, the probability that fire will persist declines from a high value to almost nil, and an important question is the way in which this change takes place. The laboratory tests indicate that the exinction velocity falls progressively as the pressure is reduced, but this is not necessarily the most important change affecting the persistence of the flame at low pressures. Air vitiation by the products of combustion, and the reduction of fuel volatility at low temperatures, have both been shown to have an enhanced quenching effect at low pressures. Hence the probability that a fire will persist in an aircraft must diminish more rapidly

at higher altitudes than the laboratory results suggest.

On the basis of this argument, we suggest that in an aircraft the probability of the persistence of fire remains high up to say 40 000 ft and then begins to decline sharply. Thus it may be much less at 50 000 ft and negligible at 60 000 ft.

However, it has been pointed out[18] that there are two practical conditions which may favour the persistence of flames at high altitudes. Ram air entering a nacelle or a damaged wing may create local high pressure regions. The same effect can be produced by air leaking from a jet engine compressor, or from pressurizing air ducts. Small localized flames might therefore persist at altitudes unfavourable to a large fire. In the absence of any data it is difficult to say to what extent this should influence the argument given above, but as the normal flow of cooling air through a nacelle creates little change in pressure, the conclusion would appear to be valid for an undamaged aircraft.

References

[1] KHUDIAKOV, G. N. *Izvest. Akad. Nauk S.S.S.R. Otdel tekh. Nauk*, 1951, **7**, 1015

[2] BURGOYNE, J. H. and KATAN, L. L. *J. Inst. Petrol.* 1947, **33**, 158

[3] RASBASH, D. J., ROGOWSKI, Z. W. and STARK, G. W. V. *Fuel, Lond.* 1956, **35**, 94

[4] SIMMONS, R. F. and WOLFHARD, H. G. *Combustion & Flame*, 1957, **1**, 155

[5] GAYDON, A. G. and WOLFHARD, H. G. *Flames: their Structure, Radiation and Temperature*, p 140. Chapman & Hall: London, 2nd ed. 1960

[6] BLINOV, V. I. and KUDIAKOV, G. N. *Dokl. Akad. Nauk S.S.S.R. (N.S.)*, 1957, **113** (5), 1094

[7] FONS, W. L. *Combustion & Flame*, 1960, **4**, 279

[8] GAYDON, A. G. and WOLFHARD, H. G. *Flames: their Structure, Radiation and Temperature*, p 140. Chapman & Hall: London, 2nd ed. 1960

[9] BARR, J. *Fourth Symposium (International) on Combustion*, p 765. Williams and Wilkins: Baltimore, 1953

[10] MULLINS, B. P. *Selected Combustion Problems*, p 477. Butterworths: London, 1954

[11] GAYDON, A. G. and WOLFHARD, H. G. *Flames: their Structure, Radiation and Temperature*, p 149. Chapman & Hall: London, 2nd ed. 1960

[12] See e.g. LEWIS, B. and VON ELBE, G. *J. chem. Phys.* 1943, **11**, 75

[13] LEVY, A. and WEINBERG, F. J. *Seventh Symposium (International) on Combustion*, p 296. Butterworths: London, 1959

[14] PALMER, G. Unpublished work, Farnborough, 1926

[15] LONGWELL, J. P. *Combustion Researches and Reviews 1955*, p 58. Butterworths: London, 1955

[16] EYRE, R. Unpublished work, Colnbrook, 1960

[17] HUGHES, C. A. U.S. Department of Commerce: Civil Aeronautics Administration. *Tech. Dev. Rep. No. 205*, 1953

[18] HANSOM, B. S. Private communication

Suggested Origin of the Anomalous Line-reversal Temperatures in the Reaction Zone of Hydrocarbon Flames†

E. M. BULEWICZ and P. J. PADLEY

Department of Physics, Duke University, Durham, North Carolina

(Received March 1961)

Measurements of electron concentrations by the method of cyclotron resonance, and of non-thermal iron line intensities in emission, as a function of composition and dilution in the reaction zone of low-pressure acetylene–oxygen–argon mixtures, reveal a marked similarity in behaviour of these two quantities. On this and other circumstantial evidence, the possible causes of the anomalous line-reversals can be narrowed down to two, neither of which can, however, be considered objection-free until further experimental evidence reveals in even more detail the nature of certain of the reaction steps proposed. One of these schemes involves postulating the bimolecular production of an excited species Y^* *by the mechanism also responsible for electron production. Species* Y^* *must be sufficiently energetic, and be present in sufficient quantity, to produce excited metal atom* M^* *by energy transfer with* M. *The other—a more specific scheme—involves reaction between* M^+ *and* e^- *to produce* M^*, *the emitted radiation being discrete. Although there is experimental evidence for all the important steps involved in this second scheme, this scheme, too, can fail if the cross sections for capture of* e^- *by* M^+ *prove to be too small. Schemes so far postulated involving termolecular reactions are eliminated as not satisfying the experimental observations presented.*

Introduction and Review of Previous Work

IT HAS been known for some time that line-reversal measurements, made on the spectral lines of various metal additives, in the reaction zone of premixed flames[1–3] often give rise to temperatures considerably above those expected on the basis of full thermodynamic equilibrium. There is, however, relatively little in the way of an understanding of the cause of this phenomenon (except in the case of hydrogen–oxygen–nitrogen mixtures[4]) nor has it been studied in great quantitative detail. The effect is most marked for premixed acetylene–oxygen–nitrogen mixtures, with lines requiring up to 174 kcal/mole for their excitation appearing in the reaction zone, but not in the burnt gases. The ammonia–oxygen, ammonia–nitrous oxide and hydrogen–nitrous oxide flames also appear to behave in a similar manner. On the other hand, flames like those of hydrogen, carbon monoxide and carbon disulphide with oxygen have often been considered to give either essentially thermal, or only slightly anomalous, line reversals.

†This research was supported by the United States Air Force under Contract No. AF 49(638)-765 monitored by the Air Force Office of Scientific Research of the Air Research and Development Command.

Suggestions put forward to date to account for this phenomenon include the following.

(*1*) A. G. GAYDON[5], in an attempt to give a general explanation for the phenomenon as observed in a wide variety of different flames, has considered whether or not lags in equipartition of energy between electronic and other modes could be responsible.

(*2*) H. P. BROIDA and K. E. SCHULER[3] have suggested a collision scheme of the type

$$CH\,(CH_2) + O + Y \longrightarrow CO + H\,(H_2) + Y^* \quad \ldots [1]$$

where Y is H_2O, O_2, H_2 or C_2H_2, followed by the efficient bimolecular exchange of energy between vibrational and electronic modes

$$Y^* + Fe\ (e.g.) \longrightarrow Fe^* + Y \quad \ldots [2]$$

(*3*) A. G. GAYDON and H. G. WOLFHARD[1] have considered the possibility of three-body collisions between a metal atom and two free radicals. They point out that it is not difficult to postulate reactions of sufficient energy involving CH, C_2, CHO or C.

(*4*) More recently, A. G. GAYDON[5] and A. G. GAYDON and H. G. WOLFHARD[6] have suggested that the effect could be connected

with the abnormally high ionization found in the reaction zone of hydrocarbon flames. Recent experimental evidence by I. R. KING[7], although not sufficiently detailed for any definite conclusions to be drawn, also suggests a qualitative parallel between these two phenomena when hydrocarbon flames are considered: for other systems (e.g. methane–nitric oxide or hydrogen–oygen), however, no such correlation is evident. All these suggestions (1) to (4) either suffer from lack of conclusiveness in such experiments as have so far been carried out, or else need reviewing in the light of more recent data on fundamental flame processes[4–14, 18–24].

First, at least two distinct types of anomalous line-reversal, or 'chemiluminescence', can now be distinguished, according to whether or not the effect persists into the burnt gases. The former type of anomaly is observed in hydrogen–oxygen–nitrogen mixtures[4], and quantitative studies of this[4,8] revealed that operation of one or both of the processes:

$$H + H + M \longrightarrow H_2 + M^* \quad \ldots . [3]$$

$$H + OH + M \longrightarrow H_2O + M^* \quad \ldots . [4]$$

can result in overpopulation of the upper state of the spectral transition by a factor as large as 1 000-fold. The relative contributions of reactions 3 and 4 could be quantitatively assessed for each metal examined, and so far the cases of sodium, thallium, lead, iron, silver and manganese have been discussed[4,8,13]. With iron, lines with excitation energies up to only 122 kcal/mole have been observed[4,14], while the 'reaction zone' chemiluminescence appears to originate from a more energetic source. This important difference is illustrated in *Figure 1*, which gives, essentially, log (no. of ground state atoms)/(no. of excited atoms) as a function of the excitation energy E of the transition, for four hydrogen flames (iron, cobalt, nickel, copper, silver, thallium, lead, potassium, sodium and lithium transitions: for more details see ref. 4), and an acetylene flame[1] (iron, lead, thallium and sodium transitions). Individual points are omitted for clarity. Regions of thermal and chemiluminescent excitation can be clearly distinguished, and an inspection of the

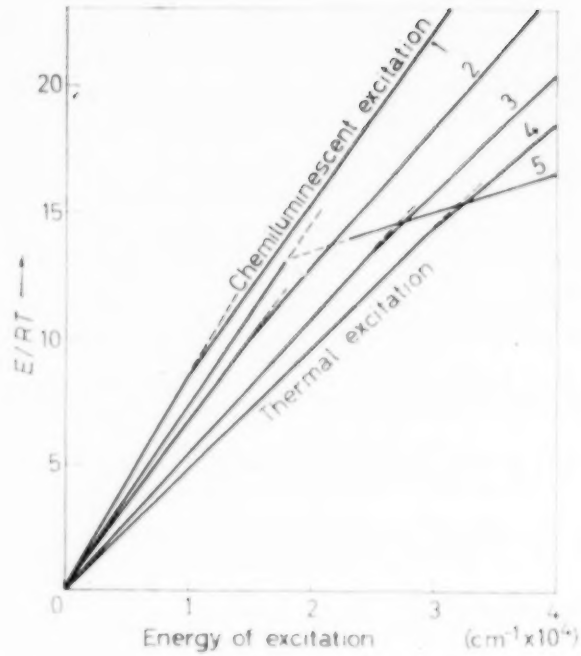

Figure 1. Degree of excitation as a function of energy of excitation of metal lines in the reaction zones of four hydrogen–oxygen–nitrogen flames (1 to 4) at atmospheric pressure[14] and an acetylene–air flame (5) at 24 mm of mercury[1]. Thermal temperatures of these flames (measured by D-line reversal, and corresponding to the slopes of the lower half of each plot): 1. 1750°K, 2. 2340°K, 3. 2600°K, 4. 2670°K, 5. 2000°K

plots reveals that for undiluted hydrogen–oxygen mixtures no overexcitation would be expected (which explains the failure of earlier workers to detect the effect) while even for the hottest acetylene–oxygen flames the overexcitation of high energy lines would still be outstanding. Thus, a systematic study of each fuel is required; and an explanation which would cover all flame systems seems highly unlikely.

The above arguments make it easier to define the problem under discussion, for it is considered that both types of chemiluminescence are, in fact, operating in acetylene flames. Preliminary studies by P. J. PADLEY and T. M. SUGDEN[15] suggest that for cool, highly diluted ($T < 2\,300$°K, preburnt nitrogen/oxygen > 4) acetylene–oxygen flames at atmospheric pressure the concentrations of species like H and OH are above the equilibrium level—as in hydrogen–oxygen–nitrogen flames—the effect being greatest near stoichiometry. The rate of

radical decay was found to be similar to that in hydrogen–oxygen–nitrogen flames[8] and consistent with the operation of reactions of the type 3 and 4. Evidence on the overexcitation of sodium and thallium lines in such flames is in line with the more detailed work on hydrogen[4,8]. Lines with excitation energies 40 to 120 kcal/mole are observed, though for $E >$ about 70 kcal/mole the reaction zone effect becomes important as well. If, however, a flame is chosen so that radical disequilibrium is low (in flames at about 15 mm of mercury, [H] and [OH] do not deviate from equilibrium[16] by more than a factor of 10) or if E for the line examined is sufficiently high, the reaction zone effect can be studied unambiguously.

It is now possible to comment briefly on the suggestions 1 to 4. Consider possibility (1). The fact that the plots of *Figure 1* in the non-thermal region are still, apparently, straight lines, both for hydrogen and acetylene, suggests that the energy of overexcitation distributes itself throughout the electronic mode in a manner which can be described as pseudo-Boltzmann. K. E. SCHULER[17] has discussed the conditions under which perturbations of the Maxwell–Boltzmann distribution law might take place in fast-reacting chemical systems. These may be due either to lags in equipartition of energy (direct physical disequilibria), i.e. suggestion (1), or to the production, in the course of the reaction, of out-of-balance concentrations of certain constituents (chemical disequilibria, which may lead to 'indirect' physical disequilibria). The anomaly in hydrogen flames is known to take the latter course—via processes 3 and 4. From the evidence of *Figure 1*, it seems reasonable to conclude that the reaction-zone anomaly in acetylene also takes the latter course, since in this respect the two effects manifest themselves so similarly, and since the 'atom electronic excitation temperature' for acetylene, i.e. the slope of the non-thermal part of the plot, at about 8 000°K, is considerably above the value of 3 000°K obtained for a hydrogen flame of similar thermal temperature. Thus this evidence is in line with Gaydon's[5] earlier suggestion that in flames the only direct physical disequilibria expected are slight lags in vibrational equipartition and persistence of metastable electronically excited species.

Turning now to suggestions (2) and (3). Broida and Schuler[3] excluded the possibility that reactions 1 and 2 might occur effectively in one step, by the reaction

$$CH + O + Fe \longrightarrow CO + H + Fe^* \quad \ldots [5]$$

on the grounds that the concentration of Fe atoms is too low for iron to act as third body, and that the overexcitation is sensibly independent of pressure[1]. Closer inspection suggests, however, that neither exclusion of reactions of the type 5, nor the inclusion of reactions 1, can be satisfactorily justified on these two counts alone. First, the degree of overexcitation is not a function of the concentration of Fe atoms. Secondly, simple steady-state calculations of Fe*/Fe, taking into account the quenching and radiation processes:

$$Y^* + X \longrightarrow Y + X \quad \ldots [6]$$

$$Fe^* + X \longrightarrow Fe + X \quad \ldots [7]$$

$$Fe^* \longrightarrow Fe + h\nu \quad \ldots [8]$$

where X is any third body, suggest that, unless the concentrations of X and Y are very different (rather unlikely), and unless the rate constants of processes 1, 2, 5 and 6 satisfy rather special conditions, then it will not be possible to distinguish kinetically between processes 1 (coupled with 2) and 5. Moreover, such explanations unfortunately do not avoid the difficulty presented by the pressure-independence of the effect. As Gaydon and Wolfhard[1] point out, three-body processes are unlikely causes of the phenomenon for this very reason, though it would be possible to invalidate this argument if the radicals producing the overexcitation were themselves destroyed predominantly by three-body processes. This, however, we consider improbable, since radicals like CH do not appear to persist into the burnt gases (suggesting bimolecular destruction) and since species like O, OH, etc., cannot be sufficiently out of equilibrium under conditions when their calculated levels are of the order of one per cent of the total gases[16]. Thus suggestions (2) and (3) need be considered no further here.

This leaves possibility (4) for comment. It is known from probe and microwave attenuation studies in flames[18–20] that the concentration of electrons in flames is often considerably above the value expected on equilibrium considerations, particularly when the reaction zone is considered. The level of ionization in hydrogen flames is still a matter of dispute, with H. F. CALCOTE and I. R. KING[18] and S. DE JAEGERE *et al.*[24] favouring a low level (in the region of 10^5 to 10^6 ions/cm^3) and with K. E. SCHULER and J. J. WEBER[19] and P. F. KNEWSTUBB and T. M. SUGDEN[23] suggesting a higher value (in the region of 10^9 ions/cm^3). Both these values are, however, considerably lower than the generally agreed-upon level of 10^{11} to 10^{12} ions/cm^3 in the reaction zone of acetylene flames at atmospheric pressure. The nature of the positive ions is now known[21–24], these being mainly H_3O^+ and, in the reaction zone of hydrocarbon flames, a large number of hydrocarbon fragments of the type $C_nH_m^+$.

In an attempt to establish a relationship, if any, between the anomalously high ionization and line-reversal measurements we have noted the following point, illustrated in *Figure 2*. The upper curve is a plot of electron concentration against λ, obtained from probe measurements made by H. F. CALCOTE[25] in the reaction zone of a series of acetylene–air flames at 22·8 mm of mercury pressure. The lower curve is a plot of the relative number of Fe atoms excited to the level giving rise to the 3 020 Å group against λ, recalculated from Gaydon and Wolfhard's temperature measurements on this group of lines in the reaction zones of a series of acetylene–air flames between 30 and 60 mm of mercury pressure. The qualitative parallel between the two effects is quite striking, bearing in mind that curves A and B were taken under completely different experimental conditions. It is evident that the establishment of a quantitative relationship here would be of the greatest importance in elucidating the cause of the chemiluminescence; and the experimental section of this work is devoted to this end.

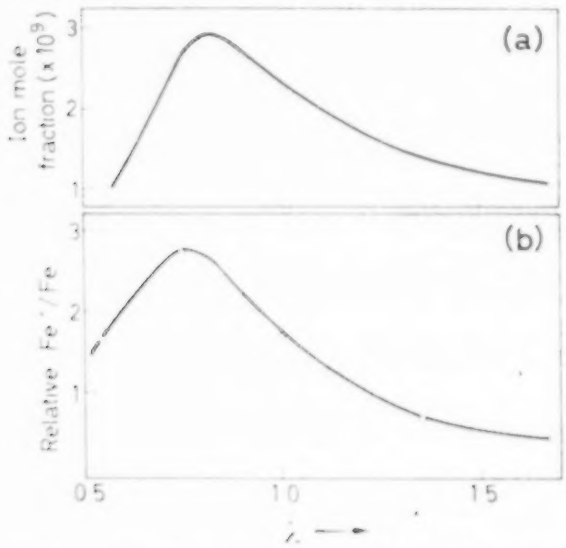

Figure 2. Electron concentration in the reaction zone of acetylene–air flames at 22·8 mm of mercury versus composition—taken from Calcote[25]. Also Fe*/Fe *(calculated from temperature measurements, made on the 3020Å line of Fe, quoted by Gaydon and Wolfhard[1]) versus composition in the reaction zone of acetylene–air flames at 30 to 60 mm of mercury. These two plots have a slightly similar appearance*

Theory and Experimental

Electron concentrations were measured by the method of cyclotron resonance, described in detail elsewhere[26–28]. The advantages of this method are, first, that no solid objects or any other form of 'indicator' are introduced into the flame. Secondly, the method to a large extent circumvents the old objections to the use of conventional microwave absorption techniques, based on the thinness of the reaction zone compared with the wavelength of the absorbed radiation, even at reduced pressure: in the latter case high sensitivity generally demands wavelengths of at least several centimetres (based both on theoretical and experimental limitations), whereas the sharpness of cyclotron resonance lines is improved if the microwave frequency and the magnetic field strength are increased. Thirdly (an important advantage over conventional microwave absorption methods), no assumptions have to be made about the electron–molecule collision frequency, which appears in the expression relating the measured attenuation to the electron concentration.

When microwave radiation is passed through the partially ionized gases so that the direction of propagation, the **E** vector and the magnetic

field are mutually perpendicular, resonance absorption takes place in the region of $\omega = \omega_e = e\mathbf{H}/mc$, where ω and ω_e are the microwave and cyclotron frequencies respectively, and $\mathbf{H}$ is the field strength in gauss, provided that ν, the electron–molecule collision frequency, $\ll \omega$. It can be shown that the number of electrons/cm^3, N, is given by

$$N = \frac{\Delta\mathbf{H} \cdot \beta_a}{d} \times \frac{1}{40\pi e \log e}$$

where β is the attenuation, in dB, at the centre of the resonance line, $\Delta\mathbf{H}$ the line width, and d the length of microwave path, in cm, through the flame.

The Pyrex glass, low pressure, air-cooled system was similar to that described by Gaydon and Wolfhard[6]. Acetylene–oxygen–diluent mixtures were burnt at pressures 8 to 40 mm of mercury, usually above a 15 mm diameter burner tube. Pressures below about 8 mm could not be used with the present arrangement, owing to the limitations imposed by the 2·3 cm gap of the magnet (12 in., 20 000 gauss maximum, Varian Research, Ser. No. 6).

Gases were obtained from commercial cylinders, and the flow-rates measured by means of calibrated rotameters. The total volume of gas used varied between 500 and 1 000 cm^3/min (usually 800 cm^3/min) at atmospheric pressure and room temperatures. Temperature measurements were made by the sodium D-line method[6], and have already been described elsewhere[27].

Microwave radiation at a frequency of about 48 kMc/s and modulated at 2 kc/s was obtained from a standard Raytheon K band klystron (type 2K33) combined with frequency multiplier. The flame vessel was placed in the magnet gap between two waveguide horns, one leading to the multiplier and the other to the detector, so that the flame, the direction of radiation propagation and the magnetic field were mutually perpendicular. The position of the burner tube was such that the microwaves traversed the flame in the immediate vicinity of the reaction zone—fine adjustment could be made by slight pressure alteration. In all the observations recorded below, the flame position giving maximum attenuation was used, since this location was the most easily reproducible. The signal from the output crystal, after suitable amplification and demodulation, was plotted as a function of magnet field strength by a pen recorder. The magnetic field was swept electrically over a range of about 3 000 gauss in two minutes, covering the whole of the cyclotron resonance line, the centre of which was in the region of 17 000 gauss.

Iron was introduced in the form of iron pentacarbonyl. The lines chosen for this study were those at 4045·8 Å, 4063·6 Å and 4071·7 Å (non-resonance lines, requiring about 105 kcal/mole for their excitation). Line intensities were measured densitometrically (Jarrell Ash JA 2 300 instrument), the photographs being taken on a conventional Hilger quarter-plate spectrograph.

Results

Figure 3(a) shows the electron/composition curve (corrected for pressure and temperature changes) obtained, and *Figure 3*(b) shows the corresponding, similarly corrected plot for the

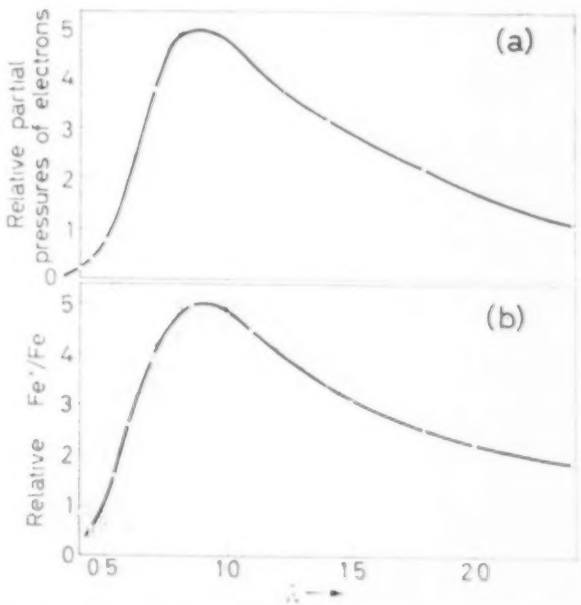

Figure 3(a). *Electron partial pressure versus composition in the zone of low-pressure acetylene–oxygen mixture.* (b). *Fe*/Fe (for 4064 Å, non-resonance line) versus composition in the same flames used to obtain Figure 3*(a). *Note the striking similarity of Figures 3*(a) *and 3*(b)

relative number of non-thermally excited iron atoms. There is a remarkable similarity between these two diagrams; this is particularly outstanding when it is remembered that no quenching corrections have been applied to *Figure 3*(b). Unfortunately there seem to be few data available[29–31] for the physical or chemical quenching of excited Fe by neutral molecules—these effects are very specific and it is difficult, therefore, to obtain information from comparisons with other metals, such as sodium, mercury, cadmium and thallium, which have been studied in detail. Using previous arguments[5], the Stern–Volmer quenching factor for excited Fe in hydrogen flames, obtained from data similar to those presented elsewhere, is very probably about 10. For a radiative lifetime of about 10^{-8} sec, a quenching cross section of 10 to 15 Å^2 is calculated. The most likely quencher expected *a priori* in this case would be water. Also carbon monoxide, carbon dioxide and oxygen might be expected to have quenching cross sections for excited Fe in this general range[29]. It seems quite probable that, owing to the way in which these molecules vary in concentration as a function of composition in low-pressure acetylene flames[6], the average collisional cross section for all flame gas molecules with excited Fe might be virtually independent of composition. It might be observed, in this connection, that the average cross sections for collisions of electrons with flame gas molecules varies only slowly[27] with λ.

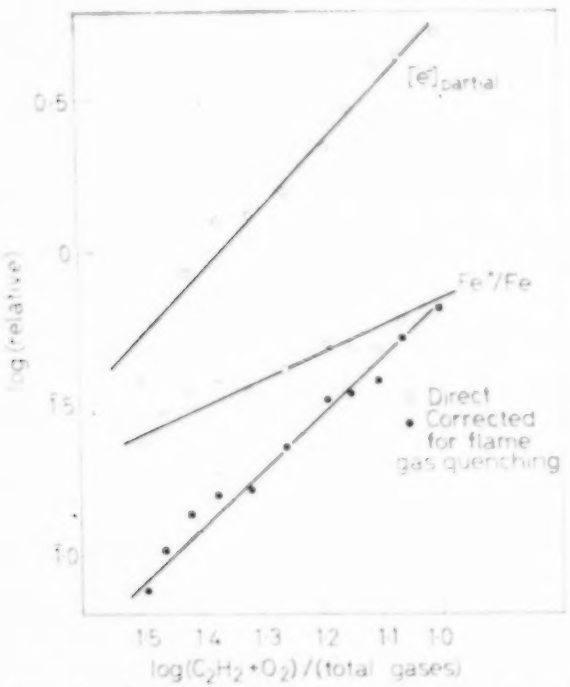

Figure 4. Electron partial pressure and Fe/Fe (for the 4064Å line) as a function of argon dilution. After correction for quenching, both plots have very similar slopes*

We have also made observations on flames diluted with argon, at constant λ and constant total gas flow of 800 cm^3/min. The partial pressure of electrons is found to be proportional to the square of the fuel-fraction present—see *Figure 4* (this result, with respect to ionization, will be discussed elsewhere). The fraction of iron atoms excited under the same conditions is found to be proportional to the fuel-fraction, in good agreement with the square-dependence of electrons, since the quenching cross section for argon can be taken as effectively zero when compared with those of the flame gas molecules.

Discussion

Mechanisms by which the connection between the two quantities measured could arise can be narrowed down to two possible alternatives.

(*1*) The excited metal atoms are produced directly by the same reaction mechanism that produces the electrons; e.g. reaction 5 coupled with

$$CH + O \longrightarrow CHO^+ + e$$

followed by

$$CHO^+ + H_2O \longrightarrow CO + H_3O^+ \text{ etc.}$$

As has been pointed out already, however, such a scheme does not explain the pressure independence of Fe*/Fe. Simple steady-state treatment suggests that this difficulty could be circumvented only if an appropriate bimolecular reaction could be found which would produce a suitable Y* (see reactions 1 and 2) with high probability, $> 0{\cdot}1$ (in order to explain ratios of M*/M as high as 10^{-7} found for some line-reversal measurements[1]).

(*2*) Gaydon and Wolfhard[1] have observed that the intensity distribution of the iron overexcitation spectrum is similar to that in the iron arc, which suggests that the overexcitation might arise directly from the presence of

charged particles. The possibility that the over-excitation is caused by electron impact is highly unlikely, particularly as some metals (e.g. the alkalis) do not, in general, show the effect at all. The closeness of the 174 kcal/mole, highest energy Fe line observed to the ionization potential of Fe^I might imply that the operative reaction is the radiative recombination of M^+ and e^-. This could manifest itself in one of the two following ways, based on other evidence which will be given shortly.

(*2, i*) Metal ions are produced in non-thermal quantities by the same reaction mechanism producing the electrons. Again following reaction 5 as an example, we have:

$$CH + O + M \longrightarrow CO + H + M^+ + e \quad k_9 \quad \ldots . [9]$$

$$M^+ + e^- \longrightarrow M^* \quad k_{10} \quad \ldots . [10]$$

$$M^* + X \longrightarrow M + X \quad k_7 \quad \ldots . [7]$$

$$M^* \longrightarrow M + h\nu \quad k_8 \quad \ldots . [8]$$

$$M^+ + e^- + X \longrightarrow M + X \quad k_{11} \quad \ldots . [11]$$

which leads to

$$\frac{[M^*]}{[M]} = \frac{k_9 k_{10} [CH] [O]}{(k_8 + k_7 [X]) (k_{10} + k_{11} [X])}$$

(*2, ii*) Metal ions are produced in non-thermal quantities by charge exchange with positive ion fragments R^+ in the reaction zone[20]. Reactions 10, 7 and 8 occur as above. Once non-thermal metal ion production has ceased, i.e. immediately downstream of the reaction zone, the free metal ion must in some way be protected from direct attack by e^-. Evidence is presented which suggests that the metal ion might become largely surrounded by a cluster of water molecules, and is also to some extent combined as hydrate MH_2O^+ or hydroxide MOH^+. Destruction of M^+ is now, effectively, bimolecular. The new reactions are:

$$R^+ + M \longrightarrow M^+ + R \text{ (disintegrates)} \quad k_{12} \quad \ldots . [12]$$

$$R^+ + e^- \longrightarrow \text{fragments} \quad k_{13} \quad \ldots . [13]$$

$$M^+ + H_2O \text{ (e.g.)} \longrightarrow MH_2O^+ \quad k_{14} \quad \ldots . [14]$$

$$MH_2O^+ + X \longrightarrow M^+ + H_2O + X \quad k_{15} \quad \ldots . [15]$$

$$MH_2O^+ + e^- \longrightarrow M + H_2O$$

$$\text{(or fragments, possibly excited)} \quad k_{16} \quad \ldots . [16]$$

This leads to an expression of the form

$$\frac{[M^*]}{[M]} = \frac{k_{10} k_{12} (k_{15} [X] + k_{16} [e^-]) [R^+]}{(k_8 + k_7 [X]) (k_{10} k_{15} [X] + k_{14} k_{16} [H_2O])}$$

for excited M^* in the reaction zone.

The evidence on which the schemes (2, i) and (2, ii) are based is the following:

(*a*) The partial electron pressure, as measured by us, in an acetylene flame burning on tubes of various diameters over the pressure range 8 to 40 mm of mercury, is sensibly independent of pressure. I. R. KING[32] has made probe measurements of partial pressures of ions in propane–air flames burning from 100 mm of mercury to 1 atmosphere pressure, and came to a similar conclusion. It is not unreasonable to assume, then, that the partial electron pressure in acetylene–oxygen mixtures (at constant λ), too, is independent of pressure over the additional range 40 mm of mercury to 1 atmosphere, thus paralleling the behaviour[1] of the ratio Fe^*/Fe.

(*b*) P. F. KNEWSTUBB and T. M. SUGDEN[33], working on the ionization of various metal additives in the burnt gases of hydrogen and acetylene flames at atmospheric pressure, found that the electron level given by certain metals in acetylene flames was considerably greater, by a factor of up to 50-fold, than that expected from the Saha equation; but, owing to experimental difficulties, a detailed study was not undertaken. The work was taken up recently by Padley and Sugden[20], who, using well-shielded flames and an improved cavity technique with spatial resolution about 2 mm, were able to study the problem kinetically. They concluded that the electrons persisted into the burnt gases by virtue of the charge transfer reaction 12 [see scheme (2, ii)]. R^+, it was suggested, normally disappeared in the reaction zone by the bimolecular process 13, but, if a proportion of the positive charge becomes locked as M^+, then charge destruction will proceed by a much slower process. This was found to be kinetically of the second order, with the experimental velocity constant for recombination k being equal to $3{\cdot}0 \times 10^{-9}$ cm^3 sec^{-1} at about 2 350°K. These observations were shown to be

consistent with operation of the 'sticky' termolecular process 11 [see scheme (2, i)]. A possible explanation not then considered is one in terms of an 'inefficient' bimolecular process of the type 15 (the inefficiency being caused by the low proportion of MH_2O^+ and the large shielding effect of the surrounding H_2O molecules), postulated in scheme (2, ii). It was inferred, however, that water is involved in the recombination, although it was, unfortunately, not possible to determine what the precise state of the water was immediately after charge destruction.

(*c*) The above-mentioned work of Knewstubb and Sugden[33] lists the excess electron levels for a number of elements at a point above 3 msec after primary combustion in a typical, fuel-rich acetylene flame at 2 500°K. The number of metals examined was extended and the level of disequilibrium confirmed in the course of the work of Padley and Sugden[20] (e.g. with tests on lead, manganese, lithium, sodium, potassium and caesium).

If all these results are plotted as a function of ionization potential, the curve shown in *Figure* 5 is obtained. For metals with ionization

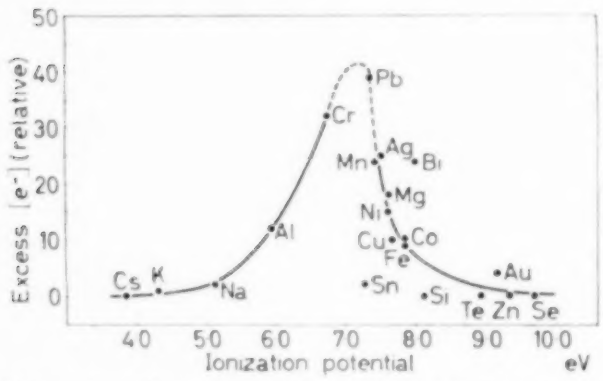

Figure 5. Measured electron concentrations/equilibrium concentrations for various metals in a fuel-rich acetylene–oxygen–nitrogen mixture at 2500°K (taken from Knewstubb and Sugden[33] and Padley and Sugden[20]) as a function of ionization potential of the metals

potential below about 5 eV, and also, apparently, for those above about 9 eV, the expected equilibrium concentrations of electrons are found. For metals of intermediate ionization potentials, however, the above-mentioned deviations occur. A fairly smooth curve can be drawn through the experimental points, reaching a maximum for metals with ionization potential near 7 eV. Although a rather fuel-rich flame ($\lambda = 0{\cdot}5$) was used in this study, it is possible that chromium (ionization potential = 6·74 eV) should be at the maximum of this curve, since no correction for (oxide) compound formation was made in the cases of chromium, tin, silicon, aluminium and zinc. The value of this evidence will be discussed shortly.

(*d*) The mobilities of univalent metal ions in flames under a constant impressed electric field are all the same, at least for the alkali metals[34]. For the divalent alkaline earths the mobilities are equal among themselves though smaller than those of the univalent alkali metals. This suggests that the ions become the nucleus of some kind of cluster. By analogy with the rather similar behaviour of metal ions in the aqueous phase[35], water might be suspected to fulfil such a role. Support for this idea is provided by the work of R. J. Munson and A. M. Tyndall[36] on the mobilities of the alkali ions in the rare gases containing various quantities of water vapour, who found that the mobility, and hence size, of the clustered ion for slow moving ions, was independent of the amount of water present. Simple ion–dipole calculations of the stability of such an arrangement (using a value of 1·8 D for water and reasonable ion–dipole distances), however, suggest a value of about 40 kcal/mole for a divalent ion, and only half this for a univalent ion. Although such a cluster, then, cannot be visualized as a stable unit at flame gas temperatures (for which its stability would have to be at least 70 kcal/mole[37]), it can be considered in terms of an increased probability of collision between M^+ and H_2O. This conclusion is in line with the early observation of J. A. McClelland[38] that the mobility of the ions decreases by about 10-fold in the cool regions, a considerable distance above the flame. Direct evidence for clustering of this type is provided by the mass-spectroscopic studies in flames, made by P. F. Knewstubb and T. M. Sugden[23, 39], in which metal ion (and even metal ion hydroxide) hydrates, sometimes involving several molecules of water, have been detected. The proportion of metal ions combined in this way is, however, small.

(*e*) F. W. HOFMANN and H. KOHN[40] have obtained direct evidence, from measurements of atom and ion emission spectra of barium, coupled with electron measurements, in flames, that the concentration of free Ba^+ is, in general, less than one per cent of the free electron concentration. They suggest that this result might be caused by formation of $BaOH^+$. How general this effect is will, of course, have to await future evidence, but it is interesting to note that this type of effect would be in line with operation of scheme (2, ii).

(*f*) It is very important to know what the efficiency of process 10 is, but unfortunately there appear to be very few data available on the cross sections for (discrete emission) radiative capture of an electron by a positive ion. Experimental and theoretical data assembled by H. S. W. MASSEY and E. H. S. BURHOP[29] for similar processes resulting in continuous emission suggest a cross section in the region 10^{-19} to 10^{-21} cm^2 for electrons with flame gas energies. Combination of this with the known electron–molecule collision frequency for acetylene–oxygen–nitrogen mixtures at 10 mm of mercury[27], i.e. $5{\cdot}0 \times 10^9$ sec^{-1} and the electron–flame gas molecule collision cross section[27] of average value 30×10^{-16} cm^2, leads to a value of k_{10} for the process 10 of about 10^{-11} to 10^{-12} cm^3/sec.

It is now possible to discuss schemes (2, i) and (2, ii) with reference to the evidence (a) to (f). Scheme (2, i) was proposed on the assumption that charge destruction proceeds according to process 11 [see evidence (b)]. Since $k_8 \lesssim k_7[X]$, and $k_{10} < k_{11}[X]$, then it can readily be seen that such a scheme, suggesting termolecular production of M^+, would be in accord with the known pressure independence of the partial pressures of M^* and e^-. The scheme does not, however, explain why the overexcitation is confined to the reaction zone. Moreover, $[M^+]$ in the reaction zone is estimated, from data quoted by Padley and Sugden[20], to be up to about 10^{-2} [M]. With the reaction zone at most about 100 μsec thick, such a proportion must be reached in probably less than 50 μsec, whereas calculations of $[M^+]$ from 9, making very generous assumptions about the concentrations of the species reacting with M, suggest that in 50 μsec only one M in 10^{-4} will be ionized. Thus scheme (2, i) can be considered highly unlikely.

Fewer such objections can be raised to scheme (2, ii). The expression for M^*/M, bearing in mind that, under flame gas conditions, $k_8 \lesssim k_7[X]$, and $k_{15}[X] > k_{16}[e^-]$, shows that M^*/M should be proportional to $[e^-]$ and should be independent of pressure, as observed. The extremely low mobility of the positive ion cluster arrangement (particularly noticeable in comparison with that for electrons[34] in flames) suggests that, once M^+ is formed (i.e. once the reaction zone is left), the metal ion might become to a large degree surrounded with H_2O molecules. Thus the probability of capture of an electron by M^+ would be considerably reduced: the anomaly could thus be effectively confined to the reaction zone. This evidence is, further, qualitatively in line with observation (e) and also the observation (b) that the overall processes 14 to 16 postulated for charge destruction are considered inefficient. This scheme would fail if such processes were predominantly termolecular.

The importance of *Figure 6* can now be assessed. With metal ions produced by the charge exchange reaction 12 (see Massey and Burhop[29] for many examples of process), this curve suggests that R^+ with which reaction 12 takes place has an average ionization potential in the region of 7 eV. This value is considerably lower than the ionization potentials measured for hydrocarbon molecules[41] (10 to 12 eV) but is of the same order of magnitude as the ionization potentials of hydrocarbon radicals. Thus, only those metals which produce the anomalously high electron concentration effect [see (b) and (c)] would show anomalous line-reversals. It is interesting to note, then, that of the metals so far examined[1, 42], tellurium, lead, iron and tin definitely do, whereas sodium definitely does not. An apparent exception is ^{43}Hg (ionization potential = 10·39 eV), but this may well be caused by charge-exchange with hydrocarbon molecule ions.

Having due regard for the arguments presented above, it seems that the weakest link in

scheme (2,ii) is reaction 10. If experiments should reveal k_{10} to be too small, then the scheme will fail. A value of 10^{-11} to 10^{-12} cm^3/sec [see (f)] was suggested for k_{10} on the basis of evidence from similar systems. Substitution of reasonable numbers into the expression for M*/M suggests a value of about 4×10^{-9} for this ratio at 20 mm of mercury, which would mean that lines with excitation energies greater than 80 kcal/mole in flames with thermal temperature 2000°K will be chemiluminescent in emission at this pressure. Values of reversal temperatures of iron lines quoted by Gaydon and Wolfhard[1] under comparable conditions suggest that, while this ratio is sufficient to account for the excitation of lines of high energies, above *ca.* 105 kcal/mole, at lower excitation energies it can be as much as 100-fold too small. Thus, for this scheme to operate, the efficiency of reaction 10 must be higher than the rather low value suggested in (f).

We would like to thank Dr Walter Gordy for his continued interest in this work, for generously making equipment available to us, and Dr T. M. Sugden, in whose laboratory and under whose guidance some of the work referred to in this paper was carried out.

References

[1] Gaydon, A. G. and Wolfhard, H. G. *Proc. Roy. Soc. A*, 1951, **205**, 118

[2] Wolfhard, H. G. and Parker, W. G. *Fifth Symposium (International) on Combustion*, p 718. Reinhold: New York, 1955

[3] Broida, H. P. and Schuler, K. E. *J. chem. Phys.* 1957, **27**, 933

[4] Padley, P. J. and Sugden, T. M. *Seventh Symposium (International) on Combustion*, p 235. Butterworths: London, 1959

[5] Gaydon, A. G. *The Spectroscopy of Flames*. Wiley: New York, 1957

[6] Gaydon, A. G. and Wolfhard, H. G. *Flames*, 2nd ed. Chapman and Hall: London, 1960

[7] King, I. R. *J. chem. Phys.* 1959, **31**, 855

[8] Padley, P. J. and Sugden, T. M. *Proc. Roy. Soc. A*, 1958, **248**, 248

[9] Bulewicz, E. M., James, C. G. and Sugden, T. M. *Proc. Roy. Soc. A*, 1956, **235**, 89

[10] James, C. G. and Sugden, T. M. *Proc. Roy. Soc. A*, 1958, **248**, 238

[11] Bulewicz, E. M. and Sugden, T. M. *Trans. Faraday Soc.* 1958, **54**, 1855

[12] Padley, P. J. *Trans. Faraday Soc.* 1960, **56**, 449

[13] Padley, P. J. and Sugden, T. M. *Trans. Faraday Soc.* 1959, **55**, 2054

[14] Padley, P. J. *Dissertation* (Cambridge, 1959)

[15] Padley, P. J. and Sugden, T. M. 1958. Unpublished work

[16] Padley, P. J. and Bulewicz, E. M. *Bull. Amer. phys. Soc.* 1961, Ser. II, **6**, 258

[17] Schuler, K. E. *Fifth Symposium (International) on Combustion*, p 56, Reinhold: New York, 1955

[18] Calcote, H. F. and King, I. R. *Fifth Symposium (International) on Combustion*, p 429. Reinhold: New York, 1955

[19] Schuler, K. E. and Weber, J. J. *J. chem. Phys.* 1954, **22**, 491

[20] Padley, P. J. and Sugden, T. M. *Eighth Symposium (International) on Combustion*, 1960. In press

[21] Deckers, J. and van Tiggelen, A. *Seventh Symposium (International) on Combustion*, p 254. Butterworths: London, 1959

[22] Knewstubb, P. F. and Sugden, T. M. *Seventh Symposium (International) on Combustion*, p 247. Butterworths: London, 1959

[23] Knewstubb, P. F. and Sugden, T. M. *Proc. Roy. Soc. A*, 1960, **255**, 520

[24] de Jaegere, S., Deckers, J. and van Tiggelen, A. *Eighth Symposium (International) on Combustion*, 1960. In press

[25] Calcote, H. F. *Combustion & Flame*, 1957, **1**, 385

[26] Schneider, J. and Hofmann, F. W. *Phys. Rev.* 1959, **116**, 244

[27] Bulewicz, E. M. *J. chem. Phys.* 1961. In press

[28] Bulewicz, E. M. and Padley, P. J. *J. chem. Phys.* 1961. In press

[29] Massey, H. S. W. and Burhop, E. H. S. *Electronic and Ionic Impact Phenomena*. Clarendon Press: Oxford, 1952

[30] Laidler, K. J. *Chemical Kinetics of Excited States*. Clarendon Press: Oxford, 1955

[31] Mitchell, A. C. G. and Zemansky, M. W. *Resonance Radiation and Excited Atoms*. Cambridge University Press: London, 1934

[32] King, I. R. *J. chem. Phys.* 1958, **29**, 681

[33] Knewstubb, P. F. and Sugden, T. M. *Research Correspondence*, 1956, **9**, A1

[34] Thomson, J. J. and Thomson, G. P. *Conduction of Electricity Through Gases*. Cambridge University Press: London, 1928

[35] Bernal, J. and Fowler, R. H. *J. chem. Phys.* 1933, **1**, 515

[36] Munson, R. J. and Tyndall, A. M. *Proc. Roy. Soc. A*, 1939, **172**, 28

[37] Sugden, T. M. *Trans. Faraday Soc.* 1956, **52**, 1465

[38] McClelland, J. A. *Phil. Mag.* 1898, **46**, 29

[39] Knewstubb, P. F. and Sugden, T. M. Unpublished data

[40] Hofmann, F. W. and Kohn, H. *J. opt. Soc. Amer.* 1961. In press

[41] Price, W. C., Bralsford, R., Harris, P. V. and Ridley, R. G. *Spectrochim. Acta*, 1958, **14**, 45

[42] Alekseeva, V. G. and Mandelshtam, S. L. *J. exp. theor. Phys., Moscow*, 1947, **17**, 759

[43] Broida, H. P. *J. chem. Phys.* 1951, **19**, 1383

A Measurement of the Temperature of Some Frictional Sparks

D. RAE

Safety in Mines Research Establishment, Ministry of Power, Buxton

(Received May 1961)

Two photocells of different cathode characteristics can be used to measure the temperature of small fragments of metals burning at T°K with maximum sensitivity provided that the reciprocals of the effective wavelengths of the cells differ by $2T/C_2$, where C_2 is the second radiation constant. Pyrophor bar and titanium particles large enough to ignite methane–air burn at about 3000°K and end explosively; magnesium particles large enough to ignite methane–air are estimated to burn at 4000°K and do not explode.

Introduction

IMPACT and friction between two bodies can produce heated fragments which are ejected from the point of impact or contact. The temperature of a frictional fragment at any time will depend on the heat given to it by friction at its formation and by subsequent chemical reactions, as well as the loss of heat to its surroundings. If the heated fragment is visibly hot it is called a frictional spark. This paper describes work carried out as part of a research programme on the ignition of methane–air mixtures by frictional sparks, and is concerned with a method of measuring the temperature of some sparks which are known to be capable of igniting these mixtures.

The only way that the temperature of a frictional spark can be conveniently measured is by the characteristics of the light emitted from it, if these are sufficiently well known; any other method is impracticable. If it is assumed that the energy radiated arises only from a heated black-body at temperature T°K then Planck's law gives the energy emitted at wavelength λ as

$$E_\lambda = AC_1\lambda^{-5}/[\exp(C_2/\lambda T) - 1] \quad \text{ergs sec}^{-1}\,\text{cm}^{-1}\,\text{steradian}^{-1} \qquad \ldots [1]$$

for an emitter area of A, at wavelength interval 1 cm, and where C_1 and C_2 are the first and second radiation constants. However, for bodies other than black-bodies only a proportion, the emissivity ε, of this energy is transmitted from the surface. In practice ε and its variation with wavelength and temperature are not usually well known, and this limits the accuracy in measuring the temperature. The intensity of radiation emitted at any wavelength is proportional to the area of the emitter, but this area is not known for a frictional spark, and it may vary with time. However, it is apparent from equation 1 that the ratio of the intensities at two wavelengths is a function of temperature independent of the area of the emitter: this is the basis of the two-colour spectral radiation pyrometer that was initially conceived to minimize the effect of ε in brightness pyrometers.

A two-colour method, with wavelengths in the red and green, was first used by H. C. HOTTEL and P. F. BROUGHTON[1] for measuring the temperature of luminous flames; G. MONNOT[2] used similar wavelengths for flame temperatures. E. C. PYATT[3] examined the errors arising from inaccurate estimation of ε. H. HERNE[4] recommended that wide band-widths should be used for each colour, which should be near to each other and at such wavelengths as to give a large signal to noise ratio.

This paper is concerned with the measurement of temperatures of particles which have been heated by combustion to about 2 500°K, and whose total life is only a few milliseconds. The radiation has then a maximum intensity at about 1·2 μ and it must be measured with a

time resolution of about 0·1 msec: vacuum photocells are therefore suitable receivers, although they do not respond to wavelengths above about 1·2 μ. The system of measurement is two photocells of different cathode characteristics acting as two wide-band receivers.

Design of Instrument

For the wavelengths and temperatures given above $\exp(C_2/\lambda T) \gg 1$ so that Wien's approximation to Planck's formula can be used. Hence the energy emitted at wavelength λ in the small interval $\Delta\lambda$ for a body of area A and emissivity $\varepsilon_{\lambda,T}$ at wavelength λ and temperature T, will be

$$\Delta E_\lambda = A\varepsilon_{\lambda,T} C_1 \lambda^{-5} \exp(-C_2/\lambda T)\,\Delta\lambda \text{ ergs sec}^{-1} \text{ steradian}^{-1} \quad \ldots [2]$$

If the receiver subtends a solid angle α at the (small) emitter and gives K_λ amperes per erg sec^{-1} of radiant energy received at wavelength λ then the measured current response for one photocell will be

$$I = \alpha A \int K_\lambda \varepsilon_{\lambda,T} C_1 \lambda^{-5} \exp(-C_2/\lambda T)\,d\lambda \text{ amperes} \quad \ldots [3]$$

where the limits of integration are the limits of response of the photocell, and where these limits are such that Wien's approximation is still valid. The area A is the same for two detectors provided that they see the same aspect of the spark. H. Herne[4] assumes that $K_\lambda\varepsilon_{\lambda,T}$ is constant over two wide wavelength ranges and calculates I_2/I_1.

However, if it is assumed that the wavebands are very narrow ($\Delta\lambda_1$ and $\Delta\lambda_2$) and lie about the wavelengths λ_1 and λ_2, which are reasonably close together (so that although $\varepsilon_{\lambda,T}$ may take any value between 0 and 1 it does not change much with λ or T) then the response ratio R is given by

$$R = \frac{I_{\lambda 2}}{I_{\lambda 1}} = \frac{\alpha_2}{\alpha_1}\frac{K_{\lambda 2}}{K_{\lambda 1}}\left(\frac{\lambda_2}{\lambda_1}\right)^{-5} \exp(-C_2/\lambda_0 T)\,\frac{\Delta\lambda_2}{\Delta\lambda_1} \quad \ldots [4]$$

where

$$1/\lambda_0 = 1/\lambda_2 - 1/\lambda_1$$

The sensitivity S can be defined as $\partial R/\partial T$: hence

$$S \propto \frac{C_2}{\lambda_0 T^2}\exp(-C_2/\lambda_0 T) \quad \ldots [5]$$

which has a maximum at $1/\lambda_0 = 2T/C_2$.

The response currents of two photocells (types VS39 and VB39, Cinema-Television Ltd) were calculated at a number of temperatures for a tungsten emitter, taking the emissivity published by J. C. de Vos[5] and the photocell response curve published by the makers. Each cell obeyed very closely the relationship

$$I = C\exp(-C_2/\lambda_e T) \quad \ldots [6]$$

where λ_e, the effective wavelength, was 0·88 μ for type VS39 and 0·59 μ for type VB39 photocell. Thus, the photocells considered behaved as if they were narrow-band receivers of wavelengths λ_e, and therefore maximum sensitivity is obtained at a temperature T given by $1/\lambda_{e_2} - 1/\lambda_{e_1} = 2T/C_2$. This temperature is about 4 000°K, and the sensitivity falls to half the maximum at about 2 000°K and 10 000°K; the combination is therefore satisfactory for determining temperatures around 2 500°K.

For temperatures lower than 2 000°K maximum sensitivity might be obtained by using filters or other means to change the effective wavelengths of the photocells.

It was deduced, from the errors involved, that a measurement could be made to within about $\pm 100°$ at 2 500°K if the photocells were calibrated for R against the true temperature of a tungsten filament: this was sufficiently accurate.

The emitting area A may change during the lifetime of a frictional spark: such a change may be detected by comparing I_1, I_2, and their ratio. From equations 3 and 6, it can be seen that C is proportional to A if $\varepsilon_{\lambda,T}$ remains constant. Thus

$$\left.\begin{aligned} I_1 &= k_1 A\exp(-C_2/\lambda_{e_1}T) \\ \text{and} \quad I_2 &= k_2 A\exp(-C_2/\lambda_{e_2}T) \end{aligned}\right\} \quad \ldots [7]$$

T is found from I_2/I_1, and can be used in equation 7 to investigate changes in A. An increase in I_1 and I_2 without any change in I_2/I_1 means an increase in A only, such as happens, for example, when a spark bursts into a number of fragments. A change in I_1 and I_2

when I_2/I_1 also changes means a change of temperature; whether A has also changed can be inferred by comparing the observed changes in I_1 and I_2 with those calculated from the measured temperatures.

Apparatus and Its Calibration

The currents I_1, I_2 produced by the two photocells were measured and recorded by amplifying the voltages produced by them across load resistors, and displaying the amplified voltages simultaneously on a two-gun cathode ray oscilloscope supplied with a time base and a camera. The circuit is shown in *Figure 1*. Potentiometers side, with only a thin metal earthed screen between them.

The oscilloscope recording the currents produced by a spark was triggered by the input signal, with the cathode ray spot suppressed. The initial small fraction of the voltage rise of the signal started the time base, and caused the spot to brighten: at the conclusion of the signal the trigger circuit was set to operate from the external voltage produced on closing switch S_1, and a zero baseline was superimposed on the photograph of the spark signal.

The displacement on the photograph was calibrated in terms of voltage by discharging a

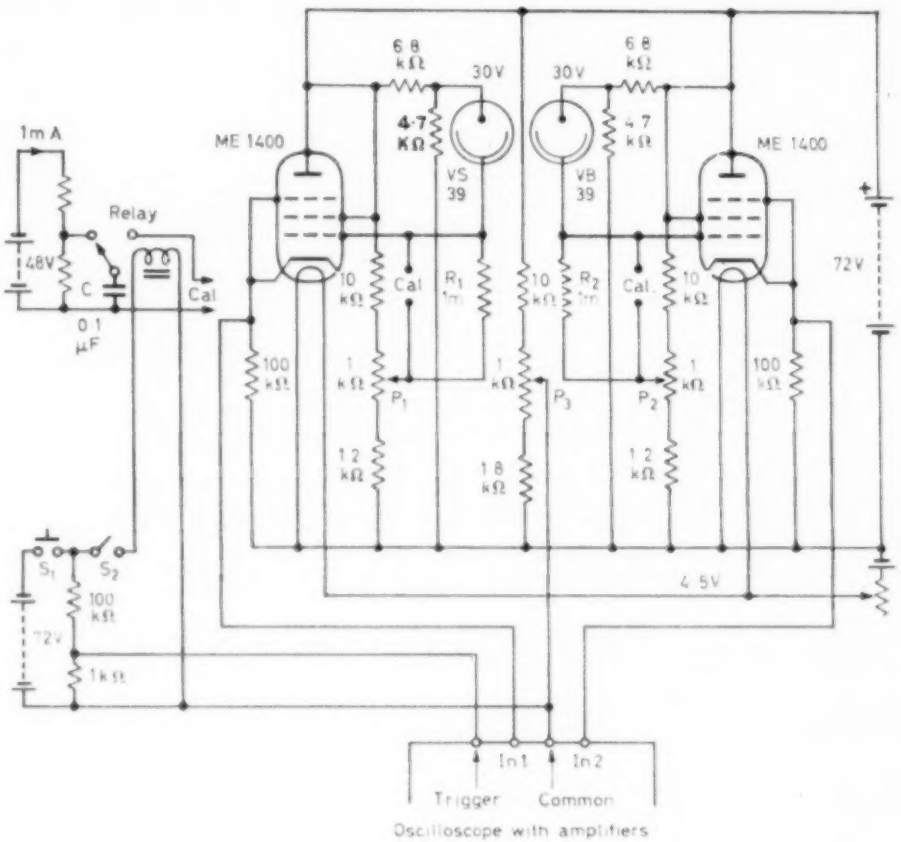

Figure 1. Photocell circuit diagram

P_1, P_2 and P_3 enable the d.c. levels of the outputs to be set at zero with respect to the amplifier inputs. The spark or tungsten strip filament calibration lamp (Mazda projector lamp type F/47) was placed 200 cm from the photocells, which were 4·2 cm diameter and placed side by

condenser, charged to a known potential similar to that produced by the spark, across the load resistors of the photocells. The resultant voltage step was arranged to come near the centre of the oscilloscope trace by introducing a delay between the time base trigger impulse and the

switching of the condenser: this delay was the delay in operation of a relay which would operate only if switch S_2 were closed. If a condenser voltage V_1 applied across the photocell load resistor R_1 gave a deflection y_1 cm on the photograph for one cell circuit, and a voltage V_2 across the load R_2 gave a deflection y_2 cm for the other circuit, and if the displacements for the spark were Y_1 and Y_2 cm, then assuming the gain of the amplifiers remained the same in the short interval between measurements

$$R = \frac{I_2}{I_1} = \frac{R_1}{R_2}\,\frac{Y_2}{Y_1}\,\frac{y_1}{y_2}\,\frac{V_2}{V_1} \qquad \ldots\ldots [8]$$

To calibrate the ratio R against temperature, the same procedure was carried out, using as the source periodically interrupted light from the centre of the filament of a tungsten lamp whose brightness temperature was measured by a disappearing filament pyrometer. If, at temperature T, the pulse of light gave deflections D_1 and D_2 cm on the photographs and the calibration voltages V_1^1 and V_2^1 gave signals y_1^1 and y_2^1 cm, then

$$R_1 = \frac{R_1}{R_2}\,\frac{D_2}{D_1}\,\frac{y_1^1}{y_2^1}\,\frac{V_2^1}{V_1^1} \qquad \ldots\ldots [9]$$

Hence a value of $Y_2y_1V_2/Y_1y_2V_1$ for a spark can be given a temperature by comparing it with the set of $D_2y_1^1V_2^1/D_1y_2^1V_1^1$ values. Brightness temperatures for tungsten are converted to true temperatures using the data given by J. C. DE VOS[5]. The linear relationship between the deflection and the intensity of light falling on the photocells was demonstrated by showing that the deflection was inversely proportional to the square of the distance of a constant light source from the photocells.

Table 1 shows the result of the calibration for seven temperatures, with repeat readings. If $\log I_1R_1/I_2R_2$ is plotted against $1/T$ the points lie close to the straight line

$$\log \frac{I_1R_1}{I_2R_2} = 1{\cdot}126 - 0{\cdot}317\,\frac{(10^4)}{(T)} \qquad \ldots\ldots [10]$$

Values of T calculated from this relation are given in the final column for the values of I_1R_1 and I_2R_2 given in *Table 1*. Since the errors are only about $\pm 90^\circ$K, equation 10 gives a reasonable representation of the calibration.

Table 1

Temperature, °K Brightness (pyrometer)	Temperature, °K True (converted)	Voltage, mV across cell loads I_1R_1	Voltage, mV across cell loads I_2R_2	$\log \frac{I_1R_1}{I_2R_2}$	Temperature, °K (from eq. 10)
2 130	2 340	122	212	$\bar{1}{\cdot}760$	2 320
2 130	2 340	123	203	$\bar{1}{\cdot}783$	2 360
2 230	2 460	207	300	$\bar{1}{\cdot}838$	2 460
2 250	2 480	229	321	$\bar{1}{\cdot}853$	2 490
2 340	2 600	373	469	$\bar{1}{\cdot}901$	2 590
2 340	2 600	369	458	$\bar{1}{\cdot}906$	2 600
2 420	2 700	573	646	$\bar{1}{\cdot}948$	2 690
2 430	2 710	563	634	$\bar{1}{\cdot}949$	2 700
2 520	2 820	850	866	$\bar{1}{\cdot}991$	2 790
2 520	2 820	855	832	0·012	2 850
2 620	2 950	1 350	1 180	0·058	2 970
2 620	2 950	1 300	1 155	0·051	2 950
2 760	3 130	2 510	1 870	0·128	3 180
2 770	3 150	2 450	1 920	0·106	3 110

From equations 9 and 4, $1/\lambda_0 = 0{\cdot}51 \times 10^4$ cm^{-1} which compares reasonably with the value $0{\cdot}56 \times 10^4$ cm^{-1} expected from the values of $\lambda_{e_1} = 0{\cdot}88\,\mu$ and $\lambda_{e_2} = 0{\cdot}59\,\mu$ calculated from the makers' response curves.

Methods of Producing Sparks

The sparks of interest here are only those that are produced as small burning fragments from friction or impact. Pyrophor bar (e.g. cigarette lighter 'flint') produced this type of spark, and D. RAE[6] has shown that its behaviour as a friction spark can be simulated by heating small fragments on an electrically heated thin wire support. Light alloys based on magnesium, aluminium or titanium when struck obliquely against rusted steel give sparking which D. RAE has shown is a result both of the thermite reaction and of burning metal which the heat of this reaction ignites. With magnesium and aluminium alloys this sparking is mainly a white flash, presumably from a cloud of burning vaporized metal, throughout which the temperature is unlikely to be uniform

the method of temperature measurement described in this paper cannot therefore be applied to their sparks. With titanium, however, a blow can be delivered that produces only one spark moving relatively slowly through the air. When titanium fragments are ignited on a heated wire, sparks are formed in which the fragment appears to break up into a number of projected particles in the same way as pyrophor bar, but with many fewer particles. However, when magnesium fragments are ignited on a heated wire support only about 1 μg is needed to ignite methane so that the cloud of burning vaporized metal is small enough to be considered as having an even temperature. Aluminium cannot be ignited on thin wires unless these are so hot that they would contribute noticeably to the light energy.

Temperature determinations were therefore made of fragments of burning pyrophor (about 100 μg), magnesium (about 1 μg) and titanium (about 10 μg), and of the sparks from the impact of titanium against rusted steel.

Spark Temperature Measurement

Pyrophor particles

The oscillogram is shown in *Figure 2*(a); it appears to consist of a varying background level on which sharp peaks are superimposed. *Table 2* shows representative values of the temperature, calculated from equation 10 by means of the voltage ratio shown. The location

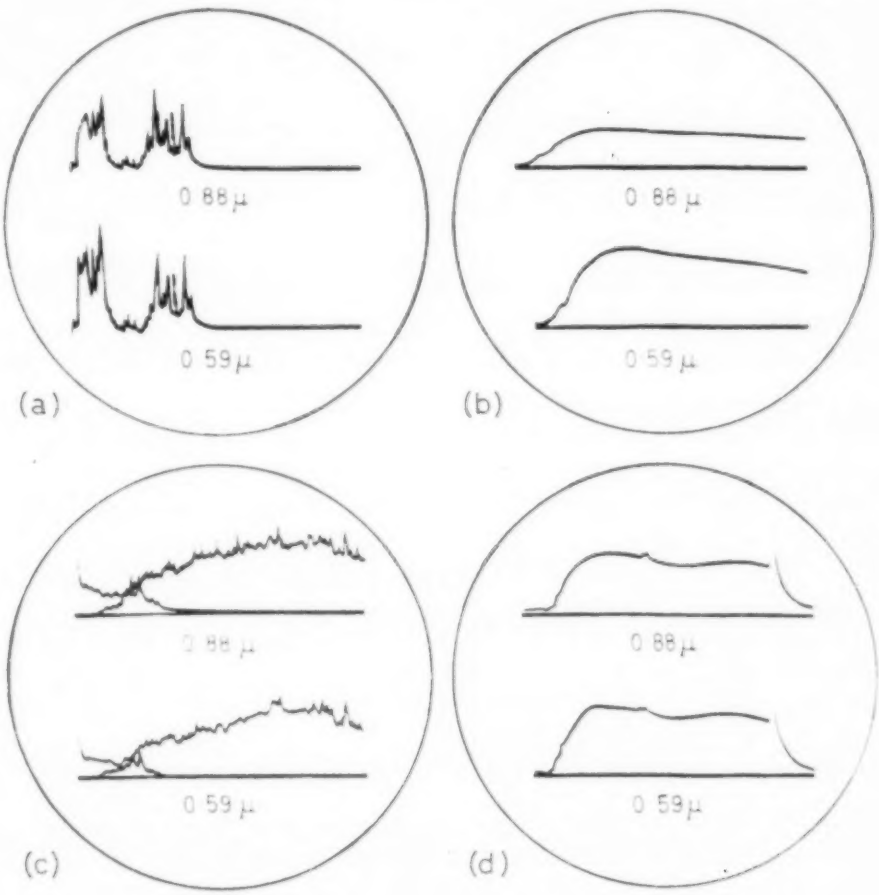

Figure 2. Oscilloscope records of photocell currents at equivalent wavelengths 0·88μ and 0·59μ (traced from the originals)

(a) *Pyrophor bar burning on hot wire at 400 mV/cm*
(b) *Magnesium burning on hot wire at 70 mV/cm*
(c) *Titanium burning on hot wire at 400 mV/cm*
(d) *Titanium on rust impact spark at 400 mV/cm*
Time base 0·1 sec: 2·3 cm long

is measured on the top trace, with its start as origin.

Table 2. Temperature of burning pyrophor bar particles

Feature	Location X mm	Location Y mm	Voltage ratio	Deduced temperature °K
Background, high level	1·03	4·45	1·11	2 940
Background, low level	9·15	1·83	0·74	2 530
Thin peak, height above background	9·78	2·20	1·00	2 810
Background for this peak	—	4·20	0·91	2 710
Thin peak at low level	5·32	1·15	0·87	2 670

The thin peaks are due to the explosive terminations of separate particle tracks which appear on photographs as substantial increases in emitter areas (see D. RAE[6]); they must, therefore, be considered as superimposed on the background, and the temperature of the phenomenon causing one of them must be, from *Table 2*, 2 810°K. The area of the single particle on explosion at 2 810°K is about 0·4 of the total area of the background at 2 710°K; this is calculated from equation 7 and the relative displacements on the record with $\lambda_r = 0{\cdot}88\,\mu$. This calculation therefore confirms the deduction from the photographs, namely, that a sudden increase in emitter area is produced by the explosion of the particles. No satisfactory reason for the explosive termination of sparks of this, or other, material is known. The experiments also show that the particles burn at temperatures up to about 2 950 ± 100°K. Records from other fragments confirm these temperatures.

Magnesium particles

A typical record from a burning magnesium particle ignited on a hot wire is shown in *Figure 2*(b). With the voltage ratios obtained equation 10 gives a burning temperature of about 4 000°K; this is well beyond the calibration range so that extrapolation is necessary and the errors are therefore increased. Representative maximum temperatures were 4 140, 4 200 and 3 950°K from three records. The measured voltage ratio varied very little as the amplitudes of the traces diminished, indicating a steady burning temperature and a steadily diminishing area of emitter as the material was consumed, presumably as vapour according to K. P. COFFIN[8], since magnesium boils at 1 370°K. There was no indication of a break-up into separate particles or of any explosive termination.

Titanium particles

A typical record of the combustion of a titanium particle is shown in *Figure 2*(c). The voltage ratio was determined at intervals for the background, ignoring the sharp peaks, and the temperatures calculated are given in *Table 3*. As the fragments burned they produced a number of small particles that ended explosively, as happens with pyrophor bar: the sharp peaks were, however, less pronounced. The background behaved in much the same way as for magnesium, although the temperature variations were relatively greater. *Table 3* shows that the burning temperature rose to about 2 800°K, but there were variations of ±200°K between similar fragments. Thus the burning temperature of these particles fell between the melting point of titanium, 2 070°K, and its boiling point, 3 270°K.

Table 3. Temperature of a burning titanium particle

	Before fly-back						After	
Distance along trace, mm	4	8	12	16	20	24	2	6
Temperature, °K	2 580	2 720	2 640	2 720	2 790	2 670	2 500	2 360

Titanium 'thermite' sparks

The record for a single spark from the impact of a solid block of titanium on a rusted steel target is shown in *Figure 2*(d). These sparks show marked constancy both in temperature and amplitude over most of their life, which ends explosively. For the example shown the temperature in the interval between 4 mm and 16 mm, at which point the explosion occurred

was calculated to be within 40° of 3 000°K. Other sparks gave maximum temperatures within this range. Since temperature and amplitude remain constant, it must be concluded that the size of the spark remains constant until the explosion occurs.

It appears likely that the sparks from impact behave as much larger but only slightly hotter versions of the single small particles produced from the fragments ignited on a heated wire. The role of the thermite reaction therefore seems to be to start a large fragment of titanium burning in air.

The figures are Crown Copyright and are reproduced by permission.

References

[1] HOTTEL, H. C. and BROUGHTON, P. F. *Industr. Engng Chem. (Anal.)*, 1932, **4**, 166
[2] MONNOT, G. *Rev. Inst. franc. Petrole*, 1954, **9**
[3] PYATT, E. C. *Brit. J. appl. Phys.* 1954 **5**, 264
[4] HERNE, H. *Brit. J. appl. Phys.* 1953, **4**, 374
[5] DE VOS, J. C. *Physica, 's Grav.* 1954, **20**, 690
[6] RAE, D. *Saf.i.-Mines Res. Rep. No.* 129, 1956
[7] RAE, D. *Saf.-i.-Mines Res. Rep. No. 177*, 1959
[8] COFFIN, K. P. *Tech. Note Nat. Adv. Comm. Aero., Wash., No. 3332*, 1954

Infra-red Analysis for Acetylene in Flame Gases at 1820°K

R. C. MILLIKAN

General Electric Research Laboratory, Schenectady, N.Y.

(*Received May 1961*)

A method of analysing flame gases for acetylene utilizing the peak absorption at 730 cm^{-1} is described. Five rich ethylene–air flames yielding burnt gases at 1820°K with between 0·012 and 0·0028 mole fraction acetylene were used as standards. The acetylene content of the gases was determined by mass analysis of probe samples. After subtraction of background absorption by water vapour and carbon dioxide, the 730 cm^{-1} absorption by the flames was found to be proportional to their acetylene content. The peak 730 cm^{-1} molecular absorption coefficients of acetylene at 1820°K for spectral passbands of 2·3 and 0·7 cm^{-1} are 5·8 ± 0·3 and 7·7 ± 0·7 respectively in units of 10^{-19} cm^2 molecules^{-1}. The effect of temperature on the absorption coefficient has been obtained approximately from similar measurements at 300°K. For a 2·3 cm^{-1}, passband, the absorption coefficient at 300°K is about 7·5 times that at 1820°K. For a 10 cm optical path in the flame, acetylene can be determined by this method when it forms 0·02 volume per cent or more of the burnt gas.

Introduction

ACETYLENE, formed in the reaction zone of rich hydrocarbon flames, is intimately connected with the deposition of soot. In a study of soot formation, a way was needed to analyse quantitatively for acetylene without disturbing the flame. Such flame gas analyses can often be made by extracting samples with a probe. Where that technique is possible, it is both powerful and versatile. Optical methods, however, have several advantages. They disturb the flame less; they measure the species *in situ*; and they can be used for sooty flames which would clog a sampling orifice. In this paper a method for determining acetylene in high temperature flame gases is described which is based on the infra-red (i.r.) absorption of acetylene at 730 cm^{-1} (13·7 μ). The required high temperature absorption coefficients have been determined experimentally by measuring the 730 cm^{-1} absorption of burnt gases containing acetylene using a large flat flame. The compositions of the gases were determined by mass analysis of probe samples. The effects of temperature and spectral resolution on the observed absorption coefficients have been determined, so that the i.r. method of analysis can be extended to cases where probe sampling might be difficult or unreliable.

The 730 cm^{-1} band of acetylene has been observed previously in flames by D. J. COLE and G. J. MINKOFF[1]. The lack of high temperature absorption coefficients, however, prevented them from doing more than observing qualitatively how the acetylene varied with flame conditions. The i.r. emission of acetylene in propellant flames has also been reported by H. A. BENT and B. CRAWFORD Jr[2], although there was interference from hydrocyanic acid in this case.

Experimental

(a) *Burner and gas supply*

The construction of the burner was similar to that described by W. E. KASKAN[3]. Briefly it consisted of a 7 cm diameter porous bronze plate sintered to a plug of copper shot containing a water cooling coil. Surrounding this central burner was an annulus 1·5 cm wide made of sintered copper shot. In operation, the combustible mixture, which was fed to the central chamber, issued from the bronze plate at a very nearly uniform linear velocity of about 11 cm/sec. This is less than the normal

burning velocity of the mixture. The flame, when ignited, propagated to the burner surface, and stabilized in close proximity to it as a steady, flat, uniform flame with flow normal to the flame. A flow of nitrogen gas was maintained through the annulus of the burner to prevent the formation of a diffusion flame between the hot gases and the atmosphere. A wire screen was placed one inch above the burner surface to impede the upward flow of hot gases and make the flow stable. It also served to make the gas column more nearly cylindrical rather than conical.

Ethylene was obtained from a cylinder, and was CP grade. Air was supplied by a 2 000 lb/in² house compressor. Both gases were metered to within 0·5 per cent with critical flow orifices.

(b) *Flames*

The rich ethylene–air flames used for determining the high temperature absorption coefficients of acetylene are characterized in *Table 1*.

Table 1. Flames used for high temperature absorption coefficient determination

Flame No.	*Vol. ratio ethylene/air*	ϕ	v_{25} *cm/sec*	$T^{\bullet}$ °K
1	0·121	1·73	11·5	1820
2	0·127	1·82	11·6	1820
3	0·134	1·92	11·7	1820
4	0·141	2·02	11·7	1815
5	0·149	2·13	11·8	1810

•12 mm above burner.

Noted there for each flame is the volumetric fuel-to-air ratio, the equivalence ratio ϕ, which is the actual fuel/air ratio divided by 0·0[illegible]8, the stoichiometric fuel/air ratio, the linear gas velocity entering the flame v_{25}, and the burnt gas temperature measured by sodium line reversal as previously described[4]. The temperature measurements are ±20°K.

(c) *Optical arrangement*

Flame absorption measurements were made with the optical arrangement shown in *Figure 1*. The source was a block of Norton stabilized zirconia whose front surface was heated by impinging upon it an approximately stoichiometric hydrogen–oxygen flame. The surface temperature of the zirconia was near 2 790°K, as determined by a pyrometer and using 0·43 for the spectral emissivity at 6 500 Å. The emissivity remains relatively high in the infrared, and the output of this source at 730 cm⁻¹ was found to be about twice that of a globar. For absorption measurements, the light chopper was located as shown between the source and the flame. Light emitted by the flame was not modulated, and did not contribute to the output of the a.c. amplifier. Emission of the flame gases was studied early in the investigation with the light chopper located between the flame and spectrometer.

The spectrometer was mounted on a vertical plate so as to make the image of the entrance slit horizontal above the burner. It was equipped with a potassium bromide foreprism, and a 75 line/mm grating blazed at 12 μ in the first order. The linear dispersion at the exit slit was computed to be 23·3 mm/micron. Thus, for 1 mm slits, the spectral slit width should be

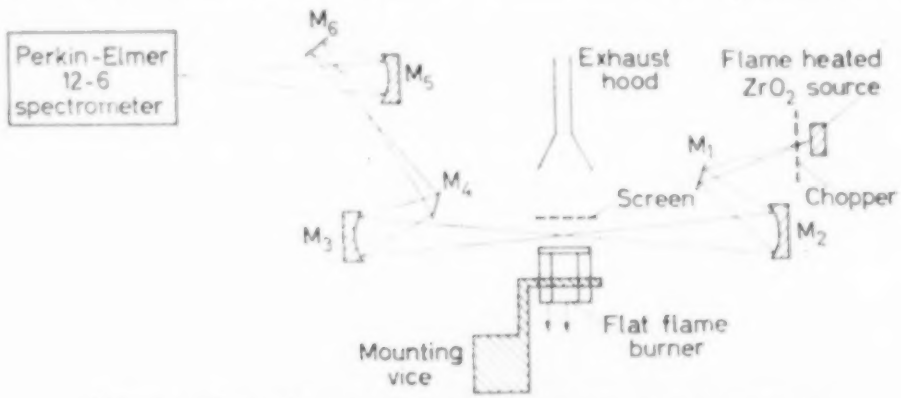

Figure 1. Optical arrangement for flame absorption measurements

2·33 cm^{-1}. This is in rough agreement with $\Delta\nu_{1/2} = 2{\cdot}9\ cm^{-1}$ measured for the room temperature Q branch absorption of acetylene at 29 cm^{-1}. The natural width of this band is much narrower, so that it serves to measure the slit function. The spectral passbands for other slit widths quoted hereafter have been computed from the given linear dispersion neglecting diffraction effects. They do not become important even for the narrowest slits used here.

(3) *Probe sampling and analysis*

Burnt gas samples were taken for analysis by sucking them through a fine quartz orifice and collecting the gases in a sample bottle at about 1 mm mercury pressure. A mass spectrometer was then used to analyse the gases.

Results

If the methods of sampling and analysing the burnt gases are to give the true composition in the flame, several conditions must be satisfied. First, the gas composition must not be changing rapidly with distance above the burner. This is necessary because the vertical divergence of the light beam across the burner was about 2 mm; the optical measurement averaged over this distance. Also, the probe cools the gases for an undetermined distance in front of it, resulting in some uncertainty in where it effectively takes its sample. Secondly, the probe must quench the sample quickly enough to prevent subsequent chemical reactions from changing the composition.

That the gas composition was approximately constant in the sampling region has been demonstrated in several ways. Temperature measurements were made as a function of distance on one of these flames[4]. It was found that beyond 6 mm from the burner the gas temperature dropped 80° ± 15°K per cm. The computed rate of temperature fall due to gas radiation was 85° ± 15°K per cm. The agreement between these rates is evidence that the gases were in thermal equilibrium. The concentration of OH radicals has also been measured as a function of distance using the u.v. line absorption method of W. E. KASKAN[5]. It was found that a large concentration of OH was produced in the reaction zone, but that this quickly dropped toward the equilibrium value as one proceeded away from the flame. The OH radicals were observed to be equilibrated with the burnt gas at distances greater than 5 mm from the burner. The species which are not in chemical equilibrium are the hydrocarbons, particularly acetylene and methane, which are produced in the reaction zone of the flame. These make up one per cent or less of the burnt gas, as will be shown later. Yet it was the acetylene we wished to measure, so the rate at which it disappeared was most important. This was determined early in the study using emission techniques.

In *Figure 2* are shown the i.r. emission of: (*1*) a hydrogen–oxygen flame, (*2*) an ethylene–oxygen flame showing the acetylene emission

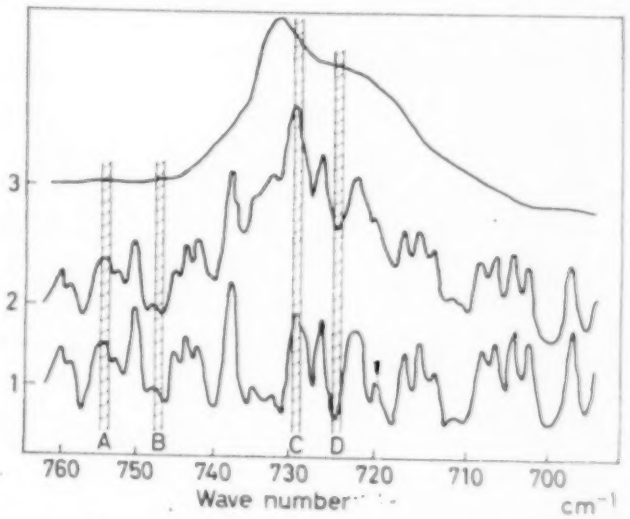

Figure 2. Infra-red flame emission. (1) Hydrogen–oxygen flame, 1 in. path. (2) Ethylene–oxygen flame, 4 in. path (3) Acetylene emission from an ethylene–oxygen flame with water emission subtracted out. A, B, C and D denote frequencies used for estimation of acetylene

added to the water emission, and (*3*) the acetylene emission observed when the water emission was subtracted out. From this figure it is evident that some care must be taken in accounting for the water emission. Initially this was done in two ways. The emission intensity at C minus that at A was used as one measure of acetylene. Alternatively D – B gave a second measure of the acetylene emission. The results of such measurements are given in *Figure 3*

where the acetylene emission for a representative flame is plotted against distance from the burner. The proportionality factors relating the emission intensity to the acetylene concentration were unknown at this stage, so the two sets of

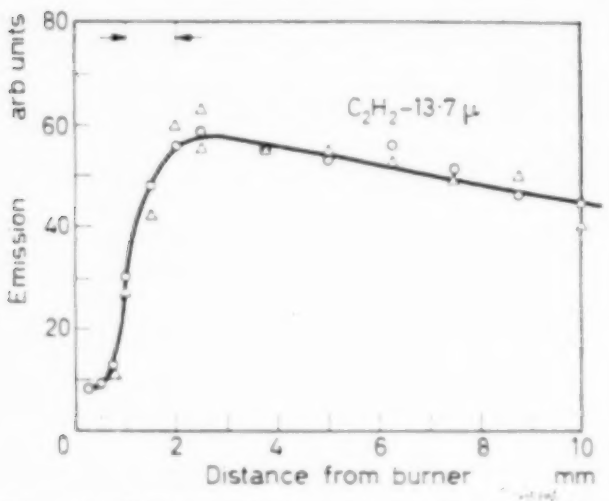

Figure 3. Emission of a 10 cm/sec ethylene–air flame of equivalence ratio 1·75 against distance from the burner. ○ Acetylene emission determined from C—A (see Figure 2). △ Acetylene emission from D—B multiplied by 2·5. Spatial resolution of light beam over the burner is indicated at the top

measurements were normalized at one point. It is seen that the two ways of accounting for the background water emission lead to the same distance profile for the acetylene emission. It is also clear that the amount of acetylene in the burnt gas is not changing very rapidly with distance. That the acetylene concentration remains nearly constant under these conditions is in agreement with the rate of oxidation of acetylene found by C. P. FENIMORE[6].

The optical absorption and probe sampling measurements were all made at a level 12 mm above the burner. It has been shown that neither the temperature nor the chemical composition of the gases were changing appreciably within 2 mm of this level. Thus this should be a favourable case for calibrating optical measurements by means of probe samples. The conclusion that the burnt gases are at chemical and thermal equilibrium, excepting of course the small amounts of acetylene, methane and soot, makes it valuable to check the gas composition determined from the probe samples against that calculated for equilibrium. In *Table 2* the analyses for three constituents of the burnt gases are given as ratios with respect to argon, which was used as an internal standard. The equilibrium composition of burnt gases from ethylene–air flames have been given as functions of temperature, pressure, and equivalence ratio by H. A. FREMONT *et al.*[7]. In order to compare the measured compositions with those tabulated in their tables, the unburnt hydrocarbons shown in columns 3 and 4 of *Table 2* must be accounted for. This has been done in the following approximate manner. It was assumed that each C_2H_2 molecule and every two CH_4 molecules which are found in the burnt gases detract from the nominal fuel/air ratio as if they were ethylene molecules. Thus from the equivalence ratio of the gases fed to the burner (column 3, *Table 1*) we subtract an amount related to the experimental methane and acetylene concentrations given in *Table 2*, to obtain an effective equivalence ratio ϕ'. For this calculation the argon content of air was taken as 0·932 volume per cent[7]. The nominal equivalence ratio was converted to a C_2H_4/A ratio. Then the effective

Table 2. Burnt gas compositions

Flame No.	Effective equivalence ratio ϕ'	Analysis of probe samples CH_4/A	C_2H_2/A	CO_2/A	Calc. equil. CO_2/A	C_2H_2 mole fract. in flame	C_2H_2 density in flame 10^{16} molecules/cm³
1	1·66	0·360	0·376	6·23	6·14	0·0028	1·12
2	1·71	0·390	0·612	5·78	5·76	0·0045	1·80
3	1·76	0·410	0·955	5·42	5·40	0·00696	2·78
4	1·81	0·485	1·31	5·05	5·06	0·00943	3·77
5	1·86	0·669	1·73	3·92	4·74	0·0123	4·92

fuel/argon ratio of the gas mixture was derived as

$$\left(\frac{\text{Fuel}}{\text{A}}\right)_{\text{eff.}} = \left(\frac{C_2H_4}{A} - \frac{C_2H_2}{A} - 2\frac{CH_4}{A}\right)$$

From this value ϕ' was computed, and is given in column 2 of *Table 2*. This procedure is obviously only an approximation, and it accounts for the unburnt carbon better than it does the unburnt hydrogen. Since the amount of hydrocarbons in the burnt gas is small, such an approach should be adequate. Using this effective equivalence ratio ϕ' and the measured flame temperatures, the equilibrium values of CO_2/A were derived from the tables by graphical interpolation, and are given in column 6 of *Table 2*. Comparison of these equilibrium values with the experimental ones in column 5 shows good agreement except for the last flame. This was a very sooty flame in which the sampling probe became badly clogged. The results for this flame must be considered as questionable. The general agreement between the calculated and measured CO_2/A ratios suggests that the gas analysis obtained by probe sampling corresponds rather well to the actual burnt gas composition. The effective equivalence ratios were also used in going from the C_2H_2/A ratios to the values for the acetylene mole fraction and density given in columns 7 and 8 of *Table 2*. These five flames with their analyses for acetylene are now taken as standards for determining the absorption coefficients.

The 730 cm^{-1} acetylene absorption band in high temperature flame gases is shown in *Figure 4*. This spectrum was obtained from point by point calculations involving three scans. First the atmospheric background was determined with no flame burning. Then an absorption spectrum was run with a very rich and sooty flame burning that contained much more acetylene than flame 5. Lastly, an absorption spectrum was taken using a nearly stoichiometric ethylene–air flame diluted with nitrogen to the point where the absorption of one of the water features in the wings of the band was the same as before. In this latter flame, no acetylene survived into the burnt gas,

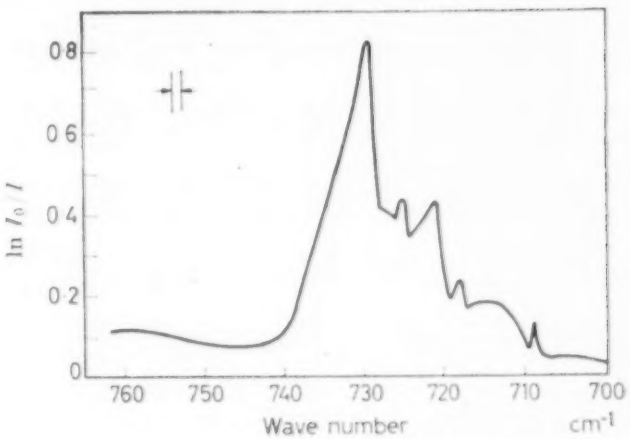

Figure 4. Infra-red absorption of acetylene in an 1820°K ethylene–air flame. See text for method of removing water absorption

so it gave a measure of the water vapour and carbon dioxide background absorptivity. It was possible to use much narrower slits for these spectra than for the emission spectra of *Figure 2*. Nevertheless, there were difficulties in accurately subtracting out the sharp water bands, and the structure shown in *Figure 4* may not truly represent that which would be observed at this spectral resolution in the absence of such interference. The sharp peak of absorption at 730 cm^{-1} is the Q branch of the bending vibration, ν_5, which falls at 729·1 cm^{-1} at room temperature[5]. The smallness of the frequency shift over this temperature interval shows that the moment of inertia of the molecule changes very little when the bending vibration is excited. This is fortunate, for it means that the absorption in all the rotational sublevels is nearly superposed, making acetylene detectable in the i.r. at much lower concentrations than is possible for substances having vibrational bands with spread out rotational structure. The sharp subsidiary peaks on the low frequency side of the 730 cm^{-1} flame band are not observed at room temperature. They are most likely due to hot bands. The lowest energy band of that type would be $\nu_4 = 1$, $\nu_5 = 0 \longrightarrow \nu_4 = 1$, $\nu_5 = 1$. It should consist of three sub-bands, and has previously been reported[5] at 716 cm^{-1}.

In order to obtain as high a sensitivity as possible for the measurement of acetylene, the peak absorptivity at 730 to 730·5 cm^{-1} was used rather than the integrated absorption. The use

of peak absorption also facilitates the removal of background absorption due to water and carbon dioxide, but introduces problems connected with the spectral resolution available. As can be seen from *Figure 2*, a rather strong water band lies under the acetylene absorption peak. In order to account for this, one would like to find a water feature of similar intensity and temperature dependence that lies just outside the acetylene absorption band. This is not possible on the low frequency side, for below about 700 cm^{-1}, carbon dioxide becomes an important absorbing species. On the high frequency side, the acetylene absorption drops to about a tenth of its peak value between 740 and 750 cm^{-1}. Its absorption then increases somewhat in the broad *R* branch of the band, and continues well beyond the convenient scanning range of the instrument. With those considerations in mind, the water band at 750 cm^{-1} was chosen to represent the background absorption. Thus for each acetylene determination, two measurements were made: (*a*) the peak absorptivity at 730 cm^{-1}, and (*b*) the peak absorptivity at 750 cm^{-1}. From these, two absorption coefficients were computed, z_{730} and z_{750} where $z = (1/l) \ln I_0/I$. The absorption coefficient due to the acetylene, $z_{C_2H_2}$, was then obtained from the formula

$$z_{C_2H_2} = z_{730} - [z_{750} - 0{\cdot}1\, z_{730}] - 0{\cdot}08$$

This equation contains corrections for two effects. At 750 cm^{-1}, the acetylene is absorbing to the extent of a tenth its peak value, hence this is subtracted from the background absorption z_{750} in the second term. The third term was found necessary to make the acetylene absorptivity pass through zero at zero concentration. The need for such a correction results from not completely taking the background absorption into account. The underlying cause is probably the carbon dioxide hot band at 720·5 cm^{-1}. The wing of this band has a greater absorptivity at 730 cm^{-1} than at 750 cm^{-1} where our determination of the background is made. In *Figure 5* the acetylene absorption coefficient so obtained is shown plotted against the mole fraction of acetylene in the five flames. It can be seen that the absorption coefficient is proportional to the amount of acetylene, but that it is not independent of the slit width. The absorption coefficients per molecule derived

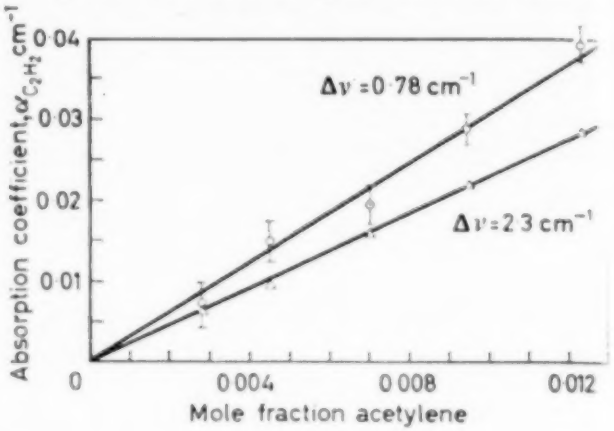

Figure 5. Peak 730 cm^{-1} absorption coefficient $\alpha_{C_2H_2} = 1/l \ln I_0/I$ against mole fraction of acetlyene. $T = 1820°K$, $P = 1$ atm

from *Figure 5* and the data of *Table 2* are given in *Table 3* where

$$z_m = (1/\rho l) \ln I_0/I$$

and ρ denotes density of acetylene in molecules per cm^3, and l is the path length in cm.

Table 3. Peak absorption coefficient per molecule for the 730 cm^{-1} band of acetylene

$\Delta\nu$ cm^{-1}	$T = 1820°K$ z_m	$T = 300°K$ z_m	$\frac{z_m^{300}}{z_m^{1820}}$	*Equation 2 constant* C
0·7	7·7 ± 0·7	96·6	12·5	0·96
2·3	5·8 ± 0·3	43·3	7·5	0·58

Units of z_m are 10^{-18} cm^2 molecules^{-1}.

In order to assess the temperature dependence of the absorption coefficient, several experiments were done at room temperature. Gaseous acetylene and air, each metered by critical flow orifice meters, were mixed to give a gas containing $8{\cdot}54 \times 10^{-4}$ mole fraction acetylene. This was allowed to issue through the 7 cm diameter burner and into the optical beam, but no flame was ignited. Thus the room temperature absorption coefficient was determined, and is given in *Table 3*. The effects of both slit width and temperature upon the acetylene molecular absorption coefficient are shown in *Figure 6*.

It is not easy to vary greatly the hot gas temperature in an experiment of this sort, yet some estimate was desired as to how the absorption coefficient changes with temperature. The simplest approach would be to assume a linear change between 300° and 1 820°K. A better approach seemed to be to consider the temperature-dependent factors which affect the absorption coefficient. One could then contrive an empirical formula of the proper functional form to connect the two experimental points. We have attempted this in what follows. No great accuracy can be expected from such an approach, but it may be possible to make the experimental data useful over a limited temperature range about 1 800°K.

Two opposing temperature effects enter into the peak absorption coefficient as determined here. First, as the temperature is raised, the number of molecules in the vibrational ground state decreases. It is from this ground state that most of the 730 cm^{-1} absorption arises. Secondly, at room temperature the band envelope is narrower than our spectral passband, hence we do not measure the full peak intensity. At flame temperature, however, the width of the absorption band is greater and we more nearly measure its true peak intensity. This is shown in *Figure 6* by the fact that at 300°K the absorption coefficient is sensitive to the slit width used, while at 1 820°K it is much less so.

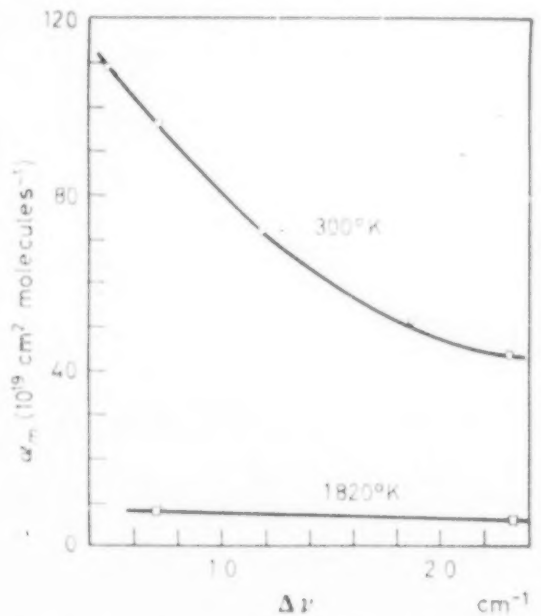

Figure 6. Acetylene molecular absorption coefficient α_m against spectral slit width at 300°K and 1820°K

The ratio of the number of molecules in the vibrational ground state at two temperatures is just the inverse of the vibrational partition function ratio. However, we must also account for the hot bands It is evident from *Figure 4* that when ν_4 is excited, the transition $\nu_5 = 0 \longrightarrow \nu_5 = 1$ still gives rise to absorption at 730 cm^{-1}. In general each hot band is shifted slightly in frequency from the fundamental. This means that in the spectral passband near 730 cm^{-1} only a few rotational lines of each hot band contribute to the measured absorption. As a guess at the magnitude of this effect, we assume that only a tenth of the molecules which give rise to a particular hot band have the proper rotational energy to make their absorption fall in the spectral passband. Thus we assume as potential absorbers at 730 cm^{-1} all molecules in the total vibrational ground state plus a tenth of the molecules which have $\nu_5 = 0$ regardless of the excitation of their other vibrations. This number can be calculated as follows

$$n_a = \frac{N}{Q}\left[1 + \frac{1}{10}\sum_{i=1}^{4}(Q_i - 1)\right] \qquad \ldots . [1]$$

where n_a denotes the number of molecules which can absorb at 730 cm^{-1} at temperature T, N is the total number of molecules, Q is the total vibrational partition function, Q_i is the partial vibrational partition function $(1 - e^{-hc\omega_i/kT})^{-1}$, and ω_i is the ith fundamental frequency.

In *Figure 7* are shown the results of such calculations for several temperatures using the molecular constants given by G. HERZBERG[8]. The upper curve gives the ratio of the number of absorbers at 300°K to the number at temperature T if only ground state molecules are considered. When molecules having vibrations other than ν_5 excited are included as in the formula above, then the lower curve of *Figure 7* is obtained. This is the curve we choose to represent the portion of the temperature dependence of the absorption coefficient that is due to the changing populations of various quantum states.

The way the width of the band changes with temperature can be treated roughly in the following way. Each rotational line in the band is about $0{\cdot}1\ cm^{-1}$ wide at 300°K and 1 atm. This width is largely due to collision broadening, and varies as $PT^{-1/2}$. However, the width of the Q branch enevelope is determined mostly by the fact that the rotational lines are not quite superposed. At 300°K the band centre lies at $729{\cdot}1\ cm^{-1}$ and the most intense rotational line is $J_{max.}=8$. At 1 820°K the peak falls at $730\pm0{\cdot}2\ cm^{-1}$ and $J_{max.}=21$. From these data, assuming the rotational lines are equally spaced, the Q band can be described as being made up of overlapping rotational lines, each $0{\cdot}1\ cm^{-1}$ wide and spaced $0{\cdot}07\ cm^{-1}$ apart. Under these conditions, the width of the band will increase with temperature approximately as does $J_{max.}$, namely as $T^{1/2}$. Taking this as our clue, we have used the following formula to fit the data on the temperature dependence of the absorption coefficient.

$$\frac{\alpha^{300}}{\alpha^{T}} = \frac{n_a^{300}}{n_a^{T}} \times C\left(\frac{300}{T}\right)^{\frac{1}{2}} \qquad \ldots\ [2]$$

where α^{300} is the molecular absorption coefficient at 300°K, α^{T} is the molecular absorption coefficient at T°K, (n_a^{300}/n_a^{T}) is obtained from *Figure 7* or equation 1, C is a constant, and T is in °K.

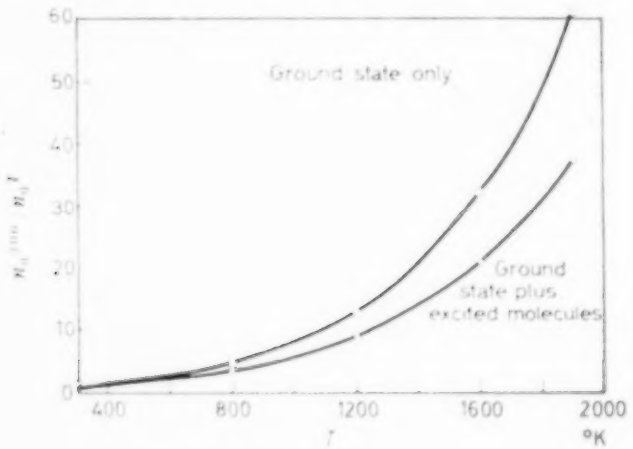

Figure 7. Temperature dependence of population ratios. n_a^{300} is the number of absorbers at 300°K. n_a^{T} is the number of absorbers at T°K. The upper curve considers only molecules in the vibrational ground state as absorbers. The lower curve includes some vibrationally excited molecules as described in the text

The constant C derived from the data of *Table 3* is given in column 5 of that table for two spectral passbands. The function of α^{300}/α^{T} so determined is plotted in *Figure 8*.

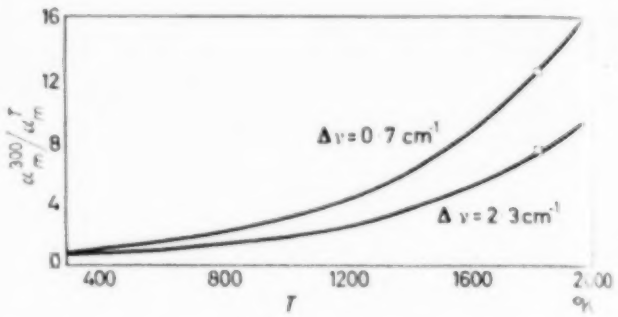

Figure 8. Ratio of acetylene molecular absorption coefficient at 300°K, α_m^{300}, to that at temperature T°K, α_m^{T}, plotted against temperature for two spectral passbands. The solid curves are given by equation 2. The points □ are experimental

The accuracy of this i.r. method of determining acetylene in flame gases is limited mainly by the difficulty of eliminating the background absorption of water and carbon dioxide. The absorption coefficients derived for 1 820°K are probably good to within 10 per cent. Those estimated for other temperatures are admittedly less accurate. At 2 000°K, for instance, an uncertainty of ±20 per cent seems likely.

The limiting sensitivity of the method can be deduced from *Figure 5*. For a 10 cm flame path, such as is easily obtained with porous plug burners, acetylene can be determined when it forms 0·02 volume per cent or more of the burnt gas.

It is often difficult, as i.r. spectroscopists are aware, to reproduce measurements of peak absorption coefficients in different laboratories. In room temperature measurements this arises largely from the difficulty of making sure the spectral passbands used are the same. However, at flame temperatures where the bands are much broader, this is less critical as shown by *Figure 6*. Instead, the major problem concerns whether or not one correctly accounts for the background absorption of water vapour and carbon dioxide. For this reason, care must be used in applying the absorption coefficients derived here in other situations. The flames described in *Table 1* have been found quite

reproducible with respect to measured burnt gas temperature on different sized porous metal burners so long as the flow velocity and mixture ratio are held constant. They could perhaps serve as calibrating standards in other work.

The author thanks G. W. Jones and C. P. Fenimore for advice and help with the mass analyses, and W. E. Kaskan for helpful discussions about this work.

References

[1] Cole, D. J. and Minkoff, G. J. *Proc. Roy. Soc. A*, 1957, **239**, 280

[2] Bent, H. A. and Crawford, B., Jr. *J. phys. Chem.* 1959, **63**, 941

[3] Kaskan, W. E. *Sixth Symposium (International) on Combustion*, p 134. Reinhold: New York, 1957

[4] Millikan, R. C. *J. opt. Soc. Amer.* 1961, **51**, 535

[5] Kaskan, W. E. *Combustion & Flame*, 1958, **2**, 229; *J. chem. phys.* 1958, **29**, 1420

[6] Fenimore, C. P. Private communication

[7] Fremont, H. A., Powell, H. N., Shaffer, A. and Suciu, S. N. *Properties of Combustion Gases, System C_nH_{2n}–Air*. General Electric Co.: New York, 1955

[8] Herzberg, G. *Molecular Spectra and Molecular Structure II*. Van Nostrand: New York, 1945

Some Experiments on Buoyant Diffusion Flames

P. H. THOMAS, C. T. WEBSTER and M. M. RAFTERY

Fire Research Station, Boreham Wood, Hertfordshire

(*Received June 1961*)

In flames produced by freely burning fuel, buoyancy may play an important role in determining the speed of the gases in the flame zone and hence the flame height. Measurements have been made of the height of flames from burning cribs of wood on a square horizontal base and a few for two other arrangements. The results are consistent with a dimensionless analysis, leading, for one particular fuel system, to the functional equation $L/D = f(Q^2/gD^5)$, *where L is the flame height, D the linear dimension of the fire or orifice, Q the volumetric flow rate of gaseous fuel at ambient temperature and g the acceleration due to gravity. In turbulent fuel jets L/D is a constant for a given fuel which is shown theoretically to be a limiting case of this relation.*

Introduction

THE thermal radiation from flames plays an important part in the spread of fire, whether the flame be travelling up a hanging fabric, along a ceiling or from a burning building, both in determining the rate of spread of flame along a combustible surface or across a roadway or a firebreak in a forest. In order to assess the magnitude of the effect of radiation it is necessary to know, amongst other factors, the height of the flame for specified conditions of burning, and the paper is concerned with this aspect of the problem. For the purpose of this paper the rate of supply of gaseous fuel will be considered as an independent variable though in fact it is itself partly determined by the radiation from the flames on to the fuel surface, be it solid or liquid.

First considered is a simple situation in which gaseous fuel emerges into an unconfined atmosphere at a volumetric rate Q through an upward facing horizontal orifice of linear dimension D, e.g. the diameter of a circular orifice or the side of a square orifice. The relation between the flame height L and the independent parameters D and Q is discussed.

The combustion of a fuel emerging from an orifice mixed with no or insufficient oxygen requires the diffusion of oxygen into the stream of gases containing unburnt fuel and combustion products. This diffusion controls the rate of heat release from the reaction over a wide range of conditions—hence the term diffusion flames.

A number of different types of diffusion flame have been studied. Thus S. P. BURKE and T. E. W. SCHUMANN[1] successfully applied a simplified theoretical model to describe the laminar flames confined in a cylindrical burner. S. YAGI[2,3], H. C. HOTTEL and W. R. HAWTHORNE[4], K. WOHL, C. GAZLEY and N. KAPP[5] have discussed unconfined laminar flames by means of diffusion theory. S. YAGI[2,3], W. R. HAWTHORNE, D. S. WEDDEL and H. C. HOTTEL[6] and K. WOHL, C. GAZLEY and N. KAPP[5] have also studied the length of turbulent fuel jets experimentally and theoretically. A review of work up to 1949 has been made by H. C. HOTTEL[7].

The studies referred to above are, however, not directly relevant to the problem at hand since they deal with flow streams which are essentially of the forced convection type whereas in this problem the flow is essentially free convection. This is because the velocity of the gaseous fuel leaving the solid or liquid surface, i.e. the orifice, may, for a wide range of conditions, be as low as of the order 10 cm/s, which corresponds to a velocity head of several orders less than the buoyancy head available from a flame which may be several metres in height.

Existing diffusion models can be extended, however, to accommodate this effect. A simple model of the kind discussed by Burke and Schumann[1], Yagi[2,3], Hottel and Hawthorne[4] is first discussed and then extended to allow for buoyancy. Although Hawthorne, Weddel and Hottel[6] did consider the effect of buoyancy in the analysis of a straight-sided conical flow system (Appendix II of their paper) their experiments were confined to the condition where it had a minor role.

Application of Diffusion Theory to Unconfined Flames Including Buoyancy Effects

The general form of the relations between flame height L, rate of fuel supply Q and burner size D, etc., for one particular fuel are determined, i.e. the dimensionless parameters which correlate flame height L with Q and D. The paper is not otherwise concerned with quantitative prediction. It is convenient to start from the direct application of diffusion theory for a moving stream of gas, and briefly derive the established results mentioned above. Hottel and Hawthorne, assuming a constant value of the diffusion coefficient D_v for laminar flames, showed that the parameter $D_v t_f / D^2$, where t_f is the time for fuel to reach the flame tip from the burner and D is the diameter of the burner orifice, is a constant for a given fuel system. Therefore, if L is the flame length and v the velocity along the flame axis x,

$$D^2/D_v \propto t_f \propto \int_0^L (1/v)\,dx \qquad \ldots [1]$$

For such a flow system containing viscous, inertia and buoyancy forces a general functional equation involving the Grashof and Reynolds numbers can be written, i.e.

$$\frac{v}{V} = f_1\left(\frac{gBD^3\Delta T}{\nu^2}, \frac{VD}{\nu}, \frac{x}{D}\right) \qquad \ldots [2]$$

where V is the velocity of the fuel emerging from the orifice, B is the coefficient of expansion of the gases, ΔT the excess temperature in the flame, g the gravitational acceleration and ν a kinematic viscosity. This functional relationship should also contain other terms, e.g. the ratio of the kinematic viscosity of the fuel to that of the air, and the ratio of absolute mean flame temperature to ambient temperature, but all such extra terms are here assumed constant for a given fuel/air system.

By definition the fuel flow rate is given by

$$Q \propto VD^2 \qquad \ldots [3]$$

It follows from equations 1, 2 and 3 that

$$\frac{Q}{D_v} \propto \frac{VD^2}{D_v} \propto Df_2\left(\frac{L}{D}, \frac{VD}{\nu}, \frac{gD^3B\Delta T}{\nu^2}\right) \qquad \ldots [4]$$

where f_2 is a second function. Henceforth different suffixes to f denote different functions.

Equation 4 can be rearranged to give

$$\frac{L}{D} = f_3\left(\frac{gD^3B\Delta T}{\nu^2}, \frac{Q}{D_vD}, \frac{D_v}{\nu}\right) \qquad \ldots [5]$$

If v/V is effectively constant and thus near to unity, then directly from equation 1

$$L \propto Q/D_v \qquad \ldots [6]$$

the result expressing the linear relationship found by S. P. Burke and T. E. W. Schumann[1], J. Barr[8] and W. A. Simmons and M. J. G. Wilson[9], which is generally acceptable for short flames[7].

In turbulent flow without boundaries it is reasonable to neglect the viscous forces, i.e. ν can be eliminated from among the parameters to be considered. Similarly D_v is not a relevant parameter since molecular diffusion is generally much less important than turbulent or eddy diffusion. If the latter diffusion can be described only in terms of V and its variation with position, and a length which is a function of the one characteristic length of the flow system D and position, it follows that the concentration of fuel along the axis of the fuel stream can be functionally described for any given fuel/air system for which the mean temperature and the temperature distribution are assumed to be the same for different values of the parameter $V^2/gBD\Delta T$ by

$$C_x = C_0 f_4\left(\frac{x}{D}, \frac{V^2}{gBD\Delta T}\right) \qquad \ldots [7]$$

where C_0 is the initial fuel concentration.

The above assumption about the description of turbulence demands that it is generated and determined by the heat source itself and not by the surrounding atmosphere.

Defining the flame tip by the point at which the concentration C_x reaches some value characteristic of the fuel C_f, it follows that for that particular fuel

$$\frac{L}{D} = f_5\left(\frac{V^2}{gBD\Delta T}\right) \qquad \ldots [8]$$

i.e. from equation 3

$$\frac{L}{D} = f_6\left(\frac{Q^2}{gD^5B\Delta T}\right) \qquad \ldots [9]$$

Given the assumptions made above this can be deduced directly from equation 5 by eliminating D_v and v.

Equation 9 is the general result which has been sought.

Alternative Derivation of Generalized Correlation

A somewhat more direct derivation is now given in slightly different terms to elaborate the significance of the above result.

The surface area S of the flame envelope can be represented by

$$S = D^2 f_7 \left(\frac{L}{D}\right) \quad \ldots . [10]$$

where f_7 is a shape factor.

The rate of air entrainment per unit area can be represented by a velocity

$$v_e \propto \varepsilon\,(1/l) \quad \ldots . [11]$$

where ε is an eddy diffusivity and l is the characteristic dimension defining the concentration gradient, or a mixing length. Conventionally ε in turbulent flow is often expressed as the product of a velocity and a distance, and for a stream of local velocity v, ε is proportional to vl which leads to

$$v_e \propto v \quad \ldots . [12]$$

This assumption is essentially the same as that used by B. L. Morton, G. I. Taylor and J. S. Turner[10].

The total air entrained is proportional to the product of S and an average value of v_e. This average value of v_e will have the same form as v in equation 2 with x replaced by L. This product is proportional to the fuel flow rate and, eliminating v from equations 2, 3, 10 and 12, gives

$$D^2 f_7 \left(\frac{L}{D}\right) \cdot V f_5 \left(\frac{gB\,\Delta T D}{V^2} \times \frac{L}{D}\right) \propto Q \propto VD^2 \quad \ldots . [13]$$

i.e.

$$\frac{L}{D} = f_9 \left(\frac{Q^2}{gD^5 B\,\Delta T}\right)$$

as before in equation 9.

It will be realized from the above discussion that Q has a dual significance. First, it is a measure of the orifice velocity and secondly, being the flow of fuel, it is a measure of the air requirements of the flame. The variable $Q^2/gD^5 B\,\Delta T$ thus affects the flame height even when orifice momentum is small compared with the gain in momentum from the buoyancy, but under these limiting conditions Q would be replaced by NQ where N is the air/fuel ratio. In view of the neglect of difference between the flame temperatures, etc., of different fuel systems the use of NQ instead of Q is only a first approximation to a generalized correlation for different fuels.

Discussion of General Equation

It might be expected that the ratios of the fuel/air molecular weights, the required fuel/air ratio, the ratio of flame temperature to ambient temperature and the fuel and air density ratios, etc., would be involved in determining flame length and it should be noted that this was implied in an equation derived by Hawthorne, Weddel and Hottel[6] when discussing a straight-edged round jet (Appendix II of their paper).

In fact, for this straight-edged round system they demonstrated the importance of a parameter

$$(gD/V^2 \tan\theta)^{1/5}\,(1 + [2L/D] \tan\theta)$$

where θ is the angle of expansion of the jet and V^2/gD is the group which appears in equation 7.

The derivation of the one-fifth power is seen from the following argument. For a long conical flame, the flame surface S becomes proportional to L^2 and independent of D as D/L tends to zero. The value of v_e tends to become independent of V if flame buoyancy is predominant over orifice momentum, i.e. if $gL \gg V^2$.

Since the conical flame can be considered to be a point source, and the influence of the flow conditions at the orifice in determining the pattern of flow becomes relatively smaller as D/L decreases, it might be expected that v_e would become independent of D as well as V for values of x large compared with D. Eliminating v, V and D from equation 2, equation 12 gives

$$v_e \propto v \propto x^{-1} \quad (x \gg D) \quad \ldots . [14]$$

and mean values of v_r are proportional to $L^{\frac{1}{2}}$. With f_7 proportional to $(L/D)^2$ and f_8 proportional to $L^{\frac{1}{2}}$ it follows that $L^{5/2}$ is proportional to Q, i.e. f_6 in equation 9 is the one-fifth power of the variable.

If gravitational effects are absent then $gB\,\Delta T$ cannot affect L and L/D must be constant. This is the well known law for turbulent fuel jets with high momentum[2-7]. A decrease in

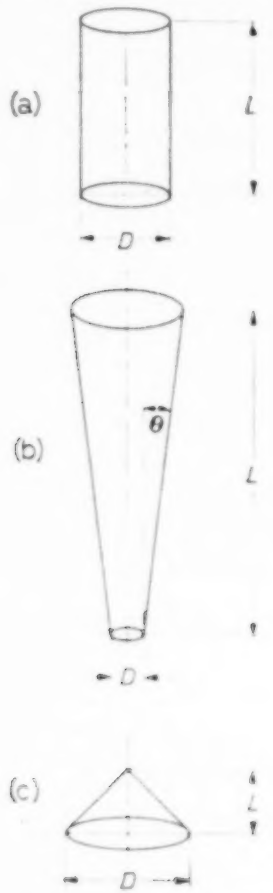

Figure 1. Diagrammatic representations of flames

buoyancy relative to orifice momentum leads to a decrease in the velocity in the fuel stream and hence less air entrainment, so that L increases. Thus L/D is an increasing function of $Q^2/gD^5B\,\Delta T$ and L/D should tend to an upper limit which has the value typical of a turbulent jet where buoyancy is of minor importance.

In equation 10 f_7 is proportional to (L/D) for cylindrical flames and to $(L/D)^2$ for conical flames [*Figures 1*(a) and *1*(b)]. If it were possible for very short flames to be idealized as shown in *Figure 1*(c) the surface area would be proportional to $D^2[1+(4L^2/D^2)]^{\frac{1}{2}}$ and so $f_7(L/D)$ would be almost independent of L or values of $L/D \ll 1$.

Thus if

$$f_7(L/D) \propto (L/D)^n \qquad \ldots . [5]$$

the index n might be expected to increase from 0 to 2 with increasing L/D.

If from equation 14 the mean value of v_r is taken as proportional to $L^{\frac{1}{2}}$ then from equations 13 and 15

$$\frac{L}{D} \propto \left(\frac{Q^2}{D^5}\right)^{\frac{1}{2n+1}} \qquad \ldots . [6]$$

This equation shows that the L/D versus Q^2/D^5 relation on a log-log basis is convex upwards. The index of Q^2/D^5 thus varies from some value equal to or less than 1 to 0·2 as L/D increases, until at high values of Q^2/D^5, when orifice momentum becomes significant, it tends to zero and L/D becomes constant. Before discussing the use of this correlation the flow criterion for the existence of a turbulent rather than laminar flame will be briefly discussed.

Transition from Laminar to Turbulent Flames

The transition from laminar to turbulent flames has been discussed in terms of a critical Reynolds number[1]; this is appropriate in determining the condition of the fuel emerging from the orifice and in the flames themselves if buoyancy effects are secondary to those of momentum at the orifice. However, Hottel and Hawthorne were not able to obtain a satisfactory criterion[1], independent of the nature of the fuel. When buoyancy is important the mean velocity of the gases increases rapidly with height, and turbulence may be induced at a height which is a small fraction of the total flame height even if the Reynolds number based on the conditions of the emerging fuel shows this flow to be laminar. It is possible therefore that buoyant diffusion flames may be effectively turbulent when the Reynolds number relevant to the fuel at the burner or orifice is below the conventional value for turbulent flow at the orifice.

Experimental Results

Cribs on square horizontal base

Results are given in this paper for cribs of wood sticks (Spruce) arranged on a square

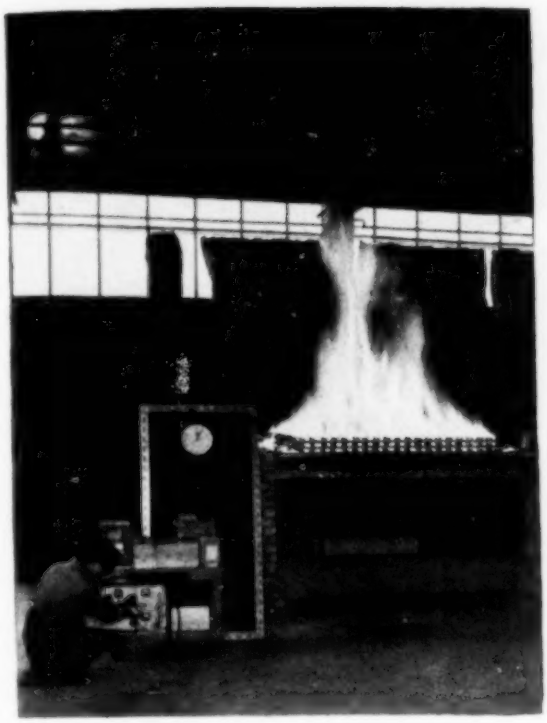

Figure 2. Flames from crib on square base of 101 cm. (Exposure time 0·1 sec)

horizontal base (*Figure 2*). By varying the amount of wood in the crib various mass rates of weight loss ρQ where ρ is the density of the cold fuel gas could be obtained for a given value of D by direct weighing. The height of the flame was in each case measured from the base of the crib and was much greater than its height. The burning rate reached a maximum value which remained steady for a period and this rate of burning and the mean height of flame visible on a photograph corresponding to it were recorded during the experiments. The flames had a short period of fluctuation in height so that the heights recorded photographically were averaged over a period considerably longer than the few seconds taken for a single fluctuation. In this period it is mainly the volatiles from the wood that are burning. Apart from a small amount of carbonaceous residue burning at the crib edge little carbon burnt until the flames subsided and the gross rate of burning fell. The results are plotted in *Figure 3*. The viscosity μ was assumed to be 10^{-4} c.g.s. units and apart from one result where

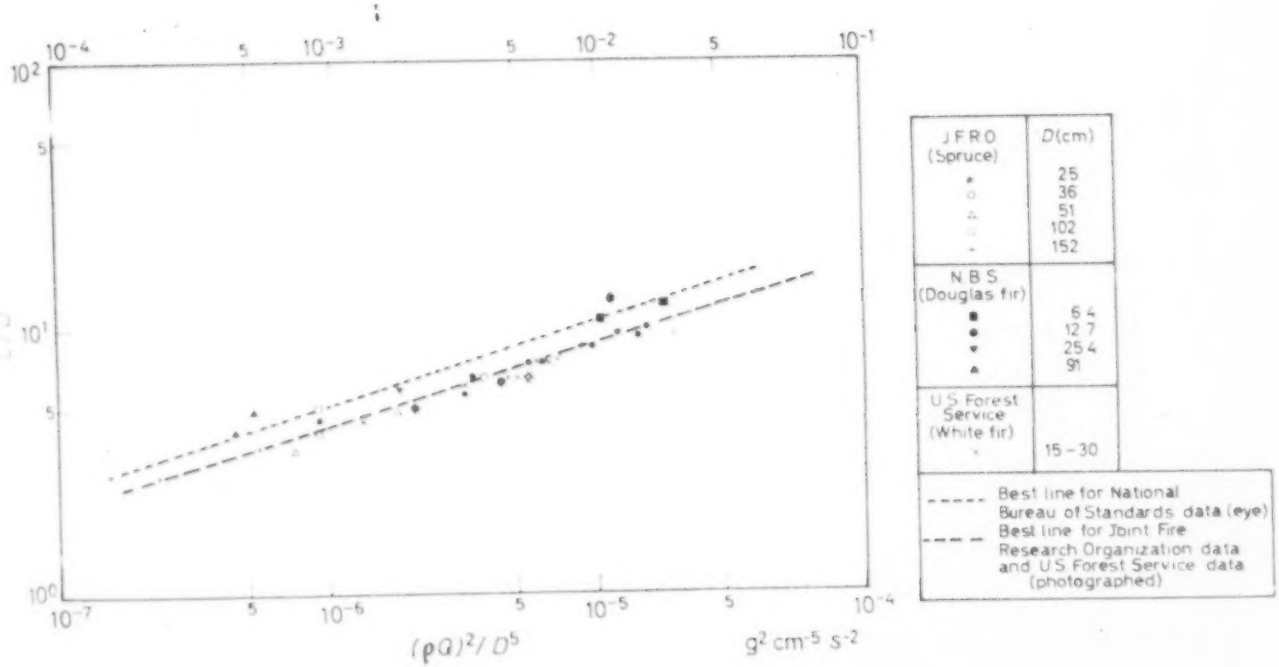

Figure 3. Correlation of flame height data. Still air—approximately radially symmetrical. The upper horizontal scale shows Q^2/gD^5 (dimensionless) with $\rho^2 g$ taken as 10^{-5} $g^2\,cm^{-5}\,s^{-2}$

it was 1 250 the Reynolds number at the orifice ($\rho Q/\mu D$) was over 2 000 in all cases. Some unpublished data are also available.

D. Gross[11], at the National Bureau of Standards, Washington, has burnt sticks of Douglas fir of square section assembled in the form of cubical cribs. These cribs varied in side from $\frac{5}{8}$ to 36 in. and some had differing numbers of sticks in the horizontal layers, thereby burning at different rates of weight loss for a given cube dimension. The Reynolds numbers based on 10^{-4} c.g.s. units for μ fell in the range 13 to 6 400. Some of the results referred to laminar flames, indeed in one case the flame was less than 2 in. high. All the data where the flames were less than 2 ft (50 cm) high have been excluded and the rest are plotted in *Figure 3*. The results measured by eye follow the same trend as the results of the Joint Fire Research Organization but are about 20 per cent higher. Since for these cubical cribs the crib height is not small compared with the linear dimension of the base it would be more appropriate to take the base of the flame half way up the crib to obtain a value of L more comparable with the other data. This reduction of L/D by 0·5 is not, however, sufficient to explain the difference in L/D between the two sets of data which as some more recent comparisons suggest may be mainly a difference between eye and photographic measurement. This may be partly a matter of spectral sensitivity and partly a matter of the different nature of the 'averaging process' on a fluctuating flame.

Use has also been made of some data given by W. L. Fons *et al.*[12]. These refer to experiments on the spread of a burning zone along a long wood crib (White fir). Data obtained photographically from these experiments have been plotted using an equivalent square base defined by $D=(D_c D_w)^{\frac{1}{2}}$, where D_c is the width of the crib and D_w the measured length of the flame zone in the direction of flame spread along the crib. The results where the flame height was not greater than three times the larger of either D_c or D_w have been excluded because they cannot be regarded as approximately radially symmetrical.

These data are also in good agreement with those described above.

Cribs in an enclosure

The second set of experimental results refers to the photographed heights of flame observed

Figure 4. General view of experimental arrangement for studying fires from cribs burning in cubical enclosures (measured scale not shown; exposure time 0·1 sec)

outside a cubical enclosure when varying amounts of wood (Spruce) were burning within it and one side of the crib was completely open (*Figure 4*). The mean rate of burning in the period when the burning was approximately constant and the corresponding mean flame height, were measured, the latter visually. The results are plotted in *Figure 5*. The Reynolds number $\rho Q/\mu D$ with μ equal to 10^{-4} c.g.s. units varied from 2 300 to 5 400 for the data recorded. It should be emphasized here that these results do not apply to the case where there is a vertical 'wall' above the opening though one would expect such results to be correlated by a relation of the same form.

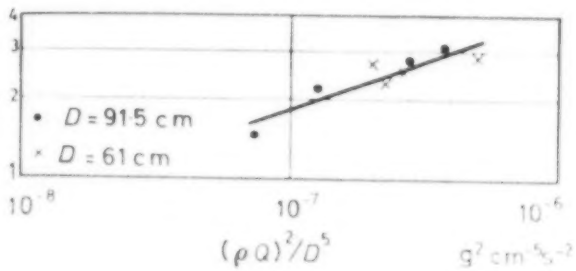

Figure 5. Flame height for flames from wood cribs in cubical enclosures with one side open

Flames on strips of hanging fabric

The third set of results refers to the photographed flames from various widths of one type of cotton fabric which was burning while hanging freely. Unlike the previous experimental arrangements the rate of burning could not be varied independently of the linear scale of the fuel arrangement, i.e. Q is a function of D, the width of fabric, and for the smallest width the flame was laminar. Despite the availability of only a few data in this case the results are given and discussed for general interest. No direct measurements were made of the loss in weight. Instead the observed rate of spread of flame up the fabric, when this had reached a constant value was measured and the flame height obtained from cinematographic records. The results could be plotted in terms of the rate of spread of flame V, and the width D since V is proportional to Q/D. However, in order to plot the data in a way comparable with the previous cases the value of the mass of fabric per unit area was used to convert the spread velocity to a rate of weight loss. This neglects the weight of the char residue and may overestimate the value of Q^2/D^5 by a factor of the order 4. The results are given in *Figure 6*.

The values of the Reynolds number $\rho Q/\mu D$ varied from 400 to 1 000 but only the flames from the two smaller widths appeared wholly or partly laminar; for the other widths the Reynolds number was over 800.

Discussion

Cribs on square horizontal base

Figure 3 shows that the results for flames from a square source can be correlated by using the terms in groups suggested by equation 9. The relationship of L/D to Q^2/D^5 is a power law but this is not of fundamental significance and can be used only over a limited, albeit a usefully wide, range. The line through the results plotted in *Figure 3* is given in c.g.s. units by

$$\frac{L}{D} = 4{\cdot}4\left(\frac{\rho^2 Q^2}{D^5}\right)^{0{\cdot}10} \quad \ldots\ldots [17]$$

For a given burning rate per unit area, i.e. a given value of V, this implies that

$$L/D \propto D^{-0{\cdot}5} \quad \ldots\ldots [18]$$

There are two reservations to the use of a power law:

(*1*) At large values of Q^2/D^5, L/D should become constant. This constant value is known for certain gases and depends markedly on the air requirement per unit quantity of fuel. For carbon monoxide which has a low air requirement the ratio is about 40 while for propane, which has a high air requirement[8], it is nearly 300. On a log-log scale these known values are not so much larger than the values found in the experiments for one to extrapolate upwards

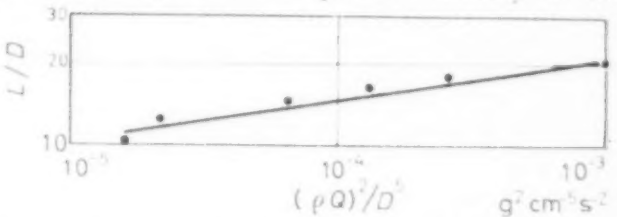

Figure 6. Flame heights for strips of fabric burning upwards

linearly over a large range. Extrapolation from small to large scale will usually decrease the value of Q^2/D^5 and thus be downward extrapolation.

(*2*) The second reservation is that, even if buoyancy were the predominant factor and Q only entered the correlation as a measure of the quantity of fuel and hence air quantity, a power law implies that the flame shape function which expresses the flame envelope surface area is also a power of the ratio L/D (equations **15** and **16**).

A straight line extrapolation in either direction based on the above arguments would tend to over-estimate flame length*.

width in a rectilinear enclosure of which the height is equal to the dimension perpendicular to the opening.

For these results where the index m is approximately $\frac{1}{5}$, L is only weakly dependent on D. In this connection it is perhaps significant that a line source of gas at constant temperature giving a straight-edged plume of constant expansion might be expected to give a two-thirds power law between height of flame L and R' based on the same arguments that led to a two-fifths power law for a point source. Thus sv_z is proportional to $L(L)^{\frac{1}{2}}$ which is proportional to R' and hence L is proportional to $(R')^{2.3}$. In an enclosure there is the added

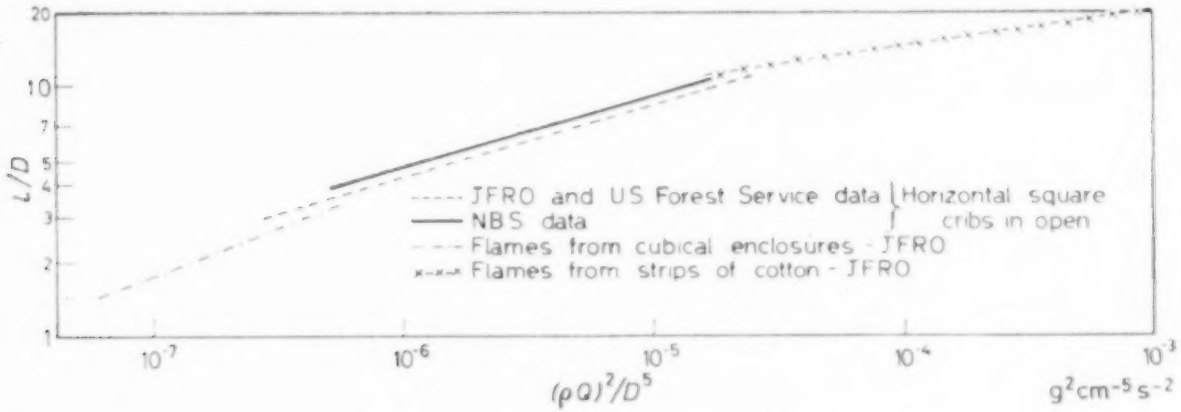

Figure 7. Best lines for Figures 3, 5 and 6

Cribs in an enclosure

The results of the experiments on flames from cubes with one side open also lie on a line of similar form to that for the open fires (*Figure 5*), but this correlation is relatively less well established in view of the fewer data available. Since the height of the flame may be expected to be independent of the width of the window it is possible (though this is only true in so far as L/D is not large compared with unity) to extend this correlation as a first approximation to the form

$$L/D \propto (R'^2/D^5)^m$$

where R' is the mass rate of burning per unit

*In theory increasing L absolutely increases the characteristic velocity (e.g. $L^{\frac{1}{2}}$) so that eventually mixing could cease to be the controlling factor and the kinetics would have to be considered.

feature of entrainment in the horizontally moving stream under the 'roof', but this might be expected to be small because of the relative difficulty of exchanging cold gas with lighter hot gas flowing over it.

Flames on strips of hanging fabric

The results for the burning fabrics are shown in *Figure 6* but because ρQ varies with D, they do not in any way prove that the form of the independent variable is Q^2/D^5 though, given this form from the experiments on cribs in the open, the correlation is as shown in *Figure 7*. As has been stated above, the smallest of the flames had a significant portion of laminar flame. The fabric data lie on a continuation of the correlation curve for the open wood cribs (*Figure 7*), despite the difference in the fuel

the definition of D and the presence of a laminar region. This is no doubt largely fortuitous.

Comparison with data on burning fuel tanks

V. I. BLINOV and G. N. KHUDIAKOV[13] have published data for flame heights from burning fuel tanks but the number of these where the Reynolds number exceeds 2 000 and which are accordingly stated to be fully turbulent[13,14] is very small (less than 5) and only three refer to one type of fuel. For the two largest fuel tanks the ratios of L/D were the same (1·7) and the authors stated that these results were in the region where such a constancy was to be expected in the light of work on turbulent fuel jets. This argument has been referred to in two reviews[14,15] of the paper by Blinov and Khudiakov. While it is true that the constancy of L/D cannot be accounted for by the arguments of the present paper since for a given V, L/D is proportional to $D^{-0.5}$ (equation 18) it is to be noted that the liquid burning rate in these tests was of the order 5 mm/min giving a gaseous velocity of the order 20 cm/s. Since the two flame heights were of the order 350 and 4 000 cm respectively giving corresponding values of $(gL)^{\frac{1}{2}}$ of 600 and 2 000 cm/s and L/D was much smaller than the values typical of turbulent fuel jets, it seems incorrect to use an argument which depends for its validity on the assumption that the velocity at the orifice determines the velocities and mixing conditions at higher levels in the flame. It would seem desirable for further experiments to be carried out as the conclusion about the constancy of L/D in these experiments depends only on the result of one of two burning tests.

Conclusion

An approximate dimensional analysis leads to a simple dimensional relationship between flame height, burning rate and orifice size for buoyant diffusion flames. Data are presented which conform to this correlation over the experimental range. The well known law for turbulent fuel jets has therefore been generalized to allow for buoyancy effects and this enables a principle of similarity to be defined for flames from fires of freely burning fuel.

The work described in this paper forms part of the programme of the Joint Fire Research Organization of the Department of Scientific and Industrial Research and Fire Offices' Committee; the paper is published by permission of the Director of Fire Research.

References

[1] BURKE, S. P. and SCHUMANN, T. E. W. *Industr. Engng Chem.* 1928, **20**, 998

[2] YAGI, S. *J. Soc. chem. Ind. Japan*, 1943, **46**, 608, 821 and 873

[3] YAGI, S. and SAJI, K. 'Problems of turbulent diffusion and flame jet'. *Fourth Symposium (International) on Combustion*, p 771. Williams and Wilkins: Baltimore, 1953

[4] HOTTEL, H. C. and HAWTHORNE, W. R. 'Diffusion in laminar flame jets'. *Third Symposium (International) on Combustion*, p 254. Williams and Wilkins: Baltimore, 1949

[5] WOHL, K., GAZLEY, C. and KAPP, N. 'Diffusion flames'. *Third Symposium (International) on Combustion*, p 288. Williams and Wilkins: Baltimore, 1949

[6] HAWTHORNE, W. R., WEDDEL, D. S. and HOTTEL, H. C. 'Mixing and combustion in turbulent fuel jets'. *Third Symposium (International) on Combustion*, p 266. Williams and Wilkins: Baltimore, 1949

[7] HOTTEL, H. C. 'Burning in laminar and turbulent fuel jets'. *Fourth Symposium (International) on Combustion*, p 97. Williams and Wilkins: Baltimore, 1953

[8] BARR, J. 'Diffusion flames'. *Fourth Symposium (International) on Combustion*, p 765. Williams and Wilkins: Baltimore, 1953

[9] SIMMONDS, W. A. and WILSON, M. J. G. 'The entrainment of air by flames'. *Commun. Gas Res. Bd No. G.R.B. 61*, November 1951

[10] MORTON, B. L., TAYLOR, G. I. and TURNER, J. S. *Proc. Roy. Soc. A*, 1956, **234** (1196), 1

[11] GROSS, D. Private communication

[12] FONS, W. L. *et al.* 'Project fire model'. *Summary Progress Report 1 Nov. 1958–30 April 1960*. U.S. Department of Agriculture Forest Service, Pacific Southwest Forest and Range Experiment Station: Berkeley, California, 1960

[13] BLINOV, V. I. and KHUDIAKOV, G. N. *Dokl. Akad. Nauk S.S.S.R.* 1957, **113**, 1094

[14] HOTTEL, H. C. *Fire Research Abstracts and Reviews* 1959 (2) 41 (3) Errata

[15] KIRKBY, W. A. *Combustion & Flame*, 1960, **4** (1) 84

Experiments on the Ignition of Cellulosic Materials by Thermal Radiation

D. L. SIMMS

Fire Research Station, Boreham Wood, Hertfordshire

(*Received June 1961*)

The temperatures in the stream of gases emitted from a cellulosic solid subjected to thermal radiation have been measured, and the effects of various factors, including the size of the area heated by the radiation and turbulence, on the likelihood of the ignition of the gases have been examined. The occurrence of turbulence in the stream of gases, even though it does not affect the temperature of the solid or the gases at their point of emission, appears to be necessary for flame to appear. External draughts, by producing turbulence, reduce the minimum intensity of radiation at which materials ignite, but if ignition occurs in the absence of an external draught, the imposition of one in the range of these experiments, does not affect the ignition time.

Introduction

WORK on the ignition of materials by radiation has hitherto been mainly concerned with conditions in the solid itself. It has been shown that the times taken for wood to ignite spontaneously when exposed to radiation in the range 1·0 to 2·5 cal cm^{-2} s^{-1} are related to the thermal properties of the wood which is assumed to be inert[1], and that wood ignites at a fixed temperature[2–4]. More recent work[5] has shown that this result may be generalized to all cellulosic materials; the ignition time may be correlated using simple heat transfer theory giving a fixed ignition temperature of about 500°C.

The use of a surface temperature criterion appears to be possible because, although the rate of evolution of volatile material increases rapidly with temperature, the surface temperature itself rises rapidly with time. Thus a precise definition of the conditions in the gas phase is of secondary importance in determining the ignition time, although ignition starts there. However, in the course of experimental work a number of observations (some summarized earlier[3–7]), some of them only qualitative, have been made which can only be interpreted by a discussion of what happens in the gas stream. It is with these aspects of ignition that this paper is concerned.

The basic experimental method is similar to that adopted earlier[1]. Blackened specimens were exposed to a known intensity of radiation either from a gas-fired radiant panel[9], a tungsten filament lamp[10] or a carbon arc[11] and the ignition time noted. Unblackened fibre insulating board, and most woods, are highly reflecting in the near infra-red and consequently they have a different absorptivity on each source. In order to compare their behaviour directly, specimens have to be blackened (usually using candle black). Measurements[8] of the temperature rise of specimens after blackening exposed to radiation from the carbon arc showed that they behaved as though they were opaque solids whereas unblackened materials were diathermanous.

Experiments[5] made to compare the time taken to ignite the same area of blackened fibre insulating board exposed to the same intensity of radiation on the three sources ignite in almost the same time. Thus blackening the surface appears to render the material opaque and give it a high absorptivity to radiation from all three sources. Details of the characteristics of the sources are given in *Table 1*.

There are two main series of experiments reported below. The discussion of these assists in interpreting some work reported previously[5].

Position of First Appearance of Flame

At high rates of heating (above 3 cal cm^{-2} s^{-1}) with the tungsten lamp source, the flow of the volatile stream appeared to become turbulent very close to its point of emission from the surface of the heated specimen, and ignition usually followed very quickly. At lower rates (below 3 cal cm^{-2} s^{-1}), the flow was clearly laminar near the heated surface and became turbulent higher up.

Table 1. Characteristics of radiation sources used

Source	*Approximate operating temperature, °K*	*Uniform irradiated area, cm²*	*Source of external draught near specimen*
Gas-fired radiant panel[2]	1000	60	*From spent gases*
Tungsten filament lamp[3]*—ellipsoidal mirror*	2800	0·5	*No draught*
Carbon arc[4]*—ellipsoidal mirror*	4000	2	*Induced by arc flame*

By focusing a ciné-camera operating at 120 frames per second on the stream of volatiles immediately above the top of the irradiated specimen, photographs were obtained showing that the flame first appeared in the volatile stream where the laminar flow became turbulent (*Figure 1*) and then travelled down to the surface. Experiments with another ciné-camera operating at 720 frames per second showed that the time taken for the flame to reach the surface from its first appearance was about 0·01 sec, at a speed of about 600 cm/s.

Influence of External Air Movements

Experiments have been made to compare the minimum intensity required to ignite blackened fibre insulating board using the three different radiation sources. The minimum intensity found by using the carbon arc source was consistent with results calculated from experiments using the gas-fired panel, allowance being made for the difference in the size of the irradiated area. However, this was not so using the tungsten filament source where a higher intensity was required for ignition than with the others. Both the gas-fired radiant panel and the carbon arc produce convection currents so that the stream of volatiles from the heated specimen becomes turbulent regardless of the rate of heating, whereas there is no such draught arising from the tungsten filament lamp affecting the neighbourhood of the specimen; this was thought to be the reason for the discrepancy between the minimum intensities required for ignition with

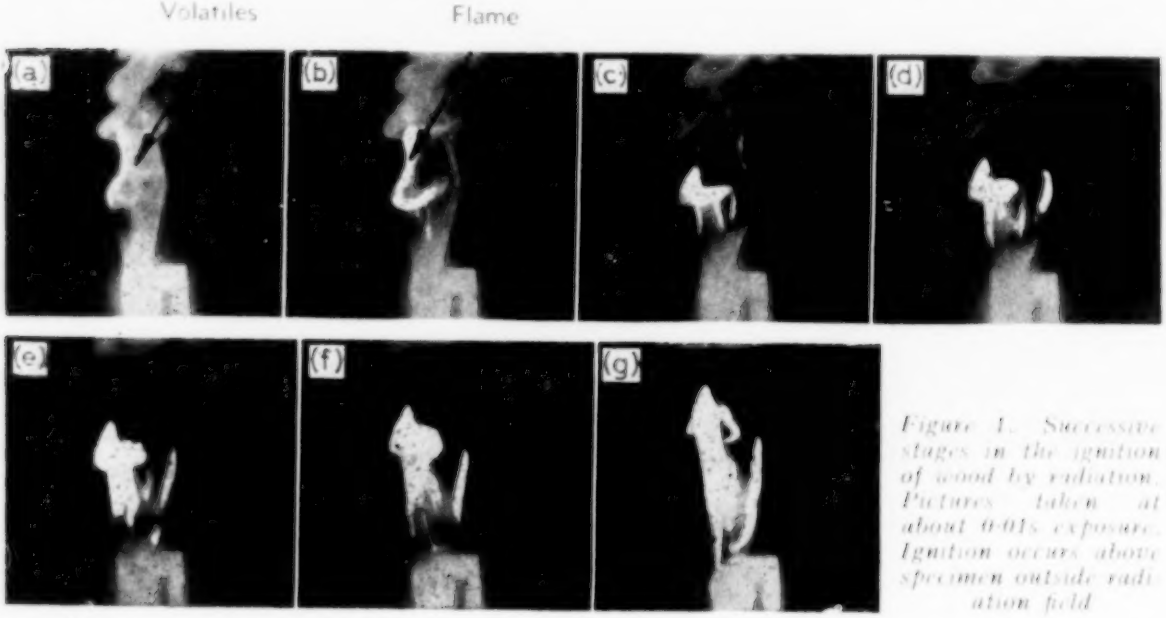

Figure 1. Successive stages in the ignition of wood by radiation. Pictures taken at about 0·01s exposure. Ignition occurs above specimen outside radiation field

different sources. Further experiments were therefore designed to find the effect of the draught from the gas-fired panel on the ignition of a specimen when this was subjected to radiation from the tungsten lamp alone.

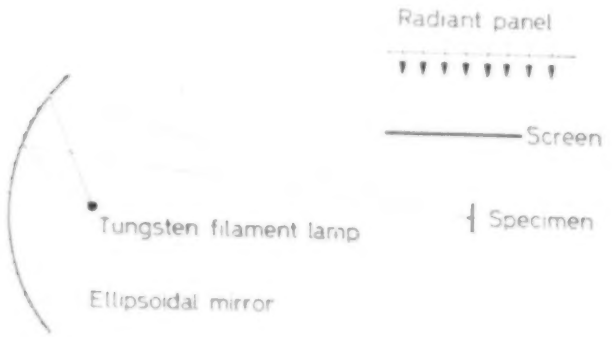

Specimen is subjected to radiation only from lamp
Draught from panel can be superimposed

Figure 2. Apparatus for studying effect of draught from radiant panel on ignition

The apparatus is shown in *Figure 2* and *Figure 3*. The specimen was placed on the central axis of the panel but perpendicular instead of parallel to it. The specimen was then subjected to the draught from the panel whilst it was exposed to radiation from the tungsten lamp. The draught from the panel was practically the same as for exposure at the minimum intensity for ignition by the panel alone.

The experiments consisted of exposing two sets of specimens to radiation from the lamp; in the first set there was no draught, while in the second, the radiant panel was operating and imposing its draught on the specimens. They were exposed to radiation of different intensities and the times taken to ignite noted. The results of the experiments are shown in *Figure 4*; each point being the mean of six readings. The minimum intensities for ignition in each set of experiments are given in *Table 2*.

Table 2. Minimum intensities for ignition, cal cm^{-2} s^{-1} (W cm^{-2})

System	Oak	Cedar	Fibre insulating board
Lamp without draught	2·8 (11·6)	2·8 (11·6)	2·2 (9·3)
Lamp and draught from panel	2·4 (10)	1·8 (7·6)	1·6 (6·5)

The value obtained for fibre insulating board with the lamp source and the draught from the panel is the same as that obtained with the panel as the radiation source, allowance again being

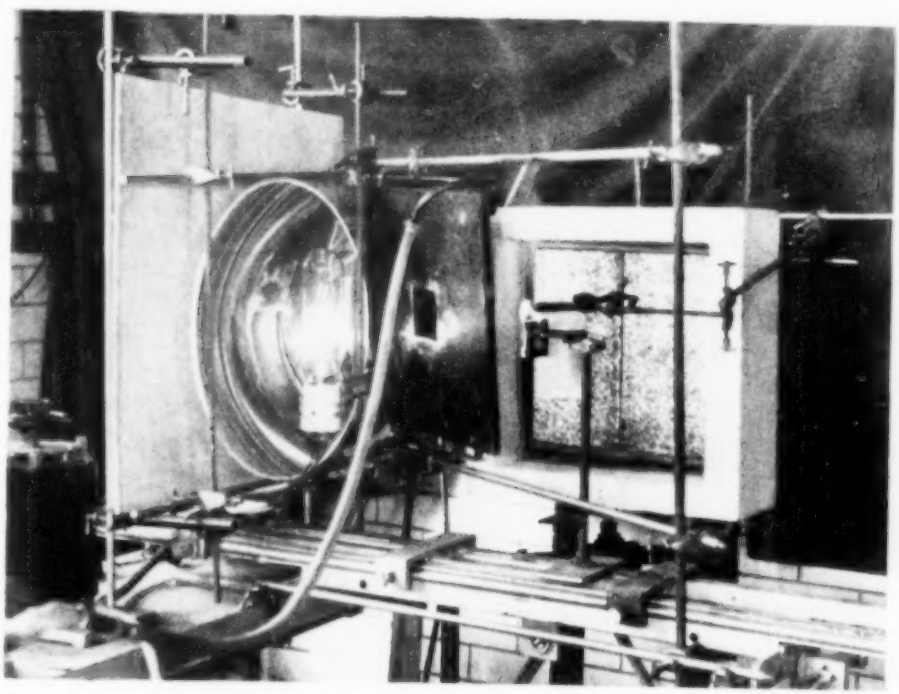

Figure 3. General arrangement of apparatus

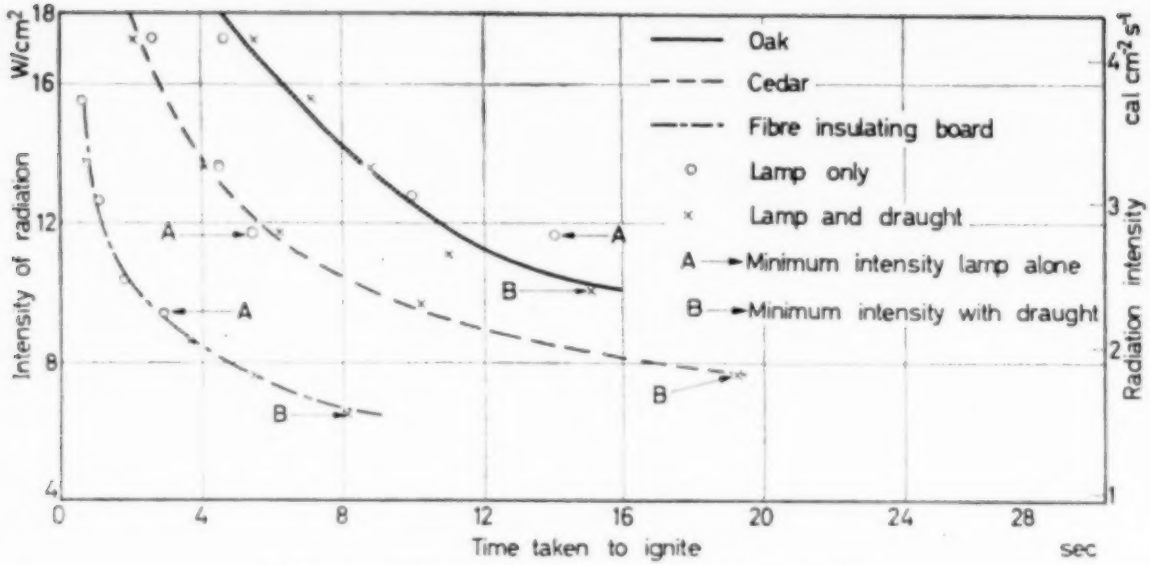

Figure 4. Effect of an external draught on ignition

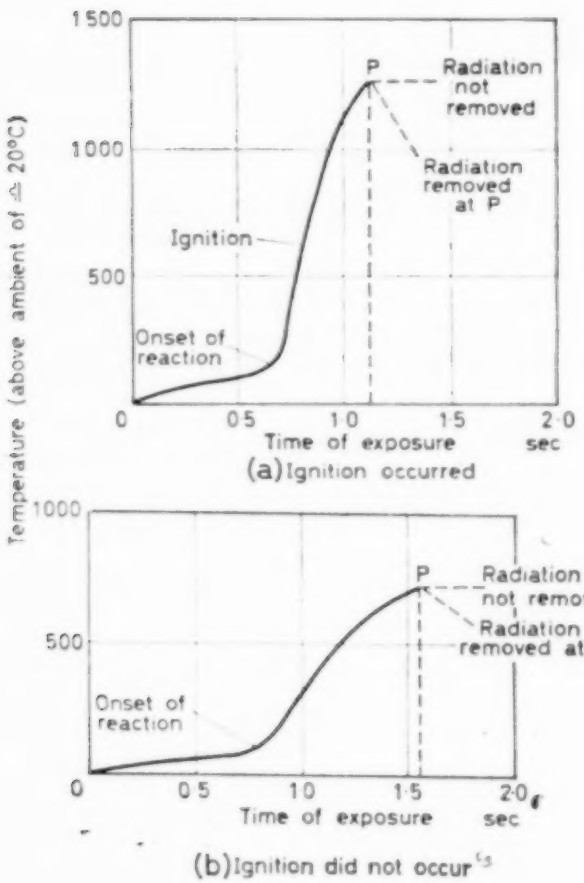

Figure 5. Temperatures in volatile stream. Radiation intensity: 4·5 cal cm⁻² s⁻¹. Thermocouple level with top of specimen

made for the effect of the difference in area[3]. Insufficient data are available on the behaviour of oak and cedar with different irradiated areas to make a similar comparison but the effect of the draught is to lower the minimum intensity by a factor of between $\frac{1}{5}$ and $\frac{1}{3}$ (*Table 1*). The absence or presence of external air movements of velocity order 25 cm/s does not affect the time taken to ignite at those intensities at which ignition normally occurs.

Temperature Measurements in the Volatile Stream

The temperatures of the surface and of the volatile stream were then investigated, both when ignition did occur and when it did not; the intensity level was the same in each and was near the threshold of ignition; the presence of an external draught was necessary to initiate ignition.

Temperatures in the volatile stream were measured by means of thermocouples placed above the specimen, temperatures on the surface by thermocouples placed in a thin slit. The thermocouples used* in these experiments were

*Specimens of fibre insulating board were exposed to an intensity of radiation of about 3 cal cm^{-2} s^{-1} to test whether the thermocouples in the volatile stream affected the ignition process. A number of wires and fibres of different thicknesses were placed in the volatile stream and the ignition times with each wire and fibre were recorded. No significant variations in ignition time were found except that the presence of a cotton fibre shortened the ignition time and the thicker metal wires (26 s.w.g.) often prevented ignition altogether, probably by cooling the volatile stream; the presence of the other fibres appeared to have no effect.

made from (45 s.w.g.) chromel–alumel wire and had a time constant of about 0·2 sec for 95 per cent full reading; their output was recorded automatically.

A typical experiment consisted of exposing a specimen to radiation, recording the temperature/time curve at *one* position in the volatile stream, and measuring the ignition time if it occurred. Each experiment was repeated several times with the thermocouples in different positions to obtain a mean profile. *Figure* 5(a) shows the mean result for two exposures in a slight draught sufficient to produce ignition and *Figure* 5(b) the mean of two without a draught where ignition did not occur. Similar results were obtained with the thermocouple in different positions in the same vertical plane.

The temperature *distribution* in a volatile stream just before and just after ignition is shown in *Figures* 6(a) and 6(b). The temperature falls rapidly once the radiation is removed and the flame does not persist. The temperature distribution in the volatile stream when ignition did not occur is given for the time just after the surface temperature reached 500°C at which temperature ignition might have been expected[3] [*Figure* 6(c)]. The corresponding rises in temperature just below the surface are given in *Figure* 7. At a rate of heating near to the threshold for ignition [*Figures* 5(a) and 5(b)] the temperatures of the volatiles as they emerge from the solid do not appear to differ whether or not ignition results; the same is true for the surface temperature (*Figure* 7).

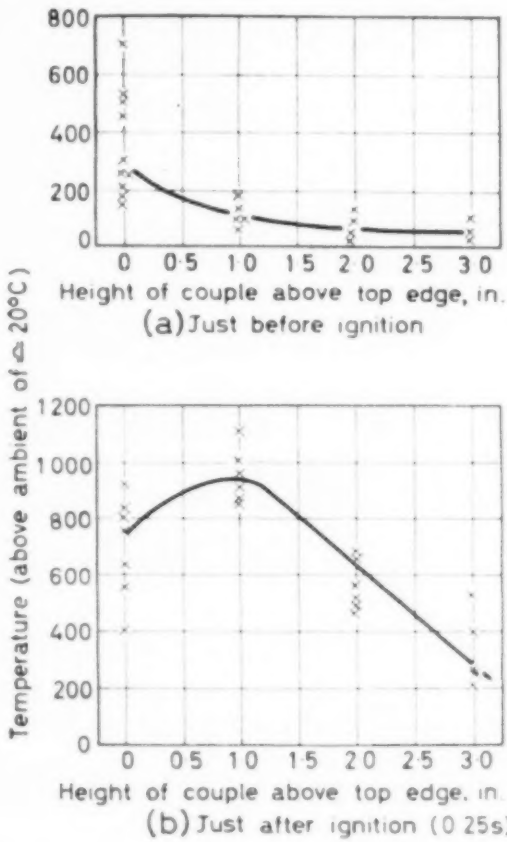

Figure 6. Stream temperature profile

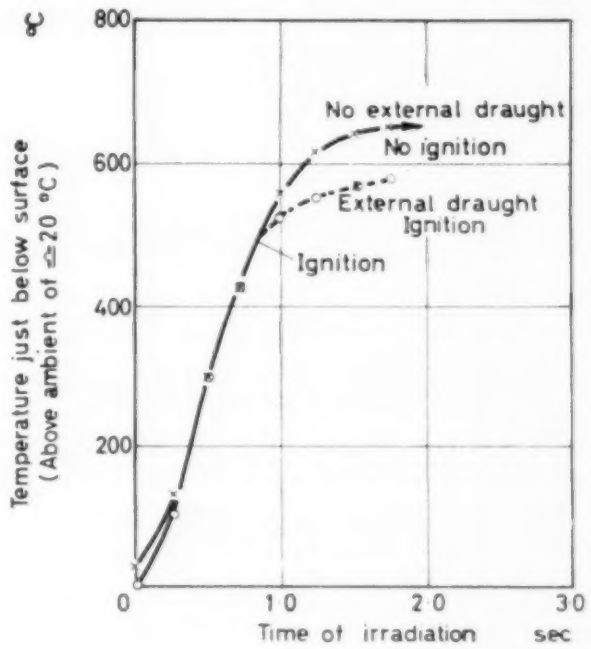

Figure 7. Temperature just below surface (intensity of radiation, 4·5 cal cm^{-2} s^{-1})

General Discussion

Turbulence and the ignition process

Superimposing a draught on the laminar part of the volatile stream produced turbulence near its point of emission and hence ignition where otherwise turbulence would develop too far from the heated surface for the volatiles to be sufficiently hot to ignite. Where turbulence occurred naturally very near the point of emission of the volatiles, an imposed external draught had no effect on the ignition time. Presumably this is because turbulence increases the rate of gross heat output by promoting mixing of air and volatiles and by extending the region in which they react together.

The present results also help to explain why large irradiated areas of the same cellulosic material are more quickly ignited than small ones at the same intensity of irradiation[5]. The smaller areas emit smaller plumes of volatiles and for a heated plume of inert gas, the smaller the total amount of gas in the originating plume, the farther away from the source is the onset of turbulence and the lower the temperature at this point. The same effect would be expected for reacting gases up to the point at which heating as a result of the reaction in the gas becomes significant. This means that the smaller areas require a longer heating time to raise the temperature of the volatiles to a given value at the greater distance where turbulence begins. Hence the ignition time is longer.

Effect of the cold areas surrounding the irradiated area

The area heated by the radiation is necessarily small when sources of high tensity are used[10,11] so that the specimen-holder may receive little of the incident radiation and remain cold. With these sources unless care is taken in mounting the specimen so that it is clear of its holder, there may be interference with the ignition process. In particular, on some occasions, the minimum intensity at which ignition occurred was found to be higher and the ignition time longer. This effect is analogous to that discussed above in connection with the size of the irradiated area. A hot surround effectively increases the amount of hot gases rising in the plume by adding heated air to the stream of volatiles and turbulence would occur more readily than with a cold surround so that the threshold time for ignition would be lower. Also with a hot surround the gases would tend to mix with air at a higher temperature and this would make ignition easier.

Conclusions

The ignition of volatiles from the heated surface, that is the first appearance of flame, occurs when the stream of volatiles becomes turbulent. If turbulence does not occur within a short distance of the point of emission of the volatiles, ignition does not occur even though the temperatures of the surface of the solid and in the volatile stream are the same as when ignition does occur. This may be due to turbulence increasing the rate of gross heat output in the volatile streams by increasing the size of the reacting zone and by increasing the rate of mixing. An external draught of about 25 cm/s, by making the volatile stream turbulent, reduces the ignition threshold, but if ignition occurs in the absence of a draught, its imposition does not, in the range of these experiments, affect the ignition time.

The interpretations of these experiments, ancillary to the main programme of work on ignition[5], show that ignition can be regarded as occurring in material which is inert up to a fixed ignition temperature for a restricted range of conditions only and that there are features of the gaseous ignition process that have relevance to experimental technique, because in some apparatus it may be difficult to avoid draughts and difficult to irradiate large areas of the material. Thus areas of different sizes need to be studied and some attempt made to extrapolate to large areas.

The work described in this paper forms part of the programme of the Department of Scientific and Industrial Research and Fire Offices' Committee Joint Fire Research Organization; the paper is published by permission of the Director of Fire Research. The author would like to thank

his colleagues for the help given both in carrying out the experiments reported in this paper and for the many discussions upon them.

References

[1] LAWSON, D. I. and SIMMS, D. L. 'The ignition of wood by radiation'. *Brit. J. appl. Phys.* 1952, **3** (9), 288

[2] LAWSON, D. I. and SIMMS, D. L. 'The ignition of wood by radiation'. *Brit. J. appl. Phys.* 1952, **3** (12), 394

[3] LAWRENCE, E. K. 'Analytical study of flame initiation'. *S.M. Thesis* in Chemical Engineering. Massachusetts Institute of Technology: Cambridge, Massachusetts, 1952

[4] AKITA, K. 'Studies on the mechanism of ignition of wood'. *Report of the Fire Research Institute of Japan 1959*, **9** (1–2)

[5] SIMMS, D. L. 'Ignition of cellulosic materials by radiation'. *Combustion & Flame*, 1960, **4** (4), 293

[6] *Fire Research 1954*. Department of Scientific and and Industrial Research and Fire Offices' Committee; Her Majesty's Stationery Office: London, 1955

[7] *Fire Research 1955*. Department of Scientific and Industrial Research and Fire Offices' Committee; Her Majesty's Stationery Office: London, 1956

[8] GARDON, R. 'Temperatures attained in wood exposed to high intensity thermal radiation'. *Ph. D. Thesis*, pp 104–8. University of London, March 1959

[9] SIMMS, D. L. and MILLER, JOAN E. 'Radiation characteristics of a gas-fired radiant panel'. Department of Scientific and Industrial Research and Fire Offices' Committee Joint Fire Research Organization *F.R. Note No. 217/1955*

[10] SIMMS, D. L., PICKARD, R. W. and LAW, MARGARET. 'A source of radiation employing a tungsten filament lamp and an ellipsoidal mirror'. Department of Scientific and Industrial Research and Fire Offices' Committee Joint Fire Research Organization *F.R. Note No. 355/1958*

[11] HINKLEY, P. L. 'Source of high intensity radiation employing an arc lamp and an ellipsoidal mirror'. Department of Scientific and Industrial Research and Fire Offices' Committee Joint Fire Research Organization *F.R. Note No. 270/1956*

Recent Developments and Notes

Height and Design of New Chimneys

The Air Pollution Panel of the Federation of British Industries at its meeting in November 1958 appointed a Working Party to make recommendations on the height of new chimneys with particular reference to Section 10 of the Clean Air Act.

The Working Party's main recommendations, contained in a handbook which has just been published, refer to industrial boiler plants with an output of 5 000 to 33 000 lb/h steam at maximum continuous rating. Proposals are also made in respect of larger plants up to an aggregate steam capacity of 450 000 lb/h. None of the recommendations refers to washed gas effluents.

It is also suggested that an F.B.I. Working Party should make a survey early in 1963 of the conditions around new chimneys built to these recommendations to check whether any modifications to the proposals are desirable.

Copies of the handbook, *Height and Design of New Chimneys*, are obtainable from FBI Print and Publications, 21 Tothill Street, London, S.W.1, price 4*s* post free.

New High Temperature Vacuum Furnace

For measuring the physical properties of materials in researches carried out in the United Aircraft Corporation Research Laboratories, East Hartford, Conn., U.S.A., a furnace was designed to operate in a high vacuum or in an inert atmosphere at temperatures up to 2 500°C, to use readily fabricated heating elements, to provide easy access to the specimen chamber, and to allow for insertion of instruments. A description of the tungsten resistance furnace which was built to meet these requirements was given by J. F. BACON, R. D. VELTRI, and J. Y. WHITTIER, in a paper at the XVIIIth International Congress of Pure and Applied Chemistry, in Montreal, in August.

The furnace has proved capable of operation at temperatures above 2 700°C and attains a vacuum of 1×10^{-7} mm of mercury when cold and 3×10^{-5} mm of mercury when at maximum operating temperature. Complete change of sample is possible with full restoration of vacuum in one hour. Radiation shielding consisting of tantalum sheets is used to prevent excessive heat loss. Typical power usage at 2 700°C is 4 600 amperes at 13 V.

Power Generation and Clean Air Equipment

From 2 to 11 May 1962 an Exhibition of Power Generation and Clean Air Equipment of an international character will be held at Olympia, London. This will be on a more extensive scale than previously and will cover every aspect of coal, oil and steam utilization, fuel economy and improvements, new materials, metals, refractories, ceramics and fabrication techniques. There will be technical meetings and special events organized in conjunction with professional and official bodies. Further information may be obtained from Provincial Exhibitions Ltd, City Hall, Deansgate, Manchester 3.

High Temperature Thermocouples

Thermocouples for detecting temperatures of up to 2 320°C are to be marketed by Honeywell Controls Ltd, Greenford, Middlesex. Materials used are combinations of tungsten, rhenium, rhodium, molybdenum, iridium and platinum. Certain of these thermocouples have maximum temperature ratings of 1 650°, others of 1 760°, 1 980°, 2 205° and 2 320°C. Types are available for both oxidizing and reducing environments.

The maximum of 2 320°C is obtained by using tungsten versus tungsten with 26 per cent rhenium. The thermoelectric output of such a thermocouple is nearly three times as great as that of the tungsten–rhenium thermocouple which it will largely supersede. The temperature/e.m.f. curve is more linear in the 1 100° to 2 200°C range. Improved uniformity of wire is

Recent Developments and Notes

Height and Design of New Chimneys

The Air Pollution Panel of the Federation of British Industries at its meeting in November 1958 appointed a Working Party to make recommendations on the height of new chimneys with particular reference to Section 10 of the Clean Air Act.

The Working Party's main recommendations, contained in a handbook which has just been published, refer to industrial boiler plants with an output of 5 000 to 33 000 lb/h steam at maximum continuous rating. Proposals are also made in respect of larger plants up to an aggregate steam capacity of 450 000 lb/h. None of the recommendations refers to washed gas effluents.

It is also suggested that an F.B.I. Working Party should make a survey early in 1963 of the conditions around new chimneys built to these recommendations to check whether any modifications to the proposals are desirable.

Copies of the handbook, *Height and Design of New Chimneys*, are obtainable from FBI Print and Publications, 21 Tothill Street, London, S.W.1, price 4*s* post free.

New High Temperature Vacuum Furnace

For measuring the physical properties of materials in researches carried out in the United Aircraft Corporation Research Laboratories, East Hartford, Conn., U.S.A., a furnace was designed to operate in a high vacuum or in an inert atmosphere at temperatures up to 2 500°C, to use readily fabricated heating elements, to provide easy access to the specimen chamber, and to allow for insertion of instruments. A description of the tungsten resistance furnace which was built to meet these requirements was given by J. F. BACON, R. D. VELTRI, and L. Y. WHITTIER, in a paper at the XVIIIth International Congress of Pure and Applied Chemistry, in Montreal, in August.

The furnace has proved capable of operation at temperatures above 2 700°C and attains a vacuum of 1×10^{-7} mm of mercury when cold and 3×10^{-5} mm of mercury when at maximum operating temperature. Complete change of sample is possible with full restoration of vacuum in one hour. Radiation shielding consisting of tantalum sheets is used to prevent excessive heat loss. Typical power usage at 2 700°C is 4 600 amperes at 13 V.

Power Generation and Clean Air Equipment

From 2 to 11 May 1962 an Exhibition of Power Generation and Clean Air Equipment of an international character will be held at Olympia, London. This will be on a more extensive scale than previously and will cover every aspect of coal, oil and steam utilization, fuel economy and improvements, new materials, metals, refractories, ceramics and fabrication techniques. There will be technical meetings and special events organized in conjunction with professional and official bodies. Further information may be obtained from Provincial Exhibitions Ltd, City Hall, Deansgate, Manchester 3.

High Temperature Thermocouples

Thermocouples for detecting temperatures of up to 2 320°C are to be marketed by Honeywell Controls Ltd, Greenford, Middlesex. Materials used are combinations of tungsten, rhenium, rhodium, molybdenum, iridium and platinum. Certain of these thermocouples have maximum temperature ratings of 1 650°, others of 1 760°, 1 980°, 2 205° and 2 320°C. Types are available for both oxidizing and reducing environments.

The maximum of 2 320°C is obtained by using tungsten versus tungsten with 26 per cent rhenium. The thermoelectric output of such a thermocouple is nearly three times as great as that of the tungsten–rhenium thermocouple which it will largely supersede. The temperature/e.m.f. curve is more linear in the 1 100° to 2 200°C range. Improved uniformity of wire is

obtained owing to the 26 per cent alloy being more homogeneous. Error is claimed to be less.

Another of the new thermocouples uses platinum with 30 per cent rhodium versus platinum with 6 per cent rhodium, and is for continuous use up to 1 500°C and intermittent service up to 1 800°C. The new alloy type does not suffer excessive grain growth, vaporization, contamination and other disadvantages of existing platinum–rhodium thermocouples.

Effect of Vorticity on Fuel Jets

An investigation of the effect of internal vorticity on the quality of atomization and the enclosed angle of an atomized diesel fuel jet has been carried out by P. I. Pobiarzhin [Dvigateli Vnutr. Sgoraniya (MVTU, **76**), Moscow, Mashgiz, 1958, 84; *Ref. Zh. Mekh.* No. 4, 1959, Rev. 3718]. In the open-type burner nozzle used the vortices were created by consecutive chokes arranged before the exit opening. Differing degrees of vorticity were achieved by throttling the fuel with a single, centrally-arranged aperture of variable size, the distance between the nozzles being adjusted by means of a movable plate between them.

The author derives relationships between the pressures in front of the entry and exit nozzles, and the rate of flow of the fuel, also between the flow coefficients of these nozzles and the pressure gradient in the nozzle, as well as the pressure in front of the nozzle. The measurements of droplet size showed that the mean droplet diameter is smaller for the burner with two nozzles than that with only one, a second throttling nozzle or choke in the burner materially influencing the droplet dimensions. The apex angle of the fuel cone for the burner with two nozzles is considerably greater than for that with only one nozzle, although with two nozzles the pressure in front of the exit nozzle is lower.

Automatic Firing of Open Hearth Furnaces

Whilst the importance of maintaining proper air/fuel ratio in the operation of open hearth furnaces has been recognized for many years, developments in the field of instrumentation have recently made this a reality. In the establishment of a system to control the air/fue ratio several factors must be considered, th chief of which are the availability of sufficien combustion air and the safe operating limits o the furnace refractories. Work on these prol lems has been progressing for a number of yea on the basic open hearth furnaces at the Sout Works of the United States Steel Corporatio Chicago, and an account of important develo ments there were given by R. E. Stoll, G. C Primm, and E. C. Rudolphy, in a pape presented to the National Open Hearth Ste Conference in Philadelphia, last April, spon sored by AIME.

The application during the past few years o continuous oxygen analysis, roof temperatur recording and automatic control is described Trials since 1958 with steam instead of wate for aspiration of the gas sample were so success ful in the continuous oxygen analyser–recorder controller system that it was decided to install the system on all open hearth furnaces at the South Works.

It was found that the operation of this system provides reliable information which can be used on a control basis. A decrease in fuel consumption resulted, together with increased furnace productivity and indications that roof refractory performance was not adversely affected, and may be improved.

In the U.K., as a result of cooperative work with certain member firms a reliable continuous waste-gas sampling system for open hearth furnaces has been developed by the British Iron and Steel Research Association. A paramagnetic oxygen analyser is used in this system. Further work is being directed towards automatic control of combustion, and equipment for this is to be installed shortly on a British open hearth furnace.

Solar Furnaces: New Techniques of Use

For high temperature experimentation and measurements, especially of physical properties solar furnaces are extremely suitable, although the unusual heating conditions existing at the focal area impose certain limitations. Chief amongst these limitations are the small size of the hot zone, the non-uniform flux across the

image area, and the fact that heating takes place only at the front of the sample. Several papers on this general subject were presented to the United Nations Conference on New Sources of Energy, held in Rome in August 1961, and in one of them T. S. LASZLO, Research and Advanced Development Division, AVCO Corporation, Wilmington, Mass., discussed these limitations and described new techniques and possibilities in solar furnaces.

Two sample holders are described in which the sample can be rotated and the atmosphere controlled. One of these holders permits the rotation of the sample around an axis perpendicular to the optical axis of the furnace. A glass or fused silica hemisphere surmounts the refractory chamber and an oscillating blade wipes condensations off the inside of the hemisphere. Refractory materials have been melted in this sample holder. Water-cooled calorimeters are used for obtaining an average value of the heat flux across the entire orifice of the furnace and the Gardon radiometer with fast response can be used to measure the flux distribution with fine resolution. The important problem of finding the optimum shape for the artificial blackbody used to absorb the incident radiation is discussed, and the author has devised a new shape consisting of a truncated right cone with the smaller end as the orifice, the bottom of the cavity being a right circular cone. A fast action on-off shutter has been designed which does not cast any shadow on the reflector when in a retracted position.

Solar Furnaces: Construction and Applications

At the United Nations Conference on New Sources of Energy, held in Rome in August 1961, P. E. GLASER, Arthur D. Little Inc., Cambridge, Mass., presented a paper dealing with research and developments in the design and construction of solar furnaces and in instrumentation. Fundamental design problems associated with the construction of large paraboloidal reflectors and supports are of first importance for the economic usefulness of solar furnaces. The glass reflectors used at present are economically unattractive and aluminium and plastic reflectors have now been developed at a fraction of the cost of glass reflecting surfaces. Because of the light weight of these new reflecting surfaces, the design of structural supports and foundations can be approached from new directions.

The construction of a large solar furnace at Tohoku University, Sendai, Japan, was described by T. SAKURAI, K. SHISHIDO, O. KAMADA and K. INAGAKI. The paraboloidal mirror has a 10 m aperture and is of 3·2 m focal length; it will be used in conjunction with a heliostat. An account of the solar distillation research at the University of California was given by E. D. HOWE. The Sea Water Conversion Project has been carried on at this University since 1952 and several variations of the simple single-effect solar still have been investigated.

Practical applications of solar furnaces and the economic possibilities of their development were described in a paper by F. TROMBE and M. FOEX, Laboratory of Solar Energy, National Commission for Scientific Research, Montluis, Pyrénées-Orientales, France. In furnaces of low or medium power, 2 kW or 50 kW, the melting or fritting of refractory oxides are eminently suitable operations, the products being used in the manufacture of various ceramics. The oxides so treated have included corundum, magnesium spinel, and zirconia. The problem of treating oxygen-free products has been solved for low-power furnaces by the use of a gas-impermeable wall, and numerous materials with special electrical, optical or magnetic properties may be prepared by this means. The melting, decomposition, roasting, reduction, treatment with reagents, of many minerals have been carried out. Centrifugal furnaces have been used. A 1 MW solar furnace is now under construction at Odeillo not only for scientific research but also as a pilot plant with the object of encouraging the construction of large solar furnaces of purely industrial character.

Heat Transfer Conference, Paris 1961

An International Conference on Heat Transfer was held in Paris from 19 to 24 June 1961, organized by l'Institut Français de Combustibles et de l'Energie, with the cooperation of la Société Française des Thermiciens, under the

presidency of Professor M. VERON. About 90 papers were presented and amongst these may be noted as of special interest to readers of this journal, in addition to two others which are the subject of separate notes here, a paper by R. KISSEL, Institut de Recherches de la Sidérurgie et Fondation des Recherches Internationales sur les Flammes, which deals with some results obtained at the IJmuiden experimental station on the radiation of gas and liquid flames, including the injection of oxygen into some flames. Another paper, by Professor H. HAUSEN, Institut de Thermodynamique de l'Ecole Polytechnique de Hanovre, describes a new method of experimentation on heat transfer in regenerators.

Convection and Surface Combustion

About twenty years ago MM. VERON and ROCARD drew attention to the possible existence of *convection vive*, a flow of heat in excess of the amount due to normal convection, at a surface situated in flowing gases undergoing chemical reaction. Since then there have been some further contributions to the subject and more recent experiments on this phenomenon were described by P. VALENTIN, Commissariat à l'Energie atomique, at the International Conference on Heat Transfer in Paris (see note above). A weak mixture of hydrogen and air was used, and a small platinum plate 0·05 mm thick, which could be electrically heated, was placed parallel to the direction of the current. Exploration of the boundary layers at the plate was carried out by means of thermocouples and for the dynamic conditions and concentrations very fine brass probes were used.

Two modes of combustion were distinguished, one solely catalytic on the surface of the plate, and another in the fluid phase for plate temperatures over 850° C. The preponderating role of diffusion in the regions reached by combustion in the fluid phase is shown and the author derives expressions which take account of the parameters concerning the onset of combustion in this phase.

The experiments have shown that if the *active* molecules possess a large coefficient of diffusion, the heat flow at the plate can be greater than that which would transmit the same fluid supposedly chemically inactive and whose temperature is the theoretical combustion temperature, provided that the reaction, at least in part, is a surface reaction.

Developments in Radiation Meters

In researches on flame radiation now being carried out at IJmuiden by the International Flame Research Foundation, a non-directional radiation pyrometer has recently been devised and was described by R. KISSEL at the International Conference on Heat Transfer held in Paris (see note above).

The usual radiation pyrometer measures the radiation in a narrow beam, but it has become necessary to be able to measure the radiation received by an absolute black-body over a wide angle. Consequently a 'spherical' or 'integrating' radiometer was devised about three years ago based on one constructed in the British Iron and Steel Research Association Laboratories. More recently the spherical form was abandoned for an ellipsoidal one, which has stable characteristics. The ellipsoid is of polished copper, internally gilded, and is placed in a water jacket. At one of the two focal planes an opening receives the incident flux and at the other a nickel-chromium thermocouple. The interior profile of the orifice has been designed so that the incident flux from a solid angle of *ca.* 85° concentrated entirely on the thermocouple. A nitrogen purge is used to keep the instrument free from dust and condensation.

A comparison was made of measurements with this non-directional pyrometer with those obtained from the calorific flux absorbed by a bundle of tubes similar to superheater tubes, and the agreement was very good.

Rocket Materials

In a recent issue of *Raketentechnik und Raumfahrtforschung* [1961, **5**, 73–101] there are published papers presented to the Conference 'Raumfahrt und Europa', held in Konstanz, May 1961, giving a review of the present position as regards rockets for space vehicles. J. FABIAN, Forschungsinstitut für Physik der

Strahlantriebe e. V., Stuttgart, gives a survey of materials for rockets and space vehicles from the viewpoint of a rocket engineer. A. DADIEU, of the same Institut, deals with liquid propellants, their performance, cost and availability. The characteristic properties of solid propellants for use in large booster rockets are examined in a paper by K. KLAGER, Aerojet-General Corporation, Sacramento, Calif. The properties of prime importance are ballistic performance, mechanical properties, ease of processing, and cost. The requirements are compared with the properties of polyurethane propellants which are particularly suited for large power plants. In a paper by G. AU, DFL-Institut für Strahltriebwerke, Braunschweig, hydromagnetic propulsion systems are described. Considerable information is given of plasma generation, constriction and acceleration in electromagnetic fields. There is a bibliography of 136 items in this paper, containing many dealing with the properties of ionized gases at high temperatures.

Combustion of Liquid Droplets

J. PAWLOWSKI, Farbenfabriken Bayer A.G., Leverkusen, has published a mathematical discussion, as stability problems, of the critical ignition and extinction processes in the combustion of a liquid droplet suspended in a turbulent atmosphere [*Internat. J. Heat Mass Transfer*, 1961, **2**, 33].

In the model used it is assumed that the homogeneous reaction takes place in a narrow zone at rest in relation to the droplet and that the reactants are highly diluted with inert gas, so that convective exchange can be neglected. The course of the reaction is treated as a quasi-stationary process. The molecular kinetic adjustment in the gaseous system takes place so rapidly under the conditions existing momentarily, that thermodynamic equilibrium prevails even in the collision waves. Moreover, it can be assumed that the adjustment of the field quantities, temperature of the reaction zone (T) and partial pressure of the reactants (p_k), under boundary conditions, takes place more rapidly than the transient change of these boundary conditions themselves.

The problem breaks down into two parts when treated from the above point of view. First, there are the usual differential equations of second order, with the appropriate boundary conditions, which give the local distribution of the values of T and p_k for the momentary boundary conditions. Secondly, first order differential equations determine the variation of some boundary quantities and therefore set the conditions for the course of the reaction at a given time. The influence of ten basic constants on the course of the reaction, especially during the induction period, and on the ignition process, is discussed.

Standardization of Tests for Explosives

The second meeting of the European Commission for the Standardization of Tests for Explosives was held at Sterrebeek, 4 and 5 May 1961, under the aegis of the Centre de Recherches pour l'Industrie des Produits Explosifs. Representatives were present from Austria, Belgium, France, Germany, Great Britain, Italy, Luxemburg, Russia and Switzerland. The general subject considered was that of methods of determination of the chief characteristics of conventional explosives and particularly exchange-ion explosives. Different sessions were concerned with tests for the transmission of detonation; explosive strength, by lead block and ballistic mortar tests; brisance; speed of detonation. A summary of the proceedings has now been published, together with three papers read to the meeting, dealing specially with exchange-ion explosives [*Explosifs*, 1961, **14**, 48]. At the third meeting of the Commission which is to be held in 1962, it is hoped that some conclusions will be reached as to international adoption of test methods.

Effect of Oxygen on the Pyrolysis of Methane

J. E. GERMAIN and R. SUEUR, Faculté des Sciences de Lille, have continued their researches on the pyrolysis of methane and have studied in more detail the induction effect of small amounts of oxygen between 950° and 1050°C, in mixtures with not more than 5 per cent of oxygen, in a flow system at atmospheric pressure in a silica tube [*Bull. Soc. chim.* 1961, 1008].

From a plot of the speed of reaction as a function of time of contact, it appears that the period of acceleration is shorter and the speed attained higher, as the oxygen concentration becomes greater. The oxygen appears in the products as carbon monoxide and traces of formaldehyde were only found at the lowest temperatures and with times of contact less than 0·2 sec.

The explanation of the quantitative results is that the oxygen acts as an initiator of the cracking chain through the formation of free radicals, due to the removal of hydrogen

$$CH_4 + O_2 \longrightarrow CH_3 + HO_2$$

This is generally recognized as the starting point for the oxidation chain for methane. Thus the cracking and oxidation reaction chains have propagating centres in common. Confirmation of this view is said to be given by the values of overall activation energy which have been calculated by the authors and agree with those of the oxidation reaction published by other investigators.

Fire Research

In the recent report of the Joint Fire Research Organization, *Fire Research 1960* [Department of Scientific and Industrial Research and Fire Offices' Committee, Joint Fire Research Organization; Her Majesty's Stationery Office: London, 1961, 5s 6*d*], the chairman of the Fire Research Board records the appointment during the year of a Committee on the Modelling of Fires, under the chairmanship of Professor M. W. Thring, of the University of Sheffield. The development of modelling techniques for experimental work on fire is considered to be of major importance. Work on an international basis is being undertaken, particularly in modelling fires in compartments, eight countries participating at present.

From the investigations on the growth of fire it is now becoming possible by means of small laboratory fires to predict the size of flames from full-scale fires. This will find application, for example, in predicting the effect of flames from a burning building on the intensity of heat radiation transmitted across a street, and hence on the exposure hazard to neighbouring buildings.

Since July 1960, the testing of the explosibility of industrial dust clouds, previously carried out at the Safety in Mines Research Establishment, Buxton, has become the responsibility of the Joint Fire Research Organization. This work is carried out on behalf of H.M. Factory Inspectorate of the Ministry of Labour. Forty one samples of dust were tested during the year. Class I, dusts that ignite and propagate flame readily, the source of heat required for ignition being small, includes polymerized methyl methacrylate, a mixture of cotton fibres and mineral dusts, dried yeast, a bronze powder, zinc, and leather dust. Class II, dusts that ignite readily but require a more severe source of ignition than those in Class I, includes tungsten, calcium citrate, and three coal dust and sand mixtures.

Reaction Zone in Detonation

H. Gg. Wagner, Institut für Physikalische Chemie der Universität Göttingen, has published recently two important papers on further experimental investigations of the reaction zone in gaseous detonations. The first, with Th. Just and F. J. Lug, deals with *Knallgas* of different compositions while the second paper, with Th. Just and W. Pusch, covers hydrocarbon-oxygen mixtures [*Z. Elektrochem.* 1961, **65**, 403, 410].

Detonation speeds, induction times and length of reaction zone were measured in hydrogen-oxygen mixtures at pressures below 100 mm of mercury, using the apparatus described earlier [*Z. Elektrochem.* 1960, **64**, 501]. By using a tube of relatively large diameter the range of stationary detonation in a stoichiometric *Knallgas* mixture could be extended to a pressure of 30 mm. From the more accurate determination of speeds, it was possible to obtain information of the stationary state of detonation and to calculate the temperature, as well as the pressure and density, immediately behind the shock front. By changing the hydrogen concentration the temperature behind the shock front could be so markedly varied that from the p

of the induction times against $1/T$, activation energies for the reactions

$$OH + H_2 \longrightarrow H_2O + H$$

or

$$O + H_2 \longrightarrow OH + H$$

and

$$H + O_2 \longrightarrow OH + O$$

could be calculated.

Similar determinations were made in mixtures of oxygen with methane, hexane, *cyclo*hexane and benzene. Considerable agreement was found between the speeds of detonation as measured at different pressures and calculated values.

Purification of Hot Flue Gases

In connection with air pollution studies, the Bureau of Mines is cooperating with the U.S. Public Health Service in investigating the use of solids for removing sulphur dioxide in concentrations of less than 0·5 per cent from combustion and waste gases. If the removal could be carried out at flue-gas temperatures, cooling of the gas which takes place in liquid scrubbing processes would no longer result and the undesirable descent of the gas to near ground level would be prevented. An account of the first phase of these investigations, bench-scale experimentation, has been published recently by D. Bienstock, J. H. Field and J. G. Myers [U.S. Department of the Interior, Bureau of Mines; *Report of Investigations No. 5735*; 1961].

A very large number of absorbents, adsorbents and oxidation catalysts at 130° and 330°C, temperatures at which flue gas may be treated in power plant practice, have been examined. Adsorption of sulphur dioxide on activated carbons and molecular sieves was found to be considerably less efficient than removal by absorption. The most active absorbents tested were the oxides of manganese, cobalt, copper and alkalized alumina: 23 to 33 g of sulphur dioxide was removed by 100 g of absorbent at 130°C, while scrubbing more than 90 per cent of the dioxide from a simulated flue gas, and 19 to 61 g was removed at 330°C. A potash-promoted vanadium pentoxide is very effective in converting sulphur dioxide to trioxide; complete conversion in a simulated flue gas containing 0·35 per cent of the dioxide was obtained at 365°C.

National Survey of Atmospheric Pollution

At the Conference at Brighton, in October 1961, organized by the National Society for Clean Air, S. R. Craxford and other members of the Warren Spring Laboratory, D.S.I.R., contributed a paper on the national air pollution survey which is being planned by the Laboratory. For many years measurements have been made by local authorities, guided and assisted by the D.S.I.R., and the new survey is an attempt to obtain more significant information by means of a smaller, more economic, and more representative selection of measurement points. This will make it possible to judge the success of any remedial measures that may have been taken in any particular locality, and also assist local authorities in considering plans for future industrial development in relation to present levels of air pollution.

Towns throughout the country with above 5 000 population, have been graded according to domestic and industrial coal consumption per unit area, and natural ventilation characteristics, making 27 different categories in all. From these a random selection of 120 towns has been made. Daily measurements will be made of smoke and sulphur dioxide suspended in the air.

Flame Research Foundation

A symposium which has been arranged jointly by The Institute of Fuel and the British Committee of the Flame Research Foundation, will take place in London on Wednesday, 13 June 1962. The object is to discuss the application of the work of the Foundation to industry in the U.K.

Five papers will be published in the *Journal of the Institute of Fuel* before the conference, bringing the account of the experimental work of the Foundation up to date, and these, together with about six papers linking the work at IJmuiden with industrial application, will provide the basis of discussion.

Diesel Smoke Regulation

A Government regulation which will come into force from 1 January 1962, has recently been made to reduce diesel vehicle smoke by control

of the use of the excess fuel device [Motor Vehicles (Construction and Use) (Amendment) Regulations, 1961. *S.I. No. 1961/1313*; H.M.S.O.].

The excess fuel device is fitted to assist in starting from cold by injecting extra fuel, but is often used by drivers to gain extra power when overtaking or ascending hills, and produces dense black smoke. The new regulations will make it an offence for the device to be kept in operation once the engine has started or to be used while the vehicle is in motion.

Russian Air Pollution Literature

The U.S. Department of Commerce, Office of Technical Services, announces that the fifth volume in a continuing survey of Russian literature on air pollution and related occupational diseases, being conducted by Dr B. S. LEVINE under a U.S. Public Health Service Research Grant, is now available through the Office of Technical Services, Business and Defence Administration, U.S. Department of Commerce, Washington 25, D.C. (Price $3.50.)

Dr LEVINE's latest survey of Soviet literature dealing with the air pollution aspects of industrial public health problems contains translations of 45 articles [*Smokeless Air*, 1961, No. 119, 37].

The Shock Tube in Fuel and Combustion Research

Professor H. B. PALMER, Head of the Department of Fuel Technology, The Pennsylvania State University, Pa, who is carrying out programmes of research involving the use of the shock tube, has published a paper describing its principles and operation, and reviewing especially its use in fuel and combustion research [*J. Inst. Fuel*, 1961, **34**, 359].

The outstanding feature of the shock-tube technique is that it heats the reacting system at an unusually fast rate, at least 1 000 times faster than by conventional methods. Temperatures may be attained at which ionization is very significant. The process under examination may be quenched abruptly and the products analysed. In effect, processes with reaction times ranging from a few thousandths of a second down to about one millionth of a second may be studied at constant temperature, under conditions where the concentrations of reacting species are known.

In studying the pyrolysis of hydrocarbons by this means, measurements have been extended into the region of temperatures corresponding to those in typical flames, and it has been also possible to examine to some extent the early stages of pyrolysis instead of relying upon final products as the only clues to the nature of the complex steps in the decomposition. The shock-tube method has the important virtue of minimizing effects of heterogeneous reactions. The use of the method for investigating the pyrolysis of oxidizers has been very fruitful. It has shown, for example, that the Arrhenius equation for the rate constant of a unimolecular reaction

$$k = A \exp(-E/RT)$$

is quite inadequate when predicting rate constants at high temperatures from those at low temperatures.

Direct studies of gaseous combustion reactions in shock tubes may be classified into measurements of flame ignition temperatures and energies; exploration of the initiation of gaseous detonation; kinetic measurements on high-temperature combustion reactions; and studies of low-temperature oxidation.

Reference is made to a small amount of work on liquid fuels and on dispersions of solid fuels in air to produce ignition, and a comprehensive bibliography of 65 items is given.

W. A. KIRKBY

Publications

GAS SAMPLING AND CHEMICAL ANALYSIS IN COMBUSTION PROCESSES

C. Tiné. Oxford and New York: Pergamon, 1961. AGARDograph 47. *xv*+94 *pp.* 42*s* or $6.00

This text deals with the experimental techniques of gas sampling and analysis as applied to combustion phenomena of interest in aeronautics. It is sponsored by the Combustion and Propulsion Panel of AGARD who felt the need for such a review; the author was enabled to visit about thirty well-known research laboratories in countries associated with AGARD in order to gather information.

A short introduction is followed by a section describing the difficulties that arise in the sampling of combustion gases. Fundamental aspects are discussed and considerable attention is devoted to various types of sampling probe and to the quenching of combustion products. Reciprocating engine combustion appears to be neglected and no mention is made of suitable valves for withdrawing samples of gas, at predetermined positions of the stroke, from the cylinders of experimental engines. Nevertheless, this is perhaps the most valuable section of the book.

In the section on gas analysis it is pointed out that the present trend is towards instrumental analysis which combines speed and accuracy. However, some of these methods are dealt with but briefly; thermal conductivity methods are dismissed in a paragraph and no reference is given; descriptions of instruments such as the paramagnetic oxygen analyser and the non-dispersive infra-red analyser do little more than illustrate the principles of their operation.

The section dealing with the analysis of intermediate oxidation products is incomplete; mention is made neither of polarographic methods in the identification and determination of peroxides and aldehydes nor of the recent application of paper chromatography to the study of peroxides. The three pages of information on gas chromatography is sparse in view of the power of this technique and the enormous volume of published work—the references quoted do not go beyond 1958. Mass spectrometry is dealt with in one page. Several of the experimental methods of analysis discussed are described fully only in unpublished reports.

On the whole this monograph is disappointing and its price is relatively high. The section on gas sampling will probably be of value to the chemist whilst that on gas analysis will serve as a brief introduction to this field for the engineer. Much of the information in this latter section is, however, available in more detail elsewhere and the individual research worker will probably prefer to make his own survey, taking due note of recent research papers and specialized reviews which nowadays appear so frequently.

R. Long

AERODYNAMIC CAPTURE OF PARTICLES

Edited by E. G. Richardson. Oxford: Pergamon, 1960. *viii*+20 *pp.* 50*s*

This book reports the papers and subsequent discussion of a conference held in 1960. In the first session, theoretical aspects were discussed including dust deposition from a turbulent air stream, electric charge effects in aerosol particle collisions and a paper on the classical computations of the capture of particles by spheres.

The second session was concerned with experimental application of capture techniques; these included deposition of radioactive particles from very low concentrations by diffusion, eddy diffusion and molecular diffusion in addition to condensation nuclei. Wood smoke particles, impingement of water drops on a surface at high speeds and removal by means of fibrous filters were also presented and discussed.

In the final session the capture of fine particles by rain drops was the main subject but also included were such subjects as the suppression of airborne dust by water spray and the theoretical collision efficiency of small drops.

The problems discussed in these papers have a very wide range of industrial applications. In both the papers and particularly in the discussions, present views on the behaviour of fine particles with special reference to their capture are given in great detail.

F. H. Garner

LONG RANGE BALLISTIC MISSILES

E. Burgess. Chapman & Hall: London, 1961. *xii*+255 *pp.* (illus.). 35*s*

The development of long range missiles began in earnest in the U.S.A. about 1953, and since then the rate of progress has been fantastic. Billions of dollars have been spent in producing a huge variegated fleet of missiles and space probes. The present volume is an attempt to describe this armoury.

The author appears at his best when he is describing actual events or pieces of machinery. His opening historical survey is detailed and interesting, and so is his description of the manufacture of the Atlas and Titan missiles. His chapter on missile support gives some idea of the immense complexity of the ground equipment needed for launching missiles. These descriptive chapters are lavishly illustrated with over a hundred photographs.

The survey is, however, quite uncritical, and no explanation is offered for such enigmas of American policy as the development of the two intermediate range missiles, Thor and Jupiter, neither of which could be used in the defence of the U.S.A., nor for the turning down of the Army project Orbiter, which

might have used current equipment to put a satellite up in 1956. Even the controversy between the champions of solid and liquid propellants gets scant mention.

The general chapters on trajectories, vehicles and re-entry bodies are poor. The matter is not presented in a coherent manner and there is endless repetition—to take a typical example, chapter four contains two virtually identical paragraphs on propellant sloshing, one on page 98 and the other on page 102! The discussion of propulsion units contains some definite mis-statements—that the jet velocity is proportional to the temperature, for example—and a good deal of muddled thinking.

The short chapter on defence is a sensible summary of present opinions, but sees no end to the current supremacy of attack over defence.

There is a short bibliography but no detailed references are included. Although the book might be useful for giving a general survey of American missiles to anyone who can easily absorb unrelated statistics, it cannot be recommended to the serious student of rocket technology.

S. L. Bragg

TECHNICAL DATA ON FUEL

Edited by H. M. Spiers. Sixth edition, published by British National Committee, World Power Conference: London, 1961. 352 *pp.* 83 *diagrams.* 393 *tables.* 60s

The sixth edition of *Technical Data* is published this year in a new larger format which has eliminated the need for folded insertions and many of the diagrams have been enlarged so as to improve their usefulness. There have been six previous revisions of the text since the first edition was published in 1928 and consequently the matter in the book has been reconsidered in every aspect for example as regards accuracy, ease of reference and general readability.

Nevertheless the text of the last impression of 1955 has again been thoroughly considered by the steering committee and a number of new sections added as for example atomic nuclear fuels, viscosity blending of oils, flow in fluidized systems and tables with the properties of some additional refrigerants. In addition the text has been thoroughly revised in the light of new information and in line with the latest British Standard specifications.

Technical Data in its new format with considerable extension in text material will be more useful to its many users who are familiar with its scope and it should be widely popular with all interested in fuel problems.

F. H. Garner

AUTOMATIC CONTROL AND COMPUTER ENGINEERING

Volume 1

Edited by V. V. Solodovnikov. Translation published by Pergamon Press: London and New York, 1961. ix + 502 *pp. (illus.).* 100s *or* $15.00

Many in the West, forgetting the Russian scientific heritage, were surprised by their revelations at the first Geneva Conference in 1955 or again when, in October 1957, they launched Sputnik 1. Yet all this is very much in the Russian tradition within which, in more recent years, the engineering sciences have been developed to take pride of place, with the physical sciences closely in support. Chemical research has met the demands made upon it by the atomic energy programme and others but, in general, the chemical industry is not in such a commanding position. In a press release of January 1960, Professor Alexander Nesmeyanov reviewed their immediate scientific aims. High priority was to be given to the development of computers for control and information handling purposes and also to the needs of the chemical industries. The Russians looked to advanced control systems as a means for increasing productivity; for the control of processes with dynamic problems which placed them beyond the reaction response of human operators; and for the control of processes requiring extreme or otherwise physically hazardous conditions where completely remote control is necessary.

With this in mind, this first volume publishing translations of papers presented at the U.S.S.R. conference on Automatic Control and Computer Engineering organized by the Scientific Technical Society of the Instrument Making Industry is likely to be eagerly sought after. However, this is a collection of specialized papers with the emphasis largely on computer engineering and then its application to control. There is little in it for the man with a general interest who would like to know more of the potentialities of advanced computer control for chemical processes.

Approximately one quarter of the papers are devoted to aspects of computer and control theory. The first article is concerned with the problem of discerning relevant information in the presence of noise. Another article on 'Extreme Control Systems' outlines an optimizing strategy. The principles of construction of a continuous-action computer applying an iterative method to the solution of integral equations which has considerable potentialities for the assessment of automatic control system dynamics from response data are described. Other papers discuss methods for the assessment of system transfer functions from the correlation of input and output fluctuations and so on.

More than half the volume is given to the 'hardware' of computers. Interest is concentrated on digital systems because of their high potential accuracy but most of the application examples are of analogue control systems. Largely, semiconductor techniques are employed in the digital system and mention is made of the need to master the mass production techniques for entire semiconductor computing elements. Memory systems; high speed pulse relay systems; logical circuits; input and output systems—the 'bottle neck' in high speed digital systems; and Western analogue/digital converter systems are all reviewed.

The few applications described are all drawn from the heavy engineering industries: the determination of optimum cutting conditions, rolling mill, steel smelting and blast furnace control and so on. An interesting article describes an analogue of a blast furnace in which 39 variables are considered. Some change slowly and are set by hand. The others, including the furnace gas temperature, hot and cold blast temperatures, pressure and quantity of the cold

blast, carbon monoxide, carbon dioxide and hydrogen content of the furnace gas can change quickly and are fed continuously to the computer and from this the course of the process can be followed. However, though accurate under generally steady operating conditions, discrepancies occur for marked disturbances due to over-simplification of the analogue model.

Since this volume was originally published in Russia in 1958, several of the contributors have visited the U.K. The time for translation and publication in the U.K. is not unduly long but it does suffer through having no index other than the contents list. The conference did not concern itself at all with the problem of an adequate criterion against which a chemical process may be optimized nor with the humbler but desperate problem of achieving accurate and consistent measurements on which the application of advanced control systems to the chemical industry must depend. There is a very real sense in which it is easier to control the launching of a Sputnik than to operate an entirely reliable integrated process control system, day in day out, through the year.

J. S. M. Botterill

RULES AND METHODS FOR CALCULATING THE PHYSICO-CHEMICAL PROPERTIES OF PARAFFINIC HYDROCARBONS

V. M. Tatevskii, V. A. Benderskii and S. S. Yarovoi. Translated by B. P. Mullins. Pergamon: London and New York, 1961. *ix*+128 *pp.* (illus.). 30s or $5.50

In spite of the vast amount of data in the technical literature on the physical and chemical properties of pure substances, most scientists and engineers must have experienced the feeling of frustration which arises when they are reluctantly forced to the conclusion that no-one has measured the property of the substance they are concerned with. In consequence, empirical correlations and techniques for the calculation of such properties fulfil an important function in applied sciences. Nevertheless, because these methods are generally regarded, often quite incorrectly, as being of no fundamental significance, they are rarely taught in formal educational courses. Teaching is generally limited to noting that the properties of homologues vary with molecular weight in a systematic manner, or that properties of molecules such as molar refractivities or heat capacities are, in suitable circumstances, approximately additive functions of the properties of the constituent atoms.

However, such simple observations are clearly inadequate when dealing with hydrocarbons and their derivatives since many structural isomers exist which possess the same numbers of each kind of atom. Because of the experimental difficulties of synthesizing high molecular weight organic compounds, particularly hydrocarbons, accurate techniques for estimating properties from structure are invaluable to those concerned with preparing or using these materials. To be of any value at all, the techniques of estimating the properties must take into account, not only the contribution from each atom to the property of the molecule, but also small corrections to it caused by the proximity of adjacent atoms in the same molecule.

The methods developed in this book achieve this requirement by relatively simple procedures. The techniques described permit the estimation of molar volumes, molar refractivities, heats of phase transformation, vapour pressures, heats of formation and combustion, boiling points and densities of alkanes. Systematically tabulated data facilitate the calculations. Other tables compare calculated values with the available experimental data and so permit assessment of the accuracy of the procedures. The methods described are clearly the result of many years of tedious computations by the Russian authors and their associates. Unfortunately few references are made to the several similar methods described in Western literature. Comparison with the group contribution method, which is similar in principle and is applicable to a wider variety of compounds although so far applied to fewer properties, would be very interesting. The methods are clearly described and easy to apply, but the user should beware of a number of minor errors in the equations and text.

C. W. Nutt

Letters to the Editors

Letters to the Editors on points of scientific interest related to combustion and flames are invited. The Editors do not hold themselves responsible for opinions expressed in correspondence. Anonymous contributions cannot be accepted.

Radiative Features of Ozone–Oxygen Mixture Decomposition Flames and Non-adiabatic Flame Theory

DR BERLAD has invited me to comment on his letter, with the above title, published on page 301 of your issue for September 1961. This letter suggests that he and I hold conflicting views about the relative magnitudes of the influences of heat losses from the reaction zone and from the combustion products on inflammability limits; he proposes to decide which of us is right by means of experiments on ozone-decomposition flames. My comments are as follows:

(*1*) I do not hold the view ascribed to me by Dr BERLAD concerning the dominance of downstream heat losses. I accept as obvious that, if the reaction products do not radiate, reaction-zone radiation cannot be ignored.

(*2*) If the differential equations on which I based my theory of inflammability limits are solved exactly, the relative importance of reaction-zone and downstream radiation can be *deduced* from the solution; no *assumption* is necessary in this regard.

(*3*) It is true that in order to obtain a simple algebraic solution, I neglected reaction-zone radiation in my paper [*Proc. Roy. Soc. A*, **1957, 240,** 83]. That paper was concerned with flames with radiating combustion products and I desired an algebraic solution which would enable the essence of the situation to be perceived without the necessity for extensive computations. My solution of the equations was therefore acknowledged to be an approximate one. Dr BERLAD, I presume, has made a different approximation, which will be more accurate than mine in some cases and less in others.

(*4*) I am not committed to my approximation in the way Dr BERLAD is to his, and decline to enter lists on its behalf. However, it seems to me that the scope and accuracy of the two approximations could only be compared by a *mathematical* investigation rather than an *experimental* one. I believe that such an investigation would show that heat losses in the reaction zone could be neglected when the products radiate strongly but not otherwise.

(*5*) An experimental study of the ozone flame cannot provide a *general* answer to the question: 'Does product or reaction-zone radiation dominate the situation?' There *is* no general answer. Nevertheless, if compared with an *exact* solution of the differential equations, such a study could strengthen our understanding of inflammability limits. I am glad Dr BERLAD is making it.

D. B. SPALDING

Department of Mechnical Engineering,
Imperial College of Science and Technology,
London, S.W.7

(*Received September 1961*)

Inflammability Limits and Flame Radiation Loss Rates

THE recent exchange of views between Professor SPALDING[1] and myself[2] bears some additional comment.

(*1*) We have noted[2] that the radiation loss pattern associated with the ozone decomposition flame *obviously demands* that any general theory consider 'reaction zone' radiative losses. Professor SPALDING now[1] agrees.

(*2*) However, the remaining part of Professor SPALDING's belief[1] '. . . that heat losses in the "reaction zone" could be neglected when the products radiate strongly . . .' is inconsistent with the theoretically deduced results[3,4] *for just such a case*, the propane–oxygen–nitrogen system:

For the propane–oxygen–nitrogen flame system we note that:

(*a*) the radiative loss rate is highest just downstream of the 'reaction zone';

(*b*) both approximate[3] *and* machine[4] solutions of the accepted conservation equations, *which include 'reaction zone' losses*, yield inflammability (as well as quenching) limits *which are insensitive to the downstream (higher) losses*;

(*c*) in these analyses[3, 4], the critical conditions for existence/non-existence of a solution of the flame equations is taken to define an extinction limit. Clearly, if the 'reaction zone' cannot physically exist (no solution), neither can the 'post reaction zone'—regardless of whether or not 'the products radiate strongly'.

A. L. BERLAD

General Dynamics/Convair,
Scientific Research Laboratory,
San Diego, California

(Received October 1961)

References

[1] SPALDING, D. B. *Combustion & Flame*, 1961 (this issue)
[2] BERLAD, A. L. *Combustion & Flame*, 1961, **5**, 301
[3] BERLAD, A. L. and YANG, C. H. *Combustion & Flame*, 1960, **4**, 325
[4] YANG, C. H. *Combustion & Flame*, 1961, **5**, 163

On the Definition of Weak Detonation Waves

THE classic theory of detonation waves assumes that the mass flow per unit area is constant through the wave. This assumption must always be true for the case of an infinite plane wave, and also applies to the typical practical case of a wave moving down a cylindrical duct. With small stationary waves, however, such as have recently been studied experimentally by J. A. NICHOLLS *et al.*[1], it is possible for the streamlines to diverge appreciably in the burning zone. Broader definitions of the terms 'weak' and 'strong' detonation, which take account of this possibility, are proposed below.

A detonation wave consists essentially of a shock wave followed and sustained by chemical reaction[2]. Solution of the equations for conservation of mass, momentum and energy in a duct of constant area yield an apparently indeterminate relationship between the wave speed, the heat added in the wave, and the velocity of the product gases relative to the wave. In the currently accepted terminology the possible solutions are grouped into weak detonations, for which the downstream velocity is supersonic relative to the wave, and strong detonations, for which it is subsonic[3]. The intermediate boundary case, where the downstream velocity is just sonic, is referred to as a Chapman–Jouguet, or C–J, wave.

Now the flow downstream of a normal shock is necessarily subsonic, and it is a well known part of the theory of compressible gas flows that, in a duct of constant area, a subsonic flow *cannot* be accelerated to supersonic velocities by adding heat to it[4]: nor are steady expansion shocks possible, from subsonic to supersonic flow, since they would contravene the Second Law of Thermodynamics. Thus, if the flow is supersonic downstream of a combustion wave of constant cross section it must in fact be supersonic throughout the wave, and there can be no shock involved. (By the same token the so-called strong deflagration, which involves a subsonic approach velocity and supersonic outlet velocity, is thermodynamically inadmissible).

Since a shock is considered an essential part of a genuine detonation, the weak wave as defined above is not a true detonation at all, but merely a case of localized heat addition in supersonic flow. No such supersonic deflagration has ever been observed in practice, and indeed the reaction rates and transfer coefficients required to support it would be fantastically high. Localized heat addition to a fully supersonic stream can certainly occur as, for example, in the so-called 'condensation shock' in supersaturated flow, but this involves no combustion and cannot by any stretch of the imagination be considered a detonation: nor, incidentally, is it likely to involve a true shock—since this would tend to raise the stream temperature back above the saturation limit—so the flow in the wave is never subsonic. Thus a weak detonation, as hitherto defined, is either impossible or a contradiction in terms, and an alternative definition appears both admissible and desirable.

It may be shown that elimination of the velocity terms from the equations of continuity of mass, momentum and energy across a wave yields the Rankine–Hugoniot equation

$$k(pr-1)-p+r=q$$

where p is the static pressure ratio across the wave, p_1/p_0; r is the inverse of the density ratio across the wave, ρ_0/ρ_1; $k=(\gamma+1)/(\gamma-1)$ is a function of the specific heat ratio, γ; and $q=2Q(\rho_0/p_0)$ is a dimensionless expression of the enthalpy change in the wave, ΔQ. *Figure 1* shows a typical plot of this hyperbolic relation between pressure and density ratios for a given value of q.

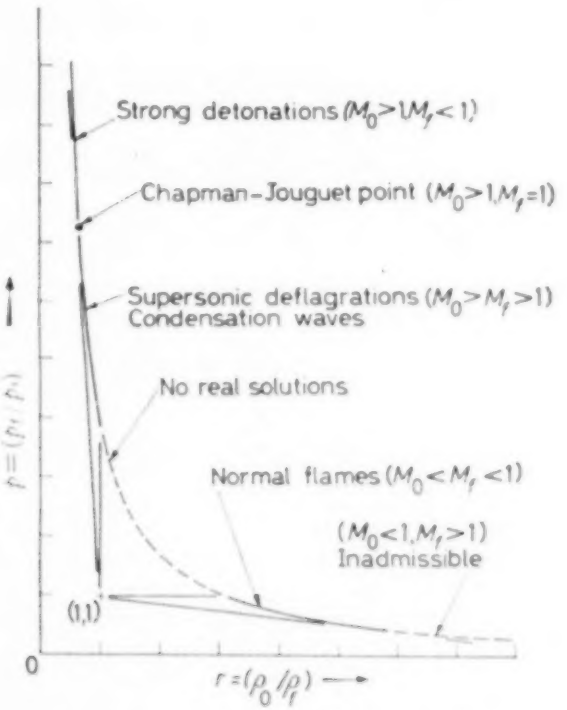

Figure 1. Rankine–Hugoniot curve for constant area flow

The slope of the line joining any point on the curve to the point (1, 1) gives the incident Mach number of the wave (M_0) via the relation

$$M_0^2=(p-1)/\gamma(1-r)$$

Examination of *Figure 1*, or perusal of the discussion in ref. 3, shows that the speed of a strong detonation wave is always greater than that of a C–J wave with the same heat release. Alternatively, a strong detonation is one in which the heat release is less than that in a C–J wave travelling at the same speed. In more rigorous terms, a strong detonation may be defined as a shock-preceded combustion wave in which the ratio of the heat release rate to the enthalpy of the undisturbed gases is *less* than that of the C–J wave travelling at the same Mach number. A more expressive description would perhaps be a 'fast' detonation wave.

In contrast, it would appear reasonable to define a weak, or 'slow', detonation as a supersonic combustion wave travelling at a *lower* speed than that of the C–J wave with the same specific heat release; or, with equal validity, as a wave in which the heat addition per unit mass was *greater* than that in a C–J wave travelling at the same speed. It may be noted that this is in opposition to the original definition by which the heat release in both weak and strong waves is less than that in the C–J wave travelling at the same speed.

It will at once be objected that the equations of continuity, momentum and energy show this new kind of weak wave to be physically impossible: according to the Rankine–Hugoniot equation, the minimum supersonic wave speed for a given specific heat release is limited to that of the Chapman–Jouguet detonation. This is quite true, *for a constant area duct*; and of course most experiments with moving waves have been carried out in such ducts. However, now that stationary detonation waves have been successfully stabilized in a free stream, there seems to be no reason why one could not conceive, at least in principle, a detonation wave, necessarily of finite width, in which the initiating shock was followed by deflagration in an expanding stream. Since there is no theoretical limit to the heat that can be added to the flow in a duct of expanding area, a heat release greater than the C–J value is possible in this case. Furthermore, it is possible for heat addition in an *expanding* duct to accelerate subsonic flow to supersonic velocities, so the flow downstream of a weak detonation, as now defined, *may* be supersonic, though it is not necessarily so.

As a proof that the possibility of such detonation waves exists one may cite the remark of J. A. NICHOLLS[5] that, in some of his later tests on stabilized detonation waves, the shock was stabilized at a velocity *below* that of a C–J wave. This observation implies that the fuel:air ratio was above the value that would produce a C–J wave at the same Mach number, so more burning was taking place than would be theoretically possible in a constant area duct, and the flow must have been diverging downstream of the shock. Nicholls mentions that the shock and combustion waves tended to separate under these conditions, but this effect may be due to the conditions of the experiment, in which the relative heat release was increased by reducing the total temperature of the flow at a particular Mach number. Had it been possible to obtain the same ratio of heat release to initial enthalpy by increasing the fuel concentration at constant temperature, such separation might not have occurred.

In other tests reported by Nicholls, when the fuel:air ratio was reduced to a value lower than that needed to sustain a C–J detonation at the approach Mach number of the shock disc, the disc moved up to a new position where the incident velocity was low enough to give either a C–J or a slightly strong detonation. The flow was then slightly subsonic behind the wave, and would presumably constrict as the pressure fell. In general, of course, any flow constriction behind a stationary detonation wave would make it a strong one.

Summarizing, then, the following definitions are suggested:

(*a*) a detonation wave is a supersonic combustion wave in which chemical reaction is initiated by a shock;

(*b*) a normal, or Chapman–Jouguet, detonation is one in which the downstream velocity is just sonic relative to the wave, the streamlines remaining parallel;

(*c*) a strong, or fast, detonation is one with a velocity greater than that of the C–J wave with the same specific heat release. Alternatively, a strong wave can be regarded as a detonation in which the specific heat release is less than that of a C–J wave propagating at the same velocity;

(*d*) a weak, or slow, detonation is one with a velocity less than that of the C–J wave with the same heat release; that is, one with a greater heat release than that of a C–J wave with the same velocity. The streamlines inevitably diverge in the combustion region of such a wave, and the final downstream velocity may be either subsonic or supersonic with respect to the wave front.

Provided that the static temperature behind the shock is high enough for ignition, but not so high that complete reaction is virtually instantaneous, Nicholls's results suggest that it is possible to produce a weak detonation wave in this new sense. On the other hand, a weak detonation in the old sense, which involved supersonic flow downstream of a shock, appears impossible on thermodynamic grounds.

S. L. BRAGG

Rolls-Royce Ltd,
P.O. Box 31, Derby

(*Received October 1961*)

References

[1] NICHOLLS, J. A., DABORA, E. K. and GEALER, R. L. *Seventh Symposium (International) on Combustion*, p. 766. Butterworths: London, 1959

[2] LEWIS, B. and VON ELBE, G. *Combustion, Flames and Explosions of Gases*. Academic Press: New York, 1951

[3] PENNER, S. S. *Explosions, Detonations, Flammability and Ignition*. AGARDograph 31, Chap. V. Pergamon: London, 1959

[4] SHAPIRO, A. H. *Compressible Fluid Flow*, Chap. 7. Ronald Press: New York, 1953

[5] NICHOLLS, J. A. University of Michigan, *Tech. Note U.M.R.I.*, Project 2874, June 1960

Classified Contents

Acetylene, high temperature pyrolysis of, 1400° to 2500°K, 55
[Acetylene, hydrogen and preheated propane flames], supersonic combustion in, 315
Acetylene, infra-red analysis for, in flame gases at 1820°K, 349

[Benzene–air system], technique for sampling reaction intermediates in, in a rapid compression machine, 229
Boron-containing flames, light scattering measurements on particles condensed from, 93
Burning rate of a fuel droplet in an oxidizing atmosphere, 207
Burning velocities of hydrogen–air and hydrogen–oxygen mixtures. Determination by burner method with schlieren photography, 7
Burning velocities of the hydrogen peroxide decomposition flame, 273
Burning velocity and reaction rates in constant temperature non-adiabatic flames, 135
Burning velocity and the structure of flames near extinction limits, 163

Cellulosic materials, experiments on the ignition of, by thermal radiation, 369
Chronology and topography of sparks at minimum energy for ignition, 235
Coal dusts, influence of coal rank and fineness on inflammability index of, 300
Combustion instability of solid propellants, experimental research in, 149
Combustion Institute meetings, 288
Combustor performance, effect of flame configuration on, 141
Comparison of temperatures of [hydrogen–air] flames on porous burners, 111
Cool flame oxidation products of diethyl ether, evidence for carbon suboxide, C_3O_2, as an intermediate product in, 65

Definition of weak detonation waves, 390
Diffusion flames, buoyant, some experiments on, 359
[*iso*Dodecane and aviation kerosine], effect of reduced pressure and airflow on liquid surface diffusion flames of, 319

Effect of flame configuration on combustor performance, 141
Effect of reduced pressure and airflow on liquid surface diffusion flames, 319
Effect of temperature on the ignition characteristics of hydrocarbons, 243
Estimate of rate of growth of lead oxide particles in engine gases, 205
[Ethylene–air mixtures], perturbation studies of flames of, by changes in composition, 45
Evidence for carbon suboxide, C_3O_2, as an intermediate product in the cool flame oxidation products of diethyl ether, 65
Experimental research in combustion instability of solid propellants, 149
Experiments on the ignition of cellulosic materials by thermal radiation, 369

Flame propagation by non-branching chain reactions, 123
Flame radiation loss rates, inflammability limits and, 389
Fluorine–ammonia flames, thermal radiation from, 1
Formaldehyde and carburetted air, inflammability ranges of, under reduced pressure, 191
Fuel droplet, burning rate of, in an oxidizing atmosphere, 207

Gaseous oxidation of *para*xylene, 249
Gas turbine combustion chamber fitted with a swirl atomizer, scale effect in, Part II, 35

High temperature pyrolysis of acetylene 1400° to 2500°K, 55
Hydrocarbon flames, suggested origin of the anomalous line-reversal temperatures in the reaction zone of, 331
Hydrocarbon fuels, knock resistance and anti-knock with, 87
Hydrocarbon–oxygen reactions, thermochemical equilibrium in, involving polyatomic forms of carbon, 257
Hydrocarbons, effect of temperature on the ignition characteristics of, 243
Hydrocarbons, liquid, rate of combustion from free surfaces of, 283
[Hydrogen and hydrocarbon] flames, burning velocity and reaction rates in constant temperature non-adiabatic, 135
Hydrogen–air and hydrogen–oxygen mixtures. Determination of burning velocities by burner method with schlieren photography, 7
[Hydrogen–air] flames, comparison of temperatures of, on porous burners, 111
Hydrogen–oxygen flame, laminar flame propagation velocities in terms of flame parameters in, 302
Hydrogen peroxide decomposition flame, burning velocities of, 273

Ignition of gases by electrically heated wires, 113
Inflammability limits, 111
Inflammability limits and flame radiation loss rates, 389
Inflammability ranges of formaldehyde and carburetted air under reduced pressure, 191
Influence of coal rank and fineness on inflammability index of coal dusts, 300
Infra-red analysis for acetylene in flame gases at 1820°K, 349
Inhibition of combustion reactions by inorganic lead compounds, 71

Knock resistance and anti-knock with hydrocarbon fuels, 87

Laminar burning velocity [of hydrogen–oxygen, methane–oxygen and ethylene–oxygen], pressure dependence of, by the spherical bomb method, 209
Laminar flame propagation velocities in terms of flame parameters in a hydrogen–oxygen flame, 302
Lead compounds, inorganic, inhibition of combustion reactions by, 71

Lead oxide particles in engine gases, estimate of rate of growth of, 205
Light scattering measurements on particles condensed from boron-containing flames, 93

Measurement of the temperature of some frictional sparks, 341
[Methane–air and hydrogen–air mixtures], ignition of, by electrically heated wires, 113
[Methane–air], measurement of the temperature of some frictional sparks [using], 341
[Methane–air mixtures], chronology and topography of sparks in, at minimum energy for ignition, 235

Ozone flames, quenching diameter of, 81
Ozone–oxygen mixture decomposition flames, radiative features of, and non-adiatic flame theory, 301, 389

Perturbation studies of flames by changes in composition, 45
Preflame reactions, shock waves from, in a motored engine, 27
Pressure dependence of laminar burning velocity by the spherical bomb method, 209
Pressure-wave, flamefront interaction, studies of screeching combustion and, 175
Propagation velocity and structure of single step reaction flames, 305

Quenching diameter of ozone flames, 81

Radiative features of ozone–oxygen mixture decomposition flames and non-adiabatic flame theory, 301, 389
Rate of combustion from free surfaces of liquid hydrocarbons, 283
Recent developments and notes, 99, 195, 291, 377
Relationship between burning velocity and space velocity of a spherical combustion wave in a closed spherical chamber, 77

Scale effect in a gas turbine combustion chamber fitted with a swirl atomizer, Part II, 35
Shock waves from preflame reactions in a motored engine, 27
Some experiments on buoyant diffusion flames, 369
Spherical combustion wave, relationship between burning velocity and space velocity of, in a closed spherical chamber, 77
Structure of flames, burning velocity and, near extinction limits, 163
Structure, propagation velocity and, of single step reaction flames, 305
Studies of screeching combustion and pressure-wave, flamefront interaction, 175
Suggested origin of the anomalous line-reversal temperatures in the reaction zone of hydrocarbon flames, 331
Supersonic combustion, 315

Technique for sampling reaction intermediates in a rapid compression machine, 229
Theoretical study of interactions between two parallel burning fuel plates, 221
Theory of steady laminar spherical flame propagation — analytical solutions, 11
— analogue solutions, 19
Thermal radiation from fluorine–ammonia flames, 1
Thermochemical equilibrium in hydrocarbon–oxygen reactions involving polyatomic forms of carbon, 257

Weak detonation waves, definition of, 390

*para*Xylene, gaseous oxidation of, 249

Author Index

ADLER, J.: review of *Computer Abstracts and Computer News*, 109
— and SPALDING, D. B.: Flame propagation by non-branching chain reactions, 123
AGNEW, J. T. and GRAIFF, L. B.: The pressure dependence of laminar burning velocity by the spherical bomb method, 209
AGNEW, J. T.: *see* GAY, N. R., AGNEW, J. T., WITZELL, O. W. and KARABELL, C. E.
—: *see* ROBLEE, Jr, L. H. S., AGNEW, J. T. and WARK, Jr, K.
ASHMAN, L. E. and BÜCHLER, A.: The ignition of gases by electrically heated wires, 113
AUEN, C. F. and GREENE, E. F.: The high temperature pyrolysis of acetylene 1400° to 2500° K, 55

BAMFORD, J. A.: *see* HERBERT, M. V. and BAMFORD, J. A.
BARDWELL, J.: Inhibition of combustion reactions by inorganic lead compounds, 71
BARNARD, J. A. and HAWTIN, P.: The gaseous oxidation of *para*xylene, 249
BERLAD, A. L.: Radiative features of ozone–oxygen mixture decomposition flames and non-adiabatic flame theory, 301
—: Inflammability limits and flame radiation loss rates, 389
BLACKMAN, A. W.: Studies of screeching combustion and pressure-wave, flamefront interaction, 175
BOTTERILL, J. S. M.: review of *Fluidization and Fluid-particle Systems*, 110
—: review of *Automatic Control and Computer Engineering*, Vol. I, 386
BRAGG, S. L.: On the definition of weak detonation waves, 390
—: review of *Long Range Ballistic Missiles*, 387
BRANSOM, S. H.: review of *Enthalpy–Entropy Chart for Air and Combustion Gases*, 109
BRUNOLD, Miss M. P., DELBOURGO, R. and LAFFITTE, P.: On the inflammability ranges of formaldehyde and carburetted air under reduced pressure, 191

BÜCHLER, A.: *see* ASHMAN, L. E. and BÜCHLER, A.
BULEWICZ, E. M. and PADLEY, P. J.: Suggested origin of the anomalous line-reversal temperatures in the reaction zone of hydrocarbon flames, 331

CARTLIDGE, J. and TIPPER, C. F. H.: Knock resistance and anti-knock with hydrocarbon fuels, 87
CRUMP, J. E.: *see* PRICE, E. W., MATHES, H. B., CRUMP, J. E. and MCGIE, M. R.

DELBOURGO, R.: *see* BRUNOLD, Miss M. P., DELBOURGO, R. and LAFFITTE, P.
DE SENDAGORTA, J. M.: Propagation velocity and structure of single step reaction flames, 305
DIXON-LEWIS, G. and ISLES, G. L.: Inflammability limits, 111
DIXON-LEWIS, G. and WILLIAMS, A: Laminar flame propagation velocities in terms of flame parameters in a hydrogen–oxygen flame, 302

EISENHIGH, R. H.: The influence of coal rank and fineness on the inflammability index of coal dusts, 300
EULNER, R., MERTENS, J. and POTTER, R. L.: Thermal radiation from fluorine–ammonia flames, 1

FENIMORE, C. P. and JONES, G. W.: Burning velocity and reaction rates in constant temperature non-adiabatic flames, 135
FINE, B.: Comparison of temperatures of flames on porous burners, 111
FIREY, J. C. and LAVI, R. R.: Shock waves from preflame reactions in a motored engine, 27
FONS, W. L.: Rate of combustion from free surfaces of liquid hydrocarbons, 283

GARNER, F. H.: review of *Aerodynamic Capture of Particles*, 385
—: review of *Technical Data on Fuel*, 386
GAY, N. R., AGNEW, J. T., WITZELL, O. W. and KARABELL, C. E.: Thermochemical equilibrium in hydrocarbon–oxygen reactions involving polyatomic forms of carbon, 257
GRAIFF, L. B.: *see* AGNEW, J. T. and GRAIFF, L. B.
GREENE, E. F.: *see* ATEN, C. F. and GREENE, E. F.
GROSSE, A. V.: *see* STRENG, A. G. and GROSSE, A. V.

HAWTIN, P.: *see* BARNARD, J. A. and HAWTIN, P.
HERBERT, M. V. and BAMFORD, J. A.: Scale effect in a gas turbine combustion chamber fitted with a swirl atomizer, Part II, 35
HIRST, R. and SUTTON, D.: The effect of reduced pressure and airflow on liquid surface diffusion flames, 319

ISLES, G. L.: *see* DIXON-LEWIS, G. and ISLES, G. L.

JAIN, V. K.: *see* SPALDING, D. B. and JAIN, V. K.
—: *see* SPALDING, D. B., JAIN, V. K. and SAMAIN, M. D.
JONES, G. W.: *see* FENIMORE, C. P. and JONES, G. W.

KARABELL, C. E.: *see* GAY, N. R., AGNEW, J. T., WITZELL, O. W. and KARABELL, C. E.
KERKAN, W. E.: Light scattering measurements on particles condensed from boron-containing flames, 93
KEHAT, E.: *see* SATTERFIELD, C. N. and KEHAT, E.
KIRKBY, W. A.: Recent developments and notes, 99, 195, 291, 377

KIRKBY, W. A.: review of *Progress in Combustion Science and Technology*, Vol. I, 203
KYDD, P. H. and MULLANEY, G. J.: Supersonic combustion, 315

LAFFITTE, P.: *see* BRUNOLD, Miss M. P., DELBOURGO, R. and LAFFITTE, P.
LAVI, R. R.: *see* FIREY, J. C. and LAVI, R. R.
LITCHFIELD, E. L.: Chronology and topography of sparks at minimum energy for ignition, 235
LONG, R.: review of *Coal Tar Fuels*, 204
—: review of *Gas Sampling and Chemical Analysis in Combustion Processes*, 385

MCGIE, M. R.: *see* PRICE, E. W., MATHES, H. B., CRUMP, J. E. and MCGIE, M. R.
MATHES, H. B.: *see* PRICE, E. W., MATHES, H. B., CRUMP, J. E. and MCGIE, M. R.
MERTENS, J.: *see* EULNER, R., MERTENS, J. and POTTER, R. L.
MIESSE, C. C.: The effect of flame configuration on combustion performance, 141
MILLIKAN, R. C.: Infra-red analysis for acetylene in flame gases at 1820°K, 349
MULLANEY, G. J.: *see* KYDD, P. H. and MULLANEY, G. J.

NEWNS, G. R.: review of *Advances in Polarography*, 204
NUTT, C. W.: review of *Elements of the Kinetic Theory of Gases*, 110
—: review of *Rules and Methods for Calculating the Physico-chemical Properties of Paraffinic Hydrocarbons*, 387

PADLEY, P. J.: *see* BULEWICZ, E. M. and PADLEY, P. J.
PARKER, W. G.: review of *The Chemistry of Propellants*, 109
POTTER, R. L.: see EULNER, R., MERTENS, J. and POTTER, R. L.
PRICE, E. W., MATHES, H. B., CRUMP, J. E. and MCGIE, M. R.: Experimental research in combustion instability of solid propellants, 149

RAE, D.: A measurement of the temperature of some frictional sparks, 341
RAEZER, S. D.: The relationship between burning velocity and space velocity of a spherical combustion wave in a closed spherical chamber, 77
RAFTERY, M. M.: *see* THOMAS, P. H., WEBSTER, C. T. and RAFTERY, M. M.
ROBLEE, Jr. L. H. S.: A technique for sampling reaction intermediates in a rapid compression machine, 229
—, AGNEW, J. T. and WARK, Jr. K.: Evidence for carbon suboxide, C_3O_2, as an intermediate product in the cool flame oxidation products of diethyl ether, 65

SALOOJA, K. C.: Effect of temperature on the ignition characteristics of hydrocarbons, 243
SAMAIN, M. D.: *see* SPALDING, D. B., JAIN, V. K. and SAMAIN, M. D
SATTERFIELD, C. N. and KEHAT, E.: Burning velocities of the hydrogen peroxide decomposition flame, 273
SCHALLA, ROSE L.: Perturbation studies of flames by changes in composition, 45

SENIOR, D. A.: Burning velocities of hydrogen–air and hydrogen–oxygen mixtures. Determination by burner method with schlieren photography, 7
SIMMS, D. L.: Experiments on the ignition of cellulosic materials by thermal radiation, 369
SPALDING, D. B.: Radiative features of ozone–oxygen mixture decomposition flames and non-adiabatic flame theory, 389
—: *see* ADLER, J. and SPALDING, D. B.
SPALDING, D. B. and JAIN, V. K.: Theory of steady laminar spherical flame propagation: analytical solutions, 11
— — and SAMAIN, M. D.: Theory of steady laminar spherical flame propagation, analogue solutions, 19
STRENG, A. G. and GROSSE, A. V.: The quenching diameter of ozone flames, 81
SUTTON, D.: *see* HIRST, R. and SUTTON, D.

TAU-YI TOONG: A theoretical study of interactions between two parallel burning fuel plates, 221
THOMAS, P. H., WEBSTER, C. T. and RAFTERY, M. M.: Some experiments on buoyant diffusion flames, 359
TIPPER, C. F. H.: *see* CARTLIDGE, J. and TIPPER, C. F. H.

WARK, Jr, K.: *see* ROBLEE, Jr, L. H. S., AGNEW, J. T. and WARK, Jr, K.
WEBSTER, C. T.: *see* THOMAS, P. H., WEBSTER, C. T. and RAFTERY, M. M.
WILLIAMS, A.: *see* DIXON-LEWIS, G. and WILLIAMS, A.
WILLIAMS, F. A.: On the burning rate of a fuel droplet in an oxidizing atmosphere, 207
WITZELL, O. W.: *see* GAY, N. R., AGNEW, J. T., WITZELL, O. W. and KARABELL, C. E.
WRIGHT, P. G.: An estimate of the rate of growth of lead oxide particles in engine gases, 205

YANG, C. H.: Burning velocity and the structure of flames near extinction limits, 163

Name Index

ADAMS, E. N. 123, 134, 305, 310, 313
ADAMS, G. K. 13, 18, 280, 282
ADLER, J. 110, 123, 134, 302
AGNEW, J. T. 65, 66, 70, 209, 216, 218, 219, 234, 257
AGNEW, W. G. 65, 66, 70, 207, 234, 289
AKITA, K. 375
ALEKSEEVA, V. G. 340
ALLEN, C. R. 206
ALLEN, Jr, H. 318
ALLEN, K. R. 237, 241
AMIEL, J. 256
ARMITAGE, J. B. 64
ARNOLD, J. S. 121, 240, 241
ASHMAN, L. E. 113, 120
ASHTON, L. A. 102
ATEN, C. F. 55, 64
AU, G. 381
AUDIBERT, E. 203
AVERY, W. H. 174, 288, 289

BACON, J. F. 377
BADIN, E. J. 74
BALLENTYNE, D. W. G. 204
BALLIK, E. A. 259, 272
BAME, J. L. 233, 234
BAMFORD, J. A. 35, 43
BARDWELL, J. 71, 75, 206
BARNARD, J. A. 249
BARR, J. 328, 330, 360, 367
BARTHOLOMÉ, E. 7, 10
BARTLESON, J. D. 73, 74
BARUSCH, M. R. 74, 91
BASEVICH, V. YA. 100
BATE, S. C. C. 102
BAULKNIGHT, C. 276, 282
BAXTER, A. D. 203
BECKERS, A. 233, 234
BECKETT, C. 289
BEER, J. M. 296, 297
BEHRENS, H. 53
BELLES, F. E. 174, 282
BENDERSKII, V. A. 387
BENEDICT, W. S. 297
BENNETT, W. J. 289
BENT, H. A. 349, 357
BERL, W. G. 289
BERLAD, A. L. 84, 85, 111, 112, 174, 281, 282, 289, 302, 389, 390
BERNAL, J. 340
BETKER, G. W. 207, 234
BIENSTOCK, D. 383
BIRD, J. F. 162
BIRD, R. B. 85, 305, 306, 310–312
BLACKHAM, A. U. 91
BLACKMAN, A. W. 175, 190
BLACKSHEAR, P. L. 178, 187, 190, 296
BLANC, M. V. 241
BLINOV, V. I. 283, 287, 328, 330, 367
BLUM, H. A. 105
BOUSE, Jr, A. B. 70
BONE, W. A. 256
BOTHA, J. P. 140, 174
BOTTERILL, J. S. M. 110, 387
BOUDART, M. 289
BOWDEN, F. P. 289
BOYS, S. F. 305, 310, 311, 313
BRADLEY, J. N. 292
BRADLEY, R. S. 206, 207
BRAGG, S. L. 289, 386, 392
BRAHAM, R. R. 291
BRALSFORD, R. 340
BRANSOM, S. H. 109
BREWER, L. 258, 272
BRICKER, C. E. 256
BRINKLEY, Jr, S. R. 148, 272, 289
BRÓIDA, H. P. 289, 331, 340
BROKAW, R. S. 120, 243, 247
BROUGHTON, P. F. 341, 346
BROWN, A. M. 104
BROWN, J. E. 91
BROWNLEE, W. G. 156, 162
BRUCE, H. D. 287
BRUNOLD, Miss M. P. 191
BÜCHLER, A. 113
BULEWICZ, E. M. 331, 340
BURGESS, E. 385
BURGOYNE, J. H. 10, 249, 258, 289, 292, 320, 330
BURHOP, E. H. S. 339, 340
BURKE, E. 219, 282
BURKE, S. P. 359, 360, 367
BURROWS, M. C. 298

CALCOTE, H. F. 282, 289, 316, 340
CALDWELL, F. R. 77, 80, 212, 219
CAMBEL, A. B. 148, 289
CAMPBELL, D. E. 85, 123, 134
CAMPBELL, K. 108
CARR, R. E. 208
CARTLIDGE, J. 87, 91
CASSEL, H. M. 289
CECKLER, W. 273, 282
CHAMBERLAIN, G. H. N. 73, 74
CHAVEN, R. 256
CHEANEY, D. E. 74, 91, 206
CHERNESKEY, M. 74, 75, 206
CHU, BOA-TEH. 53
CLARKE, J. S. 289
CLEMENTI, E. 258, 272
CLINGMAN, W. H. 219, 275, 282
CLUMPP, C. V. 86

Coffin, K. P. 346
Cohen, P. M. 74, 234
Cole, D. J. 349, 357
Conan, H. R. 7, 10
Cook, C. L. 64
Cook, E. B. 217, 219
Cook, E. C. 282
Cook, M. A. 289
Cooper, G. 174
Corner, J. 162, 305, 310, 311, 313
Coward, H. F. 100, 121, 174
Crandall, H. W. 91
Crawford, Jr. B. 349, 357
Craxford, S. R. 383
Crotty, W. 98
Crowe, T. H. 282
Crozier, W. D. 291
Crump, J. E. 149
Csaba, J. 297
Cullen, R. E. 218, 219
Cullis, C. F. 91, 254, 256
Culshaw, G. W. 282
Curtis, C. F. 85, 123, 134, 305, 306, 310–312
Cybulski, W. B. 300, 301

Dabora, E. K. 318, 390, 392
Dadieu, A. 381
Dale, P. 25
Damköhler, G. 141, 148
Daniel, W. A. 234
Daniell, P. J. 203
Da Riva, I. 313
Darling, S. M. 73, 74
Davies, D. A. 74, 91, 206
Davis, A. 74, 91, 206
Deckers, J. 140, 334, 340
Deffet, L. 199, 290
de Jaegere, S. 334, 340
Delbourgo, R. 191, 194
Demetriades, S. T. 276, 282
de Sendagorta, J. M. 305, 313
Desseine, J. 197
de Vos, J. C. 342, 346
Diederichsen, J. 218, 219
DiPerna, C. J. 101
Dixon-Lewis, G. 112, 304
Donovan, R. E. 70
Dorsch, R. G. 318
Dorsett, Jr. H. G. 107
Downs, D. 206, 207, 234
Draper, C. S. 234
Draper, P. 105
Drell, I. L. 282
Ducarme, J. 109, 203
Duff, R. E. 289
Dugger, G. L. 289
Dumoutet, P. 197

Echols, L. S. 233, 234
Edmondson, R. B. 121, 240, 241
Edse, R. 217–219, 282
Edwards, H. E. 148, 272

Egerton, Sir Alfred C. 74, 219, 256
Egloff, G. 318
Emeleus, H. J. 65, 70
Emmons, H. W. 227, 283, 287, 289
Enikolopyan, N. S. 253, 256
Entwhistle, N. 64
Erhard, K. H. L. 206
Eschenbach, R. C. 216, 218, 219
Essenhigh, R. H. 301
Eulner, R. 1
Evans, M. G. 207
Evans, Marjorie W. 289
Evans, W. H. 4, 5
Everett, A. J. 219
Eyre, R. 330
Ezrokhi, A. B. 297

Fabian, J. 380
Falconer, J. W. 99
Fay, J. A. 289
Feigenbutz, L. V. 258, 272
Fenimore, C. P. 135, 140, 352, 357
Fenn, J. B. 282, 289
Fiegl, F. 253, 256
Field, J. H. 383
Fine, B. 111
Fingerson, L. M. 296
Fiock, E. F. 77, 80, 212, 219
Firey, J. C. 27, 34
Fishenden, M. 293
Fletcher, E. A. 203, 318
Flitcroft, T. 63, 64
Foex, M. 379
Foner, S. N. 289
Fons, W. L. 283, 289, 328, 330, 364, 367
Forst, W. 276, 282
Fort, R. 256
Fortziati, A. F. 256
Foss, W. 98
Foster, P. J. 101
Fowler, R. H. 340
Frank, C. E. 91
Frank-Kamenetsky, D. A. 120
Fremont, H. A. 352, 357
Friedman, R. 282, 289
Fristrom, R. M. 171, 174, 276, 282, 289
Froede, W. 200
Fuchs, N. A. 207
Fuhs, A. E. 222, 227

Gabor, D. 199
Gardner, J. B. 256
Gardon, R. 375
Garner, F. H. 201, 298, 385, 386
Garside, J. E. 282
Garvin, D. 289
Gay, N. R. 257, 258, 272
Gaydon, A. G. 5, 10, 120, 121, 289, 297, 327, 328, 330, 331, 340
Gayhart, E. L. 121, 240, 241
Gazley, C. 359, 367

Gealer, R. L. 318, 390, 392
Geckler, R. D. 289
Germain, J. E. 381
Gerstein, M. 53, 85, 203, 243, 247, 282, 318
Gibbs, G. J. 282
Giguére, P. A. 282
Gilles, P. W. 258, 272
Glaser, P. E. 379
Glasgow, Jr. A. R. 256
Glassman, I. 289
Glasstone, S. 98
Glockler, G. 259, 272
Godsave, G. A. E. 208
Goldsmith, M. 208
Gordon, A. S. 290
Gordon, J. S. 258, 272
Gordon, S. 262, 272
Gordy, W. 340
Goulard, R. 294
Grad, H. 153, 162
Graiff, L. B. 209, 219
Grard, F. 193, 194
Gray, K. H. 108, 202
Gray, P. 256, 282, 290
Green, Jr. L. 160, 162, 197
Greene, E. F. 55, 64
Griffiths, S. T. 108, 207
Gross, D. 364, 367
Gross, R. A. 318
Grosse, A. V. 81, 86, 290
Groume-Grijmailo, W. E. 203
Grove, J. R. 282
Grumer, J. 217, 219, 282
Guenoche, H. 53
Guest, P. G. 241
Guest, P. J. 121
Guggenheim, E. A. 110
Gutman, V. R. 197

Hansom, B. S. 330
Harris, E. J. 91
Harris, P. V. 340
Hart, R. W. 150, 153, 162
Hartley, Sir Harold. 196
Hartwell, F. J. 100
Hawthorne, W. R. 359, 367
Hawtin, P. 249
Hausen, H. 380
Heath, D. J. 101
Henkel, M. H. 313
Henkel, M. J. 134
Herbert, M. V. 35, 43, 200, 203
Herne, H. 341, 342, 346
Herzberg, G. 259, 272, 302, 355, 357
Hesselberg, H. E. 207
Heyrovsky, J. 204
Hill, F. 290
Hilsenrath, J. 282
Hindersinn, K. 318
Hinkley, P. L. 375
Hinshelwood, C. N. 91, 256
Hirata, M. 222, 227
Hirschfelder, J. O. 85, 123, 134, 305, 306, 310–313
Hirst, R. 319

SENIOR, D. A.: Burning velocities of hydrogen–air and hydrogen–oxygen mixtures. Determination by burner method with schlieren photography, 7
SIMMS, D. L.: Experiments on the ignition of cellulosic materials by thermal radiation, 369
SPALDING, D. B.: Radiative features of ozone–oxygen mixture decomposition flames and non-adiabatic flame theory, 389
—: *see* ADLER, J. and SPALDING, D. B.
SPALDING, D. B. and JAIN, V. K.: Theory of steady laminar spherical flame propagation: analytical solutions, 11
— — and SAMAIN, M. D.: Theory of steady laminar spherical flame propagation, analogue solutions, 19
STRENG, A. G. and GROSSE, A. V.: The quenching diameter of ozone flames, 81
SUTTON, D.: *see* HIRST, R. and SUTTON, D.

TAU-YI TOONG: A theoretical study of interactions between two parallel burning fuel plates, 221
THOMAS, P. H., WEBSTER, C. T. and RAFTERY, M. M.: Some experiments on buoyant diffusion flames, 359
TIPPER, C. F. H.: *see* CARTLIDGE, J. and TIPPER, C. F. H.

WARK, Jr, K.: *see* ROBLEE, Jr, L. H. S., AGNEW, J. T. and WARK, Jr, K.
WEBSTER, C. T.: *see* THOMAS, P. H., WEBSTER, C. T. and RAFTERY, M. M.
WILLIAMS, A.: *see* DIXON-LEWIS, G. and WILLIAMS, A.
WILLIAMS, F. A.: On the burning rate of a fuel droplet in an oxidizing atmosphere, 207
WITZELL, O. W.: *see* GAY, N. R., AGNEW, J. T., WITZELL, O. W. and KARABELL, C. E.
WRIGHT, P. G.: An estimate of the rate of growth of lead oxide particles in engine gases, 205

YANG, C. H.: Burning velocity and the structure of flames near extinction limits, 163

Name Index

ADAMS, E. N. 123, 134, 305, 310, 313
ADAMS, G. K. 13, 18, 280, 282
ADLER, J. 110, 123, 134, 302
AGNEW, J. T. 65, 66, 70, 209, 216, 218, 219, 234, 257
AGNEW, W. G. 65, 66, 70, 207, 234, 289
AKITA, K. 375
ALEKSEEVA, V. G. 340
ALLEN, C. R. 206
ALLEN, Jr, H. 318
ALLEN, K. R. 237, 241
AMIEL, J. 256
ARMITAGE, J. B. 64
ARNOLD, J. S. 121, 240, 241
ASHMAN, L. E. 113, 120
ASHTON, L. A. 102
ATEN, C. F. 55, 64
AU, G. 381
AUDIBERT, E. 203
AVERY, W. H. 174, 288, 289

BACON, J. F. 377
BADIN, E. J. 74
BALLENTYNE, D. W. G. 204
BALLIK, E. A. 259, 272
BAME, J. L. 233, 234
BAMFORD, J. A. 35, 43
BARDWELL, J. 71, 75, 206
BARNARD, J. A. 249
BARR, J. 328, 330, 360, 367
BARTHOLOMÉ, E. 7, 10
BARTLESON, J. D. 73, 74
BARUSCH, M. R. 74, 91
BASEVICH, V. YA. 100
BATE, S. C. C. 102
BAULKNIGHT, C. 276, 282
BAXTER, A. D. 203
BECKERS, A. 233, 234
BECKETT, C. 289
BEÉR, J. M. 296, 297
BEHRENS, H. 53
BELLES, F. E. 174, 282
BENDERSKII, V. A. 387
BENEDICT, W. S. 297
BENNETT, W. J. 289
BENT, H. A. 349, 357
BERL, W. G. 289
BERLAD, A. L. 84, 85, 111, 112, 174, 281, 282, 289, 302, 389, 390
BERNAL, J. 340
BETKER, G. W. 207, 234
BIENSTOCK, D. 383
BIRD, J. F. 162
BIRD, R. B. 85, 305, 306, 310-312
BLACKHAM, A. U. 91
BLACKMAN, A. W. 175, 190
BLACKSHEAR, P. L. 178, 187, 190, 296
BLANC, M. V. 241
BLINOV, V. I. 283, 287, 328, 330, 367
BLUM, H. A. 105
BOLSE, Jr, A. B. 70
BONE, W. A. 256
BOTHA, J. P. 140, 174
BOTTERILL, J. S. M. 110, 387
BOUDART, M. 289
BOWDEN, F. P. 289
BOYS, S. F. 305, 310, 311, 313
BRADLEY, J. N. 292
BRADLEY, R. S. 206, 207
BRAGG, S. L. 289, 386, 392
BRAHAM, R. R. 291
BRALSFORD, R. 340
BRANSOM, S. H. 109
BREWER, L. 258, 272
BRICKER, C. E. 256
BRINKLEY, Jr, S. R. 148, 272, 289
BROIDA, H. P. 289, 331, 340
BROKAW, R. S. 120, 243, 247
BROUGHTON, P. F. 341, 346
BROWN, A. M. 104
BROWN, J. E. 91
BROWNLEE, W. G. 156, 162
BRUCE, H. D. 287
BRUNOLD, Miss M. P. 191
BÜCHLER, A. 113
BULEWICZ, E. M. 331, 340
BURGESS, E. 385
BURGOYNE, J. H. 10, 249, 256, 289, 292, 320, 330
BURHOP, E. H. S. 339, 340
BURKE, E. 219, 282
BURKE, S. P. 359, 360, 367
BURROWS, M. C. 298

CALCOTE, H. F. 282, 289, 334, 340
CALDWELL, F. R. 77, 80, 212, 219
CAMBEL, A. B. 148, 289
CAMPBELL, D. E. 85, 123, 134
CAMPBELL, K. 108
CARR, R. E. 208
CARTLIDGE, J. 87, 91
CASSEL, H. M. 289
CECKLER, W. 273, 282
CHAMBERLAIN, G. H. N. 73, 206
CHAYEN, R. 256
CHEANEY, D. E. 74, 91, 206
CHERNESKEY, M. 74, 75, 206
CHU, BOA-TEH. 53
CLARKE, J. S. 289
CLEMENTI, E. 258, 272
CLINGMAN, W. H. 219, 275, 282
CLUMPP, C. V. 86

Coffin, K. P. 346
Cohen, P. M. 74, 234
Cole, D. J. 349, 357
Conan, H. R. 7, 10
Cook, C. L. 64
Cook, E. B. 217, 219
Cook, E. C. 282
Cook, M. A. 289
Cooper, G. 174
Corner, J. 162, 305, 310, 311, 313
Coward, H. F. 100, 121, 174
Crandall, H. W. 91
Crawford, Jr, B. 349, 357
Craxford, S. R. 383
Crotty, W. 98
Crowe, T. H. 282
Crozier, W. D. 291
Crump, J. E. 149
Csaba, J. 297
Cullen, R. E. 218, 219
Cullis, C. F. 91, 254, 256
Culshaw, G. W. 282
Curtis, C. F. 85, 123, 134, 305, 306, 310–312
Cybulski, W. B. 300, 301

Dabora, E. K. 318, 390, 392
Dadieu, A. 381
Dale, P. 25
Damköhler, G. 141, 148
Daniel, W. A. 234
Daniell, P. J. 203
Da Riva, I. 313
Darling, S. M. 73, 74
Davies, D. A. 74, 91, 206
Davis, A. 74, 91, 206
Deckers, J. 140, 334, 340
Deffet, L. 199, 290
de Jaegere, S. 334, 340
Delbourgo, R. 191, 194
Demetriades, S. T. 276, 282
de Sendagorta, J. M. 305, 313
Desseine, J. 197
de Vos, J. C. 342, 346
Diederichsen, J. 218, 219
DiPerna, C. J. 101
Dixon-Lewis, G. 112, 304
Donovan, R. E. 70
Dorsch, R. G. 318
Dorsett, Jr, H. G. 107
Downs, D. 206, 207, 234
Draper, C. S. 234
Draper, P. 105
Drell, I. L. 282
Ducarme, J. 109, 203
Duff, R. E. 289
Dugger, G. L. 289
Dumoutet, P. 197

Echols, L. S. 233, 234
Edmondson, R. B. 121, 240, 241
Edse, R. 217–219, 282
Edwards, H. E. 148, 272
Egerton, Sir Alfred C. 74, 219, 256
Egloff, G. 318
Emeleus, H. J. 65, 70
Emmons, H. W. 227, 283, 287, 289
Enikolopyan, N. S. 253, 256
Entwhistle, N. 64
Erhard, K. H. L. 206
Eschenbach, R. C. 216, 218, 219
Essenhigh, R. H. 301
Eulner, R. 1
Evans, M. G. 207
Evans, Marjorie W. 289
Evans, W. H. 4, 5
Everett, A. J. 219
Eyre, R. 330
Ezrokhi, A. B. 297

Fabian, J. 380
Falconer, J. W. 99
Fay, J. A. 289
Feigenbutz, L. V. 258, 272
Fenimore, C. P. 135, 140, 352, 357
Fenn, J. B. 282, 289
Fiegl, F. 253, 256
Field, J. H. 383
Fine, B. 111
Fingerson, L. M. 296
Fiock, E. F. 77, 80, 212, 219
Firey, J. C. 27, 34
Fishenden, M. 293
Fletcher, E. A. 203, 318
Flitcroft, T. 63, 64
Foex, M. 379
Foner, S. N. 289
Fons, W. L. 283, 289, 328, 330, 364, 367
Forst, W. 276, 282
Fort, R. 256
Fortziati, A. F. 256
Foss, W. 98
Foster, P. J. 101
Fowler, R. H. 340
Frank, C. E. 91
Frank-Kamenetsky, D. A. 120
Fremont, H. A. 352, 357
Friedman, R. 282, 289
Fristrom, R. M. 171, 174, 276, 282, 289
Froede, W. 200
Fuchs, N. A. 207
Fuhs, A. E. 222, 227

Gabor, D. 199
Gardner, J. B. 256
Gardon, R. 375
Garner, F. H. 201, 298, 385, 386
Garside, J. E. 282
Garvin, D. 289
Gay, N. R. 257, 258, 272
Gaydon, A. G. 5, 10, 120, 121, 289, 297, 327, 328, 330, 331, 340
Gayhart, E. L. 121, 240, 241
Gazley, C. 359, 367
Gealer, R. L. 318, 390, 392
Geckler, R. D. 289
Germain, J. E. 381
Gerstein, M. 53, 85, 203, 243, 247, 282, 318
Gibbs, G. J. 282
Giguére, P. A. 282
Gilles, P. W. 258, 272
Glaser, P. E. 379
Glasgow, Jr. A. R. 256
Glassman, I. 289
Glasstone, S. 98
Glockler, G. 259, 272
Godsave, G. A. E. 208
Goldsmith, M. 208
Gordon, A. S. 290
Gordon, J. S. 258, 272
Gordon, S. 262, 272
Gordy, W. 340
Goulard, R. 294
Grad, H. 153, 162
Graiff, L. B. 209, 219
Grard, F. 193, 194
Gray, K. H. 108, 202
Gray, P. 256, 282, 290
Green, Jr, L. 160, 162, 197
Greene, E. F. 55, 64
Griffiths, S. T. 108, 207
Gross, D. 364, 367
Gross, R. A. 318
Grosse, A. V. 81, 86, 290
Groume-Grijmailo, W. E. 203
Grove, J. R. 282
Grumer, J. 217, 219, 282
Guenoche, H. 53
Guest, P. G. 241
Guest, P. J. 121
Guggenheim, E. A. 110
Gutman, V. R. 197

Hansom, B. S. 330
Harris, E. J. 91
Harris, P. V. 340
Hart, R. W. 150, 153, 162
Hartley, Sir Harold. 196
Hartwell, F. J. 100
Hawthorne, W. R. 359, 367
Hawtin, P. 249
Hausen, H. 380
Heath, D. J. 101
Henkel, M. H. 313
Henkel, M. J. 134
Herbert, M. V. 35, 43, 200, 203
Herne, H. 341, 342, 346
Herzberg, G. 259, 272, 302, 355, 357
Hesselberg, H. E. 207
Heyrovsky, J. 204
Hill, F. 290
Hilsenrath, J. 282
Hindersinn, K. 318
Hinkley, P. L. 375
Hinshelwood, C. N. 91, 256
Hirata, M. 222, 227
Hirschfelder, J. O. 85, 123, 134, 305, 306, 310–313
Hirst, R. 319

Hirth, J. P. 205, 207
Hoare, D. E. 74, 75, 206, 256, 276, 282
Hoare, M. F. 282
Hoffmann, S. K. 296
Hofmann, F. W. 339, 340
Holm, J. M. 203
Hooker, W. J. 56, 64
Hottel, H. C. 1, 5, 283, 287, 289, 290, 297, 341, 346, 359, 367
Howe, E. D. 379
Hubbard, E. H. 103
Huber, E. W. 200
Huellmantel, L. W. 148
Huff, V. N. 262, 272
Hughes, C. A. 329, 330
Hughes, E. C. 73, 74
Hulse, C. 293
Hurd, C. D. 68, 70
Huxtable, W. H. 204

Inagaki, K. 379
Ingold, K. U. 255, 256
Isles, G. L. 112

Jackson, J. L. 243, 247
Jacobson, M. 107
Jaffe, J. H. 297
Jain, V. K. 11, 18, 19, 25
James, C. G. 340
Jenkins, F. A. 258, 272
Johnson, H. R. 256
Jones, E. R. H. 64, 120
Jones, G. W. 135, 140, 174, 357
Jones, W. H. 290
Jost, W. 234
Jouy, M. 53
Jovellanos, J. V. 234
Just, Th. 382

Kamada, O. 379
Kanevsky, J. N. 222, 227
Kapp, N. M. 219, 359, 367
Karabell, C. E. 257
Karlovitz, B. 290
Kaskan, W. E. 93, 98, 111, 121, 140, 182, 190, 202, 290, 349, 351, 357
Katan, L. L. 320, 330
Katz, E. L. 258, 272
Kaufman, F. 290
Kaylor, H. M. 5
Kehat, E. 273, 282
Kelley, K. K. 207
Kerwin, E. M. 186, 187, 190
Keyes, F. G. 276, 282
Khitrin, L. N. 290
Khudiakov, G. N. 283, 287, 319, 327, 328, 330, 367
Kieffer, A. S. 86
Kinbara, T. 290
King, I. R. 332, 334, 337, 340
King, R. O. 74
Kirk, A. D. 88, 91
Kirkby, W. A. 108, 202, 204, 299, 367, 384
Kissel, R. 380
Klager, K. 381
Klein, R. 194
Klingel, A. R. 73, 74
Knewstubb, P. F. 289, 334, 337, 338, 340
Knox, J. H. 88, 91, 99
Knox, K. 55, 64
Kogarko, S. M. 100
Kohn, H. 339, 340
Kolmogorov, A. N. 303, 304
Kondratiev, V. A. 65, 70
Kunc, J. F. 234
Kunii, D. 110
Kydd, P. H. 290, 315

Ladbury, J. W. 254, 256
Laffitte, P. 191, 194, 290
Laidler, K. J. 64, 340
Laszlo, T. S. 379
Law, Margaret. 375
Lavi, R. R. 27
Lawrence, E. K. 375
Lawson, D. I. 104, 375
Leary, W. A. 207, 229, 234
Lecomte, J. 297
Lee, J. C. 282
Lees, B. 105
Lefebvre, A. H. 43, 203, 219
Legrand, J. 194
Leigh, D. 227
Lenior, J. M. 162
Levedahl, W. J. 233, 234
Levine, O. 53
Levine, R. S. 290, 384
Levy, A. 292, 328, 330
Lewis, A. 108, 202
Lewis, B. 10, 74, 80, 81, 85, 113, 119, 120, 174, 219, 241, 276, 282, 290, 330, 392
Li, Y. T. 234
Ling, S. C. 296
Linnett, J. W. 7, 10, 219, 282, 290
Lintin, D. R. 240, 241
Litchfield, E. L. 235, 241
Liu, I. D. 282
Livengood, J. C. 34, 207, 229, 234
Livingston, H. K. 91
Loefthus, A. 259, 272
Lohse, W. 109
Long, R. 204, 385
Longmuir, I. S. 204
Longwell, J. P. 148, 290, 318, 329, 330
Lorell, J. 208
Lossing, F. P. 255, 256
Lovachev, L. A. 123, 134, 298, 302–304
Lovell, W. G. 74
Ludg, F. J. 382
Lutz, O. 109
Lype, E. F. 291

McAdams, W. H. 165, 174
McClelland, J. A. 338, 340
McClure, F. T. 150, 153, 162, 290
McCone, A. 313
Macfarlane, W. A. 293
McGie, M. R. 149
McGrath, I. A. 101
McKellar, J. F. 194
Mackenzie, J. D. 98
McLane, C. K. 282
McManus, Jr, H. N. 290
McMasters, A. W. 287
Magee, E. M. 106
Mandelshtam, S. L. 340
Mandlekar, M. R. 74, 75
Mann, D. E. 98
Manton, J. 219, 278, 282
Marble, F. E. 190, 290
Markley, F. X. 91
Markstein, G. H. 53, 290
Marsel, C. J. 290
Marshall, J. G. 281, 282
Martin, F. J. 290
Marvin, C. F. 77, 80, 212, 219
Masdin, E. G. 105
Masi, J. F. 290
Maslen, S. K. 190
Mason, J. M. 89, 91, 207
Mason, T. N. 300, 301
Massey, H. S. W. 339, 340
Mathes, H. B. 149, 162
Maxwell, W. R. 295
Mayer, E. 174
Mayers, M. A. 200
Mecke, R. 297
Melentiev, P. V. 120
Mellor, J. W. 75
Mendes, M. A. T. 275, 282
Merk, H. J. 162
Mertens, J. 1
Miesse, C. C. 141, 148, 290
Millán, G. 123, 134, 306, 313
Miller, Joan E. 375
Miller, R. E. 243, 247
Millikan, R. C. 98, 349, 357
Milliken, B. B. 219, 278, 282
Minkoff, G. J. 55, 63, 219, 256, 349, 357
Minorsky, N. 162
Mitchell, A. C. G. 340
Monkhouse, A. C. 196
Monnot, G. 341, 346
Moon, C. W. 318
Moore, F. K. 190
Moore, N. P. W. 219, 290
Morey, G. W. 95, 98
Morrell, G. 203
Morrell, V. 262, 272
Morse, P. M. 190
Morton, B. L. 361, 367
Morton, F. 201
Mosher, H. S. 91
Mozer, C. F. 121
Mullaney, G. J. 315
Mullins, B. P. 243, 247, 328, 330, 387

Munson, R. J. 338, 340
Munson, T. R. 4, 5
Murphy, A. J. 106
Myers, J. G. 383
Myers, P. S. 290

Nachbar, W. 160, 162, 207
Nagy, J. 107
Nerad, A. J. 290
Nesmeyanov, A. 386
Neu, J. T. 70, 91
Neumann, R. K. 174
Newitt, D. M. 55, 63, 64, 249, 256
Newns, G. R. 204
Nicholls, J. A. 290, 318, 390, 392
Nicholls, R. W. 297
Nichols, P. 290
Nielsen, A. H. 5
Nishiwaki, N. 222, 227
Noreen, A. E. 182, 190
Norrish, R. G. W. 55, 64, 74, 194, 206, 249, 256
Nutt, C. W. 110, 387

Olsen, H. L. 240, 241
Olsen, J. L. 121
Olson, W. T. 290
Oosterhoff, L. J. 205, 206
Oppenheim, A. K. 290
Orchin, M. 91
Osborn, J. R. 48, 53
Ostrander, M. H. 1, 5
Othmer, D. F. 110

Padley, P. J. 99, 331, 332, 340
Pahnke, A. J. 74, 75, 234
Palmer, G. 328, 330
Palmer, H. B. 108, 290, 384
Parker, W. G. 109, 290, 340
Pastell, D. L. 34, 234
Patel, N. G. 103
Patrick, E. A. K. 103
Patterson, Jr, W. L. 64
Pawlowski, J. 381
Payne, J. Q. 74, 91
Pease, R. N. 219, 275, 282
PennDorf, R. B. 98
Pesner, S. S. 1, 4, 5, 85, 109, 123, 134, 141, 148, 208, 222, 227, 241, 277, 282, 290, 297, 305, 312, 392
Perry, J. H. 282
Perry, Jr, R. H. 101
Petrein, R. J. 148
Petrovsky, I. G. 303, 304
Phillips, K. 237, 241
Pickard, R. W. 375
Pidgeon, L. M. 74
Pilgrim, F. D. 68, 70
Pinkel, I. I. 318
Pirsko, A. R. 287
Piskunov, N. S. 303, 304
Pitzer, K. S. 258, 272
Pobiarzhin, P. I. 378
Pong, W. Y. 287
Porter, G. 55, 64, 290
Potter, A. E. 84, 85, 203, 281, 282
Potter, R. L. 1
Pound, G. M. 205, 207
Powell, H. N. 352, 357
Prescott, R. 174
Preston, J. 120
Price, E. W. 149, 162, 290
Price, F. 98
Price, W. C. 340
Primm, G. C. 378
Protheroe, J. 74, 91, 206, 276, 282
Pusch, W. 382
Pyatt, E. C. 341, 346
Pye, D. R. 234

Rae, D. 341, 344, 346
Raezer, S. D. 77
Raftery, M. M. 359
Ramachandran, A. 291
Ramsay, D. A. 259, 272
Rasbash, D. J. 283, 287, 290, 320, 330
Rathbone, P. 256
Raviolo, V. G. 99
Rayle, W. D. 190
Rayleigh, Lord, J. W. S. 187, 190
Reed, L. E. 200
Reid, R. C. 207, 276, 282
Rendle, L. K. 105
Rex, J. F. 222, 227
Reznyakov, A. B. 201
Richards, S. S. 287
Richardson, E. G. 385
Ridley, R. G. 340
Rifkin, E. B. 75, 89, 91, 207, 234
Roberts, R. 290
Robillard, G. 162
Roblee, Jr, L. H. S. 65, 70, 229
Roeder, C. H. 212, 219
Rögener, H. 229, 234
Rogers, D. E. 190
Rogowski, Z. W. 283, 287, 320, 330
Rosenthal, J. E. 5
Rosin, P. O. 203, 293
Ross, A. 75
Rossini, F. D. 174, 256, 258, 272, 287
Rothrock, A. 290
Rudinger, G. 53
Rudolphy, E. C. 378
Russell, W. A. 207
Rutledge, P. 55, 63, 64
Ryan, N. W. 290

Sailes, W. N. 247
Saji, K. 367
Sakurai, T. 379
Salooja, K. C. 87, 91, 243, 247, 256
Samain, M. D. 18, 19, 21, 25
Sandri, R. 85
Sanz, S. 123, 134
Satterfield, C. N. 273, 276, 282
Saunby, J. B. 201
Saunders, O. A. 219, 293
Schalla, Rose L. 45
Schiewe, R. M. 48, 53
Schmidt, E. 200
Schneider, J. 340
Schoen, L. J. 194
Schultz-Grunow, F. 292
Schumann, T. E. W. 359, 360, 367
Schumb, W. C. 282
Scurlock, A. C. 290
Seely, B. K. 291
Seery, D. J. 108
Sehon, A. H. 272
Semenov, N. N. 113, 120, 205, 207, 256, 282, 305, 313
Senior, D. A. 7
Serafini, J. S. 318
Setze, P. C. 98
Seymour, E. H. 290
Shaffer, A. 352, 357
Shapiro, A. H. 91, 223, 226, 227, 318, 392
Sharp, E. R. 203
Shchelkin, K. I. 290
Shepherd, D. G. 290
Shepherd, W. C. F. 113
Sherbourne, R. K. 121, 240, 241
Sherwood, T. K. 207, 276, 282
Shishido, K. 379
Shuler, K. E. 279, 282, 290, 331, 333, 334, 340
Shvab, V. A. 208
Silcocks, C. G. 55, 63, 64
Simmonds, W. A. 360, 367
Simmons, R. F. 322, 330
Simms, D. L. 369, 375
Simon, D. M. 53, 174, 213, 219
Singer, J. M. 217, 219, 282
Sin-I Cheng. 153, 162
Sjoblom, Miss Joan. 174
Skinner, H. A. 63, 64
Small, N. J. H. 91
Smith, D. 219
Smith, Jr, R. W. 148, 272
Smith, V. C. 1, 5
Sofferis, J. W. 162
Sokolik, A. 34
Solodovnikov, V. V. 386
Solovev, V. V. 297
Sommer, A. 98
Spakowski, A. E. 174
Spalding, D. B. 11, 18, 19, 21, 25, 111, 123, 134, 140, 174, 208, 283, 287, 288, 290, 293, 299, 301–305, 313, 389, 390
Spandinger, E. 86
Spaulding, W. P. 134, 313
Spiers, H. M. 386
Stark, G. W. V. 283, 287, 320, 330
Starkman, E. S. 288, 290
Steacie, E. W. R. 55, 64
Stein, T. W. 282

Stewart, D. G. 35, 43
Stiehl, G. L. 258, 272
Stocks, G. W. 280, 282
Stoll, R. E. 378
Stout, H. P. 120
Strang, A. 91
Strauss, W. A. 217–219
Strauss, W. F. 282
Street, J. C. 234
Streng, A. G. 81, 86
Sturgis, B. M. 74, 234, 290
Suciu, S. N. 352, 357
Sueur, R. 381
Sugden, T. M. 289, 290, 332, 334, 337, 338, 340
Summerfield, M. 290
Sutton, D. 319
Swarc, M. 256, 272
Swarts, D. E. 91

Talley, C. P. 290
Talley, R. M. 5
Tang, T. L. 249, 256
Tatevskii, V. M. 387
Tau-Yi Toong. 221, 223, 226, 227
Taylor, C. F. 34, 207, 229, 234
Taylor, E. S. 207, 234
Taylor, G. I. 361, 367
Taylor, G. W. 249, 256
Taylor, R. L. 64
Teichmann, von H. 234
Thomas, A. 247
Thomas, J. R. 91
Thomas, P. H. 290, 359
Thompson, R. 290
Thomson, G. P. 340
Thomson, J. J. 340
Thring, M. W. 101, 290, 297, 382
Thurlow, G. G. 103
Timmermanns, J. 249, 256
Tiné, G. 385
Tipper, C. F. H. 87, 91
Tizard, H. T. 234
Todes, O. M. 120
Toone, B. 204
Tower, L. K. 190
Townend, D. T. A. 74, 75
Trent, C. H. 147, 148
Trombe, F. 379
Tropsch, H. 318
Tsien, H. S. 1, 5
Turner, J. S. 361, 367
Tyndall, A. M. 338, 340

Ubbelohde, A. R. J. P. 65, 70, 91, 106, 290, 298

Vaidya, W. M. 297
Valentin, P. 380
Van deHulst, H. C. 95, 98
Vanden Berghe, R. 199
van Dolah, R. W. 290
Vanpee, M. 193, 194
van Tiggelen, A. 140, 334, 340
Veltri, R. D. 377
Veron, M. 380
Voinov, C. 34
Volmer, M. 207
von Elbe, G. 10, 74, 80, 81, 85, 113, 119, 120, 174, 219, 276, 282, 290, 330, 392
von Kármán, T. 85, 123, 134, 277, 282, 305, 306, 310–312
Vortmeyer, D. 299

Wagman, D. D. 4, 5
Wagner, H. Gg. 290, 382
Walcutt, C. 89, 91, 207, 234
Walker, L. E. Q. 204
Wallin, S. C. 200
Walsh, A. D. 73–75, 91, 206, 234, 256, 276, 282, 290
Walsh, P. N. 98
Wark, Jr, K. 65, 70
Wark, W. 234
Warren, D. R. 73, 74
Way, S. 290
Weast, R. C. 243, 247
Weber, J. J. 334, 340
Webster, C. T. 359
Weddel, D. S. 359, 367
Wedin, B. 291
Wegener, P. P. 288, 290
Weinberg, F. J. 7, 10, 203, 290, 292, 328, 330
Weiss, M. A. 148, 318
Wentworth, J. T. 234
Wentworth, R. L. 276, 282
Westenberg, A. A. 290
Wheatley, P. J. 219
Wheeler, R. V. 113, 300, 301
Wheeler, R. W. 206, 207, 234
Whelan, P. F. 108, 202
Whiffen, D. H. 70
White, D. 98, 288
White, J. 108
Whiting, M. C. 63, 64
Whittier, J. Y. 377
Whittingham, G. 101, 108
Whytlaw-Gray, R. W. 207
Wibaut, J. P. 91
Wilde, K. A. 123, 134, 305, 310, 311, 313
Wilder, Jr, J. G. 318
Williams, A. 256, 304
Williams, D. J. 256
Williams, F. A. 208, 290
Williams, G. C. 290
Williams, H. R. 91
Williams, R. P. 107
Willingham, C. B. 256
Wilson, A. 174
Wilson, M. J. G. 360, 367
Wimpress, R. N. 162
Winter, E. F. 203
Wise, H. 208, 290
Witzell, O. W. 257
Wohl, K. 359, 367
Wohl, L. 219
Wolf, F. 109
Wolfhard, H. G. 5, 10, 120, 121, 218, 219, 290, 322, 327, 328, 330, 331, 340
Wong, E. L. 53, 213, 219
Wood, A. 162
Wooding, E. R. 240, 241
Wortberg, G. 292
Wright, P. G. 205, 207
Wu, P. C. 34, 234

Yagi, S. 110, 359, 367
Yakovlevskii, O. V. 100, 201
Yang, C. H. 111, 112, 163, 174, 302, 390
Yarovoi, S. S. 387
Yeung, S. C. 277
Young, G. H. S. 295
Yowell, H. L. 234
Yumlu, V. S. 111
Yust, V. E. 233, 234

Zang, W. I. 74
Zeldovich, Y. B. 208, 305, 310, 311–313
Zemansky, M. W. 340
Zenz, F. A. 110
Ziemer, R. W. 148
Zimm, B. 98
Zucrow, M. J. 290
Zukoski, E. E. 187, 190, 290